frontiers | Research Topics

Ocean acidification in Latin America

Edited by
Alberto Acosta, Betina J. Lomovasky, Joan-Albert Sanchez-Cabeza, Jose Martin Hernandez-Ayon and Cecilia Chapa-Balcorta

Published in
Frontiers in Marine Science

ISSN 1664-8714
ISBN 978-2-8325-7401-0
DOI 10.3389/978-2-8325-7401-0

Generative AI statement
Any alternative text (Alt text) provided alongside figures in the articles in this ebook has been generated by Frontiers with the support of artificial intelligence and reasonable efforts have been made to ensure accuracy, including review by the authors wherever possible. If you identify any issues, please contact us.

About Frontiers

Frontiers is more than just an open access publisher of scholarly articles: it is a pioneering approach to the world of academia, radically improving the way scholarly research is managed. The grand vision of Frontiers is a world where all people have an equal opportunity to seek, share and generate knowledge. Frontiers provides immediate and permanent online open access to all its publications, but this alone is not enough to realize our grand goals.

Frontiers journal series

The Frontiers journal series is a multi-tier and interdisciplinary set of open-access, online journals, promising a paradigm shift from the current review, selection and dissemination processes in academic publishing. All Frontiers journals are driven by researchers for researchers; therefore, they constitute a service to the scholarly community. At the same time, the *Frontiers journal series* operates on a revolutionary invention, the tiered publishing system, initially addressing specific communities of scholars, and gradually climbing up to broader public understanding, thus serving the interests of the lay society, too.

Dedication to quality

Each Frontiers article is a landmark of the highest quality, thanks to genuinely collaborative interactions between authors and review editors, who include some of the world's best academicians. Research must be certified by peers before entering a stream of knowledge that may eventually reach the public - and shape society; therefore, Frontiers only applies the most rigorous and unbiased reviews. Frontiers revolutionizes research publishing by freely delivering the most outstanding research, evaluated with no bias from both the academic and social point of view. By applying the most advanced information technologies, Frontiers is catapulting scholarly publishing into a new generation.

What are Frontiers Research Topics?

Frontiers Research Topics are very popular trademarks of the *Frontiers journals series*: they are collections of at least ten articles, all centered on a particular subject. With their unique mix of varied contributions from Original Research to Review Articles, Frontiers Research Topics unify the most influential researchers, the latest key findings and historical advances in a hot research area.

Find out more on how to host your own Frontiers Research Topic or contribute to one as an author by contacting the Frontiers editorial office: frontiersin.org/about/contact

Ocean acidification in Latin America

Topic editors

Alberto Acosta — Pontifical Javeriana University, Colombia

Betina J. Lomovasky — Institute of Marine and Coastal Research (IIMyC), Argentina

Joan-Albert Sanchez-Cabeza — National Autonomous University of Mexico, Mexico

Jose Martin Hernandez-Ayon — Autonomous University of Baja California, Mexico

Cecilia Chapa-Balcorta — Universidad del Mar, Mexico

Citation

Acosta, A., Lomovasky, B. J., Sanchez-Cabeza, J.-A., Hernandez-Ayon, J. M., Chapa-Balcorta, C., eds. (2026). *Ocean acidification in Latin America*. Lausanne: Frontiers Media SA. doi: 10.3389/978-2-8325-7401-0

Table of contents

frontiers | Frontiers in Marine Science

TYPE Editorial
PUBLISHED 12 January 2026
DOI 10.3389/fmars.2025.1760804

OPEN ACCESS

EDITED AND REVIEWED BY
Eric 'Pieter Achterberg,
Helmholtz Association of German Research Centres (HZ), Germany

*CORRESPONDENCE
Alberto Acosta
laacosta@javeriana.edu.co

RECEIVED 04 December 2025
ACCEPTED 10 December 2025
PUBLISHED 12 January 2026

CITATION
Acosta A, Sanchez-Cabeza J-A, Lomovasky BJ, Chapa-Balcorta C and Hernandez-Ayon JM (2026) Editorial: Ocean acidification in Latin America. *Front. Mar. Sci.* 12:1760804. doi: 10.3389/fmars.2025.1760804

Editorial: Ocean acidification in Latin America

Alberto Acosta[1]*, Joan-Albert Sanchez-Cabeza[2], Betina J. Lomovasky[3], Cecilia Chapa-Balcorta[4] and José Martin Hernandez-Ayon[5]

[1]UNESIS (Unidad de Ecología y Sistemática), Departamento de Biología, Facultad de Ciencias, Pontificia Universidad Javeriana, Bogotá, Colombia, [2]Unidad Académica Mazatlán, Instituto de Ciencias del Mar y Limnología, Universidad Nacional Autónoma de México, Mazatlán, Sinaloa, Mexico, [3]Instituto de Investigaciones Marinas y Costeras (IIMyC), Facultad de Ciencias Exactas y Naturales, Universidad Nacional de Mar del Plata (UNMDP) - Consejo Nacional de Investigaciones Científicas y Técnicas (CONICET), Mar del Plata, Argentina, [4]Licenciatura en Oceanología, Instituto de Recursos, Universidad del Mar, Cd. Universitaria SN, Puerto Ángel, Oaxaca, Mexico, [5]Instituto de Investigaciones Oceanológicas, Universidad Autónoma de Baja California, Carretera Ensenada-Tijuana, Ensenada, Mexico

KEYWORDS

CO_2, Latin America, OA, ocean acidification, oceanography

Editorial on the Research Topic
Ocean acidification in Latin America

1 Advances and challenges in ocean acidification research in Latin America: towards a comprehensive regional vision

Ocean acidification is among the most significant threats to marine ecosystems worldwide, with profound implications for biodiversity, food security, and coastal economies (Gattuso et al., 2023). The Latin American region, with its vast coastline (approximately 59,960 km) and productive marine areas, hosts some of the planet's most biodiverse ecosystems, including those in the Humboldt Current, the Tropical West Atlantic, the Pacific Central-American Coastal regions, the Gulf of California and the Southwest Atlantic. These ecosystems are critical to livelihoods and climate regulation, supporting diverse habitats such as coral reefs, mangroves, salt marshes, sandy beaches and kelp forests. However, they face significant threats from pollution, degradation, and are particularly vulnerable to changes in ocean chemistry. The studies compiled in this Research Topic of *Frontiers in Marine Science* provide crucial, up-to-date evidence on the complex interactions between global climate forcings and intricate local oceanographic variability, as well as their impacts on economically and ecologically important species, providing a detailed, multidimensional picture of the region's specific vulnerabilities and resilience mechanisms. This editorial summarizes the 11 studies in this Research Topic, highlighting the advances in understanding OA in Latin America.

2 Synthesis of the Research Topic: an integrated vision of regional research

The research compiled in this Research Topic reveals a mature, multidimensional scientific landscape, where diverse methodological approaches, geographical regions, and biological groups intertwine to offer a more comprehensive understanding of ocean acidification in Latin America. The emerging body of work shows a scientific community successfully transitioning from specific descriptive studies initiated in the early 21st century toward integrative research that captures the complexity of the phenomenon and its underlying physical, chemical, and biological mechanisms.

This methodological evolution manifests through three complementary approaches that constitute the backbone of regional research. High-resolution environmental monitoring in the Colombian and Mexican Pacific has captured the variability of the carbonate system at daily and seasonal scales, while observational programs have been established in critical ecosystems such as Caribbean rhodolith beds. In parallel, controlled experimentation has generated fundamental knowledge of physiological stress response mechanisms, ranging from biochemical adaptations in Antarctic mollusks to differential tolerance in infaunal bivalves subjected to combined acidification and food limitation. Complementing these approaches, the advanced statistical modeling developed for the Gulf of Mexico represents a qualitative leap by enabling the spatial reconstruction of acidification parameters using Artificial Intelligence (AI) and machine learning algorithms, overcoming the limitations of traditional sampling.

Geographically, the studies trace a comprehensive arc spanning the Eastern Tropical Pacific, the Caribbean, the sub-Antarctic regions and Antarctica. The Pacific emerges as an area of special interest, with seminal contributions in Colombia unraveling CO_2 dynamics during La Niña events, and Costa Rica identifying key factors for coral reef development. The Caribbean region demonstrates notable scientific productivity, with advances in understanding rhodolith beds as potential biogeochemical refuges, and studies from Puerto Rico on the impact of *Sargassum* influx, and tri-national capacity assessments.

The biological dimension of the research effort spans from organismal responses to ecosystem dynamics. Mollusks emerge as a paradigmatic study group, with research ranging from physiological responses in Antarctic snails to tolerance studies in Chilean infaunal bivalves. Benthic ecosystems receive special attention, particularly Caribbean rhodolith beds and Pacific reef systems, while planktonic communities are indirectly addressed through their relationship with CO_2 fluxes in the southwestern Atlantic and the Colombian Pacific.

The studies' temporality evidences growing methodological sophistication, articulated across three complementary scales. Short-term, high-resolution investigations capture hourly and daily variability in the carbonate system in specific scenarios, while seasonal-scale studies unravel intra-annual cycles in systems subjected to ENSO events, upwelling, seasonal rainfall, and river discharge. Long-term initiatives, coupled with regional capacity assessments, lay the foundations for sustained monitoring programs and propose roadmaps for scientific development in the coming decades. Exploring innovative financing mechanisms, such as blue carbon credits, could provide a sustainable funding source for these critical long-term efforts.

3 Expanded Latin American context: scientific progress and regional complexity

The relevance and significance of these findings are considerably magnified when contextualized within the broader panorama of contemporary Latin American ocean acidification (OA) research. This region possesses an exceptional diversity of marine systems that serve as unique natural laboratories for studying ocean acidification under extreme and variable environmental conditions. From the planet's most productive upwelling systems and estuarine coastal zones to extensive tropical river mouths and complex Mesoamerican reef systems, Latin America —spanning the Gulf of Mexico, the Caribbean, and the Atlantic and Pacific Oceans— offers a complete spectrum of conditions for understanding how ocean chemistry responds to multiple climatic and oceanographic forcings.

However, this environmental richness and complexity are accompanied by a significant and persistent scarcity of systematic, long-term data, a fundamental limitation that has begun to be addressed through visionary collaborative initiatives. The creation of research networks like the tri-national network for the Gulf of Mexico (Cuba, Mexico, and the U.S.) to address the socioeconomic and ecological impacts of open and coastal acidification; the strategic formation of the GOA-ON Caribbean Hub, the Latin American Ocean Acidification Network (LAOCA), which reached its 10th anniversary in November 2025, and the Research Network of Marine-Coastal Stressors in Latin America and the Caribbean (REMARCO) represent crucial and well-oriented efforts to overcome historical barriers of technical capacity, limited infrastructure, inefficient scientific communication, and insufficient funding that have characterized regional marine research for decades.

Innovative research on the southwestern Atlantic shelf and the Colombian Pacific underscores the critical need for this collaborative approach, revealing that the spatial and seasonal variability in CO_2 fluxes is too complex for conventional large-scale climate models to capture with sufficient accuracy. Collectively, these studies illustrate a regional scientific community undergoing rapid growth and maturation, one that is beginning to produce robust, context-specific data essential for understanding the unique interplay between global stressors and local drivers that characterize our seas.

4 Future challenges and research directions

The studies presented in this Research Topic not only advance our knowledge but also critically illuminate the specific gaps that Latin America must overcome. These works represent a fundamental step in transitioning from a general diagnosis of ocean acidification to the development of applied solutions and informed policies.

4.1 Overcoming disparities in scientific capacity and governance

One of the most profound challenges is inequality in scientific production. The aforementioned network initiatives are vital strategies to counteract structural disparities. These networks promote equity in knowledge generation, standardize methodologies, and strengthen regional governance. However, persistent challenges include: technical and legal barriers to inclusive participation, the development of open-access databases and knowledge exchange platforms, and the need to incorporate considerations of food security, livelihoods, equity, transparency, and public participation.

4.2 Integrating knowledge into public policies and the transition toward decarbonization

Growing pollution and massive *Sargassum* events underscore how organic carbon fluxes exacerbate coastal acidification. Addressing this requires closing the gap between science and action through robust policies. It is fundamental to understand that acidification is a problem directly driven by CO_2, and that technological solutions like Solar Radiation Management (SRM) cannot directly address ocean acidification (Williamson and Turley, 2012). SRM, which seeks to reflect sunlight to cool the planet, does not reverse the ocean chemistry altered by CO_2 and could even redistribute acidity to greater depths. Therefore, the primary solution is the decarbonization of our economies and a drastic reduction in CO_2 emissions (Hoegh-Guldberg et al., 2023). Promoting a circular economy and implementing Integrated Coastal Zone Management (ICZM) and the restoration of blue carbon ecosystems are essential tools for this transition, transforming scientific evidence into regulatory action. Concurrently, research into marine Carbon Dioxide Removal (mCDR) techniques is accelerating. These include ocean nutrient fertilization (with N, P, Fe); macroalgal cultivation and sinking; direct ocean capture; ocean alkalinity enhancement via electrochemical or other means; ecosystem restoration; and artificial upwelling-downwelling. It is critical to note that all of these potential solutions require extensive validation, risk assessment, and scaling studies before deployment. Furthermore, implementing ethical and regulatory frameworks is essential to mitigate potential ecological risks associated with new research and technologies (mCDR).

4.3 Scaling up monitoring and addressing coastal complexity in a global context

The scarcity of historical data in the region is a critical barrier. Long-term time series, like those from the ESTOC station in the North Atlantic, are invaluable as they confirm that the surface ocean is actively absorbing anthropogenic carbon and undergoing acidification, with trends accelerating in recent decades (González-Dávila and Santana-Casiano, 2023). Statistical modeling depends on these sustained observations for validation. It is imperative to scale up monitoring efforts —potentially funded through diverse sources including private investment (e.g., carbon credits), philanthropy, and government and academic grants— to capture the complex interaction dynamics within Latin American coastal zones, where river inputs, upwelling, and extreme climate events create a mosaic of acidification conditions. Understanding these interactions is essential for refining global predictive models.

5 Conclusion: towards a unified regional vision on a warming planet

Latin American science on ocean acidification has demonstrated its technical maturity and regional relevance. The pioneering studies in this Research Topic substantially enrich global knowledge and provide a solid evidence base for decision-makers to effectively protect valuable marine resources.

However, the future health of Latin American oceans is inextricably linked to global efforts to mitigate global warming. The most recent scientific evidence confirms that we have reached the first global climate tipping point: the widespread collapse of warm-water coral reefs (Armstrong McKay et al., 2022). This finding, recently highlighted in the Global Tipping Points Report (Lenton et al., 2025), underscores the extreme urgency of the situation. The ocean, which absorbs approximately 30% of annual anthropogenic CO_2, has been a powerful ally in mitigating warming, but at an enormous cost to its chemistry and ecosystems (Hoegh-Guldberg et al., 2023). This vital service of natural decarbonization is threatened by acidification itself, which may weaken the ocean's capacity to store carbon in the future (Hu, et al., 2024). Therefore, protecting the ocean through an urgent and drastic reduction in CO_2 emissions is not only a matter of marine conservation but an essential strategy for global climate stability. OA studies are critical to this endeavor, providing insights into the species, life stages, and habitats most sensitive to changes in carbonate chemistry. This knowledge establishes the scientific baseline needed to monitor, report, and verify (MRV) the efficacy of any ocean-based CO_2 reduction or removal strategy. Given that current estimates indicate the need to remove approximately 10 gigatons of CO_2 per year from the global oceans by 2050, it is clear that traditional mitigation methods alone are insufficient, and a

portfolio of strategies, informed by robust OA research, is urgently required.

The path forward demands strengthened regional collaboration, sustained investment in local scientific capacity, and firm political determination to close the gap between knowledge and action. The visionary commitments we collectively assume today, guided by science and oriented toward a global energy transition and the responsible development of marine carbon dioxide removal methods, are the only way to ensure the health of Latin American oceans and the well-being of the millions of people who depend on them.

Author contributions

AA: Writing – original draft, Writing – review & editing. J-AS-C: Writing – review & editing. BL: Writing – review & editing. CC-B: Writing – review & editing. JH-A: Writing – review & editing.

Conflict of interest

The authors declare that the research was conducted in the absence of any commercial or financial relationships that could be construed as a potential conflict of interest.

The authors declared that they were an editorial board member of Frontiers, at the time of submission. This had no impact on the peer review process and the final decision.

Generative AI statement

The author(s) declared that generative AI was not used in the creation of this manuscript.

Any alternative text (alt text) provided alongside figures in this article has been generated by Frontiers with the support of artificial intelligence and reasonable efforts have been made to ensure accuracy, including review by the authors wherever possible. If you identify any issues, please contact us.

Publisher's note

References

Armstrong McKay, D. I., Staal, A., Abrams, J. F., Winkelmann, R., Sakschewski, B., Loriani, S., et al. (2022). Exceeding 1.5°C global warming could trigger multiple climate tipping points. *Science* 377, eabn7950. doi: 10.1126/science.abn7950

Gattuso, J. P., Magnan, A. K., Bopp, L., Cheung, W. W. L., Duarte, C. M., Hinkel, J., et al. (2023). Ocean solutions to address climate change and its effects on marine ecosystems. *Front. Mar. Sci.* 10. doi: 10.3389/fmars.2018.00337

González-Dávila, M., and Santana-Casiano, J. M. (2023). Long-term trends of pH and inorganic carbon in the Eastern North Atlantic: the ESTOC site. *Front. Mar. Sci.* 1236214. doi: 10.3389/fmars.2023.1236214

Hoegh-Guldberg, O., Jacob, D., Taylor, M., Bindi, M., Brown, S., Camilloni, I., et al. (2023). The human imperative of stabilizing global climate change at 1.5°C. *Science* 365, eaaw6974. doi: 10.1126/science.aaw6974

Hu, N., Bourdeau, P. E., and Hollander, J. (2024). Responses of marine trophic levels to the combined effects of ocean acidification and warming. *Nat. Commun.* 15, 3400. doi: 10.1038/s41467-024-47563-3

Lenton, T. M., Milkoreit, M., Willcock, S., Abrams, J. F., Armstrong McKay, D. I., Buxton, J. E., et al. (2025). The Global Tipping Points Report 2025. Exeter, UK: University of Exeter.

Williamson, P., and Turley, C. (2012). Ocean acidification in a geoengineering context. *Philos. Trans. A Math. Phys. Eng. Sci.* 370 (1974), 4317–4342. doi: 10.1098/rsta.2012.0167

frontiers | Frontiers in Marine Science

TYPE Original Research
PUBLISHED 02 June 2025
DOI 10.3389/fmars.2025.1568035

OPEN ACCESS

EDITED BY
Jose Martin Hernandez-Ayon,
Autonomous University of Baja California, Mexico

REVIEWED BY
Liqiang Zhao,
Guangdong Ocean University, China
Federica Nasi,
National Institute of Oceanography and Applied Geophysics, Italy
Araceli Rodriguez-Romero,
Spanish National Research Council (CSIC), Spain
Jay Minuti,
City University of Hong Kong, Hong Kong SAR, China

*CORRESPONDENCE
Marco A. Lardies
marco.lardies@uai.cl

RECEIVED 28 January 2025
ACCEPTED 15 May 2025
PUBLISHED 02 June 2025

CITATION
Antivero M, Caballero P, Leppes N and Lardies MA (2025) Infaunal bivalves exhibit resilience to ocean acidification but remain sensitive to food supply. *Front. Mar. Sci.* 12:1568035. doi: 10.3389/fmars.2025.1568035

Infaunal bivalves exhibit resilience to ocean acidification but remain sensitive to food supply

Montserrat Antivero[1,2], Paz Caballero[2,3], Nicolás Leppes[1,2] and Marco A. Lardies[2,4]*

[1]Facultad de Ciencias Biológicas, Pontifica Universidad Católica de Chile, Santiago, Chile, [2]Departamento de Ciencias, Facultad de Artes Liberales, Universidad Adolfo Ibañez, Santiago, Chile, [3]Facultad de Ciencias del Mar y Geografía, Pontificia Universidad Católica de Valparaíso, Valparaíso, Chile, [4]Instituto Milenio de Socio-Ecología Costera "SECOS", Santiago, Chile

Soft-sediment habitats are crucial for marine coastal ecosystems, supporting diverse biodiversity both above and below the sediment. Ocean acidification, driven by rising CO_2 and nutrient influx, enhances heterotrophic metabolism, raising CO_2 levels and lowering pH. These alterations complicate the dynamics of tidal flat, emphasizing the need for further research into their impact on biodiversity. Within these ecosystems, deposit- and suspension-feeding bivalves play crucial roles. *Tagelus dombeii*, a bivalve mollusc found in soft sediments, exhibits burrowing behavior linked to food supply and is of significant commercial value in southern Chile. This study assessed the response capacity of *T. dombeii* to key stressors associated with global ocean change, such as ocean acidification and food availability. Our results revealed significant differences in pH levels between the water column and pore water from the sediment in experimental mesocosms. *T. dombeii* was affected by ocean acidification and food availability in terms of its morphological traits (i.e. length, width, height and growth rate), while oxygen consumption was influenced only by the interaction between acidification and food supply. Notably, heart rate remained constant but increased when food supply was low. Our study suggests that *T. dombeii* exhibits partial tolerance to variations in seawater pH and carbonate chemistry, possibly due to its natural exposure to acidic pore water, but it is sensitive to food availability. These plastic physiological responses suggest that *T. dombeii* may be less vulnerable to future global change scenarios, demonstrating potential resilience and ecological success in its natural habitat.

KEYWORDS

razor clam, mollusc, metabolism, heart rate, tidal flat, mesocosm, sediments, global change

Introduction

The shallow seas found in coastal areas are highly valued ecosystems, ranking higher than open ocean systems, primarily because of their critical role in storing and cycling essential elements and nutrients (biogeochemical cycling) such as Carbon, $CaCO_3$, nitrogen, and phosphorus (Bendell et al., 2014; Kessouri et al., 2021; Iram et al., 2022). Soft-sediment habitats play a vital role in the functioning of marine coastal areas (Clements and Hunt, 2017). These habitats harbor a significant amount of marine biodiversity both above (epifaunal) and below (infaunal) the sediment surface, including various deposit-feeding and suspension-feeding bivalves (Van Colen et al., 2020). Tidal flats are notable for their infaunal inhabitants, which actively burrow into the mud and act as ecosystem engineers by shaping their surrounding microenvironment (Wethey and Woodin, 2022; Salas et al., 2022). These infauna organisms encompass a diverse array of species, including molluscs, worms, and crustaceans (Jaramillo et al., 2007; Singer et al., 2023). According to Murray et al. (2019), global tidal flats have experienced a loss of 16% in their extent from 1984 to 2016, amounting to over 20,000 km^2. These impacts are overlapped with global environmental drivers that are undergoing significant changes, including ocean warming (OW), ocean acidification (OA), and deoxygenation (DO).

The progressive escalating levels of atmospheric CO_2 driving ocean acidification, combined with the substantial influx of nutrients into coastal regions through upwelling (Torres et al., 2011) or large river systems (Liu et al., 2021) can amplify heterotrophic metabolism. This, in turn, leads to amplified CO_2 levels in the water column and exacerbates declines in pH (Carlton et al., 2023). These combined factors contribute to the intricate and ever-changing dynamics of tidal flat ecosystems, emphasizing the ongoing need for research and conservation efforts in these unique habitats. Emerging trends in ocean acidification, driven by high emissions in the 21st century, are projected to exacerbate atmospheric CO_2 concentrations, which are expected to surpass 500 parts per million and result in a doubling of ocean heat uptake – levels significantly higher than those observed over the past 420,000 years, a period during which most extant marine organisms evolved (Hoegh-Guldberg et al., 2007; Gleckler et al., 2016).

Shallow-water sediments play crucial roles in the global carbonate cycle as they serve as a significant reservoir of $CaCO_3$ (Andersson and Mackenzie, 2004). These sediments can react to the decreasing saturation state of seawater, releasing alkalinity into the overlying water column. The impact of sediment shell hash on the productivity of infaunal bivalves is still unclear and requires further investigation. The saturation state of calcium carbonate ($CaCO_3$) in seawater is a key driver of shell formation and preservation in marine invertebrates, as it directly influences their ability to deposit calcium carbonate (Barclay et al., 2020). However, this process is also strongly affected by environmental hypercapnia, which reduce carbonate ion availability and thus lower the $CaCO_3$ saturation state. As a result, hypercapnia can indirectly impair calcification. Indeed, long-term exposure to high pCO_2 has been associated with reduced growth and/or calcification rates in several marine taxa, including mussels (Michaelidis et al., 2005; Navarro et al., 2013; Leung et al., 2022), echinoderms (Asnicar and Marin, 2022), and coral species (Hoegh-Guldberg et al., 2007; Leung et al., 2022; Rathbone et al., 2022). Species with greater tolerance to such conditions often dis-play high metabolic rates, mobility, and activity levels (Medeiros and Souza, 2023). Overall, ocean acidification has been recognized as a significant threat to marine mollusks, including infaunal bivalves (Gazeau et al., 2013; Martel et al., 2022). However, these effects are often described predominantly within the context of water column acidification, overlooking or with comparatively fewer attention on the drastically different pH and carbonate system conditions that infaunal species experience below the sediment-water interface. Consequently, it is often assumed that infaunal organisms are more resilient to ocean acidification (Widdicombe et al., 2011), and several studies support their apparent tolerance to changes in seawater pH and carbonate chemistry (Vlaminck et al., 2023). However, other research has shown that sediment acidification can negatively affect infaunal organisms, particularly marine bivalves (Hu et al., 2014; Clements et al., 2016; Martel et al., 2022; Vlaminck et al., 2023).

Food supply is a factor that could potentially lead to detrimental effects on marine invertebrates, in addition to other global change effects such as ocean acidification (Lawrence et al., 2015; Flombaum and Martiny, 2021; Kwon et al., 2022). Food supply for bivalves depends on marine phytoplankton which contributes roughly 50% of global net primary production (Field, 1998), while for deposit feeders bivalves obtain their food from organic particle settling from water column, biodeposits and/or detritus (Navarro et al., 2008). A recent analysis of a 26-year time series of spatially averaged monthly mean chlorophyll-a (Chl-*a*) concentrations in the Southern Pacific Ocean revealed that the largest deviations in Chl-*a* were closely associated with El Niño–Southern Oscillation (ENSO) events, as evidenced by the strong correspondence between Chl-*a* anomalies and the Multivariate ENSO Index (Johnson and Lumpkin, 2024). These fluctuations underscore the central role of ENSO-driven variability in modulating nutrient availability, both through altered oceanographic circulation patterns and the disruption of coastal upwelling systems, which are otherwise critical sources of nutrient input sustaining primary productivity in this region. Furthermore, in the tidal flats, the intensified urbanization of coastal habitats has led to a significant degradation of food-web complexity and ecosystem services due to multiple stressors (Eriksson et al., 2010; Christianen et al., 2017). While the combined effect of both factors (OA and food supply) is not widely discussed in the literature, some studies have examined this effect in mollusks. Studies on the effect on oyster larvae (see Hettinger et al., 2013) have shown that a combination of high pCO_2 levels and low food supply results in reduced physiological performance. However, this effect occurs independently for each factor and is not additive. It is of vital importance to mention that food supply plays a crucial role in determining an organism's response to stressful situations, with significant implications for shell-forming mollusks (Ramajo et al., 2016a, 2019; Harayashiki et al., 2020). Therefore, we hypothesized that increased food supply would mitigate the negative effects of acidification in infaunal bivalves.

The tidal flats of southern Chile are characterized by the presence of numerous species of bivalve molluscs, many of which are of commercial importance (Clasing et al., 1994; Navarro et al., 2008). Several species of bivalves coexist at the lower intertidal of large tidal flats located in the enclosed or inland coast of the northern area of the North-Patagonic archipelagos on the Chilean coast (ca. 40–42°S): *Tagelus dombeii* (Lamarck), *Tawera gayi*, *Ameghinomya antiqua*, *Semele solida*, *Gari solida, Mytilus chilensis*, and *Zemysina insconspicua* (see Stead et al., 2002; Jaramillo et al., 2007). In general, studies have shown that sediments with higher densities of bivalves, particularly those where deep burrowers are most abundant, exhibited greater species richness and higher densities of macroinfauna (Stead et al., 2002; Jaramillo et al., 2007). The majority of eulamellibranch bivalves (i.e *T. dombeii*) engage in suspension feeding while deposit-feeding behavior has only been observed in the Tellinacea and Lucinacea species (Morse and Zardus, 1997; Lardies et al., 2001; Navarro et al., 2008).

In this study, we investigated the effects of ocean acidification and food supply on the morphological traits and physiological performance of the razor clam *T. dombeii* (Lamarck, 1818), which coexists with the bivalve community in the sandflats of Coihuín, Reloncaví Sound (41°29'S, 72°54'W).

Material and methods

Sampling of organisms and mesocosm setup

During spring, 100 juvenile individuals of *Tagelus dombeii* (Lamarck, 1818) (Tellinacea: Solecurtidae) with a mean of 18 mm in length, 7 mm in width, and 3 mm in height, which is below the reported size at sexual maturity (40–50 mm in length; Lépez et al., 1997; Sánchez et al., 2003), were collected from the soft sediments of the Coihuín tidal flat (41°29' S, 72°54' W), located 8 km southeast of Puerto Montt, Los Lagos Region, Chile (see Supplementary material Figures 1). Sea surface temperature follows a seasonal pattern at Coihuín, with the lowest values occurring during the winter months (8°C), increasing towards the summer maximum in January (17°C; Urrutia et al., 2001; Lardies et al., 2001). Near the sampling site, the spectral exponent (β) of seawater chemical parameters is -1.703 for temperature, -1.584 for salinity and -1.206 for pH indicating high unpredictability dominated by random short-term environmental fluctuations compared with near locations (see Castillo et al., 2024 for details). In contrast, the porewater at a depth of 5 cm in the sediment of the Coihuin tidal flat, during November, has a temperature of 13.19°C, pH of 7.72, and salinity of 30.66 (Lardies et al., unpublished data). The intertidal sediment of Coihuín tidal flat is predominantly sandy (93.81%), and the content of mud (particles < 63 mm diameter) is low in Coihuín, with an annual average of 1.83% (Lardies et al., 2001). Observed organic matter content is low (0.68%), and in the biogenic aggregates (i.e. detritus, phytoplankton, and bacteria) that represented an 0.58% (Lardies et al., 2001). The individuals were transported under humid conditions to the laboratory. No mortalities were recorded during transport. In the laboratory, individuals were acclimated for three days in a "common garden" aquarium containing filtered natural seawater at 12°C (32 ppm salinity, 12D:12N photoperiod), with daily feeding of microalgae, to minimize stress responses associated with transportation. Due to their small size and delicate shells, individuals were not marked to avoid causing harm or shell damage to the animals.

For the mesocosm experiment, random groups of 4 individuals were created and assigned to each 9-liter aquariums for an experimental trial of 67 days. Each aquarium was filled with 6 cm of commercial quartz sand (https://dondecapo.cl/project/cuarzo-32/) across the entire bottom and filled to its total capacity with filtered and UV-sterilized natural seawater (see Martel et al., 2022). It is necessary to use inert material to avoid potential effects of sediment altering the chemical properties of the water, such as pH or alkalinity (Brenner et al., 2016). Water and pore water were measured prior to the experiment for all the 16 aquariums to ensure that the system was within the desire environment condition values.

The assigned treatments included levels of acidification and food supply, simulating CO_2 concentration scenarios with a current scenario of 500 µatm and a future scenario of 1500 µatm (pH = 8.0 and 7.5, respectively; described in Navarro et al., 2013; Vargas et al., 2017). The food source used was microalgae (see below) and was assigned as either optimal or restricted food, relative to the individual's dry weight. As reported by Navarro et al. (2008), the optimal food level corresponds to 4% of individual's dry weight, while the restricted food level corresponds to 1%. Each aquarium was assigned to one of the 4 treatments, that are: 500 µatm – 1% food supply, 500 µatm – 4% food supply, 1500 µatm – 1% food supply and 1500 µatm – 4% food supply.

During the experimental period, razor clams were fed daily following this relationship with their dry weight (1% and 4%), using Reef Blizzard-O suspension (Brightwell® Aquatics) diluted in 10 mL of filtered and UV-sterilized seawater. All aquariums were monitored daily for mortality without replacement in case of death, reconsidering the food amount per aquarium. Water in all aquariums was renewed twice per week to maintain appropriate conditions. At the end of the experiment, the morphological and physiological measurement were taken from the individuals that survive and then were sacrificed.

Additionally, one aquarium with identical characteristics was subjected to the CO_2 exposure for each treatment. In each aquarium, three complete shells were placed on the sand surface, while three additional complete shells were buried approximately 3 cm deep in the sand. The buoyant weight, length, width, and height were measured, and at the end of the experiment, the same parameters were measured for each shell. This was done to estimate the rate of dissolution in the empty shells, which were not affected by biological activity. The buoyant weight (from now on referred as growth rate) served as an indicator of calcification (or decalcification; Lagos et al., 2016). During the experiment, additional individuals collected from the same site were used to analyze the relationship between shell length and dry tissue weight, as well as between oxygen uptake and dry tissue weight, using linear regression.

Seawater pCO_2 levels

The pH treatment levels (8.0 and 7.5) were achieved by adding a mixture of dry air with pure CO_2 (partial pressure of CO_2 [pCO_2] = 500 and 1500 µatm, respectively) to each aquarium with seawater in a regular continuous flow using mass flow controllers (Aalborg Instruments & Controls, Inc., Orangeburg, NY, USA; for details see Benítez et al., 2018). The pH of the water (NBS scale) was measured by extracting 60 mL of water from the aquariums with disposable syringes for each aquarium, and then measuring the pH twice with the same water sample. The sediment pH was measured using a 10 mL micropipette (Labnet BioPette Plus), extracting pore water by inserting the micropipette tip around 2–3 cm into the sediment, following the sampling method of Bendell et al. (2014). Water was extracted three times from the same aquarium, transferred to Falcon tubes, and pH was measured twice with each sample. All samples were measured using a pH meter (Mobile 826, Metrohm, Herisau, Switzerland), which was connected to a combined electrode (junction-type). During measurements, temperature was also recorded using a digital thermometer, and seawater salinity was measured using a portable salinometer (Salt6+, Oakton; precision: ± 0.1 PSU and ±0.5°C, respectively). Alkalinity samples were collected twice a week, ensuring that all aquaria were sampled in both the water column and pore water during each sampling week. The samples were fixed with a saturated solution of $HgCl_2$ and stored in 50 mL Falcon bottles in the laboratory under dark and ambient temperature conditions. At the end of the experiment, alkalinity was analyzed using a multiparameter photometer (Hanna HI83303) in the seawater alkalinity mode. For this, 10 mL of aquarium sample was used as a blank, and then 1 mL of reagent (HI755) was added, based on the colorimetric method. The results were expressed in mg/L and subsequently converted to µmol/kgSW to assess the carbonate system.

Temperature, salinity, pH, and alkalinity measurements were used to calculate the carbonate system parameters. These included the partial pressure of CO_2 (pCO_2) and the saturation states (Ω) of calcite and aragonite, which were estimated using the CO2SYS software in Excel (Pierrot et al., 2006) and the dissociation constants from Mehrbach et al. (1973), refitted by Dickson and Millero (1987), for both the water column and the sediment.

Measurements of biological traits

The measurement of growth rates and morphological changes in individuals during the experiment was obtained by measuring the buoyant weight, length, width, and height of each experimental individual. Buoyant weight corresponds to the weight of the individual in water and is used as a non-invasive estimator of calcification rate, i.e., the growth of individuals (Palmer, 1982). It was measured at the beginning and end of the experiment using an analytical balance (± 0.1 mg, AUX 220, Shimadzu, Kyoto, Japan). For measurements of length, width, and height, an electronic caliper Mitutoyo (Sakado, Japan) was used at the beginning and end of the experiment. Empty shells (without soft tissues) from aquariums under CO_2 treatments were measured for buoyant weight, without biological activity, using the same analytical balance used for measuring the buoyant weight of individuals, while for length, width, and height were measured using the electronic caliper.

At the end of the 67 days, the metabolic rate and heart rate were measured to obtain the energy expenditure value of the individuals. Metabolic rate measurements were taken before daily feeding, using 0.067 L glass respirometry chambers with a PreSens Mini Oxy-4 respirometer (PreSens GmbH, Regensburg, Germany). To measure oxygen consumption ($mgO_2\ L^{-1}\ h^{-1}$), dissolved oxygen in the chambers was quantified every 15 seconds for approximately 1 hour. Finally, the obtained measurement was standardized per gram of weight to obtain the specific metabolic rate of each individual (see Lardies et al., 2021). Background measurements (chambers without animals) were made at the same experimental conditions to quantify microbial oxygen consumption to be subtracted from each experimental measurement. No reduction over 3% of oxygen consumption was recorded (see Osores et al., 2017). Previously, the sensors were calibrated in anoxic water, using a Na_2SO_3 solution for 0% oxygen and water saturation with air bubbles for 100% oxygen. The obtained measurement was standardized per gram of weight. Heart rate measurements were taken following the methodology of Gaitán-Espitia et al. (2014) and Rodríguez-Romero et al. (2022) using as a proxy of cardiac activity at constant temperature of 12°C for all measurements. Individuals were immobilized with adhesive tape on a plate. One measurement per individual was taken in batches of 4 individuals, each in an individual chamber installed in the temperature-controlled bath (± 0.5°C, LWB-122D, LAB TECH). The protocol included 5 minutes of initial acclimation and 15 minutes of measurement. An AMP 03 heartbeat amplifier (Newshift Lda®) was used, connected to an oscilloscope. Measurements were taken for all the individuals, and the results were expressed in beats per minute.

Statistical analysis

To avoid pseudo-replication errors, variables for each individual were averaged by aquaria. First, homogeneity and normality tests were performed for the data, including Levene and Kolmogorov-Smirnov tests, respectively. To assess the difference in pH levels of both water and sediment water (pore water), a repeated ANOVA measure was performed, considering the variable place (source of water) as a within-subjects factor (within the same aquaria) and sampling time was treated as between-subjects factor.

A Two-Way ANOVA was conducted to assess the effect of CO_2 levels, food availability, and the interaction between both factors on morphological traits (length, height, width and growth rates), dissolution rates, oxygen uptake, and heart rate. This determined whether the factors separately or their interaction had significant effects on the individuals. Tukey's HSD was used as *a posteriori* test when the main factors indicated significant differences between levels of the corresponding factor (Underwood, 1997). Additionally, the effect size of the treatments on both physiological and morphological variables was calculated using the log response

ratio (lnRR), defined as lnRR = treatment/control. This approach allowed for a direct comparison of treatment effects relative to the controls. Bootstrapping was used to estimate the 95% confidence intervals of the lnRR values. All the analyses were conducted in R statistical environment (R Core Team, 2024).

Results

All environmental variables remained stable in all of the treatments throughout the experimental period, with low variations in pH, salinity, and temperature (see Table 1). Based on the analysis of characterization of the population, the relationship between length and dry tissue weight of the individuals showed an R^2 value of 0.91, while the relationship between oxygen uptake and dry tissue weight showed an R^2 of 0.57 (see Supplementary Figures S2A, B).

A significant difference in pH levels was observed between the water column and the pore water ($P < 0.01$, repeated measures ANOVA, see Supplementary Table S1, Figure S3), but no differences were found based on the sampling time. On average, the pH of the water column was 7.81 ± 0.017 SE, while the pH of the pore water was 7.54 ± 0.018 SE (see Supplementary Figures S3, S4). Particularly, a difference in pH was observed between the overlying water and the sediment, which ranged between 0.28 and 0.57 units under CO_2 levels of 500 µatm and between 0.16 and 0.34 units under CO_2 levels of 1500 µatm.

Mortality was assessed after the experimental trial. Under the 500 µatm CO_2 treatment, individuals exposed to a 4% food supply exhibited a mortality rate of 38.5%, whereas those maintained at a lower food level (1%) showed reduced mortality (14.3%). In contrast, at 1500 µatm CO_2, mortality remained at 25.0% under the 4% food condition but increased markedly to 54.0% under the 1% food supply, highlighting an interactive effect between food availability and CO_2 levels on survival.

Morphological traits

The interaction between pCO_2 and food supply affected the individuals' morphological characteristics (i.e. length, width, height, growth rate) (Figure 1; Table 2). High food supply in low pH conditions increased total width, with a marginally significant effect in the interaction of the treatments (Figure 1B; Two-Way ANOVA; $F_{1,10} = 4.90$, $P = 0.051$), while for low food supply in low pH conditions there was a decreased in total height, with a marginally significant effect in the interaction of the treatments (Figure 1C; Two-Way ANOVA; $F_{1,10} = 4.52$, $P = 0.059$). Furthermore, pH conditions and food supply affected the total increase length, and growth rate, but this effect was not significant (but see size effect, Supplementary Figure S6). Moreover, shell dissolution recorded for empty shells (see Figure 2A) was higher exposed to the water column and the interaction between the treatments pCO_2 and location in the sediment resulted in a significant effect (Two-Way ANOVA; $F_{1,4} = 7.81$, $P = 0.049$). Although shell carbonate content tended to be higher in organisms from both CO_2 treatments under 4% food supply, the difference was not statistically significant, being higher in the pCO_2 treatment (see size effect, Supplementary Figure S7 and Figure 2C).

Physiological traits

The food supply and pCO_2 treatment impacted the physiological variables of the razor clams (Table 2). A non significant effect was

TABLE 1 Mean values (± SE) of carbonate system parameters for each experimental treatment, including pCO_2 levels (500 and 1500 µatm) and food supply (1 and 4% of tissue dry weight), among the two sampling sites within the aquaria (water and pore water).

Treatments	Place	Temperature (°C)	Salinity (psu)	pH (25°C)	A_T	pCO_2	Ω_{ca}	Ω_{ar}
500 µatm – 1% Food supply	Water	12.02 ± 0.13	31.91 ± 0.36	8.03 ± 0.02	2051 ± 96	425 ± 58	2.86 ± 0.47	1.82 ± 0.30
	Pore water			7.69 ± 0.03	2087 ± 118	1288 ± 291	1.57 ± 0.52	1.00 ± 0.33
500 µatm – 4% Food supply	Water	12.28 ± 0.11	31.63 ± 0.46	7.97 ± 0.02	2135 ± 49	542 ± 67	2.47 ± 0.24	1.57 ± 0.15
	Pore water			7.55 ± 0.03	2323 ± 58	1514 ± 218	1.25 ± 0.15	0.79 ± 0.09
1500 µatm – 1% Food supply	Water	12.44 ± 0.13	31.46 ± 0.42	7.63 ± 0.01	2035 ± 100	942 ± 94	1.39 ± 0.09	0.88 ± 0.06
	Pore water			7.25 ± 0.086	2472 ± 380	2451 ± 375	0.86 ± 0.16	0.55 ± 0.10
1500 µatm – 4% Food supply	Water	12.44 ± 0.05	31.95 ± 0.34	7.61 ± 0.01	2097 ± 29	1023 ± 77	1.36 ± 0.06	0.86 ± 0.03
	Pore water			7.36 ± 0.02	2226 ± 58	2332 ± 168	0.72 ± 0.04	0.46 ± 0.03

The pH is reported on NBS scale, AT refers to total alkalinity expressed in µmol kg^{-1}, and Ω_{ca} and Ω_{ar} represent the calcite and aragonite saturation states in seawater.

10.3389/fmars.2025.1568035

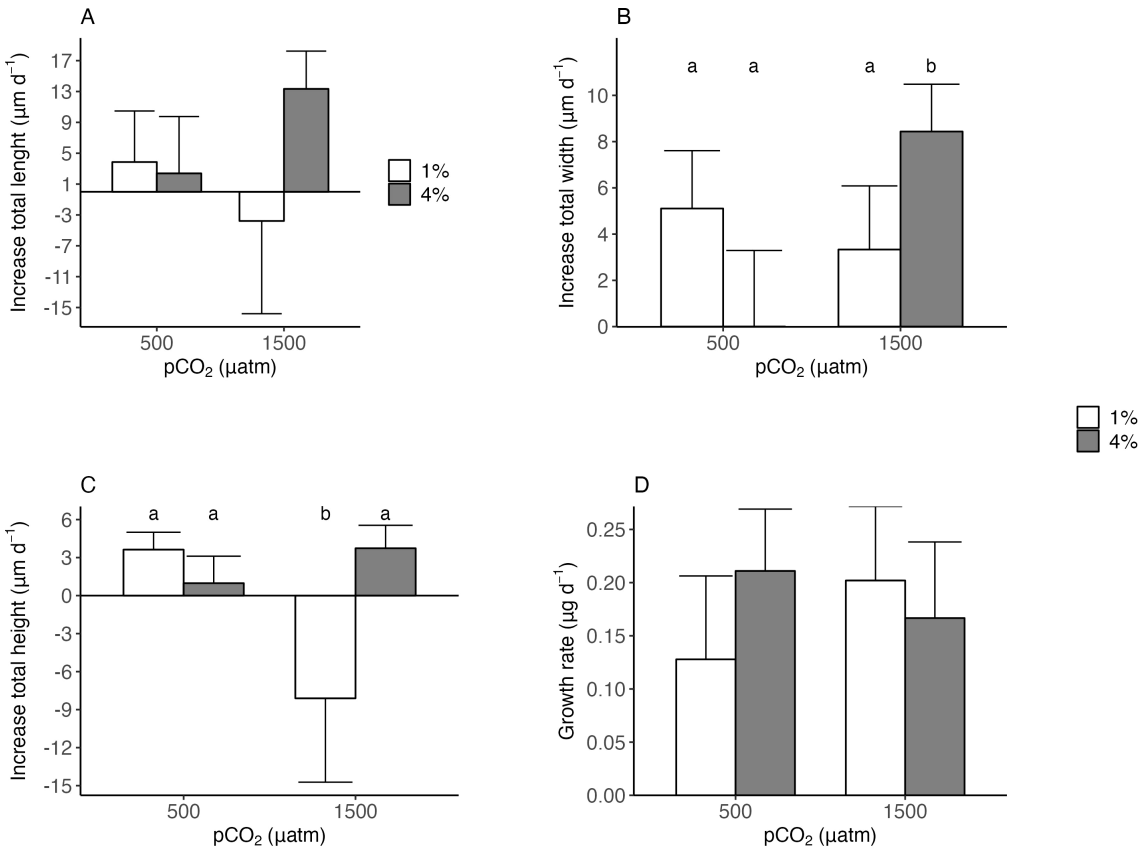

FIGURE 1
Tagelus dombeii: morphological changes with increase of total length **(A)**, increase of total width **(B)**, increase of total height **(C)**, and growth rate **(D)** in each experimental condition. The treatments were conditions of pH (500 µatm and 1500 µatm) and food supply (1% and 4% dry weight). The letters in lowercase indicate and mark the significance.

observed on the oxygen uptake rate, which decreased when the organisms were exposed to low pH (Two-Way ANOVA; $F_{1,10}$ = 4.47, P = 0.06), and the interaction between CO_2 and food supply (Two-Way ANOVA; $F_{1,10}$ = 4.556, P = 0.058; Figure 3; but see size effect Supplementary Figure S8.). The interaction between the treatments food supply and pCO_2 did not influence heart rate (Figure 4). However, the individuals tended to increase their heart rate in conditions of low food supply (see Figure 4).

Discussion

The ongoing rise in CO_2 emissions is accelerating both climate change and ocean acidification, significantly impacting various marine invertebrates (Shi and Li, 2024). However, the magnitude and direction of these effects vary according to the specific characteristics of each species (Goethel et al., 2017; Vargas et al., 2017; Harvey et al., 2013). In this context, infaunal bivalves could show greater resilience to these disturbances, attributable, among other factors, to their exposure to pore water, which has an intrinsically lower pH compared to the water column. Our results indicate that *T. dombeii* possesses adaptive mechanisms that allow it to cope with environmental stress, such as ocean acidification, but not for limited food supply. These mechanisms include morphological modifications and physiological trade-offs that optimize its ability to survive under unfavorable conditions.

The characteristics of pore water are strongly influenced by the dynamics of the overlying water (Zhang et al., 2013; Precht et al., 2004). Various processes, such as the decomposition of organic matter, the sedimentation of materials of terrestrial origin, and the biological activity of both microorganisms and infaunal organisms, can generate a decrease in the pH of sediments (Hohaia et al., 2014) in addition to other processes that can contribute to pH reduction in sediments, such as sulfide oxidation or metal presence (see Bonner et al, 1990). This localized acidification of the benthic environment could have significant implications for key processes in bivalves, such as settlement, recruitment, and survival (Meseck et al., 2018; Clements and Hunt, 2018; Cummings et al., 2009). The pH of pore water tends to be more acidic than that of surface water, a condition attributed to the processes previously described (Hu et al., 2014; Cummings et al., 2009). The observed pH gradient between the overlying water and the sediment highlights the potential for differential buffering capacities at the sediment–water interface. These results are consistent with those reported by McGarrigle and Hunt (2024), who, in controlled experiments, documented that the pH of the water under constant acidification

10.3389/fmars.2025.1568035

TABLE 2 Summary of Two-way ANOVA for the effects of pH conditions, food supply, and interaction among both, upon morphological physiological variables (large, width, height, and growth rate).

Dependent Variable	Source of variation	d.f	MS (Mean)	F	P
Increase total large	CO_2	1	5.5530	0.069	0.797
	Food supply	1	320.74	4.024	0.072
	CO_2 x Food supply	1	35.255	0.442	0.521
	Residuals	10	79.692		
Increase total width	CO_2	1	15.727	1.072	0.324
	Food supply	1	6.8348	0.465	0.510
	CO_2 x Food supply	1	71.876	4.900	0.051
	Residuals	10	14.668		
Increase total height	CO_2	1	34.530	1.306	0.279
	Food supply	1	49.247	1.862	0.202
	CO_2 x Food supply	1	119.72	4.528	0.059
	Residuals	10	26.439		
Growth rate	CO_2	1	0.0001	0.001	0.992
	Food supply	1	0.0072	0.697	0.423
	CO_2 x Food supply	1	0.0259	2.508	0.144
	Residuals	10	0.0103		
Shell dissolution rate	CO_2	1	0.0353213	1.809489	0.250
	Location	1	0.0263002	1.347344	0.310
	CO_2 x Location	1	0.1525338	7.814213	**0.049**
	Residuals	4	0.0195200		
Shell carbonate content	CO_2	1	0.0037139	4.219588	0.070
	Food supply	1	0.0034304	3.897520	0.079
	CO_2 x Food supply	1	0.0014170	1.609966	0.236
	Residuals	9	0.0008802		
Oxygen uptake	CO_2	1	15.637	4.479	0.060
	Food supply	1	6.7483	1.932	0.194
	CO_2 x Food supply	1	15.908	4.556	0.058
	Residuals	10	3.4911		
Heart rate	CO_2	1	166.70	0.545	0.477
	Food supply	1	601.58	1.969	0.191
	CO_2 x Food supply	1	324.15	1.061	0.327

The significant P-values are highlighted in bold.

conditions was 7.73 ± 0.13, while that of the sediment was 7.29 ± 0.19, evidencing an average difference of 0.44 units. Such micro-scale heterogeneity is ecologically significant, as it may influence the exposure of benthic organisms to acidified conditions and thus mediate their physiological responses. Although ocean acidification has been a central research topic in recent decades, the carbonate system in sediments has yet to be fully explored. Our results reveal, in addition to a difference in pH between the water column and pore water, variations in the carbonate systems of both environments. The sediments exhibited more acidic conditions, with higher partial pressure of CO_2 (pCO_2), accompanied by a decrease in the saturation states of calcite and aragonite. Under these undersaturated conditions ($\Omega_{ca} < 1$ and $\Omega_{ar} < 1$; see Table 1), such as the pore water, the shell's mineral phase is likely to undergo dissolution, leading to higher energy demands for maintaining its structure and function. In our case, the findings indicate a higher

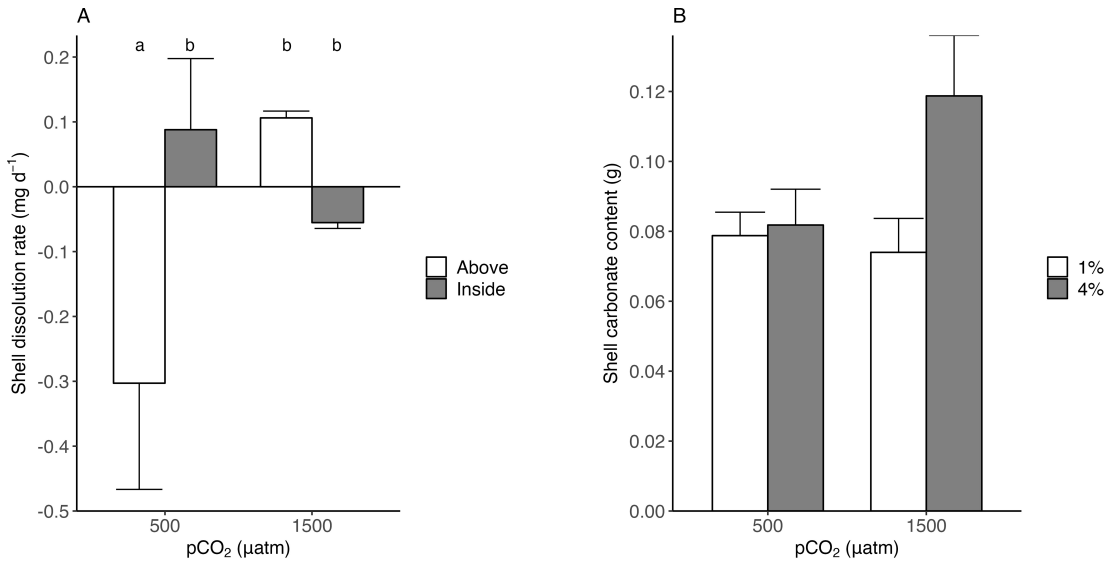

FIGURE 2
Shell dissolution rate **(A)**, measured above and below the sediment, and shell carbonate content **(B)** in empty shells of *Tagelus dombeii* after 67 days of exposure to experimental conditions. The treatments in panel B correspond to pH levels (500 µatm and 1500 µatm) combined with food supply (1% and 4% dry weight). The letters in lowercase indicate and mark the significance.

carbonate content in individuals exposed to acidified conditions with 4% food supply, despite the low saturation states of calcite (Ω_{ca} = 0.72) and aragonite (Ω_{ar} = 0.46). This suggests an increased investment in shell production under ocean acidification, potentially as a compensatory response when food availability is optimal. Such a response may help maintain shell integrity despite the thermodynamically unfavorable conditions for calcification. However, sustained low aragonite/calcite saturation states in sediments may have long-term consequences for bivalve shell integrity and calcification capacity. While significant short-term effects were detected, chronic exposure to undersaturated conditions could progressively impair shell formation.

The outcomes revealed variable morphological effects, highlighting a significant impact on the increase in total height and width, attributed to the interaction between both treatments. However, measurements related to the growth rate in terms of increase in total length, calcification (change in growth rate), and shell carbonate content did not show significant differences. These findings coincide with those reported by Liang et al. (2022), who observed that individuals of the infaunal bivalve *Sinonovacula constricta* subjected to controlled pH conditions (pH = 8.1) and projected future scenarios (pH = 7.7) did not show significant changes in their growth performance. The fact that the treatments have generated mostly non-significant morphological effects suggests that this species could possess some resistance to acidification. Previous studies have indicated that infaunal organisms, which are regularly exposed to acidified conditions in their natural habitats, such as in our case, where individuals

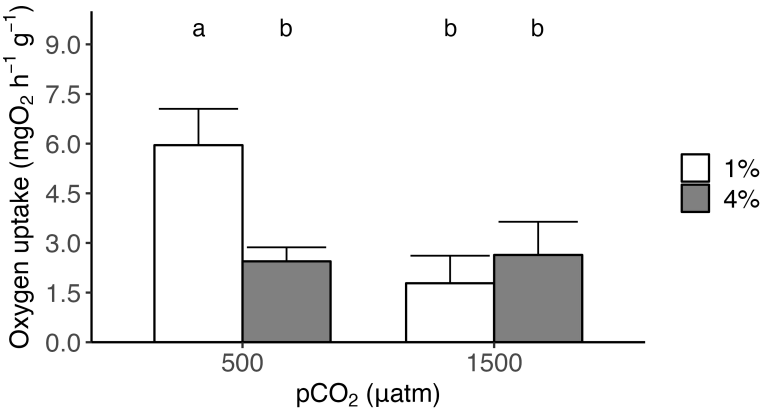

FIGURE 3
Tagelus dombeii: metabolic rate as oxygen uptake ($mgO_2h^{-1}g^{-1}$) for razor clams in each experimental condition. The treatments were conditions of pH (500 µatm and 1500 µatm) and food supply (1% and 4% dry weight). The letters in lowercase indicate and mark the significance.

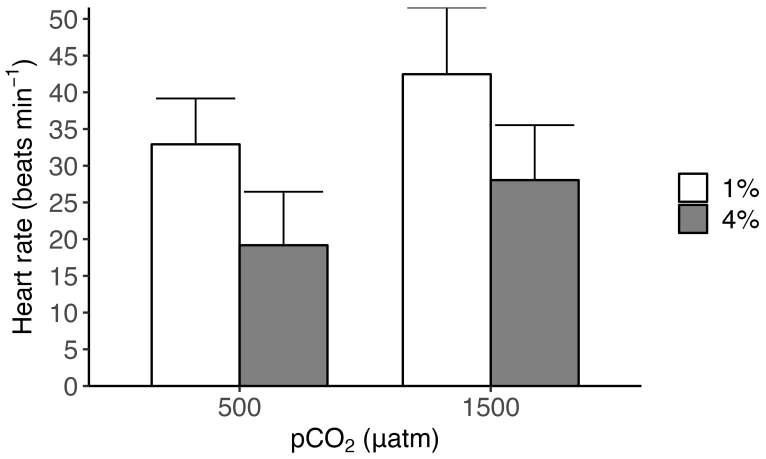

FIGURE 4
Tagelus dombeii: heart rate as beats min^{-1} for razor clams in each experimental condition in a mesocosm for 67 days. The treatments for B were conditions of pH (500 µatm and 1500 µatm) and food supply (1% and 4% dry weight).

originate from an environment with a pH of 7.7, may exhibit greater tolerance and experience fewer morphological effects under acidification scenarios (Liang et al., 2022; Hu et al., 2014). On the other hand, McGarrigle and Hunt (2024) propose that, during periods of stress, such as exposure to constant elevated levels of CO_2, organisms tend to prioritize survival overgrowth, strategically redistributing the available energy. Additionally, it has been suggested that calcifying organisms could overcome the energetic limitations associated with ocean acidification as long as they have sufficient amounts of food (Clements and Darrow, 2018). In this context, food supply could play a key role in physiologically compensating for the stress induced by acidification conditions (Goethel et al., 2017; Ramajo et al., 2016a). Furthermore, individuals of *T. dombeii* show a dual feeding behavior, using both suspension feeding and deposit feeding strategies (Lardies et al., 2001). This species can alternate between these strategies according to the conditions, obtaining food from both the water column (suspension) and the sediment surface (detritus; Navarro et al., 2008). Additionally, individuals tend to employ suspension feeding when they are at greater depths in the sediment, while they opt for deposit feeding when they are closer to the surface (Lardies et al., 2001; Navarro et al., 2008) thus increasing the likelihood of sustaining feeding activity and coping with adverse conditions, such as environmental stressors like OA and limited food supply.

The results indicate a significant decrease in oxygen consumption under acidification conditions, suggesting metabolic depression in organisms exposed to these conditions. Metabolic depression is a strategy adopted by organisms to extend short-term survival in adverse environments (Ramajo et al., 2016b; Hu et al., 2014). Although this metabolic depression may represent an acute response to environmental stressors, its persistence and long-term consequences remain uncertain. Prolonged exposure to low pH conditions could either lead to physiological acclimation or, conversely, to cumulative energetic deficits that compromise growth, reproduction, or survival. Further studies with longer exposure periods are needed to determine whether this response is transient or maintained over time, and whether it translates into reduced fitness or population-level impacts.

Previous studies have documented this response in various species, including the infaunal brittlestar (Hu et al., 2014), scallops (Ramajo et al., 2016b), and infaunal clams (Martel et al., 2022). Food supply has been shown to enhance resilience to ocean acidification (Ramajo et al., 2016a), as organisms with access to adequate food exhibit higher growth, metabolism, calcification, and ingestion rates compared to those with limited food supply, both under control conditions and acidification scenarios (Navarro et al., 2016). In line with these findings, our study shows that organisms exposed to high food availability and low pH exhibit greater survival than those under low food availability and low pH conditions (see Supplementary Figure S5). However, food availability alone does not always guarantee effective intake and assimilation. Under acidified conditions, metabolic depression can impair feeding and nutrient processing, thereby limiting the benefits of increased food supply. This decoupling between external resource availability and internal energy acquisition has been observed in other bivalves and may compromise energy allocation to growth and reproduction (Ramajo et al., 2016b; Clements and Darrow, 2018).

Heart rate (HR) in mollusks is a fundamental physiological indicator that reflects their health status and their ability to adapt to different environmental conditions (Davis et al., 2023; Fernández et al., 2024). This parameter responds to a variety of stress factors, showing notable plasticity in populations inhabiting variable environments. In the present study, *Tagelus dombeii* showed a higher (but not significant) heart rate with lower food supply, would

indicate an increase in stress experienced by the organism (Davis et al., 2023). Under extreme conditions, the relationship between HR and metabolic rate may decouple (Marshall and McQuaid, 2020); mollusks can maintain a constant HR while decreasing their metabolic rate, adopting alternative strategies to ensure their survival (Marshall and McQuaid, 2020). Consistent with these findings, our results show that *T. dombeii* exhibited a reduced oxygen consumption rate under low pH conditions, while heart rate increased when food supply was limited. This suggests a decoupling between HR and metabolic rate, likely reflecting an adaptive response to the combined stressors of ocean acidification and food supply. Likewise, ocean acidification can induce metabolic depression, evidenced by a reduction in metabolism, which constitutes an energy-saving strategy against the stress associated with low pH, regardless of changes in heart rate (Martel et al., 2022).

Our results indicate an effect of the interaction between pH and food supply on oxygen consumption but not on food supply. This finding could be explained by the ability of *T. dombeii* to employ both types of feeding, which allows it to obtain nutrients from two different sources, thus improving its efficiency in food acquisition (Navarro et al., 2008). Although this study did not quantify the time spent on each type of feeding, we suggest that these organisms could alternate between suspension feeding and deposit feeding to minimize the ingestion of low-pH water under acidification conditions (see Vlaminck et al., 2023). This feeding flexibility allows infaunal filter-feeding bivalves to mitigate the effects of acidification, maintaining acid-base balance and avoiding physiological alterations (see Vlaminck et al., 2023), which reinforces the resilience and robustness of these organisms, in line with the results obtained in *M. calcarea* (Goethel et al., 2017).

The variability in responses to adverse conditions of marine invertebrates depends on the habitat of origin, the scales of environmental variability, and the simultaneous presence of other stress factors (Lefevre, 2016; Castillo et al., 2024; Gaitán-Espitia et al., 2017). These elements influence the physiological responses of organisms to cope with unfavorable conditions. In this study, the razor clams analyzed come from Coihuín, a site near the Reloncaví fjord, which is characterized by high variability in pCO_2 and food supply (Vergara-Jara et al., 2019; Lardies et al., 2001; Castillo et al., 2024). This suggests that infaunal organisms in the tidal flat would show greater signs of phenotypic plasticity, given the wide environmental variability of this quasi-estuarine system (see Osores et al., 2017; Castillo et al., 2024).

Global change, particularly ocean acidification, poses significant threats to marine species and fisheries, including *T dombeii*. The species metabolic depression in response to acidification could reduce its harvestable biomass, thereby affecting the maximum sustainable yield and threatening economic stability in affected regions. The previous plus pressure of artisanal fisheries on *T. dombeii*, with an annual harvest of 2,203 Mt (100 Mt from the Los Lagos Region), face potential losses. For example, between 1996 and 2007, the selectivity for *T. dombeii* dropped from a mean size of 76 mm to 54 mm (legal commercial size 65 mm), indicating a shift toward smaller harvestable individuals in the Bio-Bio region (Hernández et al., 2011). This trend could lead to significant economic losses, underlining the need for adaptive fisheries management that accounts for both climate stressors and ecological dynamics.

Tagelus dombeii demonstrates partial resilience to ocean acidification due to its natural exposure to acidic pore water and flexible feeding strategies. This adaptability allows it to optimize nutrient acquisition and maintain physiological balance under stressful conditions. However, its survival and performance are compromised under low food supply, highlighting the importance of trophic conditions. These findings highlight the complexity of infaunal marine invertebrate responses to global change, emphasizing the need to consider multiple stressors in future projections and fisheries.

Data availability statement

The raw data supporting the conclusions of this article will be made available by the authors, without undue reservation.

Ethics statement

The manuscript presents research on animals that do not require ethical approval for their study.

Author contributions

MA: Formal Analysis, Investigation, Writing – original draft, Writing – review & editing, Data curation, Methodology, Visualization. NL: Data curation, Formal Analysis, Investigation, Visualization, Writing – original draft, Writing – review & editing, Software. PC: Conceptualization, Data curation, Investigation, Methodology, Writing – original draft. ML: Conceptualization, Formal Analysis, Funding acquisition, Investigation, Project administration, Resources, Supervision, Validation, Writing – original draft, Writing – review & editing.

Funding

The author(s) declare that financial support was received for the research and/or publication of this article. This work was funded by ANID FONDECYT N° 1240367. ML acknowledges the ANID-Millennium Science Initiative Program-Code ICN2019_015 and also thanks the support from PIA ANID ANILLOS ACT240004.

Conflict of interest

The authors declare that the research was conducted in the absence of any commercial or financial relationships that could be construed as a potential conflict of interest.

Generative AI statement

The author(s) declare that no Generative AI was used in the creation of this manuscript.

Publisher's note

All claims expressed in this article are solely those of the authors and do not necessarily represent those of their affiliated organizations, or those of the publisher, the editors and the reviewers. Any product that may be evaluated in this article, or claim that may be made by its manufacturer, is not guaranteed or endorsed by the publisher.

Supplementary material

The Supplementary for this article can be found online at: https://www.frontiersin.org/articles/10.3389/fmars.2025.1568035/full#supplementary-material

References

Andersson, A. J., and Mackenzie, F. T. (2004). Shallow-water oceans: a source or sink of atmospheric CO_2? *Front. Ecol. Environ.* 2, 348–353. doi: 10.1890/1540-9295(2004)002[0348:SOASOS]2.0.CO;2

Asnicar, D., and Marin, M. G. (2022). Effects of seawater acidification on echinoid adult stage: A review. *J. Mar. Sci. Eng.* 10, 477. doi: 10.3390/jmse10040477

Barclay, K. M., Gingras, M. K., Packer, S. T., and Leighton, L. R. (2020). The role of gastropod shell composition and microstructure in resisting dissolution caused by ocean acidification. *Mar. Environ. Res.* 162, 105105. doi: 10.1016/j.marenvres.2020.105105

Bendell, L. I., Chan, K., Crevecoeur, S., and Prigent, C. (2014). Changes in ammonium and pH within intertidal sediments in relation to temperature and the occurrence of nonindigenous bivalves. *Open J. Mar. Sci.* 4, 151–162. doi: 10.4236/ojms.2014.43015

Benítez, S., Lagos, N. A., Osores, S., Opitz, T., Duarte, C., Navarro, J. M., et al. (2018). High pCO_2 levels affect metabolic rate, but not feeding behavior and fitness, of farmed giant mussel *Choromytilus chorus*. *Aquac. Environ. Interac.* 10, 267–278. doi: 10.3354/aei00271

Brenner, H., Braeckman, U., Le Guitton, M., and Meysman, F. J. R. (2016). The impact of sedimentary alkalinity release on the water column CO2 system in the North Sea. *Biogeosciences* 13, 841–863. doi: 10.5194/bg-13-841-2016

Bonner, J. S., Autenrieth, R. L., and Schreiber, L. (1990). Aquatic Sediments. *Research Journal of the Water Pollution Control Federation* 62(4), 593–614. Available online at: http://www.jstor.org/stable/25043883.

Carlton, H., Champlin, L., Jeppesen, R., Haskins, J. C., Rahman, F. I., and Watson, E. B. (2023). Tidal restrictions in a central Californian estuarine system are associated with higher mean pH, but increased low-pH exposure. *Mar. Ecol. Prog. Ser.* 703, 177–182. doi: 10.3354/meps14209

Castillo, N., Gaitán-Espitia, J. D., Quintero-Galvis, J. F., Saldías, G. S., Martel, S. I., Lardies, M. A., et al. (2024). Small-scale geographic differences in multiple-driver environmental variability can modulate contrasting phenotypic plasticity despite high levels of gene flow. *Sci. Total Environ.* 954, 176772. doi: 10.1016/j.scitotenv.2024.176772

Christianen, M. J. A., van der Heide, T., Holthuijsen, S. J., van der Reijden, K. J., Borst, A. C. W., and Olff, H. (2017). Biodiversity and food web indicators of community recovery in intertidal shellfish reefs. *Biol. Conserv.* 213, 317–324. doi: 10.1016/j.biocon.2016.09.028

Clasing, E., Brey, T., Stead, R., Navarro, J., and Asencio, G. (1994). Population dynamics of *Venus antiqua* (Bivalvia: Veneracea) in the Bahía de Yaldad, Isla de Chiloé, southern Chile. *J. Exp. Mar. Biol. Ecol.* 177, 171–186. doi: 10.1016/0022-0981(94)90235-6

Clements, J. C., and Darrow, E. S. (2018). Eating in an acidifying ocean: a quantitative review of elevated CO 2 effects on the feeding rates of calcifying marine invertebrates. *Hydrobiologia* 820, 1–21. doi: 10.1007/s10750-018-3665-1

Clements, J. C., and Hunt, H. L. (2017). Effects of CO2-driven sediment acidification on infaunal marine bivalves: a synthesis. *Mar. pollut. Bull.* 117, 6–16. doi: 10.1016/j.marpolbul.2017.01.053

Clements, J. C., and Hunt, H. L. (2018). Testing for sediment acidification effects on within-season variability in juvenile soft-shell clam (*Mya arenaria*) abundance on the northern shore of the Bay of Fundy. *Estuar. Coasts* 41, 471–483. doi: 10.1007/s12237-017-0270-x

Clements, J. C., Woodard, K. D., and Hunt, H. L. (2016). Porewater acidification alters the burrowing behavior and post-settlement dispersal of juvenile soft-shell clams (Mya arenaria). *J. Exp. Mar. Biol. Ecol.* 477, 103–111. doi: 10.1016/j.jembe.2016.01.013

Cummings, V., Vopel, K., and Thrush, S. (2009). Terrigenous deposits in coastal marine habitats: influences on sediment geochemistry and behaviour of post-settlement bivalves. *Mar. Ecol. Prog. Ser.* 383, 173–185. doi: 10.3354/meps07983

Davis, A. M., Plough, L. V., and Paynter, K. T. (2023). Intraspecific patterns of mortality and cardiac response to hypoxia in the eastern oyster, *Crassostrea virginica*. *J. Exp. Mar. Biol. Ecol.* 566, 151921. doi: 10.1016/j.jembe.2023.151921

Dickson, A. G., and Millero, F. J. (1987). A comparison of the equilibrium constants for the dissociation of carbonic acid in seawater media. *Deep-Sea Res.* 34, 1733–1743. doi: 10.1016/0198-0149(87)90021-5

Eriksson, B. K., van der Heide, T., van de Koppel, J., Piersma, T., van der Veer, H. W., and Olff, H. (2010). Major changes in the ecology of the Wadden Sea: human impacts, ecosystem engineering and sediment dynamics. *Ecosystems* 13, 752–764. doi: 10.1007/s10021-010-9352-3

Fernández, C., Poupin, M. J., Lagos, N. A., Broitman, B. R., and Lardies, M. A. (2024). Physiological resilience of intertidal chitons in a persistent upwelling coastal region. *Scient. Rep.* 14, 21401. doi: 10.1038/s41598-024-72488-8

Field, C. B. (1998). Primary production of the biosphere: integrating terrestrial and oceanic components. *Science* 281, 237–240. doi: 10.1126/science.281.5374.237

Flombaum, P., and Martiny, A. C. (2021). Diverse but uncertain responses of picophytoplankton lineages to future climate change. *Limnology Oceanography* 66, 4171–4181. doi: 10.1002/lno.v66.12

Gaitán-Espitia, J. D., Bacigalupe, L. D., Opitz, T., Lagos, N. A., Timmermann, T., and Lardies, M. A. (2014). Geographic variation in thermal physiological performance of the intertidal crab Petrolisthes violaceus along a latitudinal gradient. *J. Exp. Biol.* 217, 4379–4386. doi: 10.1242/jeb.108217

Gaitán-Espitia, J. D., Marshall, D., Dupont, S., Bacigalupe, L. D., Bodrossy, L., and Hobday, A. J. (2017). Geographical gradients in selection can reveal genetic constraints for evolutionary responses to ocean acidification. *Biol. Lett.* 13, 20160784. doi: 10.1098/rsbl.2016.0784

Gazeau, F., Parker, L. M., Comeau, S., Gattuso, J.-P., O'connor, W. A., Martin, S., et al. (2013). Impacts of ocean acidification on marine shelled molluscs. *Mar. Biol.* 160, 2207–2245. doi: 10.1007/s00227-013-2219-3

Gleckler, P. J., Durack, P. J., Stouffer, R. J., Johnson, G. C., and Forest, C. E. (2016). Industrial-era global ocean heat uptake doubles in recent decades. *Nat. Clim. Change* 6, 394–398. doi: 10.1038/nclimate2915

Goethel, C. L., Grebmeier, J. M., Cooper, L. W., and Miller, T. J. (2017). Implications of ocean acidification in the Pacific Arctic: experimental responses of three arctic bivalves to decreased pH and food availability. *Deep Sea Res. Part II: Trop. Stud. Oceanogr.* 144, 112–124. doi: 10.1016/j.dsr2.2017.08.01

Harayashiki, C. A. Y., Márquez, F., Cariou, E., and Castro, Í.B. (2020). Mollusk shell alterations resulting from coastal contamination and other environmental factors. *Environmen. Pollut.* 265, 114881. doi: 10.1016/j.envpol.2020.114881

Harvey, B. P., Gwynn-Jones, D., and Moore, P. J. (2013). Meta-analysis reveals complex marine biological responses to the interactive effects of ocean acidification and warming. *Ecol. Evol.* 3, 1016–1030. doi: 10.1002/ece3.2013.3.issue-4

Hernández, A. F., Cubillos, L. A., and Quiñones, R. A. (2011). Evaluación talla estructurada de los stocks de *Ensis macha* y *Tagelus dombeii* en el Golfo de Arauco, Chile. *Rev. Biol. Mar. Oceanogr.* 46, 157–176. doi: 10.4067/S0718-19572011000200006

Hettinger, A., Sanford, E., Hill, T. M., Hosfelt, J. D., Russell, A. D., and Gaylord, B. (2013). The influence of food supply on the response of Olympia oyster larvae to ocean acidification. *Biogeosciences* 10, 6629–6638. doi: 10.5194/bg-10-6629-2013

Hoegh-Guldberg, O., Mumby, P. J., Hooten, A. J., Steneck, R. S., Greenfield, P., Gomez, E., et al. (2007). Coral reefs under rapid climate change and ocean acidification. *Science* 318, 1737–1742. doi: 10.1126/science.1152509

Hohaia, A., Vopel, K., and Pilditch, C. A. (2014). Thin terrestrial sediment deposits on intertidal sandflats: effects on pore-water solutes and juvenile bivalve burial behaviour. *Biogeosciences* 11, 2225–2235. doi: 10.5194/bg-11-2225-2014

Hu, M. Y., Casties, I., Stumpp, M., Ortega-Martinez, O., and Dupont, S. (2014). Energy metabolism and regeneration are impaired by seawater acidification in the

infaunal brittlestar *Amphiura filiformis*. *J. Exp. Biol.* 217, 2411–2421. doi: 10.1242/jeb.100024

Iram, N., Maher, D. T., Lovelock, C. E., Baker, T., Cadier, C., and Adame, M. F. (2022). Climate change mitigation and improvement of water quality from the restoration of a subtropical coastal wetland. *Ecol. Appl.* 32, e2620. doi: 10.1002/eap.v32.5

Jaramillo, E., Contreras, H., and Duarte, C. (2007). "Community structure of the macroinfauna inhabiting tidal flats characterized by the presence of different species of burrowing bivalves in Southern Chile," in *Biodiversity in Enclosed Seas and Artificial Marine Habitats. Developments in Hydrobiology*, vol. 193 . Eds. G. Relini and J. Ryland (Dordrecht: Springer). doi: 10.1007/978-1-4020-6156-1_7

Johnson, G. C., and Lumpkin, R. L. (2024). Global oceans [in "State of the climate in 2023". *Bull. Amer. Meteor. Soc* 105, S156–S213. doi: 10.1175/BAMS-D-24-0100.1

Kessouri, F., McWilliams, J. C., Bianchi, D., Sutula, M., Renault, L., Deutsch, C., et al. (2021). Coastal eutrophication drives acidification, oxygen loss, and ecosystem change in a major oceanic upwelling system. *PNAS* 118, e2018856118. doi: 10.1073/pnas.2018856118

Kwon, E. Y., Sreeush, M. G., Timmermann, A., Karl, D. M., Church, M. J., Lee, S. S., et al. (2022). Nutrient uptake plasticity in phytoplankton sustains future ocean net primary production. *Sci. Adv.* 8, eadd2475. doi: 10.1126/sciadv.add2475

Lagos, N. A., Benitez, S., Duarte, C., Lardies, M. A., Broitman, B. R., Tapia, C., et al. (2016). Effects of temperature and ocean acidification on shell characteristics of *Argopecten purpuratus*: implications for scallop aquaculture in an upwelling-influenced area. *Aquacult. Environ. Interact.* 8, 357–370. doi: 10.3354/aei00183

Lardies, M. A., Caballero, P., Duarte, C., and Poupin, M. J. (2021). Geographical variation in phenotypic plasticity of intertidal sister limpet's species under ocean acidification scenarios. *Front. Mar. Sci.* 8. doi: 10.3389/fmars.2021.647087

Lardies, M. A., Clasing, E., Navarro, J. M., and Stead, R. (2001). Effects of environmental variables on burial depth of two infaunal bivalves inhabiting a tidal flat in southern Chile. *J. Mar. Biol. Assoc. UK.* 81, 809–816. doi: 10.1017/S0025315401004635

Lawrence, J., Popova, E., Yool, A., and Srokosz, M. (2015). On the vertical phytoplankton response to an ice-free Arctic Ocean. *J. Geophys. Res. Oceans* 120, 8571–8582. doi: 10.1002/2015JC011180

Lefevre, S. (2016). Are global warming and ocean acidification conspiring against marine ectotherms? A meta-analysis of the respiratory effects of elevated temperature, high CO_2 and their interaction. *Conserv. Physiol.* 4 (1), cow009. doi: 10.1093/conphys/cow009

Lépez, I., Aracena, O., Carmona, A., Espinoza, A., Fuentes, L., Sánchez, J., et al. (1997). "Caracterización bioeconómica de las pesquerías de huepo (Ensis macha) y navajuela (Tagelus dombeii) en la VIII Región," in *Informe Final Proyecto FIP N°95-20a*. (Chile: Subsecretaría de Pesca, Valparaíso).

Leung, J. Y., Zhang, S., and Connell, S. D. (2022). Is ocean acidification really a threat to marine calcifiers? A systematic review and meta-analysis of 980+ studies spanning two decades. *Small* 18, 2107407. doi: 10.1002/smll.202107407

Liang, J., Liu, Y., Zhu, F., Li, Y., Liang, S., and Guo, Y. (2022). Impact of ocean acidification on the physiology of digestive gland of razor clams *Sinonovacula constricta*. *Front. Mar. Sci.* 9. doi: 10.3389/fmars.2022.1010350

Liu, X., Stock, C. A., Dunne, J. P., Lee, M., Shevliakova, E., Malyshev, S., et al. (2021). Simulated global coastal ecosystem responses to a half-century increase in river nitrogen loads. *Geophysical Res. Lett.* 48, e2021GL094367. doi: 10.1029/2021GL094367

Marshall, D. J., and McQuaid, C. D. (2020). Metabolic regulation, oxygen limitation and heat tolerance in a subtidal marine gastropod reveal the complexity of predicting climate change vulnerability. *Front. Physiol.* 11, 1106. doi: 10.3389/fphys.2020.01106

Martel, S. I., Fernández, C., Lagos, N. A., Labra, F. A., Duarte, C., Vivanco, J. F., et al. (2022). Acidification and high- temperature impacts on energetics and shell production of the edible clam *Ameghinomya antiqua*. *Front. Mar. Sci.* 9. doi: 10.3389/fmars.2022.972135

McGarrigle, S. A., and Hunt, H. L. (2024). Infaunal invertebrate community relationships to water column and sediment abiotic conditions. *Mar. Biol.* 171, 3. doi: 10.1007/s00227-023-04318-w

Medeiros, I. P. M., and Souza, M. M. (2023). Acid times in physiology: a systematic review of the effects of ocean acidification on calcifying invertebrates. *Environmen. Res.* 231, 116019. doi: 10.1016/j.envres.2023.116019

Mehrbach, C., Culberson, C. H., Hawley, J. E., and Pytkowicx, R. M. (1973). Measurement of the apparent dissociation constants of carbonic acid in seawater at atmospheric pressure. *Limnol. Oceanogr.* 18, 897–907. doi: 10.4319/lo.1973.18.6.0897

Meseck, S. L., Mercaldo-Allen, R., Kuropat, C., Clark, P., and Goldberg, R. (2018). Variability in sediment-water carbonate chemistry and bivalve abundance after bivalve settlement in Long Island Sound, Milford, Connecticut. *Mar. pollut. Bull.* 135, 165–175. doi: 10.1016/j.marpolbul.2018.07.025

Michaelidis, B., Ouzounis, C., Paleras, A., and Pörtner, H. O. (2005). Effects of long-term moderate hypercapnia on acid–base balance and growth rate in marine mussels *Mytilus galloprovincialis*. *Mar. Ecol. Prog. Ser.* 293, 109–118. doi: 10.3354/meps293109

Morse, M. P., and Zardus, J. D. (1997). "Bivalvia," in *Microscopic anatomy of invertebrates*, vol. 6A . Eds. F. W. Harrison and A. J. I. Kohn (John Wiley & Sons Inc, New York), 7–118. Mollusca.

Murray, N. J., Phinn, S. R., DeWitt, M., Ferrari, R., Johnston, R., Lyons, M. B., et al. (2019). The global distribution and trajectory of tidal flats. *Nature* 565, 222. doi: 10.1038/s41586-018-0805-8

Navarro, J. M., Clasing, E., Lardies, M. A., and Stead, R. A. (2008). Feeding behavior of the infaunal bivalve Tagelus dombeii (Lamarck 1818). Suspension vs. deposit feeding. *Rev. Biol. Mar. Oceanogr.* 43, 599–605. doi: 10.4067/S0718-19572008000300019

Navarro, J. M., Duarte, C., Manríquez, P. H., Lardies, M. A., Torres, R., Acuña, K., et al. (2016). Ocean warming and elevated carbon dioxide: multiple stressor impacts on juvenile mussels from southern Chile. *ICES J. Mar. Sci.* 73, 764–771. doi: 10.1093/icesjms/fsv249

Navarro, J. M., Duarte, C., Manríquez, P. H., Torres, R., Vargas, C. A., Lardies, M. A., et al. (2013). Impact of medium-term exposure to elevated pCO2 levels on the physiological energetics of the mussel Mytilus Chilensis. *Chemosphere* 90, 242–248. doi: 10.1016/j.chemosphere.2012.09.063

Osores, S. J., Lagos, N. A., San Martín, V., Manríquez, P. H., Vargas, C. A., Torres, R., et al. (2017). Plasticity and inter-population variability in physiological and life-history traits of the mussel *Mytilus Chilensis*: A reciprocal transplant experiment. *J. Exp. Mar. Biol. Ecol.* 490, 1–12. doi: 10.1016/j.jembe.2017.02.005

Palmer, A. R. (1982). Growth in marine gastropods. A non-destructive technique for independently measuring shell and body weight. *Malacologia* 23, 63–74.

Pierrot, D., Lewis, E., and Wallace, D. W. R. (2006). "MS excel program developed for CO2 system calculations., ORNL/CDIAC-105," in *Carbon Dioxide Information Analysis Center Oak Ridge National Laboratory US Department of Energy*(Oak Ridge Tennessee: ORNL Environmental Sciences Division).

Precht, E., Franke, U., Polerecky, L., and Huettel, M. (2004). Oxygen dynamics in permeable sediments with wave-driven pore water exchange. *Limnol. Oceanogr.* 49, 693–705. doi: 10.4319/lo.2004.49.3.0693

Ramajo, L., Fernández, C., Núñez, Y., Caballero, P., Lardies, M. A., and Poupin, M. J. (2019). Physiological responses of juvenile Chilean scallops (*Argopecten purpuratus*) to isolated and combined environmental drivers of coastal upwelling. *ICES J. Mar. Sci.* 76, 1836–1849. doi: 10.1093/icesjms/fsz080

Ramajo, L., Hendriks, I. E., Marbà, N., Sejr, M. K., Blicher, M. E., Lagos, N. A., et al. (2016a). Food supply confers calcifiers resistance to ocean acidification. *Scient. Rep.* 6, 1–6. doi: 10.1038/srep19374

Ramajo, L., Marba, N., Prado, L., Peron, S., Lardies, M. A., Rodríguez-Navarro, A. B., et al. (2016b). Biomineralization changes with food supply confer juvenile scallops (*Argopecten purpuratus*) resistance to ocean acidification. *Glob. Change Biol.* 22, 2025–2037. doi: 10.1111/gcb.13179

Rathbone, M., Brown, K. T., and Dove, S. (2022). Tolerance to a highly variable environment does not infer resilience to future ocean warming and acidification in a branching coral. *Limnol. Oceanogr.* 67, 272–284. doi: 10.1002/lno.11991

R Core Team (2024). *A Language and Environment for Statistical Computing*. R 4.5.0. version: 2025-04-11. (Vienna, Austria: R Foundation for Statistical Computing). Available at: https://www.R-project.org/.

Rodríguez-Romero, A., Gaitán-Espitia, J. D., Opitz, T., and Lardies, M. A. (2022). Heterogeneous environmental seascape across a biogeographic break influences the thermal physiology and tolerances to ocean acidification in an ecosystem engineer. *Divers. Distrib.* 28, 1542–1553. doi: 10.1111/ddi.13478

Salas, M. C., Defeo, O., Firstater, F., and Narvarte, M. (2022). Impact of a macrofaunal ecosystem engineer on its assemblage and its habitat in mixed sediments as assessed through manipulative experiments. *J. Exp. Mar. Biol. Ecol.* 554, 151766. doi: 10.1016/j.jembe.2022.151766

Sánchez, J., Hernández, A., Agüero, M., González, E., Miranda, L., Vásquez, C., et al. (2003). "Ordenamiento de la pesquería de huepo y navajuela," in *Informe Final Proyecto FIP N°2002- 26*. (Chile: Subsecretaría de Pesca, Valparaíso).

Shi, Y., and Li, Y. (2024). Impacts of ocean acidification on physiology and ecology of marine invertebrates: a comprehensive review. *Aquat. Ecol.* 58, 207–226. doi: 10.1007/s10452-023-10058-2

Singer, A., Bijleveld, A. I., Hahner, F., Holthuijsen, S. J., Hubert, K., Kerimoglu, O., et al. (2023). Long-term response of coastal macrofauna communities to de-eutrophication and sea level rise mediated habitat changes, (1980s versus 2018). *Front. Mar. Sci.* 9, 1–20. doi: 10.3389/fmars.2022.963325

Stead, R. A., Clasing, E., Lardies, M. A., Arratia, L. P., and Urrutia, G. (2002). The significance of contrasting feeding strategies on the reproductive cycle in two coexisting tellinacean bivalves. *J. Mar. Biol. Assoc. United Kingdom* 82, 443–453. doi: 10.1017/S0025315402005702

Torres, R., Pantoja, S., Harada, N., González, H. E., Daneri, G., Frangopulos, M., et al. (2011). Air-sea CO2 fluxes along the coast of Chile: From CO2 outgassing in central northern upwelling waters to CO2 uptake in southern Patagonian fjords. *J. Geophysical Research: Oceans* 116 (C9). doi: 10.1029/2010JC006344

Underwood, A. J. (1997). *Experiments in ecology* (United Kingdom: Cambridge University Press).

Urrutia, G. X., Navarro, J. M., Clasing, E., and Stead, R. A. (2001). The effects of environmental factors on the biochemical composition of the bivalve *Tagelus dombeii* (Lamarck 1818) (Tellinacea: Solecurtidae) from the intertidal flat of Coihuín, Puerto Montt, Chile. *J. Shellfish Res.* 20, 1077–1088.

Van Colen, C., Ong, E. Z., Briffa, M., Wethey, D. S., Abatih, E., Moens, T., et al. (2020). Clam feeding plasticity reduces herbivore vulnerability to ocean warming and acidification. *Nat. Clim. Change* 10, 162–166. doi: 10.1038/s41558-019-0679-2

Vargas, C. A., Lagos, N. A., Lardies, M. A., Duarte, C., Manríquez, P. H., Aguilera, V. M., et al. (2017). Species-specific responses to ocean acidification should account for local adaptation and adaptive plasticity. *Nat. Ecol. Evol.* 1, 0084. doi: 10.1038/s41559-017-0084

Vergara-Jara, M. J., DeGrandpre, M. D., Torres, R., Beatty, C. M., Cuevas, L. A., Alarcón, E., et al. (2019). Seasonal changes in carbonate saturation state and air-sea CO_2 fluxes during an annual cycle in a stratified-temperate fjord (Reloncaví Fjord, Chilean Patagonia). *J. Geophys.l Res. Biogeosciences* 124, 2851–2865. doi: 10.1029/2019JG005028

Vlaminck, E., Moens, T., Braeckman, U., and Van Colen, C. (2023). Ocean acidification and warming modify stimulatory benthos effects on sediment functioning: An experimental study on two ecosystem engineers. *Front. Mar. Sci.* 10. doi: 10.3389/fmars.2023.1101972

Wethey, D. S., and Woodin, S. A. (2022). Climate change and Arenicola marina: Heat waves and the southern limit of an ecosystem engineer. *Estuar. Coast. Shelf Sci.* 276, 108015. doi: 10.1016/j.ecss.2022.108015

Widdicombe, S., Spicer, J. I., and Kitidis, V. (2011). "Effects of ocean acidification on sediment fauna," in *Ocean acidification*. Eds. J. P. Gattuso and L. Hansson (Oxford University Press, Oxford), 176–191.

Zhang, L., Wang, L., Yin, K., Lü, Y., Zhang, D., Yang, Y., et al. (2013). Pore water nutrient characteristics and the fluxes across the sediment in the Pearl River estuary and adjacent waters, China. *Estuar. Coast. Shelf Sci.* 133, 182–192. doi: 10.1016/j.ecss.2013.08.028

frontiers | Frontiers in Marine Science

TYPE Original Research
PUBLISHED 09 June 2025
DOI 10.3389/fmars.2025.1595911

OPEN ACCESS

EDITED BY
Jose Martin Hernandez-Ayon,
Autonomous University of Baja California, Mexico

REVIEWED BY
Diana L. Stram,
North Pacific Fishery Management Council, United States
Mihailov Maria Emanuela,
Maritime Hydrographic Directorate, Romania

*CORRESPONDENCE
Kalina C. Grabb
kgrabb@whoi.edu
Natalie Lord
natalie.lord@unh.edu

RECEIVED 18 March 2025
ACCEPTED 19 May 2025
PUBLISHED 09 June 2025

CITATION
Grabb KC, Lord N, Dobson KL, Gordon-Smith D-ADS, Escobar-Briones E, Ford MC, Lander S, Kitch GD, Meléndez M, Morell J, Caravaca AM, Newton J, Packard A, Valauri-Orton A, Valladarez J, Vondriska C and Wright-Fairbanks E (2025) Building ocean acidification research and policy capacity in the wider Caribbean region: a case study for advancing regional resilience. *Front. Mar. Sci.* 12:1595911. doi: 10.3389/fmars.2025.1595911

Building ocean acidification research and policy capacity in the wider Caribbean region: a case study for advancing regional resilience

Kalina C. Grabb [1*], Natalie Lord [2*], Kerri L. Dobson [3], Debbie-Ann D. S. Gordon-Smith [4], Elva Escobar-Briones [5], Marcia Creary Ford [6], Sylvia Lander [7], Gabriella D. Kitch [8], Melissa Meléndez [9], Julio Morell[10], Alain Muñoz Caravaca [11], Jan Newton [12], Amber Packard [13], Alexis Valauri-Orton [14], Jair Valladarez [15], Clayton Vondriska [16,17] and Elizabeth Wright-Fairbanks [18]

[1]Marine Policy Center, Woods Hole Oceanographic Institution, Woods Hole, MA, United States, [2]Natural Resources and the Environment, University of New Hampshire, Durham, NH, United States, [3]Department of Biology and Marine Biology, Center for Marine Science, University of North Carolina Wilmington, Wilmington, NC, United States, [4]Department of Chemistry, The University of the West Indies, Kingston, Jamaica, [5]Universidad Nacional Autónoma de México, Instituto de Ciencias del Mar y Limnología, Ciudad Universitaria, Mexico City, Mexico, [6]Centre for Marine Sciences, The University of the West Indies, Kingston, Jamaica, [7]National Center of Testing Excellence, Dominica Bureau Of Standards, Roseau, Dominica, [8]Ocean Acidification Program, National Oceanic and Atmospheric Administration, Silver Spring, MD, United States, [9]Oceanography Department, University of Hawai'i at Mānoa, Honolulu, HI, United States, [10]Caribbean Coastal Ocean Observing System, Mayagüez, Puerto Rico, [11]Departamento de Gestión e Ingeniería Ambiental, Centro de Estudios Ambientales de Cienfuegos, Cienfuegos, Cuba, [12]Applied Physics Laboratory and School of Oceanography, University of Washington, Seattle, WA, United States, [13]Center for Marine and Environmental Studies, University of the Virgin Islands, St. Thomas, VI, United States, [14]The Ocean Foundation, Washington, DC, United States, [15]Faculty of Science and Technology, University of Belize, Belmopan, Belize, [16]Department of Biology, College of Science and Mathematics, University of the Virgin Islands, St Thomas, VI, United States, [17]Department of Marine Biology and Ecology, Rosenstiel School of Marine, Atmospheric, and Earth Science, University of Miami, Miami, FL, United States, [18]University Corporation for Atmospheric Research, under contract to NOAA Ocean Acidification Program, Oceanic and Atmospheric Research, National Oceanic and Atmospheric Administration, Silver Spring, MD, United States

To meet scientific, policy, and community goals, there is a critical need to strengthen research capacity, increase monitoring, and inform adaptation and mitigation policies to enhance resilience against ocean acidification (OA) and associated multi-stressors in the Caribbean. In 2023, an OA Needs Based Assessment survey of ocean professionals was conducted, engaging 59 participants from across the wider Caribbean to evaluate regional challenges and opportunities in OA research and monitoring. To understand differences in OA research capacity related to training and funding, we divide the respondents into four groups: those that have received 1) training and funding, 2) training only, 3) funding only, and 4) neither training nor funding. Results indicate regional strengths include awareness of local oceanic conditions, access to nearshore sites, and strong social support networks in ocean research. Regional barriers include limited technical capacity and funding to conduct oceanographic research and monitoring, and in particular, carbonate measurements. The four training and funding groups vary significantly, suggesting that access to training

and funding are important factors to increasing the amount of access that respondents have to different types of equipment, the number of different types of measurements they conduct, the number of different habitats they research, and the amount of experience they have conducting OA research. This study also demonstrates the community-led efforts to address local OA challenges by presenting a case study on the formation of the Global Ocean Acidification Network (GOA-ON) OA Caribbean Hub that was founded by local leaders (co-authors of this study) who were inspired through the survey process and engagement that was conducted by co-authors. This study provides examples of avenues and challenges to build OA capacity for research and monitoring from the ground up within the wider Caribbean to advance towards global sustainability goals.

KEYWORDS

OA, sustainable development goals, capacity building, regional networks, Caribbean, OA training, OA funding, OA research

Introduction

As global climate continues to change, the ocean has absorbed around one-third of anthropogenic carbon dioxide emissions, causing the carbon content within the ocean to increase along with atmospheric carbon dioxide (CO_2) concentrations (Caldeira and Wickett, 2003; Doney et al., 2009). The absorption of CO_2 by the ocean leads to ocean acidification (OA) due to higher concentrations of hydrogen ions (decreased pH; increased acidity) and decreased availability of carbonate ions, which impacts marine ecosystems and organisms (Friedlingstein et al., 2022; Gruber et al., 2023).

Globally, ocean pH has decreased by 0.1 pH units over the past century, corresponding to a ~26% increase in acidity (IPCC, 2023). While OA is a global issue, local variability and its specific effects necessitate measuring it at the community scale. Localized approaches help to understand drivers and synergies, develop targeted adaptation and mitigation strategies, and create predictive capabilities to identify early warning signs for timely decision making (Cross et al., 2019).

In response to the rising threat, OA monitoring and research has been set as a priority for global policy frameworks. These include the international Kunming-Montreal Global Biodiversity Framework Target 8 and the national and regional frameworks within the U.S. (Federal Ocean Acidification Research and Monitoring Act of 2009, FOARAM Act, U.S. Code under Title 33, Chapter 50), European Union (Marine Strategy Framework Directive), and North-East Atlantic's Oslo and Paris Conventions (OSPAR) Commission (Galdies et al., 2021; Grabb et al., 2024). To achieve widespread global OA measurements, the United Nations Sustainable Development Goal (SDG) 14 (*Conserve and sustainably use the oceans, seas and marine resources for sustainable development*) aims to address and increase measurements of OA through its Target 14.3 (*Minimize and address the impacts of ocean acidification, including through enhanced scientific cooperation at all levels*) and Indicator 14.3.1 (*Average marine acidity (pH) measured at agreed suite of representative sampling stations*) (United Nations, 2024; See Appendix B for list of acronyms and policies). The SDG 14.3.1 methodology provides written guidance on how to conduct and collect OA observations, including identifying designated parameters to measure for OA (United Nations, 2024).

However, many countries lack the resources, policy, and technical capacity to monitor OA (Cooley et al., 2022), particularly Small Island Developing States (SIDS), which depend heavily on ocean resources for their livelihoods and economies (Meléndez and Salisbury, 2017; Grabb et al., 2024). Increasing the global capacity for OA research can help preserve ocean-based ecosystem services (i.e. coastal protection, food security, economies, and health) that directly support human livelihoods and provide up-to-date information and tools to assess these marine resources under changing climates (Gill et al., 2017; Hughes et al., 2017; Miloslavich et al., 2019). Depending on a number of factors including the future demand for shellfish and the extent of economic sectors that OA can impact, OA is predicted to result in an annual loss between US $6 billion (Narita et al., 2012) to US $400 billion (Moore and Fuller, 2020) globally. Under future climate scenarios, increased capacity for measuring, monitoring, and reporting OA must be a global and regional policy priority in order to inform mitigation, adaptation and resilience plans and to meet climate goals.

OA in the Caribbean

The Caribbean region consists of nearly 30 SIDS, yet is often discussed as the wider Caribbean region, which includes all countries and territories bordering the Caribbean Sea and Gulf of Mexico (Cartagena Convention, Article 2). Seventy percent of the

Caribbean population lives on the coast and relies on marine ecosystems for food security, coastal protection, the tourism industry, and cultural practices (Meléndez and Salisbury, 2017). The region is also a global marine biodiversity hotspot and one of the most diverse marine regions in the Atlantic (Roberts et al., 2002). Coastal ecosystems include coral reefs, seagrass beds, mangroves, rocky shorelines, and sandy beaches (Roberts et al., 2002; Miloslavich et al., 2010). However, climate stressors like OA threaten these ecosystems and associated resources (Gledhill et al., 2008; Cooley et al., 2022). For example, the categories of Caribbean species that had the highest commercial values in 2020 have the potential to be negatively affected by OA (Doney et al., 2009). Surface aragonite saturation state within the Caribbean has also declined by ~3% since pre-industrial levels (Gledhill et al., 2008; Meléndez and Salisbury, 2017), which can affect the availability of carbonate ions. This can negatively affect behavior, growth, survival, and larval development across a broad range of marine species, especially those that have larval stages requiring calcification, which can be further restricted if their larval development occurs during a tightly constrained time frame (Fabry et al., 2008; Spalding et al., 2017). In addition to the physiological challenges, OA also exacerbates other environmental stressors, including ocean warming, harmful algal blooms, and deoxygenation (Siedlecki et al., 2021).

Systematic remote sensing and *in situ* carbonate system measurements in the Caribbean SIDS began only in the past two decades, leaving significant gaps in both spatial and temporal data coverage. Despite these limitations, existing studies have successfully captured an OA signal across the region (Gledhill et al., 2008; Bates, 2012; Meléndez and Salisbury, 2017; Land et al., 2019; Meléndez et al., 2020). On a regional scale, remote sensing and model-based data indicate a ~10% increase in surface OA from 1992-2015, with significant spatial and temporal variability (Meléndez and Salisbury, 2017). At a local scale, the first long-term OA time series within Caribbean SIDS was established in 2009 at La Parguera Marine Reserve, Puerto Rico (Meléndez et al., 2020). This collaborative initiative between federal and state programs monitors nearshore carbonate dynamics along with other chemical, biological, geological, and physical parameters. La Parguera MAPCO$_2$ buoy is the only coastal buoy in the U.S. National Ocean Acidification Observing Network (NOAON) within the Caribbean Sea. In the wider Caribbean region, the CArbon Retention In A Colored Ocean (CARIACO) time series measured CO_2 concentrations within the Cariaco Basin off of Venezuela between 1995 and 2017, and observed some of the highest rates of decreasing pH compared to other ocean time series around the world (-0.0025 pH yr^{-1}) (Bates et al., 2014). The Research Network of Marine-Coastal Stressors in Latin America and the Caribbean (Red de Investigación Marino-Costera; REMARCO) has also established a network across the Caribbean and Latin America to increase measurements of OA, resulting in two countries (Colombia and Cuba) reporting data within the Caribbean Sea to SDG 14.3.1 and six countries (Colombia, Costa Rica, Cuba, Dominican Republic, Panama, and Venezuela) with monitoring stations for carbonate parameters within Caribbean Sea (Espinosa, 2023). These efforts to establish monitoring stations at various locations across the Caribbean Sea have provided enough data to show that OA is occurring throughout the region, yet more widespread, routine, and robust monitoring across the wider Caribbean region is needed to drastically increase the spatial and temporal OA data coverage. Higher resolution OA data throughout the region is necessary to understand the local variability in OA and inform local and regional decisions about mitigation and adaptation approaches.

Two significant sea level and climate monitoring networks were also established in the Caribbean in 1997 and measured physical parameters along with pH. However, they did not measure additional carbonate chemistry components to constrain the carbonate system and provide data on OA. The first was under the World Bank funded Caribbean Planning for Adaptation to Climate Change (CPACC) Project, during which 18 stations were established in 12 countries between 1997 and 2001. The second network consisted of the Coral Reef Early Warning System (CREWS) stations established in 11 countries over the period of 1997–2016 with funding provided by the U.S. National Oceanic and Atmospheric Administration (NOAA). These networks have faced challenges due to the lack of technical support and funding for routine maintenance and repairs, which were especially needed following severe damage from storm events and hurricanes (Hendee et al., 2016). Despite some advances in establishing OA monitoring programs, the limited number of functional monitoring sites, challenges with environmental conditions, and significant regional and local variability underscore the need for expanded capacity to help establish and strengthen observation and monitoring efforts to fully understand OA dynamics across the wider Caribbean region (IOC-UNESCO, 2024b).

Expanding OA monitoring throughout the Caribbean will be crucial to inform mitigation and adaptation strategies tailored to vulnerable local communities across the region. To achieve this access to resources such as sustained funding, training opportunities, collaborations, and regional networks are needed to strengthen OA research and monitoring (Miloslavich et al., 2019; Whitefield et al., 2021). Additionally, integrating place-based knowledge into scientific research and capacity-building efforts is essential, as it will provide vital insights, enhance adaptation strategies, and strengthen engagement throughout the community (Cross et al., 2019; Miloslavich et al., 2022).

Global initiatives to share ocean research capacity

Programs have been developed across regions to share research capacity amongst ocean professionals, yet few are focused on ocean carbonate chemistry measurements and even fewer are designed for and/or implemented within the Caribbean. In other regions of the world, networks have been established to help share OA research capacity, including the Global Ocean Acidification Network (GOA-ON) (Newton et al., 2015). GOA-ON is a collaborative international network designed to improve understanding of global OA

conditions and ecosystem responses to OA. GOA-ON also works to acquire, exchange, and consolidate data and knowledge necessary to optimize modeling for OA and its impacts. GOA-ON has a dedicated Secretariat that coordinates over 1,000 members from over 100 countries and territories, as well as the UN Ocean Decade endorsed program Ocean Acidification Research for Sustainability (OARS) (Dobson et al., 2023; IOC-UNESCO, 2024a). To achieve a global approach that addresses local OA needs, GOA-ON has facilitated the grassroots formation of regional hubs that are purposefully built by local ocean professionals. GOA-ON and its partners also coordinate the Pier2Peer mentorship program (led by NOAA and The Ocean Foundation, TOF) and GOA-ON in a Box Kits (led by TOF), which are low-cost kits used for collecting weather-quality ocean acidification measurements. The Pier2Peer program awards scholarships for small projects and five have been awarded within the wider Caribbean (two in Mexico, one in Costa Rica, and one in Honduras). The Kits have been distributed to scientists in over 25 different countries with ongoing training and support including a few countries within the wider Caribbean (i.e. Mexico, Panama, Jamaica, and Colombia). Best practice guides for science, monitoring, and mentorship have also been developed as resources by the international OA community such as the Practical Best Practices to Ocean Acidification Monitoring (Currie et al., 2024) and the Guide for Developing Mentoring Programs for the International Ocean Community (Lang et al., 2024). These resources offer insights to OA measurements and mentoring programs that can also be translated to communities within the Caribbean.

OA policy and collaborations in the Caribbean

Given the major threat of OA to the Caribbean, policy and community efforts have been made to address OA within the region. For example, the IOC-UNESCO Subcommission for the Caribbean and Adjacent Regions, IOCARIBE, developed a Regional Action Plan on Ocean Acidification for Latin America and the Caribbean (Laffoley et al., 2018). This Action Plan highlighted priorities throughout the region for science, policy, communication, and outreach, and provided a framework of priorities to support collaboration and funding to prioritize OA research and monitoring. Following this, the Scientific and Technical Advisory Committee (STAC) to the Protocol Concerning Specially Protected Areas and Wildlife in the wider Caribbean region (SPAW Protocol, STAC8, December 2018 in Panama with TOF staff) and the Cartagena Convention (COP15, June 2019 in Honduras) signed a Memorandum of Understanding to work with TOF to address OA within the Caribbean region. REMARCO also recognizes OA as a major threat within the region and supports collaborative actions to measure OA, develop policies to reduce CO_2 emissions, and disseminate scientific information to inform policy and decision making.

Another well-established and highly productive network within the region that focuses on OA research and policy efforts is the GOA-ON Latin American and Caribbean OA Regional Hub (LAOCA). Since LAOCA primarily includes Spanish-speaking countries from Latin America, Central America, and the Caribbean, its meetings are often conducted in Spanish to accommodate the majority of its members. However, this can create challenges for non-Spanish-speaking Caribbean countries and territories, which have broad linguistic diversity (Ferreira, 2012) with English being the unofficial language of tourism (which is the largest industry) throughout the Caribbean. Beyond language barriers, the Caribbean SIDS face unique socio-cultural, logistical, and capacity-related challenges (Allahar, 1993; Fanning et al., 2021) that may not align with the priorities of LAOCA. Compared to larger Latin American countries, SIDS often have fewer resources and face distinct vulnerabilities that may not align with the broader regional priorities, potentially limiting their influence in policy discussions and capacity-building initiatives.

Despite these differences, LAOCA's progress serves as an excellent example of how regional collaboration can advance OA research and policy. Acknowledging this success, an opportunity was identified to establish a dedicated OA hub tailored to the unique needs of the wider Caribbean region, where many nations are SIDS. A new hub within the wider Caribbean region would address not only linguistic accessibility and the unique priorities of the region's islands but also foster complementary collaboration with LAOCA, REMARCO, and other existing regional networks to build on their successes and enhance collective efforts in addressing OA impacts across Latin America and the Caribbean.

In recognizing this need to establish an OA network within the Caribbean, the Caribbean Ocean Acidification Community of Practice (CoP) was formed in 2021. The CoP was developed following the 2021 UNESCO Intergovernmental Oceanographic Committee Assembly and the accepted IOCARIBE Decision. The CoP consisted of a core task team of members from the U.S. (i.e., NOAA Ocean Acidification Program (OAP), NOAA's Office of Oceanic and Atmospheric Research International Activities Office, and TOF) and the Caribbean (i.e., representatives from university partners, government, and non-profit/non-governmental organizations). The goals of the CoP were to increase connectivity and engagement and to identify and strengthen current OA research and capacity gaps within the region. The CoP brought together individuals with deep knowledge, strong connections, and a vested interest in the region. It played a key role in advancing OA research, addressing capacity gaps, and laying the foundation for long-term regional networks, such as the GOA-ON OA Caribbean Regional Hub and the Caribbean Coastal Acidification Network (CariCAN).

To better understand the unique regional needs and priorities of the wider Caribbean region, our co-author at TOF led members of the CoP to design an OA Needs Based Assessment survey in 2022. This survey aimed to evaluate OA research capacity and identify priorities and challenges related to OA research as well as strategies to strengthen the region's ability to address these challenges effectively.

In this paper, we present the results of the OA Needs Based Assessment survey, which indicate the current state of OA activities, including strengths and barriers in conducting OA research and

monitoring in the wider Caribbean. We evaluate the OA research aspects that benefit from OA training and funding and present a case study on the establishment of the GOA-ON OA Caribbean Hub, which was initiated following the engagement from this survey. Finally, we provide a brief discussion on the challenges along with recommendations for sustained research, capacity building, and policies that support OA efforts in the wider Caribbean moving forward.

Methods

Survey design

The survey was designed by the CoP in collaboration with TOF to leverage their existing survey design which has been implemented in other regions as part of their OA capacity building efforts (Valauri-Orton et al., 2025; See Appendix A for survey). All survey questions were written in English. The survey was designed to: 1) assess the current state of OA sampling methodologies and ocean observing capacity for the region, and 2) identify regional priorities and areas for improvement and resource focus. A non-probability purposive sampling framework (Carr et al., 2021; Lune and Berg, 2017) was developed to select cases with the following criteria 1) ocean professional currently conducting ocean observations (with a demonstrated focus on OA parameters) and 2) individuals conducting broader water quality monitoring and oceanographic research within countries and territories that have waters bordering the Caribbean Sea. Therefore, this was a targeted survey that is not generalizable with an unknown probability of selection into the sample.

The survey assessment and follow-up activities within this study encompassed the wider Caribbean region (Cartagena Convention, Article 2). Responses from individuals located in the mainland U.S. were not included in the analysis per request of the Caribbean community members who participated in these efforts, given that the intent of this study was to understand the barriers to increasing OA capacity that are unique to the wider Caribbean. The mainland U.S. has had access to an abundance of resources in comparison to the rest of the wider Caribbean and typically does not face the same socio-cultural, logistical, and capacity-related challenges as the other countries and territories within the wider Caribbean, including the U.S. Territories (Allahar, 1993; Fanning et al., 2021). The sampling frame included individuals in the U.S. territories of Puerto Rico and U.S. Virgin Islands because Puerto Rico maintains the only MAPCO2 buoy currently collecting data in the region and both territories have research institutions that conduct OA research in collaboration with others within the region and act as funding pathways for other institutions in the wider Caribbean.

The survey distribution and follow-up activities were facilitated by the co-leads of this study (Grabb and Lord) during their tenure as Sea Grant Knauss Fellows at NOAA OAP in 2023. The survey was distributed between February and June of 2023 via email contact and the Google Forms survey platform. Efforts were made to distribute the survey widely amongst ocean professionals within all countries and territories within the wider Caribbean region; the survey was distributed through direct emails to contacts within the Caribbean by identified research institutions, academic departments, professors, and other ocean professionals with special attention to reach at least several representatives from each country and territory in the wider Caribbean. We also distributed the survey via snowball sampling through existing networks (i.e. the CoP, NOAA Southeast and Caribbean Regional offices, the UNESCO Intergovernmental Oceanographic Commission Subcommission for the Caribbean and Adjacent Regions (IOCARIBE), Caribbean Coastal Ocean Observing System (CARICOOS), United Nations Environmental Program Specially Protected Areas Protocol (SPAW)), at conferences in the Caribbean, through virtual presentations to Caribbean members, and through survey respondents' networks. Survey respondents were given up to five months (February to June) to respond and reminders were sent monthly to encourage respondents to fill out the survey and share it throughout their networks. Additional outreach was focused on encouraging responses from professionals within countries with low or no response rates, for example those within the Eastern Caribbean where there is limited existing research expertise. While snowball sampling methods enabled the survey to be sent to broad groups of ocean professionals, they restricted the ability to track the exact number of people who received the survey and determine the response rate, which is a limitation of the study.

Responses were removed if the entirety of the survey was not complete or if participants identified their location in the mainland U.S. or outside of the wider Caribbean region. The participants were not compensated. Due to the unknown probability of selection into the sample, there are no survey weights, and these results do not represent the entirety of the marine research community in the Caribbean region. The non-probability sampling has limitations, and this work cannot claim generalizability to the entire population of regional researchers. Purposive and snowball sampling may be biased based on existing network access of individuals, with some researchers being left out (Lune and Berg, 2017). Purposive sampling was used to narrow the sampling frame to identify researchers studying ocean acidification and adjacent oceanographic research, therefore not allowing generalizability for all marine researchers in the region. Snowball sampling was used to leverage the social networks of researchers in the region and identify respondents that were difficult to reach, however the networks do not represent the full population of researchers in the region. Despite the limitations of the sample size and the ability for representativeness in statistical analysis, this OA Needs Based Assessment provides descriptive results in an understudied area of research in a data poor region and may be used to inform future funding and policy mechanisms for OA research.

Survey analysis

Survey responses were anonymized, translated into English, and processed using Microsoft Excel and Python programming languages for data analyses and visualization. The survey design included a combined use of quantitative (multiple choice) and qualitative questions (open-ended), so mixed-methods were used for analysis (Creswell and Creswell, 2017), combining both quantitative and qualitative data for more context. The quantitative questions included multiple choice answers where respondents could select all that applied. For the qualitative portion of the survey questions, the responses were open-ended and analyzed using inductive coding based on the themes presented in the responses and the literature (Carr et al., 2021). For questions with multiple categorical responses (i.e. number of different types of equipment accessible, number of different types of measurements conducted, etc.), the total number of responses for each category was quantified to facilitate further quantitative analysis. Based on answers about receiving training or funding, survey respondents were classified into four groups: respondents that have received 1) training and funding (T&F), 2) training only (T), 3) funding only (F), and 4) neither training nor funding (N). For those questions that had quantitative answers the average and standard deviation were calculated for the respondents within each of the four training and funding groups. To compare the significance between averages of each training and funding group, ANOVA single-factor p-values (<0.05) were calculated, followed by Tukey t-test p-values (<0.05) to determine individual variation.

To emphasize transparency in data collection and distribution, all survey responses were anonymized and shared with participants, and have since been reported at international conferences, regional meetings, community gatherings of ocean professionals, and with interested partners within the region. Anonymized responses to the multiple-choice questions are provided in Appendix C with personalized responses removed to protect anonymity. All data has been archived in the password-protected NOAA Google Drive platform.

Results and discussion

The findings presented here are based on the OA Needs Based Assessment survey, associated engagement, and the specific case study on establishing the GOA-ON OA Caribbean Hub. Given the limited sample size in relation to all ocean professionals within the wider Caribbean, this survey offers the viewpoint of those that participated; Most of the respondents have a working knowledge of OA, are involved in ocean research, and are connected in some way to a broader community, given the methods used to distribute the survey (see Methods). The survey results were self-reported and, therefore, may contain biases. The results presented suggest trends across survey participants, yet additional follow-up studies are needed to further investigate the cause of these trends and confirm if the smaller sample size in this study is representative for broader groups throughout the Caribbean. Regardless, these survey results and this study offer insights into the current state of ocean research and a case study on establishing a network dedicated to OA within the wider Caribbean that has not been published previously. It also lays the groundwork for follow-up investigations on OA research, policy, and capacity needs within the wider Caribbean while offering a model for other regions to follow.

Survey respondent demographics

A total of 76 ocean professionals responded to the survey. Of these, 59 were from the wider Caribbean (excluding the mainland U.S.) and were included in the analysis (Appendix C). The remaining 17 respondents - 10 from the mainland U.S. and 7 from other regions outside the Caribbean - were excluded. Representatives from the mainland U.S. were excluded in the survey responses and engagement activities per request from the Caribbean community members who participated in the survey engagement, and therefore, references to the wider Caribbean within this study will exclude the mainland U.S. The purpose of this request was to tailor the survey, capacity building efforts, policy recommendations, and follow-up actions to the priorities of the countries and territories within the wider Caribbean region (including U.S. territories), which differ socio-economically from the mainland U.S (Allahar, 1993; Fanning et al., 2021). The respondents from the wider Caribbean (n=59) were from 25 different countries and territories (Figure 1, Appendix C). Almost half of the participants (47.5%) were from academic and research institutions (n=28), 23% of them work in governmental roles (n=14), 22% work at non-governmental organizations (n=13), and one works for a private company (Supplementary Figure S1).

Of the 59 respondents, 79% currently conduct ocean monitoring. 40% of the respondents monitor biological parameters, with 23% conducting chemical monitoring, 26% conducting physical monitoring, and 13% conducting socioeconomic monitoring. A majority of the respondents have a working knowledge of OA (63%), while nearly a third (31%) lack the resources and instruments necessary to study and monitor OA, and another third (32%) are able to conduct their research but noted that they have limited resources. Another large portion (20%) of the respondents have some knowledge of OA but would like to learn more and potentially build a research and monitoring program (Figure 2; Appendix C).

The current state of OA research in the Caribbean

Ocean professionals in the Caribbean rely on nearshore marine environments due to their accessibility, and therefore, their strengths, interests, and expertise focus mainly on nearshore environments. Across the region, respondents are most concerned about coral reef health (58%) and water quality (51%) within their local marine environments. Over half of the respondents conduct research in nearshore environments (59%) compared to a much

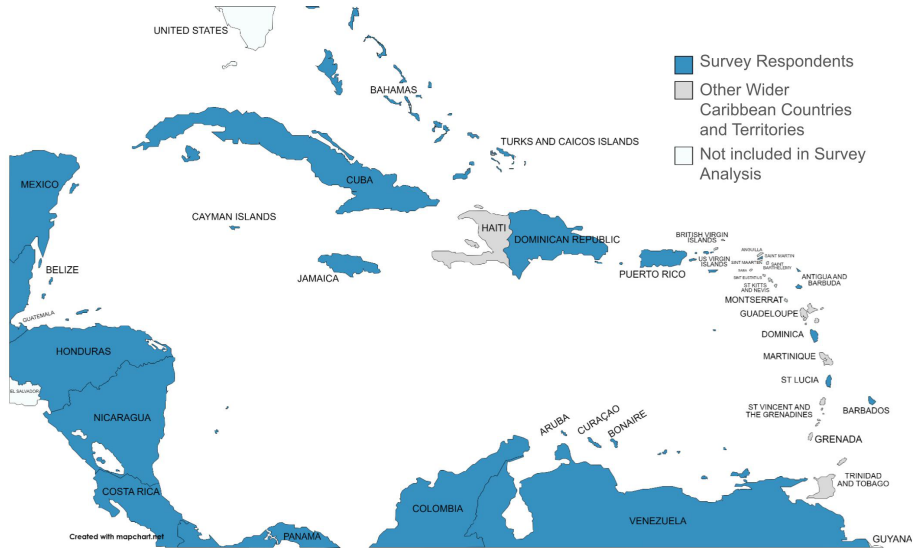

FIGURE 1
Map indicating countries and territories in the wider Caribbean where survey respondents reside (blue), the countries and territories that do not have survey respondents (grey), and those that are not included within the survey analysis (white, mainland U.S., excluded to focus survey on needs specific to wider Caribbean excluding mainland U.S.).

smaller fraction that work in the open ocean and offshore environments (22%). The most frequently studied ecosystems are coral reefs (64%), yet respondents also monitor other nearshore environments such as mangroves (49%), estuaries and bays (40%), and seagrasses (35%) (Figure 3). Other concerns for ocean health expressed by respondents, include harmful algal blooms (31%), sargassum inundation (27%), ocean acidification (21%), overfishing (22%), and climate change impacts such as hurricanes and sea level rise (29%) (Appendix C).

Respondents collect a wide range of ocean measurements, the most common include temperature (74%), salinity (68%), pH (66%), and dissolved oxygen (54%) (Figure 4). These parameters can be collected with methods that are easy to use, affordable, and require minimal training (Wang et al., 2019; Busch et al., 2016; Bittig et al., 2018), such as thermometers, refractometers, electrodes, optodes, and spectrophotometers. Chlorophyll measurements and water depth are conducted by 42% of respondents, and 36% of participants measure nutrients even though relatively affordable methods are available that require little expertise (Wernand, 2010; Beaton et al., 2012; Leeuw et al., 2013; Busch et al., 2016; Clinton-Bailey et al., 2017).

In order to constrain the carbonate system and OA, two of the four carbonate measurements are needed (i.e. dissolved inorganic carbon (DIC), total alkalinity (TA), pH, or partial pressure of carbon dioxide (pCO_2)), therefore requiring researchers to measure another carbonate parameter in addition to pH. Of the other carbonate parameters besides pH, 32% of respondents are measuring TA, 14% are measuring pCO_2, and 15% are measuring DIC (Figure 4). A total of 34% of respondents are measuring two or more of these four carbonate parameters (i.e., pH, DIC, TA, and/or pCO_2), and this percentage could be related to the pending distribution of low-cost sensors and/or complex laboratory methods that require specific training and lab infrastructure for DIC, TA, and pCO_2 measurements (Pardis et al., 2022; Li et al., 2023; Currie et al., 2024). Underlying this need for training and infrastructure to enhance the ability to make carbonate chemistry measurements are the required funds for the initial investment in establishing labs that can conduct these measurements and the continued financial support to maintain the equipment, workforce, and on-going research and monitoring.

While respondents often highlighted awareness of local oceanic conditions as a strength, they also recognized the need for additional formal technical scientific training and support in advanced chemical and physical monitoring techniques. Many respondents expressed a strong commitment to ocean research, motivated by both local knowledge and the desire to contribute to broader scientific understanding. One participant highlighted several strengths of their research program: “long standing relationships with local communities, close network of local scientists, and access to talented students”. Underlying most of the barriers that respondents identified to building and enhancing OA research and monitoring efforts were limitations in training to achieve greater technical capacity and access to sufficient funding, which is needed to sustain research, purchase equipment, and increase overall resources.

The role of training and funding

Training and continuous funding acquisition are paramount to advancing global observations by increasing scientific expertise, instrumentation, data management, and infrastructure to conduct ocean measurements (Venkatesan et al., 2019). For countries with limited resources to conduct oceanographic research, long-term

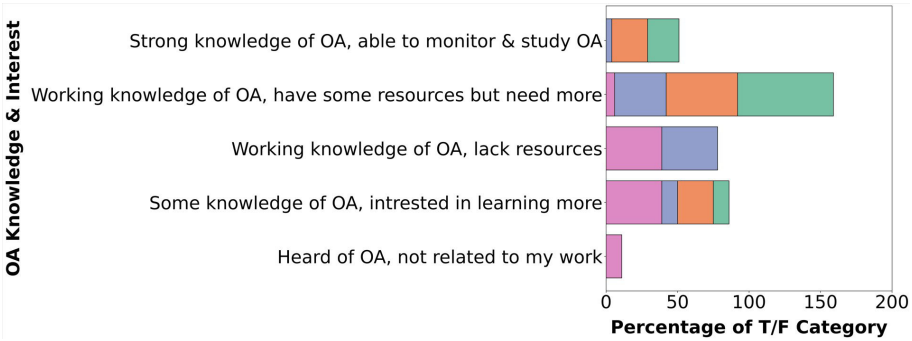

FIGURE 2
Ocean acidification knowledge and interest of survey respondents (y-axis) for each of the training and funding (T/F) categories (training only in blue, n=28; funding only in orange, n=4; training and funding in green, n=9; neither training nor funding in pink, n=18), displayed by percentage of each respective category normalized to the sample size for each training and funding category (x-axis).

monitoring of OA can be particularly challenging, especially for nations with coral reef ecosystems, such as those within the wider Caribbean, where carbonate chemistry budgets add complexity. Due to the lack of resources and sustained funding, baseline assessments for acidification conditions across the Caribbean are deficient (Meléndez and Salisbury, 2017) with only one sustained time series that continues to measure CO_2 within the Caribbean (La Parguera, Meléndez et al., 2020). The one other previous time series (CARIACO) within the region measured the highest rates of decreasing pH compared to any other ocean time series around the world (-0.0025 pH yr^{-1}) (Bates et al., 2014) and was one of only three total time series (CARIACO, Bermuda Atlantic Time-series Study, BATS, and Hawaii Ocean Time-series, HOT) that have been funded by the U.S. National Science Foundation for over two decades to measure ecology and biogeochemistry in ocean waters (Muller-Kargo et al., 2019). Unfortunately, in 2017 the CARIACO time series was discontinued due to budget constraints even though BATS and HOT continue to be funded to date, thus limiting data collection within the Caribbean (Kusek, 2019).

In this study, over half of the survey respondents (62%) indicated that they have received some amount of training on OA across a wide range of techniques. Of the 62% that have received training, the majority have learned techniques such as conducting pH analysis in the lab (86%), collecting bottle samples for lab analysis (81%), and/or conducting alkalinity analysis in the lab (70%). Techniques that respondents have received less training on include deployment of autonomous sensors (38%); data offloading, quality control, and analysis (30%); and pCO_2 analysis in the lab (27%). Fewer trainees have received training on OA biological effects and modeling aspects, such as designing biological experiments (19%), running analysis and analyzing results (14%), monitoring the effects of OA on species *in situ* (11%), and using

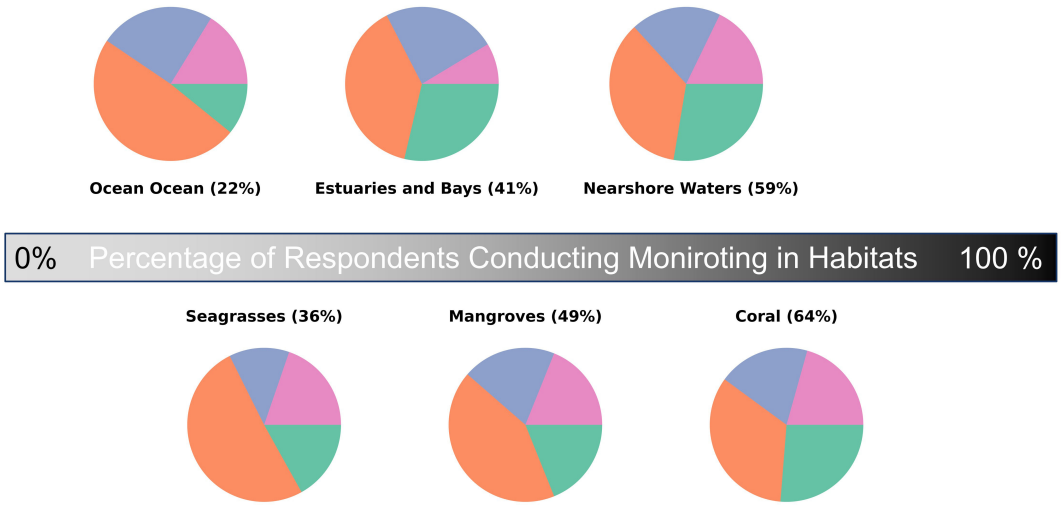

FIGURE 3
Percentage of respondents that are currently conducting monitoring in different habitats (indicated by percentage next to parameter), listed along the continuum from lowest (left, 0%) to highest (right, 100%). Pie charts show the percentage of each training and funding (T/F) categories (training only in blue, n=28; funding only in orange, n=4; training and funding in green, n=9; neither training nor funding in pink, n=18) normalized to the sample size for each respective category.

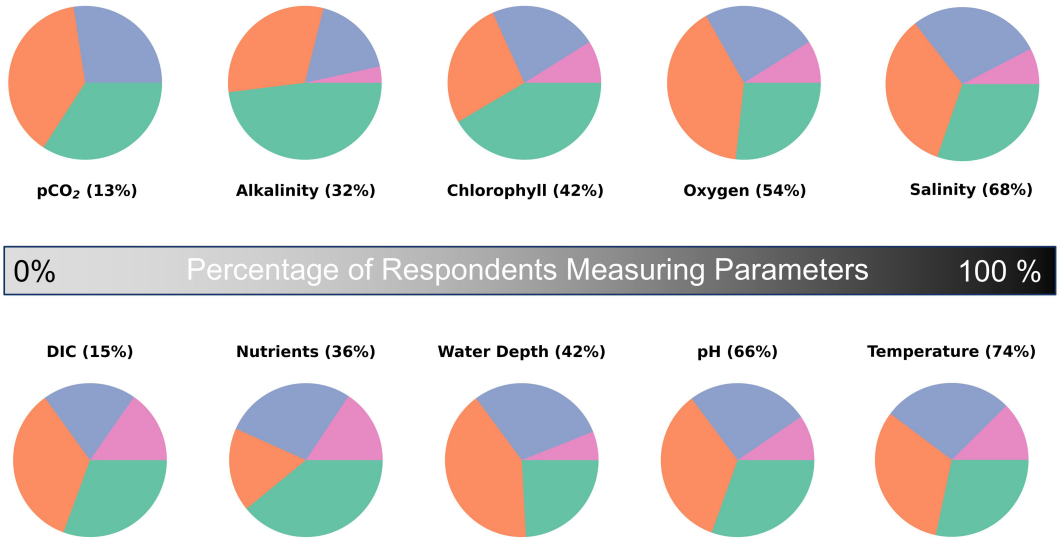

FIGURE 4
Percentage of respondents that are measuring specific parameters in coastal or offshore waters (indicated by percentage next to parameter), listed along the continuum from lowest (left, 0%) to highest (right, 100%). Pie charts show the percentage of each training and funding (T/F) categories (training only in blue, n=28; funding only in orange, n=4; training and funding in green, n=9; neither training nor funding in pink, n=18) normalized to the sample size for each respective category.

computer models to understand OA (11%) (Appendix C). While exposure to some OA training has been accessible by majority of the survey respondents, this study did not explore the type of training, quality, or quantity of training received nor what type of training would be most beneficial to respondents in the future.

When categorizing the respondents into four groups based on the training and funding received, we find that around one in six have received both training and funding (15%), nearly half received training only (47%), a small portion received funding only (7%), and nearly a third have received neither (31%) (Supplementary Figure S2). There is a significant difference between these four groups in relation to the amount of access to different types of equipment (ANOVA, p-value < 0.001), types of measurements conducted (ANOVA, p-value < 0.001), number of habitats researched (ANOVA, p-value = 0.041), and OA experience level (ANOVA, p-value = 0.025) (Table 1).

There is a major funding gap for Caribbean SIDS to meet their ocean-based Nationally Determined Contributions (NDCs) and ocean acidification scientific research projects lack funding and policy support, requiring additional allocation of domestic resources and leveraging of international climate finance and private sector funds (VanderZwaag et al., 2021; Mohan, 2023). In this survey, responses suggest that funding may play a significant role in the different types of equipment and ecosystems that ocean professionals can access for ocean monitoring. For example, access to different types of equipment is significantly higher (tukey-t test, p-value < 0.001) when both funding and training are provided compared to providing neither (Table 1; Supplementary Figure S3). Funding may be more of a driver than training to increase access to different types of equipment (Tukey-t test p-value, T&F v T < 0.001, F v N = 0.041) (Table 1; Supplementary Table S1), however the group that has received funding only is small (n=4) and therefore follow-up studies are required to confirm these trends. Funding alone is correlated with higher diversity of habitats in which ocean professionals conduct ocean monitoring (tukey-t test p-value, T v F = 0.043, F v N = 0.035) (Table 1, Supplementary Table S1, Figure 3). Compared to receiving neither option, providing either training and/or funding to ocean professionals significantly increases the different types of measurements that they can conduct to monitor the ocean (tukey-t test p-value, T v N = 0.001, F v N = 0.012, T&F v N = 0.001) (Supplementary Table S1). While OA experience is significantly different between the four training and funding groups (ANOVA p-value = 0.025), a specific combination of training and funding is not driving this variation (Supplementary Table S1). There is a higher average level of OA experience within the training and funding (4 +/- 0.8 out of 5) and funding only (4.3 +/- 0.4 out of 5) groups compared to those that only received training (3.5 +/- 0.7 out of 5) or neither training nor funding (3.1 +/- 1.1 out of 5) (Table 1). This suggests that funding may be slightly more impactful to increase OA experience than training, although additional research is necessary to investigate the types of training and funding that would be most beneficial to the community and confirm this trend since the groups that received funding were the smallest in sample size (4 respondents received funding only and 9 received training and funding). This small sample size also suggests that there is only a small proportion of ocean practitioners within the Caribbean that has received funding compared to training for OA research and monitoring, further supporting the conclusion that additional funding support is needed in the region. One participant noted that "most problems are related to financial

TABLE 1 Table indicating the average amount of access to different types of ocean observing capabilities based on the max value for each of the capabilities.

Amount of Access to Different Types of Ocean Observing Capabilities	Max value	Entity	Training and Funding (T&F) (n=9)	Training (T) (n=28)	Funding (F) (n=4)	Neither (N) (n=18)	ANOVA p-value	Tukey t-test (p-value < 0.05)
Training techniques	11	Avg	4.89	4.04	1.75	0.00	*6.485E-5	T&F v. N (0.000) T v. N (0.000)
		Std Dev	1.59	2.15	2.05	0.00		
Access to Equipment	17	Avg	11.56	5.75	9.75	4.39	*3.025E-5	T&F v. T (0.000) T&F v. N (0.000) F v. N (0.041)
		Std Dev	1.71	3.87	3.56	3.32		
Types of Measurements Conducted	10	Avg	6.22	4.89	6.50	1.67	*0.000	T&F v. N (0.001) T v. N (0.001) F v. N (0.012)
		Std Dev	2.94	2.81	0.50	2.49		
Habitats researched	6	Avg	3.11	2.50	5.00	2.33	*0.041	T v. F (0.043) F v. N (0.035)
		Std Dev	1.97	1.57	0.71	1.80		
OA Experience Level	5	Avg	4.00	3.54	4.25	3.11	*0.025	
		Std Dev	0.82	0.68	0.43	1.05		

Averages and standard deviations are displayed for the four training and funding categories along with the ANOVA p-value for the difference between the four training and funding categories. The Tukey t-test indicates which group-to-group comparisons between the different training and funding categories (T&F, Training and Funding; T, training only; F, funding only; N, neither training nor funding) are significantly different (p-value < 0.05) with the p-value stated in parenthesis. For example, when considering the number of training techniques each group on average has access to, the T&F group varies significantly from the N group with a p-value of 0.000 and is therefore listed in the table as "T&F v. N (0.000)".

capacity including the ability to hire qualified staff, maintain equipment, instruments and facilities and opportunities for training in data collection and data management." Unfortunately, even though this study found that training and funding are critical for capacity building, only 22% of the survey respondents have received funding for OA research. While 62% have received training, around 76% of those who have received training did not receive funding, which would make it difficult to conduct and sustain the techniques that were learned during training and highlight the limited nature of funding within the Caribbean for OA research.

This study showcases the need for both training and funding to be provided to make a significant impact on research capacity, which has also been shown in previous studies (e.g. Venkatesan et al., 2019; VanderZwaag et al., 2021; Mohan, 2023). While both increased training and funding are necessary, training can be passed on through various formal and informal avenues while funding requires continuous investment to sustain the workforce, maintain equipment, and support on-going research and monitoring. Training and funding are especially important for complex techniques that require specific lab infrastructure, such as TA, DIC, and pCO2, which are needed in addition to pH to constrain the carbonate system (Pardis et al., 2022; Li et al., 2023; Currie et al., 2024). Therefore, this study suggests that financial support for OA research may be a factor in increasing the amount and diversity of equipment available, measurements conducted, habitats research, and level of OA expertise. Future studies should be conducted to confirm these trends across a broader group of ocean professionals throughout the Caribbean and investigate which training and funding resources would be most impactful for the region.

Application of OA measurements to SDG requirements

Clearly, gaps remain in regional OA research and monitoring, making it difficult for Caribbean nations to not only meet their ocean-based NDCs (Mohan, 2023), but also contribute to the indicator methodology required under international data reporting obligations for UN SDG Target 14.3 (*Minimize and address the impacts of ocean acidification, including through enhanced scientific cooperation at all levels*). Of the survey respondents, 64% are aware that OA monitoring is required to meet the SDG Indicator 14.3.1 (*Average marine acidity (pH) measured at agreed suite of representative sampling stations*). However, only 37% of participants could name the entity responsible for submitting the required OA monitoring data for their nation. This result highlights a gap between the OA data collection and submission process, which could be due to many different factors which we did not investigate in this study. This gap does, however, suggest that communication and engagement could be strengthened either within and/or across nations to better familiarize ocean professionals and researchers collecting OA data with the governmental entities submitting the data on the SDG Indicator 14.3.1 Data Portal. While SDG 14.3 is considered a target, it does not account for a scientifically verifiable baseline, nor contain binding elements, which could make it more effective (Houghton, 2014; Loewe and Rippin, 2015; Recuero Virto, 2018). The SDG Indicator 14.3.1 is one of the quantifiable aspects of SDG Target 14.3 that can produce scientific data to inform practitioners of OA trends across temporal and spatial scales. Regions with more OA monitoring and research capabilities, such as many regions within the Global North, maintain a record of incorporating OA mitigation and adaptation

strategies into their local and regional policies (Grabb et al., 2024). However, there is a comparable lack of OA research capacity and regulation frameworks addressing OA within SIDS and the Global South (Grabb et al., 2024). Given that the wider Caribbean region includes a few dozen SIDS that rely heavily on the marine environment (Meléndez and Salisbury, 2017), the wider Caribbean is an example of a region that could benefit from increasing research capacity to address SDG Indicator 14.3.1 by expansion of OA data collection and research dissemination. Although further research is required to investigate the factors underlying this gap, this study suggests that additional access to OA training and funding may help ocean professionals increase OA research capacity to contribute to SDG Indicator 14.3.1 and conduct more OA measurements using a larger variety of instrumentation across a wider range of habitats including offshore and deep-sea ecosystems (Bell et al., 2023). Training and funding opportunities may help increase the ability to meet policy commitments such as NDCs and the SDG Indicator 14.3.1, yet additional efforts are also required to strengthen conduits to apply OA science to inform mitigation, adaptation, and policy decisions, which were not investigated within this study.

Interest in GOA-ON hub

This study identified the opportunity to create a coordinated regional effort in the wider Caribbean to support OA capacity building and facilitate the sharing of OA research findings and methodologies. Indicated by previous studies on OA, a key recommendation to address OA is to create a strong regional monitoring network to inform policy actions (Chan et al., 2016; Whitefield et al., 2021). Therefore, as a case study to explore possible mechanisms to build capacity through a regional network for OA research and monitoring within the Caribbean, this study explored the option to establish a regional GOA-ON OA Caribbean Hub. 39% of the survey respondents were already GOA-ON members, however, when all survey respondents were asked if they thought a regional GOA-ON OA Caribbean Hub would be beneficial, 78% responded "Yes", 17% responded "Maybe", and only 2% responded "No". The majority of respondents felt that strong benefits of a regional GOA-ON OA Caribbean Hub included increased access to equipment (88%), capacity building (85%), regional organization and communication (83%), development of policy and decision-making resources (81%), help with SDG Indicator 14.3.1 reporting (75%), data sharing (66%), and collaborations and joint activities (54%). Survey respondents also had the opportunity to indicate if they were interested in future leadership opportunities in capacity building efforts.

GOA-ON regional hubs are built from the ground up with local community leaders to ensure alignment with regional goals and they are also provided with staff support from the GOA-ON Secretariat to facilitate meetings and connect GOA-ON members and Hubs to opportunities within the international network (Newton et al., 2015). Previously established GOA-ON regional hubs have demonstrated that benefits similar to those expressed by the survey respondents are achievable (Newton et al., 2015). For example, through opportunities within the GOA-ON network, many regional hubs have benefited from OA trainings and workshops, Pier2Peer mentorship and scholarships, increased access to technical equipment (i.e., GOA-ON in a Box Kits), increased opportunities for research funding, and international collaborations. While the needs within each GOA-ON regional hub are unique, the successes to establish and sustain OA monitoring and research within other regional hubs serve as examples for the potential resources that can be developed through the GOA-ON network.

GOA-ON OA Caribbean hub formation

To inform the Caribbean OA research community of the needs assessment results, the survey results were shared via email to respondents, presented during virtual meetings with Caribbean community members, and presented at a conference in the Caribbean where local OA practitioners were engaged in further conversations and discussions. Following these engagements, those interested in leadership positions for future capacity building networks were encouraged to attend an initial virtual meeting in May 2023, which was facilitated by the co-leads of this study, who were Sea Grant Knauss Fellows at NOAA OAP. After several virtual informational meetings where the survey results were presented, the Caribbean OA community leaders (who are co-authors of this study) decided to establish and lead monthly meetings to design the goals, scope, and direction of a collaborative network. Upon learning about the opportunities that GOA-ON regional hubs have provided other regions, the Caribbean OA community leaders decided to pursue the formation of a GOA-ON OA Caribbean Hub in November 2023 by creating and agreeing upon terms of reference and naming the steering committee members (https://www.goa-on.org/regional_hubs/caribbean/about/introduction.php). The GOA-ON OA Caribbean Hub was formed with two co-chairs hailing from Jamaica and the U.S. Virgin Islands, and five additional steering committee members located in Belize, Commonwealth of Dominica, Cuba, Puerto Rico, and the U.S. Virgin Islands. The GOA-ON OA Caribbean Hub welcomes members from the wider Caribbean region, including U.S. Territories, and as of February 2025 had 28 members from 14 different countries and territories.

The steering committee designed the GOA-ON OA Caribbean Hub goals to address the needs of the wider Caribbean region that were expressed in the needs assessment. The goals of the hub are to: (1) Grow involvement within the Caribbean OA community and promote activities within the hub; (2) Encourage coordination of efforts and collaboration with organizations and projects involved in ocean acidification observations, impacts, and data delivery; (3) Promote the awareness of the OA Caribbean Hub to the public, policymakers, and scientific community; and (4) Engage national and international funding agencies to support the activities of the OA Caribbean Hub.

Since its establishment, the GOA-ON OA Caribbean Hub has interacted with other GOA-ON regional hubs to learn about successful regional initiatives for building and sustaining OA research and monitoring capacity. Like other hubs, the OA

Caribbean Hub has GOA-ON secretariat support to assist with connections throughout the international network as well as two seats on the GOA-ON Executive Council to help increase international networking and knowledge sharing with other GOA-ON regional hubs and international partners (Newton et al., 2015). The GOA-ON OA Caribbean Hub also has a dedicated early career steering committee member who sits on the International Carbon Ocean Network for Early Career (ICONEC) steering committee. International partners and networks have expressed interest in engaging with the OA Caribbean GOA-ON Hub including IOCARIBE, CARICOOS, UN Environmental Program (UNEP) SPAW, Caribbean Fishery Management Council, International Atomic Energy Agency (IAEA), and IOC-UNESCO.

Within a year of establishment, the GOA-ON OA Caribbean Hub maintained monthly steering committee meetings and made progress towards increased collaboration and expansion of its network with sessions at both 2023 and 2024 GOA-ON OA Week, a presence at international conferences such as the CariCOOS 2023 General Assembly, and facilitation of an OA workshop for regional collaboration on OA research. The Hub has worked to disseminate OA research updates and funding announcements via a monthly newsletter and created a policy brief in 2024 to communicate OA issues in the Caribbean to better inform local officials.

At the same time the GOA-ON OA Caribbean Hub was forming, there was also a strong push to establish the Caribbean-based Coastal Acidification Network (CariCAN) for the U.S. territories within the Caribbean: Puerto Rico and the U.S. Virgin Islands. While the Hub itself did not directly lead to the creation of the CariCAN, the growing momentum for OA research driven by researchers and NOAA's programs like CariCOOS and OAP helped facilitate its formation in 2024. Throughout the U.S., there are seven CANs that are regionally located and they are designed to bring together collaborative partnerships across scientists, academics, Tribal community leaders, industry professionals, and policymakers to build capacity for regionally-specific OA science and disseminate research for U.S. states and territories (McLaughlin et al., 2015; Cross et al., 2019; Gassett et al., 2021). Coupling the GOA-ON OA Caribbean Hub with the CariCAN will complement the international GOA-ON network with U.S. capacity building and funding opportunities to expand the reach beyond scientific sectors.

Continued policy and community directions for sustained future capacity

This study suggests that there is a need to strengthen the resulting actions from high level policies to increase tangible support for funding, training opportunities, and access to regional networks that can help sustain OA research and assist with the translation of this research into mitigation and adaptation policies. Example models of the successful, sustained future capacity required in the Caribbean can be seen in The Pacific Islands Ocean Acidification Center (PIOAC), as well as in collaborative actions in the Gulf of Guinea. Both examples were made possible by significant collaborative funding investments, and they are already yielding high returns in improving OA research and policy capacity. Policymakers play a crucial role in increasing the regional awareness around OA and can advocate for increased support for OA research and monitoring within the existing regional networks (i.e., IOCARIBE, SPAW, etc.) and international communities and organizations (i.e., GOA-ON, IOC-UNESCO, NOAA, IAEA, etc.). Continued support for the recently established GOA-ON OA Caribbean Hub, CariCAN, and associated efforts for training and capacity building can ensure reliable science is being produced across the region that can inform mitigation and adaptation policies.

The GOA-ON OA Caribbean Hub's policy brief produced in 2024 conveys OA data and possible OA mitigation solutions to regional policymakers to bolster efforts to include OA priorities in national and regional climate change policy. For example, the brief suggests policies should support increased collaboration, innovation, protection, and mitigation of OA. The ability to manage marine ecosystems and minimize the negative effects of OA and other stressors relies on targeted science that is conducted in collaboration with and supported by policy initiatives. Policies need to prioritize, fund, and direct sustained resources towards efforts to establish and reinforce robust monitoring programs at local and region-wide scales and support research efforts on OA impacts. Developing methods to convey OA data and solutions to policymakers at the regional and international levels requires collaboration amongst scientists and decision makers and open communication lines, which can further strengthen the scientific goals and ensure that scientific priorities also align with policy needs. Additional science-policy coordination and engagement with the communities can also help distribute resources for OA education.

Conclusion

The results of the wider Caribbean OA Needs Based Assessment Survey reflect the challenges to develop sustained regional OA monitoring projects that are designed *by the community for the community* to enhance research capacity in a data poor region. This study indicates that training to achieve greater technical capacity supported by sustained funding is essential to build research capacity at the community level. Since OA has unique local impacts that need continuous monitoring to understand natural variation, addressing OA requires sustained financial investment and commitment across communities and sectors, including policy and decision makers, to combat OA at a global scale (Weller et al., 2019). Dedicated support and funding for staff time is essential since many actors are involved in a variety of initiatives and commitments. Leaders within the Caribbean (including co-authors of this study) have stepped up to pioneer the field of OA within their communities in addition to many other responsibilities and need continued financial support and resources to carry on these efforts. External research collaborations, training, and funding initiatives should prioritize community needs by investing in grassroots leadership, co-designing and co-developing collaborative projects from the onset, and ensuring that the resources remain within the local community to sustain the initiatives. Only by creating policies that empower local community members and

commit resources that align with their priorities can we begin to address the impacts of OA and meet climate goals.

Data availability statement

The original contributions presented in the study are included in the article/Supplementary Material. Further inquiries can be directed to the corresponding authors.

Ethics statement

Ethical approval was not required for the study involving humans in accordance with the local legislation and institutional requirements. Written informed consent to participate in this study was not required from the participants or the participants' legal guardians/next of kin in accordance with the national legislation and the institutional requirements.

Author contributions

KG: Conceptualization, Data curation, Formal Analysis, Investigation, Methodology, Project administration, Visualization, Writing – original draft, Writing – review & editing. NL: Conceptualization, Data curation, Formal Analysis, Investigation, Methodology, Project administration, Visualization, Writing – original draft, Writing – review & editing. KD: Conceptualization, Investigation, Methodology, Project administration, Writing – review & editing. D-AG-S: Investigation, Methodology, Writing – review & editing. EE-B: Investigation, Methodology, Writing – review & editing. MF: Investigation, Methodology, Writing – review & editing. SL: Investigation, Methodology, Writing – review & editing. GK: Conceptualization, Investigation, Methodology, Project administration, Resources, Writing – review & editing. MM: Conceptualization, Investigation, Methodology, Writing – review & editing. JM: Investigation, Methodology, Writing – review & editing. AM: Investigation, Methodology, Writing – review & editing. JN: Conceptualization, Investigation, Methodology, Project administration, Supervision, Writing – review & editing. AP: Investigation, Methodology, Writing – review & editing. AV-O: Conceptualization, Investigation, Methodology, Writing – review & editing. JV: Investigation, Methodology, Writing – review & editing. CV: Investigation, Methodology, Writing – review & editing. EW-F: Conceptualization, Investigation, Methodology, Project administration, Resources, Writing – review & editing.

Funding

The author(s) declare that financial support was received for the research and/or publication of this article. Funding for Grabb and Lord was provided by the 2023 Knauss Marine Policy Fellowship in the NOAA OAP and supported by the Woods Hole Sea Grant and New Hampshire Sea Grant, respectively. Escobar-Briones was supported by grant PE-207024 with funding from DGAPA PAPIME UNAM. Valauri-Orton and Meléndez were supported by NOAA Ocean Acidification Program Regional Vulnerability Assessment grant. Valauri-Orton was further supported by the Government of Sweden.

Acknowledgments

We would like to thank all the Caribbean OA Community of Practice members who contributed to the early efforts of the Caribbean capacity building. Specifically, we would like to acknowledge everyone who was a part of the Caribbean OA Community of Practice Strategic Plan: Alicia Cheripka (NOAA OAR International Activities Office); Kerri Dobson (formerly a Sea Grant Knauss Fellow at NOAA Ocean Acidification Program); Kaitlyn Lowder (The Ocean Foundation); Bobbi-Jo Dobush (The Ocean Foundation, consultant); Gabriel Smith (Regional Environmental Hub for Central America and the Caribbean, Department of State); Tadzio Bervoets (Dutch Caribbean Nature Alliance); Melissa Meléndez (University of Hawai'i at Manoa), Ileana C Lopez (UNEP Cartagena Convention); Gabby Kitch (NOAA Ocean Acidification Program); Marcia Creary Ford (Centre for Marine Sciences, The University of the West Indies). This research was supported by NOAA Ocean Acidification Program (OAP).

Conflict of interest

The authors declare that the research was conducted in the absence of any commercial or financial relationships that could be construed as a potential conflict of interest.

Generative AI statement

The author(s) declare that no Generative AI was used in the creation of this manuscript.

Publisher's note

Author disclaimer

The scientific results and conclusions, as well as any views or opinions expressed herein, are those of the author(s) and do not necessarily reflect the views of NOAA or the Department of Commerce.

Supplementary material

The Supplementary Material for this article can be found online at: https://www.frontiersin.org/articles/10.3389/fmars.2025.1595911/full#supplementary-material

References

Allahar, A. L. (1993). Unity and diversity in caribbean ethnicity and culture. *Can. Ethnic Stud. (XXV)* 1, 70–84.

Bates, N., Astor, Y., Church, M., Currie, K., Dore, J., Gonaález-Dávila, M., et al. (2014). A time-series view of changing ocean chemistry due to ocean uptake of anthropogenic CO2 and ocean acidification. *Oceanography* 27, 126–141. doi: 10.5670/oceanog.2014.16

Bates, N. R. (2012). Multi-decadal uptake of carbon dioxide into subtropical mode water of the North Atlantic Ocean. *Biogeosciences* 9, 2649–2659. doi: 10.5194/bg-9-2649-2012

Beaton, A. D., Cardwell, C. L., Thomas, R. S., Sieben, V. J., Legiret, F.-E., Waugh, E. M., et al. (2012). Lab-on-chip measurement of nitrate and nitrite for *in situ* analysis of natural waters. *Environ. Sci. Technol.* 46, 9548–9556. doi: 10.1021/es300419u

Bell, K. L. C., Quinzin, M. C., Amon, D., Poulton, S., Hope, A., Sarti, O., et al. (2023). Exposing inequities in deep-sea exploration and research: results of the 2022 Global Deep-Sea Capacity Assessment. *Front. Marine Sci.* 10. doi: 10.3389/fmars.2023.1217227

Bittig, H. C., Steinhoff, T., Claustre, H., Fiedler, B., Williams, N. L., Sauzède, R., et al. (2018). An alternative to static climatologies: Robust estimation of open ocean CO_2 variables and nutrient concentrations from T, S, and O_2 data using Bayesian neural networks. *Front. Mar. Sci* 5. doi: 10.3389/fmars.2018.00328

Busch, J., Bardaji, R., Ceccaroni, L., Friedrichs, A., Piera, J., Simon, C., et al. (2016). Citizen bio-optical observations from coast- and ocean and their compatibility with ocean colour satellite measurements. *Remote Sens.* 8, 879. doi: 10.3390/rs8110879

Caldeira, K., and Wickett, M. E. (2003). Anthropogenic carbon and ocean pH. *Nature* 425, 365. doi: 10.1038/425365a

Carr, D., Boyle, E. H., Cornwell, B., Correll, S., Crosnoe, R., Freese, J., et al. (2021). "Art and Science of Social Research: with Ebook," in *Quizitive, Writing for Sociology Tutorials, and Author Videos* (WW Norton & Company).

Chan, F., Boehm, A. B., Barth, J. A., Chornesky, E. A., Dickson, A. G., Feely, R. A., et al. (2016). *The West Coast Ocean Acidification and Hypoxia Science Panel: Major Findings, Recommendations, and Actions* (Oakland, California, USA: California Ocean Science Trust).

Clinton-Bailey, G. S., Grand, M. M., Beaton, A. D., Nightingale, A. M., Owsianka, D. R., Slavik, G. J., et al. (2017). A lab-on-chip analyzer for in situ measurement of soluble reactive phosphate: improved phosphate blue assay and application to fluvial monitoring. *Environ. Sci. Technol.* 51, 9989–9995. doi: 10.1021/acs.est.7b01581

Cooley, S., Schoeman, D., Bopp, L., Boyd, P., Donner, S., Ghebrehiwet, D. Y., et al. (2022). "Oceans and Coastal Ecosystems and Their Services," in *Climate Change 2022: Impacts, Adaptation and Vulnerability. Contribution of Working Group II to the Sixth Assessment Report of the Intergovernmental Panel on Climate Change*. Eds. H.-O. Pörtner, D. C. Roberts, M. Tignor, E. S. Poloczanska, K. Mintenbeck, A. Alegría, M. Craig, S. Langsdorf, S. Löschke, V. Möller, A. Okem and B. Rama (Cambridge University Press, Cambridge, UK and New York, NY, USA), 379–550. doi: 10.1017/9781009325844.005

Creswell, J. W., and Creswell, J. D. (2017). *Research design: Qualitative, quantitative, and mixed methods approaches* (Sage publications).

Cross, J. N., Turner, J. A., Cooley, S. R., Newton, J. A., Azetsu-Scott, K., Chambers, R. C., et al. (2019). Building the knowledge-to-action pipeline in North America: Connecting ocean acidification research and actionable decision support. *Front. Marine Sci.* 6, 356. doi: 10.3389/fmars.2019.00356

Currie, C., Sabine,, Lowder, K., Hassoun, A. E. R., Meléndez, M., Chu, S., et al. (2024). *Practical Best Practices for Ocean Acidification Monitoring (1.1)* (The Ocean Foundation). doi: 10.5281/zenodo.13876198

Dobson, K. L., Newton, J. A., Widdicombe, S., Schoo, K. L., Acquafredda, M. P., Kitch, G., et al. (2023). Ocean acidification research for sustainability: co-designing global action on local scales. *ICES J. Marine Sci.* 80, 362–366. doi: 10.1093/icesjms/fsac158

Doney, S. C., Fabry, V. J., Feely, R. A., and Kleypas, J. A. (2009). Ocean acidification: the other CO2 problem. *Annu. Rev. Marine Sci.* 1, 169–192. doi: 10.1146/annurev.marine.010908.163834

Espinosa, L. F. (2023). *REMARCO – NETWORK FOR RESEARCH ON MARINE – COASTAL STRESSORS IN LATIN AMERICA AND THE CARIBBEAN* (UNEP(DEPI)/CAR).

Fabry, V. J., Seibel, B. A., Feely, R. A., and Orr, J. C. (2008). Impacts of ocean acidification on marine fauna and ecosystem processes. *ICES J. Marine Sci.* 65, 414–432. doi: 10.1093/icesjms/fsn048

Fanning, L., Mahon, R., Compton, S., Corbin, C., Debels, P., Haughton, M., et al. (2021). Challenges to implementing regional ocean governance in the wider caribbean region. *Front. Mar. Sci.* 8. doi: 10.3389/fmars.2021.667273

Ferreira (2012). "Caribbean Languages and Caribbean Linguistics," in *Caribbean Heritage* (University of West Indies Press).

Friedlingstein, P., Jones, M., O'Sullivan, M., Andrew, R., Bakker, D., Hauck, J., et al. (2022). Global carbon budget 2021. *Earth System Sci. Data* 14, 1917–2005. doi: 10.5194/essd-14-1917-2022

Galdies, C., Tiller, R., and Martinez Romera, B. (2021). "Global Ocean Governance and Ocean Acidification," in *Life Below Water*. Eds. W. Leal Filho, A. M. Azul, L. Brandli, A. Lange Salvia and T. Wall (Springer International Publishing, Cham), 1–12. doi: 10.1007/978-3-319-71064-8_109-1

Gassett, P. R., OBrien-Clayton, K., Bastidas, C., Rheuban, J. E., Hunt, C. W., Turner, E., et al. (2021). Community science for coastal acidification monitoring and research. *Coastal Manage.* 49, 510–531. doi: 10.1080/08920753.2021.1947131

Gill, D. A., Mascia, M., Ahmadia, G., Glew, L., Lester, S., Barnes, M., et al. (2017). Capacity shortfalls hinder the performance of marine protected areas globally. *Nature* 543, 665–669. doi: 10.1038/nature21708

Gledhill, D. K., Wanninkhof, R., Millero, F. J., and Eakin, M. (2008). Ocean acidification of the greater Caribbean region 1996–2006. *J. Geophysical Research: Oceans* 113, 1–11. doi: 10.1029/2007JC004629

Grabb, K. C., Ghosh, A., Adekunbi, F. O., Williamson, P., and Widdicombe, S. (2024). "Ocean acidification: Causes, impacts, and policy actions," in *Reference Module in Earth Systems and Environmental Sciences* (Elsevier), B9780443140822000119. doi: 10.1016/B978-0-443-14082-2.00011-9

Gruber, N., Bakker, D. C. E., DeVries, T., Gregor, L., Hauck, J., Landschützer, P., et al. (2023). Trends and variability in the ocean carbon sink. *Nat. Rev. Earth Environ.* 4, 119–134. doi: 10.1038/s43017-022-00381-x

Hendee, J. C., Halas, J., Fletcher, P. J., Jankulak, M., and Gramer, L. J. (2016). Expansion of the coral reef early warning system (CREWS) network throughout the caribbean. *Proc. 13th Int. Coral Reef Symposium Honolulu*, 517–522. Available online at: https://coralreefs.org/wp-content/uploads/2019/01/Session-73-1-Hendee-et-al-CREWS-Expansion-13ICRS-Session73A-Final-1NS-1.pdf.

Houghton, K. (2014). *A Sustainable Development Goal for the Ocean: Moving from Goal Framing Towards Targets and Indicators for Implementation* (IASS Potsdam).

Hughes, T. P., Kerry, J., Alvarez-Noriega, M., Alvarez-Romero, J., Anderson, K., Baird, A., et al. (2017). Global warming and recurrent mass bleaching of corals. *Nature* 543, 373–377. doi: 10.1038/nature21707

IOC-UNESCO (2024a). *Ocean Acidification Research for Sustainability - A Community Vision for the Ocean Decade* (IOC-UNESCO). doi: 10.25607/YPE3-0H04

IOC-UNESCO (2024b). *IOCARIBE Medium-Term Strategic Science Plan, 2023–2029* (Paris: IOC Information document).

IPCC (2023). *Climate Change 2022 – Impacts, Adaptation and Vulnerability: Working Group II Contribution to the Sixth Assessment Report of the Intergovernmental Panel on Climate Change. 1st edn* (Cambridge University Press). doi: 10.1017/9781009325844

Kusek, K. (2019). 21-Year CARIACO Ocean Time Series Ends: That's a Wrap! ¡Fin del Día!. *USF College of Marine Science*. Available online at: https://www.usf.edu/marine-science/news/2019/21-year-caricao-ocean-time-series-ends.aspx (Accessed May 27, 2025).

D. Laffoley, J. M. Baxter, F. A. Arias-Isaza, P. C. Sierra-Correa, N. Lagos, M. Graco, E. B. Jewett and K. Isensee (Eds.) (2018). *Regional Action Plan on Ocean Acidification for Latin America and the Caribbean – Encouraging Collaboration and Inspiring Action. Serie de Publicaciones Generales No. 99* (Santa Marta, Colombia: INVEMAR), 37pp.

Land, P. E., Findlay, H. S., Shutler, J. D., Ashton, I. G. C., Holding, T., Grouazel, A., et al. (2019). Optimum satellite remote sensing of the marine carbonate system using empirical algorithms in the global ocean, the Greater Caribbean, the Amazon Plume and the Bay of Bengal. *Remote Sens. Environ.* 235, 111469. doi: 10.1016/j.rse.2019.111469

Lang, F., Gwinn, J., Grabb, K., Valauri-Orton, A., and Spencer, G. (2024). *Guide to Developing Mentoring Programs for the International Ocean Community* (The Ocean Foundation). Available online at: https://oceanfdn.org/guide-to-ocean-mentoring.

Leeuw, T., Boss, E., and Wright, D. (2013). *In situ* measurements of phytoplankton fluorescence using low cost electronics. *Sensors* 13, 7872–7883. doi: 10.3390/s130607872

Li, H., Zheng, S., Tan, Q.-G., Zhan, L., Martz, T. R., and Ma, J. (2023). Toward citizen science-based ocean acidification observations using smartphone devices. *Analytical Chem.* 95, 15409–15417. doi: 10.1021/acs.analchem.3c03720

Loewe, M., and Rippin, N. (2015). The sustainable development goals of the post-2015 agenda: comments on the OWG and SDSN proposals. *SSRN Electronic J*, 1–92. doi: 10.2139/ssrn.2567302

Lune, H., and Berg, B. L. (2017). *Qualitative research methods for the social sciences* (Pearson Education Limited).

McLaughlin, K., Weisberg, S., Dickson, A., Hofmann, G., Newton, J., Aseltine-Neilson, D., et al. (2015). Core principles of the California Current Acidification Network: linking chemistry, physics, and ecological effects. *Oceanography* 25, 160–169. doi: 10.5670/oceanog.2015.39

Meléndez, M., and Salisbury, J. (2017). Impacts of ocean acidification in the coastal and marine environments of caribbean small island developing states (SIDS). *Caribbean Marine Climate Change Rep. Card: Sci. Rev.* 2017, 31–39.

Meléndez, M., Salisbury, J., Gledhill, D., Langdon, C., Morell, J. M., Manzello, D., et al. (2020). Seasonal variations of carbonate chemistry at two western atlantic coral reefs. *J. Geophysical Research: Oceans* 125, e2020JC016108. doi: 10.1029/2020JC016108

Miloslavich, P., Díaz, J. M., Klein, E., Alvarado, J. J., Díaz, C., Gobin, J., et al. (2010). Marine biodiversity in the caribbean: regional estimates and distribution patterns. *PloS One* 5, e11916. doi: 10.1371/journal.pone.0011916

Miloslavich, P., Seeyave, S., Muller-Karger, F., Bax, N., Ali, E., Delgado, C., et al. (2019). Challenges for global ocean observation: the need for increased human capacity. *J. Operational Oceanography* 12, S137–S156. doi: 10.1080/1755876X.2018.1526463

Miloslavich, P., Zitoun, R., Urban, E. R., Muller-Karger, F., Bax, N. J., Arbic, B. K., et al. (2022). "Developing Capacity for Ocean Science and Technology," in *Blue Economy*. Eds. E. R. Urban and V. Ittekkot (Springer Nature Singapore, Singapore), 467–504. doi: 10.1007/978-981-19-5065-0_15

Mohan, P. S. (2023). Implementing nationally determined contributions under the Paris Agreement: An assessment of ocean-based climate action in Caribbean Small Island Developing States. *Marine Policy* 155, 105787. doi: 10.1016/j.marpol.2023.105787

Moore, C., and Fuller, J. (2020). Economic impacts of ocean acidification: A meta-analysis. *Marine Resource Economics* 37, 201–219. doi: 10.1086/718986

Muller-Karger, F. E., Astor, Y. M., Benitez-Nelson, C. R., Buck, K. N., Fanning, K. A., Lorenzoni, L., et al. (2019). The scientific legacy of the CARIACO Ocean Time-Series Program. *Ann. Rev. Mar. Sci.* 11, 413–437. doi: 10.1146/annurev-marine-010318-095150

Narita, D., Rehdanz, K., and Tol, R. S. J. (2012). Economic costs of ocean acidification: a look into the impacts on shellfish production. *Climatic Change* 113, 1049–1063. doi: 10.1007/s10584-011-0383-3

Newton, J. A., Feely, R. A., Jewett, E. B., Williamson, P., and Mathis, J. (2015). *Global Ocean Acidification Observing Network: Requirements and Governance Plan* (IAEA, GOA-ON), 57.

Pardis, W., Grabb, K. C., DeGrandpre, M. D., Spaulding, R., Beck, J., Pfeifer, J. A., et al. (2022). Measuring protons with photons: A hand-held, spectrophotometric pH analyzer for ocean acidification research, community science and education. *Sensors* 22, 7924. doi: 10.3390/s22207924

Recuero Virto, L. (2018). A preliminary assessment of the indicators for Sustainable Development Goal (SDG) 14 "Conserve and sustainably use the oceans, seas and marine resources for sustainable development. *Marine Policy* 98, 47–57. doi: 10.1016/j.marpol.2018.08.036

Roberts, C. M., McClean, C. J., Veron, J. E. N., Hawkins, J. P., Allen, G. R., McAllister, D. E., et al. (2002). Marine biodiversity hotspots and conservation priorities for tropical reefs. *Science* 295, 1280–1284. doi: 10.1126/science.1067728

Siedlecki, S. A., Pilcher, D., Howard, E. M., Deutsch, C., MacCready, P., Norton, E. L., et al. (2021). Coastal processes modify projections of some climate-driven stressors in the California Current System. *Biogeosciences* 18, 2871–2890. doi: 10.5194/bg-18-2871-2021

Spalding, C., Finnegan, S., and Fischer, W. W. (2017). Energetic costs of calcification under ocean acidification. *Global Biogeochemical Cycles* 31, 866–877. doi: 10.1002/2016GB005597

United Nations (2024). Measure and report ocean acidification: Sustainable Development Goal 14.3.1 indicator. UN Sustainable Development Goals. Available online at: https://sdgs.un.org/partnerships/measure-and-report-ocean-acidification-sustainable-development-goal-1431-indicator (Accessed February 9, 2025).

Valauri-Orton, A., Lowder, K. B., Currie, K., Sabine, C. L., Dickson, A. G., Chu, S. N., et al. (2025). Perspectives from developers and users of the GOA-ON in a box kit: A model for capacity sharing in ocean sciences. *Oceanography* 38, 96–98. doi: 10.5670/oceanog.2025.135

VanderZwaag, D., Oral, N., and Stephens, T. (2021). *Research Handbook on Ocean Acidification Law and Policy* (Edward Elgar Publishing). doi: 10.4337/9781789900149

Venkatesan, R., Navaneeth, K. N., Vedachalam, N., and Atmanand, M. A. (2019). "Observing the oceans in real time—need for affordable technology and capacity development," in *OCEANS 2019 MTS/IEEE SEATTLE* (IEEE, Seattle, WA, USA), 1–7. doi: 10.23919/OCEANS40490.2019.8962684

Wang, Z. A., Moustahfid, H., Mueller, A. V., Michel, A. P. M., Mowlem, M., Glazer, B. T., et al. (2019). Advancing observation of ocean biogeochemistry, biology, and ecosystems with cost-effective *in situ* sensing technologies. *Front. Mar. Sci.* 6, 519. doi: 10.3389/fmars.2019.00519

Weller, R. A., Baker, D. J., Glackin, M. M., Roberts, S. J., Schmitt, R. W., Twigg, E. S., et al. (2019). The challenge of sustaining ocean observations. *Front. Marine Sci.* 6. doi: 10.3389/fmars.2019.00105

Wernand, M. R. (2010). On the history of the Secchi disc. *J. Eur. Optical Society-Rapid Publications* 5, 10013s. doi: 10.2971/jeos.2010.10013s

Whitefield, C. R., Braby, C. E., and Barth, J. A. (2021). Capacity building to address ocean change: organizing across communities of place, practice and governance to achieve ocean acidification and hypoxia resilience in Oregon. *Coastal Manage.* 49, 532–546. doi: 10.1080/08920753.2021.1947133

frontiers | Frontiers in Marine Science

TYPE Original Research
PUBLISHED 04 July 2025
DOI 10.3389/fmars.2025.1612438

OPEN ACCESS

EDITED BY
Betina J. Lomovasky,
Institute of Marine and Coastal Research (IIMyC), Argentina

REVIEWED BY
Emma Rocke,
University of Cape Town, South Africa
Alberto Sánchez-González,
National Polytechnic Institute (IPN), Mexico

*CORRESPONDENCE
Priscilla N. Molina-Cora
priscilla.molina@upr.edu
Julio M. Morell
julio.morell@upr.edu
Loraine Martell-Bonet
loraine.martelll@upr.edu

RECEIVED 15 April 2025
ACCEPTED 18 June 2025
PUBLISHED 04 July 2025

CITATION
Molina-Cora PN, Morell JM, Martell-Bonet L, Rodriguez-Matos LR, Morell JE and Vélez-Rivera M (2025) Observations of *Sargassum* carbon influx and biogeochemical impact in La Parguera Marine Reserve. *Front. Mar. Sci.* 12:1612438. doi: 10.3389/fmars.2025.1612438

Observations of *Sargassum* carbon influx and biogeochemical impact in La Parguera Marine Reserve

Priscilla N. Molina-Cora[1,2*], Julio M. Morell[1,2*], Loraine Martell-Bonet[2*], Luis R. Rodriguez-Matos[2], Julián E. Morell[2] and Maribel Vélez-Rivera[2]

[1]Department of Marine Sciences, University of Puerto Rico, Mayagüez, Puerto Rico, [2]Caribbean Coastal Ocean Observing System, Lajas, Puerto Rico

The massive influx of pelagic *Sargassum* spp. species, also known as *Sargassum* inundation events (SIEs), first arrived at the Caribbean's coastal waters in 2011. These events have been linked to hypoxia, among other ecological disturbances. Here, we report data from 2022 on (1) an assessment of the relative magnitude of particulate organic carbon (POC) load arising from SIEs into the La Parguera Marine Reserve (LPMR) basin off the southwest coast of Puerto Rico and (2) the biogeochemical impact of SIE in a nearshore mangrove key within the reserve, Monsio Jose Key Bay (MJKB). Our analysis yields that the carbon influx increased by 20% in the LPMR basin and by 103% in MJKB. Weekly observations of *Sargassum* input, along with the collection and analysis of water samples in MJKB, evidenced a cause-effect relation between *Sargassum* carbon loading and frequency of hypoxic (DO < 2 $mg{\cdot}L^{-1}$) and critically acidic conditions (Aragonite saturation, $\Omega < 2.0$). During the 2022 *Sargassum* season, hypoxic conditions were detected in 43% of samples collected in MJKB. Considering the modulation of biogeochemical parameters by changes in tide height (Δh) and wind speed ($m{\cdot}s^{-1}$), stepwise multiple regression analyses (RDA-AIC model selection) showed that significant parameters influencing DO, pH, and Ω include the *Sargassum* carbon influx and Δh ($p < 0.05$). These findings strongly support the hypothesis that the additional input of POC influx enhances microbial mineralization rates responsible for depressed oxygen concentrations and acidic conditions, which could be detrimental to coastal ecosystems. This is particularly concerning in areas prone to SIEs where geomorphological features facilitate the entrainment of floating materials. Proper management requires the identification of vulnerable sites and *Sargassum* removal. Ongoing efforts towards that goal are underway for LPMR.

KEYWORDS

carbon input, tropical coastal ecosystem, pelagic Sargassum, hypoxia, biogeochemistry, ocean acidification

1 Introduction

Pelagic *Sargassum* blooms form aggregations or 'rafts' (Brooks et al., 2018), of which significant amounts are advected into Caribbean waters. Rafts support a drifting ecosystem hosting a wide variety of marine species (Weis, 1968; Casazza and Ross, 2008; Brown, 2020) and are recognized by the South-Atlantic Fisheries Council of the National Oceanic and Atmospheric Administration as an essential fish habitat (NOAA, 2003; Huffard et al., 2014; Cashman and Nagdee, 2017). Since 2011, the seasonal occurrence of large pelagic blooms of *Sargassum*, including two predominant species (*S. fluitans* and *S. natans*), has become the new normal in the Tropical and Subtropical North Atlantic from Brazil to Africa (de Széchy et al., 2012; Hu et al., 2016; Putman et al., 2018; Wang et al., 2019; Johns et al., 2020). Pelagic *Sargassum* blooms have attracted attention due to their substantial arrival in vast quantities, also known as *Sargassum* inundation events (SIEs), along the coasts of the Greater Caribbean and the Tropical Atlantic Regions (Moreira and Alfonso, 2013; Mendez-Tejeda and Rosado, 2019; Wang et al., 2019). Once brought ashore by currents and winds (Putman et al., 2018; Wang et al., 2019), the accumulation of *Sargassum* on the coast has been reported to lead to detrimental conditions for coastal ecosystems, fisheries, and tourism (Cashman and Nagdee, 2017; van Tussenbroek et al., 2017; Cabanillas-Teran et al., 2019; Mendez-Tejeda and Rosado, 2019; Brown, 2020; Bernard et al., 2022; Sánchez et al., 2023). Although SIEs have been considered a temporary phenomenon (Marsh et al., 2022), recent studies indicate that recurrent blooms could be associated with climate change, fluctuations in hydrodynamic patterns, and the introduction of anthropogenic nutrients (Djakouré et al., 2017; Sonter et al., 2017; Putman et al., 2018; Wang et al., 2019; Gouvêa et al., 2020). *Sargassum* accumulates seasonally under the Intertropical Convergence Zone (ITCZ) (Johns et al., 2020). In this zone the equatorial and Northwest Africa coastal upwelling regions, the Amazon and Orinoco River outflows, and the Saharan dust transported by the easterly trade winds supply a significant amount of nutrients (Wang et al., 2019; Oviatt et al., 2019), providing optimal conditions to sustain a *Sargassum* bloom in the North Equatorial Recirculation Region (NERR) (Gower et al., 2013; Wang and Hu, 2016; Djakouré et al., 2017). Following the bloom, the *Sargassum* is transported westward and eastward, creating the great Atlantic *Sargassum* belt (Wang et al., 2019; Johns et al., 2020; Skliris et al., 2022).

Given its effectiveness as a primary producer and storehouse of organic carbon (Krause-Jensen and Duarte, 2016; Gouvêa et al., 2020), SIEs can represent a significant exogenous source of particulate organic carbon (POC) (Valiela et al., 1997). POC influx can be expected to result in hypoxia and ocean acidification due to increased metabolic demands (Burkholder et al., 2007; Lee et al., 2007; Martínez-Lüscher and Holmer, 2010; van Tussenbroek et al., 2017). Hypoxic conditions associated with *Sargassum* have been linked to neritic fish and crustacean mortality (Rodríguez-Martínez et al., 2019). However, although *Sargassum's* role in carbon dynamics in the Tropical and Subtropical Atlantic oceanic domains has been well-documented (Krause-Jensen and Duarte, 2016; Wang et al., 2018; Gouvêa et al., 2020; Hu et al., 2021), the impact of pelagic *Sargassum* carbon that inundates Caribbean coastal ecosystems remains to be adequately assessed. Further studies identifying the magnitude and frequency of SIEs driven hypoxia and acidification events in representative critical ecosystems should provide a baseline for the development of models predicting biomass influx and retention as well as the resulting hypoxia and acidification. Said forecasting tools would support resource managers responsible for deploying impact mitigation measures.

Here, we present data from a year-long (2022) time-series of observations focused on assessing the temporal variability of *Sargassum* biomass influx rates into the La Parguera Marine Reserve (LPMR) basin and at Monsio Jose Key Bay (MJKB) within the basin. The relative increase in POC loading resulting from *Sargassum* influx, both at the basin-wide scale and at MJKB, is estimated using available data on mangrove litterfall (Vega-Rodríguez et al., 2008; Pérez-Pérez et al., 2022) and seagrass production for LPMR basin (Liboy, 1976; Hertler, 2002). Below we report serial observations of dissolved oxygen (DO) concentration, total alkalinity (TA) and pH at MJKB, collected in parallel to biomass influx measurements provided for assessing the magnitude, frequency and duration of hypoxia and acidification events in a mangrove key, a typical ecosystem in LPMR basin, arising from SIEs.

2 Materials and methods

2.1 Area of study

This study was conducted in the coastal waters of LPMR off the southwestern coast of Puerto Rico (Figure 1), an area designated as a Nature Reserve in September 1979. The reserve consists of a series of reef cays with a dispersed distribution along the interior insular shelf hosting ecosystems, including coral reefs, seagrass meadows, and mangroves (Valdés-Pizzini and Schärer-Umpierre, 2014). Due to the prevalence of south-southeasterly winds, the area is particularly susceptible to SIEs (Hernández et al., 2022). Meteorologically, the LPMR basin is characterized by a wet season extending from August to November, and semiarid conditions prevail during the rest of the year (García-Troche et al., 2021; Ayala-Torres and Otero, 2023). Mangrove litterfall and seagrasses are the major organic carbon sources in LPMR. Net carbon production by planktonic autotrophs was not included as a source of POC in LPMR basin, as the only published information available (Odum et al., 1959) reports net autotrophy presumably supported by dissolved organic carbon (DOC) exported by mangrove forests. Moreover, Meléndez et al. (2022), using data from a decade of observations collected by La Parguera MapCO_2 buoy, located off a mid-shelf reef key in the LPMR basin, reported net heterotrophic conditions during the year as slightly autotrophic conditions only prevailing during winter months.

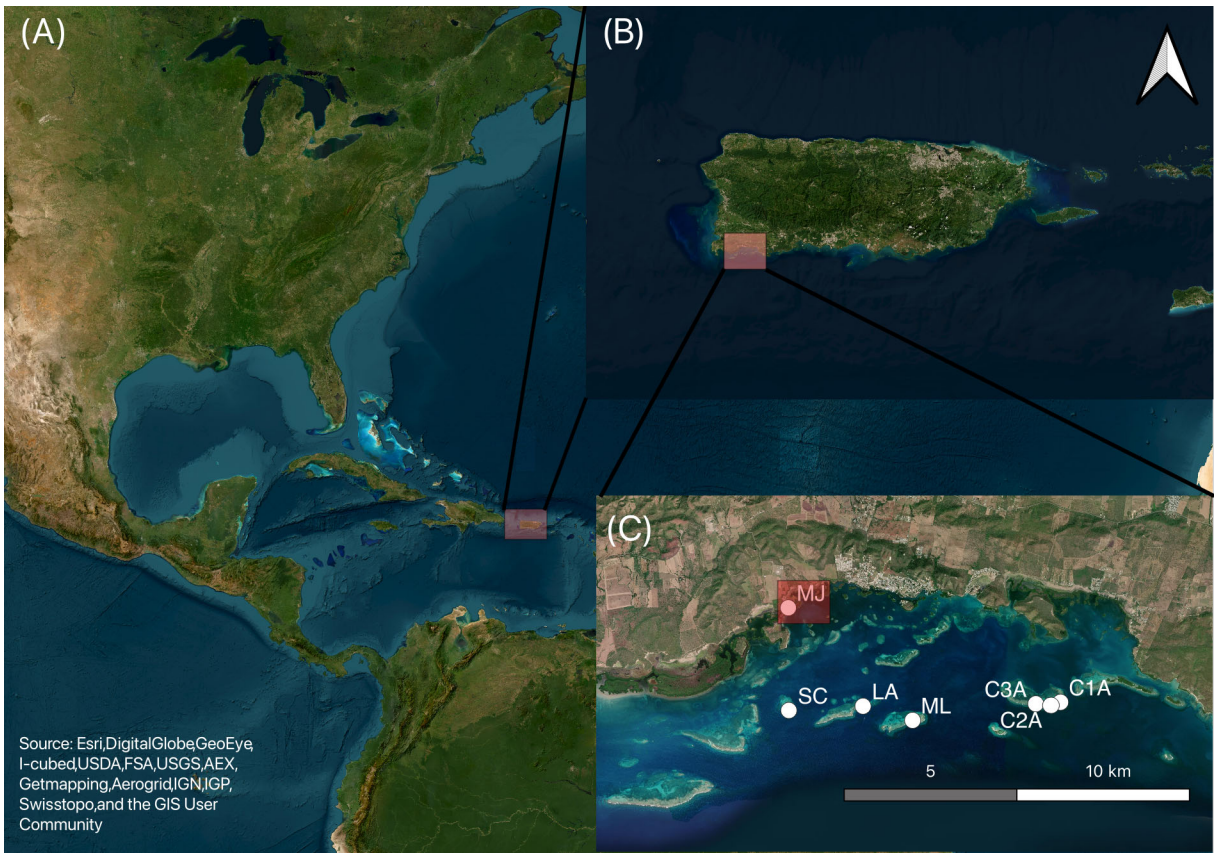

FIGURE 1
Satellite images showing **(A)** Puerto Rico in the Caribbean Sea, **(B)** the study area off the southwestern coast of Puerto Rico, and **(C)** the geographical distribution of *Sargassum* trap location around La Parguera Marine Reserve, Lajas, Puerto Rico. The white circles indicate study sites: SC (San Cristobal key; 17.942074°N, 67.076714°W), LA (Laurel key; 17.943191°N, 67.056441°W), ML (Media Luna key; 17.9395°N, 67.042871°W), C3A (17.9438° N, 67.009188°W), C2A (17.9434°N, 67.005127°W), and C1A (17.9442°N, 67.002603°W) (Corral Key) and MJKB (Monsio José Key Bay; 17.9688°N, 67.076871°W). The red squared in MJKB marks the location where a *Sargassum* trap was located, and biogeochemical samples were collected.

2.2 Estimation of *Sargassum* carbon influx

Six (6) *Sargassum* traps (Supplementary Figure A.1 in Supplementary Materials), constructed using PVC pipe and plastic mesh and measuring 0.63 x 0.5 x 0.63 m (depth x width x height), were deployed facing the prevailing southeasterly winds on the seaward edge of four reef islands on the outer southern boundary of LPMR basin. An additional trap was deployed in Monsio Jose Key Bay (MJKB) (17.9688°N, 67.076871°W), a nearshore mangrove-lined embayment (Figure 1). Traps were placed in 10 cm deep water to ensure water inflow even at low tide. Weekly sampling facilitated trap maintenance, allowing for continuous assessment of their condition. Traps were replaced as needed to ensure optimal functionality and uninterrupted sampling.

Quantification of the weekly *Sargassum* biomass influx ($kg{\cdot}m^{-1}{\cdot}Wk^{-1}$) into the LPMR basin and MJKB was estimated by collecting the *Sargassum* accumulated in the traps, transferring it to a mesh bag, and weighing it on-site using an electronic fish scale. The *Sargassum* wet weight was converted to POC using an averaged carbon-to-wet weight ratio of 0.05 ± 0.01 published by Laffoley et al. (2014); Wang et al. (2018, 2019); and Gouvea et al. (2020) (Supplementary Table A.1 in Supplementary Materials). The total weekly *Sargassum* carbon influx to the LPMR basin was estimated using the weekly mean capture of all traps located in the outer reefs, normalized by the trap width (meters) and multiplied by the width of the basin's windward boundary (10.4 km). For MJKB, weekly mean values were multiplied by the width of the channel (69 m) facing the prevailing wind. *Sargassum* carbon influx rates to MJKB nearshore station were contrasted with estimates of carbon influx from mangrove litterfall. To achieve a more comprehensive assessment of the carbon contribution, we also estimated DOC from *Sargassum* using values reported by Powers et al. (2019).

2.3 Estimating mangrove POC influx

The mangrove litterfall rate for the LPMR basin and MJKB were estimated using the mean of reported litterfall observations in LPMR, 476 dry $weights{\cdot}m^{-2}{\cdot}yr^{-1}$ (Vega-Rodríguez et al., 2008; Pérez-Pérez et al., 2022) and area estimates were derived from satellite imagery. Mangrove litter mass was converted to carbon using the 0.5 carbon/litter weight ratio reported by Golley et al.

(1962) (Supplementary Table A.2 in Supplementary Materials). The estimated POC was converted to DOC using the 0.13 reported by Adame and Lovelock (2011).

2.4 Estimating seagrass POC input

Estimates of net carbon input from seagrasses are based on seagrass growth studies carried out in LPMR basin by Liboy (1976) and Hertler (2002). The mean seagrass productivity rate (4.56 ± 2.01 $g{\cdot}m^{-2}{\cdot}day^{-1}$) calculated from data from both studies was used to obtain the seagrass POC production rate for the basin. Said rate is consistent with reports from other areas in the Caribbean (Linton and Fisher, 2004; Juman, 2005). Seagrass biomass was converted to carbon using the carbon-to-biomass ratio (0.32) reported by Bay et al. (1996) (Supplementary Table A.3 in Supplementary Materials). We estimated the exudation carbon by using the POC-to-DOC ratio (0.126) reported by Robertson et al. (1982).

2.5 Biogeochemical observations at MJKB

Although *Sargassum* traps were deployed throughout LPMR, the analysis of weekly seawater samples for assessing the biogeochemical impact of SIEs was exclusively conducted for MJKB in this study. Samples were collected within 3.5 meters of the MJKB *Sargassum* trap (17.968766°N, 67.076871°W) from January 2022 to December 2022 between 7:00 and 10:00 a.m. (local time) at 1-meter depth using a Van Dorn 3.5 L sampler, following the best practices guidelines (Dickson et al., 2007). One seawater sample was collected for each parameter, which allowed for duplicate analyses in the lab. Conductivity and temperature data were collected with an SBE25 CTD. Seawater samples for pH and TA were fixed immediately with a saturated solution of mercury chloride ($HgCl_2$) to prevent biological alteration. Analysis for pH on the Total Scale was performed using a spectrophotometer with m-cresol purple indicator dye (pH_T ± 0.003) (Dickson and Goyet, 1996; Grasshoff et al., 2007). Total alkalinity determinations (TA ± 2 $\mu mol{\cdot}kg^{-1}$) (Dickson et al., 2007) were carried out following the protocol described by García-Troche et al. (2021). DO sample analysis was performed following the Winkler method (DO ± 0.50 $mg{\cdot}L^{-1}$) (Grasshoff et al., 2007; Astor et al., 2013). Aragonite saturation state (Ω) values were estimated from pH and TA measurements using the CO2SYS program (Lewis and Wallace, 1998).

2.6 Statistical analysis

Pearson's correlation analysis was used to identify significant time-lagged correlations between the explanatory variable (i.e., weekly *Sargassum* carbon influx) and the dependent variables (i.e., DO). A MATLAB function was created to identify different weekly lags between the variables and show the significant Pearson's correlation coefficient. The lagged *Sargassum* carbon influx ($kgC{\cdot}m^{-1}$) and physical parameters, such as wind speed ($m{\cdot}s^{-1}$) and changes in tide height, calculated as Δh = (tide height at sampling time)/(mean low tide), were included in data analyses to determine their significance in modulating the measured and calculated biogeochemical parameters (i.e., DO, pH, Ω). Wind speed data were sourced from the National Buoy Center, and tidal data were obtained from NOAA Tides & Currents for Station 9759110, Magueyes Islands, PR.

The MATLAB Fathom toolbox (Jones, 2017) was used to perform a stepwise forward selection of explanatory variables in Redundancy Analysis (RDA) using Akaike Information Criteria (AIC). This analysis identified optimal variables that substantially explained the variation of biogeochemical parameters (i.e., response variables; DO, pH, Ω). Explanatory variables included in the RDA-AIC analysis were *Sargassum* carbon influx, wind speed, and Δh. Subsequently, a permutation-based RDA with 1000 iterations was conducted using the optimal explanatory variables identified through the RDA-AIC analyses to derive the model statistics. Lastly, to gain a clearer understanding of the individual effects of the optimal explanatory variables on the response variables, a permutation-based Multiple Linear Regression via Least Squares Estimation with 1000 iterations were performed for each response variable independently. This enabled a more precise interpretation of the impact of each explanatory variable on the response variables, offering insights into their distinct roles within the broader model.

3 Results

3.1 *Sargassum* biomass influx

During 2022, SIEs at LPMR basin started in April and extended until November. The mean weekly *Sargassum* biomass influx for the six (6) traps, located in the outer keys of the LPMR basin (Figure 2), ranged from non-detectable to a maximum of 24.80 $kg{\cdot}m^{-1}{\cdot}Wk^{-1}$ occurring on the second week of May. An estimate of the mean weekly *Sargassum* biomass influx into the basin yields 7.85 ± 6.60 $kg{\cdot}m^{-1}{\cdot}Wk^{-1}$ or 81,725 $kg{\cdot}Wk^{-1}$ for the whole basin. For the same period, the weekly *Sargassum* biomass influx rate into the MJKB averaged 2.13 ± 5.08 $kg{\cdot}m^{-1}{\cdot}Wk^{-1}$ with a maximum *Sargassum* input rate of 23.22 $kg{\cdot}m^{-1}{\cdot}Wk^{-1}$ (Figure 3). Extrapolation using the width of MJKB channel (69 m) aligned with the prevailing wind direction, yields a weekly mean *Sargassum* biomass loading rate for the embayment of 155 ± 327 $kg{\cdot}Wk^{-1}$.

3.2 Carbon inputs to LPMR basin

Figure 4 presents the estimates of POC production by mangroves (as litterfall) and seagrasses (leaf growth) as well as estimates of *Sargassum* POC influx into the LPMR basin. The weekly POC production of seagrasses and mangroves totaled 18,209 $kgC{\cdot}Wk^{-1}$, while the POC loading arising from the *Sargassum* influx during high season in 2022 averaged 3,617 ± 3,452 $kgC{\cdot}Wk^{-1}$ with a standard error of 241 $kgC{\cdot}Wk^{-1}$, thus

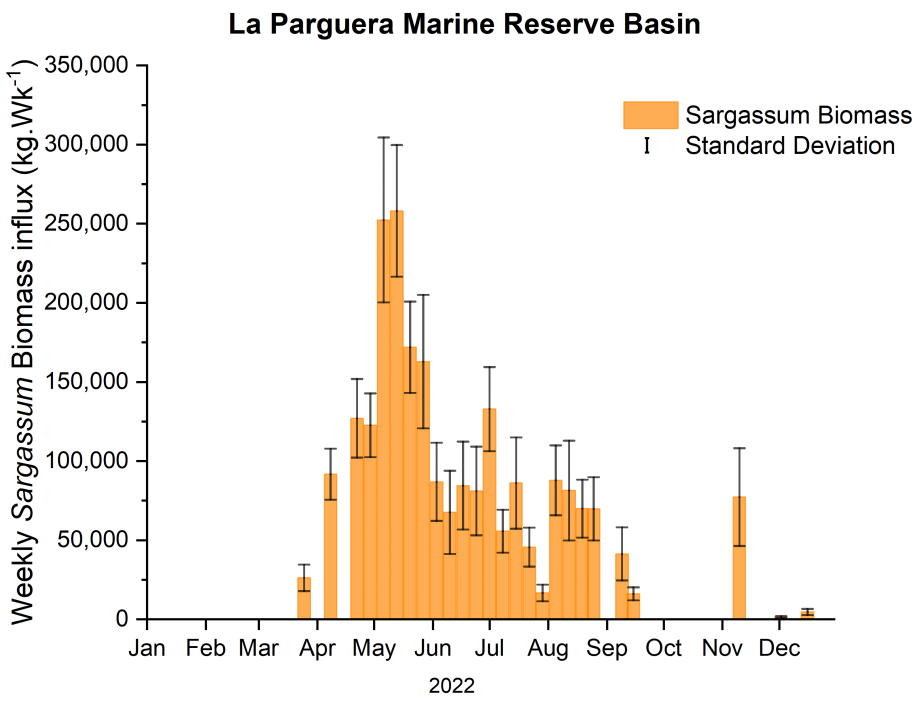

FIGURE 2
Estimated average over-trap (n = 6) of *Sargassum* biomass influx on the outer keys extrapolated by the width of the LPMR basin during the 2022 season.

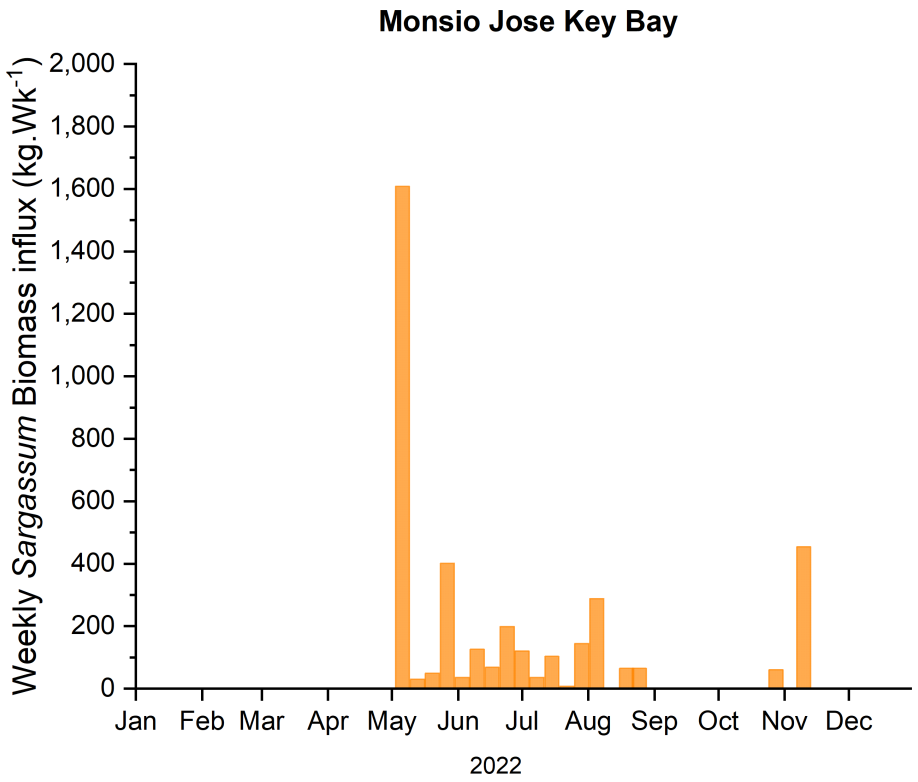

FIGURE 3
Estimated *Sargassum* biomass influx to MJKB, extrapolated by the width of the channel, during the 2022 season.

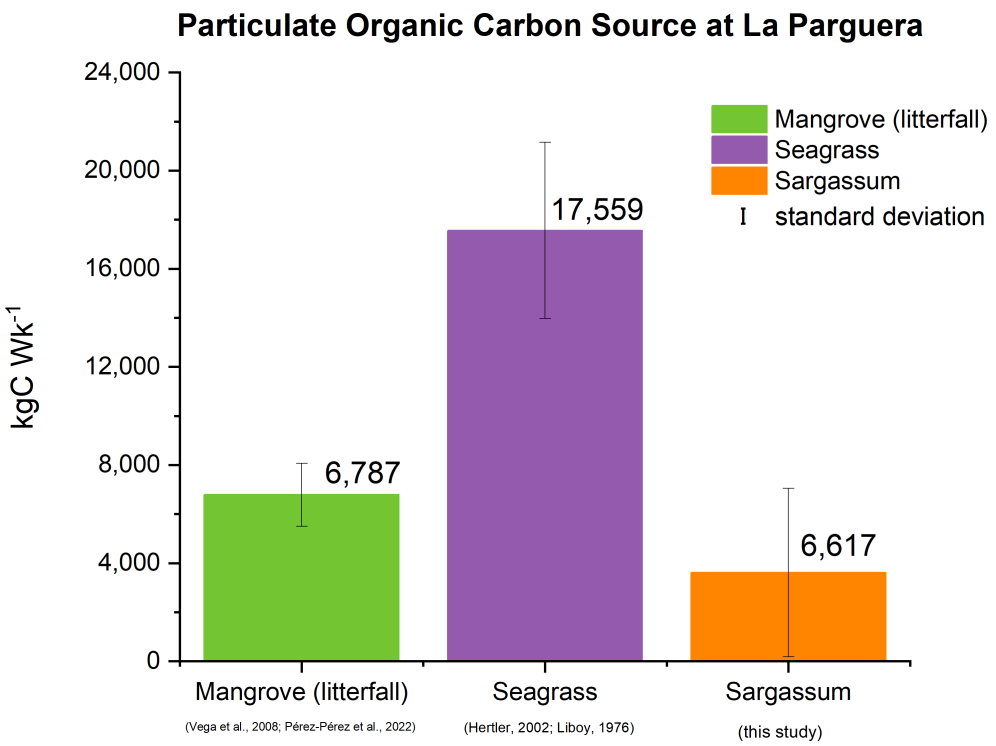

FIGURE 4
Estimated weekly POC input rates from *Sargassum* and other primary sources in LPMR basin.

representing about 20 ± 19% increase in POC input to LPMR basin (Figure 4).

The weekly estimated exudates of DOC from the production of seagrasses and mangroves in the LPMR basin are 3,041 kgC·Wk^{-1} (Supplementary Table A.4 in Supplementary Materials). At the same time, the DOC loading arising from the *Sargassum* influx during the high season in 2022 averaged 6 kgC·Wk^{-1}, thus representing a 0.2% minor fraction increase in DOC input to the LPMR basin. The comparison of the calculated POC and DOC fractions from *Sargassum* suggests that POC is the predominant contributor to the organic carbon pool in the LPMR basin.

3.3 Carbon input to MJKB

Weekly estimates of carbon loading from mangroves (as litterfall) and *Sargassum* to MJKB are presented in Figure 5. Nonetheless, for MJKB, the seagrass carbon was not considered because the study site does not harbor seagrasses. While carbon production by mangroves for the area in the MJKB, is estimated at 7.5 ± 1.4 kgC·Wk^{-1}, *Sargassum*, POC influx averaged 7.7 ± 16.3 kgC·Wk^{-1}, thus representing a 103% net increase in POC.

The carbon exudation estimates by mangroves, primarily through litterfall, for MJKB are approximately 1.0 kgC·Wk^{-1} (Supplementary Table A.5 in Supplementary Materials). In contrast, the DOC influx from *Sargassum* into the MJKB averaged 0.013 kgC, contributing to a minor increase of 1.3% in DOC.

3.4 Biogeochemistry at MJKB

Observations of biogeochemical data indicate that during the months before the arrival of *Sargassum* (winter season), pH ranged from 7.7 to 7.9, while $\Omega_{aragonite}$ ranged from 2.2 to 3.0. DO values ranged from 3.28 to 5.24 mg·L^{-1}, while temperature ranged from 26.11 to 28.21°C (Supplementary Table A.6 in Supplementary Materials). After the onset of the *Sargassum* season in early May, we observed a sharp decrease in pH, $\Omega_{aragonite,}$ and DO (Figure 6). Simultaneously, we observed a warmer seawater temperature. For this period, pH values ranged between 7.0 – 7.8, with increased seawater acidity observed during the summer months when $\Omega_{aragonite}$ ranged between 0.5 – 2.8, values under critical levels are $\Omega <$ 2.0. During the same period, DO values ranged from non-detectable to 4.67 mg·L^{-1}, frequently reaching hypoxic or anoxic conditions. Temperature values ranged from 27.90 to 30.77°C, with higher temperature levels occurring between late summer and fall. The ecosystem's gradual and modest recovery is evident towards the end of the season, albeit with sustained low DO and pH levels. These conditions persisted from mid-June to September.

Data analyses were performed using a one-week lag on the *Sargassum* carbon influx based on the significant time lagged correlations identified by the Pearson's correlation analysis using DO, pH and Ω data (Supplementary Table A.7 in Supplementary Materials). These results suggest that biogeochemical parameters exhibit measurable changes one week after a SIE, indicating *Sargassum* impact on the system's chemical dynamics. The stepwise RDA-AIC analyses showed that Δh and *Sargassum*

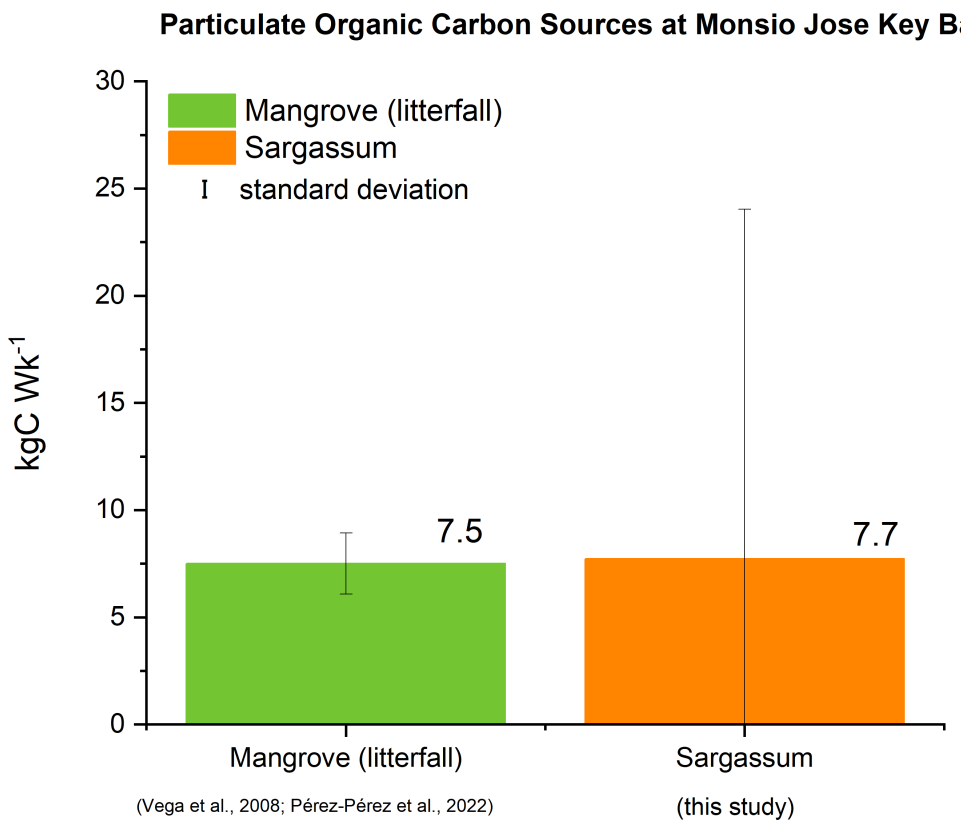

FIGURE 5
Estimates of POC sources at MJKB during the 2022 Sargassum season.

carbon influx were the optimal explanatory variables for the variance of DO, pH and Ω (Table 1). A significant portion of the response variables is explained by Δh independently, but adding *Sargassum* carbon influx further improves the model. Wind speed was not identified as an optimal explanatory variable by the AIC analyses. The RDA permutation test demonstrated that the model incorporating the optimal explanatory variables identified through RDA-AIC accounted for a significant proportion of the variance in the response variables ($p < 0.05$, $r^2 = 0.34$; Supplementary Table A.8 in Supplementary Materials).

Multiple linear regressions to assess the individual effects of Δh and *Sargassum* carbon influx on response variables (i.e., DO, pH, Ω) showed that DO is significantly influenced by Δh and *Sargassum* carbon influx ($p < 0.05$, $r^2 = 0.35$; Table 2), with *Sargassum* carbon influx having a negative relationship and Δh having a positive relationship with DO. However, the response of pH and Ω is less well explained by Δh and *Sargassum* carbon influx ($r^2 = 0.14$). The variation in Δh has a marginal influence on pH, whereas the influx of carbon from *Sargassum* has a minimal impact on Ω (Table 2).

4 Discussion

Sargassum inundation events in LPMR basin and MJKB exhibit a marked seasonal variability, with peak influx rates occurring in spring and summer and quickly subsiding between August and December. In May 2022, the LPMR basin and MJKB experienced a major influx of *Sargassum* biomass, which has been corroborated by satellite image analyses reported by the University of South Florida Optical Oceanography Lab, which sets a new historical record for the month of May for all Caribbean regions, exceeding all major *Sargassum* blooms in previous years (Hu, 2022). The mean estimate of *Sargassum* biomass loading in LPMR basin indicates a substantial influx. The assumption is that the *Sargassum* collected in the traps represents the total *Sargassum* accumulation in the LPMR basin, which can lead to an overestimation of biomass influx. We emphasize that the purpose of this research is to estimate the amount of *Sargassum* POC entering the basin compared to well-known local POC sources. However, we compared our 2022 data on *Sargassum* biomass (wet weight) with data from Mexico in 2015. This comparison provides an insight into the influx estimate. Our data indicate that the LPMR basin received a monthly influx of 49,360 kg·km^{-1} for July-August, an amount notably lower compared to the monthly ~817,000 kg·km^{-1} accumulated on Mexico's coastline in 2015 (van Tussenbroek et al., 2017).

The estimates reported in Section 4 for POC inputs to the LPMR basin indicate that, at the basin scale, *Sargassum* input represents a significant increase in carbon load (20%) over POC inputs from seagrass and mangrove litter. However, in MJKB, where the shoreline favors entrainment of buoyant material, the *Sargassum* inundation represented a 103% increase in carbon loading comparable with local carbon input from mangrove

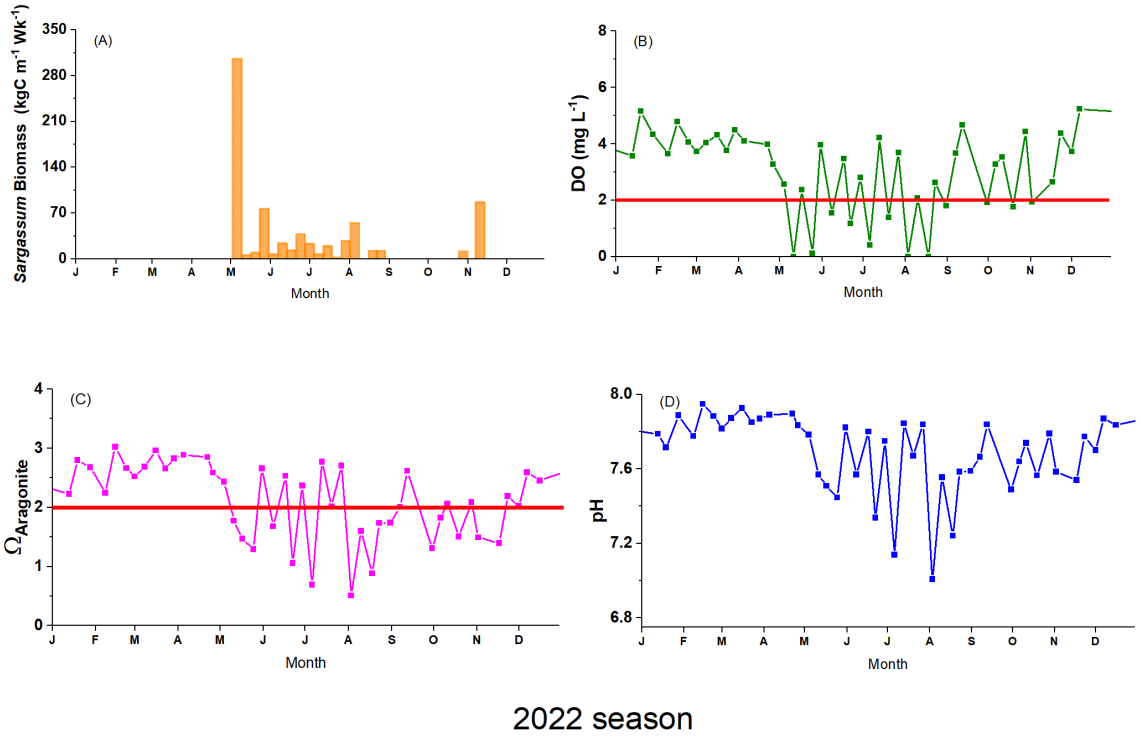

FIGURE 6
Time series of **(A)** *Sargassum* carbon influx, **(B)** Dissolved oxygen, **(C)** Ω aragonite, and **(D)** pH, for the 2022 season at Monsio Jose Key Bay (MJKB). The red line represents the critical level for DO (<2 mg·L^{-1}) and Ω (< 2).

litterfall. This means that environmental conditions (e.g., prevailing winds, hydrodynamics) at specific geographical areas with shoreline characteristics that are conducive to the retention of *Sargassum*, are particularly vulnerable to SIE (León-Pérez et al., 2023). In MJKB, this additional input of POC into the ecosystem most probably leads to hypoxia and acidification enhancement due to increased metabolic demands in the benthos and water column (Burkholder et al., 2007; Lee et al., 2007; Martínez-Lüscher and Holmer, 2010; van Tussenbroek et al., 2017; Valiela et al., 1997; Rabalais et al., 2002; Wallace et al., 2014).

TABLE 1 Akaike Information Criterion (AIC) model with explanatory variables (Δh, *Sargassum* carbon influx) that explained DO, pH, Ω at Monsio Jose.

Variable	r^2	r^2Adjusted	AIC
Δh	0.21	0.19	34.69
Sargassum carbon influx	0.32	0.28	31.27

The tidal height differential (Δh) plays a significant role in regulating DO, pH, and Ω through physical and biogeochemical processes. During periods of larger Δh, the influx of offshore water into MJKB facilitates water mass flushing, promoting oxygenation and mitigating declines in pH and Ω. Conversely, when Δh is minimal and tidal exchange is limited, the "residence time" of water masses in MJKB may become stagnant, allowing biological processes such as respiration and the decomposition of *Sargassum* and other organic matter to drive reductions in DO, pH, and Ω. These findings indicate that tides actively shape the ecological and biogeochemical conditions at MJKB, even during SIEs.

Monsio Jose Key Bay is characterized by fringe mangroves, which are host to a varied community of autotrophs and heterotrophs and function as essential nursery grounds for juvenile fish (Nagelkerken et al., 2008), SIEs may disrupt these ecosystems, leading to direct mortality, forced migration, heightened vulnerability to predation, shifts in food availability, and changes to life cycles (Rabalais et al., 2002; Vaquer-Sunyer and Duarte, 2008; Dubuc et al., 2019; Pérez-Posada et al., 2023).

TABLE 2 Results of multiple regressions for DO, pH and Ω against Δh and *Sargassum* carbon influx.

Response variable	r^2	Adjusted r^2	*p*	Intercept (beta, p)	*Sargassum* carbon influx (beta, p)	Δh (beta, p)
DO	0.35	0.32	**$1{\cdot}10^{-3}$**	1.75, **$2.00{\cdot}10^{-3}$**	-0.03, **$2.00{\cdot}10^{-3}$**	1.33, **$2.00{\cdot}10^{-3}$**
pH	0.14	0.10	**$1{\cdot}10^{-3}$**	7.56, **$2.00{\cdot}10^{-3}$**	$-3.12{\cdot}10^{-3}$, 0.06	0.13, **$2.00{\cdot}10^{-3}$**
Ω	0.14	0.09	**$1{\cdot}10^{-3}$**	1.86, **$2.00{\cdot}10^{-3}$**	-0.01, **$2.00{\cdot}10^{-3}$**	0.30, 0.08

Significant p values are in bold.

Therefore, the constant arrival of *Sargassum* poses a threat to both flora and fauna. Hernández et al. (2022) suggest that the persistent influx of *Sargassum* may have negatively impacted vegetation cover, including mangroves and seagrasses, resulting in a decline in La Parguera. MJKB experienced 10 weeks of hypoxic conditions due to the accumulation of carbon-rich *Sargassum* biomass, with DO levels decreasing below the critical lethal concentration 50% (LC50) threshold of 2 mg O_2/L (Vaquer-Sunyer and Duarte, 2008). According to Vaquer-Sunyer and Duarte (2008), fish and crustaceans would perish from hypoxia in these circumstances before they could reach the critical threshold.

The evolution of hypoxia was paralleled by a decline in aragonite saturation, which dropped below the critical threshold of $\Omega < 2.0$ following SIEs (Sánchez-Beristain et al., 2016), as illustrated in Figure 6. The decrease in Ω could be disadvantageous for many marine organisms, such as corals, clams, echinoderms, mussels, oysters, etc (Morse et al., 2006; Bates et al., 2009; Millero, 2013; Mollica et al., 2018). Also, the low pH and Ω levels could affect commercially important species' breeding areas and the food web dynamics at lower trophic levels (Branch et al., 2013; Sutton et al., 2016; Clements and Chopin, 2017).

The SIEs have a significant impact on the ecosystem and socio-economic consequences, disrupting tourism, limiting local recreational activities, and constraining fisheries due to reduced fish availability (Rodríguez-Martínez et al., 2019; Hamel et al., 2024). Additionally, there are challenges in developing cost-effective management strategies to remove *Sargassum* from shorelines (Hamel et al., 2024; León-Pérez et al., 2024). Our observations highlight the need for further assessment of impacts arising from *Sargassum* and the development of tools capable of forecasting SIEs and their biogeochemical impacts. The time series presented in this study was used to develop the CARICOOS' coastal *Sargassum* inundation forecasting products (caricoos.org/sargassum) and is an ongoing effort to validate the models. In this way we are enhancing predictive models and providing tools for coastal management strategies.

Data availability statement

The datasets presented in this study can be found in online repositories. The names of the repository/repositories and accession number(s) can be found below: http://dm1.caricoos.org/thredds/catalog/content/Parguera_Sargassum/catalog.html.

Author contributions

PM-C: Writing – review & editing, Project administration, Writing – original draft, Formal analysis, Methodology, Data curation, Conceptualization, Investigation. JMM: Funding acquisition, Resources, Project administration, Formal analysis, Supervision, Conceptualization, Writing – review & editing, Methodology. LM-B: Formal analysis, Methodology, Writing – review & editing. LR-M: Methodology, Writing – review & editing, Investigation. JEM: Methodology, Investigation, Writing – review & editing. MV-R: Formal analysis, Writing – review & editing, Methodology.

Funding

The author(s) declare that financial support was received for the research and/or publication of this article. This project was funded by the NOAA Ocean Service, National Centers for Coastal Ocean Science, Competitive Research Program under NOAA award #NA23NOS4780291. This is contribution number 267 from the NOAA Monitoring and Event Response for Harmful Algal Blooms (MERHAB) Research Program.

Acknowledgments

We acknowledge the financial support provided by NOAA's NCCOS and IOOS programs and the Department of Marine Science at the University of Puerto Rico Mayagüez for their assistance with field logistics.

Conflict of interest

The authors declare that the research was conducted in the absence of any commercial or financial relationships that could be construed as a potential conflict of interest.

Generative AI statement

The author(s) declare that no Generative AI was used in the creation of this manuscript.

Publisher's note

Supplementary material

The Supplementary Material for this article can be found online at: https://www.frontiersin.org/articles/10.3389/fmars.2025.1612438/full#supplementary-material

References

Adame, M. F., and Lovelock, C. E. (2011). Carbon and nutrient exchange of mangrove forests with the coastal ocean. *Hydrobiologia* 663, 23–50. doi: 10.1007/s10750-010-0554-7

Astor, Y., Fanning, K., Guzman, L., Li, X., Lorenzoni, L., Masserini, R., et al. (2013). *Cariaco Time Series Study Handbook of Methods for the Analysis of Oceanographic Parameters at the CARIACO Time-series Station Serie Ciencia y Tecnología N ° 12 Fundación La Salle de Ciencias Naturales Caracas 2013*. Fundación La Salle de Ciencias Naturales Caracas: CARIACO Time-Series Study Handbook of Methods Methods.

Ayala-Torres, R., and Otero, E. (2023). Seasonal dissolved oxygen depletion in bottom waters may be linked to bioluminescence in a shallow Caribbean bay. *Regional. Stud. Mar. Sci.* 66, 103139. doi: 10.1016/j.rsma.2023.103139

Bates, N. R., Mathis, J. T., and Cooper, L. W. (2009). Ocean acidification and biologically induced seasonality of carbonate mineral saturation states in the western Arctic Ocean. *J. Geophys. Res. Oceans.* 114, 1–21. doi: 10.1029/2008JC004862

Bay, C., Lee, K.-S., and Dunton, K. H. (1996). *Production and carbon reserve dynamics of the seagrass Thalassia testudinum in Corpus Christi Bay, Texas, USA*.

Bernard, D., Biabiany, E., Cécé, R., Chery, R., and Sekkat, N. (2022). Clustering analysis of the Sargassum transport process: application to beaching prediction in the Lesser Antilles. *Ocean. Sci.* 18, 915–935. doi: 10.5194/os-18-915-2022

Branch, T. A., DeJoseph, B. M., Ray, L. J., and Wagner, C. A. (2013). Impacts of ocean acidification on marine seafood. *Trends Ecol. Evol.* 28, 178–186. doi: 10.1016/j.tree.2012.10.001

Brooks, M. T., Coles, V. J., Hood, R. R., and Gower, J. F. R. (2018). Factors controlling the seasonal distribution of pelagic Sargassum. *Mar. Ecol. Prog. Ser.* 599, 1–18. doi: 10.3354/meps12646

Brown, P. (2020). Rethinking Sargassum Seaweed: Could It Be the New Normal in Jamaica? Available online at: https://nacla.org/news/2020/03/12/rethinking-sargassum-seaweed-Jamaica (Accessed April 26, 2020).

Burkholder, J. A. M., Tomasko, D. A., and Touchette, B. W. (2007). Seagrasses and eutrophication. *J. Exp. Mar. Biol. Ecol.* 350, 46–72. doi: 10.1016/j.jembe.2007.06.024

Cabanillas-Teran, N., Hernandez-Arana, H. A., Ruiz-Zarate, M. A., Vega-Zepeda, A., and Sanchez-Gonzalez, A. (2019). Sargassum blooms in the Caribbean alter the trophic structure of the sea urchin Diadema antillarum. *PeerJ* 2019, 1–32. doi: 10.7717/peerj.7589

Casazza, T. L., and Ross, S. W. (2008). Fishes associated with pelagic Sargassum and open water lacking Sargassum in the Gulf Stream off North Carolina. Available online at: http://hdl.handle.net/1834/25466 (Accessed October 11, 2023).

Cashman, A., and Nagdee, M. R. (2017). Impacts of climate change on settlements and infrastructure in the coastal and marine environments of caribbean small island developing states (SIDS). *Sci. Rev.* 2017, 155–173.

Clements, J. C., and Chopin, T. (2017). Ocean acidification and marine aquaculture in North America: potential impacts and mitigation strategies. *Rev. Aquac.* 9, 326–341. doi: 10.1111/raq.12140

de Széchy, M. T. M., Guedes, P. M., Baeta-Neves, M. H., and Oliveira, E. N. (2012). Verification of Sargassum natans (Linnaeus) Gaillon (Heterokontophyta: Phaeophyceae) from the Sargasso Sea off the coast of Brazil, western Atlantic Ocean. *Check. List.* 8, 638–641. doi: 10.15560/8.4.638

Dickson, A. G., Andrew, G., Sabine, C. L., Christian, J. R., and North Pacific Marine Science Organization (2007). *Guide to best practices for ocean CO_2 measurements* (Sidney, British Columbia: North Pacific Marine Science Organization).

Dickson, A. G., and Goyet, C. (1994). "Determination of the pH of sea water using the indicator dye m-cresol purple," in *Handbook of Methods for the Analysis of the various parameters of the carbon dioxide system in Sea Water* (Oak Ridge, TN: Oak Ridge National Lab. (ORNL)), 3–10. doi: 10.2172/10107773

Djakouré, S., Araujo, M., Hounsou-Gbo, A., Noriega, C., and Bourlès, B. (2017). On the potential causes of the recent Pelagic Sargassum blooms events in the tropical North Atlantic Ocean. *Biogeosci. Discuss.* 2017, 1–20. doi: 10.5194/bg-2017-346

Dubuc, A., Baker, R., Marchand, C., Waltham, N. J., and Sheaves, M. (2019). Hypoxia in mangroves: Occurrence and impact on valuable tropical fish habitat. *Biogeosciences* 16, 3959–3976. doi: 10.5194/bg-16-3959-2019

García-Troche, E. M., Morell, J. M., Meléndez, M., and Salisbury, J. E. (2021). Carbonate chemistry seasonality in a tropical mangrove lagoon in La Parguera, Puerto Rico. *PloS One* 16, e0250069. doi: 10.1371/journal.pone.0250069

Golley, F., Odum, H. T., and Wilson, R. F. (1962). The structure and metabolism of a puerto rican red mangrove forest in may. *Ecology* 43, 9–19. doi: 10.2307/1932034

Gouvea, L. P., Assis, J., Gurgel, C. F. D., Serrão, E. A., Silveira, T. C. L., Santos, R., et al. (2020). Golden carbon of Sargassum forests revealed as an opportunity for climate change mitigation. *Sci. Total. Environ.* 729, 138745. doi: 10.1016/j.scitotenv.2020.138745

Gower, J., Young, E., and King, S. (2013). Satellite images suggest a new Sargassum source region in 2011. *Remote Sens. Lett.* 4, 764–773. doi: 10.1080/2150704X.2013.796433

Grasshoff, K., Kremling, K., and Ehrhardt, M. (2007). *Methods of Seawater Analysis: Third, Completely Revised and Extended Edition* (Weinheim, Germany: Wiley-VCH). doi: 10.1002/9783527613984

Hamel, K., Garcia-Quijano, C., Jin, D., and Dalton, T. (2024). Perceived Sargassum event incidence, impacts, and management response in the Caribbean Basin. *Mar. Policy* 165, 106214. doi: 10.1016/j.marpol.2024.106214

Hernández, W. J., Morell, J. M., and Armstrong, R. A. (2022). Using high-resolution satellite imagery to assess the impact of Sargassum inundation on coastal areas. *Remote Sens. Lett.* 13, 24–34. doi: 10.1080/2150704X.2021.1981558

Hertler, H. (2002). Implications of resource management in La Parguera, Puerto Rico. Available online at: https://www.researchgate.net/publication/28673803 (Accessed October 20, 2023).

Hu, C. (2022). Outlook of 2022 Sargassum blooms in the Caribbean Sea and Gulf of Mexico. Available online at: https://optics.marine.usf.edu/projects/SaWS/pdf/Sargassum_outlook_2022_bulletin05_USF.pdf (Accessed May 22, 2024).

Hu, C., Hardy, R., Ruder, E., Geggel, A., Feng, L., Powers, S., et al. (2016). Sargassum coverage in the northeastern Gulf of Mexico during 2010 from Landsat and airborne observations: Implications for the Deepwater Horizon oil spill impact assessment. *Mar. pollut. Bull.* 107, 15–21. doi: 10.1016/j.marpolbul.2016.04.045

Hu, C., Wang, M., Lapointe, B. E., Brewton, R. A., and Hernandez, F. J. (2021). On the Atlantic pelagic Sargassum's role in carbon fixation and sequestration. *Sci. Total. Environ.* 781, 146801. doi: 10.1016/j.scitotenv.2021.146801

Huffard, C. L., von Thun, S., Sherman, A. D., Sealey, K., and Smith, K. L. (2014). Pelagic Sargassum community change over a 40-year period: temporal and spatial variability. *Mar. Biol.* 161, 2735–2751. doi: 10.1007/s00227-014-2539-y

Johns, E. M., Lumpkin, R., Putman, N. F., Smith, R. H., Muller-Karger, F. E., T. Rueda-Roa, D., et al. (2020). The establishment of a pelagic Sargassum population in the tropical Atlantic: Biological consequences of a basin-scale long distance dispersal event. *Prog. Oceanogr.* 182, 102269. doi: 10.1016/j.pocean.2020.102269

Jones, D. L. (2017). Fathom Toolbox for MATLAB: software for multivariate ecological and oceanographic data analysis (St. Petersburg, FL, USA: College of Marine Science, University of South Florida). Available online at: https://www.usf.edu/marine-science/research/matlab-resources/index.aspx/ (Accessed March 3, 2025).

Juman, R. A. (2005). The structure and productivity of the Thalassia testudinum community in Bon Accord Lagoon,Tobago. *Rev. Biol. Trop.* 53, 219–227. Available at: http://www.scielo.sa.cr/scielo.php?script=sci_arttext&pid=S0034-77442005000300027&lng=en&nrm=iso&tlng=en.

Krause-Jensen, D., and Duarte, C. M. (2016). Substantial role of macroalgae in marine carbon sequestration. *Nat. Geosci.* 9, 737–742. doi: 10.1038/ngeo2790

Laffoley, D., Baxter, J. M., Thevenon, F., Oliver, J. D., Baxter, J. M., Thevenon, F., et al. (2014). *The significance and management of natural carbon stores in the open ocean* (Gland, Switzerland: IUCN (International Union for Conservation of Nature)).

Lee, K. S., Park, S. R., and Kim, Y. K. (2007). Effects of irradiance, temperature, and nutrients on growth dynamics of seagrasses: A review. *J. Exp. Mar. Biol. Ecol.* 350, 144–175. doi: 10.1016/j.jembe.2007.06.016

León-Pérez, M. C., McLaughlin, R. J., Gibeaut, J. C., Carrubba, L., Colón-Rivera, R. J., and Esteves, R. (2024). First steps towards untangling the sargassum legal regime in Puerto Rico. *Mar. Policy* 165, 106202. doi: 10.1016/j.marpol.2024.106202

León-Pérez, M. C., Reisinger, A. S., and Gibeaut, J. C. (2023). Spatial-temporal dynamics of decaying stages of pelagic Sargassum spp. along shorelines in Puerto Rico using Google Earth Engine. *Mar. pollut. Bull.* 188, 114715. doi: 10.1016/j.marpolbul.2023.114715

Lewis, E., and Wallace, D. (1998). *Program developed for CO2 system calculations* (Oak Ridge, Tennessee, USA: Carbon Dioxide Information Analysis Center (CDIAC), Oak Ridge National Laboratory).

Liboy, J. G. (1976). *An Examination of the Present Condition of Seagrass Meadows in La Parguera, Puerto Rico* (Puerto Rico: Department of Natural Resources, Puerto Rico).

Linton, D., and Fisher, T. (2004). *CARICOMP: Caribbean Coastal Marine Productivity Program, 1993-2003*. (Kingston, Jamaica: CARICOMP).

Marsh, R., Oxenford, H. A., Cox, S. A. L., Johnson, D. R., and Bellamy, J. (2022). Forecasting seasonal sargassum events across the tropical Atlantic: Overview and challenges. *Front. Mar. Sci.* 9. doi: 10.3389/fmars.2022.914501

Martínez-Lüscher, J., and Holmer, M. (2010). Potential effects of the invasive species Gracilaria vermiculophylla on Zostera marina metabolism and survival. *Mar. Environ. Res.* 69, 345–349. doi: 10.1016/j.marenvres.2009.12.009

Meléndez, M., Salisbury, J., Gledhill, D., Langdon, C., Morell, J. M., Manzello, D., et al. (2022). Net ecosystem dissolution and respiration dominate metabolic rates at two western Atlantic reef sites. *Limnol. Oceanogr.* 67, 527–539. doi: 10.1002/lno.12009

Mendez-Tejeda, R., and Rosado, J. G. A. (2019). Influence of climatic factors on Sargassum arrivals to the coasts of the Dominican Republic. *J. Oceanogr. Mar. Sci.* 10, 22–32. doi: 10.5897/joms2019.0156

Millero, F. (2013). *Chemical Oceanography*, *4th ed*. (Boca Raton, Florida, USA: CRC Press). doi: 10.1201/b14753

Mollica, N. R., Guo, W., Cohen, A. L., Huang, K. F., Foster, G. L., Donald, H. K., et al. (2018). Ocean acidification affects coral growth by reducing skeletal density. *Proc. Natl. Acad. Sci. U.S.A.* 115, 1754–1759. doi: 10.1073/pnas.1712806115

Moreira, Á., and Alfonso, G. (2013). Inusual arribazón de Sargassum fluitans (Børgesen) Børgesen en la costa centro-sur de Cuba. *Rev. Investig. Mar.* 33, 17–20.

Morse, J. W., Andersson, A. J., and Mackenzie, F. T. (2006). Initial responses of carbonate-rich shelf sediments to rising atmospheric pCO2 and "ocean acidification": Role of high Mg-calcites. *Geochim. Cosmochim. Acta* 70, 5814–5830. doi: 10.1016/j.gca.2006.08.017

Nagelkerken, I., Blaber, S. J. M., Bouillon, S., Green, P., Haywood, M., Kirton, L. G., et al. (2008). The habitat function of mangroves for terrestrial and marine fauna: A review. *Aquat. Bot.* 89, 155–185. doi: 10.1016/j.aquabot.2007.12.007

NOAA (2003). Rule to implement fishery management plan for pelagic sargassum habitat of the south atlantic region. *Fed. Regist.* 68.

Odum, H., Burkholder, P., and Rivero, J. (1959). Measurement of productivity of turtle grass flats, reefs, and the bahia fosforescente of southern Puerto Rico. *Inst. Mar. Sci.* VI, 159–170.

Oviatt, C. A., Huizenga, K., Rogers, C. S., and Miller, W. J. (2019). What nutrient sources support anomalous growth and the recent Sargassum mass stranding on Caribbean beaches? A review. *Mar. pollut. Bull.* 145, 517–525. doi: 10.1016/j.marpolbul.2019.06.049

Pérez-Pérez, J., Cruz Motta, J. J., Hernández López, W. J., and Morales Payán, J. P. (2022). *Impacts of floating Sargassum accumulation on the fringing mangrove Rhizophora mangle in Southwestern Puerto Rico: A Case Study* (Mayagüez, Puerto Rico: University of Puerto Rico at Mayagüez).

Pérez-Posada, I., Cabanillas-Terán, N., Rosas-Luis, R., Hernández-Arana, H. A., and Sánchez-Gonzalez, A. (2023). Isotopic niche shift in the sea urchins Echinometra lucunter and E. viridis after massive arrivals of Sargassum in the Mexican Caribbean. *Regional. Stud. Mar. Sci.* 65, 103064. doi: 10.1016/j.rsma.2023.103064

Powers, L. C., Hertkorn, N., McDonald, N., Schmitt-Kopplin, P., Del Vecchio, R., Blough, N. V., et al. (2019). Sargassum sp. Act as a large regional source of marine dissolved organic carbon and polyphenols. *Global Biogeochem. Cycles.* 33, 1423–1439. doi: 10.1029/2019GB006225

Putman, N. F., Goni, G. J., Gramer, L. J., Hu, C., Johns, E. M., Trinanes, J., et al. (2018). Simulating transport pathways of pelagic Sargassum from the Equatorial Atlantic into the Caribbean Sea. *Prog. Oceanogr.* 165, 205–214. doi: 10.1016/j.pocean.2018.06.009

Rabalais, N. N., Turner, R. E., and Wiseman, W. J. (2002). Gulf of Mexico hypoxia, a.k.a. "The dead zone. *Annu. Rev. Ecol. Syst.* 33, 235–263. doi: 10.1146/annurev.ecolsys.33.010802.150513

Robertson, M. L., Mills, A. L., and Zieman, J. C. (1982). Microbial synthesis of detritus-like particulates from dissolved organic carbon released by tropical seagrasses. *Mar. Ecol. Prog. Ser.* 7, 279–285. doi: 10.3354/meps007279

Rodríguez-Martínez, R. E., Medina-Valmaseda, A. E., Blanchon, P., Monroy-Velázquez, L. V., Almazán-Becerril, A., Delgado-Pech, B., et al. (2019). Faunal mortality associated with massive beaching and decomposition of pelagic Sargassum. *Mar. pollut. Bull.* 146, 201–205. doi: 10.1016/j.marpolbul.2019.06.015

Sánchez, A., Gonzalez-Jones, P., Camacho-Cruz, K. A., Anguas-Cabrera, D., Ortiz-Hernández, M. C., and Rey-Villiers, N. (2023). Influence of pelagic sargassum influxes on the δ15N in Thalassia testudinum of the Mexican Caribbean coastal ecosystem. *Mar. pollut. Bull.* 192, 115091. doi: 10.1016/j.marpolbul.2023.115091

Sánchez-Beristain, F., García-Barrera, P., and Calvillo-Canadell, L. (2016). Mares calcíticos y aragoníticos: efectos en organismos formadores de arrecifes a través del tiempo. *TIP* 19, 45–53. doi: 10.1016/j.recqb.2016.02.005

Skliris, N., Marsh, R., Appeaning Addo, K., and Oxenford, H. (2022). Physical drivers of pelagic sargassum bloom interannual variability in the Central West Atlantic over 2010–2020. *Ocean. Dynamics.* 72, 383–404. doi: 10.1007/s10236-022-01511-1

Sonter, L. J., Herrera, D., Barrett, D. J., Galford, G. L., Moran, C. J., and Soares-Filho, B. S. (2017). Mining drives extensive deforestation in the Brazilian Amazon. *Nat. Commun.* 8, 1013. doi: 10.1038/s41467-017-00557-w

Sutton, A. J., Sabine, C. L., Feely, R. A., Cai, W. J., Cronin, M. F., McPhaden, M. J., et al. (2016). Using present-day observations to detect when anthropogenic change forces surface ocean carbonate chemistry outside preindustrial bounds. *Biogeosciences* 13, 5065–5083. doi: 10.5194/bg-13-5065-2016

Valdés-Pizzini, M., and Schärer-Umpierre, M. (2014). People, habitats, Species, and Governance: An Assessment of the Social-Ecological System of La Parguera, Puerto Rico. Available online at: http://www.seagrantpr.org/catalog/files/books/La_Parguera.pdf (Accessed February 18, 2025).

Valiela, I., McClelland, J., Hauxwell, J., Behr, P. J., Hersh, D., and Foreman, K. (1997). Macroalgal blooms in shallow estuaries: Controls and ecophysiological and ecosystem consequences. *Limnol. Oceanogr.* 42, 1105–1118. doi: 10.4319/lo.1997.42.5_part_2.1105

van Tussenbroek, B. I., Hernández Arana, H. A., Rodríguez-Martínez, R. E., Espinoza-Avalos, J., Canizales-Flores, H. M., González-Godoy, C. E., et al. (2017). Severe impacts of brown tides caused by Sargassum spp. on near-shore Caribbean seagrass communities. *Mar. pollut. Bull.* 122, 272–281. doi: 10.1016/j.marpolbul.2017.06.057

Vaquer-Sunyer, R., and Duarte, C. M. (2008). Thresholds of hypoxia for marine biodiversity. *Proc. Natl. Acad. Sci.* 105, 15452–7. doi: 10.1073/pnas.0803833105

Vega-Rodríguez, M., Armstrong, R. A., Gilbes, F., López, J., and Fernandez del Viso, D. (2008). *Estimating primary productivity of red mangroves in southwestern Puerto Rico from remote sensing and field measurements (Master's thesis).* (Mayagüez, Puerto Rico: University of Puerto Rico at Mayagüez).

Wallace, R. B., Baumann, H., Grear, J. S., Aller, R. C., and Gobler, C. J. (2014). Coastal ocean acidification: The other eutrophication problem. *Estuar. Coast. Shelf. Sci.* 148, 1–13. doi: 10.1016/j.ecss.2014.05.027

Wang, M., and Hu, C. (2016). Mapping and quantifying Sargassum distribution and coverage in the Central West Atlantic using MODIS observations. *Remote Sens. Environ.* 183, 356–367. doi: 10.1016/j.rse.2016.04.019

Wang, M., Hu, C., Barnes, B. B., Mitchum, G., Lapointe, B., and Montoya, J. P. (2019). The great Atlantic Sargassum belt. *Sci. (1979).* 365, 83–87. doi: 10.1126/science.aaw7912

Wang, M., Hu, C., Cannizzaro, J., English, D., Han, X., Naar, D., et al. (2018). Remote sensing of sargassum biomass, nutrients, and pigments. *Geophys. Res. Lett.* 45, 12,359–12,367. doi: 10.1029/2018GL078858

Weis, J. S. (1968). Fauna associated with pelagic sargassum in the gulf stream. *Source.: Am. Midland. Nat.* 80, 554–558. doi: 10.2307/2423550

frontiers | Frontiers in Marine Science

TYPE Original Research
PUBLISHED 12 August 2025
DOI 10.3389/fmars.2025.1595871

OPEN ACCESS

EDITED BY
Martin F. Soto-Jimenez,
National Autonomous University of Mexico, Mexico

REVIEWED BY
Juan Carlos Carrasco Navas-Parejo,
University of Cádiz, Spain
Raffi Isah,
University of Hawaii at Manoa, United States
Maria Lourdes San Diego-McGlone,
University of the Philippines Diliman, Philippines

*CORRESPONDENCE
Alberto Acosta
laacosta@javeriana.edu.co

RECEIVED 18 March 2025
ACCEPTED 22 July 2025
PUBLISHED 12 August 2025

CITATION
Murcia A, Acosta A, Garcia AP, Corredor-Acosta A, Hernández-Ayón JM, Guitiérrez S, Celis C and Ruiz-Pino D (2025) High-resolution monitoring of the pH under strong La Niña conditions in Gorgona Island, Colombian Pacific, Panama Bight. *Front. Mar. Sci.* 12:1595871. doi: 10.3389/fmars.2025.1595871

High-resolution monitoring of the pH under strong La Niña conditions in Gorgona Island, Colombian Pacific, Panama Bight

Andrea Murcia[1], Alberto Acosta[1*], Alejandro P. Garcia[1], Andrea Corredor-Acosta[2,3], José Martín Hernández-Ayón[4], Simón Guitiérrez[1], Crispín Celis[5] and Diana Ruiz-Pino[6]

[1]UNESIS (Unidad de Ecología y Sistemática), Departamento de Biología, Facultad de Ciencias, Pontificia Universidad Javeriana, Bogotá, Colombia, [2]División de Investigación en Acuicultura, Instituto de Fomento Pesquero (IFOP), Putemún, Chile, [3]Centro FONDAP de Investigación en Dinámica de Ecosistemas Marinos de Altas Latitudes (IDEAL), Instituto de Acuicultura y Ciencias Ambientales, Universidad Austral de Chile, Puerto Montt, Chile, [4]Instituto de Investigaciones Oceanológicas, Universidad Autónoma de Baja California, Ensenada, Baja California, Mexico, [5]Laboratorio de Fitoquímica, Línea de Investigación en Tecnología Ambiental y de Materiales, Departamento de Química, Facultad de Ciencias, Pontificia Universidad Javeriana, Bogotá, Colombia, [6]Sorbonne Universités (UPMC, Univ Paris 06)-CNRS-IRD-MNHN, LOCEAN Laboratory-IPSL, Paris, France

Few studies have investigated the potential drivers of high-resolution (daily and 24-hour scales) on ocean acidification (OA) and the carbonate system in a coastal estuary during an intense La Niña event. Therefore, we conducted the first high-resolution total scale pH (pH_T) monitoring every three hours for 56 days (13 September to 7 November 2021) at the Colombian Pacific in El Muelle reef, Gorgona National Natural Park. Two moored autonomous submersible instruments (iSAMI-pH and CTD-Diver) were deployed at a depth of 2 m in an area influenced by extreme precipitation, river discharge, semi-diurnal tides, and southwest winds during La Niña 2020-2023. Total alkalinity was derived from salinity data and used alongside pH_T to calculate sea surface seawater partial pressure of CO_2 (pCO_{2w}; µatm), dissolved inorganic carbon (DIC; µmol kg^{-1}), and omega aragonite saturation (Ω_a). The findings suggest that the observed low pH (7.93) and aragonite saturation state (Ω_a = 2.22) values are likely attributed to increased precipitation. This enhanced precipitation resulted in higher river discharge, transporting naturally low-pH water to the island via mixing mechanisms (RiOMar type 2). Daily, decreasing solar radiation may reduce the seawater temperature, simultaneously elevating the pCO_{2w} levels and reducing pH_T. In contrast, elevated precipitation may reduce surface seawater salinity through freshwater dilution. Throughout the diurnal cycle, peak pH_T values were recorded during late afternoon hours, likely driven by photosynthetic activity, while minimum values coincided with early morning periods of maximal respiratory activity. These results underscore the dynamic nature of this area and emphasize the need for long-term evaluation.

KEYWORDS

ocean acidification, riverine input, ENSO, RioMar, coral reef

1 Introduction

Ocean acidification (OA) driven by human-induced increases in atmospheric carbon dioxide (CO_2) (Sabine et al., 2004; Feely et al., 2009) has significantly altered carbonate chemistry, leading to increased concentration of hydrogen ions [H^+] and reduced global pH levels (Kleypas et al., 1999; Caldeira and Wickett, 2003; Gattuso et al., 2015). The El Niño–Southern Oscillation (ENSO) modulates OA. During El Niño events in the Eastern Tropical Pacific, reduced trade winds weaken equatorial upwelling, limiting the transport of cold, nutrient- and carbon-rich waters from the deep ocean to the surface (Vaittinada Ayar et al., 2022). As a result, surface dissolved inorganic carbon (DIC) concentrations decrease, leading to relatively lower seawater pCO_{2w} and reduced CO_2 outgassing to the atmosphere (Feely et al., 2006; Ishii et al., 2014; Espinoza-Morriberón et al., 2019). In contrast, La Niña events strengthen the trade winds and enhance upwelling, bringing DIC and nutrient-rich waters to the surface (Vaittinada Ayar et al., 2022). This increase in upwelling elevates pCO_{2w} levels, thereby increasing CO_2 outgassing (Yasunaka et al., 2019) and can lead to lower pH levels in coastal waters, intensifying OA (Oliva-Méndez et al., 2018).

La Niña event also induces increased rainfall, which enhances river discharge in coastal areas (Restrepo and Kjerfve, 2000; Hernández et al., 2006; Blanco, 2009). This influx of freshwater significantly reduces the buffering capacity of estuaries to neutralize acids and maintain stable pH levels, because freshwater lacks the carbonate buffer system found in seawater. These conditions increase the solubility of CO_2 and reduce the dissociation of bicarbonates (HCO_3^-) into carbonate ions (CO_3^{-2}; Cai et al., 2021). Additionally, rivers contribute to pH reduction by transporting organic matter, which releases carbon dioxide as it oxidizes upon reaching the sea (Salisbury et al., 2008; Zhai et al., 2015; Vargas et al., 2016). Moreover, nutrients from land and rivers are transported to coastal waters via runoff, forming low-salt river plumes that extend to the continental shelf, driven by winds and tides (Dai et al., 2022a). The areas influenced by these plumes, associated with the 19 largest rivers globally, cover an average of 3.7×10^6 km^2 annually (Kang et al., 2013), representing approximately 14% of the total global continental shelf area (Dai et al., 2022a). Thus, salinity variations in estuary systems are determined by the mixing process influenced by tidal movements, precipitation, river discharges, and seawater influx (Atekwana et al., 2022).

In the Colombian Caribbean, La Niña events have been observed to intensify precipitation, leading to increased freshwater inflow and a subsequent dilution that significantly reduces DIC and total alkalinity (TA) (Ricaurte-Villota et al., 2025). Furthermore, heavy rains in the tropical Pacific Ocean can modify salinity, with dilution effects persisting for over 10 days (Henocq et al., 2010). This phenomenon decreases two key parameters of the carbonate system: TA and DIC (Turk et al., 2010; Ashton et al., 2016; Ho and Schanze, 2020). The relationship between low salinity and variations in the carbonate system has also been documented in other coastal regions of the Eastern Tropical Pacific (10°N), where precipitation influences can extend over 40,000 km^2, due to surface ocean currents dispersing freshwater over larger areas (Ho and Schanze, 2020).

Estuaries and coastal waters present greater complexity compared to open ocean waters when estimating OA and the carbonate system, as they are highly variable environments due to the mixing of seawater and freshwater (Wang et al., 2019; Nehir et al., 2022). Additionally, these Tropical Pacific waters, often influenced by anthropogenic activities, are critical for acidification studies. However, their complexity and the time scales (ranging from hours to interannual changes) require high-resolution monitoring to accurately assess OA (Carstensen et al., 2018; Nehir et al., 2022). One of the key parameters to monitor in estuaries is the natural variation of water pH (Nehir et al., 2022), which is typically measured using the National Bureau of Standards scale (pH_{NBS}) and total pH scales (pH_T). The pH_T is preferred in oceanography due to its accuracy. It also considers other factors that affect proton activity in complex solutions such as seawater, including the presence of salts (Fassbender et al., 2021).

The equatorial Pacific waters are characterized by lower pH values (8.00; Zhong et al., 2025) compared to the global average (8.05; von Schuckmann et al., 2024), making this region a key area for analyzing OA and its ecological impacts. To address this, continuous monitoring efforts using *in situ* submersible spectrophotometric sensors, such as Lab-on-Chip (Yin et al., 2021; Nehir et al., 2022) and the iSAMI-pH (Valauri-Orton et al., 2025), have proven effective for small-scale autonomous monitoring of the total pH scale (pH_T). For example, in the Pacific Coastal Ocean, significant pH_T variation (7.93 to 8.37) has been associated with upwelling events (Monterey Bay, USA) which increase pCO_{2w} and reduce pH_T (Gray et al., 2011). In contrast, during periods without upwelling and in the rainy season, a more minor pH_T variation (ranging from 7.98 to 8.06) has been observed along the Pacific coast of Costa Rica (Bahia Culebra; Sánchez-Noguera et al., 2018). In this region, a distinct 24-hour cycle was detected, with the lowest pH_T occurring in the early morning hours, due to organic matter respiration at night, and the highest pH_T values recorded in the late afternoon, associated with photosynthesis (Sánchez-Noguera et al., 2018).

In the Colombian Pacific Ocean, high-resolution measurements of pH_T have not been conducted. Instead, discrete measurements related to carbonate chemistry and pH_{NBS} have primarily been performed in the Caribbean Sea and the Pacific Ocean, including sampling sites around Gorgona National Natural Park (GNNP) by Instituto de Investigaciones Marinas y Costeras José Benito Vives de Andréis (INVEMAR) as part of the program "Red de Vigilancia para la Conservación y Protección de las Aguas Marinas y Costeras de Colombia (REDCAM)". In Tayrona National Natural Park, studies such as those by Ricaurte-Villota et al. (2025) have collected discrete samples of pH_{NBS}, TA, and DIC, revealing high variability strongly influenced by coastal upwelling, precipitation, and river runoff, which are further affected by ENSO events. The high variability of oceanographic processes in coastal regions underscores the need for high-resolution monitoring, as discrete measurements are limited in their ability to capture natural variability and achieve sufficient temporal resolution (Nehir et al.,

2022). Gorgona National Natural Park, located on the Colombian Pacific continental shelf, is a potential hotspot for OA due to its exposure to frequent ENSO events, which drive significant climate variability through El Niño and La Niña events (Lavín et al., 2006; Emerton et al., 2017; Fiedler and Lavín, 2017; Berri et al., 2019). As part of the Eastern Tropical Pacific (ETP), it is influenced by the Choco Jet, which brings intense precipitation from September to November (Serna et al., 2018; Guzmán et al., 2014), further increasing the already high fluvial discharge from the Patia-Sanquianga deltaic complex, the largest in Colombia (Díaz, 2007). Additionally, the Intertropical Convergence Zone (ITCZ) intensifies cloudiness and precipitation during this period, reducing solar radiation and potentially impacting the carbonate system and OA by altering water temperature and CO_2 solubility, as observed in other regions (Webster, 2020; Cai et al., 2021).

Therefore, this study investigates fine-scale, high-frequency dynamics in coastal carbonate chemistry using continuous measurements of pH_T, temperature, salinity, and derivation of TA, DIC, $pCO_{2w,}$ and omega aragonite saturation (Ω_a). Focusing on Gorgona National Natural Park (GNNP) in the Colombian Pacific Ocean (Panama Bight), it examines how freshwater pulses during strong rainy season La Niña events modulate coastal carbonate buffering capacity and influence pH stability and ecosystem resilience to ocean acidification under climatic stress. This study uses a fixed mooring equipped with autonomous sensors to characterize high-frequency variability (daily over 56 days and hourly over 24 hours) of pH_T and other carbon chemistry variables (TA, pCO_{2w}, and DIC). Additionally, it explores the influence of tidal dynamics (ebb vs. flood) on variations in pH_T, salinity, temperature, pCO_{2w}, DIC, and TA, synchronizing high-resolution measurements from the iSAMI-pH and CTD-Diver with tide height data to identify primary sources of pH_T variation (oceanic vs. riverine influences). Furthermore, the relationships, both in magnitude and direction, between pH_T, salinity, temperature, pCO_{2w}, DIC, and TA, with external drivers such as daily solar radiation and daily precipitation (influenced by the Intertropical Convergence Zone, ITCZ) were analyzed. Daily mean values of the dependent variables were calculated to assess their response to these environmental factors under extreme climatic and hydrological dynamics. Finally, the study evaluates whether pH_T, salinity, temperature, pCO_{2w}, DIC, and TA exhibit significant differences between early morning and late afternoon within a 24-hour daily cycle, providing insights into diurnal variability in the study area. By addressing the critical role of fine-scale processes in shaping coastal carbonate chemistry, this research fills a significant gap in understanding the dynamics of coastal systems under extreme conditions.

2 Methods

2.1 Study area

The Gorgona National Natural Park (GNNP; 2° 55'45" - 3° 00' 55" N, 78° 09' 00″ - 78° 14' 30" W) is located on the continental shelf of the Colombian Pacific basin (Figure 1). This region is characterized by warm and low-salinity surface waters (Giraldo López, 2008; Giraldo et al., 2008, 2011, 2014), and constitutes one of the rainiest regions of the world, being also the rainiest area of Colombia with annual values ranging from 2500 mm to 8000 mm (Rangel and Rudas, 1990; Blanco, 2009). This condition is mainly associated with the latitudinal migration of the Intertropical Convergence Zone (ITCZ; Díaz Guevara et al., 2008) and the Choco Jet Stream, which increases cloudiness and precipitation due to the convergence of trade winds from the northern and southern hemispheres (Prahl et al., 1990; Díaz Guevara et al., 2008; Guzmán et al., 2014; Serna et al., 2018). During the second half of the year, the ITCZ moves north, altering the wind direction near 3° N latitude, which becomes dominant in the southwesterlies and forms the Choco Jet off western Colombia (Poveda and Mesa, 2000; Amador et al., 2006; Guerrero Gallego et al., 2012). During the study period (September 13 to November 7, 2021), the area was affected by the strong La Niña 2020–2023 event (thermal anomalies of -1.4 ± 0.1°C; Supplementary Table 1, IDEAM, 2021) that increased total precipitation in the Colombian Pacific.

Gorgona Park is in front of the Patia-Sanquianga delta complex (Figure 1B), the largest in the country, which contributes approximately 23% of the total freshwater discharged to the Colombian Pacific (2045 m^3 s^{-1}; Díaz, 2007). This delta comprises several rivers, including the Guapi, Patia, Iscuande, Tapaje, and Sanquianga (Díaz, 2007, Figure 1B). Likewise, the tidal regime around GNNP is semi-diurnal, repeating twice in 24 hours, with two alternating high tides (5.82 m) and two low tides (-0.78 m; Flanders Marine Institute [VLIZ] and Intergovernmental Oceanographic Commission [IOC], 2025).

The Pacific coast has an average daily solar radiation of 3500 to 4000 Wh m^{-2} and an annual availability of solar radiation that varies between 1,080,000 and 1,440,000 Wh m^{-2} (UPME, 2005). During the year's second half, solar radiation decreases until it reaches its minimum in December (Rangel and Rudas, 1990). Regarding its biodiversity, GNNP hosts one of the most critical coral reef areas in the Eastern Tropical Pacific (ETP) region in terms of structure and species diversity (Glynn et al., 1982; Zapata, 2001; Díaz et al., 2001) and connects the ETP with other Pacific regions (e.g., Hawaii, Polynesia) via larval potential dispersion (Romero-Torres et al., 2018). Remarkably, these reefs persist despite being regularly exposed to multiple environmental stressors. At the beginning of the year, they experience sub-aerial exposure during extreme low tides (Zapata, 2001; Zapata et al., 2010), low pH levels reaching as low as 7.4 (Giraldo and Valencia, 2013), cooler temperatures (16.69 °C; Giraldo et al., 2008), and hypoxic conditions (< 3.7 mg L^{-1}) associated with seasonal upwelling (Castrillón-Cifuentes et al., 2023a, b). During the second half of the year, these reefs are subjected to low salinity levels during the rainy season (as low as 25; Giraldo et al., 2008), warmer temperatures (27 °C; Giraldo et al., 2008), and increased sedimentation rates (23.30 ± 4.34 g m^{-2} d^{-1}; Lozano-Cortés et al., 2014). Coral species such as *Pocillopora* spp. and *Pavona* spp. dominate the eastern (leeward) and southern areas of Gorgona Island, while occurring more sparsely in the western and northern areas (Figure 1A, Zapata, 2001). The sampling point (Figure 1A) was located at the north end of El Muelle reef

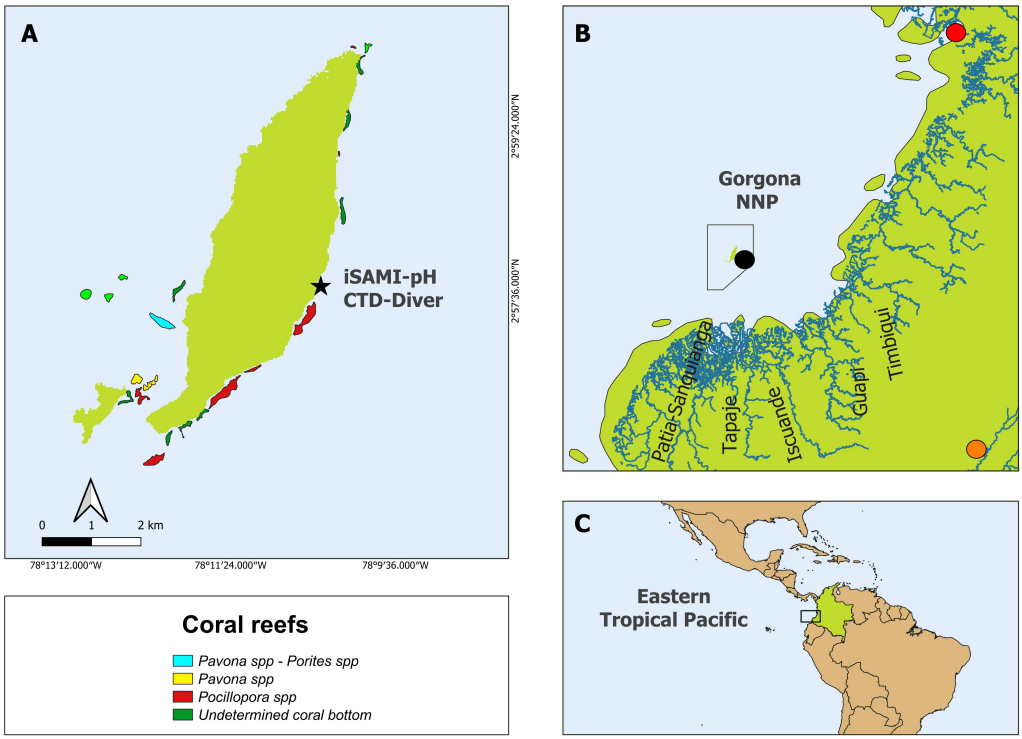

FIGURE 1
Location of Gorgona National Natural Park in the Colombian Pacific Ocean, Eastern Tropical Pacific (ETP). **(A)** iSAMI-pH and CTD-Diver measurements at El Muelle reef (black star). The colored polygons show the coral reefs (*Pavona* spp - *Porites* spp, *Pavona* spp, and *Pocillopora* spp) around Gorgona according to Colombia's Atlas of Coral Areas until 2020 (INVEMAR, 2020a). **(B)** The black polygon shows the protected area of Gorgona Park and its proximity to the Pacific coast (around 50 km), as well as the main rivers influencing the island (Guapi River, Patia - Sanquianga Rivers, Tapaje River, and Iscuande River). The black dot represents the "57025020 Gorgona Guapi" pluviometric station (DHIME, 2025), the orange dot represents the "26015040 Arrayanales" for solar radiation measurements (DHIME, 2025), while the red point represents the Buenaventura station for tide height measurements (Flanders Marine Institute [VLIZ] and Intergovernmental Oceanographic Commission [IOC], 2025). **(C)** Square showed the island's position within the ETP. The red polygon shows the Panama Bight, which includes the Panama and Colombian Pacific basins.

(northward surface current), where the genus *Pocillopora* spp. predominantly dominates this and the major eastern coral patch of Azufrada (Zapata, 2001; Romero-Torres and Acosta, 2010).

2.2 *In situ* measurements

Continuous measurements of pH_T, conductivity (mS cm^{-1}), and temperature (°C) were made at a fixed depth of around 2 meters in El Muelle reef, GNNP (2° 57' 39" N, 78° 10' 25" W; Figure 1A) from 13 September to 07 November 2021, every three hours, using a buoy anchoring system designed to compensate the tidal changes and to keep the equipment at a similar depth. The iSAMI-pH equipment (programmed with SAMI Client v2.5 software) was used to record pH_T (accuracy: 0.0004 and precision: ± 0.0024) and temperature (accuracy: ± 0.14°C; at 24.55 °C Tris bottle number 10 Sunburst Sensors). The CTD Diver equipment (programmed with Diver Field software, Van Essen Instruments) was used to take conductivity measurements (accuracy: ± 1% mS cm^{-1}). Conductivity data were also downloaded using Diver Field software. The salinity was calculated using the practical scaling relationship proposed by Aminot and Kérouel (2004). The iSAMI-pH data were downloaded with the SAMI program (QC pH v4.4). Because the QC pH v4.4 program handles a constant salinity of 35 units by default, the pH_T data were corrected for salinity. To do the correction, the program was set to the corresponding average salinity (29.74 ± 0.94, 31.29; mean ± SD, maximum, n = 403) of the sampling point (2° 57' 39" N, 78° 10' 25" W). With the correction, differences in pH_T of ± 0.01 units were observed. We used the average salinity value to ensure consistency in salinity correction, as the CTD Diver recorded salinity 30 minutes after iSAMI-pH measurements from October 10 to November 7. When both devices recorded simultaneously between September 13 and October 10, the difference between pH corrected with average and measured salinity was insignificant (± 0.0001). iSAMI recorded 49 outliers out of 441 data points, which were excluded from the analysis as iSAMI-pH identified them as measurement anomalies (error codes 100, 1001, 1010, and 1000) associated with issues related to pumping, dye supply, or blank measurement. Additionally, 19 temperature and 38 salinity data points were identified as outliers when plotting variables and their relationship to total pH_T. These points were excluded from the analysis after applying a criterion based on standard deviation to consecutive measurements. Any change greater than 0.030 in pH,

0.30°C in temperature, or 0.94°C in salinity between measurements was considered a potential outlier. Flagged data points underwent contextual evaluation, considering environmental consistency (e.g., salinity-TA relationships, diel cycles, water mass characteristics), sensor artifacts, and physical plausibility. Only measurements inconsistent both statistically and contextually were excluded.

2.3 Carbonate system derivation

Total alkalinity (TA; µmol kg^{-1}) was calculated using a regression line between salinity (*in situ* data taken with CastAway-CTD equipment) and TA. Preciado (2023) built the regression (y = 57.479x+249.08; R2 = 0.94; n=268) using measured local discrete TA data obtained from 8 sampling stations around Gorgona, one of which included the iSAMI-pH deployment site. The data were collected over 13 sampling months, from September 2021 to October 2022, at depths ranging from 2 to 80 meters, following the SOP-3b protocol (Dickson et al., 2007). Discrete samples of TA (± 13 µmol kg^{-1}, Batch #182 2230.91µmol kg^{-1}) were collected monthly at the iSAMI-pH site from November 2021 to July 2022. Comparing the measured TA values with those estimated from salinity, a mean difference of 11 ± 5 µmol kg^{-1} and a regression coefficient of $R^2 = 0.91$ were observed (Supplementary Figure 1). Specifically, in November 2021, the difference was 10 ± 3 µmol kg^{-1}. This regression approach for estimating TA through salinity has been validated in previous studies (Lee et al., 2006; Takatani et al., 2014; Carter et al., 2016; Fassbender et al., 2017; Metzl et al., 2024).

For the derivation of the carbonate system pCO_{2w} (µatm), dissolved inorganic carbon (DIC; µmol kg^{-1}), and omega aragonite (Ω_a), we used the Carbonate System equation solution (CO2sys v3.0, Pierrot et al., 2021), with the pair pH_T (n = 392) from iSAMI-pH and TA derived from the former regression, as well as salinity from CTD (Aminot and Kérouel, 2004) and temperature (iSAMI-pH). Propagation error analysis using CO2sys v3.0 estimated uncertainties of ±52 µmol·kg^{-1} for DIC, ± 33 µatm for pCO_2, and ±0.16 for Ω_a. In the carbonate system equation solution, the following constants were used: (i) Dissociation constants for K_1 and K_2 from Millero, 2010) for waters ranging from 0 to 40, given that the study area the salinities variation are between 27.03 to 31.29, (ii) $KHSO_4$ dissociation constant from Dickson (1990), (iii) KHF from Perez and Fraga (1987), (iv) Total pH scale (mol-kg SW), (v) [B]T value from Lee et al. (2010), and (vi) EOS-80 standard.

To evaluate the influence of temperature and salinity, pH_T was normalized using the mean temperature (27.39°C) and salinity (29.74), as recommended by Terlouw et al. (2019). Additionally, normalization was performed using constant values representing the minimum observed temperature (26.72°C) and salinity (27.03), to account for the most extreme conditions in the dataset (Supplementary Figure 2). This normalization process isolates the potential effect of temperature and salinity on pH_T, following the methodology outlined by Sarmiento and Gruber (2006). The influence of temperature and salinity corresponds to the difference between the normalized pH_T and the *in situ* measured pH_T.

2.4 Statistical analysis: evaluation of external forcing on carbon chemistry

2.4.1 Tidal movement data

Daily tide measurements (m) between 13 September and 07 November 2021 were obtained from the UNESCO Sea Level Monitoring Facility database (Flanders Marine Institute [VLIZ] and Intergovernmental Oceanographic Commission [IOC], 2025), specifically from the Buenaventura station (3° 53' 26" N, 77° 4' 51" W), which measures the tide using a radar sensor. These tide measurements were temporally synchronized with iSAMI-pH and CTD-Diver data and subsequently labeled according to the water movement (ebb or flood; Supplementary Figure 3). The dependent variables do not meet the assumptions of normality, so non-parametric tests were chosen (Supplementary Table 2). The Kruskal-Wallis nonparametric test was used to determine if there were significant differences ($p < 0.05$) in the dependent variables (pH_T, salinity, temperature, pCO_{2W}, DIC, and TA) when comparing tidal movements (ebb and flood tides).

2.4.2 Atmospheric variables, solar radiation, and precipitation, and correlation with carbon chemistry

For the study period, 56 days, daily solar radiation (Wh m^{-2}) was obtained from the "26015040 Arrayanales" fixed station (2° 26' 53" N, 76° 26' 9" W; DHIME, 2025), and daily total precipitation (mm) from the "57025020 Gorgona Guapi" fixed station (2° 57' 47" N, 78° 10' 28" W; DHIME, 2025).

Daily means of the dependent variables (pH_T, salinity, temperature, pCO_{2W}, DIC, and TA) were calculated. A Spearman correlation analysis was performed between the dependent physical and chemical parameters and atmospheric variables (solar radiation and total precipitation) to evaluate the importance and direction of their relationship (rho value).

2.4.3 Hour carbon chemistry cycle analysis

The hourly cycle analysis was performed by calculating the average of the variables (pH_T, salinity, temperature, pCO_{2W}, DIC, and TA) taken at the same hour every three hours between 13 September and 7 November 2021. Carbonate alkalinity was also calculated following the equation proposed by Munhoven, 2013:

$$Alk_C = [HCO_3^-] + 2[CO_3^{2-}]$$

The Kruskal-Wallis test executed in RStudio was used to determine if there were significant differences (p-value < 0.05) in the dependent variables (pH_T, salinity, temperature, pCO_{2W}, DIC, TA, and carbonate alkalinity) when comparing the early morning hours (5:00 - 6:00) with the late afternoon hours (17:00 - 18:00).

3 Results

The sampling period took place during a year with strong La Niña conditions displaying atmospheric thermal anomalies of -1.4

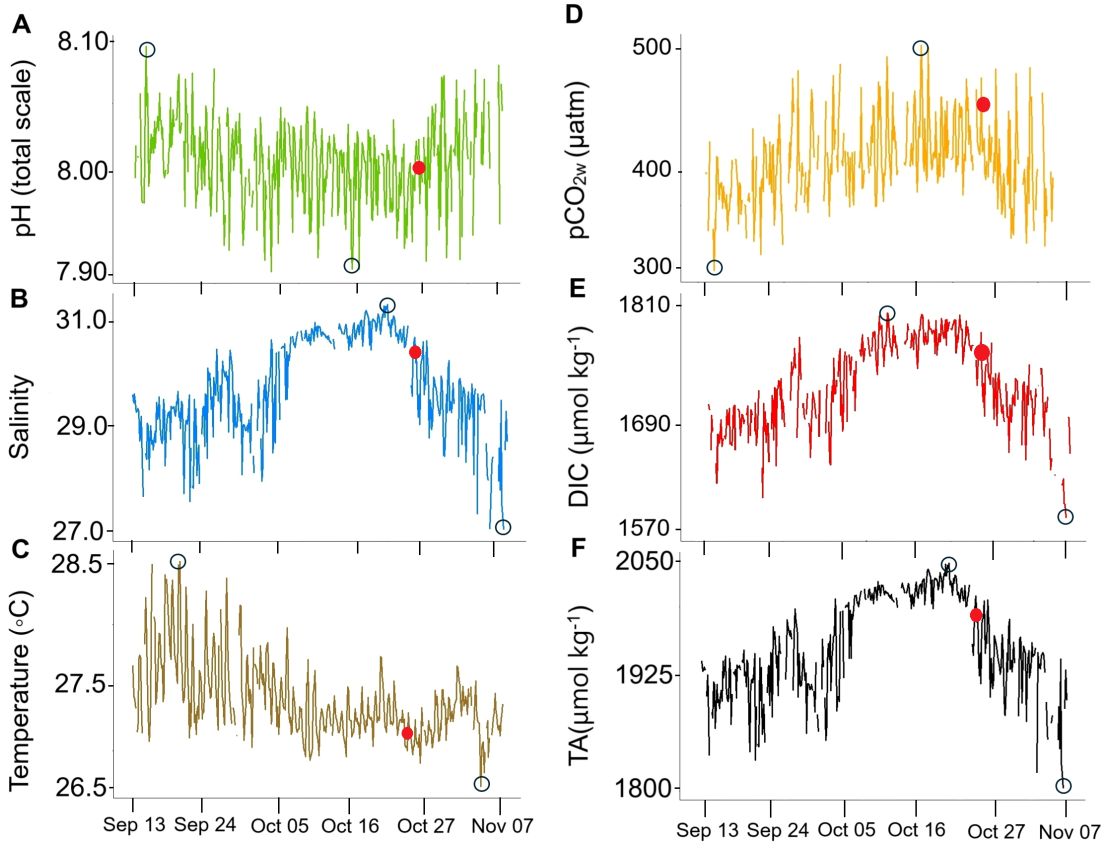

FIGURE 2
High-frequency measurements of **(A)** pH_T (green), **(B)** salinity (blue), **(C)** temperature (brown), **(D)** pCO_{2w} (orange), **(E)** dissolved inorganic carbon (DIC; red), and **(F)** total alkalinity (TA; black) every three hours between September 13 and November 07, 2021. The black circles highlight each variable's highest and lowest values, while the red dot marks October 25, when pH_T began to increase and pCO_{2w}, salinity, TA, and DIC began to decrease.

± 0.1°C (Supplementary Table 1; IDEAM, 2021) and extreme precipitation values (959 ± 316 mm/monthly; DHIME, 2025). Throughout the study period, pH_T decreased from September until October 25 (Figure 2), after which it increased until November 7, while pCO_{2w}, DIC, and salinity increased until October 25 and then decreased until November 7. Throughout the study period, pH_T and pCO_{2w} exhibited opposite trends (Figure 2), with lower pH_T values corresponding to higher pCO_{2w} levels and vice versa (Table 1). pH_T averaged 8.01 ± 0.03, peaking on September 15 (8.09), then decreasing until October 25, reaching a minimum on October 16 (7.93), before increasing again until November 7. In contrast, pCO_{2w} averaged 397 ± 36 µatm, reaching its minimum on September 15 (302 µatm), increasing until October 25, reaching a maximum on October 16 (499 µatm), and then decreasing until November 7. Salinity averaged 29.74 ± 0.94, increasing until October 25, with a peak on October 20 (31.29), then decreasing until November 7, reaching its minimum on that date (27.03). Similarly, TA averaged 1959 ± 54 µmol kg^{-1}, increasing until October 25, with a maximum on October 20 (2048 µmol kg^{-1}), then decreasing until November 7, when it reached its minimum (1803 µmol kg^{-1}). DIC followed a similar pattern, averaging 1728 ± 49 µmol kg^{-1}, increasing until October 25, with a maximum on October 11 (1807 µmol kg^{-1}), and decreasing until November 7, with a minimum on November 5 (1574 µmol kg^{-1}). The temperature averaged 27.39 ± 0.30°C, with a peak on September 20 (28.50°C), decreasing until October 9 and remaining stable until October 25 (27.25 ± 0.16°C), before oscillating until November 7, when it reached a minimum on November 4 (26.72°C).

When pH_T was normalized using salinity and temperature, the variation attributed to mean salinity reached up to 0.001 pH units, and up to 0.047 pH units when using the minimum salinity. In contrast, minor temperature-related variations reached only 0.000028 pH units with the mean temperature and 0.017 pH units with the minimum temperature. These results suggest that salinity plays a more significant role than temperature in driving pH_T variability (Supplementary Figure 2).

3.1 Tidal movement

No significant differences were found between high and low tides for the dependent variables of pH_T, salinity, temperature, pCO_{2w}, DIC, and TA (Supplementary Table 3). However, pH_T during flood tide (8.010 ± 0.031) was slightly higher than during ebb tide (8.008 ± 0.029), with a lower positive slope on the regression line (Figure 3A). pCO_{2w} and DIC showed similar values during the

10.3389/fmars.2025.1595871

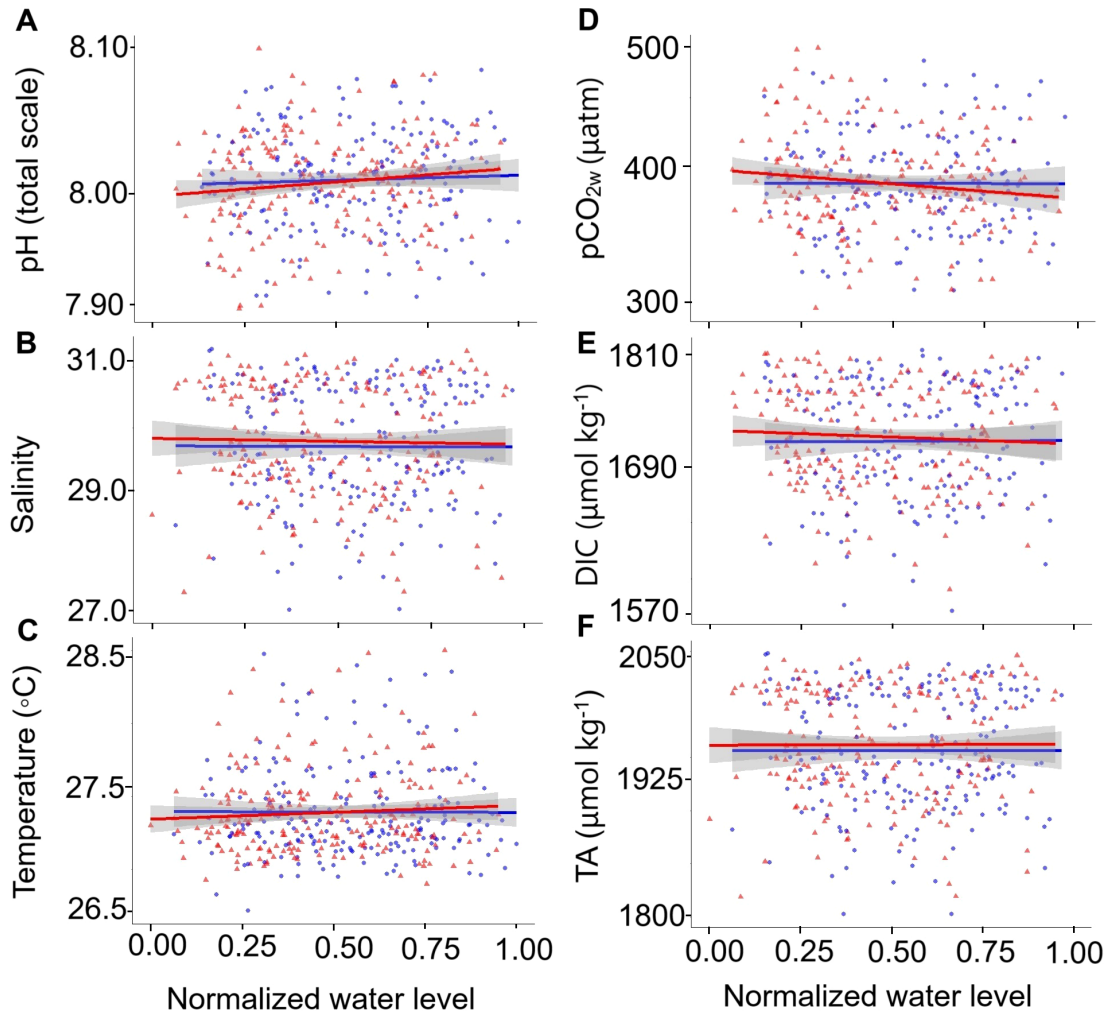

FIGURE 3
Normalized water level (0.00–1.00) plotted against the dependent variables: **(A)** pH_T, **(B)** salinity, **(C)** temperature, **(D)** pCO_{2W}, **(E)** dissolved inorganic carbon (DIC), and **(F)** total alkalinity (TA). The blue regression line and dots represent flood, while the red regression line and triangles represent ebb. A normalized tide value of 0.00 corresponds to a minimum low tide, and 1.00 corresponds to a maximum high tide.

flood tide (396 ± 38 µatm and 1726 ± 52 µmol kg^{-1}, respectively) and the ebb tide (397 ± 35 µatm and 1730 ± 46 µmol kg^{-1}, respectively), with a slight negative slope observed in the regression trend (Figures 3D, E, respectively). Variables such as temperature, salinity, and TA exhibited slopes close to zero, indicating that this area's seawater and river water are well-mixed.

3.2 Physico-chemical seawater parameters and atmospheric variables (56 days' time scale)

The independent atmospheric variables (solar radiation and total precipitation) were correlated with water type (sea surface temperature and salinity) and carbon chemistry data (pH_T, pCO_{2w}, DIC, and TA). Total daily solar radiation showed the strongest correlations with all dependent variables; suggesting that average radiation values of 3078 ± 1098 Wh m^{-2} (n= 56), as well as radiation values in a range of 1378 to 5968 Wh m^{-2} displayed positively correlations with mean daily temperature and pH_T, and negative correlations with salinity, pCO_{2w}, DIC, and TA (Table 2). In contrast, total daily precipitation (mean average of 31 ± 27 mm; n= 56) within the 0 to 115 mm range only correlated negatively with mean daily salinity (Table 2). No significant correlation was observed between daily precipitation and pH_T, temperature, pCO_{2W}, DIC, and TA (Table 2). In addition, rainwater samples collected during the high rainfall season (May 2022) in GNNP showed the lowest salinity values (0.26).

3.3 Diurnal, 24-hour cycle of the carbonate system

pH_T, temperature, pCO_{2W}, and DIC followed a pronounced diurnal cycle with significant differences ($p < 0.05$; Supplementary Table 4) between early morning and late evening hours (Figure 4).

TABLE 1 Descriptive statistics of the measured and derived variables (*) from September 13 to November 07, 2021, in El Muelle reef, GNNP, Colombian Pacific.

Statistics	pH (total scale)	Salinity	Temperature (°C)	pCO_{2w}* (µatm)	DIC * (µmol kg^{-1})	TA * (µmol kg^{-1})	Ω_a*
Mean ± SD	8.01 ± 0.03	29.74 ± 0.94	27.39 ± 0.30	396.78 ± 36.25	1728.10 ± 49.06	1959.42 ± 54.14	2.71 ± 0.17
Maximum	8.09	31.29	28.50	498.94	1806.97	2047.60	3.09
Minimum	7.93	27.03	26.72	302.29	1574.23	1802.74	2.22
N	392	403	422	354	355	391	355

The mean value, standard deviation (SD), maximum, minimum, and sample size of the measured variables pH_T, salinity, temperature, and derived variables pCO_{2w}, DIC, TA, and Ω_a are described.

TABLE 2 Spearman correlation between the dependent variables (daily average) pH_T, salinity, temperature, pCO_{2W}, dissolved inorganic carbon (DIC), total alkalinity (TA), and the independent variables (daily total) solar radiation and precipitation.

Variables	Statistics	pH_T	Salinity	T	pCO_{2w}*	DIC *	TA*
Radiation	p value	**0.01**	**0.00**	**0.00**	**0.00**	**0.00**	**0.00**
	rho	0.37	-0.41	0.51	-0.46	-0.42	-0.41
Precipitation	p value	0.22	**0.04**	0.85	0.13	0.06	0.06
	rho	0.17	-0.28	0.03	-0.21	-0.26	-0.26
pH	p value		**0.00**	**0.03**	**0.00**	**0.00**	**0.00**
	rho		-0.54	0.29	-0.95	-0.63	-0.53
N		56	56	56	56	56	56

In bold, the variables that were significantly correlated ($p < 0.05$). Dependent variables marked with an asterisk (*) indicate values derived either from a regression with salinity (e.g., TA) or calculated using CO2sys (e.g., pCO_{2W} and DIC). In contrast, unmarked variables were directly measured in the field.

During early morning hours, after sunrise (5:00 - 6:00), at 8:00 the lowest values of pH_T (7.993 ± 0.040; Figure 4A) and temperature (27.23 ± 0.18; Figure 4B) were recorded, as well as the highest values of pCO_{2W} (413 ± 40 µatm; Figure 4C) and DIC (1739 ± 46 µmol kg^{-1}; Figure D). In the late afternoon (17:00 - 18:00), during sunset, the highest values of pH_T (8.030 ± 0.025; Figure 4A) and temperature (27.61 ± 0.36; Figure 4B) were found, together with the lowest pCO_{2W} (374 ± 25 µatm; Figure 4C) and DIC (1718 ± 50 µmol kg^{-1}; Figure 4D). In contrast, salinity (Figure 4E), TA (Figure 4F), and carbonate alkalinity did not show significant differences ($p > 0.05$, Supplementary Table 4) between early morning and late evening hours.

4 Discussion

4.1 Freshwater input, precipitation, and river discharges play a key role in the Pacific Colombian GNNP region

The high variability found in variables pH_T, salinity, temperature, pCO_{2w}, DIC, and TA at El Muelle reef highlights the influence of La Niña 2020–2023 event. La Niña event strengthened the Choco Jet (Hoyos et al., 2013; Arias et al., 2015; Serna et al., 2018), which caused an increase in precipitation in the Colombian Pacific basin and, consequently, an increase in the river flow into the sea (Restrepo and Kjerfve, 2000; Blanco, 2009; Serna et al., 2018). During the sampling period from September to November 2021, the station "57025020 Gorgona Guapi" recorded a total precipitation of 2878 mm, exceeding the total multiannual monthly average by more than 59% to 1815 mm.

Likewise, the station "53047010 Sangaral" recorded a monthly average flow of the Guapi River of 447 $m^3 s^{-1}$, exceeding by 44% the total multiannual monthly average of 309 $m^3 s^{-1}$. Thus, the sampling period was characterized by a considerable inflow of freshwater from river discharges and high rainfall that explained the reduced recorded salinity values and part of the pH_T variability (Figure 2). The salinity normalization and correlation (Table 2) suggest that salinity plays a significant role in pH_T variability. The interplay between low salinity and reduced alkalinity (directly correlated) and pH variability underscores its critical role in coastal biogeochemical cycles. Reduced salinity not only dilutes carbonate and bicarbonate ions but also disrupts the equilibrium of the CO_2 system, as observed in estuarine zones by Feely et al. (2010) and Cai et al. (2021), where freshwater influx exacerbates anthropogenic CO_2 uptake. These dynamics challenge the buffering capacity and resilience, particularly in reefs, where a range of water pH is essential for calcification.

Additionally, high rainfall and the consequent excess of freshwater (characteristic of a RioMar system) acted as a surface layer dilution factor (Zeebe and Wolf-Gladrow, 2001; Turk et al., 2010; Trujillo and Thurman, 2016; Ho and Schanze, 2020),

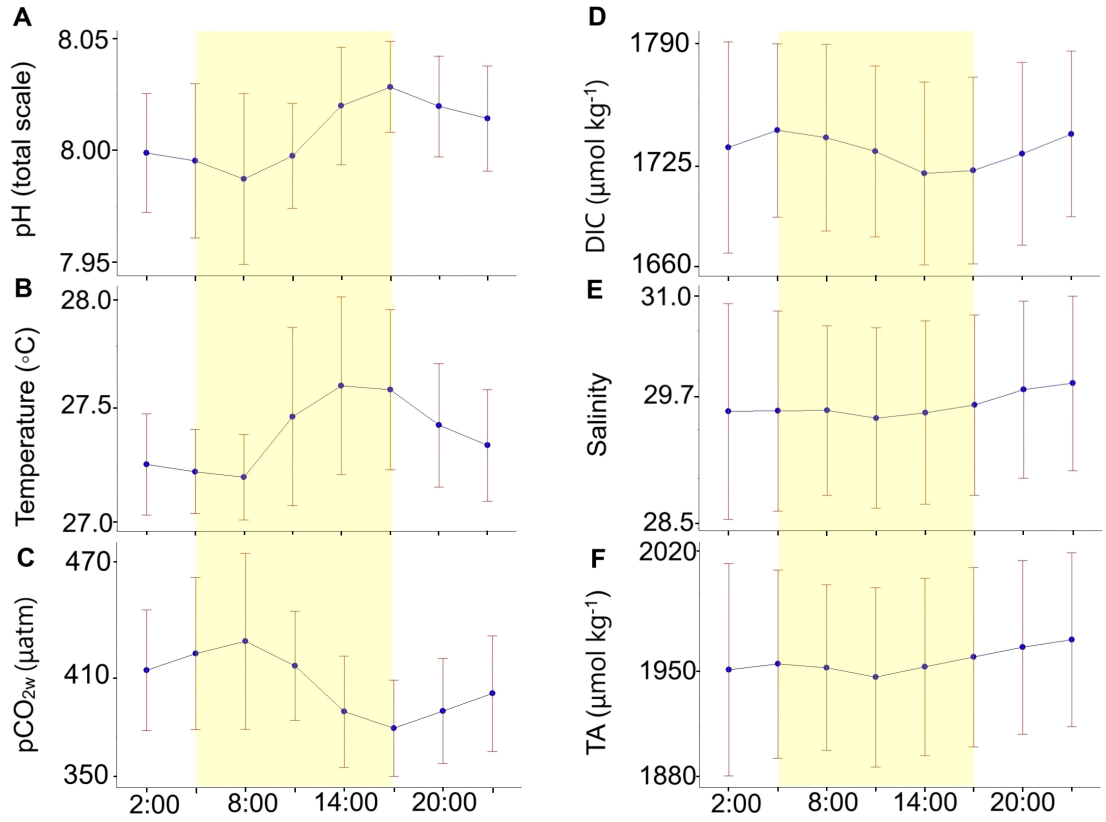

FIGURE 4
The diurnal scale (24 hours) of **(A)** pH_T, **(B)** temperature, **(C)** pCO_{2W}, **(D)** dissolved inorganic carbon (DIC), **(E)** salinity, and **(F)** total alkalinity (TA). The points represent the daily averages of measurements recorded every 3 hours over 56 consecutive days, with the red lines indicating the standard deviation of the daily averages. The shaded area highlights the daylight hours.

contributing to reducing, even more, the salinity over time. For example, Ho and Schanze (2020) reported a rapid decrease in salinity of 4.4 at depths of 2 to 3 cm in response to heavy rainfall in the Eastern Equatorial Pacific, highlighting the impact of precipitation on coastal salinity dynamics. Salinity gradients and alkalinity depletion may act as synergistic stressors, which align with broader concerns about coastal acidification (Doney et al., 2009) and the ecological risks associated with climate change scenarios.

The tides exert a continuous physical influence, due considerable tidal variation, having maximum amplitudes of 5.82 m and minimum of -0.78 m in 2021 (3.39 ± 1.20 m; Flanders Marine Institute [VLIZ] and Intergovernmental Oceanographic Commission [IOC], 2025), implying millions of cubic meters of freshwater entering and leaving the coastal system, mixing oceanic water with freshwater coming from the Patia-Sanquianga complex plus the rainfall. The well-mixed RioMar water has minimal salinity variations throughout a full ebb and flow cycle (Figure 3). This high mixing condition persists up to 55 km downstream of the river mouth. As indicated by Palacios Moreno and Pinto Tovar (1992), due to the high tide, mixing begins at the river mouth, where seawater enters through the bottom of the Guapi River, resulting in waters with a salinity of 25.60 at 10 m, compared to 17 at 1 m. Furthermore, tides and the southern trade winds during La Niña events generate coastal currents and a strong swell (Osorio et al., 2014) that contribute to mixing these two water types, creating an estuary environment. Consequently, this coastal zone can be classified as a Type 2 RiOMar regime (Dai et al., 2022a), characterized by a high-energy tidal system and significant mixing near the river mouths (Lamarque et al., 2022).

In this scenario, the riverine influence reaching GNNP may explain the observed decrease in pH_T over the study period. This trend is likely driven by the input of CO_2 derived from riverine DIC, potentially due to the input and decomposition of organic matter, which increases H^+ ion concentrations, as observed in other coastal regions (Vargas et al., 2016; Cai et al., 2021). In fact, in the Eastern Colombian Pacific, the observed decrease and low values of pH_T were strongly correlated with salinity, pCO_{2w}, and DIC (Table 2). Between 2018 and 2021, data collected at 13 river stations near the GNNP showed pH_{NBS} values ranging from 6.3 to 8.3. Suspended solids ranged from 11 to 407 mg L^{-1}, while nitrate (NO_3^-) concentrations ranged from 2 to 90.9 µg L^{-1}. Phosphate ($P\text{-}PO_4^{3-}$) levels fluctuated between 2 and 3.3 µg L^{-1}, and chlorophyll-a concentrations ranged from 0.07 to 9.8 µg L^{-1}. The highest values for these parameters were recorded during the year's second half, coinciding with the rainy season (INVEMAR, 2020b; INVEMAR, 2022), which could contribute to acidification. This phenomenon aligns with RiOMar systems, where high DIC and nutrient inputs

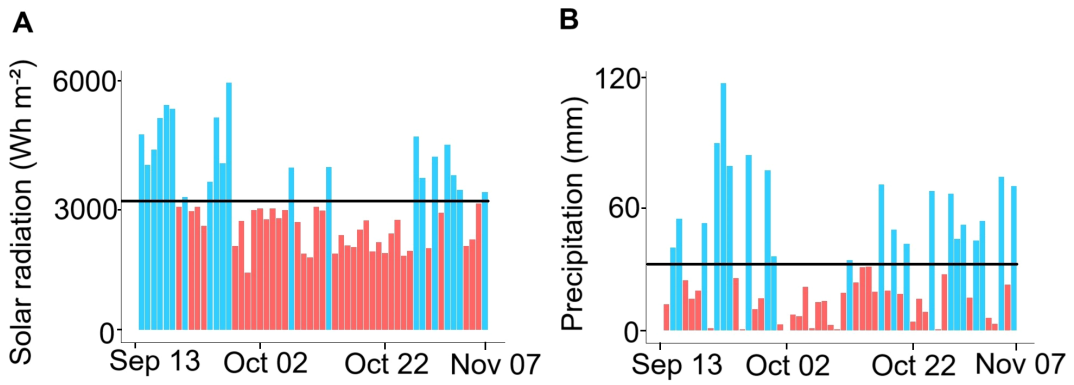

FIGURE 5
Atmospheric variables in the study area from September 13 to November 7, 2021. **(A)** Solar radiation was recorded at station 26015040 (Arrayanales). The black line indicates the daily (September to 7 November 2021) for solar radiation (3078 Wh m^{-2}) and precipitation (31 mm), and **(B)** Total precipitation was recorded at station 57025020 (Gorgona). Periods above the daily average are highlighted in blue, while periods below the daily average are shown in red.

TABLE 3 Comparison between autonomous sensors recorded total scale pH (pH_T) across various geographical zones.

Location	Long.	Lat.	Ocean	Instrument	pH_T range	Reference
Bahia Monterrey, EEUU	121° 54′ 0″ W	36° 49′ 48″ N	Pacific Ocean	iSAMI-pH	7.93 - 8.37	Gray et al., 2011
Bahia Culebra, Costa Rica	85° 36′ 0″ W	10° 30′ 0″ N	Pacific Ocean	iSAMI-pH	7.98 - 8.06	Sánchez-Noguera et al., 2018
East China Sea	128° 30′ 0″ E	30° 0′ 0″ N	Pacific Ocean	SeaFET Ocean pH sensor	7.98 - 8.07	Wu et al., 2021
Northwest European Shelf Seas	10° 0′ 0″ W to 10° 0′ 0″ E	45° 0′ 0″ N to 60° 0′ 0″ N	Atlantic Ocean	Lab-on-Chip	7.99 - 8.21	Rérolle et al., 2018
Algoa Bay, South Africa	25° 48′ 0″ E	33° 48′ 0″ S	Atlantic Ocean	iSAMI-pH	7.98 - 8.44	Edworthy et al., 2022
Gorgona, Colombia	78° 6′ 0″ W	2° 54′ 0″ N	Pacific Ocean	iSAMI-pH	7.93 - 8.09	This study (2021)

Note that the minimum pH_T recorded at Gorgona Island, Colombia, is lower than in other regions.

from rivers reach nearshore waters, and organic matter is subsequently exported to the continental shelf (Gan et al., 2009; Dai et al., 2022a). Decreases in pH_T in other estuaries have been indirectly linked to fluvial discharges. For example, along the central-southern Chilean Pacific coast (Biobío River basin), the expansion of the river plume seaward led to reduced pH_T conditions (7.6) during periods of maximum higher river discharge, compared to more oceanic stations where pH_T ranged from 7.95 to 8.15 (Vargas et al., 2016). Likewise, in the South Pacific Ocean, in Coral Bay, fluvial discharges from low-pH rivers (7.739 ± 0.022) cause coastal areas with low pH_T (8.014 ± 0.015) (Aguilera et al., 2013), similar to low pH observed across the GNNP Colombian Pacific Region. Indeed, the surface values (2m) of pH_T (8.01 ± 0.03), salinity (29.74 ± 0.94), TA (1959 ± 54 µmol kg^{-1}), DIC (1728 ± 49 µmol kg^{-1}) and Ω_a (2.71 ± 0.17) at El Muelle reef (GNNP) are below the surface averages reported for the North Pacific (8. 105 ± 0.06, 34.05 ± 0.86, 2255 ± 34 µmol kg^{-1}, 1959 ± 42 µmol kg^{-1} and 3.30 ± 0.7; respectively) and the South Pacific (8.079 ± 0.03, 35.29 ± 0.55, 2319 ± 35 µmol kg^{-1}, 2003 ± 39 µmol kg^{-1} and 3.52 ± 0.4) (Feely et al., 2009).

On the contrary, oceanic areas without river input, such as North Pacific Monterey Bay, have recorded relatively high pH_T (Gray et al., 2011). However, at higher latitudes on the Pacific coast of Costa Rica, low pH_T levels were associated with the rainy season (Sánchez-Noguera et al., 2018). A drop in pH_T is also known to occur in the estuaries of Swartkops and Sundays in South Africa, where, due to strong inflows of freshwater, a high pH_T decrease of 0,46 pH units was produced (Edworthy et al., 2022). The relatively low pH_T of the Pacific Colombian Coast (El Muelle, GNNP, Table 3) is similar to studies in the East River China Sea, where the low pH_T (7.98 to 8.07) was attributed to the high river inputs from the Changjiang plume, known to carry organic carbon, nutrients, and CO_2 supersaturated water (Wu et al., 2021). We already know that freshwater inputs from rivers play a critical role in shaping carbonate chemistry in coastal systems, particularly in the continental shelf. As well as in our study site, Rérolle et al.

(2018) have identified riverine discharges, characterized by high DIC and TA, as key drivers of reduced pH_T in the Irish Sea, southern North Sea, and Skagerrak region. Further studies on carbon chemistry in the region are needed, including direct measurements of DIC and dissolved organic matter in the Patia-Sanquianga complex during wet and dry seasons. These and other chemical parameters, such as nutrients, are crucial to evaluating rivers' contribution to coastal carbonate chemistry, particularly near reef systems, and the impact on ocean acidification (Borges et al., 2005; Cai et al., 2021). The main knowledge gaps include the effects of remineralization on pH in tropical estuaries (Dai et al., 2022b; Vargas et al., 2016) to understand the vulnerability of ecosystems to OA.

4.2 Daily scale of carbon and physical seawater variability and atmospheric variables, solar radiation, and precipitation

During the study period, the ITCZ was located close to the equator in the Colombian Pacific Ocean (Díaz Guevara et al., 2008), which intensified cloudiness and precipitation due to the convergence of trade winds from the northern and southern hemispheres (Díaz Guevara et al., 2008). The increase in cloudiness likely contributed to the decline in solar radiation, which diminished from 3,709 ± 1,205 Wh m^{-2} in September to 2,501 ± 789 Wh m^{-2} in November, with a marked reduction between October 1 and 25 (2,488 ± 590 Wh m^{-2}; Figure 5A). Given the positive correlation between solar radiation and temperature (Trujillo and Thurman, 2016; Webster, 2020), the decrease in solar radiation may explain the low SST observed from September 13 to November 7. According to Millero (2007, 2013) lower temperatures increase CO_2 solubility in seawater, suggesting that the temperature decline likely improved oceanic CO_2 uptake by enabling its transfer from the atmosphere to the ocean during the study period. The resulting CO_2 increase could explain pCO_{2w} and DIC's highest values (Figure 2), particularly between October 1 and 25, when solar radiation was at its lowest (Figure 5). Thus, the solar radiation and temperature reduction may partially explain the observed decline in pH_T during this period. The inverse correlation between pH_T and pCO_{2w} also suggests that fluctuations in pCO_{2w} (indirectly DIC) could help explain pH_T variations over September-November (Table 2; Zeebe and Wolf-Gladrow, 2001; Millero, 2013; Cai et al., 2021). After October 25, the rise in solar radiation and temperature may have led to a pH_T increment by approximately 0.028 units, along with a decrease in pCO_{2w} by 41 µatm and DIC by 100 µmol kg^{-1} (Figures 2D, E).

Between October 3 and 16, total precipitation amounted to 22 mm (Figure 5B), with most days recording values below the mean daily precipitation of 31 mm. The observed reduction in precipitation likely diminished freshwater inflow relative to seawater, thereby enhancing salinity levels and elevating TA and DIC concentrations during this period. During the sampling period (September 13 to November 7), evaporation (Copernicus Climate Change Service, 2024) was highest in October (-62 mm), followed by September (-36 mm) and November (-15 mm). However, in all cases, the monthly accumulated evaporation remained well below the corresponding monthly precipitation totals of 680 mm, 727 mm, and 261 mm, respectively (DHIME, 2025).

In addition to previously discussed mechanisms, the elevated levels of pCO_{2w}, DIC, and salinity observed between October 1 and 25 may also be influenced by a coastal upwelling event. This hypothesis is supported by the positive values of zonal Ekman transport (ZET) during this period, which indicates eastward surface water movement, given the regional coastline orientation and prevailing wind patterns (Corredor-Acosta et al., 2020). The eastward Ekman transport suggests offshore water displacement and the potential for deeper, carbon- and nutrient-rich water upwelling (Supplementary Figure 4).

4.3 24-hour cycle of the carbonate system

During early morning hours (5:00 - 6:00 am), we registered the lowest pH_T and temperature values, along with the highest concentration of pCO_{2w} and DIC, suggesting the influence of night-time respiration processes before daylight (Millero, 2013; Albright et al., 2013; Sánchez-Noguera et al., 2018). On the other hand, the highest values of pH_T and temperature and the lowest values of pCO_{2w} and DIC recorded during the late afternoon (17:00 - 18:00) suggest photosynthetic processes during daylight driven by increased solar radiation (Cyronak et al., 2013). The mean diel change of 0.037 units in pH_T and 0.38 °C in temperature between early morning and afternoon hours fall within the expected diel variability for shallow environments (0.7–17 m), where biological and physical processes significantly influence pH and temperature dynamics (Cyronak et al., 2013).

The absence of a significant difference in TA and carbonate alkalinity between early morning and late afternoon hours may be due to the derivation of TA using a TA-salinity relationship, which primarily accounts for processes such as evaporation, precipitation, and mixing tides (Spaulding et al., 2014). In contrast, calcification and dissolution, more likely to exhibit variations over a 24-hour cycle, may not be adequately reflected (Zeebe and Wolf-Gladrow, 2001; Millero, 2013; Cai et al., 2021). However, the data indicate that the El Muelle reef, close to the sampling point, is composed predominantly of *Pocillopora* spp. (Figure 1; Zapata, 2001; Acosta et al., 2007), was exposed during the sampling period to low pH_T (8.01 ± 0.03), salinity (29.32 ± 1.01), and Ω_a (2.71 ± 0.17). These environmental conditions are considered challenging for *Pocillopora* spp., which are known to be highly sensitive to reduced pH and lowered salinity associated with river discharge (Alvarado et al., 2005; Lizcano-Sandoval et al., 2018; Sánchez-Noguera, 2019). Notably, the global, annually averaged tolerance limit for coral reefs is an Ω_a of 2.82, indicating that corals at this site live below the threshold commonly reported in the literature (Guan et al., 2015).

Despite these adverse conditions and frequent riverine influence, especially during the rainy season in the latter half of the year (Giraldo et al., 2008, 2011), *Pocillopora* spp. persist and even dominate the area (Zapata, 2001; Acosta et al., 2007; Lizcano-

Sandoval et al., 2018). Previous studies have shown that *Pocillopora* spp. in GNNP can maintain growth rates (Lizcano-Sandoval et al., 2018) and tolerate hypoxia, low salinity, and temperature fluctuations by reducing reproductive output rather than growth (Castrillón-Cifuentes et al., 2023a, 2023). This suggests that these corals are either locally adapted or possess a degree of physiological tolerance to low pH, salinity, and Ω_a. Similar findings from the Pearl River Estuary in Southeast China indicate that long-term hypo-salinity acclimation can enhance the tolerance of *Pocillopora* spp. to low salinity by reducing energy consumption, slowing metabolism, improving the energy metabolism of their symbiotic algae (Symbiodiniaceae), and altering their symbiotic bacterial communities to avoid bleaching (Chen et al., 2024). Nevertheless, *Pocillopora* spp. corals at Gorgona Island exhibit lower calcification rates (3.16 g $CaCO_3$ cm^{-2} yr^{-1}; Lizcano-Sandoval et al., 2018) compared to those reported in other reef systems, such as Panama (5–6 g $CaCO_3$ cm^{-2} yr^{-1}; Manzello, 2010) and Mexico (2.99–6.02 g $CaCO_3$ cm^{-2} yr^{-1}; Medellín-Maldonado et al., 2016; González-Pabón et al., 2021; Tortolero-Langarica et al., 2022). To establish a more robust correlation between the carbonate system and calcification rates in *Pocillopora* spp. at GNNP, future research efforts should prioritize *in situ* measurements of TA, dissolved oxygen, and direct calcification assessments (e.g., via buoyant weight or alkalinity anomaly techniques) on a 24-h scale during both rainy and dry seasons, to better quantify metabolic dynamics and clarify the adaptive capacity of this species under adverse environmental conditions.

In addition, future research should prioritize high-frequency measurements of pH, nutrient concentrations, and stable isotopes across diurnal, seasonal, and interannual timescales. These efforts should encompass both rainy and dry seasons and different ENSO phases, such as El Niño and neutral conditions, to better distinguish water sources in the region and assess the influence of these temporal scales on carbonate chemistry variability.

5 Conclusions

The natural variability of the Ocean Acidification on 24-hour and daily scales and during 56 days at El Muelle reef, Colombian Pacific, Gorgona Island, was assessed in a fixed station using high-resolution measurements of seawater pH_T, salinity, and temperature taken every three hours during a year with a strong La Niña event and extreme precipitation months. The prolonged 2020–2023 La Niña event amplified rainfall and freshwater discharges from the Guapi River, establishing a Type 2 RIOMar (river-marine) system dominated by high-energy tidal dynamics and intense river-sea mixing. This freshwater influx likely contributed to localized declines in seawater pH_T. Concurrently, the southward migration of the ITCZ triggered persistent cloud cover and strong southwesterly winds, attenuating solar radiation and lowering both sea surface temperatures and pH_T. Enhanced rainfall within the RIOMar system further diluted the surface layer, progressively reducing salinity and TA, thereby diminishing the system's buffering capacity against carbonate chemistry fluctuations. Biological processes such as photosynthesis and respiration shaped pronounced diurnal patterns within the 24-hour cycles, driving decreased and increased pH, pCO_{2w}, and DIC. These results highlight the substantial and high-frequency variability of pH and acidification conditions formed by the heavy rainfall and runoff that characterize this Pacific Colombian region. Therefore, we strongly recommend implementing long-term monitoring programs (COCAS Ocean Decade Project) to support acidification impact studies and adaptive management and conservation efforts within this National Natural Park.

Data availability statement

The datasets generated for this study can be found in the NOAA - National Centers for Environmental Information (NCEI; Accession Number 0300707). https://www.ncei.noaa.gov/data/oceans/ncei/ocads/metadata/0300707.html).

Author contributions

AM: Conceptualization, Investigation, Methodology, Supervision, Validation, Visualization, Writing – original draft, Writing – review & editing, Data curation, Formal Analysis. AA: Conceptualization, Formal Analysis, Funding acquisition, Investigation, Methodology, Project administration, Resources, Supervision, Validation, Visualization, Writing – original draft, Writing – review & editing. AG: Conceptualization, Investigation, Methodology, Writing – review & editing. AC: Formal Analysis, Investigation, Supervision, Validation, Visualization, Writing – review & editing. JH: Conceptualization, Formal Analysis, Supervision, Validation, Visualization, Writing – review & editing. SG: Investigation, Methodology, Validation, Visualization, Writing – review & editing. CC: Methodology, Validation, Writing – review & editing. DR: Conceptualization, Supervision, Validation, Visualization, Writing – review & editing.

Funding

The author(s) declare financial support was received for the research and/or publication of this article. The Principal Investigator (PI), AA, acknowledges receiving financial support for various research activities, including purchasing equipment, acquiring laboratory and field materials, and funding field trips. Additionally, these funds were used to establish and equip a laboratory at the Pontificia Universidad Javeriana. Partial resources from the same fund were also allocated to cover the publication costs of this article (ID 21346). The National Geographic Explorer program funded this research through the project titled *"Ocean Acidification Vulnerability in Colombia: First Monitoring Program in the Tropical Pacific"* (Grant No. NGS-64756R-19), with additional COVID-19 grant support (Grant No. NGS-81727R-20). The Pontificia Universidad Javeriana provided further funding under the project *"Monitoreo de acidificación marina en el Pacífico colombiano"* (Project ID: 120132C0401200, No. 20019).

Acknowledgments

Dr. Cristian Vargas of the Laboratory of Aquatic Ecosystems Performance (LAFE) at the University of Concepción (EULA Chile) supported getting the iSAMI-pH equipment. The Ocean Foundation donated the GOA-ON in a Box kit, OA training, and grant support for equipment maintenance under the Memorandum of Understanding between Pontificia Universidad Javeriana and The Ocean Foundation ("TOF"). Dra. Andrea Corredor-Acosta thanks FONDECYT Postdoctoral Project No. 3230740, granted by the Chilean Agency for Research and Development (ANID). This research is part of the collaboration with the International COCAS project (2021-2030), Ocean Decade-United Nations (Leader Diana Ruiz Pino and Alban Lazar) https://oceandecade.org/fr/actions/coastal-observatory-for-climate-co2-and-acidification-for-theglobal-south-society-cocas/. We also thank Parques Nacionales Naturales de Colombia - Gorgona for their logistical support at Gorgona (Christian Díaz – research head & Monitoring of the Gorgona park), accommodation, boat, and the research permit No. 004 de 2020 - file number: OTRP 004-2020. To Dra. Reggie Spaulding, James Beck, and Dr. Christopher Sabine for their technical support with the iSAMI-pH equipment. To Camilo, Freddy, and Jaime for their help in the Ocean Acidification laboratory. To Juan Felipe Cifuentes for his assistance deploying the iSAMI-pH at El Muelle Reef. Thanks to Dr. Alan Giraldo of Universidad del Valle for funding research interns Cristian Claros, Sebastián Ortiz, and Natalia Londoño, who collaborated with us in the field sampling. We thank Camilo Rodríguez and Enrique Herman for their help during the long days of boat sampling and for hosting us in their home during our stay at Guapi.

Conflict of interest

The authors declare that the research was conducted in the absence of any commercial or financial relationships that could be construed as a potential conflict of interest.

The author(s) declared that they were an editorial board member of Frontiers, at the time of submission. This had no impact on the peer review process and the final decision.

Generative AI statement

The author(s) declare that no Generative AI was used in the creation of this manuscript.

Publisher's note

Supplementary material

The Supplementary Material for this article can be found online at: https://www.frontiersin.org/articles/10.3389/fmars.2025.1595871/full#supplementary-material

References

Acosta, L. A., Uribe, D. G., and Isaacs, P. (2007). Estudio de línea base de las formaciones coralinas de Yundigua y el muelle, isla Gorgona, Pacífico Colombiano. *Universitas Scientiarum* 12, 65–81.

Aguilera, V. M., Vargas, C. A., Manríquez, P. H., Navarro, J. M., and Duarte, C. (2013). Low-pH freshwater discharges drive spatial and temporal variations in life history traits of the neritic copepod. *Acartia tonsa. Estuaries Coasts* 36, 1084–1092. doi: 10.1007/s12237-013-9615-2

Albright, R., Langdon, C., and Anthony, K. R. N. (2013). Dynamics of seawater carbonate chemistry, production, and calcification of a coral reef flat, central Great Barrier Reef. *Biogeosciences* 10, 6747–6758. doi: 10.5194/bg-10-6747-2013

Alvarado, J. J., Cortés, J., Fernández, C., and Nivia, J. (2005). Comunidades y arrecifes coralinos del Parque Nacional Marino Ballena, costa del Pacífico de Costa Rica. *Rev. Biología Trop.* 31, 1–20.

Amador, J. A., Alfaro, E. J., Lizano, O. G., and Magaña, V. O. (2006). Atmospheric forcing of the eastern tropical Pacific: A review. *Prog. Oceanography* 69, 101–142. doi: 10.1016/j.pocean.2006.03.007

Aminot, A., and Kérouel, R. (2004). *Hydrologie des écosystèmes marins: paramètres et analyses* (Editions Quae).

Arias, P. A., Martínez, J. A., and Vieira, S. C. (2015). Moisture sources to the 2010–2012 anomalous wet season in northern South America. *Climate Dynamics* 45, 2861–2884. doi: 10.1007/s00382-015-2511-7

Ashton, I. G., Shutler, J. D., Land, P. E., Woolf, D. K., and Quartly, G. D. (2016). A sensitivity analysis of the impact of rain on regional and global sea-air fluxes of CO2. *PloS One* 11. doi: 10.1371/journal.pone.0161105

Atekwana, E. A., Ramatlapeng, G. J., Ali, H. N., Njilah, I. K., and Ndondo, G. R. N. (2022). Tide-salinity patterns reveal seawater-freshwater mixing behavior at a river mouth and tidal creeks in a tropical mangrove estuary. *J. Afr. Earth Sci.* 196. doi: 10.1016/j.jafrearsci.2022.104684

Berri, G. J., Bianchi, E., and Müller, G. v. (2019). El Niño and la Niña influence on mean river flows of southern South America in the 20th century. *Hydrological Sci. J.* 64, 900–909. doi: 10.1080/02626667.2019.1609681

Blanco, J. F. (2009). The hydroclimatology of Gorgona island: seasonal and ENSO-related patterns. *Actualidades Biológicas* 31, 111–121. doi: 10.17533/udea.acbi.331494

Borges, A. V., Delille, B., and Frankignoulle, M. (2005). Budgeting sinks and sources of CO2 in the coastal ocean: Diversity of ecosystems counts. *Geophys. Res. Lett.* 32, L14601. doi: 10.1029/2005GL023053

Cai, W. J., Feely, R. A., Testa, J. M., Li, M., Evans, W., Alin, S. R., et al. (2021). Natural and anthropogenic drivers of acidification in large estuaries. *Annu. Rev. Mar. Sci.* 13, 23–55. doi: 10.1146/annurev-marine-010419-011004

Caldeira, K., and Wickett, M. E. (2003). Anthropogenic carbon and ocean pH. *Nature* 425, 365–365. doi: 10.1038/425365a

Carstensen, J., Chierici, M., Gustafsson, B. G., and Gustafsson, E. (2018). Long-term and seasonal trends in estuarine and coastal carbonate systems. *Global Biogeochemical Cycles* 32, 497–513. doi: 10.1002/2017GB005781

Carter, B. R., Williams, N. L., Gray, A. R., and Feely, R. A. (2016). Locally interpolated alkalinity regression for global alkalinity estimation. *Limnology Oceanography: Methods* 14, 268–277. doi: 10.1002/lom3.10087

Castrillón-Cifuentes, A. L., Zapata, F. A., Giraldo, A., and Wild, C. (2023a). Spatiotemporal variability of oxygen concentration in coral reefs of Gorgona Island (Eastern Tropical Pacific) and its effect on the coral Pocillopora capitata. *PeerJ* 11, e14586. doi: 10.7717/peerj.14586

Castrillón-Cifuentes, A. L., Zapata, F. A., and Wild, C. (2023b). Physiological responses of Pocillopora corals to upwelling events in the Eastern Tropical Pacific. *Front. Mar. Sci.* 10. doi: 10.3389/fmars.2023.1212717

Chen, J., Yu, X., Yu, K., Chen, B., Qin, Z., Liao, Z., et al. (2024). Potential adaptation of scleractinian coral *Pocillopora damicornis* during hypo-salinity stress caused by

extreme pre-flood rainfall over south China. *Environ. Res.* 262, 119848. doi: 10.1016/j.envres.2024.119848

Copernicus Climate Change Service, Climate Data Store (2024). *ERA5 post-processed daily-statistics on single levels from 1940 to present* (Copernicus Climate Change Service (C3S) Climate Data Store (CDS). doi: 10.24381/cds.4991cf48

Corredor-Acosta, A., Cortés-Chong, N., Acosta, A., Pizarro-Koch, M., Vargas, A., Medellín-Mora, J., et al. (2020). Spatio-temporal variability of chlorophyll-a and environmental variables in the Panama bight. *Remote Sens.* 12, 2150. doi: 10.3390/rs12132150

Cyronak, T., Santos, I. R., and Eyre, B. D. (2013). Permeable coral reef sediment dissolution driven by elevated CO_2 and porewater advection. *Geophysical Res. Lett.* 40, 4876–4881. doi: 10.1002/grl.50948

Dai, M., Lu, Z., Zhai, W., Chen, B., Cao, Z., Zhou, K., et al. (2022a). Carbon cycling in the river-dominated ocean margins: Mechanisms, fluxes, and global significance. *Front. Mar. Sci.* 9. doi: 10.3389/fmars.2022.789234

Dai, M., Su, J., Zhao, Y., Hofmann, E. E., Cao, Z., Cai, W.-J., et al. (2022b). Carbon fluxes in the coastal ocean: synthesis, boundary processes and future trends. *Annu. Rev. Earth Planetary Sci.* 50, 593–626. doi: 10.1146/annurev-earth-032320

Datos Hidroclimatologicos y Meteorológicos. (DHIME) (2025).Consulta y Descarga de Datos Hidrometeorológicos. Available online at: http://dhime.ideam.gov.co/atencionciudadano/ (Accessed April 17, 2023).

Díaz, M. J. (2007). "Deltas y Estuarios del Pacífico Colombiano," in *Deltas y estuarios de Colombia* (Banco de Occidente, Cali).

Díaz, J. M., Pinzón, J. H., Perdomo, A. M., Barrios, L. M., and López-Victoria, M. (2001). "Generalidades: 17-26," in *Gorgona Marina: Contribución al conocimiento de una isla única.*, vol. 7 . Eds. L. M. En Barrios and M. López-Victoria (INVEMAR, Serie de Publicaciones Especiales, Santa Marta, Colombia), 160 pp.

Díaz Guevara, D. C., Málikov, I., and Villegas Bolaños, N. L. (2008). Características de las zonas de surgencia de la cuenca del Pacífico Colombiano y su relación con la zona de convergencia intertropical. *Boletín Científico CIOH* 26, 59–71. doi: 10.26640/01200542.26.59_71

Dickson, A. G. (1990). Standard potential of the reaction: AgCl (s)+ 12H2 (g)= Ag (s) + HCl (aq), and the standard acidity constant of the ion HSO4– in synthetic sea water from 273.15 to 318.15 K. The. *J. Chem. Thermodynamics* 22, 113–127. doi: 10.1016/0021-9614(90)90074-Z

Dickson, A. G., Sabine, C. L., and Christian, J. R. (2007). *Guide to best practices for ocean CO2 measurements* (North Pacific Marine Science Organization).

Doney, S. C., Fabry, V. J., Feely, R. A., and Kleypas, J. A. (2009). Ocean acidification: The other CO_2 problem. *Annu. Rev. Mar. Sci.* 1, 169–192. doi: 10.1146/annurev.marine.010908.163834

Edworthy, C., Potts, W. M., Dupont, S., Duncan, M. I., Bornman, T. G., James, N. C., et al. (2022). A baseline assessment of coastal pH variability in a temperate South African embayment: implications for biological ocean acidification research. *Afr. J. Mar. Sci.* 44, 367–381. doi: 10.2989/1814232X.2022.2147999

Emerton, R., Cloke, H. L., Stephens, E. M., Zsoter, E., Woolnough, S. J., and Pappenberger, F. (2017). Complex picture for likelihood of ENSO-driven flood hazard. *Nat. Commun.* 8. doi: 10.1038/ncomms14796

Espinoza-Morriberón, D., Echevin, V., Colas, F., Tam, J., Gutierrez, D., Graco, M., et al. (2019). Oxygen variability during ENSO in the tropical South Eastern Pacific. *Front. Mar. Sci.* 5. doi: 10.3389/fmars.2018.00526

Fassbender, A. J., Alin, S. R., Feely, R. A., Sutton, A. J., Newton, J. A., and Byrne, R. H. (2017). Estimating total alkalinity in the Washington State coastal zone: complexities and surprising utility for ocean acidification research. *Estuaries Coasts* 40, 404–418. doi: 10.1007/s12237-016-0168-z

Fassbender, A. J., Orr, J. C., and Dickson, A. G. (2021). Interpreting pH changes. *Biogeosciences* 18, 1407–1415. doi: 10.5194/bg-18-1407-2021

Feely, R. A., Alin, S. R., Newton, J., Sabine, C. L., Warner, M., Devol, A. H., et al. (2010). The combined effects of ocean acidification and low salinity on carbonate chemistry. *Estuarine Coast. Shelf Science.* 88, 442–449. doi: 10.1016/j.ecss.2009.12.021

Feely, R. A., Doney, S. C., and Cooley, S. R. (2009). Ocean acidification: Present conditions and future changes in a high-CO_2 world. *Oceanography* 22, 36–47. doi: 10.5670/oceanog.2009.95

Feely, R. A., Takahashi, T., Wanninkhof, R., McPhaden, M. J., Cosca, C. E., Sutherland, S. C., et al. (2006). Decadal variability of the air-sea CO2 fluxes in the equatorial Pacific Ocean. *J. Geophysical Research: Oceans* 111. doi: 10.1029/2005JC003129

Fiedler, P. C., and Lavín, M. F. (2017). "Oceanographic conditions of the eastern tropical Pacific," in *Coral Reefs of the Eastern Tropical Pacific*, vol. 8 . Eds. P. Glynn, D. Manzello and I. Enochs (Springer, Dordrecht). Coral Reefs of the World. doi: 10.1007/978-94-017-7499-4_3

Flanders Marine Institute (VLIZ) and Intergovernmental Oceanographic Commission (IOC) (2025).Sea level station monitoring facility. Available online at: https://www.ioc-sealevelmonitoring.org (Accessed May 18, 2024).

Gan, J., Li, L., Wang, D., and Guo, X. (2009). Interaction of a river plume with coastal upwelling in the northeastern South China Sea. *Continental Shelf Res.* 29, 728–740. doi: 10.1016/j.csr.2008.12.002

Gattuso, J. P., Magnan, A., Billé, R., Cheung, W. W., Howes, E. L., Joos, F., et al. (2015). Contrasting futures for ocean and society from different anthropogenic CO2 emissions scenarios. *Science* 349. doi: 10.1126/science.aac4722

Giraldo, A., Rodríguez-Rubio, E., and Zapata, F. (2008). Condiciones oceanográficas en isla Gorgona, Pacífico oriental tropical de Colombia. *Latin Am. J. Aquat. Res.* 36, 121–128. doi: 10.3856/vol36-issue1-fulltext-12

Giraldo, A., and Valencia, B. (2013). "Monitoreo del ambiente pelágico del PNN Gorgona: marzo 2013," in *Informe Técnico producto No. 8 del proyecto de investigación* (Monitoreo de los valores objeto de conservación priorizados para las áreas protegidas Gorgona y Utría adscritas a la Dirección Terri, Cali).

Giraldo, A., Valencia, B., Acevedo, J. D., and Rivera, M. (2014). Fitoplancton y zooplancton en el área marina protegida de Isla Gorgona, Colombia, y su relación con variables oceanográficas en estaciones lluviosa y seca. *Rev. Biología Trop.* 62, 117–132. doi: 10.15517/rbt.v62i0.15982

Giraldo, A., Valencia, B., and Ramírez, D. G. (2011). Productividad planctónica y condiciones oceanográficas locales en Isla Gorgona durante julio 2006. *Boletín Investigaciones Marinas y Costeras-INVEMAR* 40, 185–201.

Giraldo López, A. (2008). Variabilidad espacial de temperatura, salinidad y transparencia en el ambiente pelágico del PNN Gorgona durante septiembre 2007 y marzo 2008. *Boletín Científico CIOH* 26, 157–163. doi: 10.26640/01200542.26.157_163

Glynn, P. W., Prahl, H. V., and Guhl, F. (1982). Coral reefs of Gorgona Island, Colombia, with special reference to corallivores and their influence on community structure and reef development. *Annales l'Institut Océanographique* 58, 243–277.

González-Pabón, M. A., Tortolero-Langarica, J. A., Calderon-Aguilera, L. E., Solana-Arellano, E., Rodríguez-Troncoso, A. P., Cupul-Magaña, A. L., et al. (2021). Low calcification rate, structural complexity, and calcium carbonate production of Pocillopora corals in a biosphere reserve of the central Mexican Pacific. *Mar. Ecol.* 42, e12678. doi: 10.1111/maec.12678

Gray, S. E. C., DeGrandpre, M. D., Moore, T. S., Martz, T. R., Friederich, G. E., and Johnson, K. S. (2011). Applications of in *situ* pH measurements for inorganic carbon calculations. *Mar. Chem.* 125, 82–90. doi: 10.1016/j.marchem.2011.02.005

Guan, Y., Hohn, S., and Merico, A. (2015). Suitable environmental ranges for potential coral reef habitats in the tropical ocean. *PloS One* 10, e0128831. doi: 10.1371/journal.pone.0128831

Guerrero Gallego, J., Toro Botero, F. M., Osorio Arias, A. F., Álvarez Silva, O. A., and Giraldo, A. (2012). Modelación hidrodinámica de los patrones de circulación en isla Gorgona (Colombia), para el año 2011. *Escuela Geociencias y Medio Ambiente.*

Guzmán, D., Ruiz, J. F., and Cadena, M. (2014). *Regionalización de Colombia según la estacionalidad de la precipitación media mensual, a través análisis de componentes principales (ACP)* (Bogotá DC: Informe Técnico. IDEAM).

Henocq, C., Boutin, J., Petitcolin, F., Reverdin, G., Arnault, S., and Lattes, P. (2010). Vertical variability of near-surface salinity in the tropics: Consequences for L-band radiometer calibration and validation. *J. Atmospheric Oceanic Technol.* 27, 192–209. doi: 10.1175/2009JTECHO670.1

Hernández, D., Málikov, I., and Villegas, N. (2006). Relaciones espacio-temporales entre la temperatura superficial del mar de la Cuenca del Pacífico Colombiano y el ciclo El Niño oscilación del sur. *Memorias*, 6 (1-2012).

Ho, D. T., and Schanze, J. J. (2020). Precipitation-induced reduction in surface ocean pCO2: observations from the eastern tropical Pacific ocean. *Geophysical Res. Lett.* 47. doi: 10.1029/2020GL088252

Hoyos, N., Escobar, J., Restrepo, J. C., Arango, A. M., and Ortiz, J. C. (2013). Impact of the 2010–2011 La Niña phenomenon in Colombia, South America: The human toll of an extreme weather event. *Appl. Geogr.* 39, 16–25. doi: 10.1016/j.apgeog.2012.11.018

Instituto de Hidrología, Meteorología y Estudios Ambientales [IDEAM] (2021). *Boletín Climatológico Septiembre de 2021* (Instituto de Hidrología, Meteorología y Estudios Ambientales).

Instituto de Investigaciones Marinas y Costeras José Benito Vives de Andréis [INVEMAR] (2020a). GDB *Atlas de Áreas Coralinas de Colombia Fase II*. Available online at: https://areas-coralinas-de-Colombia-invemar.hub.arcgis.com/maps/35e85cca85ca42b3a0a8be987b1c5fa3/about (Accessed August 30, 2023).

Instituto de Investigaciones Marinas y Costeras José Benito Vives de Andréis [INVEMAR] (2020b). *Diagnóstico y evaluación de la calidad de las aguas marinas y costeras en el Caribe y Pacífico Colombianos* (Instituto de Investigaciones Marinas y Costeras José Benito Vives de Andréis).

Instituto de Investigaciones Marinas y Costeras José Benito Vives de Andréis [INVEMAR] (2022). *Diagnóstico y evaluación de la calidad de las aguas marinas y costeras en el Caribe y Pacífico Colombianos* (Instituto de Investigaciones Marinas y Costeras José Benito Vives de Andréis).

Ishii, M., Feely, R. A., Rodgers, K. B., Park, G. H., Wanninkhof, R., Sasano, D., et al. (2014). Air–sea CO 2 flux in the Pacific Ocean for the period 1990–2009. *Biogeosciences* 11, 709–734. doi: 10.5194/bg-11-709-2014

Kang, Y., Pan, D., Bai, Y., He, X., Chen, X., Chen, C. T. A., et al. (2013). Areas of the global major river plumes. *Acta Oceanologica Sin.* 32, 79–88. doi: 10.1007/s13131-013-0269-5

Kleypas, J. A., Buddemeier, R. W., Archer, D., Gattuso, J. P., Langdon, C., and Opdyke, B. N. (1999). Geochemical consequences of increased atmospheric carbon dioxide on coral reefs. *Science* 284, 118–120. doi: 10.1126/science.284.5411.118

Lamarque, B., Deflandre, B., Schmidt, S., Bernard, G., Dubosq, N., Diaz, M., et al. (2022). Spatiotemporal dynamics of surface sediment characteristics and benthic macrofauna compositions in a temperate high-energy River-dominated Ocean Margin. *Continental Shelf Res.* 247. doi: 10.1016/j.csr.2022.104833

Lavín, M. F., Fiedler, P. C., Amador, J. A., Ballance, L. T., Färber-Lorda, J., and Mestas-Nuñez, A. M. (2006). A review of eastern tropical Pacific oceanography: Summary. *Prog. Oceanography* 69, 391–398. doi: 10.1016/j.pocean.2006.03.005

Lee, K., Kim, T. W., Byrne, R. H., Millero, F. J., Feely, R. A., and Liu, Y. M. (2010). The universal ratio of boron to chlorinity for the North Pacific and North Atlantic oceans. *Geochimica Cosmochimica Acta* 74, 1801–1811. doi: 10.1016/j.gca.2009.12.027

Lee, K., Tong, L. T., Millero, F. J., Sabine, C. L., Dickson, A. G., Goyet, C., et al. (2006). Global relationships of total alkalinity with salinity and temperature in surface waters of the world's oceans. *Geophysical Res. Lett.* 33. doi: 10.1029/2006GL027207

Lizcano-Sandoval, L. D., Londoño-Cruz, E., and Zapata, F. A. (2018). Growth and survival of *Pocillopora damicornis* (Scleractinia: Pocilloporidae) coral fragments and their potential for coral reef restoration in the Tropical Eastern Pacific. *Mar. Biol. Res.* 14, 887–897. doi: 10.1080/17451000.2018.1528011

Lozano-Cortés, D. F., Giraldo, A., and Izquierdo, V. (2014). Short-term assessment of the sediment deposition rate and water conditions during a rainy season on La Azufrada coral reef, Gorgona Island, Colombia. *Rev. Biología Trop.* 62, 107–116. doi: 10.15517/rbt.v62i0.15981

Manzello, D. P. (2010). Coral growth with thermal stress and ocean acidification: lessons from the eastern tropical Pacific. *Coral Reefs* 29, 749–758. doi: 10.1007/s00338-010-0623-4

Medellín-Maldonado, F., Cabral-Tena, R. A., López-Pérez, A., Calderón-Aguilera, L. E., Norzagaray-López, C., Chapa-Balcorta, C., et al. (2016). Calcification of the main reef-building coral species on the Pacific coast of southern Mexico. *Cienc. Marinas* 42, 209–225. doi: 10.7773/cm.v42i3.2650

Metzl, N., Fin, J., Lo Monaco, C., Mignon, C., Alliouane, S., Antoine, D., et al. (2024). A synthesis of ocean total alkalinity and dissolved inorganic carbon measurements from 1993 to 2022: the SNAPO-CO2-v1 dataset. *Earth System Sci. Data* 16, 89–120. doi: 10.5194/essd-16-89-2024

Millero, F. J. (2007). The marine inorganic carbon cycle. *Chem. Rev.* 107, 308–341. doi: 10.1021/cr0503557

Millero, F. J. (2010). Carbonate constants for estuarine waters. *Mar. Freshw. Res.* 61, 139–142. doi: 10.1071/MF09254

Millero, F. J. (2013). *Chemical Oceanography. 4th ed* (Boca Raton: CRC Press).

Munhoven, G. (2013). Mathematics of the total alkalinity–pH equation–pathway to robust and universal solution algorithms: the SolveSAPHE package v1. 0.1. *Geoscientific Model. Dev.* 6, 1367–1388. doi: 10.5194/gmd-6-1367-2013

Nehir, M., Esposito, M., Loucaides, S., and Achterberg, E. P. (2022). Field application of automated spectrophotometric analyzer for high-resolution in situ monitoring of pH in dynamic estuarine and coastal waters. *Front. Mar. Sci.* 9. doi: 10.3389/fmars.2022.891876

Oliva-Méndez, N., Delgadillo-Hinojosa, F., Pérez-Brunius, P., Valencia-Gasti, A., Huerta-Diaz, M. A., Palacios-Coria, E., et al. (2018). The carbonate system in coastal waters off the northern region of the Baja California Peninsula under La Niña conditions. *Cienc. Marinas* 44, 203–220. doi: 10.7773/cm.v44i3.2833

Osorio, A. F. A., Peláez-Zapata, D. S., Guerrero-Gallego, J., Álvarez-Silva, O., Osorio-Cano, J. D., Toro, F. M., et al. (2014). Hydrodynamics applied to the management and conservation of marine and coastal ecosystems: Gorgona Island, Colombian Pacific Ocean. *Rev. Biol. Trop.* 62, 133–147. doi: 10.15517/rbt.v62i0.15983

Palacios Moreno, M. A., and Pinto Tovar, C. A. (1992). Estudio de la influencia de la marea en el río Guapi. *Boletín Científico Centro Control Contaminación Del Pacífic* 3, 3–13. doi: 10.26640/01213423.3.3_13

Perez, F. F., and Fraga, F. (1987). Association constant of fluoride and hydrogen ions in seawater. *Mar. Chem.* 21, 161–168. doi: 10.1016/0304-4203(87)90036-3

Pierrot, D., Epitalon, J.-M., Orr, J. C., Lewis, E., and Wallace, D. W. R. (2021). *MS Excel program developed for CO2 system calculations – version 3.0*. Available online at: https://github.com/dpierrot/co2sys_xl (Accessed June 20, 2025).

Poveda, G., and Mesa, O. J. (2000). On the existence of Lloró (the rainiest locality on Earth): Enhanced ocean-land-atmosphere interaction by a low-level jet. *Geophysical Res. Lett.* 27, 1675–1678. doi: 10.1029/1999GL006091

Prahl, H. V., Cantera, J. R., and Contreras R, R. (1990). *Manglares y hombres del Pacífico Colombiano* (Colciencias).

Preciado, R. A. (2023). *Variabilidad espacio-temporal del sistema carbonatos en Isla Gorgona, Pacífico Colombiano, Panamá Bight [Trabajo de grado, maestría en Ciencias Biológicas]* (Pontificia Universidad Javeriana).

Rangel, O., and Rudas, A. (1990). Aspectos microclimáticos. *Biota y ecosistemas Gorgona*, 41–51.

Rérolle, V. M., Achterberg, E. P., Ribas-Ribas, M., Kitidis, V., Brown, I., Bakker, D. C., et al. (2018). High resolution pH measurements using a lab-on-chip sensor in surface waters of Northwest European shelf seas. *Sensors* 18, 2622. doi: 10.3390/s18082622

Restrepo, J. D., and Kjerfve, B. (2000). Water discharge and sediment load from the western slopes of the Colombian Andes with focus on Rio San Juan. *J. Geology* 108, 17–33. doi: 10.1086/314390

Ricaurte-Villota, C., Murcia-Riaño, M., and Hernandez-Ayon, J. M. (2025). Dynamics and drivers of the carbonate system: response to terrestrial runoff and upwelling along the Northeastern Colombian Caribbean coast. *Front. Mar. Sci.* 11. doi: 10.3389/fmars.2024.1305542

Romero-Torres, M., and Acosta, A. (2010). *Corales duros del Pacífico Colombiano: guía visual de identificación* Vol. 41 (Bogotá DC Colombia: Unión Gráfica Ltda.).

Romero-Torres, M., Treml, E. A., Acosta, A., and Paz-Garciá, D. A. (2018). The Eastern Tropical Pacific coral population connectivity and the role of the Eastern Pacific Barrier. *Sci. Rep.* 8. doi: 10.1038/s41598-018-27644-2

Sabine, C. L., Feely, R. A., Gruber, N., Key, R. M., Lee, K., Bullister, J. L., et al. (2004). The oceanic sink for anthropogenic CO2. *Science* 305, 367–371. doi: 10.1126/science.1097403

Salisbury, J., Green, M., Hunt, C., and Campbell, J. (2008). Coastal acidification by rivers: a threat to shellfish? *Eos Trans. Am. Geophysical Union* 89, 513–513. doi: 10.1029/2008EO500001

Sánchez-Noguera, C. (2019). Carbonate chemistry and coral reefs in the Pacific coast of Costa Rica *[Doctoral dissertation]* (Universität Hamburg).

Sánchez-Noguera, C., Stuhldreier, I., Cortés, J., Jiménez, C., Morales, Á., Wild, C., et al. (2018). Natural ocean acidification at Papagayo upwelling system (north Pacific Costa Rica): Implications for reef development. *Biogeosciences* 15, 2349–2360. doi: 10.5194/bg-15-2349-2018

Sarmiento, J. L., and Gruber, N. (2006). *Ocean Biogeochemical Dynamics* (Princeton University Press). doi: 10.2307/j.ctt3fgxqx

Serna, L. M., Arias, P. A., and Vieira, S. C. (2018). The Choco and Caribbean low-level jets during El Niño and El Niño Modoki events. *Rev. la Academia Colombiana Cienc. Exactas Fisicas y Naturales* 42, 410–421. doi: 10.18257/raccefyn.705

Spaulding, R. S., DeGrandpre, M. D., Beck, J. C., Hart, R. D., Peterson, B., De Carlo, E. H., et al. (2014). Autonomous in *situ* measurements of seawater alkalinity. *Environ. Sci. Technol.* 48, 9573–9581. doi: 10.1021/es501615x

Takatani, Y., Enyo, K., Iida, Y., Kojima, A., Nakano, T., Sasano, D., et al. (2014). Relationships between total alkalinity in surface water and sea surface dynamic height in the Pacific Ocean. *J. Geophysical Research: Oceans* 119, 2806–2814. doi: 10.1002/2013JC009739

Terlouw, G. J., Knor, L. A., De Carlo, E. H., Drupp, P. S., Mackenzie, F. T., Li, Y. H., et al. (2019). Hawaii coastal seawater CO2 network: A statistical evaluation of a decade of observations on tropical coral reefs. *Front. Mar. Sci.* 6. doi: 10.3389/fmars.2019.00226

Tortolero-Langarica, J. J. A., Rodríguez-Troncoso, A. P., Cupul-Magaña, A. L., Morales-de-Anda, D. E., Caselle, J. E., and Carricart-Ganivet, J. P. (2022). Coral calcification and carbonate production in the eastern tropical Pacific: The role of branching and massive corals in the reef maintenance. *Geobiology* 20, 533–545. doi: 10.1111/gbi.12491

Trujillo, A. P., and Thurman, H. V. (2016). *Essentials of Oceanography. 12th ed* (Hoboken: Pearson Educación).

Turk, D., Zappa, C. J., Meinen, C. S., Christian, J. R., Ho, D. T., Dickson, A. G., et al. (2010). Rain impacts on CO2 exchange in the western equatorial Pacific Ocean. *Geophysical Res. Lett.* 37. doi: 10.1029/2010GL045520

Unidad de Planeación Minero Energética [UPME] (2005). *Atlas de Radiación solar de Colombia*. Bogotá: UPME. 175 pp. Available at: http://www.upme.gov.co/Atlas_Radiacion.htm

Vaittinada Ayar, P., Tjiputra, J., Bopp, L., Christian, J. R., Ilyina, T., Krasting, J. P., et al. (2022). Contrasting projection of the ENSO-driven CO 2 flux variability in the Equatorial Pacific under high warming scenario. *Earth System Dynamics Discussions* 2022, 1–31. doi: 10.5194/esd-13-1097-2022

Valauri-Orton, A., Lowder, K. B., Currie, K., Sabine, C. L., Dickson, A. G., Chu, S. N., et al. (2025). Perspectives from developers and users of the GOA-ON in a Box kit: A model for capacity sharing in ocean sciences. *Oceanography* 38. doi: 10.5670/oceanog.2025.135

Vargas, C. A., Contreras, P. Y., Pérez, C. A., Sobarzo, M., Saldías, G. S., and Salisbury, J. (2016). Influences of riverine and upwelling waters on the coastal carbonate system off Central Chile and their ocean acidification implications. *J. Geophysical Research: Biogeosciences* 121, 1468–1483. doi: 10.1002/2015JG003213

von Schuckmann, K., Moreira, L., Cancet, M., Gues, F., Autret, E., Baker, J., et al. (2024). The state of the global ocean. *State Planet* 4, 1–30. doi: 10.5194/sp-4-osr8-1-2024

Wang, Z. A., Moustahfid, H., Mueller, A., Michel, A. P. M., Mowlem, M., Glazer, B. T., et al. (2019). Advancing observation of ocean biogeochemistry, biology, and ecosystems with cost-effective *in situ* sensing technologies. *Front. Mar. Sci.* 6. doi: 10.3389/fmars.2019.00519

Webster, P. J. (2020). *Dynamics of the tropical atmosphere and oceans* (John Wiley and Sons).

Wu, Y., Dai, M., Guo, X., Chen, J., Xu, Y., Dong, X., et al. (2021). High-frequency time-series autonomous observations of sea surface p CO2 and pH. *Limnology Oceanography* 66, 588–606. doi: 10.1002/lno.11625

Yasunaka, S., Kouketsu, S., Strutton, P. G., Sutton, A. J., Murata, A., Nakaoka, S., et al. (2019). Spatio-temporal variability of surface water pCO2 and nutrients in the tropical

Pacific from 1981 to 2015. *Deep Sea Res. Part II: Topical Stud. Oceanography* 169, 104680. doi: 10.1016/j.dsr2.2019.104680

Yin, T., Papadimitriou, S., Rérolle, V. M., Arundell, M., Cardwell, C. L., Walk, J., et al. (2021). A novel lab-on-chip spectrophotometric pH sensor for autonomous in situ seawater measurements to 6000 m depth on stationary and moving observing platforms. *Environ. Sci. Technol.* 55, 14968–14978. doi: 10.1021/acs.est.1c03517

Zapata, F. A. (2001). "Formaciones coralinas de la isla Gorgona," in *Gorgona marina: contribución al conocimiento de una isla única*. Eds. L. M. Barrios and M. López-Victoria (Instituto de Investigaciones Marinas y Costeras [INVEMAR]), 27–40.

Zapata, F. A., Rodríguez-Ramírez, A., Caro-Zambrano, C., and Garzón-Ferreira, J. (2010). Mid-term coral-algal dynamics and conservation status of a Gorgona Island (Tropical Eastern Pacific) coral reef. *Rev. Biología Trop.* 58, 81–94. doi: 10.15517/rbt.v58i1.20025

Zeebe, R. E., and Wolf-Gladrow, D. (2001). *CO2 in seawater: equilibrium, kinetics, isotopes* Vol. 65 (Gulf Professional Publishing).

Zhai, W. D., Zang, K. P., Huo, C., Zheng, N., and Xu, X. M. (2015). Occurrence of aragonite corrosive water in the North Yellow Sea, near the Yalu River estuary, during a summer flood. *Estuarine Coast. Shelf Sci.* 166, 199–208. doi: 10.1016/j.ecss.2015.02.010

Zhong, G., Li, X., Song, J., Qu, B., Wang, F., Wang, Y., et al. (2025). A global monthly 3D field of seawater pH over 3 decades: a machine learning approach. *Earth System Sci. Data* 17, 719–740. doi: 10.5194/essd-17-719-2025

frontiers | Frontiers in Marine Science

TYPE Original Research
PUBLISHED 28 August 2025
DOI 10.3389/fmars.2025.1626578

OPEN ACCESS

EDITED BY
Jose Martin Hernandez-Ayon,
Autonomous University of Baja California, Mexico

REVIEWED BY
Peng Zhang,
Guangdong Ocean University, China
Cecilia Chapa-Balcorta,
Universidad del Mar, Mexico

*CORRESPONDENCE
Natalia Rincón-Díaz
mnrincon@unimagdalena.edu.co

RECEIVED 11 May 2025
ACCEPTED 29 July 2025
PUBLISHED 28 August 2025

CITATION
Rincón-Díaz N, Gómez CE, Piñeros-Pérez V, Alvarado-Jiménez F, Núñez S and García-Urueña R (2025) Temporal dynamics of the carbonate system in a tropical rhodolith bed from a protected Caribbean bay. *Front. Mar. Sci.* 12:1626578. doi: 10.3389/fmars.2025.1626578

Temporal dynamics of the carbonate system in a tropical rhodolith bed from a protected Caribbean bay

Natalia Rincón-Díaz[1]*, Carlos E. Gómez[2], Valentina Piñeros-Pérez[1], Félix Alvarado-Jiménez[1], Samuel Núñez[3] and Rocío García-Urueña[1]

[1]Grupo de Investigación en Ecología y Diversidad de Algas Marinas y Arrecifes Coralinos, Universidad del Magdalena, Santa Marta, Colombia, [2]Laboratorio de Biología Molecular Marina (BIOMMAR), Universidad de los Andes, Bogotá, Colombia, [3]Universidad del Magdalena, Santa Marta, Colombia

Coastal zones are key players in the global carbon cycle, yet the temporal dynamics of their carbonate system, particularly in tropical rhodolith habitats, remain understudied. This study assessed seasonal and spatial variability in carbonate chemistry in Gairaca Bay, a protected tropical bay within Tayrona National Natural Park, Colombian Caribbean. Sampling was conducted in 2023–2024 across three habitats: a rhodolith bed (1, 7, 15 m depth), the bay entrance (outer bay, 10 m depth), and a shallow sandy-bottom area (inner bay, 1 and 6 m depths). Temperature, salinity, and total scale pH (pH_T) were measured *in situ*; total alkalinity (TA) was determined via open-cell titration, and dissolved inorganic carbon (DIC), pCO_2, bicarbonate (HCO_3^-), carbonate (CO_3^{2-}), and aragonite saturation state (Ω_{arag}) were calculated. Seasonal and spatial patterns were analyzed using PERMANOVA. Significant seasonal differences were found in temperature ($F = 248.42$, $p < 0.05$), salinity ($F = 49.02$, $p < 0.05$), TA ($F = 7.65$, $p < 0.001$), and DIC ($F = 2.54$, $p < 0.001$), with no significant variation among sites or depths. Upwelling periods were cooler and saltier (25.9 ± 1.14 °C; 34.48 ± 0.46), with elevated TA and DIC, and slightly lower pH_T and Ω_{arag}. Non-upwelling periods were warmer (30.0 ± 0.76 °C), less saline (33.36 ± 0.28), and had higher pH_T and Ω_{arag}. Seasonal delta analysis indicated greater variability during non-upwelling, linked to enhanced freshwater discharge. The outer bay showed the highest variability in pH_T and Ω_{arag}, while the inner bay was most stable for TA and DIC. The rhodolith bed bottom exhibited high TA variability but stability in pH_T and Ω_{arag}, especially during non-upwelling. Seasonal processes, including upwelling and freshwater inputs, drive carbonate system variability in Gairaca Bay. The stability of pH_T and Ω_{arag} in the rhodolith bed bottom suggests a potential role as a biogeochemical refuge in acidification-prone tropical environments.

KEYWORDS

carbonate chemistry, upwelling, rhodolith beds, tropical coastal ecosystems, runoff

1 Introduction

The coastal marine carbonate system is increasingly recognized as critical components of the global carbon cycle, particularly in light of ongoing climate change and ocean acidification (Martin and Hall-Spencer, 2017; Padin et al., 2020). Although coastal ecosystems occupy a relatively small fraction of the ocean's surface, they contribute disproportionately to marine primary production, fisheries, and biodiversity, supporting essential ecosystem services (Doney et al., 2012; Silbiger and Sorte, 2018). In 2013, demersal and pelagic fisheries yielded approximately 2×10^{10} kg and 8×10^{9} kg of catch, respectively, together accounting for 28% of global fish production (Lu et al., 2018). These habitats also excel at carbon sequestration, salt marshes, mangroves, and seagrasses store more carbon per unit area than most terrestrial forests (Lu et al., 2018). Consequently, developing a comprehensive understanding of natural carbonate chemistry dynamics in coastal systems is essential for predicting their resilience to future environmental change (Pedersen et al., 2024).

Within tropical coastal zones, the interplay between physical, chemical, and biological processes generates high spatial and temporal variability in carbonate system parameters (Roberts et al., 2021; García-Ibáñez et al., 2024). Seasonal drivers, such as coastal upwelling and freshwater inflows, exert a influence on carbonate chemistry by modulating temperature, salinity, dissolved inorganic carbon (DIC), and total alkalinity (TA) (Ricaurte-Villota et al., 2025). Despite their importance, tropical upwelling systems remain understudied compared to their temperate counterparts, limiting our understanding of their natural variability and resilience.

Upwelling processes, which transport cold deeper nutrient-rich waters to the surface, can alter coastal carbonate chemistry. These changes include reductions in pH and aragonite saturation state (Ω_{arag}) associated with increased partial pressure of CO_2 (pCO_2), TA and DIC concentrations (Reum et al., 2016; Xiu et al., 2018; Gómez et al., 2023). However, the magnitude and consequences of these fluctuations can vary depending on regional oceanography, local biogeochemical processes, and climatic phenomena such as the El Niño–Southern Oscillation (ENSO) (Reithmaier et al., 2023).

In the Colombian Caribbean region, the North Atlantic Subtropical Underwater (SUW) enters the basin from the tropical Atlantic and becomes shallower along the continental slope, reaching depths of approximately 50 m near Santa Marta and Tayrona National Natural Park (TNNP) (Correa-Ramirez et al., 2020). Before reaching these coastal upwelling zones, the SUW mixes with fresher waters influenced by the Caribbean Coastal Countercurrent within the Panama-Colombia Gyre. This mixing reduces salinity and alter the carbonate chemistry and nutrient content of upwelled waters (Bayraktarov et al., 2012; Correa-Ramirez et al., 2020), ultimately impacting coastal ecosystems.

Gairaca Bay (TNNP), offers a unique setting to study the seasonal and interannual variability of carbonate system dynamics in a tropical upwelling-influenced environment. Seasonal upwelling events within the TNNP, deliver cooler, more saline, carbon-enriched waters to the bay, lowering pH and increasing DIC and TA, while during non-upwelling periods dominated by freshwater input, dilution effects elevate pH and reduce DIC and TA, creating contrasting biogeochemical conditions (Ricaurte-Villota et al., 2025). In TNNP, ENSO drives interannual variability, whereas seasonal changes are primarily influenced by coastal upwelling and freshwater discharge from the Magdalena River (Ricaurte-Villota et al., 2025).

Among the key habitats within Gairaca Bay are rhodolith beds, composed of free-living coralline algae, which were originally referred to as *Lithothamnion* meadows by Garzón-Ferreira and Cano (1991). These structures play vital ecological and biogeochemical roles, serving as biodiversity hotspots, stabilizing sediments, and significantly contributing to carbonate production in marine sediments (Foster, 2001; van der Heijden and Kamenos, 2015; Martin and Hall-Spencer, 2017). Unlike coral reefs, which are generally considered carbon sources, rhodolith beds can act as either carbon sinks or sources depending on species composition and environmental conditions (Schubert et al., 2024). Their resilience to extreme environmental conditions (Martin and Hall-Spencer, 2017) and capacity for photosynthesis and calcification make them potential buffers against local acidification (Riosmena-Rodríguez et al., 2017). Moreover, while mangroves are recognized as blue carbon sinks (Yong et al., 2011; Yeemin et al., 2024), rhodolith beds offer a complementary biogeochemical function. However, their ecological functionality may be threatened under future environmental scenarios due to projected changes in temperature, nutrient availability, and carbonate chemistry (McCoy and Ragazzola, 2014; Mccoy and Kamenos, 2015).

In this study, we analyzed carbonate system variability across three contrasting environments within Gairaca Bay: a rhodolith bed, the bay entrance (Outer bay), and a shallow sandy-bottom area (Inner bay). Our goals were to (i) characterize spatial and temporal patterns in carbonate system parameters (TA, DIC, pH_T, pCO_2, Ω_{arag}) across these habitats; (ii) evaluate the influence of seasonal climatic phases (upwelling vs. non-upwelling) on the carbonate chemistry; and (iii) explore the potential role of rhodolith beds as a proxy for understanding local modulation of carbonate system dynamics under natural upwelling conditions.

2 Materials and methods

2.1 Study area

This study was conducted from March 2023 to July 2024 in Gairaca Bay, a protected bay located within TNNP, on the Caribbean coast of Colombia (11°15'33'' N, 73°24'06'' W) (Figure 1). The bay is situated between the eastern sector of Taganga and the Piedras River basin, and features diverse geomorphology including rhodolith beds, coral reefs, rocky shores, sandy beaches, shallow sandy-bottom areas, and a transitional zone at the bay's entrance influenced by open ocean processes (Figure 1).

The region experiences pronounced seasonal variability, modulated by the interplay of coastal upwelling, precipitation,

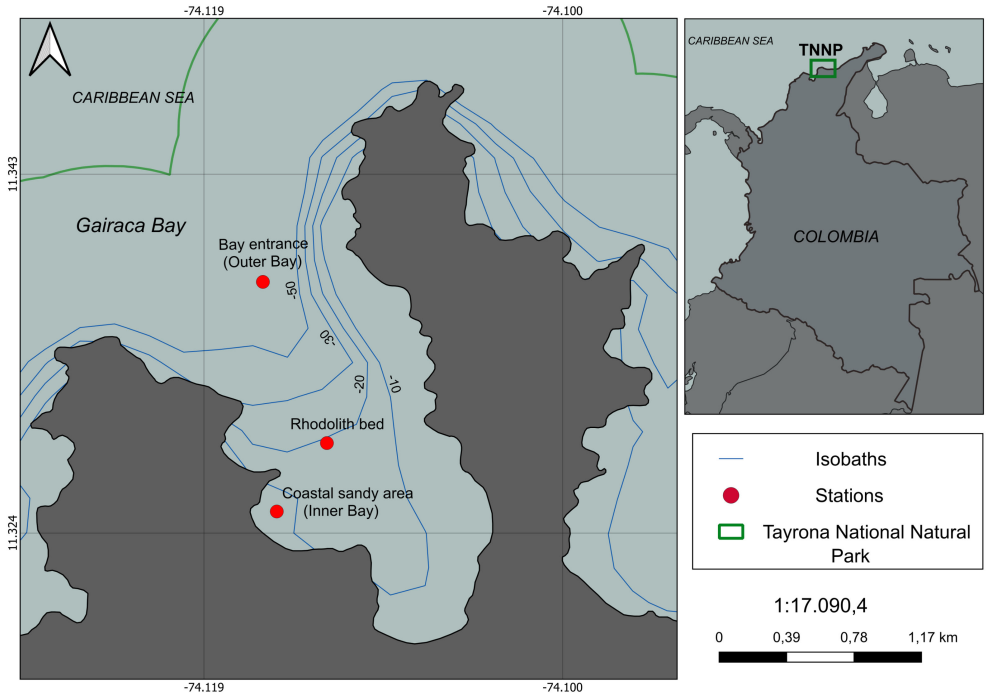

FIGURE 1
Map of Gairaca Bay within Tayrona National Natural Park, showing the sampling stations used for carbonate chemistry characterization. Depth contours (isobaths) are shown to illustrate the bathymetry of the bay.

and freshwater inflow (Bayraktarov et al., 2014) (Ricaurte-Villota et al., 2025). The local climate follows a bimodal seasonal pattern, with alternating wet and dry periods throughout the year. The rainy season typically extends from August to November, while the dry season occurs between December and April. During the dry season, intensified northeasterly trade winds promote upwelling of SUW with sea surface temperatures between 19–25 °C and salinities exceeding 36.5 (Paramo et al., 2011; Correa-Ramirez et al., 2020). In contrast, rainy season conditions are characterized by warmer surface waters (average 28.7 °C, reaching up to 30.3 °C) and reduced salinity (~34.7) due to increased freshwater input from the Magdalena river and local tributaries draining from the Sierra Nevada de Santa Marta (Arévalo-Martínez and Franco-Herrera, 2008; Bayraktarov et al., 2013; Alvarado-Jiménez et al., 2024) that alters salinity, total alkalinity (TA), and dissolved inorganic carbon (DIC) within the bay (Ricaurte-Villota et al., 2025). These seasonal changes in water mass properties are driven by the alternating dominance of coastal upwelling and fluvial inputs.

To further characterize the upwelled water mass, we used ARGO profiling float data to identify the presence of SUW in the offshore region of the Colombian Caribbean. The gridded distribution of potential temperature (θ) was derived from validated ARGO profiles (WOD code: 12; originator's flag set to use = 12), collected in April 2024 approximately 200 km off the coast during oceanographic cruises. The figure was generated using the "Two Scatter Windows" tool in Ocean Data View (ODV) with gridded field interpolation enabled. SUW was identified by its characteristic high-salinity core (~37.16 ± 0.18) located at ~120 m depth (Correa-Ramirez et al., 2020). This thermohaline signature is consistent with SUW properties previously described for the western tropical Atlantic, supporting the notion that this water mass is the primary source of upwelled water in the region during the dry season (Supplementary Figure SM_1).

2.2 Sampling station selection and environmental variable collection

Three stations were strategically selected to represent different habitats and hydrodynamic conditions: A rhodolith bed located at the center of the bay (sampled at 1, 7, and 15 m depths), the outer bay at the entrance (10 m depth), and the inner bay, a shallow sandy-bottom zone near the beach (sampled at 1 and 6 m depths). The selection of the three sampling sites within Gairaca Bay, was guided by the objective of capturing environmental contrasts within a relatively small spatial scale, such as physical and oceanographic features related to depth, exposure to oceanic exchange, and proximity to terrestrial inputs (Figure 1).

At each station and depth, *in situ* measurements of temperature, salinity, and pH were taken immediately after sample collection. The pH on the total scale (pH_T) was measured using a SI Analytics HandyLab 100 meter equipped with a WTW Sentix 41 pH electrode. The instrument had a resolution setting of 0.001 pH units (3 decimal places) and an accuracy of ≤ 0.005 pH ±1 digit. pH measurements were recorded in millivolts and later converted to pH_T using the values of Tris buffer (Batch T41) and the *in situ*

temperature, following standard operating procedures (Dickson et al., 2007). The electrode was calibrated monthly using NBS buffers (pH 4.01, 7.00, and 10.00), and during each calibration, the slope was checked and consistently exceeded 97%, indicating a near-Nernstian response (Dickson et al., 2007). Dissolved oxygen was measured *in situ* using a WTW Oxi 3310 meter, with a manufacturer-reported accuracy of ≤ 0.1 K ±1 digit. Salinity and conductivity were measured using an SI Analytics HandyLab 200 meter, with an accuracy of ≤ 0.5% of the measured value ±1 digit. These measurements were taken immediately after water sample collection at each station and depth to ensure reliable representation of ambient conditions. Additionally, 500 mL seawater samples were collected monthly either by SCUBA diving or using a 7-liter Niskin bottle. Samples for TA analysis were preserved with saturated mercuric chloride to prevent chemical alterations. All samples were transported to the Water Quality Laboratory at the University of Magdalena and stored at temperatures below 17 °C until further analysis.

Precipitation data for the study period were obtained from the Institute of Hydrology, Meteorology, and Environmental Studies (IDEAM), using records from the Simón Bolívar Airport station near Gairaca Bay. Wind speed and wind direction data were retrieved from the Copernicus product Global Ocean Hourly Sea Surface Wind and Stress, with a spatial resolution of 0.125° (DOI: 10.48670/moi-00305). Continuous temperature monitoring was performed *in situ* at the rhodolith bed (15 m depth) using an Onset HOBO UA-002–64 data logger, programmed to record every 2 hours.

All nutrient analyses were performed following the methodology described by Garay et al. (2003). Dissolved inorganic nutrient concentrations were determined using standard colorimetric techniques. Ammonium (NH_4^+) was quantified using the indophenol blue method, which involves its reaction with phenol and sodium nitroprusside in an alkaline medium in the presence of hypochlorite. Nitrite (NO_2^-) was measured via diazotization, using sulfanilamide and N-(1-naphthyl) ethylenediamine as reagents. Nitrate (NO_3^-) was first reduced to nitrite using a cadmium column activated with copper sulfate and then analyzed using the same procedure as for nitrite. Inorganic phosphate (PO_4^{3-}) was quantified using the molybdenum blue method, employing a reagent mixture of ammonium heptamolybdate, ascorbic acid, sulfuric acid, and potassium antimonyl tartrate. Absorbance measurements were performed using a UV-Vis spectrophotometer, with wavelengths ranging from 543 to 885 nm depending on the nutrient analyzed.

2.3 Sample analysis and carbonate system calculations

TA was determined via open-cell potentiometric titration with 0.1 mol L^{-1} hydrochloric acid buffered in 0.6 mol L^{-1} NaCl (Certified Reference Material - CRM, Dickson Laboratory, Batch 205), following the Remarco protocol (Bernal et al., 2021). The titration's analytical accuracy was monitored using the CRM with an uncertainty of ±10 µmol kg^{-1}.

Using the measured TA and pH_T values, additional carbonate system parameters, dissolved inorganic carbon (DIC), partial pressure of carbon dioxide (pCO_2), bicarbonate (HCO_3^-) and carbonate ions (CO_3^{2-}), and saturation state for calcite (Ω_{cal}) and aragonite (Ω_{arag}), were calculated using the Excel-CO2SYS software version 2.5 (Pierrot et al., 2006). Dissociation constants K1, K2 were taken from (Mehrbach et al., 1973) refit by (Dickson and Millero, 1987), $KHSO_4$ by (Dickson, 1990) and boron concentration following (Lee et al., 2010).

2.4 Data analysis: temporal and spatial variability of environmental and carbonate system variables

Trends in sea surface temperature, wind velocity, and precipitation were analyzed through time series plots to identify fluctuations associated with different climatic phases (upwelling, non-upwelling, transition pre-upwelling, and transition post-upwelling). Climatic classifications were based on temporal patterns of these environmental drivers.

Descriptive statistics compiling the mean ± standard deviation values of carbonate system variables such as TA, DIC, pH_T, Ω_{arag}, and CO_3^{2-} were done per site, climatic season, and year (2023–2024). To illustrate the relative temporal deviations in the carbonate system (increases or decreases of the carbonate variables over the study time), minimum and maximum seasonal deltas (Δ - deviations from the mean) were calculated for TA, DIC, Salinity, and Ω_{arag} across the rhodolith bed bottom, outer bay, and inner bay sites for each climatic season in 2023 and 2024.

Deltas (Δ_i) were computed as:

$$\Delta i = Xi - \bar{X}$$

Where Xi is the observed value and $\overline{X}$ is the overall mean of each variable, calculated using all available observations across sites, seasons, and years. The mean was chosen as the reference value to center the data around a consistent baseline, facilitating the comparison of variability across sites and time frames. This method allowed for the identification of relative increases or decreases in carbonate system parameters with respect to their average behavior.

Sectional plots of each parameter were then generated in Ocean Data View (ODV) using the Gridded Field option with DIVA gridding, with sampling date (month–year) on the X-axis, depth (m) on the Y-axis, and parameter concentration on the Z-axis. To enhance interpretability, the X-axis scale was set to 50 and the Y-axis scale increased to 350 ‰, a vertical extrapolation of ± 0.5 m was applied, and contour lines were added to highlight gradients throughout the water column.

PERMANOVA was performed to detect differences in the carbonate system parameters (TA, DIC, pCO_2, Ω_{cal}, Ω_{arag}, pH_T, salinity) among sites, depths, and seasons. A Euclidean distance

matrix was computed using standardized data with the vegdist function (vegan package, R version 4.3.2). PERMANOVA was performed using the adonis2 function, with 9,999 permutations and type II sums of squares. The homogeneity of multivariate dispersion was tested using the betadisper function and confirmed by ANOVA ($p > 0.05$).

To assess the predictive capacity of temperature on carbonate system variables, we fitted both simple and multiple linear regression models to estimate dissolved inorganic carbon (DIC, μmol kg^{-1}) and partial pressure of CO_2 (pCO_2, μatm). The analysis used discrete *in situ* data collected from three representative sites within Gairaca Bay: rhodolith bed bottom, inner bay and outer bay. The following models were applied:

Simple regression model for DIC:

$$DIC = a \,.\, Temp + b$$

Simple regression model for pCO_2:

$$PCO_2 = a \,.\, Temp + b$$

Multiple regression model for pCO_2:

$$pCO_2 = a \,.\, Temp + b - Salinity + c \,.\, TA + d \,.\, DIC + e \,.\, \left(\frac{DIC}{TA}\right)$$

Model fitting was conducted in R using the lm () function. Model performance was assessed using the coefficient of determination (R^2) and root mean square error (RMSE).

An additional PERMANOVA was performed between seasons at the rhodolith bed bottom site. SIMPER analyses were carried out to identify the contribution of individual variables to the observed dissimilarities between seasons, with 9,999 permutations. Spearman's rank correlation was used to assess relationships between environment and carbonate system variables (T°C, pCO_2, CO_3^{2-}, salinity, pH_T, DIC, Ω_{arag}) and nutrient concentrations (ammonium - NH_4^+, nitrate - NO_3^-, nitrite - NO_2^-, and phosphate - PO_4^{3-}) at the rhodolith bed bottom. All statistical analyses were performed in RStudio (version 2024.12.1 Build 563; Posit Software, PBC, 2025), using the packages vegan (Oksanen et al., 2025), ggplot2 (Wickham, 2016), car (Fox et al., 2024) (Fox and Weisberg, 2019), dplyr (Wickham et al., 2023a), and tidyr (Wickham et al., 2023b).

3 Results

3.1 Descriptive analysis of environmental variables

Seasonal and spatial variability in discrete *in situ* measurements of temperature, salinity, and dissolved oxygen was evident across the main sampling sites and depths in Gairaca Bay between March 2023 and July 2024. At the rhodolith bed bottom (15 m depth), temperatures ranged from 26.2 °C during upwelling (March 2024) to 30.5 °C in the post-upwelling transition (June 2024), with salinity between 33.5 and 35.9 and oxygen concentrations inversely correlated with temperature (3.50–7.28 $mg{\cdot}L^{-1}$). At the inner bay (6 m depth), temperatures varied from 27.0 to 30.8 °C, salinity ranged from 33.0 to 35.9, and oxygen concentrations declined from a peak of 7.93 $mg{\cdot}L^{-1}$ (March 2023) to 4.03 $mg{\cdot}L^{-1}$ (October 2023). The outer bay (10 m depth) showed intermediate conditions, with temperatures between 26.4 and 30.5 °C, salinity from 32.7 to 35.8, and dissolved oxygen following the seasonal temperature pattern (3.51–7.67 $mg{\cdot}L^{-1}$) (Table 1). Additional *in situ* data from 1 m and 7 m depths at the rhodolith bed, and from 1 m depth at the inner bay, are presented in Supplementary Material (Supplementary Table SM_1).

Mean wind speeds and water temperatures (the latter continuously measured with a HOBO sensor at the rhodolith bed bottom) exhibited a clear seasonal pattern influenced by climatic and oceanographic processes. Unless otherwise noted, all mean values are presented with their corresponding standard deviations (mean ± SD). In 2023, water temperature and wind speed exhibited marked seasonal variability associated with the upwelling season. The lowest mean water temperature was observed in March (24.73 ± 0.66 °C), corresponding to the peak of the upwelling season, while the highest was recorded in June (28.67 ± 0.98 °C), followed by a slight decrease in July (28.14 ± 0.60 °C), reflecting the transition out of the upwelling phase. Wind speeds during this period peaked in July, reaching a monthly average of 7.80 ± 1.62 $m{\cdot}s^{-1}$, with a maximum of 10.28 $m{\cdot}s^{-1}$. The lowest wind speeds occurred in May and June, with daily minima of 2.04 $m{\cdot}s^{-1}$ and 1.69 $m{\cdot}s^{-1}$, respectively, indicating a relaxation phase before re-intensification (Figure 2).

In 2024, the seasonal pattern remained consistent, but wind speeds were generally stronger and temperatures slightly higher during the post-upwelling transition. The highest mean wind speed was observed in January (10.06 ± 1.16 $m{\cdot}s^{-1}$), and high wind activity persisted through February to April (means between 8.30 and 8.53 $m{\cdot}s^{-1}$), with peak gusts exceeding 13 $m{\cdot}s^{-1}$ in February (Figure 2). As wind strength declined in May (5.83 ± 1.97 $m{\cdot}s^{-1}$), water temperatures rose to a maximum monthly mean of 27.95 ± 0.44 °C, marking the post-upwelling transition. The coldest daily temperature in 2024 was 23.27 °C, recorded in January, slightly earlier than in 2023.

Wind direction also followed a seasonal pattern, with prevailing northeasterly and easterly winds during upwelling months (January to March and December), reinforcing the wind-driven upwelling dynamics. In contrast, during transitional and non-upwelling periods, wind direction became more variable, with increased frequencies from the southeast, south, and southwest, indicating a weakening of the trade wind system and reduced upwelling potential (Supplementary Figure SM_2).

Precipitation in 2023 showed a pronounced seasonal pattern influenced by the upwelling season and associated climatic transitions. During the upwelling season (March to April) only 0.1 mm of rain was recorded on a single day in March, and a moderate onset of rainfall in April, for a total of 81.9 mm over 3 rainy days, with a peak of 54.1 mm. During the post-upwelling transition (May to July), rainfall initially decreased to 12.8 mm in May, but increased considerable in June, reaching 175.6 mm, with

10.3389/fmars.2025.1626578

TABLE 1 Monthly summary of carbonate system parameters (e.g., pH_T, TA, DIC, Ω_{arag}, CO_3^{2-}) and *in situ* environmental variables (temperature, salinity, dissolved oxygen) across sites and depths (Rhodolith bed: 15 m, Inner bay: 6 m, Outer bay: 10 m) in Gairaca Bay, categorized by climatic season.

Site/ year-month	Season	TA (µmol kg $^{-1}$)	ph_T	DIC (µmol kg $^{-1}$)	Ω_{arag}	CO_3 (µmol kg $^{-1}$)	Salinity	Temperature °C	O_2 mg·L^{-1}
Rhodolith bed bottom (15 m depth)									
2023-3	Upwelling	2469.30	7.99	2166.24	3.55	220.51	34.50	27.20	7.04
2023-4	Upwelling	2411.50	7.99	2115.74	3.46	214.33	34.00	27.40	4.37
2023-5	Transition post-upwelling	2376.80	7.97	2089.15	3.38	208.17	34.00	28.30	5.64
2023-6	Transition post-upwelling	2357.80	7.94	2080.12	3.24	200.22	35.00	28.70	7.28
2023-7	Transition post-upwelling	2451.70	8.00	2138.33	3.64	226.14	35.00	27.70	7.19
2023-8	Transition post-upwelling	2295.90	7.96	2007.64	3.41	206.83	33.50	30.50	6.26
2023-9	Non-upwelling	2365.50	8.02	2036.28	3.88	235.66	33.50	29.90	5.02
2023-10	Non-upwelling	2287.30	8.01	1977.78	3.60	219.57	33.60	29.30	4.17
2023-11	Transition pre-upwelling	2375.80	7.92	2108.56	3.14	194.21	35.00	28.50	4.63
2023-12	Transition pre-upwelling	2446.40	7.91	2196.89	3.00	185.70	34.20	27.30	4.04
2024-1	Upwelling	2435.00	7.92	2175.97	3.06	190.66	34.80	26.90	4.23
2024-2	Upwelling	2372.00	7.93	2113.12	3.06	189.19	34.20	27.50	4.99
2024-3	Upwelling	2380.10	7.94	2125.23	2.97	185.98	34.70	26.20	4.23
2024-4	Upwelling	2358.10	7.98	2063.97	3.37	210.08	35.10	27.40	4.67
2024-5	Transition post-upwelling	2388.10	8.00	2075.15	3.57	222.85	35.60	28.00	5.10
2024-6	Transition post-upwelling	2355.90	7.99	2034.46	3.70	228.02	35.30	30.00	3.50
2024-7	Transition post-upwelling	2412.10	7.89	2150.61	3.07	191.16	35.90	28.80	5.49
Inner bay (6 m depth)									
2023-3	Upwelling	2420.20	8.13	2031.37	4.42	274.54	34.50	27.30	7.93
2023-4	Upwelling	2416.10	7.98	2124.03	3.43	212.15	34.00	27.50	3.62
2023-5	Transition post-upwelling	2436.40	8.00	2116.75	3.73	230.33	34.70	28.70	5.20
2023-6	Transition post-upwelling	2391.10	7.98	2095.02	3.43	213.03	34.80	27.80	7.20
2023-7	Transition post-upwelling	2457.60	7.96	2161.41	3.49	215.69	34.90	28.50	6.50
2023-8	Transition post-upwelling	2294.30	7.95	2006.03	3.42	206.87	33.50	30.80	6.94
2023-9	Non-upwelling	2317.00	8.03	1986.73	3.86	234.33	33.60	30.20	6.32
2023-10	Non-upwelling	2281.50	7.99	1970.95	3.68	221.30	33.00	31.20	4.03
2023-11	Transition pre-upwelling	2432.10	7.98	2133.12	3.49	216.44	34.70	27.60	5.01

(Continued)

10.3389/fmars.2025.1626578

TABLE 1 Continued

Site/ year-month	Season	TA (μmol kg $^{-1}$)	ph_T	DIC (μmol kg $^{-1}$)	Ω_{arag}	CO_3 (μmol kg $^{-1}$)	Salinity	Temperature °C	O_2 mg·L^{-1}
Inner bay (6 m depth)									
2023-12	Transition pre-upwelling	2342.50	7.86	2123.33	2.62	162.96	34.50	27.00	4.43
2024-1	Upwelling	2365.20	7.76	2188.48	2.25	138.59	34.20	28.10	4.50
2024-2	Upwelling	2316.40	7.91	2071.33	2.88	178.40	34.50	27.70	4.66
2024-3	Upwelling	2422.20	7.85	2192.47	2.77	172.00	35.20	28.10	4.86
2024-4	Upwelling	2371.10	8.00	2054.55	3.61	224.67	35.50	28.20	4.91
2024-5	Transition post-upwelling	2288.20	7.92	2020.34	3.17	193.08	34.00	30.40	4.32
2024-6	Transition post-upwelling	2371.30	7.89	2113.71	3.01	187.25	35.90	28.70	5.48
Outer bay (10 m depth)									
2023-3	Upwelling	2440.00	7.97	2152.81	3.37	209.43	34.30	27.20	7.04
2023-4	Upwelling	2399.20	8	2105.32	3.43	212.63	33.90	27.00	3.46
2023-5	Transition post-upwelling	2443.90	8	2127.37	3.69	228.46	34.70	28.30	5.52
2023-6	Transition post-upwelling	2431.80	7.97	2138.51	3.41	212.45	35.00	27.60	6.88
2023-7	Transition post-upwelling	2335.90	8.03	2019.29	3.6	223.81	34.90	27.50	7.67
2023-8	Transition post-upwelling	2457.60	7.95	2163.25	3.55	216.34	33.60	29.70	5.61
2023-9	Non-upwelling	2333.40	7.95	2046.94	3.41	206.97	33.50	30.10	5.35
2023-10	Non-upwelling	2320.50	8.01	2005.63	3.75	225.82	32.70	30.50	3.87
2023-11	Transition pre-upwelling	2335.00	7.97	2053.41	3.23	201.46	34.90	27.30	4.78
2023-12	Transition pre-upwelling	2478.00	7.9	2234.49	2.92	182.24	34.60	26.40	4.58
2024-1	Upwelling	2420.90	7.91	2159.99	3.09	191.64	35.00	28.10	5.00
2024-2	Upwelling	2330.80	7.96	2058.48	3.18	196.49	34.10	27.90	5.26
2024-3	Upwelling	2435.80	8.01	2127.88	3.56	221.97	34.70	26.60	4.73
2024-4	Upwelling	2421.00	7.99	2122.72	3.45	215.07	35.00	27.10	4.71
2024-5	Transition post-upwelling	2363.20	7.94	2085.04	3.21	200.1	35.40	28.10	5.02
2024-6	Transition post-upwelling	2332.00	7.94	2045.35	3.35	205.41	35.00	30.10	3.51
2024-7	Transition post-upwelling	2388.20	7.88	2135.68	2.97	184.81	35.80	28.80	4.93

an extreme event of 102.4 mm on a single day. Rainfall decreased again in July to 51.1 mm, although distributed over 13 rainy days. In 2024, the first quarter of the year was extremely dry, with only 0.4 mm of rain in February. A slight increase occurred in April (5.9 mm) and May (6.8 mm), with isolated light rain events. June, marked the onset of the rainy season, with 126.9 mm, including 7 days with rainfall exceeding 5 mm, and a maximum daily value of 43.0 mm. In July, rainfall was 72.2 mm, although concentrated in fewer events, with one day of heavy rainfall peaking at 63.1 mm (Figure 3).

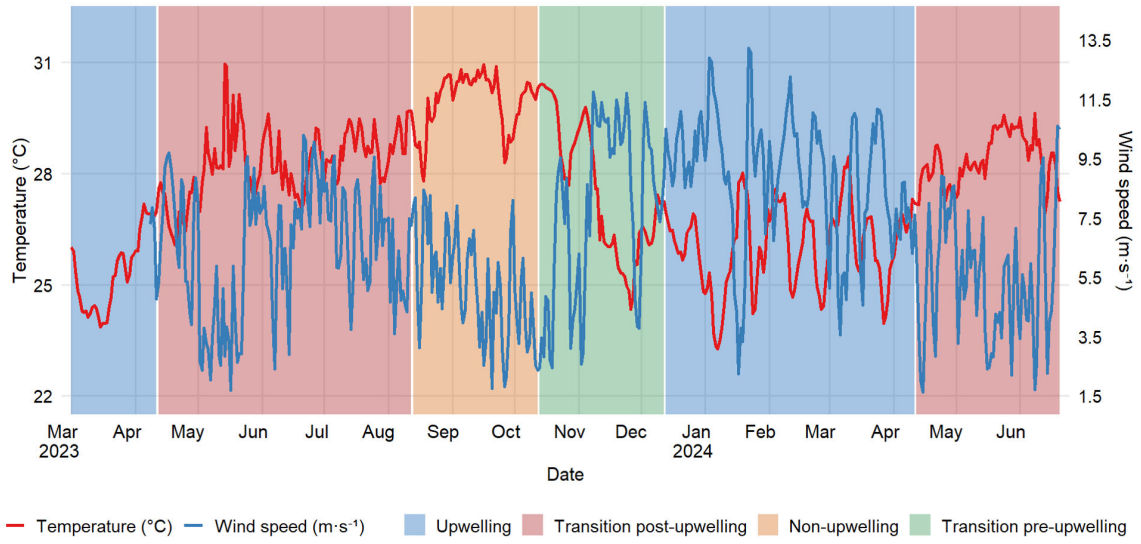

FIGURE 2
Average monthly wind speed and water temperature at the study site. Temperature was recorded *in situ* at the rhodolith bed (15 m depth) using HOBO data loggers.

3.2 Carbonate system dynamics

A summary of carbonate system variables and *in situ* environmental parameters across the three main sites, rhodolith bed bottom (15 m), inner bay (6 m), and outer bay (10 m), is shown in Table 1. A full dataset including additional depths and sites (e.g., rhodolith bed surface (1 m depth) and midwater (7 m depth), inner bay surface (1 m depth)) is provided in Supplementary Material (Supplementary Table SM_1).

The seasonal averages and standard deviations reported below were calculated from the raw data presented in Table 1 and Supplementary Table SM_1. For clarity and synthesis, values were grouped by site and climatic period (upwelling, non-upwelling, and transitional seasons), to better describe temporal variability across the study period.

Temporal variations were observed in the main physicochemical parameters and carbonate system variables in Gairaca Bay from April 2023 to July 2024. Total alkalinity (TA) exhibited higher values during the upwelling season in both years, reaching 2427.95 ± 29.4 µmol kg^{-1} in 2023 at the rhodolith bed bottom (Table 1) (Figure 4). In 2024, the highest TA was recorded at the outer bay, with 2377.46 ± 35.2 µmol kg^{-1} (Supplementary Figure SM_7A). In contrast, the lowest TA values occurred during the non-upwelling season at the inner bay (1 m depth) in 2023

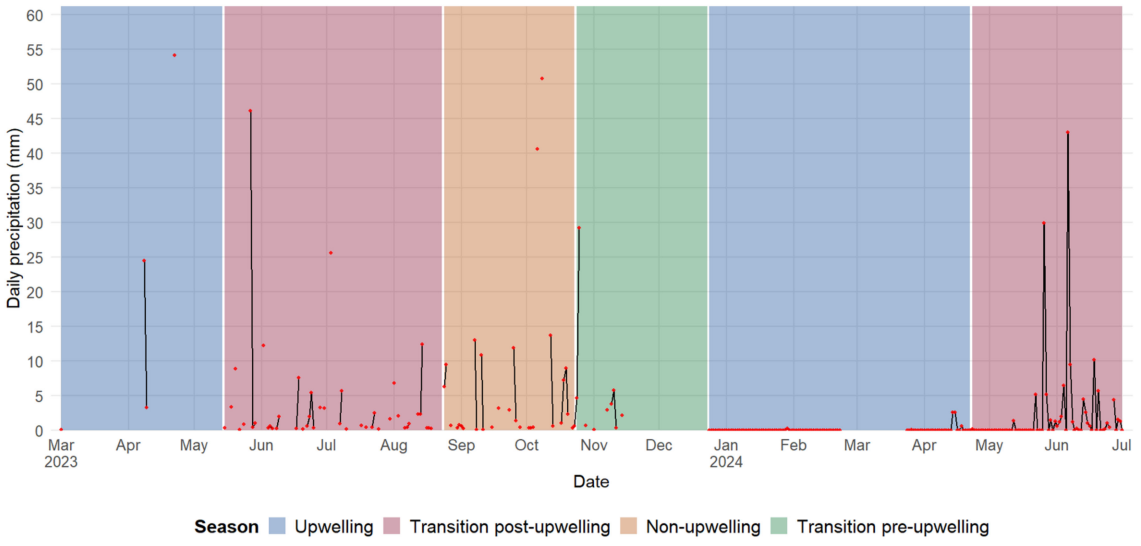

FIGURE 3
Seasonal precipitation trends in the area near Gairaca Bay during 2023 and 2024.

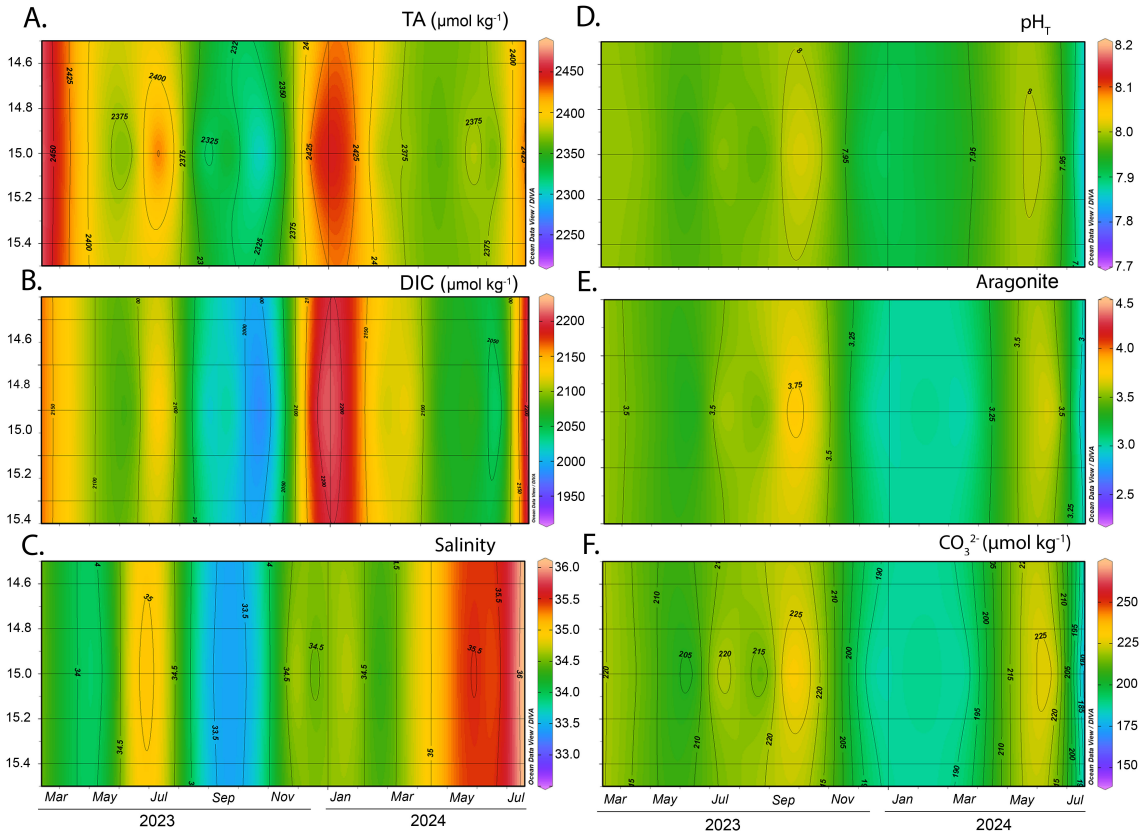

FIGURE 4
Monthly and interannual variation of carbonate system parameters at the rhodolith bed bottom. Panels show: **(A)** total alkalinity (TA, µmol kg^{-1}), **(B)** dissolved inorganic carbon (DIC, µmol kg^{-1}), **(C)** salinity, **(D)** pH_T (total scale), **(E)** aragonite saturation state (Ω_{arag}), and **(F)** carbonate ion concentration (CO_3^{2-}, µmol kg^{-1}).

(2316.3 ± 37.0 µmol kg^{-1}), reflecting the influence of less alkaline surface waters over sandy bottoms (Supplementary Figure SM_5A).

The total pH (pH_T) showed a seasonal pattern consistent with TA fluctuations. The highest values were recorded during the non-upwelling season in 2023 at the rhodolith bed midwater (7 m depth), averaging 7.99 ± 0.03 (Supplementary Table SM_1; Supplementary Figure SM_4). A decrease in pH_T was observed during the upwelling season, particularly in 2024, when the lowest value (7.94 ± 0.05) was recorded at the inner bay at 6 m depth (Table 1; Supplementary Figure SM_6). However, overall variations in this variable across sites and seasons were relatively small, indicating a general stability of the carbonate system's pH throughout the study period.

Dissolved inorganic carbon (DIC) showed the highest concentrations during the pre-upwelling transition in 2023 at the outer bay (2134.05 ± 46.5 µmol kg^{-1}), and during upwelling at the rhodolith bed bottom in both years (2122.60 ± 40.7 µmol kg^{-1} in 2023 and 2109.86 ± 40.9 µmol kg^{-1} in 2024) (Table 1).

Salinity exhibited both spatial and interannual variability. In 2023, the lowest salinity values were recorded at the inner bay (1 m depth) during the non-upwelling season (33.36 ± 0.29) (Supplementary Table SM_1; Supplementary Figure SM_5C). In contrast, in 2024, salinity increased significantly at the rhodolith bed midwater, reaching 35.17 ± 0.97 during the post-upwelling transition season (Supplementary Table SM_1; Supplementary Figure SM_4C).

The aragonite saturation state (Ω_{arag}) exhibited a seasonal pattern similar to pH_T. In 2023, the highest Ω_{arag} values were recorded at the rhodolith bed surface during the non-upwelling season (3.65 ± 0.17) (Supplementary Table SM_1; Supplementary Figure SM_3E). However, a general decline in Ω_{arag} was observed across all sites in 2024, with the most pronounced decrease at the inner bay (6 m depth) during the upwelling season (average 3.13 ± 0.31), representing the lowest value recorded during the study (Table 1; Supplementary Figure SM_6E).

The carbonate ion concentration (CO_3^{2-}) showed pronounced seasonal and between year variability. In 2023, the highest average CO_3^{2-} concentration was recorded at the inner Bay (6 m depth) during upwelling (274.54 ± 22.1 µmol kg^{-1}) (Supplementary Figure SM_6F). Conversely, in 2024 at the same site and season, the lowest values were observed, averaging 138.59 ± 19.5 µmol kg^{-1}. Overall, CO_3^{2-} concentrations tended to be higher during non-upwelling and transitional periods, and lower during upwelling events, particularly in 2024 across most sites (Table 1; Supplementary Table SM_1).

3.3 Seasonal and spatial variability of carbonate system

Seasonal deltas, calculated as deviations from the mean, revealed interannual and spatial variability in carbonate system variables across the three sites: rhodolith bed bottom (15 m depth) (Figure 5), inner bay (6 m depth) (Figure 6), and outer bay (10 m depth) (Figure 7). In 2023, the strongest deviations were observed at rhodolith bed bottom, ΔTA reaching a maximum delta of +92.5 µmol kg^{-1} during upwelling and a minimum of −89.5 µmol kg^{-1} during non-upwelling (Figure 5A). Similar but less pronounced patterns were detected in 2024, with ΔTA ranging from +58.2 to −20.9 µmol kg^{-1}. At inner bay, ΔTA in 2023 ranged approximately from −27.7 to +88.7 µmol kg^{-1}, while in 2024 the spread was narrower (Figure 6A). Outer bay showed more moderate fluctuations across both years, with most ΔTA values remaining within approximately ±45 µmol kg^{-1} (range: −71 to 85 µmol kg^{-1}) (Figure 7A).

ΔDIC at rhodolith bed bottom showed the widest range in 2023, peaking at +88.3 µmol kg^{-1} during the transition pre-upwelling and dropping to −130.8 µmol kg^{-1} during non-upwelling. In 2024, ΔDIC remained high, with values between +67.4 and −74.1 µmol kg^{-1} (Figure 5B). At inner bay, ΔDIC in 2023 followed a similar pattern but did not reach the same extremes, with the most negative value (−115.89 µmol kg^{-1}) recorded in October during the non-upwelling season. In 2024, the variation decreased overall, although a maximum positive ΔDIC of 105.62 µmol kg^{-1} was observed during the upwelling season (Figure 6B).

The general behavior of salinity across the three sites shows a decreasing trend during the non-upwelling season, especially at outer bay and rhodolith bed bottom. In 2023, rhodolith bed bottom showed the strongest salinity deviations, reaching −1.08 during the wet season and +0.42 during the transition post and pre-upwelling (Figure 5C). These patterns persisted in 2024 with similar magnitude. At inner bay, the salinity deltas show a contrasting pattern between 2023 and 2024. In 2023, there was a slight decreasing trend in salinity (mean of -0.25), with a higher proportion of negative values. In 2024, however, a clear increasing trend was observed (mean of 0.41) (Figure 6C).

At the rhodolith bed bottom, ΔpH_T values were generally negative during upwelling and positive during non-upwelling. In 2023, they ranged from −0.06 to +0.06, with peaks during the non-upwelling season. In 2024, the largest deviations occurred during the transition post-upwelling (−0.07 to +0.03), while changes during upwelling remained moderate (−0.04 to +0.02) (Figure 5D). At inner Bay, ΔpH_T values in 2023 were mostly positive across all seasons, reaching up to +0.18 during upwelling and +0.08 during non-upwelling. However, negative values were

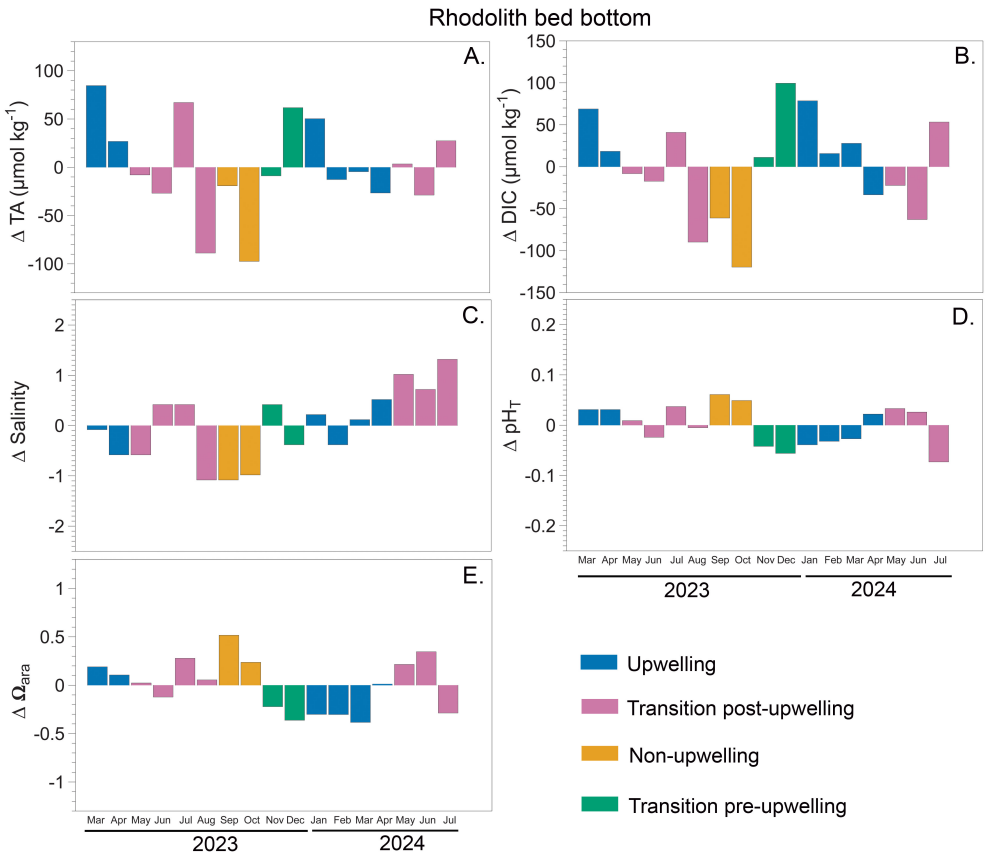

FIGURE 5
Seasonal deltas for carbonate system variables measured in Gairaca Bay between 2023 and 2024 at rhodolith bed bottom (15 m). Panels show: **(A)** total alkalinity (TA), **(B)** dissolved inorganic carbon (DIC), **(C)** salinity, **(D)** total pH (pH_T), and **(E)** saturation state aragonite (Ω_{arag}).

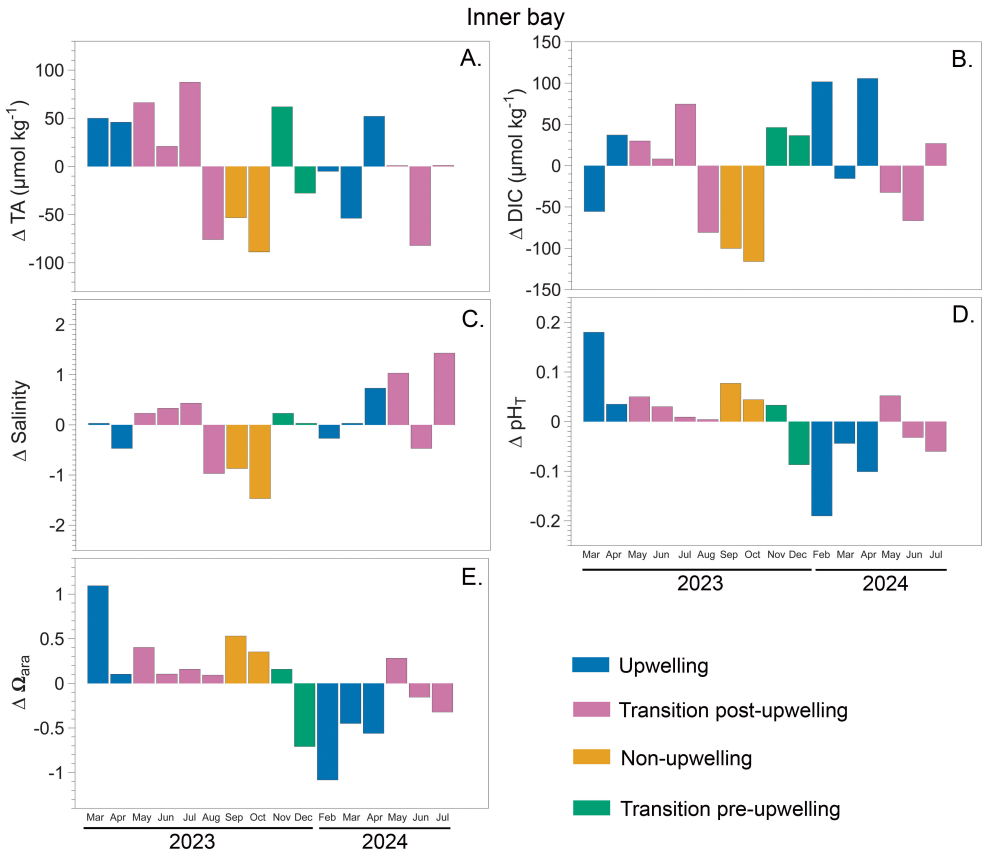

FIGURE 6
Seasonal deltas for carbonate system variables measured in Gairaca Bay between 2023 and 2024 at inner bay (6 m). Panels show: **(A)** total alkalinity (TA), **(B)** dissolved inorganic carbon (DIC), **(C)** salinity, **(D)** total pH (pH_T), and **(E)** saturation state aragonite (Ω_{arag}).

observed during the transition pre-upwelling (as low as −0.09). In contrast, in 2024, ΔpH_T values at inner bay were predominantly negative, particularly during the upwelling season, reaching as low as −0.19. During the transition post-upwelling, fluctuations were more moderate, ranging from −0.06 to +0.05 (Figure 6D). At outer bay, ΔpH_T values in 2023 were mostly positive, with peaks during the transition post-upwelling (+0.06) and non-upwelling (+0.05) periods. In 2024, however, values exhibited greater variability, with a pronounced minimum of −0.09 during the transition post-upwelling and a maximum of +0.05 during upwelling. Overall, both positive and negative ΔpH_T values remained within ±0.1 units across years (Figure 7D).

Ω_{arag} deltas were generally lowest during upwelling and highest during non-upwelling across all sites. At the rhodolith bed bottom, 2023 showed the largest amplitude, with deltas ranging from −0.36 to +0.52, while 2024 displayed a slightly narrower and more negative range (−0.38 to +0.35) (Figure 5E). Inner bay exhibited a different pattern, with much greater variability. In 2023, deltas ranged widely from −0.71 to +1.09, and in 2024 the extremes were even more pronounced (−1.08 to +0.28), indicating fluctuations in carbonate saturation (Figure 6E). At outer bay, Ω_{arag} remained relatively stable in both years, with deltas mostly contained between −0.44 and +0.38 in 2023 and between −0.39 and +0.19 in 2024 (Figure 7E).

Although no statistically significant differences were found between sites (PERMANOVA: $R^2 = 0.04$, $F = 0.76$, $p = 0.66$), the outer bay exhibited the greatest changes in DIC ($\Delta \approx 229$ μmol kg^{-1}) and salinity ($\Delta = 3.1$), whereas the inner bay showed the highest variability in pH_T ($\Delta \approx 0.37$) and aragonite saturation state ($\Delta\Omega_{arag} \approx 2.18$). Meanwhile, the rhodolith bed bottom recorded the largest variation in total alkalinity ($\Delta TA \approx 182$ μmol kg^{-1}). Overall, DIC was the most variable parameter across all sites.

3.4 Seasonal variability in carbonate system parameters and contribution of key variables

PERMANOVA indicated no significant differences in carbonate system composition among sites or depths ($p > 0.05$). However, seasonal differences were detected between the non-upwelling and upwelling periods. The transition pre-upwelling season closely resembled the upwelling period. Significant seasonal variation was also observed for temperature ($F = 248.42$, $p < 0.05$), salinity ($F = 49.02$, $p < 0.05$), TA ($F = 7.65$, $p < 0.00$), and DIC ($F = 2.54$, $p < 0.00$). The SIMPER analysis identified the carbonate system variables contributing most significantly to seasonal dissimilarities. In the upwelling versus non-upwelling contrast,

10.3389/fmars.2025.1626578

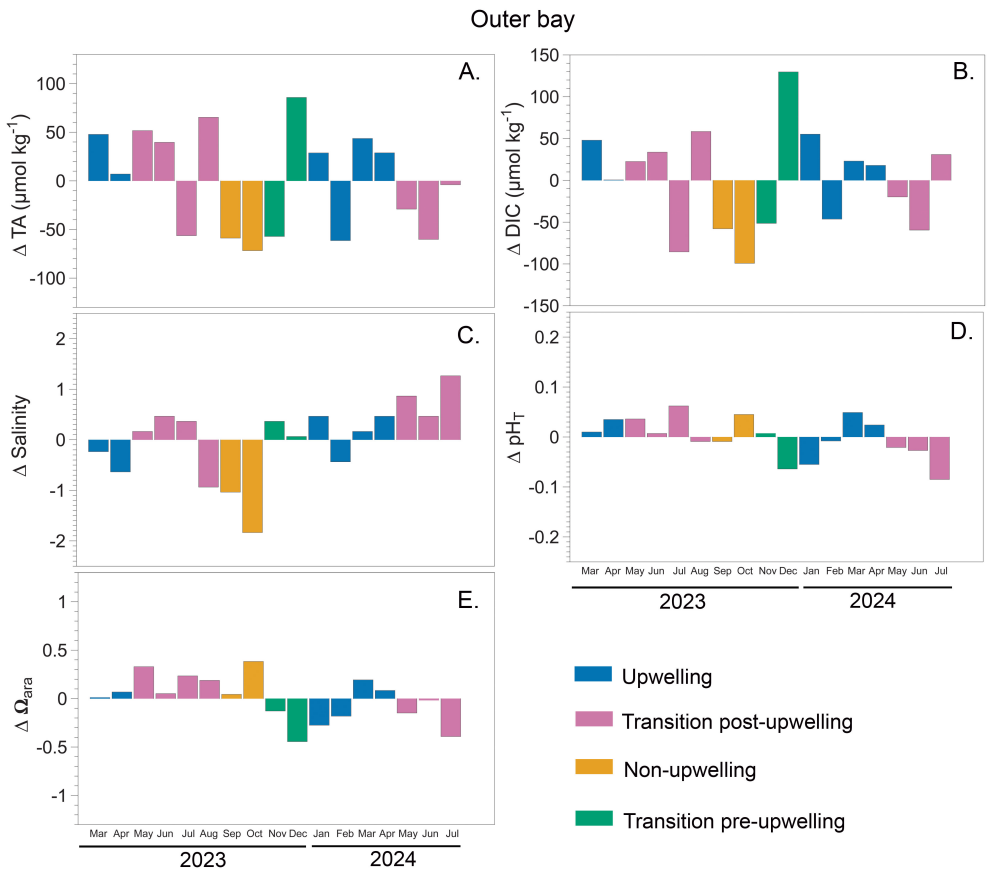

FIGURE 7
Seasonal deltas for carbonate system variables measured in Gairaca Bay between 2023 and 2024 at outer bay (10 m). Panels show: **(A)** total alkalinity (TA), **(B)** dissolved inorganic carbon (DIC), **(C)** salinity, **(D)** total pH (pH_T), and **(E)** saturation state aragonite (Ω_{arag}).

TABLE 2 SIMPER analysis summary showing carbonate system variables contributing most significantly to differences between climatic seasons.

Contrast	Variable	Contribution (%)	P-value
Upwelling vs non-upwelling	DIC	38.9	***
	TA	28.6	**
	Salinity	0.4	**
	Ω_{cal}	0.2	**
	Ω_{arag}	0.2	**
Transition post-upwelling vs non-upwelling	DIC	36.9	*
	Salinity	0.7	***
Non-upwelling vs transition pre-upwelling	DIC	39	***
	pCO_2	34.6	*
	TA	25.6	**
	Salinity	0.4	***
	Ω_{cal}	0.2	***
	Ω_{arag}	0.2	***
	pH_T	0.07	*

Significance: ***p ≤ 0.001, **p ≤ 0.01, *p ≤ 0.05.

DIC (38.9%) and TA (28.6%) were the major contributors to observed differences, both statistically significant (p ≤ 0.05). Other variables such as salinity, aragonite saturation state (Ω_{arag}), and calcite saturation state (Ω_{cal}) contributed less than 0.4% (Table 2).

In the transition post-upwelling vs. non-upwelling comparison, DIC accounted for 36.9% of the dissimilarity (p = 0.03), while salinity contributed only 0.7% (p ≤ 0.00), despite its low explanatory power. In the non-upwelling versus transition pre-upwelling contrast, DIC again emerged as the dominant factor (39.0%, p ≤ 0.00), followed by pCO_2 (34.6%, p = 0.01) and TA (25.6%, p = 0.00). Although salinity, Ω_{cal}, Ω_{arag}, and pH_T contributed to the differences, their individual contributions were relatively small (Table 2). These results highlight the importance of DIC and TA in the seasonal differentiation of the carbonate system. However, the interaction between different variables can further modulate the variability of the carbonate system.

3.5 Factors driving carbonate system variability

The variability of the carbonate system cannot be explained solely by individual factors. Temperature explained 39% of DIC

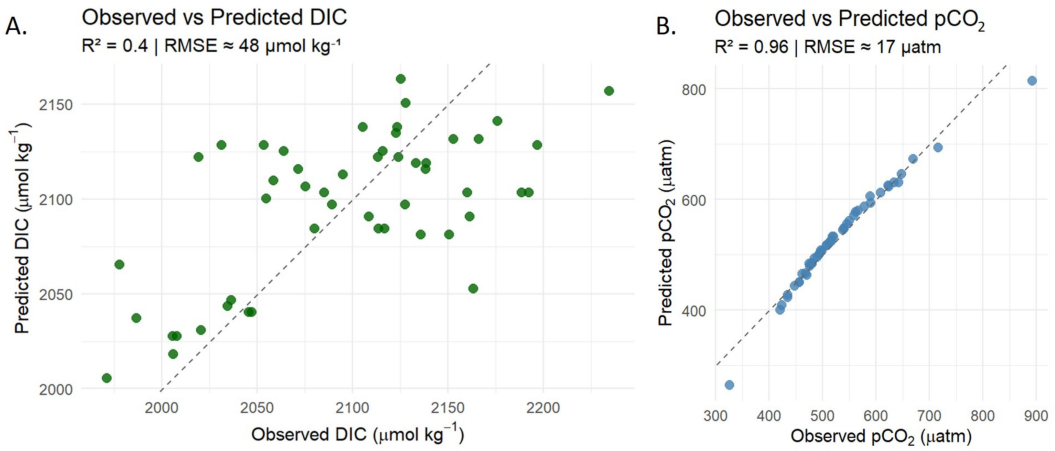

FIGURE 8
Observed versus predicted values for **(A)** DIC and **(B)** pCO_2 in seawater samples from Gairaca Bay. **(A)** shows the simple linear regression between observed and predicted DIC using temperature as the sole predictor (R^2 = 0.04; RMSE ≈ 48 µmol kg^{-1}). **(B)** presents the results of a multiple linear regression predicting pCO_2 based on temperature, salinity, total alkalinity (TA), DIC, and the DIC: TA ratio (R^2 = 0.96; RMSE = 17 µmol kg^{-1}). Dashed lines indicate the 1:1 relationship.

variability, showing a statistically significant relationship (R^2 = 0.39, $p < 0.001$) (Figure 8A). In contrast, no significant relationship was found between temperature and pCO_2 (R^2 = 0.02, p = 0.32), indicating that temperature alone was not a good predictor of pCO_2 variability in the study area (Table 3).

When considering additional hydrochemical variables, the multiple regression model achieved a markedly improved fit for pCO_2 (adjusted R^2 = 0.96, RMSE = 18.1 µatm) (Table 4; Figure 8B). In this model, temperature, salinity, and the DIC/TA ratio emerged as significant predictors, whereas total alkalinity (TA) and DIC alone did not significantly contribute to the explained variance.

3.6 Carbonate system dynamics at the rhodolith bed bottom

At the rhodolith bed bottom site, the carbonate system parameters and salinity exhibited relatively stable average values, with notable seasonal variability (Figure 4). TA had a mean value of 2384.66 ± 49.87 µmol kg^{-1}, ranging from 2287.30 to 2469.30 µmol kg^{-1} (Figure 4A), DIC averaged 2097.37 ± 60.64 µmol kg^{-1}, with a range between 1977.78 and 2196.89 µmol kg^{-1} (Figure 4B) and salinity averaged 34.58 ± 0.73, fluctuating between 33.5 and 35.9 (Figure 4C). The pH_T showed limited variability across seasons, with an overall mean of 7.96 ± 0.04. The maximum value (8.02) was recorded during the non-upwelling season in September 2023, while the minimum (7.89) occurred in July 2024 during the post-upwelling transition (Figure 4D). The Ω_{arag} averaged 3.36 ± 0.28 (Figure 4E). The CO_3^{2-} had a mean value of 211.38 ± 13.28 µmol kg^{-1}, the highest concentration (235.66 µmol kg^{-1}) was observed in September 2023 during the non-upwelling period, coinciding with elevated Ω_{arag} and lower DIC values, while the lowest value (185.70 µmol kg^{-1}) was observed in December 2023 during the pre-upwelling transition, when pCO_2 peaked and Ω_{arag} declined (Figure 4F).

PERMANOVA revealed statistically significant differences among seasons (F = 3.0596; p = 0.01). SIMPER analysis further identified the variables contributing most to these seasonal dissimilarities at the rhodolith bed bottom site. The transition post-upwelling vs. transition pre-upwelling comparison exhibited

TABLE 3 Simple linear regression models of temperature on carbonate system variables.

Variable	Formula	R^2	RMSE (µmol kg^{-1} or µatm)	Temp significance
DIC	$DIC = a \cdot Temp + b$	0.39	49.0 µmol kg^{-1}	*** p < 0.001
pCO_2	$PCO_2 = a \cdot Temp + b$	0.02	90.1 µatm	p = 0.32

***p ≤ 0.001.

TABLE 4 Multiple linear regression model predicting pCO_2 from carbonate system variables.

Predictor	Estimate	P-value
Intercept	-18618.5	0.04 *
Temp	20.86	<0.00 ***
Salinity	10.25	0.02 *
TA	5.28	0.15
DIC	-5.86	0.16
DIC/TA	20339.4	0.04 *

-Adjusted R^2: 0.96; RMSE: 18.1 µatm.
***p ≤ 0.001, *p ≤ 0.05.

the strongest dissimilarities, with DIC (41.4%, p = 0.04) and TA (92.7%, p = 0.03) showing statistically significant differences. In the upwelling vs. transition post-upwelling comparison, the major contributors were Ω_{arag} (34.7%) and Ω_{calc} (30.1%), followed by DIC (18.8%) and TA (6.7%) with no significant differences (p > 0.1). In the upwelling vs. non-upwelling contrast, DIC (19.6%), Ω_{arag} (19.1%), and Ω_{calc} (18.3%) contributed most, followed by TA (16.8%), salinity (12.3%), and pCO_2 (12.1%) with no statistically significant differences detected (p > 0.75).

Similarly, in the upwelling vs. transition pre-upwelling comparison, Ω_{calc} (31.7%), Ω_{arag} (29.4%), and pCO_2 (27.2%) were the dominant contributors without significant differences. The transition post-upwelling vs. non-upwelling comparison revealed salinity as the main contributor (21.6%), with no significant differences (p > 0.30), likewise, no significant differences were found between non-upwelling and transition pre-upwelling periods, despite salinity accounting for 100% of the observed dissimilarity (p = 0.80).

3.7 Nutrient dynamics and their relationship with carbonate chemistry at the rhodolith bed bottom site

The analysis of nutrient concentrations revealed clear seasonal and between year variation. Maximum nitrate concentrations were recorded in June 2023, reaching 0.08 $mg{\cdot}L^{-1}$. Regarding nitrite, the highest values were observed in July 2023 and April 2024, while the lowest concentration was recorded in December 2023 (0.03 $mg{\cdot}L^{-1}$). For ammonium, the highest concentration was detected in August 2023 (0.01 $mg{\cdot}L^{-1}$); however, from June to December 2023 and throughout 2024, ammonium levels were consistently below the detection limit. Phosphate concentrations also varied notably between years. In 2023, the highest concentration occurred in September (0.31 $mg{\cdot}L^{-1}$), whereas the lowest was measured in December (0.22 $mg{\cdot}L^{-1}$). In contrast, 2024 exhibited a significant increase, with a peak concentration of 0.39 $mg{\cdot}L^{-1}$ recorded in May; in all other sampled months, phosphate concentrations were below the detection limit (Table 5). Among the nutrient variables, a positive correlation was found between nitrite (NO_2^-) and both CO_3^{2-} (r = 0.59, p = 0.02) and Ω_{arag} (r = 0.54, p = 0.04). Additionally, nitrate (NO_3^-) was positively correlated with phosphate (PO_4^{3-}) (r = 0.53, p = 0.04).

Correlations between carbonate chemistry variables and nutrient concentrations at the rhodolith bed bottom site revealed strong internal coherence within the carbonate system, but weak associations with nutrient dynamics (Figure 9). Total alkalinity (TA) showed a strong positive correlation with dissolved inorganic carbon (DIC) (ρ = 0.91, p < 0.00), while DIC was also positively correlated with pCO_2 (ρ = 0.67, p = 0.00) and negatively with pH_T (ρ = –0.51, p = 0.04) and CO_3^{2-} (ρ = –0.51, p = 0.04). Aragonite saturation state proxies (pH_T and CO_3^{2-}) were highly correlated with each other (ρ = 0.89, p < 0.00), and both were strongly and negatively correlated with pCO_2 (ρ = –0.96 and –0.89, respectively, p < 0.00). Among the nutrients, only nitrite (NO_2^-) showed a significant positive correlation with CO_3^{2-} (ρ = 0.59, p = 0.02). All

TABLE 5 Monthly concentrations of dissolved inorganic nutrients at the rhodolith bed bottom in Gairaca Bay during 2023 and 2024.

Year-month	Season	Ammonium (NH_4^+, $mg{\cdot}L^{-1}$)	Nitrate (NO_3^-, $mg{\cdot}L^{-1}$)	Nitrite (NO_2^-, $mg{\cdot}L^{-1}$)	Phosphate (PO_4^{3-}, $mg{\cdot}L^{-1}$)
2023-5	Transition post-upwelling	0.001	0.043	0.038	0.310
2023-6	Transition post-upwelling	<0.0001	0.077	0.042	0.296
2023-7	Transition post-upwelling	0.000	0.056	0.056	0.287
2023-8	Transition post-upwelling	0.010	0.043	0.036	0.287
2023-9	Non-upwelling	<0.0001	0.068	0.047	0.315
2023-10	Non-upwelling	<0.0001	0.040	0.037	0.301
2023-11	Transition pre-upwelling	<0.0001	0.050	0.036	0.313
2023-12	Transition pre-upwelling	<0.0001	0.042	0.031	0.219
2024-1	Upwelling	<0.0002	0.023	0.035	<0.004
2024-2	Upwelling	<0.0002	0.012	0.037	<0.004
2024-3	Upwelling	<0.0002	0.048	0.035	<0.004
2024-4	Upwelling	<0.0002	0.001	0.049	<0.004
2024-5	Transition post-upwelling	<0.0002	0.015	0.035	0.390
2024-6	Transition post-upwelling	<0.0002	0.015	0.038	<0.004
2024-7	Transition post-upwelling	<0.0002	0.008	0.046	<0.004

Values are expressed in $mg{\cdot}L^{-1}$ for ammonium (NH_4^+), nitrate (NO_3^-), nitrite (NO_2^-), and phosphate (PO_4^{3-}). Values below the detection limit are indicated with "<".

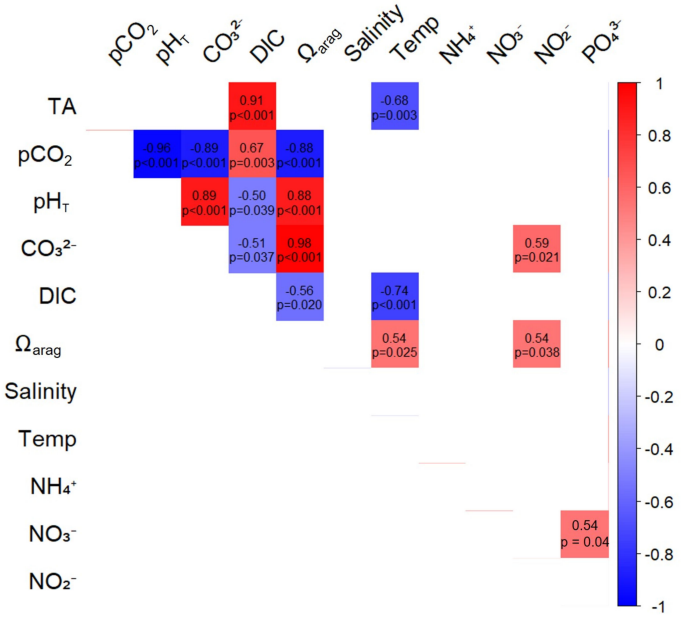

FIGURE 9
Spearman correlation matrix between carbonate system variables and nutrients at the rhodolith bed bottom site (n = 15). The color scale represents the strength and direction of the correlation coefficients (r), with blue indicating positive correlations and red indicating negative correlations. Blank cells indicate non-significant correlations (p > 0.05).

other correlations between nutrients (NH_4^+, NO_3^-, PO_4^{3-}) and carbonate system variables were not statistically significant ($p > 0.05$). Temperature also exhibited significant relationships with carbonate parameters. It was negatively correlated with TA ($\rho = -0.68$, $p = 0.00$) and DIC ($\rho = -0.74$, $p = 0.00$), and positively correlated with Ω_{arag} ($\rho = 0.54$, $p = 0.02$) (Figure 9).

4 Discussion

4.1 Seasonal and spatial patterns of the carbonate system

This study highlights the significant influence of seasonal variability on carbonate chemistry in tropical coastal ecosystems, particularly those affected by upwelling. Our results show a clear connection between the non-upwelling season, characterized by the rainy period and increased runoff from the Magdalena River (Ricaurte-Villota et al., 2025), and significant fluctuations in the carbonate system parameters in Gairaca Bay. These patterns are comparable to those reported for Moorea reef flats (Kleypas et al., 2011) and suggest that continental runoff plays a central role in modulating water chemistry in Gairaca, setting it apart from other tropical coastal systems where oceanic upwelling exerts a more dominant influence (Sánchez-Noguera et al., 2018). Notably, freshwater inputs contribute substantially to the spatial variability of carbonate chemistry, reinforcing the importance of accounting for runoff in coastal biogeochemical assessments.

During upwelling peaks, DIC and TA increase, while pH_T drops below 7.95 and Ω_{arag} decreases to ~3.0, similar to conditions observed in the Gulf of Papagayo (Sánchez-Noguera et al., 2018). In contrast, the non-upwelling season reflects a diminished influence of cold, CO_2-rich subsurface waters (Ricaurte-Villota et al., 2025), with pH_T rising from 7.93–7.99 (upwelling) to 8.01–8.03 at sites such as the rhodolith bed surface and inner bay (Table 1; Supplementary Table SM_1). This increase in pH_T is accompanied by a decrease in DIC, which drops from 2115.77 µmol kg^{-1} in April 2023 (upwelling, inner bay) to around 1973.10 µmol kg^{-1} in October (Table 1). Similarly, TA shows a slight decline, such as at rhodolith bed surface, where it decreases from 2487.40 µmol kg^{-1} in March to 2268.00 µmol kg^{-1} in October (Supplementary Table SM_1). These changes are coupled with a decline in DIC, from 2115.77 µmol kg^{-1} in April (inner bay) to ~1973.10 µmol kg^{-1} in October, and a moderate decrease in TA, for example from 2487.40 to 2268.00 µmol kg^{-1} at the rhodolith bed surface. Conversely, Ω_{arag} and CO_3 concentrations increase during this period, reaching up to 3.88 and 235.66 µmol kg^{-1} at the rhodolith bed bottom, respectively.

Salinity also decreases (e.g., from 34.4 in March to 33.2 in October), while temperature rises to 30.5 °C, compared to 27.0–27.5 °C during upwelling. Dissolved oxygen concentrations tend to decline, as observed at the rhodolith bed bottom (from 7.04 to 4.17 $mg{\cdot}L^{-1}$). These warmer, fresher waters exhibit higher pH_T and Ω_{arag}, which thermodynamically lowers the energy barrier for $CaCO_3$ precipitation (Mucci, 1983; Cyronak et al., 2016). Carbonate speciation under elevated pH shifts the equilibrium toward CO_3^{2-}, enhancing local carbonate ion availability (Dickson and Millero, 1987).

The freshwater influx into Gairaca Bay during the rainy season results in a distinct carbonate chemistry response, differentiating it

from systems like Papagayo, dominated by oceanic upwelling with minimal freshwater influence (Sánchez-Noguera et al., 2018), and Bocas del Toro, which experiences moderate terrestrial runoff (Pedersen et al., 2024). Gairaca is subjected to pronounced seasonal and interannual variability in runoff, particularly from the Magdalena River during the rainy, non-upwelling season. This input amplifies fluctuations in pH_T, TA, DIC, and Ω_{arag}, especially during periods of intense rainfall and river discharge, when upwelling is absent (Table 1, Figure 4). Additionally, the Magdalena River transports organic matter and nutrients (Restrepo et al., 2006), whose remineralization can further alter DIC and pH_T dynamics. Maximum runoff typically occurs from September to November, coinciding with weakened trade winds, enhanced coastal countercurrents, and the suppression of upwelling, thereby strongly influencing the carbonate system (Ricaurte-Villota et al., 2025). Although spatial variability in water chemistry exists within Bocas del Toro due to terrestrial runoff and benthic metabolism (Pedersen et al., 2024), Gairaca shows notably higher temporal variability driven by the strong seasonal freshwater inputs during the non-upwelling season. Nonetheless, the three sites evaluated within Gairaca Bay exhibit similar responses to these runoff and rainy conditions.

Spatial differences among the rhodolith bed bottom, inner bay, and outer bay sites were minimal, likely due to a generally well-mixed water column (see Section 4.3). However, the pronounced seasonal shifts highlight the interplay between oceanic and terrestrial influences, which may enable site-specific buffering mechanisms, such as localized photosynthesis or sediment-driven alkalinity release (Savoie et al., 2022; Ricaurte-Villota et al., 2025). These seasonal shifts in carbonate chemistry not only reflect oceanographic-terrestrial interactions but may also have significant implications for the physiological performance of calcifying organisms (Li et al., 2022).

Finally, it is important to consider the analytical uncertainty associated with TA and DIC measurements in this study, which is estimated at ±10 μmol kg^{-1}. This level of precision corresponds to the "weather goal" defined by the Global Ocean Acidification Observing Network (GOA-ON), which is considered adequate for characterizing short-term variability and spatial gradients in coastal systems (Kortazar et al., 2020). Although not suitable for detecting long-term anthropogenic trends, this uncertainty is acceptable in highly dynamic environments like Gairaca Bay, where variability in TA and DIC often exceeded 100 μmol kg^{-1}, ensuring that the observed patterns remain robust and interpretable.

4.2 Influence of seasonal variability and climatic conditions

During the study period, rainy days were recorded even during months that are typically dry, resulting in unusual hydrological conditions for that time of year (Figure 3). These unexpected rainfall events likely intensified freshwater inputs, leading to dilution effects, changes in salinity and alkalinity, and potential decoupling among carbonate system parameters. Elevated runoff may also have altered water column structure and enhanced biogeochemical fluxes, contributing to the variability observed in carbonate chemistry (Correa-Ramirez et al., 2020; Norzagaray et al., 2020; Cai et al., 2021; Reithmaier et al., 2023).

During the non-upwelling months, which coincide with the rainy season, Gairaca Bay exhibited reduced salinity, lower TA and DIC concentrations, and elevated pCO_2 levels. These shifts likely resulted from increased remineralization and microbial respiration, stimulated by the influx of terrestrial organic matter during intense rainfall. In coastal ecosystems, remineralization refers to the breakdown of organic matter into inorganic constituents. This process, particularly when driven by microbial activity, generates CO_2 and modifies porewater chemistry (Bayraktarov and Wild, 2014; Quintana et al., 2015; Cohn et al., 2024). However, the observed decrease in TA during the rainy season suggests that the dilution effect of freshwater inputs, which are typically low in TA, may outweigh any potential increase in TA from remineralization processes (Pedersen et al., 2024).

Terrestrial–marine interactions, especially those involving organic matter inputs from river discharge, mangroves, and seagrass meadows, are known to modulate carbonate chemistry in Caribbean coastal systems by altering TA and DIC concentrations (Meléndez et al., 2020; Pedersen et al., 2024). These biogeochemical dynamics are ecologically relevant for calcifying organisms such as corals and coralline algae, which are particularly sensitive to fluctuations in pH and carbonate saturation state (Martin and Hall-Spencer, 2017; Silbiger and Sorte, 2018). Increased freshwater runoff can suppress calcification and alter benthic community composition (Fabricius, 2005). However, rhodolith beds may partially buffer these effects by maintaining relatively stable micro-environmental conditions through photosynthesis, calcification, and microbial mediation (Isah et al., 2022).

4.3 Carbonate chemistry responses and delta patterns

Delta patterns revealed that climatic seasonality is a major driver of carbonate system variability across Gairaca Bay. Although statistically significant differences between sites were not detected, the magnitude of variation in parameters such as TA, DIC, Ω_{arag}, and pH_T, differed notably across seasons (Figures 5-7).

During the non-upwelling season, the variability between sampling locations was markedly higher for all measured parameters. TA showed the greatest inter-site difference, with a 90.7% relative difference, followed by pH_T (83.2%), DIC (80.5%), and Ω_{arag} (68.7%). These pronounced variations suggest that localized processes, such as freshwater input, biological activity, and water column stratification, exert greater influence under low-mixing conditions when upwelling is absent. The rhodolith bed bottom recorded the highest TA variability, while the outer bay exhibited the greatest fluctuations in DIC and pH_T. Conversely, the inner bay consistently showed lower variability across most parameters during this period. These findings highlight the

complex interplay of regional and local factors in shaping carbonate system dynamics in tropical coastal environments (Sánchez-Noguera et al., 2018; Norzagaray et al., 2020).

Consistent with these observations, temperature emerged as a key driver of DIC variability, due to its effects on solubility and biologically mediated processes such as calcification and respiration. Warmer temperatures generally reduce DIC solubility (Bakker et al., 1999), while biological processes are also temperature-dependent: enhanced respiration increases DIC concentrations, and decreased calcification reduces DIC uptake (Pedersen et al., 2024). In contrast, pCO_2 was influenced by multiple interacting variables. The strong performance of the multiple linear model ($R^2 = 0.96$; RMSE ≈ 18 µatm) indicates that including salinity and the DIC/TA ratio significantly improves prediction accuracy, capturing the combined influence of freshwater input, mixing, and net community metabolism. Such complexity is typical in estuarine and coastal systems, where biogeochemical and physical drivers interact dynamically (Cai et al., 2021).

These findings emphasize that, while DIC dynamics are influenced by temperature, pCO_2 is shaped by a broader suite of environmental factors, including carbonate equilibrium and the balance between DIC and TA, which determines buffering capacity and resistance to pH changes (Khan et al., 2020). Understanding these interactions is crucial for predicting the impacts of environmental variability on coastal carbonate chemistry (Carstensen and Duarte, 2019).

Observed reductions in salinity, TA, and DIC during the non-upwelling season support the central role of freshwater inputs in modulating carbonate conditions (Pérez et al., 2015). Biological processes, particularly photosynthesis, may further contribute to DIC drawdown (Isah et al., 2022), while decoupling between production and respiration can amplify pH variability in stratified coastal waters (Carstensen and Duarte, 2019).

In contrast, during the upwelling season, spatial differences across sampling sites diminished considerably. Relative differences in pH_T (48.9%), TA (42.9%), DIC (20.0%), and Ω_{arag} (18.9%) were all lower, suggesting a homogenizing effect of upwelling, driven by the intrusion of cold, CO_2-rich subsurface and enhanced vertical mixing across the water column, which together affect the entire bay. This influence was most pronounced at the outer bay, where pH_T and Ω_{arag} variability peaked, while the rhodolith bed bottom and inner bay showed more moderate changes. The predominance of northeasterly and easterly winds during this season plays a key role in sustaining upwelling-favorable conditions, enhancing the upward advection of DIC-enriched subsurface water masses. This mechanism likely contributes to the observed increase in DIC concentrations during upwelling, compared to the more variable and stratified conditions of the non-upwelling season. The stronger divergence observed during the non-upwelling period may be further intensified by unusually high rainfall and riverine discharge (Restrepo and Kjerfve, 2000; Ricaurte-Villota et al., 2025), which enhance the effects of local processes under stratified conditions and limited vertical mixing (Pedersen et al., 2024). On average, Ω_{arag} remained above the aragonite saturation threshold (>1) at all sites (see Supplementary Table SM_1), indicating generally favorable conditions for marine calcification (McGrath et al., 2019). Slightly higher values were observed at the outer bay, followed by the rhodolith bed bottom and inner bay.

Rhodolith bed bottom site exhibited the most stable Ω_{arag} values across seasons, while outer and inner bay sites showed greater variability. This stability supports the buffering potential of rhodolith habitats, consistent with previous findings that suggest rhodolith beds may act as microhabitat refugia under ocean acidification scenarios (Costa et al., 2023). Their capacity to maintain stable chemical conditions through biological and sedimentary processes may offer protection to vulnerable calcifiers. In contrast, shallow inner bay areas, dominated by sandy bottoms, are more susceptible to fluctuations in carbonate availability. These results highlight the interplay between regional climatic drivers and local environmental features in shaping the chemical mosaic of tropical marine systems (Gómez et al., 2023).

Although direct measurements of metabolic or calcification rates were not conducted, the consistently elevated and stable Ω_{arag} values at the rhodolith bed suggest the presence of biologically mediated buffering. While average values across sites and depths were relatively similar, SIMPER analysis revealed that variables such as TA and DIC contributed significantly to seasonal dissimilarities at the rhodolith bed bottom, particularly between transition phases. These patterns support the notion that, despite limited spatial contrast in mean values, rhodolith beds may play a role in modulating carbonate chemistry under fluctuating conditions, especially during periods of environmental stress such as upwelling pulses or freshwater inputs (Pedersen et al., 2024; Ricaurte-Villota et al., 2025).

4.4 Nutrients and biogeochemical interactions

Nutrient dynamics at the rhodolith bed bottom revealed clear seasonal trends driven by upwelling, freshwater inputs, and biological processes. Nitrate concentrations peaked during June and July 2023 (0.07 and 0.06 $mg{\cdot}L^{-1}$ respectively), coinciding with the post-upwelling transition. These peaks likely reflect enhanced remineralization following the intrusion of subsurface waters (Schubert et al., 2019; Ricaurte-Villota et al., 2025). In contrast, ammonium remained largely undetectable throughout 2024, while phosphate concentrations increased notably in May 2024 (0.39 $mg{\cdot}L^{-1}$), coinciding with the onset of the rainy season and heightened river discharge.

Interestingly, Ω_{arag} showed a positive correlation with NO_2^- y PO_4^{3-}. While this relationship is not necessarily causal, it may reflect the combined influence of terrestrial runoff and *in situ* biogeochemical processes in this tropical coastal environment. Seasonal runoff in Gairaca Bay, particularly during the rainy season, introduces nutrients and organic matter that can stimulate biological activity and indirectly affect carbonate chemistry (Aronson et al., 2014). In coastal waters, nutrient enrichment and remineralization can influence pH and DIC,

sometimes resulting in complex or even counterintuitive correlations with Ω_{arag} (Cai et al., 2021). Therefore, the observed positive correlation may be the result of overlapping hydrological and biological processes rather than a direct mechanistic link.

The carbonate system at the rhodolith bed is shaped by a complex interplay between pH_T, DIC, Ω_{arag}, and nutrient concentrations. A significant inverse relationship was found between DIC and both pH_T and Ω_{arag}, consistent with acid-base dynamics in marine systems: as DIC increases, pH_T and Ω_{arag} decrease. This pattern aligns with observations in other tropical regions, such as the northern South China Sea, where similar relationships were reported by Roberts et al. (2021), highlighting the widespread influence of DIC on carbonate chemistry across diverse marine environments.

The positive correlation observed between temperature and aragonite saturation state (Ω_{arag}) can be attributed to the seasonal dynamics of the studied tropical coastal system. During the rainy season, surface water temperatures rise while upwelling intensity decreases, reducing the input of cold, CO_2-rich subsurface waters and thereby limiting acidification from vertical mixing. Consequently, pH_T and carbonate ion (CO_3^{2-}) concentrations increase, resulting in elevated Ω_{arag} values. This pattern, characteristic of shallow tropical environments with seasonal forcing, contrasts with systems dominated by persistent upwelling, where the influx of subsurface waters typically lowers Ω_{arag} despite cooler temperatures (Mucci, 1983; Zeebe and Wolf-Gladrow, 2001; Manzello, 2010). However, the hysteresis effect described by (McMahon et al., 2013) underscores the importance of considering diel variability and metabolic feedbacks when interpreting correlations between Ω_{arag} and environmental drivers such as temperature.

Nevertheless, most correlations between pH_T or DIC and nutrient concentrations were not statistically significant, indicating that nutrient variability does not directly control carbonate system dynamics in this setting. Although nutrients are essential for biological productivity, their short-term influence on pH_T and DIC appears less pronounced than other drivers such as temperature, salinity, or air–sea CO_2 exchange (Gattuso et al., 1998; Zeebe and Wolf-Gladrow, 2001). In tropical coastal systems, these physical and chemical factors often dominate carbonate chemistry, especially under stratified or runoff-influenced conditions (Salisbury et al., 2008; Cai et al., 2021).

This nutrient enrichment pattern supports the role of freshwater inputs in modulating carbonate dynamics in Gairaca Bay (Ricaurte-Villota et al., 2025). Riverine waters are typically low in TA and DIC but high in nutrients and temperature, promoting seawater dilution and enhanced biological CO_2 uptake through primary production (Borges and Gypens, 2010). Such correlations likely reflect the contribution of remineralization and biologically driven CO_2 uptake in shaping local carbonate dynamics (Borges and Gypens, 2010). These interactions likely explain some of the shifts in carbonate chemistry observed during transition periods, when freshwater delivery and biological activity are both elevated.

Although freshwater inputs from rainfall and runoff are well-documented drivers of biogeochemical variability in this region (Ricaurte-Villota et al., 2025) our data suggest that internal metabolic activity within rhodolith beds may help maintain conditions favorable to calcification, even under elevated pCO_2 and DIC levels. Future studies should investigate diel metabolic variability and long-term biogeochemical trends to better understand the mechanisms sustaining rhodolith bed resilience under changing oceanographic conditions.

5 Conclusion

This study highlights the role of seasonal dynamics in modulating the carbonate system of Gairaca Bay, a tropical coastal ecosystem influenced by oceanic upwelling and freshwater runoff. Marked seasonal variations were observed in total alkalinity (TA), dissolved inorganic carbon (DIC), pH_T, and aragonite saturation state (Ω_{arag}), reflecting the combined effects of oceanographic forcing and terrestrial inputs.

Non-upwelling periods, coinciding with increased rainfall and riverine discharge, intensified spatial variability in TA and DIC, emphasizing the significance of localized processes such as water column stratification, organic matter inputs, and benthic remineralization. Conversely, upwelling periods produced more homogeneous carbonate conditions across all sites due to the influence of cold, CO_2-rich subsurface waters.

Notably, rhodolith beds exhibited the most stable Ω_{arag} values, especially relative to the greater seasonal variability observed at the outer and inner bay sites, reinforcing their potential role as localized buffers under fluctuating environmental conditions. This buffering capacity likely results from biological activities including photosynthesis, calcification, microbial processes, and sediment-mediated alkalinity release. Collectively, these processes may offer significant ecological protection to vulnerable calcifying organisms inhabiting or adjacent to rhodolith beds, particularly during episodic acidification events linked to upwelling pulses.

In contrast, (inner bay) shallow sandy-bottom areas demonstrated greater fluctuations in carbonate chemistry, making them more susceptible to variations in carbonate availability. This variability underscores the intricate interplay between regional climatic drivers and local environmental conditions, highlighting the necessity of considering both regional oceanographic processes and site-specific factors in managing and understanding tropical coastal carbonate chemistry.

Seasonal nutrient dynamics, influenced by rainfall-driven hydrological changes, showed elevated nitrate and phosphate concentrations during periods of increased precipitation. These nutrient influxes likely stimulated primary productivity and microbial respiration, further influencing local carbonate chemistry and demonstrating the interconnectedness of nutrient and carbonate system variability.

Additionally, our analysis indicated that temperature significantly influenced DIC variability due to its direct impact on carbon solubility and biologically mediated processes such as respiration and calcification. While temperature was a primary driver of DIC dynamics, pCO_2 variability was regulated by

multiple interacting factors, including salinity and the DIC/TA ratio, highlighting the complex regulation of carbonate chemistry in coastal ecosystems.

Overall, this study emphasizes the functional importance of rhodolith beds in buffering carbonate chemistry fluctuations under variable climatic conditions. Although direct measurements of metabolic and calcification rates were beyond the scope of this study, consistently elevated and stable Ω_{arag} values in rhodolith habitats strongly suggest biologically mediated buffering. Future research should prioritize *in situ* assessments of photosynthesis, respiration, and calcification rates in diverse rhodolith species, and investigate the role of associated microbial communities in modulating carbonate chemistry. Such research is essential for advancing our understanding of the resilience mechanisms within rhodolith beds and their broader ecological implications under ongoing climatic variability and ocean acidification scenarios.

Data availability statement

The original contributions presented in the study are included in the article/Supplementary Material. Further inquiries can be directed to the corresponding authors.

Author contributions

NR: Conceptualization, Data curation, Formal analysis, Funding acquisition, Investigation, Methodology, Project administration, Resources, Software, Validation, Visualization, Writing – original draft, Writing – review & editing. CG: Conceptualization, Data curation, Formal analysis, Investigation, Methodology, Supervision, Writing – original draft, Writing – review & editing. VP: Data curation, Formal analysis, Investigation, Methodology, Visualization, Writing – review & editing. FA: Data curation, Investigation, Methodology, Software, Writing – review & editing. SN: Conceptualization, Data curation, Formal analysis, Project administration, Supervision, Validation, Writing – review & editing. RG: Conceptualization, Funding acquisition, Investigation, Methodology, Project administration, Resources, Supervision, Validation, Visualization, Writing – review & editing.

Funding

The author(s) declare financial support was received for the research and/or publication of this article. This research was supported by the Colombian Institute for Educational Credit and Technical Studies Abroad (ICETEX) and the Ministry of Science, Technology, and Innovation of Colombia (MINCIENCIAS) under project code CD 82611 CT ICETEX 2021-1032. The lead author's doctoral studies were also funded through the Bicentennial Doctoral Scholarship Program. The funders had no role in the study design, data collection and analysis, decision to publish, or preparation of the manuscript.

Acknowledgments

We are grateful to Cleimar Cayón and Jair López, for their assistance during fieldwork, as well as to Andrés Alvarado and Juan García for their help with logistics. We extend our thanks to the staff of the Water Quality Laboratory (Carlos España, Laudys Gutiérrez, and Isaac Romero) for their support in total alkalinity analyses; and to César Bernal and Marco Correa (INVEMAR) for their technical guidance in sample processing and ODV plotting. We also acknowledge the support of Iván Villamil and the Mollusk Research Group for assisting in assembling the alkalinity measurement system and lending equipment. Special thanks to Colombia's National Natural Parks System (permit AUR 003-2021) and the Vice-Rectorate for Research at Universidad del Magdalena (especially Heidy Pérez) for their support in permit management.

Conflict of interest

The authors declare that the research was conducted in the absence of any commercial or financial relationships that could be construed as a potential conflict of interest.

Generative AI statement

The author(s) declare that Generative AI was used in the creation of this manuscript. The author(s) verify and take full responsibility for the use of generative AI in the preparation of this manuscript. Generative AI was used to assist in improving the clarity, structure, and grammar of selected paragraphs. All content was critically reviewed and validated by the authors to ensure accuracy and scientific integrity.

Any alternative text (alt text) provided alongside figures in this article has been generated by Frontiers with the support of artificial intelligence and reasonable efforts have been made to ensure accuracy, including review by the authors wherever possible. If you identify any issues, please contact us.

Publisher's note

Supplementary material

The Supplementary Material for this article can be found online at: https://www.frontiersin.org/articles/10.3389/fmars.2025.1626578/full#supplementary-material

References

Alvarado-Jiménez, F., Rincón-Díaz, N., and García-Urueña, R. (2024). Reproductive phenology of coralline algae *Porolithon antillarum* and *Lithophyllum* sp. under seasonal upwelling conditions, Colombian Caribbean. *Aquat. Bot.* 190, 0–2. doi: 10.1016/j.aquabot.2023.103726

Arévalo-Martínez, D. L., and Franco-Herrera, A. (2008). Características oceanográficas de la surgencia frente a la ensenada de Gaira, departamento de Magdalena, época seca menor de 2006. *Boletin Investigaciones Marinas y Costeras* 37, 131–162. doi: 10.25268/bimc.invemar.2008.37.2.195

Aronson, R. B., Hilbun, N. L., Bianchi, T. S., Filley, T. R., and McKee, B. A. (2014). Land use, water quality, and the history of coral assemblages at Bocas del Toro, Panamá. *Mar. Ecol. Prog. Ser.* 504, 159–170. doi: 10.3354/MEPS10765

Bakker, D. C. E., De Baar, H. J. W., and De Jong, E. (1999). The dependence on temperature and salinity of dissolved inorganic carbon in East Atlantic surface waters. *Mar. Chem.* 65, 263–280. doi: 10.1016/S0304-4203(99)00017-1

Bayraktarov, E., Pizarro, V., Eidens, C., Wilke, T., and Wild, C. (2012). "Upwelling mitigates coral bleaching in the Colombian Caribbean," in *Proceedings of the 12th International Coral Reef Symposium*. (Cairns: James Cook University) 9–13.

Bayraktarov, E., Pizarro, V., Eidens, C., Wilke, T., and Wild, C. (2013). Bleaching susceptibility and recovery of Colombian Caribbean corals in response to water current exposure and seasonal upwelling. *PLoS One* 8. doi: 10.1371/journal.pone.0080536

Bayraktarov, E., Pizarro, V., and Wild, C. (2014). Spatial and temporal variability of water quality in the coral reefs of Tayrona National Natural Park, Colombian Caribbean. *Environ. Monit. Assess.* 186, 3641–3659. doi: 10.1007/s10661-014-3647-3

Bayraktarov, E., and Wild, C. (2014). Spatiotemporal variability of sedimentary organic matter supply and recycling processes in coral reefs of Tayrona National Natural Park, Colombian Caribbean. *Biogeosciences* 11, 2977–2990. doi: 10.5194/bg-11-2977-2014

Bernal, C. A., Gómez, M., Sánchez-Cabeza, J. A., Cartas Aguila, H., and Herrera Merlo, J. (2021). *Determinación De Alcalinidad Total En Agua De Mar Utilizando Dispensador* (Santa Marta, Colombia: Red de Investigación de Estresores Marinos - Costeros en Latinoamérica y El Caribe – REMARCO).

Borges, A. V., and Gypens, N. (2010). Carbonate chemistry in the coastal zone responds more strongly to eutrophication than to ocean acidification. *Limnology Oceanography* 55, 346–353. doi: 10.4319/lo.2010.55.1.0346

Cai, W. J., Feely, R. A., Testa, J. M., Li, M., Evans, W., Alin, S. R., et al. (2021). Natural and anthropogenic drivers of acidification in large estuaries. *Annu. Rev. Mar. Sci.* 13, 23–55. doi: 10.1146/ANNUREV-MARINE-010419-011004/CITE/REFWORKS

Carstensen, J., and Duarte, C. M. (2019). Drivers of pH variability in coastal ecosystems. *Environ. Sci. Technol.* 53, 4020–4029. doi: 10.1021/ACS.EST.8B03655/SUPPL_FILE/ES8B03655_SI_001.XLS

Cohn, M. R., Stephens, B. M., Meyer, M. G., Sharpe, G., Niebergall, A. K., Graff, J. R., et al. (2024). Microbial respiration in contrasting ocean provinces via high-frequency optode assays. *Front. Mar. Sci.* 11. doi: 10.3389/FMARS.2024.1395799/BIBTEX

Correa-Ramirez, M., Rodriguez-Santana, Á., Ricaurte-Villota, C., and Paramo, J. (2020). The Southern Caribbean upwelling system off Colombia: Water masses and mixing processes. *Deep-Sea Res. Part I: Oceanographic Res. Papers* 155. doi: 10.1016/j.dsr.2019.103145

Costa, D., de, A., Dolbeth, M., Christoffersen, M. L., Zúñiga-Upegui, P. T., Venâncio, M., et al. (2023). An overview of rhodoliths: ecological importance and conservation emergency. *Life* 13. doi: 10.3390/life13071556

Cyronak, T., Schulz, K. G., and Jokiel, P. L. (2016). The Omega myth: What really drives lower calcification rates in an acidifying ocean. *ICES J. Mar. Sci.* 73, 558–562. doi: 10.1093/icesjms/fsv075

Dickson, A. G. (1990). Thermodynamics of the dissociation of boric acid in synthetic seawater from 273.15 to 318.15 K. *Deep Sea Res. Part A. Oceanographic Res. Papers* 37, 755–766. doi: 10.1016/0198-0149(90)90004-F

Dickson, A. G., and Millero, F. J. (1987). A comparison of the equilibrium constants for the dissociation of carbonic acid in seawater media. *Deep Sea Research Part A, Oceanographic Research Papers* 34. 1733–1743. doi: 10.1016/0198-0149(87)90021-5

Dickson, A. G., Sabine, C. L., and Christian, J. R. (2007). *Guide to Best Practices for Ocean CO2 measurements* (Sidney, British Columbia, Canada: PICES Special Publication).

Doney, S. C., Ruckelshaus, M., Emmett Duffy, J., Barry, J. P., Chan, F., English, C. A., et al. (2012). Climate change impacts on marine ecosystems. *Annu. Rev. Mar. Sci.* 4, 11–37. doi: 10.1146/annurev-marine-041911-111611

Fabricius, K. E. (2005). Effects of terrestrial runoff on the ecology of corals and coral reefs: Review and synthesis. *Mar. pollut. Bull.* 50, 125–146. doi: 10.1016/j.marpolbul.2004.11.028

Foster, M. S. (2001). Rhodoliths: Between rocks and soft places. *J. Phycology* 37, 659–667. doi: 10.1046/j.1529-8817.2001.00195.x

Fox, J., and Weisberg, S. (2019). *An R Companion to Applied Regression*. Sage, Thousand Oaks CA, *3rd* edition. Available at: http://z.umn.edu/carbook.

Fox, J., Weisberg, S., Price, B., Adler, D., Bates, D., Baud-Bovy, G., et al. (2024). *car: An R Companion to Applied Regression. R package version 3.1-3*. Vienna, Austria: R Foundation for Statistical Computing. doi: 10.32614/CRAN.package.car

Garay, J., Ramírez, G., Betancourt, J., Marín, B., Cadavid, B., Panizzo, L., et al. (2003). *Manual de Técnicas Analíticas para la Determinación de Parámetros Fisicoquímicos y Contaminantes Marinos: Aguas, Sedimentos y Organismos*. Santa Marta, Colombia: Instituto de Investigaciones Marinas y Costeras – INVEMAR.

García-Ibáñez, M. I., Guallart, E. F., Lucas, A., Pascual, J., Gasol, J. M., Marrasé, C., et al. (2024). Two new coastal time-series of seawater carbonate system variables in the NW Mediterranean Sea: rates and mechanisms controlling pH changes. *Front. Mar. Sci.* 11. doi: 10.3389/fmars.2024.1348133

Garzón-Ferreira, J., and Cano, M. (1991). "Tipos, distribución, extensión y estado de conservación de los ecosistemas marinos costeros del Parque Nacional Natural Tayrona," in *Versión presentada al Séptimo Concurso Nacional de Ecología*, vol. 82. (Fondo Para la Protección del Medio Ambiente - FEN Colmbia, Santa Marta).

Gattuso, J. P., Frankignoulle, M., Bourge, I., Romaine, S., and Buddemeier, R. W. (1998). Effect of calcium carbonate saturation of seawater on coral calcification. *Global Planetary Change* 18, 37–46. doi: 10.1016/S0921-8181(98)00035-6

Gómez, C. E., Acosta-Chaparro, A., Bernal, C. A., Gómez-López, D., Navas-Camacho, R., and Alonso, D. (2023). Seasonal upwelling conditions modulate the calcification response of a tropical scleractinian coral. *Oceans* 4, 170–184. doi: 10.3390/oceans4020012

Isah, R. R., Enochs, I. C., and San Diego-McGlone, M. L. (2022). Sea surface carbonate dynamics at reefs of Bolinao, Philippines: Seasonal variation and fish mariculture-induced forcing. *Front. Mar. Sci.* 9. doi: 10.3389/fmars.2022.858853

Khan, H., Laas, A., Marcé, R., and Obrador, B. (2020). Major effects of alkalinity on the relationship between metabolism and dissolved inorganic carbon dynamics in lakes. *Ecosystems* 23, 1566–1580. doi: 10.1007/S10021-020-00488-6/TABLES/3

Kleypas, J. A., Anthony, K. R. N., and Gattuso, J. P. (2011). Coral reefs modify their seawater carbon chemistry - case study from a barrier reef (Moorea, French Polynesia). *Global Change Biol.* 17, 3667–3678. doi: 10.1111/j.1365-2486.2011.02530.x

Kortazar, L., Duval, B., Liñero, O., Olamendi, O., Angulo, A., Amouroux, D., et al. (2020). Accurate determination of the total alkalinity and the CO2 system parameters in high-altitude lakes from the Western Pyrenees (France – Spain). *Microchemical J.* 152, 104345. doi: 10.1016/j.microc.2019.104345

Lee, K., Kim, T. W., Byrne, R. H., Millero, F. J., Feely, R. A., and Liu, Y. M. (2010). The universal ratio of boron to chlorinity for the North Pacific and North Atlantic oceans. *Geochimica Cosmochimica Acta* 74, 1801–1811. doi: 10.1016/j.gca.2009.12.027

Li, H., Moon, H., Kang, E. J., Kim, J. M., Kim, M., Lee, K., et al. (2022). The diel and seasonal heterogeneity of carbonate chemistry and dissolved oxygen in three types of macroalgal habitats. *Front. Mar. Sci.* 9. doi: 10.3389/fmars.2022.857153

Lu, Y., Yuan, J., Lu, X., Su, C., Zhang, Y., Wang, C., et al. (2018). Major threats of pollution and climate change to global coastal ecosystems and enhanced management for sustainability. *Environ. pollut.* 239, 670–680. doi: 10.1016/j.envpol.2018.04.016

Manzello, D. P. (2010). Coral growth with thermal stress and ocean acidification: Lessons from the eastern tropical Pacific. *Coral Reefs* 29, 749–758. doi: 10.1007/S00338-010-0623-4/METRICS

Martin, S., and Hall-Spencer, J. M. (2017). "Effects of ocean warming and acidification on rhodolith/maërl bed," in *Rhodolith/Maërl Beds: A Global Perspective*. Eds. R. Riosmena-rodríguez, W. Nelson and J. Aguirre (Springer US, Boca Raton, FL), 368. doi: 10.1007/978-3-319-29315-8_1

Mccoy, S. J., and Kamenos, N. A. (2015). Coralline algae (Rhodophyta) in a changing world: Integrating ecological, physiological, and geochemical responses to global change. *J. Phycology* 51, 6–24. doi: 10.1111/jpy.12262

McCoy, S. J., and Ragazzola, F. (2014). Skeletal trade-offs in coralline algae in response to ocean acidification. *Nat. Climate Change* 4, 719–723. doi: 10.1038/nclimate2273

McGrath, T., McGovern, E., Gregory, C., and Cave, R. R. (2019). Local drivers of the seasonal carbonate cycle across four contrasting coastal systems. *Regional Stud. Mar. Sci.* 30, 100733. doi: 10.1016/J.RSMA.2019.100733

McMahon, A., Santos, I. R., Cyronak, T., and Eyre, B. D. (2013). Hysteresis between coral reef calcification and the seawater aragonite saturation state. *Geophysical Res. Lett.* 40, 4675–4679. doi: 10.1002/grl.50802

Mehrbach, C., Culberson, C. H., Hawley, J. E., and Pytkowicx, R. M. (1973). Measurement of the apparent dissociation constants of carbonic acid in seawater at atmospheric pressure. *Limnology Oceanography* 18, 897–907. doi: 10.4319/lo.1973.18.6.0897

Meléndez, M., Salisbury, J., Gledhill, D., Langdon, C., Morell, J. M., Manzello, D., et al. (2020). Seasonal variations of carbonate chemistry at two western Atlantic coral reefs. *J. Geophysical Research: Oceans* 125, 1–21. doi: 10.1029/2020JC016108

Mucci, A. (1983). The solubility of calcite and aragonite in seawater at various salinities, temperatures, and one atmosphere total pressure. *Am. J. Sci.* 283, 780–799. doi: 10.2475/AJS.283.7.780

Norzagaray, C. O., Hernández-Ayón, J. M., Castro, R., Calderón-Aguilera, L. E., Martz, T., Valdivieso-Ojeda, J. A., et al. (2020). Seasonal controls of the carbon biogeochemistry of a fringing coral reef in the Gulf of California, Mexico. *Continental Shelf Res.* 211. doi: 10.1016/j.csr.2020.104279

Oksanen, J., Simpson, G. L., Blanchet, F. G., Kindt, R., Legendre, P., Minchin, P. R., et al. (2025). *vegan: Community Ecology Package. R package version 2.6-8.* Vienna, Austria: R Foundation for Statistical Computing. Available at: https://CRAN.R-project.org/package=vegan.

Padin, X. A., Velo, A., and Pérez, F. F. (2020). ARIOS: A database for ocean acidification assessment in the Iberian upwelling system, (1976-2018. *Earth System Science Data* 12, 2647–2663. doi: 10.5194/essd-12-2647-2020

Paramo, J., Correa, M., and Núñez, S. (2011). Evidencias de desacople físico-biológico en el sistema de surgencia en la Guajira, caribe Colombiano. *Rev. Biol. Marina y Oceanografia* 46, 421–430. doi: 10.4067/S0718-19572011000300011

Pedersen, K., Cyronak, T., Goodrich, M., Kline, D. I., Linsmayer, L. B., Torres, R., et al. (2024). Short-Term Spatiotemporal Variability in Seawater Carbonate Chemistry at Two Contrasting Reef Locations in Bocas del Toro, Panama. *Aquat. Geochemistry*. 30, 13. doi: 10.1007/s10498-024-09421-y

Pérez, C. A., DeGrandpre, M. D., Lagos, N. A., Saldías, G. S., Cascales, E.-K., and Vargas, C. A. (2015). Influence of climate and land use in carbon biogeochemistry in lower reaches of rivers in central southern Chile: Implications for the carbonate system in river-influenced rocky shore environments. *J. Geophysical Research: Biogeosciences* 120, 965–978. doi: 10.1002/2014JG002699

Pierrot, D. E., Lewis, E., and Wallace, D. W. (2006). MS excel program developed for CO2 system calculations. Oak Ridge, TN: Carbon Dioxide Information Analysis Center, Oak Ridge National Laboratory. doi: 10.3334/CDIAC/otg.CO2SYS_XLS_CDIAC105a

Quintana, C. O., Shimabukuro, M., Pereira, C. O., Alves, B. G. R., Moraes, P. C., Valdemarsen, T., et al. (2015). Carbon mineralization pathways and bioturbation in coastal Brazilian sediments. *Sci. Rep.* 5, 1–13. doi: 10.1038/srep16122

Reithmaier, G. M. S., Cabral, A., Akhand, A., Bogard, M. J., Borges, A. V., Bouillon, S., et al. (2023). Carbonate chemistry and carbon sequestration driven by inorganic carbon outwelling from mangroves and saltmarshes. *Nat. Commun.* 14, 1–8. doi: 10.1038/s41467-023-44037-w

Restrepo, J. D., and Kjerfve, B. (2000). Magdalena river: interannual variability, (1975–1995) and revised water discharge and sediment load estimates. *J. Hydrology* 235, 137–149. doi: 10.1016/S0022-1694(00)00269-9

Restrepo, J. D., Zapata, P., Díaz, J. M., Garzón-Ferreira, J., and García, C. B. (2006). Fluvial fluxes into the Caribbean Sea and their impact on coastal ecosystems: The Magdalena River, Colombia. *Global Planetary Change* 50, 33–49. doi: 10.1016/j.gloplacha.2005.09.002

Reum, J. C. P., Alin, S. R., Harvey, C. J., Bednaršek, N., Evans, W., Feely, R. A., et al. (2016). Interpretation and design of ocean acidification experiments in upwelling systems in the context of carbonate chemistry co-variation with temperature and oxygen. *ICES J. Mar. Sci.* 73, 582–595. doi: 10.1093/icesjms/fsu231

Ricaurte-Villota, C., Murcia-Riaño, M., and Hernádez-Ayón, J. M. (2025). Dynamics and drivers of the carbonate system: response to terrestrial runoff and upwelling along the Northeastern Colombian Caribbean coast. *Front. Mar. Sci.* 11. doi: 10.3389/fmars.2024.1305542

Riosmena-Rodríguez, R., Nelson, W., and Aguirre, J. (2017). *Rhodolith/Maërl Beds : A Global Perspective*. Eds. R. Riosmena-rodríguez, W. Nelson and J. Aguirre (Boca Raton, FL: Springer US). doi: 10.1007/978-3-319-29315-8

Roberts, E. G., Dai, M., Cao, Z., Zhai, W., Guo, L., Shen, S. S. P., et al. (2021). The carbonate system of the northern South China Sea: Seasonality and exchange with the western North Pacific. *Prog. Oceanography* 191, 102464. doi: 10.1016/j.pocean.2020.102464

Salisbury, J., Green, M., Hunt, C., and Campbell, J. (2008). Coastal acidification by rivers: A threat to shellfish? *Eos* 89, 513. doi: 10.1029/2008EO500001

Sánchez-Noguera, C., Stuhldreier, I., Cortés, J., Jiménez, C., Morales, Á., Wild, C., et al. (2018). Natural ocean acidification at Papagayo upwelling system (north Pacific Costa Rica): Implications for reef development. *Biogeosciences* 15, 2349–2360. doi: 10.5194/bg-15-2349-2018

Savoie, A. M., Moody, A., Gilbert, M., Dillon, K. S., Howden, S. D., Shiller, A. M., et al. (2022). Impact of local rivers on coastal acidification. *Limnology Oceanography* 67, 2779–2795. doi: 10.1002/lno.12237

Schubert, N., Salazar, V. W., Rich, W. A., Vivanco Bercovich, M., Almeida Saá, A. C., Fadigas, S. D., et al. (2019). Rhodolith primary and carbonate production in a changing ocean: The interplay of warming and nutrients. *Sci. Total Environ.* 676, 455–468. doi: 10.1016/j.scitotenv.2019.04.280

Schubert, N., Tuya, F., Peña, V., Horta, P. A., Salazar, V. W., Neves, P., et al. (2024). Pink power"—the importance of coralline algal beds in the oceanic carbon cycle. *Nat. Commun.* 15, 8282. doi: 10.1038/s41467-024-52697-5

Silbiger, N. J., and Sorte, C. J. B. (2018). Biophysical feedbacks mediate carbonate chemistry in coastal ecosystems across spatiotemporal gradients. *Sci. Rep.* 8, 1–11. doi: 10.1038/s41598-017-18736-6

van der Heijden, L. H., and Kamenos, N. A. (2015). Reviews and syntheses: Calculating the global contribution of coralline algae to total carbon burial. *Biogeosciences* 12, 6429–6441. doi: 10.5194/bg-12-6429-2015

Wickham, H. (2016). *ggplot2: Elegant Graphics for Data Analysis* (Springer-Verlag New York).

Wickham, H., François, R., Henry, L., Müller, K., and Vaughan, D. (2023a). *dplyr: A Grammar of Data Manipulation. R package version 1.1.4.* Vienna, Austria: R Foundation for Statistical Computing. Available at: https://CRAN.R-project.org/package=tidyr.

Wickham, H., Vaughan, D., Girlich, M., and Ushey, K. (2023b). *tidyr: Tidy Messy Data. R package version 1.3.0.* Vienna, Austria: R Foundation for Statistical Computing. Available at: https://CRAN.R-project.org/package=dplyr.

Xiu, P., Chai, F., Curchitser, E. N., and Castruccio, F. S. (2018). Future changes in coastal upwelling ecosystems with global warming: The case of the California Current System. *Sci. Rep.* 8, 1–9. doi: 10.1038/s41598-018-21247-7

Yeemin, T., Sutthacheep, M., Pengsakun, S., Klinthong, W., Chamchoy, C., and Suebpala, W. (2024). Quantifying blue carbon stocks in interconnected seagrass, coral reef, and sandy coastline ecosystems in the Western Gulf of Thailand. *Front. Mar. Sci.* 11. doi: 10.3389/fmars.2024.1297286

Yong, Y., Baipeng, P., Guangcheng, C., and Yan, C. (2011). Processes of organic carbon in mangrove ecosystems. *Acta Ecologica Sin.* 31, 169–173. doi: 10.1016/j.chnaes.2011.03.008

Zeebe, R. E., and Wolf-Gladrow, D. (2001). *CO2 in seawater: Equilibrium, kinetics, isotopes | ScienceDirect.com by Elsevier* Vol. 65 (Amsterdam, Netherlands: Elsevier Oceanography Series).

frontiers | Frontiers in Marine Science

TYPE Original Research
PUBLISHED 03 September 2025
DOI 10.3389/fmars.2025.1621280

OPEN ACCESS

EDITED BY
Joan-Albert Sanchez-Cabeza,
National Autonomous University of Mexico, Mexico

REVIEWED BY
Xinyu Li,
University of Washington, United States
David Moriña,
Autonomous University of Barcelona, Spain
Zhentao Sun,
University of Delaware, United States

*CORRESPONDENCE
EvaLynn Jundt
evalynnjundt@gmail.com
Xinping Hu
xinping.hu@austin.utexas.edu

RECEIVED 30 April 2025
ACCEPTED 29 July 2025
PUBLISHED 03 September 2025

CITATION
Jundt E and Hu X (2025) Statistical models for the estimation of pH and aragonite saturation state in the Northwestern Gulf of Mexico. *Front. Mar. Sci.* 12:1621280. doi: 10.3389/fmars.2025.1621280

Statistical models for the estimation of pH and aragonite saturation state in the Northwestern Gulf of Mexico

EvaLynn Jundt[1]* and Xinping Hu[1,2]*

[1]Harte Research Institute, Texas A&M University-Corpus Christi, Corpus Christi, TX, United States, [2]Marine Science Institute, The University of Texas at Austin, Port Aransas, TX, United States

Historical water column carbonate measurements have been scarce in the Gulf of Mexico (GOM); thus, the progression of ocean acidification (OA) is still poorly understood, especially in the subsurface waters. In the literature, statistical models, such as multiple linear regression (MLR), have been created to fill OA data gaps in different ocean regions. Additionally, machine learning techniques such as random forest (RF) have been used in model creations for both the open ocean and marginal seas. However, there is no statistical model for subsurface carbonate chemistry parameters (i.e., pH and Ω_{Arag}) in the GOM. By creating models with various architectures built upon the relationships between commonly measured hydrographic properties (e.g., salinity, temperature, pressure, and dissolved oxygen or DO) and carbonate chemistry parameters (e.g., pH and aragonite saturation state, or Ω_{Arag}), data gaps can be potentially filled in areas with insufficient sampling coverage. In this study, two statistical models were created for pH and Ω_{Arag} in the northwestern GOM (nwGOM) within the range of 27.1–29.0 °N and 89–95.1 °W using both MLR and RF methods. The calibration data used in the models include salinity, temperature, pressure, and DO collected from seven cruises that took place between July 2007 and February 2023. The models predict Ω_{Arag} with $R^2 \geq 0.94$, mean square error (MSE) ≤ 0.04, and pH with $R^2 \geq 0.93$, MSE ≤ 0.0005. Both the MLR and RF models perform similarly. These models are valuable tools for reconstructing pH and Ω_{Arag} data where direct chemical observations are absent but hydrographic information is available in the nwGOM. Nevertheless, potential shifts in circulation, water mass changes, and accumulation of anthropogenic CO_2 need to be accounted for to improve and revise these models in the future.

KEYWORDS

ocean acidification, Gulf of Mexico, statistical models, carbonate chemistry, predictive models

Introduction

The capability of oceans to store absorbed CO_2 from the atmosphere is attributed to seawater's buffering capability. Through a chain of processes, from CO_2 dissolution to carbonic acid dissociation, only a small amount of absorbed CO_2 remains undissociated (i.e., aqueous CO_2, or CO_2*) (Zeebe et al., 2011). Due to this reaction, CO_2 invasion into seawater results in changes to the speciation of the carbonate system. Thus, while the increase in CO_2* is proportional to the CO_2 increase in the atmosphere, the extent of the total dissolved inorganic carbon (DIC) concentration increase is lower than that in the atmosphere. As a result, carbonate ion (CO_3^{2-}) concentration decreases along with the release of H^+, and carbonate saturation state (Ω) decreases following Equation 1.

$$\Omega_{sp} = [Ca^{2+}][CO_3^{2-}] / K_{sp'} \quad (1)$$

Here, $[Ca^{2+}]$ is the concentration of calcium ions, and $K_{sp'}$ is the stoichiometric solubility product (Zeebe and Wolf-Gladrow, 2001). K_{sp}' is a function of the mineral phase (calcite or aragonite), pressure, salinity, and temperature. Based on thermodynamics, calcification is favored when $\Omega > 1$ (supersaturation), while dissolution is favored when $\Omega < 1$ (undersaturation). Ocean acidification (OA) can lead to unfavorable conditions for calcareous organisms such as corals, shellfish, calcareous algae, and other important calcifying species on the ocean food web (such as pteropods) by affecting their calcification (Bednaršek et al., 2012; Erez et al., 2011; Eyre et al., 2014; Hoegh-Guldberg et al., 2007).

Although there has been increasing effort in collecting carbonate chemistry data, creating novel applications of models to supplement existing datasets in many areas, especially the coastal ocean, including the GOM, is still needed. Currently, the data coverage in the nwGOM is limited to infrequent water chemistry data collections from several NOAA-led cruises (Barbero et al., 2024, 2017; Peng and Langdon, 2007; Wanninkhof et al., 2012) and those from our study. New methods are being put into practice to remedy the missing data, including autonomous measurements, although many of these platforms are limited with measuring pH and CO_2 partial pressure (pCO_2), hence, available datasets often lack the necessary information for characterizing OA conditions in the coastal region.

In recent years, statistical modeling based on hydrographic data has been used to fill in data gaps in water column carbonate chemistry datasets (Juranek et al., 2009), as such data (including salinity, temperature, dissolved oxygen or DO, and sometimes nutrients) are much more widely available. By creating models using commonly measured hydrographic data, information such as Ω_{Arag} (i.e., aragonite saturation state), pH, total dissolved inorganic carbon (DIC), and total alkalinity (TA) can be calculated (e.g., Carter et al., 2018). An early example of these studies was done for Ω_{Arag} on the continental shelf of central Oregon (Juranek et al., 2009), where a multilinear regression (MLR) model using temperature and oxygen was developed for Ω_{Arag} (coefficient of determination or $R^2 = 0.987$, with mean standard error or MSE of 0.003). This MLR model was used for constructing comprehensive water-column Ω_{Arag} values to evaluate the seasonal evolution of Ω_{Arag}. The application of MLR models with adjustments for anthropogenic CO_2 to determine Ω_{Arag} using historical datasets was done in a study in the Sea of Japan (East Sea), where a similar model was applied to a historical dataset lacking Ω_{Arag}, resulting in an Ω_{Arag} dataset from 1960 to 2000 (Kim et al., 2010). Similar models have also been proven effective for the prediction of Ω_{Arag} in other locations, with some model applications including TA and DIC (Alin et al., 2012; Bostock et al., 2013; Hare et al., 2025; McGarry et al., 2021; Carter at al., 2021).

Our study developed statistical models using both and random forest (RF) architectures for the purpose of predicting pH and Ω_{Arag} in the northwestern Gulf of Mexico (nwGOM). Equation 2 was used to represent the MLR model, where Y is the target variable, β_0 is the y-intercept, β_x represents the slope intercept, X_x is the predictor variables and ε is the error term. MLR is a popular and effective linear modeling technique that has been applied in a vast number of research areas, including the aforementioned successful applications to marine carbonate chemistry, and thus was a clear choice.

$$Y = \beta_0 + \beta_1 X_1 + \beta_2 X_2 + \ldots + \varepsilon \quad (2)$$

Machine learning has emerged as an alternative to linear models in numerous fields (Thessen, 2016). The proliferation of machine learning techniques has led to the development of methods for a wide variety of datasets and goals. The simplest machine learning models, such as decision trees and RF models, which are constructed from a group of decision trees, each trained on a distinct subset of data. These three based models are frequently preferred when applicable due to their explanatory capability through feature importance, low computing power requirements, and ability to operate on relatively small datasets (Cutler et al., 2007). RF is a versatile and powerful ensemble learning method capable of producing high-quality predictions while effectively handling noisy data and mitigating common challenges such as overfitting (Breiman, 2001). By aggregating the predictions of multiple decision trees, each trained on distinct subsets of data, the randomness introduced by this approach enhances prediction accuracy and diminishes the risk of overfitting (Thessen, 2016). Moreover, RF offers interpretability that many other machine learning models lack, through assessment of feature importance, which measures how much each feature contributes to reducing impurity (like variance) across all the trees in the forest, indicating its overall influence on the model's predictions. This combination of robustness, accuracy, and interpretability makes RF well suited for both classification and regression tasks (Thessen, 2016). For this study, statistical and machine learning methods were used to create MLR and RF models using measured hydrographic data (salinity, temperature, pressure, DO) to estimate pH and Ω_{Arag}. These models will have the capacity not only to estimate pH and Ω_{Arag} using existing datasets but also could pair with current and potentially future autonomous observation platforms to create near real-time estimated pH and Ω_{Arag} coverage within the recommended timeframe (i.e., the next 10 years). This study will also serve as a valuable baseline of data for future OA research in the nwGOM.

Methods

Dataset description

Water column studies focusing on the carbonate system in the GOM shelf and upper slope (up to 1000 m) region include GOMECC cruises 1–4 in 2007, 2012, 2017, and 2021 (Barbero et al., 2024, 2017; Peng and Langdon, 2007; Wanninkhof et al., 2012) (Table 1). In addition to these large-scale expeditions, regional datasets also exist from individual studies focusing largely on the northern GOM shelf (Cai et al., 2020, 2011; Hu et al., 2017; Huang et al., 2015).

From April 2021 to February 2023, five cruises were conducted in the nwGOM shelf and upper slope to collect both surface and water column data across different seasons as a part of the project "Ocean Acidification at a Crossroad" (XR) (Figure 1). Among the stations sampled were those along the Galveston transect, which is a transect along the 95° W longitude first taken during GOMECC-1 cruise. This transect was sampled on GOMECCs 3 and 4 and again by the XR project in April and August of 2021, December of 2022, and February of 2023 (Table 1; Figure 1). The combined dataset before circulations QC and preparation included 960 data points from 36 stations, out of which 94 of these data points from the GOMECC-4 cruise were to be used for testing the models while the remaining 866 data points were to be split (90:10) and used for model training and calibration.

Sampling and analytical methods

Seawater sampling for the XR cruises was done following the best practices for carbonate chemistry analysis (Dickson et al., 2007). Briefly, samples were taken from the Niskin bottles into 250-ml ground-neck borosilicate glass bottles. Preservation of samples for carbonate chemistry analyses was done by adding 100 µl of saturated $HgCl_2$ solution. Glass stoppers with the aid of Apiezon® L grease and rubber bands were used to seal the samples. The GOMECC samples were analyzed on board the ship, including DO, DIC, and TA; nutrient samples were analyzed at the Atlantic Oceanographic and Meteorological Laboratory (AOML) (Barbero et al., 2017, 2024; Peng and Langdon, 2007; Wanninkhof et al., 2012). All XR carbonate chemistry (DIC, pH, and TA) samples were analyzed in our lab at Texas A&M University-Corpus Christi (Hu et al., 2018), and DO was analyzed on board the ship. Nutrient samples were analyzed at the Geochemical and Environmental Research Group at Texas A&M University.

For the GOMECC samples, DO was determined using an automated oxygen titrator with amperometric end-point detection (Culberson and Huang, 1987). DIC was determined using gas calibrations and Certified Reference Material (CRM) stability checks to ensure proper performance (with precisions of ± 1.37 µmol/kg) (Johnson et al., 1985). For the XR samples, DO was determined on a selected subset of the samples using Winkler titration (Culberson, 1991; Winkler, 1888), as these water samples were used to verify the DO sensor on the onboard the CTD (DiMarco et al., 2012). DIC was determined using infrared methodology on a DIC analyzer (Apollo SciTech Inc.) with CRM to ensure optimal instrument performance (with precisions of ±0.1%) (Chen et al., 2015). For all cruises, TA was analyzed using open-cell Gran titration (Gran, 1952), and pH was analyzed using a spectrophotometric method with purified m-cresol purple (Liu et al., 2011). Due to the COVID-19-caused interruption to CRM supply in early 2021, XR1 samples were analyzed using CRM Batch #181 and a homemade secondary reference (based on CRM Batch #181) taken from filtered (0.2 µm) and $HgCl_2$-dosed Aransas Ship Channel water. XR2 samples used CRM Batch #194, 197, and 198; XR3 samples used CRM Batch #202 and 204; and XR4 samples used Batch #204 only, while XR5 samples used Batch #204 and 205.

TABLE 1 Summary of datasets included in this research study.

Name		Date	# Observations
GOMECC	1	July 2007	90
	3	July 2017	131
	4	October 2021	59
XR	1	April 2021	104
	2	August 2021	107
	3	December 2022	57
	4	February 2023	121

Number of observations column indicates the total number of observations from each cruise included in modeling after modification for target depth and calculation of necessary parameters.

Calculations, QC, and data preparation

Speciation calculations for the GOMECC-1 data used TA, DIC, and nutrients as input variables as direct pH measurement using the spectrophotometric method was not available. Estimated uncertainties using the average surface water conditions for pH and Ω_{Arag} were ±0.01 and ±0.17, respectively (Orr et al., 2018); then DIC and pH were used for speciation calculations in all other GOMECC datasets as well as the XR ones without nutrient data, resulting in an uncertainty in Ω_{Arag} of ±0.18. Though some calculations were done without nutrients, uncertainty contributed to the combined standard uncertainty are negligible even in high-nutrient regions, except in high-nutrient waters with TA as a member of the input pair (Orr et al., 2018). Carbonate speciation calculation was done using the MatLab version program CO2SYS (Sharp et al., 2023; van Heuven et al., 2011). Carbonate dissociation constants from Mehrbach et al. (1973) refit by Dickson and Millero (1987), the dissociation constant of bisulfate reported in Dickson et al. (1990), the total boron concentration provided in Uppström (1974), and the aragonite solubility constant from Mucci (1983) were used in these calculations. As nutrient data were not available for the XR cruises due to technical issues encountered during the pandemic, we were not able to do a strict internal consistency analysis because using TA as one of the input variables would

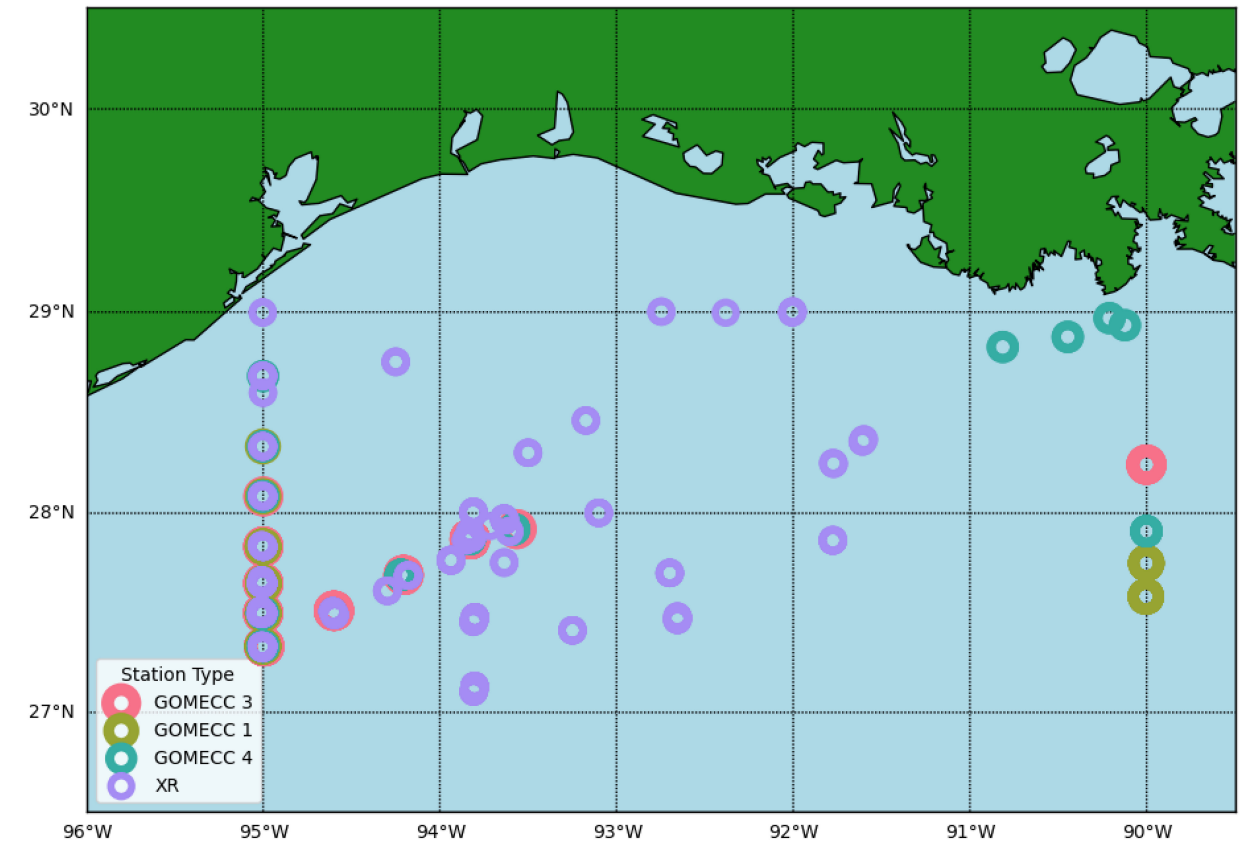

FIGURE 1
A map of the study area and stations where data was collected.

require nutrient information. However, the offset between calculated (using DIC/pH without nutrients, except for GOMECC-1) and measured TA values, was compared across all cruises to ensure that data quality was consistent among these trips (Figure 2) (Patsavas et al., 2015).

When modeling carbonate chemistry, it is crucial to focus on a geographic area where local processes and water masses exert similar control. This ensures that the relationships between parameters remain consistent throughout the area and are accurately captured in the models. Hence, data used for our model development were limited spatially within the range of 27.1–29.0°N and 89–95.1°W. Removal of the upper water column of various depths is regularly done in some capacity in carbonate modeling studies in an attempt to remove large, short-term, unconstrained variabilities, such as surface water gas exchange, physical, biological, and seasonal changes (Juranek et al., 2009; Kim et al., 2010; Lima et al., 2023; McGarry et al., 2021). Depth ranges of the mixed layer to be removed vary by location and season. Some models do not require exclusion of air-surface water interactions due to predictor variables being unaffected by this exchange, and others have used removal of additional surface water as a means of removing the effect of seasonality (Juranek et al., 2009; Kim et al., 2010; Lima et al., 2023; McGarry et al., 2021; Montes et al., 2016). Since the models produced in this study could contain DO, removing air-sea interaction was necessary. However, the removal of the mixed layer to eliminate seasonality as done by Kim et al. (2010) would equate to a removal of more than 100 m to account for the seasonal changes in mixed layer depth, as winter mixed layer depth in nwGOM can be more than 100 m (Muller-Karger et al., 2015). To retain as much data as possible while removing seasonality, removal of the upper 30 m of data was arbitrarily chosen. Note this removal should more than cover the depth of the mixed layer in summer but is shallower than those depths in winter and spring. The predictor parameters (salinity, temperature, pressure, and DO) were normalized to avoid collinearity, which causes computational problems that make parameter estimates unstable (Quinn and Keough, 2002). This was done through computing *Z*-scores using Equation 3, where X_i is the predictor variable data point, X_m is the mean of the calibration set, and X_{SD} is the standard deviation of the calibration set. This can be described as centering by subtracting the mean and dividing by the standard deviation, resulting in predictor variables having a mean of 0 and a standard deviation of 1.

$$X_n = \frac{X_i - X_m}{X_{SD}} \tag{3}$$

This approach uses normalized predictor variables to estimate nonnormalized target variables, so the relative importance of multiple parameters can be compared within one model through the magnitude of the coefficients. The normalized predictor variables were tested for collinearity by calculating the variance

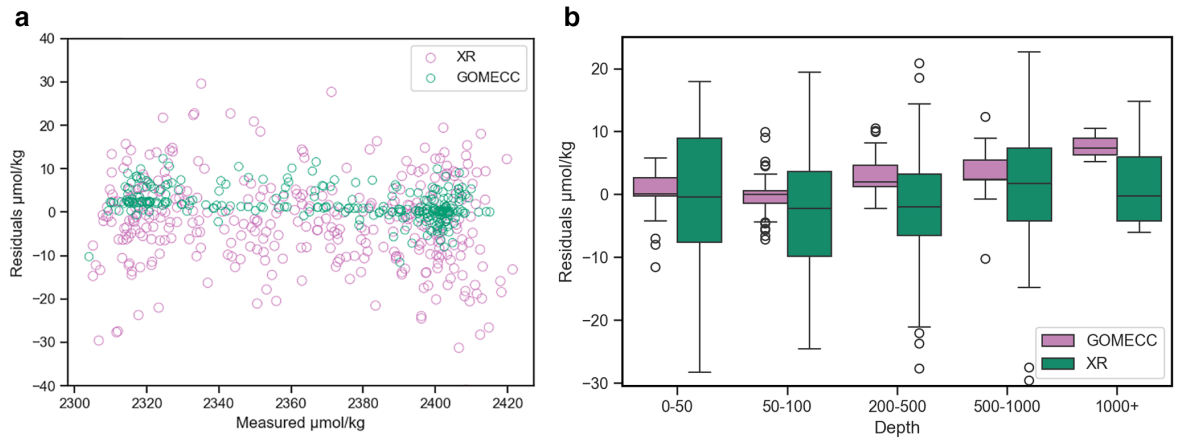

FIGURE 2
Visuals for quality control comparisons of analysis between XR and GOMECC datasets. Boxplot **(a)** showing distribution of ΔTA by calculation inputs separated by depth. Scatterplot **(b)** visualizing the spread of ΔTA by calculation inputs by measured TA values.

inflation factor (VIF) for each predictor. Combinations of terms resulting in a VIF greater than 10, indicating excessive collinearity, were not used in any model (Kutner et al., 2005). Outliers were identified using studentized residuals, which are more effective for detecting outlying Y observations than standardized residuals. Studentized residuals larger than 3 (which are classified as outliers) were further examined. Each data point was individually evaluated, considering corresponding measurements from the same sample for consistency. Data flagged as questionable across multiple parameters were carefully considered, and if multiple indicators suggested potential error, the observation was excluded from the dataset. Any data points with studentized residuals >5 were removed due to the likelihood of being erroneous or anomalous.

Model creation

The modeling exercise was conducted in Python using the *Scikit-learn* packages (Pederegosa et al., 2011). Using a combination of the measured data (salinity or S; temperature or T; DO; and pressure, or P), these techniques produced RF and MLR models for pH and Ω_{Arag}. The predictor variables were selected by dredge for MLR models or variable importance for RF models (see below for details). The process was repeated until either R^2 values were <0.90 or only one predictor variable remained. Final predictor variable selections were used to create final models that were evaluated.

MLR - Empirical models were developed for each target variable (i.e., pH and Ω_{Arag}) using least squares multiple linear regression on each combination of hydrographic variables, following the methods of Juranek et al. (2009) and Alin et al. (2012). All parameters (DO, S, T, P) in the training data were given as predictors to a full MLR model. Dredge methodology was used to evaluate every possible combination of the four parameters. From among the combinations, all models were ranked based on minimizing the Akaike information criterion (AIC), a metric for model selection that incorporates both the goodness of fit and a penalty for complexity (Burnham and Anderson, 2004). The best performing models with $R^2 > 0.90$ and correlation coefficients with correct signs (±) were selected for further evaluation.

RF - An initial RF model was created including all four variables. Hyperparameter tuning is the process of optimizing a model's configuration settings to improve performance by specifying tuned values for the number of trees, max tree depth, and minimum samples split. Hyperparameters for tuning were decided using scickit-learn GridSearchCV (Supplementary Table S2). Selected hyperparameters were applied using an RF regressor function (Probst et al., 2019). After this step, the variable importance was analyzed, and a stepwise procedure was followed to create a new model without the variable of least importance. The new model was then tuned and evaluated, if the model's R2 > 0.90 it would be considered in the final model valuation. In addition, the process starting by analyzing feature importance to create a simpler model was continued until the resulting model did not meet previously stated criteria.

Model evaluation

The models were used to predict their target variable while using predictor variable data from the completely "unseen data," or data uninvolved in the training process, in this instance, the GOMECC-4 data. By using data from a cruise, which also took place within the time period that the modeled data were collected, separate from the training data, this ensures that the model performance results will accurately represent the models' efficacy on new data. To ensure that the test dataset is representative of the training dataset and that the distributions of the variables are not problematically different, a two-step evaluation process was conducted. First, the distribution of each variable in both the training and test datasets was visually examined using graphical representations, such as histograms, density plots, or boxplots, to

identify any noticeable differences. Second, the Kolmogorov–Smirnov (KS) test, a non-parametric statistical test, was applied to each variable to evaluate whether two samples are drawn from the same underlying distribution by comparing their cumulative distribution functions (Massey, 1951). These analyses collectively concluded that the training and test datasets are statistically comparable, minimizing the risk of bias in model evaluation due to distributional differences.

After confirmation of the representative quality of the test data, model evaluations were based on the performance across multiple metrics, including mean absolute error (MAE), mean square error (MSE), mean absolute percent error (MAPE), correlation coefficient R^2, and spatial bias (Vujovic, 2021). MAE and MSE represent the absolute-difference and the squared-difference metrics, respectively. MLR model variable coefficients were used for interpretation of relative variable effect. The RF model variable importance best describes model fit, not direct variable relationships, and therefore was not interpreted this way, that is, variable effect. Additional analysis of the residual data to identify normality and potential signals was done using QQ-plots and Shapiro–Wilks tests (Chen et al., 2019) (Supplementary Figures S1-S8).

Results

The models chosen to predict both Ω_{Arag} and pH included different combinations of the following parameters: salinity, temperature, pressure, and DO (Table 2). All linear combinations of hydrographic parameters in the models presented here resulted in VIFs less than 10, suggesting that there is no statistical evidence of coupling between any of the predictor variables. The MLR and RF models for Ω_{Arag} had adjusted R^2 values between 0.94 and 0.99 and MAE values between 0.06 and 0.14. The MLR and RF models for pH had adjusted R^2 values between 0.93 and 0.96 and MAE values between 0.01 and 0.02. As shown in Figures 3 and 4, the residuals for all model versions displayed some visually identifiable tendency for greater error in shallower depths. This, in combination with poorer performance of models including all depths, supports the choice made to mitigate uncertainty caused by air-sea interaction by the exclusion of the mixed layer in some capacity (Supplementary Table S2). MAPE statistics indicate the models for pH displayed less deviation between predicted and actual values and may perform better when used with new data (Table 2). These model evaluative criteria indicate that both models produced reliable results across the range of observed values in the calibration dataset (Figures 3, 4).

$$E_{est} = \sqrt{E_{Response}^2 + E_{Input}^2 + E_{MLR}^2} \quad (4)$$

$$E_{est} = \sqrt{\sum_{i=1}^{n} (U_i B_i)^2} \quad (5)$$

Uncertainty propagations were calculated using Equation 4 (Carter et al., 2018; Li et al., 2022). E_{MLR} refers to the model RMSE. $E_{Response}$ represents measurement uncertainties; for pH, this is the spectrophotometric measurement uncertainty, which was set conservatively to be a constant 0.005 (Carter et al., 2024). For Ω_{Arag} this is the uncertainty from input pairs propagated through calculations of Ω_{Arag} which was set as 0.085 (Orr et al., 2018). E_{input} is the uncertainty of the input parameters propagated in the regression, which can be calculated using Equation 5, where U_i is the i-th input uncertainties of the predictor properties. We set the U_i values at 0.005, 0.005°C, and 2.2 µmol kg^{-1} for S, T, and DO,

TABLE 2 Summary of all models for the prediction of pH including their performance metrics and variable importance for RF models and coefficients for MLR models.

	MSE	MAE	MAPE	R^2	MSE	MAE	R^2	Temperature	Dissolved Oxygen	Pressure	Salinity	Intercept
Ω_{Arag} RF 3	0.010	0.071	0.029	0.987	0.011	0.068	0.985	0.56	0.09	0.35		
Ω_{Arag} RF 2	0.021	0.095	0.039	0.971	0.025	0.095	0.966	0.61		0.39		
Ω_{Arag} RF 1	0.037	0.130	0.051	0.949	0.044	0.135	0.94	1				
Ω_{Arag} MLR 4	0.009	0.072	0.032	0.987	0.01	0.056	0.986	0.3982	0.3722	-0.0544	0.0989	2.5369
Ω_{Arag} MLR 3	**0.010**	**0.071**	**0.032**	**0.987**	**0.011**	**0.063**	**0.984**	**0.4367**	**0.3687**	**-0.1127**		**2.537**
pH RF 3	**0.0003**	**0.013**	**0.002**	**0.959**	**0.0002**	**0.013**	**0.961**		**0.15**	**0.75**	**0.1**	
pH MLR 3	0.001	0.018	0.002	0.929	0.0005	0.017	0.929	-0.0078	0.0647	-0.0432		7.9512
pH MLR 4	0.000	0.016	0.002	0.946	0.0003	0.011	0.955	-0.0232	0.0661	-0.0198	0.0396	7.9511

Unshaded area includes results from performance of validation dataset; shaded area indicates performance of unseen test data. Number in the model ID reflects the number of variables used in the model. MSE is mean square error, MAE is mean absolute error, MAPE is mean absolute percent error, R^2 is the correlation coefficient. The rows with the bold fonts indicate the best models. Note the first column includes modeled parameter (Ω_{Arag} and pH), and the numbers after the statistical models (RF or MLR) indicate the number of predicting variables used.

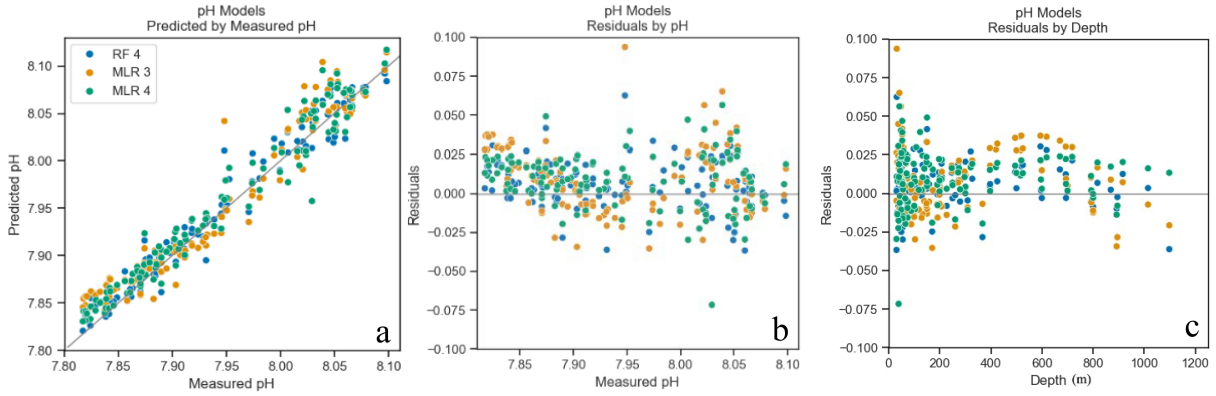

FIGURE 3
pH models predicted values plotted by measured values from models' application to test dataset (GOMECC4) **(a)**, residuals plotted by measured Ω_{Arag} **(b)**, and depth **(c)**. Points color coded for each model (Table 2).

respectively (Carter et al., 2018). Total uncertainty calculated is 0.12 for Ω_{Arag} and 0.0173 for pH. Other information that can be inferred from these calculations is the relative sources of uncertainty by the comparison of $E_{Response}$, E_{Input}, and E_{MLR}. In both cases the E_{MLR} value was the largest contributor of uncertainty, followed by $E_{Response}$.

In addition to the total uncertainty calculations, a better understanding of the source of the uncertainty described by the E_{MLR} can be achieved by examining the calculations of error used to describe model performance, such as MAPE and MAE. Ω_{Arag} models produced MAPE scores of 2.9%–5.1% and MAE of 0.05–0.13 in comparison to estimates of error propagation for calculation of Ω_{Arag} being ±0.16 depending on input pairs (Orr et al., 2018). Most of the uncertainty from calculation comes from the pair-constants curve, meaning methodological uncertainties for the input pairs result in little effect on the overall propagated uncertainties. Therefore, the relative uncertainty due to error of model Ω_{Arag} values has similar reliability to calculations of Ω_{Arag} from measured DIC, TA, or pH values. This was not true for pH models, as MAPE scores ranged from 0.16% to 0.22%, with an MAE of 0.011–0.018 in comparison to a relative uncertainty of measurement methods of 0.008–0.0012, meaning that there is a higher confidence of measured values as opposed to predicted (Takeshita et al., 2021).

The best model for Ω_{Arag} was the MLR model, which included all variables with an R^2 = 0.99. (Ω_{Arag} MLR 4; Table 2). MLR equation coefficients indicate that for the Ω_{Arag} model, variable importance, or contribution to explainability, is as follows, from most to least important: temperature, DO, pressure, and salinity, with temperature and DO being >77% larger than pressure and salinity. The second-best performing model with R^2 = 0.98 is the MLR model with three variables, which, in order of importance, are temperature, DO, and pressure (Ω_{Arag} MLR 3; Table 2). The RF models did not outperform MLR models but came close behind, with the best RF model (Ω_{Arag} RF 3; Table 2) having an R^2 = 0.99 while using the same three variables as the second-best MLR model. For the RF models, poorer performance on test data than validation data would indicate overfitting and that the model has poor ability to generalize. However, minimal difference ($\Delta R^2 < 0.01$) was observed in performance on testing versus validation data. This

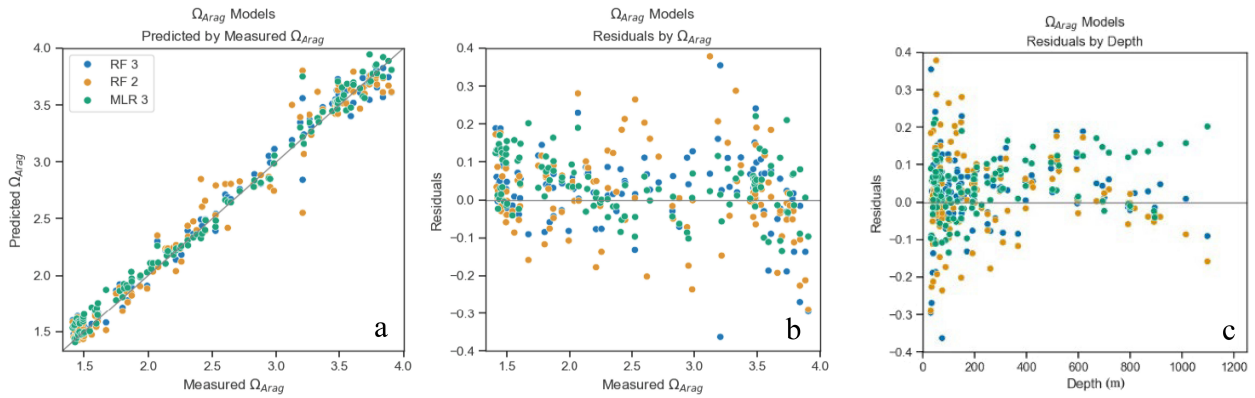

FIGURE 4
Ω_{Arag} models predicted values plotted by measured values from models' application to test dataset (GOMECC4) **(a)**, residuals plotted by measured Ω_{Arag} **(b)** and depth **(c)**. Points color coded for each model (Table 2).

indicates that the model is not overfitted, generalized well, and can be expected to perform similarly (as it did on the test data) on new data (Domingos, 2012).

For pH, the best-performing model was the RF model that included three variables with an $R^2 = 0.96$. (pH RF 3; Table 2). The second-best performing model with $R^2 = 0.975$ was the MLR model with all variables, which, in order of importance, are DO, temperature, pressure, and salinity (pH MLR 4). The RF models outperformed the MLR models for pH prediction, but again by a narrow gap. Differences were observed in performance on validation and test datasets of $R^2 > 0.6$, indicating which models may be slightly overfitted. The RF model containing all four variables performed poorly, possibly due to overfitting or collinearity and thus is not included.

All residuals indicated nonnormality as seen in QQ-plots, histograms, and through Shapiro-Wilks p-values < 0.05 (Supplementary Figures S1–S8). To further investigate the non-normality of residuals and determine if it could be an indicator of other problems, the Durbin-Watson and Breusch-Pagan tests were used to test the assumptions for independent and homoscedastic residuals. A Durbin-Watson test for independence resulting in a value close to 2 suggests that the residuals an autocorrelated. Breusch–Pagan test for homoscedasticity, where a $p > 0.05$ suggests homoscedasticity. Therefore, despite the nonnormality of the residuals, it is unlikely to be problematic due to their independence, homoscedasticity, the size of the dataset, and the robust nature of the models (Breiman, 2001).

Discussion

Data selection considerations

The nwGOM area (latitudes 27.1–29.0˚N and longitudes 89–95.1˚W) was selected to isolate a relatively small geographic area where controlling factors on the carbonate system are expected to remain similar in the examined window of time and included the same stations surveyed repeatedly along the same transect (i.e., the 90° line). This study area lies almost entirely on the Texas shelf and far enough to the west so that the effects of the freshwater discharge transported westward are less pronounced than on the bulk of the Louisiana Shelf (Androulidakis et al., 2015; Morey et al., 2003). Under heavy influence from the large river's watershed, salinity would be a key variable for models, although it is not detected as such in our models. Therefore, salinity was only included as a predictor variable in one of the Ω_{Arag} models and only half of the pH models.

Removal of the surface layer of the water column was done strategically to remove large, short-term temporally unconstrained variabilities, such as surface water gas exchange, physical, biological, and seasonal changes (Juranek et al., 2009; Kim et al., 2010; McGarry et al., 2021). In the nwGOM, removal of shallow water can potentially mitigate the minimal effects of freshwater outflow as the low-salinity river discharge is buoyant. Removal of surface water can be less important when air-surface water interactions do not affect predictor variables. Even still, removal can serve as a means of removing the effect of seasonality, though depth ranges of the mixed layer to be removed vary by location and season (Juranek et al., 2009; Kim et al., 2010; McGarry et al., 2021; Montes et al., 2016). Since most of the models produced in this study contain DO, removing air-sea interaction was necessary. Based on the final models chosen for Ω_{Arag} and pH, the relationships showed that the exclusion of the upper 30 m of the water column did improve the performance of all Ω_{Arag} models. When models are compared with the model containing the same spatial data but all depths, models with the upper 30 m removed, except for pH MLR models, had either greater R^2, lower MSE or MAPE, or a combination of the three (Supplementary Table S2). The improvements in all models indicate that the removal of surface water increases the performance of the models, though it should be noted that there may be bias across seasons due to unaccounted-for surface water and mixed-layer inclusion in the datasets used for training. Seasonal bias could also occur due to a greater quantity of summer observations in the training dataset. Further data beyond the 2007–2023 time series, as well as the inclusion of more seasonal data, are needed to properly assess the potential existence of these biases.

Aragonite models

There are many known relationships between Ω_{Arag} and physical and chemical parameters, which is why the variables salinity, temperature, pressure, and DO were chosen in developing Ω_{Arag} models. However, the degree to which each of these variables is intertwined with Ω_{Arag} is not so easy to identify but can be inferred by their selection and importance in the models with the highest performance.

Temperature was the most prominent predictor for Ω_{Arag} in all models (Table 2). The strength of the relationship can be explained by Ω_{Arag} as a function of K_{sp} and $[CO_3^{2-}]$, and K_{sp} as a function of temperature, salinity, and pressure. Temperature as a dominant predictor variable aligns well with models built for Ω_{Arag} prediction in other areas, which also found temperature to be a primary predictor for Ω_{Arag} (Alin et al., 2012; Juranek et al., 2009; Kim et al., 2010; McGarry et al., 2021). Pressure was included in all MLR models and two out of three RF models (Table 2). The pressure term in the models can be in part explained by Ω_{Arag} as a function of K_{sp} and $[CO_3^{2-}]$, and K_{sp} is also a function of pressure, that is, increasing solubility with depth. DO was included in both MLR models and one RF model (Table 2). The inclusion of DO is likely due to the close coupling of DO and DIC in subsurface waters, which includes CO_2 uptake (photosynthesis) and release (respiration) and lacks exchange with the atmosphere in the subsurface (>30 m). Although salinity was also tested, it was only included in one MLR model based on selection criteria and was the least important predictor variable by coefficient (Table 2). The lack of salinity could be in part because salinity in the modeled dataset has small variability from 33.2 to 36.7 without outliers and an interquartile range (IQR) of from 35.2 to 36.4. This means salinity has a relatively small contribution to variability, either due to the

hydrography of the area or possibly in part to the limitation of the dataset's spatial and depth coverage. By focusing on the nwGOM and removing the upper 30 m it is possible that freshwater outflow transported from the Mississippi-Atchafalaya watershed westward over the Louisiana-Texas shelf in the surface water has been partially or wholly avoided (Morey et al., 2003).

pH models

Although anthropogenic CO_2 is the dominant driver for long-term, that is, multidecadal, change in pH in the upper ocean water column, the variations observed in coastal waters on decadal time scales are largely attributed to driving forces including production shift due to changes in nutrient input (Wang et al., 2013) and ocean circulation changes (e.g., upwelling) (Feely et al., 2008) and terrestrial influences (Cai, 2003; Duarte et al., 2013; Gomez et al., 2021). The fact that DO was included as an important predictor variable suggests that biological activities are a major driving force for the carbonate system. Similarly, DO was also found to be the strongest predictor of pH in the Northeast US (McGarry et al., 2021). Pressure was also important in all the models, as carbonate system equilibria are affected by pressure (Table 2). There is a visually notable trend of overprediction of pH from 400 to 800 m; this is an area with lower pH and Ω than the rest of the water column. We attribute this bias to the non-linearity of the carbonate system. This type of bias has also been seen in other similar models in different geographic locations as well (Juranek et al., 2011, 2009).

Comparison with previous models

One of the primary motivations behind the use of the MLR modeling with standardized variables is the ability to use empirical relationships among predictor variables to accurately describe the controlling processes in the study area, whereas RF modeling can only provide relative feature importance, which is not a quantification of the correlation between variables but of the relative impact on the performance of the model, or reduced impurity, that can be attributed to that predictor variable (Breiman, 2001). Due to standardization, the strength of the predictor variable correlation with the target variable can be inferred by the absolute value of the coefficients of predictor variables included in the models. However, it is important to note that statistical models reflect correlations between predictor variables and target variables but do not necessarily reveal mechanistic relationships (Quinn and Keough, 2002) (Table 2).

Because of differences in hydrography, river influences, and location of the drivers of the carbonate system, statistical models for carbonate system parameters are often specific to the geographic areas where they were created for. Although many of the primary drivers of the carbonate system remain the same, the secondary variables shift, as does the degree to which they influence.

In the literature, Ω_{Arag} models have been created for the northwestern Atlantic (McGarry et al., 2021), northern Gulf of Alaska (Evans et al., 2013), Central Oregon Coast (Juranek et al., 2011, 2009), southern California Current system (Alin et al., 2012), Queen Charlotte Sound (Hare et al., 2025), U.S. east coast (Li et al., 2022), and the Sea of Japan (East Sea) (Kim et al., 2010). These models all have between two and three variables and an adjusted $R^2 \geq 0.91$ compared to between one and four variables with an adjusted $R^2 \geq 0.94$ in this study. The primary predictor variable in all previous models except two (Evans et al., 2013; Juranek et al., 2011) is temperature, as is the case in this study. Most models also include some combination of temperature with salinity, oxygen, and interaction terms; one model also used pressure (Kim et al., 2010), and one used NO_3^- (Evans et al., 2013). The models created here and those created previously for Ω_{Arag} agreed on the use of temperature as a primary predictor variable in combination with other predictor variables.

pH models have been created for the eastern US coast (McGarry et al., 2021; Li et al., 2022), the northeast Pacific (Juranek et al., 2011), the southern California Current System (Alin et al., 2012), Queen Charlotte Sound (Hare et al., 2025), and the global ocean (Carter et al., 2021). All those models also used temperature and DO (Alin et al., 2012; Juranek et al., 2011; McGarry et al., 2021; Li et al., 2022), with one model also using an interaction term between DO and temperature (Alin et al., 2012), one using nutrients, salinity, and multiple interaction terms (McGarry et al., 2021) and, lastly, one using AOU and salinity (Hare et al., 2025). They included between two and seven variables and resulted in adjusted $R^2 \geq 0.89$ in comparison to our models, which have between three and four variables and adjusted $R^2 \geq 0.93$. Our MLR models are consistent with previous models that DO was an important predictor variable for pH.

Model applicability

The GOMECC-1 survey in 2007 was among the first to collect comprehensive, high-quality, measurements of the inorganic carbonate system parameters in the GOM. However, the capacity for autonomous observation of ocean carbonate chemistry is growing rapidly. By combining real-time, high-resolution data with modeling methods, it is possible to create comprehensive data coverage while simultaneously providing data validation via comparison between different data sources. With the use of MLR in combination with a single Argo profile float containing DO and temperature sensors, Juranek et al. (2011) were able to create a 14-month comprehensive time series containing Ω_{Arag} and pH, which were verified by comparisons to independently measured values. Evans et al. (2013) applied models to field data from glider flight and a GLOBEC mesoscale SeaSoar survey (Cowles, 2002) to create complete datasets, allowing for identification of variability of Ω_{Arag}. Hare et al. (2025) also had success with this in Queen Charlotte Sound, British Columbia, where regression models were applied to regional autonomous glider data. Although autonomous measurements for biogeochemical parameters in the GOM have just begun (Osborne et al., 2024), successful combination of

models and autonomous data collection should greatly improve geochemical data coverage and advance carbonate chemistry studies.

In addition to long-term changes, there is strong motivation to apply empirical models to year-round hydrographic data to reconstruct the seasonal cycle of carbonate chemistry. For example, Juranek et al. (2009) created a model using data collected in spring and successfully used it to predict the seasonal changes in Ω_{Arag} under the assumption that the seasonal variability of the primary independent variables (temperature and DO) would be comparable to the variations encountered spatially during the initial data collection. One method to mitigate effects of the lack of seasonal variation data on the relationships between physical and chemical data is by excluding depths influenced by local meteorological conditions from the analysis (Kim et al., 2010). Most models were calibrated using mostly summer data and none with subsurface seasonal data for the GOM. Our models contain data from all seasons with slightly more data points from summer months. Seasonal application is expected to be viable in the produced models for pH as it was explained primarily by biologically driven changes, that is, the coupling between DIC and DO. Seasonal application is also expected to be viable for Ω_{Arag} at depths of 30–300 m, as biological changes are primarily driven by DIC rather than TA (Anglès et al., 2019; Hu et al., 2018). It is expected that changes in DIC should be captured in these models due to their relationship with DO in the subsurface (Anderson and Sarmiento, 1994; Hales et al., 2005).

Furthermore, there is also motivation to apply statistical models to forecast the carbonate system conditions as OA progresses. Previously created MLRs have been applied to generate hindcasts (up to 40 years) on carbonate chemistry (Evans et al., 2013; Kim et al., 2010). However, the temporal applicability of a model is expected to be limited. To use the model for predictions beyond the timeframe of training data, even with relatively unchanged circulation and watershed conditions, it is necessary to make corrections for shifts caused by changes in the anthropogenic CO_2 inventory in the water column, increasing error beyond model uncertainty. This is because empirical models do not account for anthropogenic addition of CO_2, which changes the ratio of DIC/DO. Due to atmospheric CO_2 input, previous modeling studies have calculated that the statistical relationships will need to be updated every 5–10 years to account for changes in target variables (Alin et al., 2012; Juranek et al., 2011, 2009). The models can be used for estimation of data within the timeframe of the training data (2007–2023), with the requirement that seasonality or waterbody changes are captured, hindcasting up to 10 years (1997–2007), and predicting up to 10 years (2023–2033) (Juranek et al., 2011). For example, Juranek et al. (2009) created a model using data collected in spring, and they successfully used it to predict the seasonal changes in $\Omega_{Arag.}$ The assumption of this study was that the seasonal variability of the primary independent variables (temperature and DO) would be comparable to the variation encountered spatially during the initial data collection just a year prior. However, to extend the reconstruction further than 10 years, it would be necessary to account for the progressive addition of anthropogenic CO_2 to the water column over time. For example, Kim et al. (2010) used estimates of anthropogenic CO_2 invasion to subtract anthropogenic CO_2 and apply modeling estimates of DIC in the Sea of Japan (East Sea) to create a 40-year reconstruction. In our study, the total uncertainty values are 0.12 for Ω_{Arag} and 0.0173 for pH. The rate of pH decline at the surface during the 2013–2022 period is 0.0025 ± 0.0005 year^{1-}, while there is no discernable trend in Ω_{Arag} (Hu, unpublished data). Based on this, it would take 14 years for the accumulation of anthropogenic carbon to surpass two times the uncertainty for pH (i.e., the time of emergence, Turk et al., 2019). Due to the lack of trend in Ω_{Arag}, these models could be applicable for a longer period in this region. However, we recommend conservatively applying caution when using beyond the 10-year window. For all models but particularly $\Omega_{Arag,}$ it seems likely that other factors such as changing climatology may be the first to influence model applicability rather than anthropogenic CO_2 intrusion.

Data scarcity

Technological advancements (e.g., satellites, floats, and gliders) have made autonomous measurements for selected variables possible. Even though satellites provide large volumes of invaluable data, their scope is limited not only to the surface layer but also to measurements of temperature and ocean color, which can be used for estimations of productivity, dissolved organic matter, and sea surface CO_2 partial pressure (e.g., Chen et al., 2019). Some remedies for the lack of data beyond the surface have come in the form of novel technologies, including Argo floats and gliders (Osborne et al., 2024). The Argo array supports more than 3,000 floats across the global ocean, supplying profiles of T and S, of which about 200 are also equipped with a DO sensor. Biogeochemical-Argo (BGC-Argo) floats can take measurements from the surface to 2,000 dbar and provide high-resolution autonomous measurements for some combinations of chlorophyll, particle backscatter, DO, nitrate, pH, or irradiance (Roemmich et al., 2019). Nevertheless, this equipment is limited in coverage ability; BGC-Argos have yet to reach the comprehensive coverage of traditional Argos, and they usually do not operate on continental shelves. Gliders share the similar biogeochemical sensors used by the BGC-Argo floats with a similar mode of operation but perform sawtooth trajectories from the surface to the bottom, or to 200–1,000 m depth, and their deployments are limited largely by biofouling, battery life, and payload space, hindering their ability to carry many sensors (Saba et al., 2019; Testor et al., 2019). Additionally, all data from floats and gliders must undergo rigorous quality control and correction of potential errors in sensors, such as drift and be compared to lab-measured samples when possible (Roemmich et al., 2019).

Given the performance of the models created here, it would be reasonable to expect that in combination with datasets from data collection via these platforms, one or both of pH and Ω_{Arag} could be estimated. Traditional Argos, as well as most gliders, have temperature and pressure (or depth) measurements, meaning Ω_{Arag} could be estimated using either of the two RF models with

R^2 values of 0.94 and 0.97. With the addition of DO, which is included in a subset of the Argos and in the BGC-Argos, the Ω_{Arag} model with an R^2 of 0.98 could be applied. Additionally, the pH model with R^2 of 0.94 could be used; even though pH sensors are included in many BGC-Argos, the modeled results could provide robust data quality check capability.

Recommendations

The models developed in this study serve as valuable tools for reconstructing pH and Ω_{Arag} data in the absence of direct chemical observations, leveraging available hydrographic information. The models can also be used for hindcasting over a 10-year period (1997–2007) and for forecasting over the next ~10 years (2023–2033) in the nwGOM, if seasonality and watermass changes are adequately captured. Through modeling, our results showed that RF models do not have any distinct advantage over the MLR models which are commonly used. It is crucial to examine potential shifts in circulation, water mass composition, and anthropogenic CO_2 accumulation to refine and update the models over time. Despite their robustness, several potential issues remain across all models, suggesting room for improvement, such as difficulties estimating target variables due to significant variation in the shallow and mixed layers, a need for additional data points, or the application of more complex models. Future work to enhance these models could involve incorporating additional data, as well as exploring the application of neural network AI models and locally interpolated regressions, such as those employed by Carter et al. (2021).

Data availability statement

The original contributions presented in the study are publicly available. This data can be found here: https://github.com/ejundt/XRModel.git and https://wq.gcoos.org/oa/data/csv/. Publicly available datasets were analyzed in this study. This data can be found here: https://glodap.info/.

Author contributions

EJ: Conceptualization, Data curation, Formal analysis, Investigation, Methodology, Software, Validation, Visualization, Writing – original draft, Writing – review & editing. XH: Conceptualization, Funding acquisition, Resources, Supervision, Writing – review & editing.

Funding

The author(s) declare financial support was received for the research and/or publication of this article. This study was funded by NOAA Ocean Acidification Program (award #NA19OAR0170354).

Acknowledgments

This publication was made possible by the National Oceanic and Atmospheric Administration, Office of Education Educational Partnership Program with Minority Serving Institutions award (NA21SEC4810004). We would like to thank Steven DiMarco, Piers Chapman, Sakib Mahmud, students and postdocs from Texas A&M University, and the captain and crew on board R/V Pelican for their assistance with sample collection and analyses. We would also like to thank the scientific party on previous GOMECC cruises for their contributions to the data used in this study.

Conflict of interest

The authors declare that the research was conducted in the absence of any commercial or financial relationships that could be construed as a potential conflict of interest.

Generative AI statement

The author(s) declare that no Generative AI was used in the creation of this manuscript.

Any alternative text (alt text) provided alongside figures in this article has been generated by Frontiers with the support of artificial intelligence and reasonable efforts have been made to ensure accuracy, including review by the authors wherever possible. If you identify any issues, please contact us.

Publisher's note

Author disclaimer

Its contents are solely the responsibility of the award recipient and do not necessarily represent the official views of the U.S. Department of Commerce, National Oceanic and Atmospheric Administration.

Supplementary material

The Supplementary Material for this article can be found online at: https://www.frontiersin.org/articles/10.3389/fmars.2025.1621280/full#supplementary-material

References

Alin, S. R., Feely, R. A., Dickson, A. G., Martín Hernández-Ayón, J., Juranek, L. W., Ohman, M. D., et al. (2012). Robust empirical relationships for estimating the carbonate system in the southern California Current System and application to CalCOFI hydrographic cruise data, (2005–2011). *J. Geophys Res. Oceans* 117, 5033. doi: 10.1029/2011JC007511

Anderson, L. A., and Sarmiento, J. L. (1994). Redfield ratios of remineralization determined by nutrient data analysis. *Global Biogeochem Cycles* 8, 65–80. doi: 10.1029/93GB03318

Androulidakis, Y. S., Kourafalou, V. H., and Schiller, R. V. (2015). Process studies on the evolution of the Mississippi River plume: Impact of topography, wind and discharge conditions. *Cont Shelf Res.* 107, 33–49. doi: 10.1016/j.csr.2015.07.014

Anglès, S., Jordi, A., Henrichs, D. W., and Campbell, L. (2019). Influence of coastal upwelling and river discharge on the phytoplankton community composition in the northwestern Gulf of Mexico. *Prog. Oceanogr* 173, 26–36. doi: 10.1016/j.pocean.2019.02.001

Barbero, L., Pierrot, D., Wanninkhof, R., Baringer, M., Hooper, J., Zhang, J. Z., et al. (2017). *Cruise Report: Third Gulf of Mexico Ecosystems and Carbon Cycle (GOMECC-3) Cruise*. Miami, FL 33149: NOAA Atlantic Oceanographic and Meteorological Laboratory. doi: 10.25923/y6m9-fy08

Barbero, L., Stefanick, A., Hooper, J., Wanninkhof, R., Baringer, M., Smith, I., et al. (2024). *Cruise Report: Fourth Gulf of Mexico Ecosystems and Carbon Cycle (GOMECC-4) Cruise*. Atlantic Oceanographic and Meteorological Laboratory, Miami, FL 33149. doi: 10.25923/rwx5-s713

Bednaršek, N., Tarling, G. A., Bakker, D. C. E., Fielding, S., Jones, E. M., Venables, H. J., et al. (2012). Extensive dissolution of live pteropods in the Southern Ocean. *Nat. Geosci* 5, 881–885. doi: 10.1038/NGEO1635

Bostock, H. C., Mikaloff Fletcher, S. E., and Williams, M. J. M. (2013). Estimating carbonate parameters from hydrographic data for the intermediate and deep waters of the Southern Hemisphere oceans. *Biogeosciences* 10 (10), 6199–6213. doi: 10.5194/BG-10-6199-2013

Breiman, L. (2001). Random forests. *Mach. Learn* 45, 5–32. doi: 10.1023/A:1010933404324/METRICS

Burnham, K. P., and Anderson, D. R. (2004). Multimodel inference: understanding AIC and BIC in model selection. *Sociological Methods & Research* 33, 261–304. doi: 10.1177/0049124104268644

Cai, W. J. (2003). Riverine inorganic carbon flux and rate of biological uptake in the Mississippi River plume. *Geophys Res. Lett.* 30, 1032. doi: 10.1029/2002GL016312

Cai, W. J., Hu, X., Huang, W. J., Murrell, M. C., Lehrter, J. C., Lohrenz, S. E., et al. (2011). Acidification of subsurface coastal waters enhanced by eutrophication. *Nat. Geosci.* 11, 766–770. doi: 10.1038/ngeo1297

Cai, W. J., Xu, Y. Y., Feely, R. A., Wanninkhof, R., Jönsson, B., Alin, S. R., et al. (2020). Controls on surface water carbonate chemistry along North American ocean margins. *Nat. Commun.* 11, 1–13. doi: 10.1038/s41467-020-16530-z

Carter, B. R., Bittig, H. C., Fassbender, A. J., Sharp, J. D., Takeshita, Y., Xu, Y.-Y., et al. (2021). New and updated global empirical seawater property estimation routines. *Limnology and Oceanography: Methods*. 19, 785–809. doi: 10.1002/lom3.10461

Carter, B. R., Feely, R. A., Williams, N. L., Dickson, A. G., Fong, M. B., and Takeshita, Y. (2018). Updated methods for global locally interpolated estimation of alkalinity, pH, and nitrate. *Limnol Oceanogr Methods* 16, 119–131. doi: 10.1002/LOM3.10232;JOURNAL:JOURNAL:15415856;WGROUP:STRING:PUBLICATION

Carter, B. R., Sharp, J. D., Dickson, A. G., Álvarez, M., Fong, M. B., García-Ibáñez, M. I., et al. (2024). Uncertainty sources for measurable ocean carbonate chemistry variables. *Limnol Oceanogr* 69, 1–21. doi: 10.1002/LNO.12477

Chen, B., Cai, W. J., and Chen, L. (2015). The marine carbonate system of the Arctic Ocean: Assessment of internal consistency and sampling considerations, summer 2010. *Mar. Chem.* 176, 174–188. doi: 10.1016/J.MARCHEM.2015.09.007

Chen, S., Hu, C., Barnes, B. B., Wanninkhof, R., Cai, W.-J., Barbero, L., et al. (2019). A machine learning approach to estimate surface ocean pCO 2 from satellite measurements. *Remote Sens Environ.* 228, 203–226. doi: 10.1016/j.rse.2019.04.019

Cowles, T. (2002). *GLOBEC Northeast Pacific California Current Cruise Report, R/V Thomas G. Thompson (T0205) Alternative Cruise ID: Mesoscale Survey TN147 Chief Scientist: Cruise Objectives*. College of Oceanic and Atmospheric Sciences Oregon State University Corvallis, OR.

Culberson, C. H. (1991). *WHO Operations and Methods: Dissolved Oxygen. Newark*. College of Marine Studies. University of Delaware. Newark, U.S.A.

Culberson, C. H., and Huang, S. (1987). An automated amperometric oxygen titration. *Deep Sea Res.* 34, 875–880. doi: 10.1016/0198-0149(87)90042-2

Cutler, D. R., Edwards, T. C., Beard, K. H., Cutler, A., Hess, K. T., Gibson, J., et al. (2007). Random forests for classification in ecology. *Ecology* 88, 2783–2792. doi: 10.1890/07-0539.1

Dickson, A. G., and Millero, F. J. (1987). A comparison of the equilibrium constants for the dissociation of carbonic acid in seawater media. *Deep Sea Research Part A, Oceanographic Research Papers* 34 (10), 1733–1743. doi: 10.1016/0198-0149(87)90021-5

Dickson, A. G., Wesolowski, D. J., Palmer, D. A., and Mesmer, R. E. (1990). Dissociation constant of bisulfate ion in aqueous sodium chloride solutions to 250° C. *J. Physical Chem.* 94 (20), 7978–7985. doi: 0.1021/J100383A042/ASSET/J100383A042.FP.PNG_V03

Dickson, A. G., Sabine, C. L., and Christian, J. R. (2007). "Guide to best practices for ocean CO2 measurements," in *PICES Special Publication, Guide to Best Practices for Ocean CO2 measurements* (North Pacific Marine Science Organization Sidney, British Columbia, Canada: PICES Special Publication).

DiMarco, S. F., Strauss, J., May, N., Mullins-Perry, R. L., Grossman, E. L., and Shormann, D. (2012). Texas coastal hypoxia linked to Brazos river discharge as revealed by oxygen isotopes. *Aquat Geochem* 18, 159–181. doi: 10.1007/S10498-011-9156-X/METRICS

Domingos, P. (2012). A few useful things to know about machine learning. *Commun. ACM*. 55 (10), 78–87. doi: 10.1145/2347736.2347755

Duarte, C. M., Hendriks, I. E., Moore, T. S., Olsen, Y. S., Steckbauer, A., Ramajo, L., et al. (2013). Is ocean acidification an open-ocean syndrome? Understanding anthropogenic impacts on seawater pH. *Estuaries Coasts* 36, 221–236. doi: 10.1007/S12237-013-9594-3/TABLES/1

Erez, J., Reynaud, S., Silverman, J., Schneider, K., and Allemand, D. (2011). "Coral calcification under ocean acidification and global change," in *Coral Reefs: An Ecosystem in Transition* (Springer Dordrecht, Netherlands: Springer Netherlands), 151–176. doi: 10.1007/978-94-007-0114-4_10

Evans, W., Mathis, J. T., Winsor, P., Statscewich, H., and Whitledge, T. E. (2013). A regression modeling approach for studying carbonate system variability in the northern Gulf of Alaska. *J. Geophys Res. Oceans* 118, 476–489. doi: 10.1029/2012JC008246

Eyre, B. D., Andersson, A. J., and Cyronak, T. (2014). Benthic coral reef calcium carbonate dissolution in an acidifying ocean. *Nat. Climate Change* 11, 969–976. doi: 10.1038/nclimate2380

Feely, R. A., Sabine, C. L., Hernandez-Ayon, J. M., Ianson, D., and Hales, B. (2008). Evidence for upwelling of corrosive "acidified" water onto the continental shelf. *Science (1979)* 320, 1490–1492. doi: 10.1126/science.1155676

Gomez, F. A., Wanninkhof, R., Barbero, L., and Lee, S. K. (2021). Increasing river alkalinity slows ocean acidification in the northern Gulf of Mexico. *Geophys Res. Lett.* 48, e2021GL096521. doi: 10.1029/2021GL096521

Gran, G. (1952). Determination of the equivalence point in potentiometric titrations. *Part II Analyst* 77, 661–671. doi: 10.1039/an9527700661

Hales, B., Takahashi, T., and Bandstra, L. (2005). Atmospheric CO2 uptake by a coastal upwelling system. *Global Biogeochem Cycles* 19, 1–11. doi: 10.1029/2004GB002295

Hare, A. A., Evans, W., Dosser, H. V., Jackson, J. M., Alin, S. R., Hannah, C., et al. (2025). Regression-based characterization of the marine carbonate system across shelf and nearshore waters of Queen Charlotte Sound. *Mar. Chem.* 270, 104511. doi: 10.1016/J.MARCHEM.2025.104511

Hoegh-Guldberg, O., Mumby, P. J., Hooten, A. J., Steneck, R. S., Greenfield, P., Gomez, E., et al. (2007). Coral reefs under rapid climate change and ocean acidification. *Science* 318, 1737–1742. doi: 10.1126/SCIENCE.1152509/SUPPL_FILE/HOEGH-GULDBERG.SOM.PDF

Hu, X., Li, Q., Huang, W. J., Chen, B., Cai, W. J., Rabalais, N. N., et al. (2017). Effects of eutrophication and benthic respiration on water column carbonate chemistry in a traditional hypoxic zone in the Northern Gulf of Mexico. *Mar. Chem.* 194, 33–42. doi: 10.1016/J.MARCHEM.2017.04.004

Hu, X., Nuttall, M. F., Wang, H., Yao, H., Staryk, C. J., McCutcheon, M. R., et al. (2018). Seasonal variability of carbonate chemistry and decadal changes in waters of a marine sanctuary in the Northwestern Gulf of Mexico. *Mar. Chem.* 205, 16–28. doi: 10.1016/j.marchem.2018.07.006

Huang, W. J., Cai, W. J., Wang, Y., Hu, X., Chen, B., Lohrenz, S. E., et al. (2015). The response of inorganic carbon distributions and dynamics to upwelling-favorable winds on the northern Gulf of Mexico during summer. *Cont Shelf Res.* 111, 211–222. doi: 10.1016/J.CSR.2015.08.020

Johnson, K. M., King, A. E., and Sieburth, J. M. N. (1985). Coulometric TCO2 analyses for marine studies; an introduction. *Mar. Chem.* 16, 61–82. doi: 10.1016/0304-4203(85)90028-3

Juranek, L. W., Feely, R. A., Gilbert, D., Freeland, H., and Miller, L. A. (2011). Real-time estimation of pH and aragonite saturation state from Argo profiling floats: Prospects for an autonomous carbon observing strategy. *Geophys Res. Lett.* 38. doi: 10.1029/2011GL048580

Juranek, L. W., Feely, R. A., Peterson, W. T., Alin, S. R., Hales, B., Lee, K., et al. (2009). A novel method for determination of aragonite saturation state on the continental shelf of central Oregon using multi-parameter relationships with hydrographic data. *Geophys Res. Lett.* 36, 1–6. doi: 10.1029/2009GL040778

Kim, T. W., Lee, K., Feely, R. A., Sabine, C. L., Chen, C. T. A., Jeong, H. J., et al. (2010). Prediction of Sea of Japan (East Sea) acidification over the past 40 years using a multiparameter regression model. *Global Biogeochem Cycles* 24, 1–14. doi: 10.1029/2009GB003637

Kutner, M. H., Nachtsheim, C., Neter, J., and Li, W. (2005). *Applied linear statistical models* (McGraw-Hill/Irwin New York, NY, USA: McGraw-Hill Irwin).

Li, X., Xu, Y. Y., Kirchman, D. L., and Cai, W. J. (2022). Carbonate parameter estimation and its application in revealing temporal and spatial variation in the south and Mid-Atlantic Bight, USA. *J. Geophys Res. Oceans* 127, e2022JC018811. doi: 10.1029/2022JC018811

Lima, I. D., Wang, Z. A., Cameron, L. P., Grabowski, J. H., and Rheuban, J. E. (2023). Predicting carbonate chemistry on the northwest Atlantic shelf using neural networks. *J. Geophys Res. Biogeosci* 128. doi: 10.1029/2023JG007536

Liu, X., Patsavas, M. C., and Byrne, R. H. (2011). Purification and characterization of meta-cresol purple for spectrophotometric seawater ph measurements. *Environ. Sci. Technol.* 45, 4862–4868. doi: 10.1021/es200665d

Massey, F. J. (1951). The Kolmogorov-Smirnov test for goodness of fit. *J. Am. Stat. Assoc.* 46, 68–78. doi: 10.1080/01621459.1951.10500769

McGarry, K., Siedlecki, S. A., Salisbury, J., and Alin, S. R. (2021). Multiple linear regression models for reconstructing and exploring processes controlling the carbonate system of the northeast US from basic hydrographic data. *J. Geophys Res. Oceans* 126, 1–19. doi: 10.1029/2020JC016480

Mehrbach, C., Culberson, C. H., Hawley, J. E., and Pytkowicx, R. M. (1973). Measurement of the apparent dissociation constants of carbonic acid in seawater at atmospheric pressure. *Limnology and Oceanography* 18 (6), 897–907.

Montes, E., Muller-Karger, F. E., Cianca, A., Lomas, M. W., Lorenzoni, L., and Habtes, S. (2016). Decadal variability in the oxygen inventory of North Atlantic subtropical underwater captured by sustained, long-term oceanographic time series observations. *Global Biogeochem Cycles* 30, 460–478. doi: 10.1002/2015GB005183

Morey, S. L., Martin, P. J., O'Brien, J. J., Wallcraft, A. A., Zavala-Hidalgo, J., Morey, C., et al. (2003). Export pathways for river discharged fresh water in the northern Gulf of Mexico. *J. Geophys Res. Oceans* 108, 3303. doi: 10.1029/2002JC001674

Muller-Karger, F. E., Smith, J. P., Werner, S., Chen, R., Roffer, M., Liu, Y., et al. (2015). Natural variability of surface oceanographic conditions in the offshore Gulf of Mexico. *Prog. Oceanogr* 134, 54–76. doi: 10.1016/j.pocean.2014.12.007

Mucci, A.. (1983). The solubility of calcite and aragonite in seawater at various salinities, temperatures, and one atmosphere total pressure. *American Journal of Science* 283, 780–799.

Orr, J. C., Epitalon, J. M., Dickson, A. G., and Gattuso, J. P. (2018). Routine uncertainty propagation for the marine carbon dioxide system. *Mar. Chem.* 207, 84–107. doi: 10.1016/J.MARCHEM.2018.10.006

Osborne, E., Xu, Y. Y., Soden, M., McWhorter, J., Barbero, L., and Wanninkhof, R. (2024). A neural network algorithm for quantifying seawater pH using Biogeochemical-Argo floats in the open Gulf of Mexico. *Front. Mar. Sci.* 11. doi: 10.3389/FMARS.2024.1468909/BIBTEX

Patsavas, M. C., Byrne, R. H., Wanninkhof, R., Feely, R. A., and Cai, W. J. (2015). Internal consistency of marine carbonate system measurements and assessments of aragonite saturation state: Insights from two U.S. coastal cruises. *Mar. Chem.* 176, 9–20. doi: 10.1016/J.MARCHEM.2015.06.022

Pedregosa, F., Duchesnay, E., Varoquaux, G., Gramfort, A., Michel, V., Thirion, B., et al. (2011). Scikit-learn. *Journal of Machine Learning Research* 12, 2825–2830.

Peng, T.-H., and Langdon, C. (2007). *Gulf of Mexico and East Coast Carbon Cruise (GOMECC) Chief Scientists: Tsung-Hung Peng and Chris Langdon NOAA Atlantic Oceanographic and Meteorological Laboratory Cruise Report*. College of Marine Studies. University of Delaware. Newark, U.S.A.

Probst, P., Wright, M. N., and Boulesteix, A. L. (2019). Hyperparameters and tuning strategies for random forest. *Wiley Interdiscip Rev. Data Min Knowl. Discov.* 9, e1301. doi: 10.1002/WIDM.1301

Quinn, G. P., and Keough, M. J. (2002). *Experimental Design and Data Analysis for Biologists* (Cambridge, England: Cambridge University Press).

Roemmich, D., Alford, M. H., Claustre, H., Johnson, K. S., King, B., Moum, J., et al. (2019). On the future of Argo: A global, full-depth, multi-disciplinary array. *Front. Mar. Sci.* 6. doi: 10.3389/FMARS.2019.00439/BIBTEX

Saba, G. K., Wright-Fairbanks, E., Chen, B., Cai, W. J., Barnard, A. H., Jones, C. P., et al. (2019). The development and validation of a profiling glider deep ISFET-based pH sensor for high resolution observations of coastal and ocean acidification. *Front. Mar. Sci.* 6. doi: 10.3389/FMARS.2019.00664/BIBTEX

Sharp, J. D., Pierrot, D., Orr, J. C., Epitalon, J.-M., Humphreys, M. P., Wallace, D. W. R., et al. (2023). *CO2SYSv3 for MATLAB (Version v3.2.1)*. European Organization for Nuclear Research, Genève Switzerland.

Takeshita, Y., Warren, J. K., Liu, X., Spaulding, R. S., Byrne, R. H., Carter, B. R., et al. (2021). Consistency and stability of purified meta-cresol purple for spectrophotometric pH measurements in seawater. *Mar. Chem.* 236, 104018. doi: 10.1016/J.MARCHEM.2021.104018

Testor, P., DeYoung, B., Rudnick, D. L., Glenn, S., Hayes, D., Lee, C., et al. (2019). OceanGliders: A component of the integrated GOOS. *Front. Mar. Sci.* 6. doi: 10.3389/FMARS.2019.00422/BIBTEX

Thessen, A. E. (2016). Adoption of machine learning techniques in ecology and earth science. *One Ecosystem* 1. doi: 10.3897/oneeco.1.e8621

Turk, D., Wang, H., Hu, X., Gledhill, D. K., Wang, Z. A., Jiang, L., et al. (2019). Time of emergence of surface ocean carbon dioxide trends in the North American coastal margins in support of ocean acidification observing system design. *Front. Mar. Sci.* 6. doi: 10.3389/fmars.2019.00091

Uppström, L. R.. (1974). The boron/chlorinity ratio of deep-sea water from the Pacific Ocean. *DSRA* 21 (2), 161–162. doi: 10.1016/0011-7471(74)90074-6

van Heuven, S., Pierrot, D., Rae, J. W. B., Lewis, E., and Wallace, D. W. R. (2011). *MATLAB Program Developed for CO2 System Calculations*. Carbon Dioxide Information Analysis Center, Oak Ridge National Laboratory, U.S. DoE, Oak Ridge, TN.

Vujovic, Z. (2021). Classification model evaluation metrics. *Int. J. Advanced Comput. Sci. Appl.* doi: 10.14569/IJACSA.2021.0120670

Wang, Z. A., Wanninkhof, R., Cai, W. J., Byrne, R. H., Hu, X., Peng, T. H., et al. (2013). The marine inorganic carbon system along the Gulf of Mexico and Atlantic coasts of the United States: Insights from a transregional coastal carbon study. *Limnol Oceanogr* 58, 325–342. doi: 10.4319/lo.2013.58.1.0325

Wanninkhof, R., Wood, M., and Barbero, L. (2012). *Gulf of Mexico and East Coast Carbon Cruise #2 (GOMECC-2)* (NOAA Atlantic Oceanographic and Meteorological Laboratory).

Winkler, L. W. (1888). The determination of oxygen dissolved in water. *Rep. German Chem. Soc.* 21, 2843–2855. doi: 10.1002/cber.188802102122

Zeebe, R. E., Ridgwell, A., Zeebe, R. E., and Ridgwell, A. (2011). Past changes in ocean carbonate chemistry. *Ocean Acidification* 6, 21–40. doi: 10.1093/oso/9780199591091.003.0007

Zeebe, R. E., and Wolf-Gladrow, D. (2001). *CO2 in Seawater: Equilibrium, Kinetics, Isotopes. 1st Edition* Vol. 65 (Amsterdam, Netherlands: Elsevier Science). Available online at: https://www.elsevier.com/books/co2-in-seawater-equilibrium-kinetics-isotopes/zeebe/978-0-444-50946-8.

frontiers | Frontiers in Marine Science

TYPE Original Research
PUBLISHED 01 October 2025
DOI 10.3389/fmars.2025.1623344

OPEN ACCESS

EDITED BY
Jose Martin Hernandez-Ayon,
Autonomous University of Baja California, Mexico

REVIEWED BY
Solomon Dan,
Beibu Gulf University, China
Nicolas Metzl,
Centre National de la Recherche Scientifique (CNRS), France

*CORRESPONDENCE
Cíntia Albuquerque
albuquerque.cintia@ce.uerj.br

RECEIVED 05 May 2025
ACCEPTED 29 August 2025
PUBLISHED 01 October 2025

CITATION
Albuquerque C, Miguel G, Lencina-Avila JM, Pinho L, Marotta H, Fernandes AM, Passos EN, Amora-Nogueira L, Campos E and Cotrim da Cunha L (2025) Linking surface pCO_2 variability to physical processes along a continental shelf–ocean transect in the southwestern Atlantic Ocean during austral autumn and winter. *Front. Mar. Sci.* 12:1623344. doi: 10.3389/fmars.2025.1623344

Linking surface pCO_2 variability to physical processes along a continental shelf–ocean transect in the southwestern Atlantic Ocean during austral autumn and winter

Cíntia Albuquerque[1,2,3]*, Gizyelle Miguel[1], Jannine M. Lencina-Avila[1,2,3], Luana Pinho[2,3], Humberto Marotta[3,4,5], Alexandre Macedo Fernandes[1,6], Elisa Nóbrega Passos[1,6], Leonardo Amora-Nogueira[4,5], Edmo Campos[7] and Leticia Cotrim da Cunha[1,2,3,8]

[1]Programa de Pós-Graduação em Oceanografia, Universidade do Estado do Rio de Janeiro – UERJ, Rio de Janeiro, Brazil, [2]Laboratório de Oceanografia Química LABOQUI, Faculdade de Oceanografia, UERJ, Rio de Janeiro, Brazil, [3]Brazilian Ocean Acidification Network – BrOA, Rio Grande, Brazil, [4]Ecosystems and Global Change Laboratory (LEMG-UFF), Biomass and Water Management Research Center (NAB-UFF), Graduate Program in Geosciences (Environmental Geochemistry), Universidade Federal Fluminense – UFF, Niterói, Brazil, [5]Physical Geography Laboratory (LAGEF-UFF), Department of Geography, Graduate Program in Geography, Fluminense Federal University (UFF), Niterói, Brazil, [6]Laboratório de Oceanografia Física, Faculdade de Oceanografia Universidade do Estado do Rio de Janeiro (UERJ), Rio de Janeiro, Brazil, [7]Instituto Oceanográfico, Universidade de São Paulo, Brazil, [8]Brazilian Research Network on Global Climate Change (Rede CLIMA), INPE, São José dos Campos, Brazil

The southwestern South Atlantic Ocean is an important global sink of atmospheric carbon dioxide (CO_2), driven by increased primary productivity in a nearby region where oligotrophic warm currents converge with nutrient-rich cold waters. However, uncertainties remain regarding CO_2 dynamics and the role of physical processes in CO_2 uptake across this region. Here, we assess variations in surface partial pressure of CO_2 (pCO_2) and air–sea CO_2 fluxes in the Southwest Atlantic, along a transect from the continental shelf to the open ocean at 34.5°S during austral autumn 2018 and winter 2019. High-resolution spatial measurements of the temperature, salinity, and molar fraction of surface CO_2 were conducted. In autumn 2018, the shelf region acted as a source of CO_2 to the atmosphere (median of 3.2 mmol CO_2 m^{-2} d^{-1}), which was partially offset by a sink (median of −2.5 mmol CO_2 m^{-2} d^{-1}) in the open ocean. In contrast, the entire transect in winter 2019 presented median CO_2 emissions of ~1.5 mmol CO_2 m^{-2} d^{-1}, which differs from climatological estimates. The spatial and seasonal variations in surface ocean pCO_2 were linked to variable hydrodynamic processes, including water masses and mesoscale structures. Our findings reveal that, in one of the most productive oceanic waters worldwide, pCO_2 may be influenced by distinct continental inputs (e.g., rivers, runoff, and groundwater discharge) and water masses (e.g., Tropical Water, Plata Plume Water and Subtropical Shelf Water). Therefore, the local hydrodynamic processes can modulate high spatial and seasonal variability in CO_2 exchange at the ocean–

atmosphere interface, with potential implications for regional and global carbon budgets. General results, such as climatological, cannot fully capture the influence of regional upwelling and continental water input, which highlights the importance of high-resolution regional observations.

KEYWORDS

air–sea CO2 fluxes, SAMOC, seasonality, partial pressure of CO2, subtropical South Atlantic Ocean, shelf region, open ocean

1 Introduction

Globally, the ocean is a net sink of carbon dioxide (CO_2) in the atmosphere with a global average CO_2 flux of ~2.9 ± 0.4 Pg C yr^{-1} from 2014 to 2023 (Friedlingstein et al., 2025). The coastal ocean accounts for a net CO_2 sink with estimates ranging from –0.44 Pg C yr^{-1} to –0.72 Pg C yr^{-1} (Resplandy et al., 2024), but it presents a more spatially heterogeneous pattern, acting as either a source or sink associated with local processes, such as river plumes (Parc et al., 2024) and coastal upwelling (e.g., Lefèvre et al., 2023; Siddiqui et al., 2023).

The Atlantic Ocean, which includes both the continental shelf and open-ocean regions, accounts for ~25% of the global oceanic CO_2 sink, corresponding to –393 ± 29 Tg C yr^{-1} (Roobaert et al., 2019). However, these estimates may be biased due to the lower frequency of high resolution spatial measurements in the South Atlantic Ocean than in the North portion (Bakker et al., 2016, 2024; Liu et al., 2025). The CO_2 sink in the Southwest Atlantic Ocean (SWAO) is particularly intense, with estimates of –3.7 mmol m^{-2} d^{-1} south of 40°S (Bianchi et al., 2009). More recent climatologies for the broader SWAO report fluxes of ~–3 to –5 mmol m^{-2} d^{-1} for April and June, respectively near 35°S/54–44°W (Fay et al., 2024), where the circulation patterns influence sea surface temperature (SST) variability and subsequent physical processes, e.g., upwelling (Takahashi et al., 2009; Ito et al., 2016), fronts and eddies (Pezzi et al., 2005; Ito et al., 2016; Orselli et al., 2019).

In this context, the South Atlantic Meridional Overturning Circulation (SAMOC) is an important feature of the SWAO and redistributes mass, heat, salt, oxygen, nutrients and carbon across the ocean (Kersalé et al., 2020). It presents a dynamic and complex water mass structure, characterized by intense boundary currents and mesoscale eddies (Manta et al., 2021). In the SWAO, around 34.5°S, there is still limited data coverage (Meinen et al., 2018). Thus, in 2009 the SAMOC array was initially deployed at 34.5°S to monitor the meridional flow of the western boundary currents (Meinen et al., 2013, 2017). Additionally, the Brazil– Malvinas Confluence (BMC), around 38°S, introduces further variability by facilitating vertical mixing and supporting high biological productivity (Chelton et al., 1990; Moura-Falcão et al., 2024).

The SAMOC system directly influences the spatial and temporal variability of the partial pressure of CO_2 (pCO_2) at the sea surface (Boot et al., 2022), as it regulates the transport and distribution of different water masses, each with distinct physical –chemical properties. Fluxes of CO_2 (FCO_2) variability is known to be controlled primarily by pCO_2; thus, understanding the drivers of pCO_2 is crucial for determining the ocean carbon sink (e.g., Landschützer et al., 2016). In the SWAO shelf break and continental slope regions, the upper layer of the water column is dominated by two main water masses: the Tropical Water (TW) and South Atlantic Central Water (SACW) (Campos et al., 1995; Castro and Miranda, 1998; Silveira et al., 2000). The surface layer (0–100 m) of the tropical southwestern South Atlantic is dominated by the TW, a relatively warm and salty water mass with SST greater than 18.5°C and sea surface salinity (SSS) values greater than 36. It is characterized by being nutrient poor (Campos et al., 1995; Möller et al., 2008) and typically has high pCO_2 values due to lower CO_2 solubility and limited biological drawdown. The SACW occupies the central layer of the South Atlantic Gyre and upwells to the surface at ~23°S 42°W, exhibiting cooler and more saline characteristics than the surrounding water, with average SSS and SST values of ~35°C and 16–18°C, respectively. In contrast, this water mass is nutrient-rich (De Souza et al., 2018; Azar et al., 2021), increasing the pCO_2 values. Two other important water masses are the Plata Plume Water (PPW) and Subtropical Shelf Water (STSW). Surface waters with a salinity of ~32.5 indicate the presence of PPW, which originates from the Plata River and reaches southern Brazil via wind-driven transport. The PPW, being freshwater diluted and nutrient rich, tends to promote high biological activity and CO_2 uptake, reducing surface pCO_2 (Lencina-Avila et al., 2016). In turn, the STSW consists of modified warm TW and SACW diluted by the PPW, which is characterized by SSTs less than 18°C and SSS values between 33 and 36 (Möller et al., 2008).

Despite global predictions of changes in ocean biogeochemistry under climate change (Sabine et al., 2004; Gallego et al., 2020; Matthews et al., 2020; Pérez et al., 2024), regional responses in the SWAO remain poorly understood. There is still a gap in the information needed to assess the regional impacts of climate change along the SWAO areas. Here, we present a unique high resolution dataset of underway surface pCO_2 observations obtained during two oceanographic cruises in the austral autumn of 2018 and winter of 2019 — seasons that remain underrepresented in the literature. The temporal resolution and spatial coverage across the

SWAO shelf and slope provide unprecedented detail on short-term variability in surface CO_2 dynamics during cooler months, which are critical for understanding carbon fluxes driven by physical processes such as deep-water ventilation and mesoscale activity. By integrating continuous pCO_2, SST, and SSS data with hydrographic and regional circulation patterns, this study extends the findings of Moura-Falcão et al. (2024) by offering new insight with high–resolution into the seasonal drivers of surface ocean pCO_2 variability in a region of high biogeochemical and dynamic complexity. Furthermore, we discussed the regional hydrographic conditions, the air–sea CO_2 fluxes, the mesoscale dynamics and their implications.

2 Materials and methods

2.1 Sampling strategy

The study area comprises the SWAO, over a longitudinal transect along 34.5°S latitude, from the coast of Brazil to 44.5° W (Figure 1). Data were acquired during two oceanographic campaigns onboard RV Alpha Crucis (Universidade de São Paulo, Brazil) between 23–30 April 2018 (austral autumn) and 17 June–2 July 2019 (austral winter) as part of the 'South Atlantic Meridional Overturning Circulation Basin-wide Array' project (Fundação de Amparo à Pesquisa do Estado de São Paulo - FAPESP; FAPESP; Chidichimo et al., 2021).

2.2 Surface seawater sampling

The surface hydrographic properties were measured using a Sea-Bird Electronics (SBE) 9*plus* conductivity–temperature–depth (CTD) profiler equipped with sensors for temperature, conductivity and pH during campaigns aboard the RV Alpha Crucis.

In the study area, SSS and SST data from the ship's thermosalinograph (SBE 45 MicroTSG) were integrated into the continuous pumping system to determine the high-resolution spatial distribution of seawater pCO_2 (pCO_{2SW}) (Section 2.3). The SST and SSS errors of the CTD are ±0.00014 °C for SST and ± 0.002 for SSS. The pCO_2 error is ± 2 µatm, according to Fernandes et al. (2025). We have named "continental shelf" all sampling stations where local bottom depth was equal or shallower than 200 m (region corresponding to stations 1 to 7) and the other sampling stations (8 to 23) are referred to as "open ocean".

2.3 CO_2 partial pressure calculations

For the acquisition of the ongoing molar fraction of CO_2, a water–air equilibrator coupled to an infrared gas analyzer (IRGA)-type CO_2 detector (EGM-4 Environmental Gas Monitor for CO_2, PP Systems) was used along the entire trajectory of the ship. After data acquisition, we applied a treatment routine to correct for atmospheric pressure and water vapor partial pressure according to Weiss and Price (1980). *In situ* variations in temperature and internal equilibrator temperature were corrected following the methods of Takahashi et al. (2009). The initial results generated by the IRGA readings are in xCO_2, which refers to the number of CO_2 molecules in each number of air molecules. This estimate is generally used because a gas molecule in dry air tends not to change when there are variations in temperature and pressure.

There is also a necessary adjustment in relation to the *in-situ* temperature, as suggested by Takahashi et al. (1993). The value of 0.0423°C in Equation 1 is considered a constant and was determined by Takahashi et al. (2009).

$$(pCO_2)_{corrected} = (pCO_2)_{eq} xEXP[0.0423x(T_{insitu} - T_{eq}) \quad (1)$$

where $T_{in\ situ}$= *in situ* surface temperature; T_{eq} = seawater temperature in the balancer; $(pCO_2)_{eq}$ = pCO_2 in the balancer.

To remove the effect of the SST on the sampled pCO_2 data, the data were normalized to the average SST during the sampling periods (autumn and winter). The average observed SST value for 2018 was 22.54°C (autumn), and in 2019, it was 17.88 °C (winter). The calculations follow the precepts indicated by Takahashi et al. (2002) and Takahashi et al. (2009) according to Equation 2:

$$NpCO_2 = (pCO_2)xEXP[0.0423(SST_M - SST) - 4.35x10^{-5}((SST_M)^2 - (SST)^2)] \quad (2)$$

where SST_M = average temperature (°C) observed at the sea surface.

To calculate the CO_2 diffusion rate at the ocean–atmosphere interface, FCO_2 were calculated (Equation 3):

$$FCO_2 = k\ x\ k_0 x\ (\Delta pCO_2)_{oc-atm} \quad (3)$$

where k = the gas transfer speed as a function of the wind speed; k_o = the solubility of CO_2 in sea water (according to Weiss, 1974); and $(\Delta pCO_2)_{oc\text{-}atm}$ = the difference between ocean pCO_2 and atmosphere pCO_2. The pCO_2 in atmospheric equilibrium was assumed to be 405.295 µatm in autumn 2018 and 408.186 µatm in winter 2019. These values correspond to the monthly averages of the estimated atmospheric concentration in the mid-latitude range of the sampling, with uncertainty values of 0.178 µatm in 2018 and 0.075 µatm in 2019. These estimates were taken from the database of the U.S. agency National Oceanic and Atmospheric Administration (NOAA) for Greenhouse Gas Reference - Atmospheric Carbon Dioxide. Wind speed data were obtained continuously onboard from the Alpha Crucis meteorological station.

The difference in pCO_2 (ΔpCO_2) between the two compartments determines the direction of net transfer between the ocean and the atmosphere. The ratio between the viscosity and molecular diffusion rate is represented by k (Weiss, 1974). In this study, the calculated coefficients of k were compared between 3 works: Wanninkhof (1992); Nightingale et al. (2000); Wanninkhof (2014), which are represented as W92, N00 and W14, respectively. The equations used for k calculations are summarized in Supplementary Table S1. Although W14 is a central choice, we also include other parameterizations (such as N00 and W92) (Supplementary Tables S2, S3) to provide different perspectives/

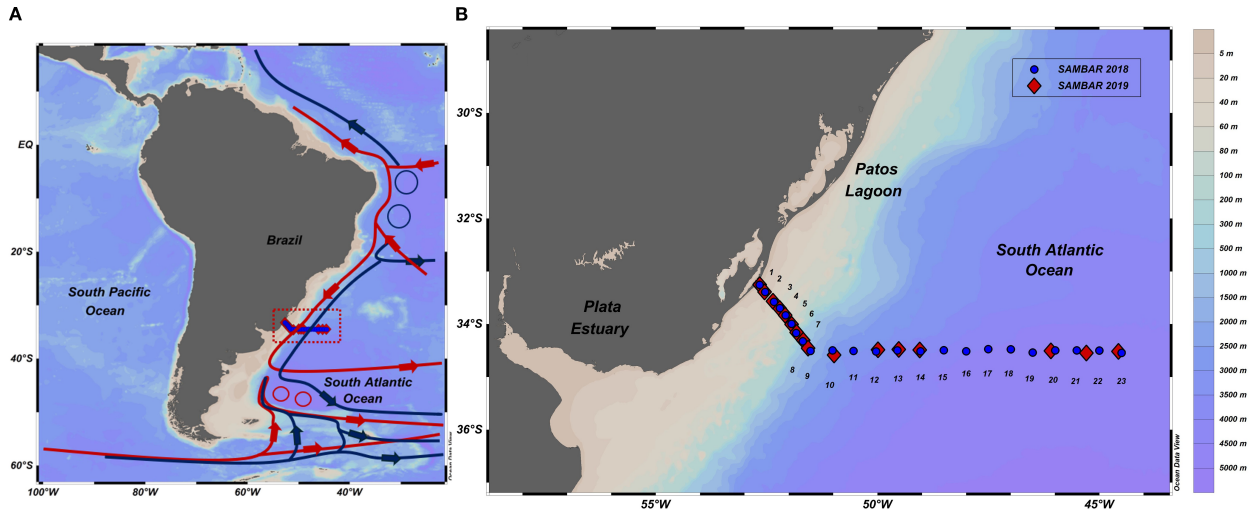

FIGURE 1
(A) Idealized schematic of the overturning circulation in the Southwestern Atlantic Ocean with the location of the study area marked with a red-dotted rectangle. The lines, circles and arrows represent the pathways of the surface (red) and deep waters (blue) based on Chidichimo et al. (2023). **(B)** Map of the CTD sampling stations along the southwestern South Atlantic Ocean margin off the Brazilian coast. The sampling stations from the autumn of 2018 are represented by blue dots, and the sampling stations from the winter of 2019 are represented by red diamonds.

scenarios of the flux given the complexity of the region and to compare with other studies that might have used different parametrizations. The wind speed data fit these k and they have already been used in previous studies and have shown good representation for the region. The figures was performed in Ocean Data View software (ODV - Schlitzer, 2021).

2.4 Statistical analysis

Normality was not achieved, as indicated by the D'Agostino and Pearson (1973), even after data transformation. Therefore, non-parametric statistical methods were applied. Seasonal differences between autumn and winter within each region (continental shelf and open ocean) were assessed using multiple Mann–Whitney U tests ($p < 0.05$), resulting in six pairwise comparisons (Supplementary Table S4; Supplementary Figure S1). To evaluate differences across both seasons and regions (four groups), the Kruskal–Wallis test was applied, followed by the two-stage linear step-up procedure of Benjamini, Krieger, and Yekutieli to control the false discovery rate (FDR), totaling 18 comparisons (Supplementary Table S5; Supplementary Figure S2). In addition, Spearman's rank correlation analysis ($p < 0.05$) was conducted to examine the relationships among pCO_2, SST, and SSS (Supplementary Table S6; Supplementary Figure S3).

2.5 Oceanographic modelling data

Oceanographic modelling data of surface anomalies (SSH) and current velocity derived from satellite images were used to understand and compare ocean conditions and identify mesoscale structures between the autumn (2018) and winter (2019) periods in the southwestern Atlantic Ocean.

To investigate ocean dynamics and physical properties during the transect periods, we utilized global ocean physics reanalysis data from the Copernicus Marine Environment Monitoring Service (CMEMS) (https://resources.marine.copernicus.eu/). The dataset is derived from version v3.6_STABLE of the Nucleus for European Modelling of the Ocean (NEMO) model, which features a 1/12›···» horizontal resolution (~9 km) and 50 vertical levels. Although only data from the SAMBAR transect periods were analyzed, reanalysis data are available from 1993 to 2019. The model's initial conditions were obtained from the European Centre for Medium-Range Weather Forecasts (ECMWF) ERA-Interim and ERA5 reanalysis datasets, which incorporate data assimilation from altimetry, satellite-derived sea surface temperature, sea ice concentration, and *in situ* vertical profiles of temperature and salinity. In this study, we specifically used daily mean fields of sea surface temperature, sea surface height, and velocity. The selected model domain extends from 44°W to 59°W longitude and 30°S to 37°S latitude.

The CMEMS reanalysis dataset was selected due to its robustness, global coverage (e.g., Wang et al., 2023), and widespread use within the oceanographic research community. As described previously, the product is based on the NEMO model (v3.6_STABLE), which provides daily mean physical fields with sufficient resolution to analyze mesoscale ocean dynamics in the southwestern Atlantic Ocean. Notably, no interpolation or spatial resampling of the model output was performed. In addition, no direct validation was conducted compare the *in-situ* measurements and model data, as the primary objective of this study was not to assess model performance but rather to utilize the modeled fields as contextual support for interpreting the oceanographic patterns

observed during the SAMBAR transect campaigns. Nevertheless, we recognize the limitations of the reanalysis product, such as the smoothing of fine-scale variability and the inability to resolve submesoscale processes, which were considered during the analysis and discussion of the results.

3 Results

3.1 Spatial and temporal distributions of physical–chemical parameters

Warmer (>21°C) waters during autumn 2018 dominated continental and open ocean areas up to approximately 47°W, and we found colder surface waters in the open ocean area (stations 18 and 21) (Figure 2A). On the other hand, during the winter of 2019, the SST in the open ocean area were patchy, with colder water intrusions. In addition, prominent cooler (<19°C) and fresher (<30) (Figure 3B) water extended over the continental shelf, identified as the PPW (Figure 3B). The CMEMS data clearly revealed a difference in the distribution of SSTs between autumn 2018 and winter 2019 across the study region (Figure 2). Similarly, the SST and SSS data from the thermosalinograph (Supplementary Tables S2, S3) showed significant spatial and seasonal differences between the continental shelf and open ocean (Mann–Whitney, $p < 0.05$). Along these transects, the SST and SSS reached higher median values in autumn 2018 (22.5°C and 36.2) than in winter 2019 (20.5°C and 35.5) (Supplementary Tables S2, S3).

For the SST and SSS, the surface seawater pCO_2 significantly differed between the autumn of 2018 and winter of 2019 (Mann–

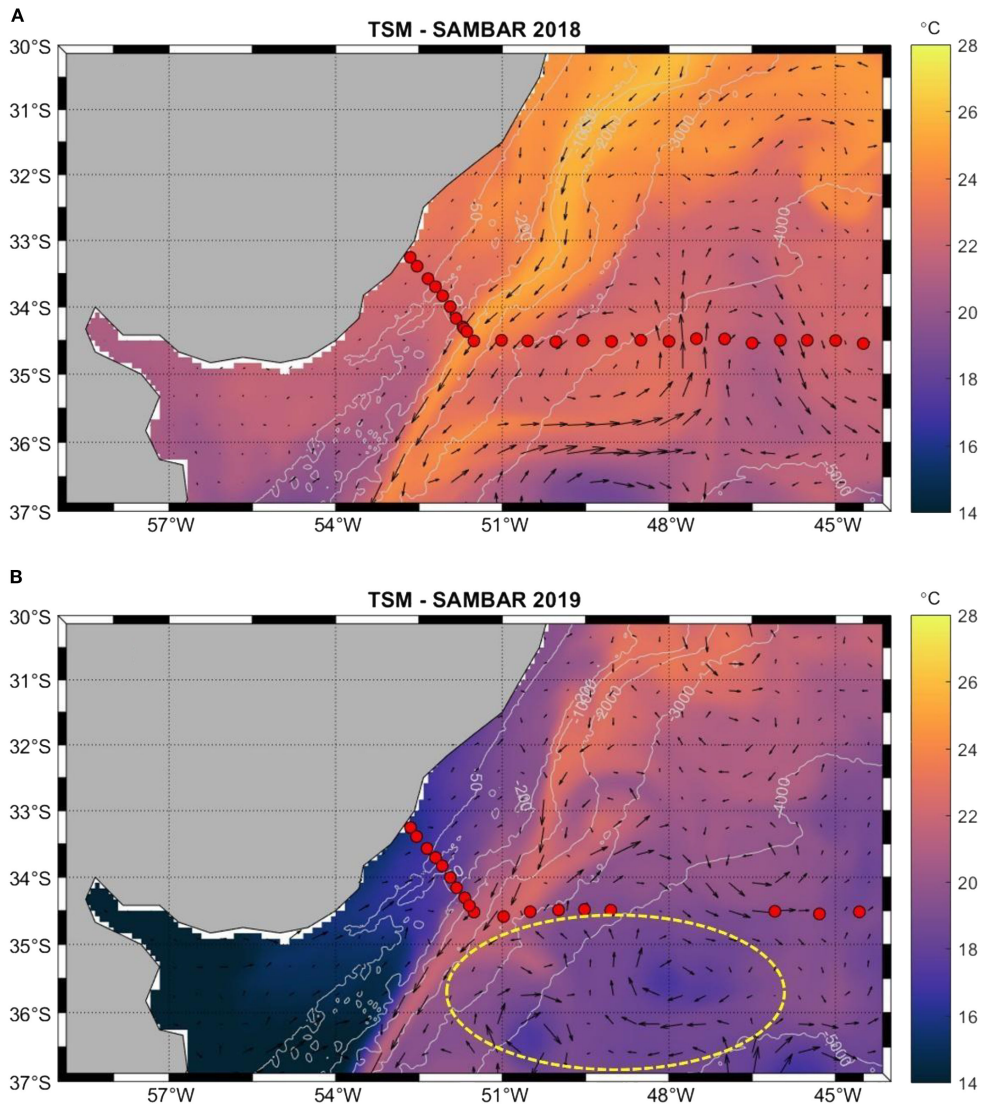

FIGURE 2
Sea surface temperature (SST; °C) in the southwestern Atlantic Ocean during the **(A)** 2018 and **(B)** 2019 campaigns, derived from the CMEMS reanalysis. The SST data have a 9 km resolution and represent an 8-day average (April 23–May 1, 2018, and June 18–26, 2019). The grey contours indicate isobaths, whereas the red dots represent sampling stations from both campaigns over the continental shelf and open ocean. The arrows indicate the currents. The yellow circle indicates the presence of eddies.

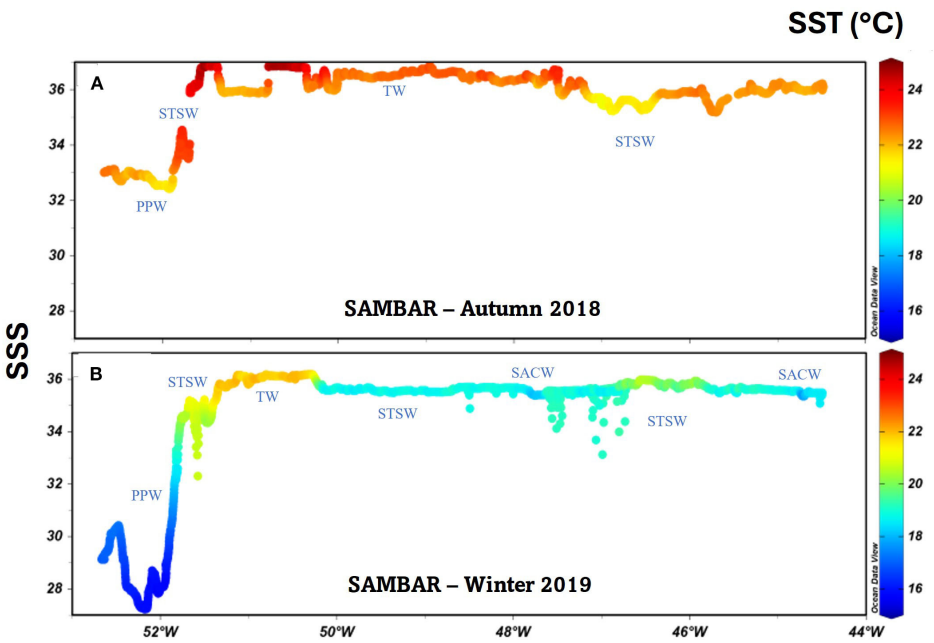

FIGURE 3
Continuous salinity (SSS) and sea surface temperature (SST; °C) data from the vessel's thermosalinograph in the transect region during campaigns **(A)** in the autumn of 2018 and **(B)** winter of 2019. The water masses are indicated in the figure: Plata Plume Water (PPW), Subtropical Shelf Water (STSW), Tropical Water (TW) and South Atlantic Central Water (SACW).

Whitney, $p < 0.05$). The median pCO_2 value in the winter 2019 (434 µatm) was higher (Supplementary Table S3) than that in the autumn of 2018 (380 µatm) (Supplementary Table S2). Moreover, there was a clear division ($p<0.05$) between the relatively higher (>450 µatm) pCO_2 values on the continental shelf and the relatively lower (<400 µatm) pCO_2 values in the open ocean waters at the continental slope in the autumn of 2018 (Figure 4A), with higher median in shelf waters (445 µatm) (Supplementary Table S2). On the other hand, during winter 2019, the pCO_2 did not significantly differ spatially ($p > 0.05$), and both areas presented the same median (433 µatm) (Supplementary Tables S2, S3). The same features are observed for the spatial variation in ΔpCO_2 values (Figures 4C, D). In 2019 (winter), the median ΔpCO_2 was 28 µatm both on the shelf and in the open ocean. During 2018 (autumn), the shelf region had a median ΔpCO_2 of 39 µatm, whereas in the open ocean, it was –28 µatm. These results highlight strong seasonal and spatial patterns in the SST, SSS, and pCO_2, while also indicating continental freshwater mixing — particularly in autumn—when cross-shelf gradients become less pronounced. Spearman correlation analyses indicated a negative correlation between pCO_2 and the SST, as well as between pCO_2 and the SSS. Both correlations were statistically significant at $\alpha = 0.05$.

3.2 SSH and ΔpCO_2

The spatial distributions of the SSH and ΔpCO_2 values significantly differed between the 2018 and 2019 campaigns (Figure 5). In 2018, a well-defined gradient was observed along the transect, with strongly positive (reddish tones) and negative (bluish tones) ΔpCO_2 values. Notably, the westernmost portion of the transect predominantly indicated CO_2 release to the atmosphere, whereas the eastern portion was characterized by CO_2 uptake by the ocean. In contrast, during the winter of 2019, the ΔpCO_2 gradient was less pronounced, with a predominance of positive values and near-equilibrium conditions with the atmosphere (white tones).

The variation in SSH, represented by green and red tones, suggests distinct ocean circulation patterns between the two analyzed years. In 2018, a positive SSH anomaly (> 0.2 m) east of the transect may have been associated with the influence of an oceanic feature, such as an anticyclonic eddy. In 2019, the more uniform SSH distribution indicated a weaker influence of mesoscale structures in the study area. Mesoscale dynamics, defined here as features with horizontal scales of ~10–100 km (Martínez-Moreno et al., 2022), were less evident during this period. Although a SSH anomaly was detected around 48°W, it likely represents a smaller-scale or transient feature rather than a well-developed mesoscale eddy.

The observed SSH anomalies were associated with ΔpCO_2 variability, consistent with the influence of mesoscale structures. These results point to the importance of mesoscale circulation in driving surface CO_2 variability in the SWAO.

3.3 Ocean–atmosphere CO_2 fluxes

The shelf region acted as a weak source and the open ocean region acted as a CO_2 weak sink during the autumn campaign (2018). The median FCO_2 was 0.1 mmol CO_2 $m^{-2}h^{-1}$ for the shelf and –0.1 mmol CO_2 $m^{-2}h^{-1}$ for the ocean (Wanninkoff 2014 parameterization)

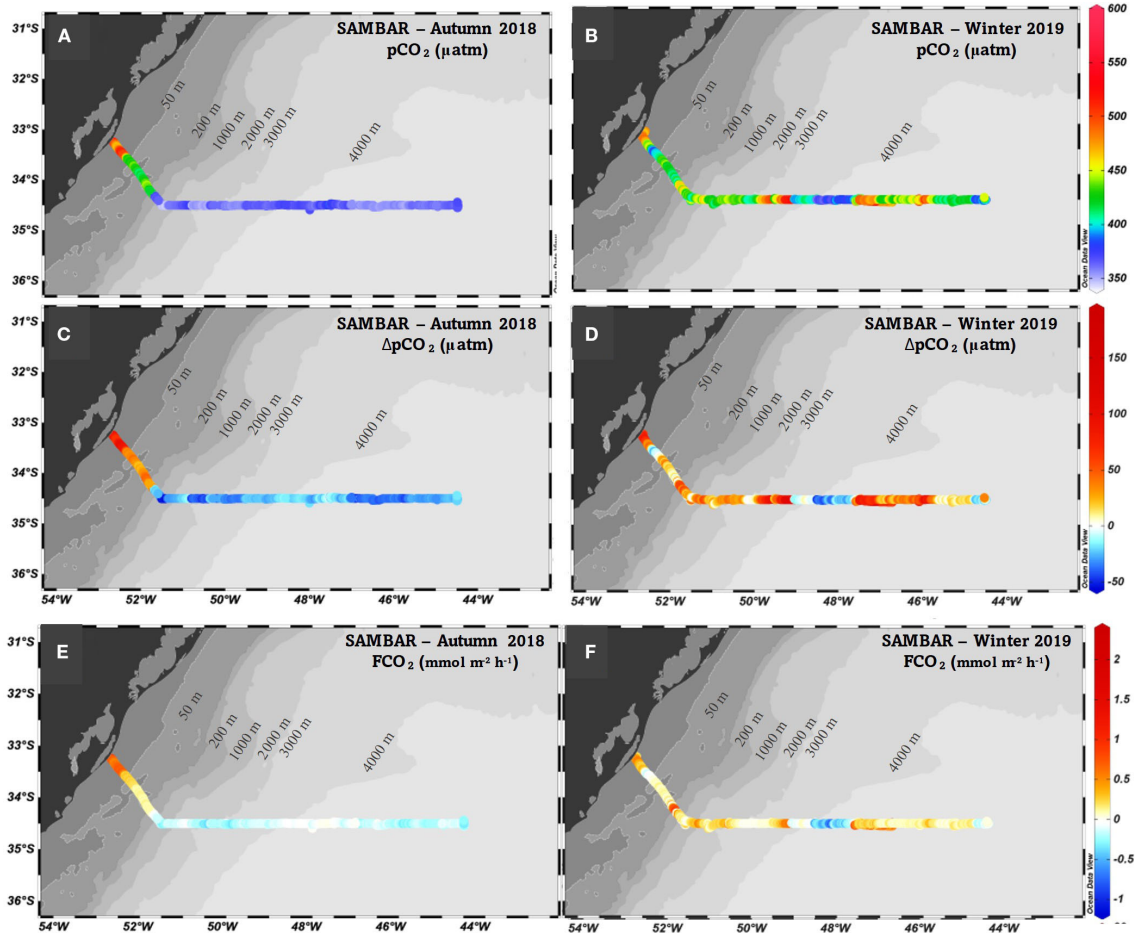

FIGURE 4
Continuous **(A, B)** partial pressure of CO_2 (pCO_2; µatm), **(C, D)** difference between ocean pCO_2 and atmospheric pCO_2 (ΔpCO_2; µatm) and **(E, F)** fluxes of CO_2 (FCO_2; mmol m^{-2} h^{-1}) data in the transect region during the campaigns in the **(A, C, E)** autumn of 2018 and **(B, D, F)** winter of 2019. The grayscale shading represents the variation in bathymetry, with the shallowest areas being identified by darker grey and the deepest areas represented by lighter grey. The lines represent the isobaths.

(Supplementary Table S2). Although the shelf region acted as a source, when considering the entire transect, there was a weak CO_2 sink with a median FCO_2 of –0.1 mmol CO_2 $m^{-2}h^{-1}$ (Figure 4E). The wind speed was constant throughout the autumn campaign, with overall median values of ~10 m s^{-1} (Supplementary Figure S5a). On the other hand, during the entire winter 2019 campaign, the region behaved as a weak CO_2 source (Figure 4F), with some areas showing CO_2 equilibrium between the ocean and the atmosphere along the transect. A relatively strong CO_2 sink area was observed ~48°W, where wind speeds with 10 m s^{-1} were also observed (Supplementary Figure S5b).

4 Discussion

4.1 Hydrographic conditions in the southwestern Atlantic Ocean

The analyzed period exhibited SST and SSS patterns consistent with the water masses typically found in the southwestern Atlantic Ocean (Bianchi et al., 1993; Piola et al., 2000; Möller et al., 2008). The pattern of wind directions in the study region changed from predominantly northerly winds in autumn to predominantly southerly and southwesterly winds in winter (Möller et al., 2008). Our observed thermohaline properties indicated that the relatively fresher, cooler and nutrient rich PPW was more common off the Argentine–Uruguay coastal area in autumn, with the STSW covering the northern portion of the shelf.

The surface haline front (100–200 m) divides the outer shelf and the open ocean regions (Brandini et al., 2018). Warmer and more saline waters predominated on the shelf and in the open ocean up to approximately 47°W in autumn 2018, suggesting a lesser influence of PPW, allowing greater penetration of TW and STSW in the region. On the other hand, in 2019 (winter), a significant reduction in SST and SSS was observed on the continental shelf, indicating an expansion of the PPW (Figure 3B). This pattern is consistent with studies (e.g., Möller et al., 2008) that showed that the Plata River discharge and the consequent expansion of the plume are intensified in winter. During this period, the prevailing winds from the south and southeast favored the dispersion of less saline water to the north.

Additionally, the SACW was observed during the winter of 2019, between the STSW and TW in the open ocean area (Figure 3). The presence of cooler and less saline waters in winter is also associated with the displacement of the BMC to more northern latitudes (Combes and Matano, 2014). The BMC marks the meeting point between the warm and salty BC and the cold and less saline MC. During winter, the MC intensifies its influence on the shelf, promoting the cooling of surface waters and contributing to the intrusion of subantarctic water masses.

Although no direct comparison was made between the model outputs and the *in-situ* measurements — as model validation was not the aim of this work — the CMEMS modeled fields were useful for supporting the interpretation of circulation patterns and thermohaline structures observed across the shelf and open ocean. The limitations of the CMEMS fields were considered during the interpretation of results, and care was taken to avoid overinterpreting features below the model's resolution capability. No interpolation was applied to the model fields, and only daily mean values were used as provided by CMEMS.

4.2 Distribution of pCO_2

The median pCO_2 concentration in the winter of 2019 (434 µatm) was greater than that in the autumn of 2018 (380 µatm). In addition, the behavior of the regions (continental shelf *vs.* open ocean) was different during the study period. The pCO_2 was greater than that of open ocean waters in autumn 2018, while both areas presented the same median (433 µatm) during the winter of 2019. One of the factors associated with these variations may be associated with the SST. SST highly modulates pCO_2 variations (e.g., Takahashi et al., 2009; 2014). In this region, Ito et al. (2016) reported that the thermal effect is the main factor controlling the solubility of CO_2. However, several processes can stimulate seasonal variations in ocean surface pCO_2 (e.g., respiration, production, carbonate dissolution, and precipitation) (Sarmiento and Gruber, 2006).

In autumn 2018, when the influence of the PPW was lower, the shelf had higher pCO_2 values. The observed warmer and saltier water conditions suggest a lower renewal of water masses and the predominance of oligotrophic TW, which tends to have higher pCO_2 values (Ito et al., 2016).

Lencina-Avila et al. (2016) and Ito et al. (2016) noted that less saline water (<30), which is rich in organic matter and nutrients, can considerably reduce pCO_2 by stimulating primary productivity. The PPW is rich in nutrients and may play a key role in promoting phytoplankton blooms (Lima et al., 2019), as does the SACW (Pezzi et al., 2009). After blooms, these organisms produce organic matter and decompose, potentially generating carbon in the water (Carvalho et al., 2022). Similarly, Bordin et al. (2019) demonstrated that CO_2-rich waters at the surface increase pCO_2, even at lower temperatures. During the 2019 winter cruise, the combination of enhanced vertical mixing and the presence of SACW likely increased surface carbon, raising pCO_2 despite cooler temperature. In this context, variations in total alkalinity further modulate the signal: lower total alkalinity in river-influenced sectors reduces buffering and amplifies pCO_2, whereas higher total alkalinity locally mitigates it. This interpretation is consistent with the temperature-normalized patterns and with regional total alkalinity–salinity relationships documented by Albuquerque et al. (2025). Together, these findings suggest that the observed homogenization of surface pCO_2 in winter of 2019 resulted from an interplay of physical mixing, biological processes, and carbonate chemistry. However, full seasonal studies are still required to confirm these dynamics, and a complete carbonate-system decomposition (e.g., Kerr et al., 2024) will be addressed in future work.

4.3 Ocean–atmosphere FCO_2

Several authors have discussed the importance of the South Atlantic Ocean region in the absorption of atmospheric CO_2 (e.g., Ito et al., 2016; Lencina-Avila et al., 2016; Padin et al., 2010). During the study period, the SWAO area behaved as both a sink and a source of CO_2 to the atmosphere. In the autumn of 2018, the shelf region acted as a weak source, and the open ocean region acted as a weak CO_2 sink. However, during the winter of 2019, the region behaved as a CO_2 source with some areas showing CO_2 equilibrium. In general, open ocean region behaves as an ocean CO_2 sink in the SWAO, whereas the shelf region is considered a CO_2 source for the atmosphere during all seasons (Ito et al., 2005; Arruda et al., 2015). The same was found in our study in the autumn of 2018. In contrast, the transect region acted as a weak source of CO_2 to the atmosphere during the winter of 2019, except in the SACW observed areas (Supplementary Tables S2, S3; Figure 4). Lencina-Avila et al. (2016) reported that the continental shelf region acted as a sink for atmospheric CO_2 during the spring of 2011 in the southwestern Atlantic Ocean, with a mean flux of −0.5 ± 0.2 mmol CO_2 m^{-2} d^{-1} in the shelf region and −3.1 ± 2.2 mmol CO_2 m^{-2} d^{-1} in the open ocean region. The values found in this study were in accordance with those in the literature (Table 1) (e.g., Padin et al., 2010). These seasonal contrasts highlight only the large dynamics of the study region due to the intensity of physical processes (Lencina-Avila et al., 2016).

When compared to climatological estimates, our observations show broadly consistent magnitudes. For the open ocean region, Fay et al. (2024) reported climatological fluxes of ~ – 3 mmol m^{-2} d^{-1} in April (autumn) and ~ –5 mmol C m^{-2} d^{-1} in June (winter), with an annual mean flux at 35°S/54–44°W of –1.94 mol m^{-2} yr^{-1}. However, our results diverge from these climatological means, particularly in winter of 2019 when a CO_2 source was observed instead of the expected sink. This highlights that while climatologies are useful for large-scale generalizations, they may smooth out short-term or mesoscale variability, underscoring the importance of high-resolution regional observations to accurately represent local carbon dynamics, which are still sparse in this dynamic region (Affe et al., 2023).

The contrast in air–sea CO_2 fluxes between the autumn of 2018 and winter of 2019 reflects the interplay among thermal

TABLE 1 Average or median air-sea fluxes of CO_2 (FCO_2; mmol CO_2 m^{-2} d^{-1}) with standard deviation or interquartile, season and year from several studies along 34.5°S and the surrounding area.

Area	Year	Season	FCO_2 (mmol CO2 m−2 d −1)	Reference
Shelf region	2018	Austral autumn	3.2 (1.6 – 9.9) (W14)	This study – 34.5°S
	2019	Austral winter	2.4 (1.0 – 5.2) (W14)	This study – 34.5°S
	2011	Austral spring	−0.001 ± 0.005 (W14)	Carvalho et al., 2021 – 35°S
	2011	Austral spring	−0.5 ± 0.2 (W92)	Lencina-Avila et al., 2016 – 35°S
	2010	Austral spring	0.0 ± 1.1 (W92)	Ito et al., 2016 – 34° to 34.9°S
	2000 to 2008	Austral autumn	−8.8 ± 7.4 (W92)	Padin et al., 2010 – 31° to 40°S
Open ocean	2018	Austral autumn	−2.5 (−3.8 – −1.1) (W14)	This study – 34.5°S
	2019	Austral winter	1.2 (−0.1 – 3.7) (W14)	This study – 34.5°S
	2011	Austral spring	−3.1 ± 2.2 (W92)	Lencina-Avila et al., 2016 – 35°S
	2000 to 2008	Austral autumn	−6.0 ± 5.8 (W92)	Padin et al., 2010 – 31° to 40°S

W14 and W92 correspond to the equations used by Wanninkhof 2014 and Wanninkhof 1992.

structure, freshwater inputs, and wind forcing. The relatively warm surface temperatures (>21°C) and constant moderate wind speeds (~10 m s^{-1}) likely maintained stratification and limited vertical mixing, while allowing for localized biological CO_2 uptake offshore in autumn. In winter, however, colder waters and pronounced PPW intrusion (SST < 19°C; SSS < 30) spread over the continental shelf, altering surface water chemistry, as already observed by Albuquerque et al. (2025). Concurrently, stronger and more variable wind speeds (with values >15 m s^{-1}) increased the gas transfer velocity and promoted deeper mixing, reducing the pCO_2 gradient and leading to near-equilibrium conditions along the shelf region. The heterogeneity in the SST and SSS, also evident in CMEMS data, supports the influence of mesoscale dynamics and water mass mixing in shaping these seasonal differences. The heterogeneity in the SST and SSS, also evident in CMEMS data, supports the influence of mesoscale dynamics and water mass mixing in shaping these seasonal differences. During winter 2019, strong gradients of SST and SSS along ~36–38°S (Figure 2) were linked to frontal zones and cyclonic eddies, while at ~34–35°S (Figure 3) the influence of PPW further contributed to the observed variability.

Surface pCO_2 distribution with a similar spatial structure farther south in the SWAO was also reported along the COSTAL-AR section (Berghoff et al., 2023), where three distinct systems were identified. Their study found significant differences in FCO_2 between these domains and in different seasons. In both cases, high average FCO_2 values were observed in the coastal zone, with minimum values occurring near the shelf-break front, followed by an increase in offshore waters. These observations support the hypothesis that horizontal gradients in pCO_2 are shaped by shelf −ocean exchange and frontal dynamics and reinforce the idea that the shelf-break may act as a biogeochemical transition zone. Our findings align with this spatial pattern, particularly the tendency for lower pCO_2 and fluxes near the open ocean in the autumn of 2018 and more homogenized values in winter of 2019.

The observed pCO_2 dynamics reinforce the variable behavior of the southwestern Atlantic Ocean, which can act as both a sink and a source of CO_2, tending towards CO_2 equilibrium, depending on the season and the dominant processes. Lefèvre et al. (2010) highlighted this variability, indicating that the waters of the South Atlantic Ocean respond rapidly to changes in water masses and the influence of the BMC. Furthermore, this seasonal variation alternating between periods of CO_2 uptake and release depends on the SST, riverine influence and upwelling (Landschützer et al., 2016).

In addition, lower temperatures can promote the uptake of CO_2 through the solubility pump. This process may have contributed to the in gassing of CO_2 in the open ocean region during both seasons, as demonstrated by Ito et al. (2005) and Lencina-Avila et al. (2016).

The coastal zone receives larger inputs of nutrients and organic matter because of the greater contribution from the continent (rivers, runoff, and groundwater discharge) (Möller et al., 2008). In addition to the influence of the plumes of the Plata River and Patos Lagoon on the supply of nutrients, Carvalho et al. (2021) reported that physical instability at the water surface and relatively cold water tend to increase phytoplankton permanence in the euphotic zone and favor the dominance of diatoms close to 35°S

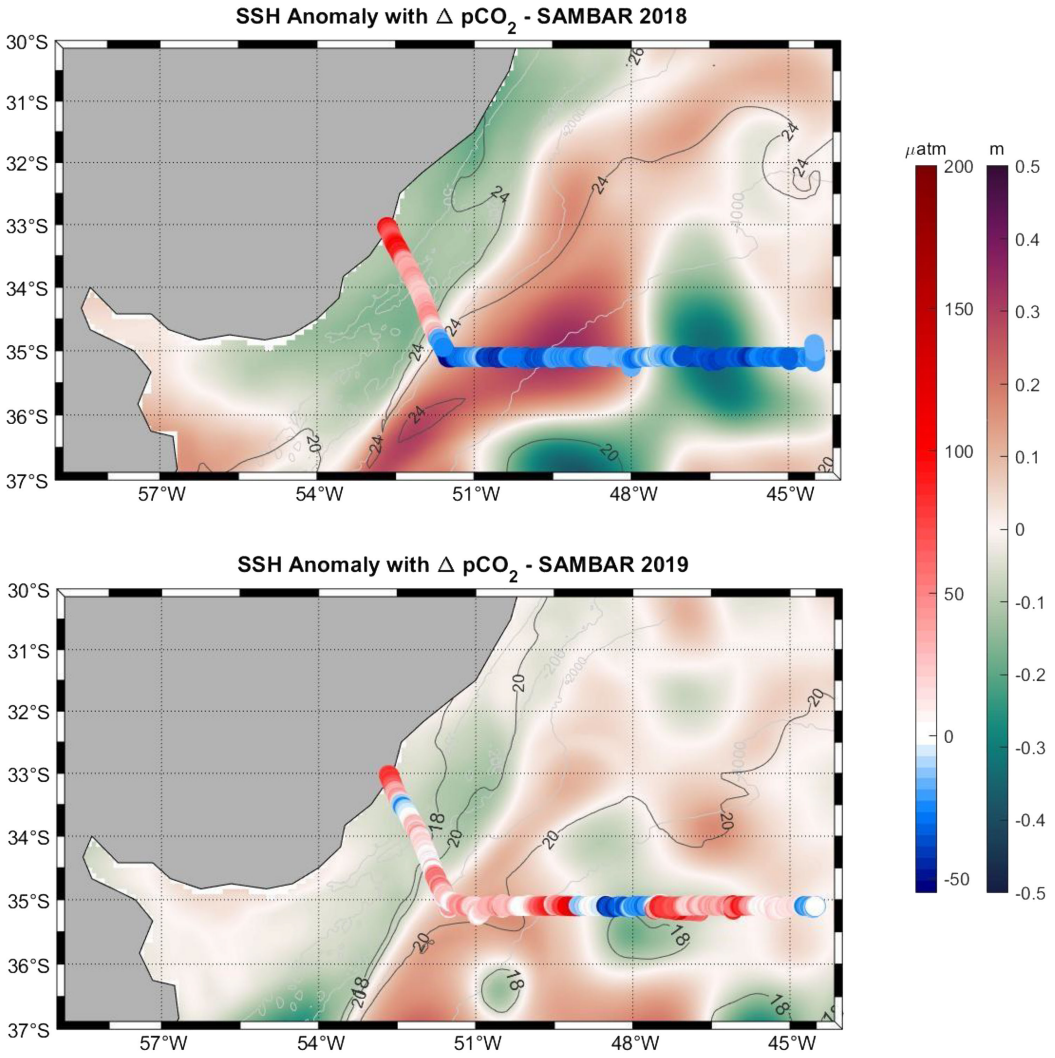

FIGURE 5
Map of the study region, showing the surface height anomaly (SSH; m) and continuous data of the difference between ocean and atmospheric pCO_2 (ΔpCO_2; µatm; https://resources.marine.copernicus.eu). The top map refers to the 2018 campaign (autumn), whereas the bottom map refers to the 2019 campaign (winter). The first bar indicates the variation in ΔpCO_2 values along the transect (red, white, and blue), where red tones represent CO_2 sources to the atmosphere, white tones indicate equilibrium, and blue tones denote CO_2 uptake. The second color bar (orange, white and green) corresponds to SSH variations across the study area. The black contour lines represent temperature isolines (°C).

latitude. Therefore, high pCO_2 values are generally observed in shelf water and waters and are influenced by both the physical dynamics of the BC and biological processes (Ito et al., 2016). While photosynthesis tends to lower pCO_2, respiration and remineralization in productive shelf environments often enhance carbon concentrations and increase pCO_2 values. In the SWAO shelf, this balance is further modulated by nutrient supply from upwelling and riverine input, which can stimulate biological production and subsequently reduce pCO_2 at longer timescales. Our observations suggest that, during the study period, the net effect of physical dynamics and remineralization dominated, leading to higher pCO_2 in shelf waters. Furthermore, carbon inputs from continents may be associated with groundwater from Patos Lagoon, since records in this region of groundwater discharge represent a potentially important source of dissolved nutrients to the coastal ocean (Souza et al., 2021). Once on the coast, this groundwater can mix with the PPW and influence the pCO_2.

Upwelling and deep mixing processes can indeed contribute to the elevated pCO_2 values observed in winter. These processes bring subsurface waters, enriched in carbon due to remineralization at depth, to the surface. The excess of carbon increases surface pCO_2, often offsetting the cooling effect that would otherwise lower pCO_2 in winter. Moreover, the stronger winds typical of this season enhance vertical mixing and air–sea gas exchange, favoring CO_2 outgassing. The formation of the western SACW in this area enhances this effect (Liu and Tanhua, 2021). Similar mechanisms have been described for other upwelling systems and regions influenced by the SACW (e.g., Ito et al., 2016; Azar et al., 2021). Thus, the high pCO_2 observed during our winter cruise may reflect the combined effect of deep-water ventilation and physical forcing.

Hydrodynamic processes, including mesoscale eddies, influence the regional variability in surface ocean pCO_2 (Orselli et al., 2019). Along the transect, in both campaigns, the normalized pCO_2 results indicate that this parameter is strongly dependent on the SST. The presence of cyclonic eddies in the region (Figure 2), detected from satellite-derived current velocities, suggests that these structures may be associated with variations in pCO_2. Cyclonic eddies are characterized in the Southern Hemisphere by clockwise rotation and low-pressure centers, displacing the isopycnals upwards, thus presenting a typical signature of cooling of the sea surface (e.g., Azevedo and Mata, 2010; Talley et al., 2011). Therefore, they are associated with negative heat flux anomalies, which means that in the regions where they can be identified, the ocean takes up heat from the atmosphere and thus tends to cool the atmospheric boundary layer (Villas Bôas et al., 2015). Furthermore, the solubility of CO_2 in seawater is greater when the water is cold and less salty. Consequently, cyclonic eddies increase the solubility of CO_2 (Figure 2) (Smith et al., 2023), changing the pCO_2 values, where cooler SST within the eddy core coincided with higher pCO_2 compared to surrounding waters.

4.4 Mesoscale dynamics

The surface velocity field significantly differed between the two campaigns. In 2018, the BC region displayed more intense activity, extending its influence farther south to the BMC region. Upon reaching the BMC, the BC underwent retroflection, generating a coastward jet that changes course northwards near 48°W, reaching the SAMBAR transect. In 2019, the BC region was weaker than that in 2018, and the velocity field along with the sea surface height anomaly was characterized by multiple smaller vortical structures (Figure 5). Two cyclonic eddies, centered at 51°W 36°30'S and 48° W 35°30'S, present temperatures lower than 18 °C. This spatial variation suggests the influence of physical processes, such as upwelling and horizontal advection. Thus, the BC ocean boundary and its anticyclones are associated with positive sea surface height anomalies. Additionally, cyclonic vortices are characterized by negative sea surface height anomalies (Angel-Benavides et al., 2016; Carvalho et al., 2019) due to the upwelling of cold water (McGillicuddy and Robinson, 1997) and consequent thermal contraction in their interior. This spatial variation suggests the influence of physical processes, such as upwelling and horizontal advection.

Lencina-Avila et al. (2016) identified vortices in the region (open ocean) that promote the absorption of atmospheric CO_2 through vertical and horizontal mixing processes and suggested the influence of frontal structures along the subtropical convergence region. This agrees with the results of this study for the open ocean in both periods. This finding reinforces our suggestion that mesoscale structures influence pCO_2 dynamics in the study area along 34.5°S. Furthermore, Orselli et al. (2019) reported that eddies in the Agulhas region act as CO_2 sinks in the South Atlantic Ocean. The authors explain that cyclonic structures can act in the upwelling of CO_2-rich water masses, behaving as a source of CO_2 to the atmosphere, despite the presence of anticyclonic vortices acting as CO_2 sink zones. This means that the presence of a vortex near the transect region may affect the sink capacity of the southwestern Atlantic Ocean. However, a more detailed investigation should be performed to verify this conclusion.

5 Conclusion

In this study, the variations in surface ocean pCO_2 and net CO_2 fluxes at the ocean–atmosphere interface at 34.5°S in the SWAO during the autumn of 2018 and winter of 2019 were evaluated. Water mass distributions and physicochemical properties on the sea surface, which are strongly associated with seasonal variation, were considered in the spatial assessment of pCO_2. The shelf region acted as a source, whereas the open sea tended towards a weak sink of CO_2 in the autumn of 2018. In the winter of 2019, CO_2 was predominantly weakly released into the atmosphere, both in the open ocean and on the continental shelf, while it was expected that it would act as a sink. In addition, a relatively strong CO_2 sink area was observed ~48°W, where wind speeds with 10 m s^{-1} were also observed. This highlights that while climatologies are useful for largescale generalizations, they may smooth out short-term or mesoscale variability, underscoring the importance of high-resolution regional observations to accurately represent local carbon dynamics. This study contributes to the understanding of how different mechanisms lead to CO_2 exchanges in the outer shelf and open ocean waters in the southwestern Atlantic Ocean. This knowledge provides support for establishing the influence of each factor involved in carbon exchange (e.g., thermal effects and hydrodynamic processes) while considering spatial and seasonal gradients, in addition to contributing to the quantification of the global carbon cycle. For this reason, we suggest further studies of biogeochemical parameters to better understand the variation in pCO_2 and its influences.

Data availability statement

The original contributions presented in the study are included in the article/Supplementary Material. Further inquiries can be directed to the corresponding author.

Author contributions

CA: Software, Conceptualization, Methodology, Investigation, Writing – original draft. GM: Investigation, Methodology, Writing – original draft, Formal analysis, Software, Data curation. JL-A: Writing – review & editing, Conceptualization, Investigation. LP: Writing – review & editing, Supervision, Conceptualization, Investigation. HM: Formal analysis, Methodology, Conceptualization, Investigation, Writing – review & editing. AF:

Writing – review & editing, Data curation, Methodology. EP: Writing – review & editing, Methodology, Software, Investigation, Conceptualization. LA-N: Writing – review & editing, Methodology, Software, Data curation, Validation. EC: Resources, Funding acquisition, Project administration, Writing – review & editing. LC: Visualization, Investigation, Project administration, Conceptualization, Resources, Funding acquisition, Writing – original draft, Supervision.

Funding

The author(s) declare financial support was received for the research and/or publication of this article. This study was financed in part by the Coordenação de Aperfeiçoamento de Pessoal de Nível Superior – Brasil (CAPES) – Finance Code 001, with a Master fellowship to GCM. The dataset analysed in this study is part of the SAMBAR project (Variabilidade interanual dos transportes meridionais através da rede transatlântica Samoc, process n° 17/09659-6, financed by Fundação de Amparo à Pesquisa do Estado de São Paulo – FAPESP). We acknowledge the contributions of Ms. Camilla Caetano and Ms. Julia Arouca for measuring underway surface ocean pCO2 during the 2 sampling campaigns, Fundação Carlos Chagas Filho de Amparo à Pesquisa do Estado do Rio de Janeiro (FAPERJ) for the fellowships awarded to Julia Arouca, the whole crew at RV Alpha Crucis for the onboard physicochemical data and SAMBAR campaigns, and Rede Nacional de Observação e Monitoramento Oceânico (RENOMO – financed by Conselho Nacional de Desenvolvimento Científico e Tecnológico – CNPq – process n° 409666/2022-0). LQP, AMF and LCC acknowledge the Prociência/UERJ+FAPERJ Scholarship Program. LCC acknowledges the CNPq-PQ2 309708/2021-4 and FAPERJ-CNE E-26/201.156/2022 grants.

Conflict of interest

The authors declare that the research was conducted in the absence of any commercial or financial relationships that could be construed as a potential conflict of interest.

Generative AI statement

The author(s) declare that no Generative AI was used in the creation of this manuscript.

Any alternative text (alt text) provided alongside figures in this article has been generated by Frontiers with the support of artificial intelligence and reasonable efforts have been made to ensure accuracy, including review by the authors wherever possible. If you identify any issues, please contact us.

Publisher's note

Supplementary material

The Supplementary Material for this article can be found online at: https://www.frontiersin.org/articles/10.3389/fmars.2025.1623344/full#supplementary-material

References

Affe, H. M. J., Rocha, D. S. B., Piedras, F. R., Moser, G. A. O., Araujo, M. C., and da Cunha, L. C. (2023).) Sea-air CO2 fluxes along the Brazilian continental margin. *Ocean Coast. Res.* 71. doi: 10.1590/2675-2824071.22051hmdja

Albuquerque, C., Miguel, G., Faria, C. O., Pinho, L., Marotta, H., Orselli, I. B. M., et al. (2025). Regional relationship between total alkalinity and salinity in the surface waters of the western South Atlantic margin. *Regional Stud. Mar. Sci.* 81, 103992. doi: 10.1016/j.rsma.2024.103992

Angel-Benavides, I. M., Pilo, G. S., Dias, F. B., and Garcia, C. A. (2016). Influência de vórtices na concentração de clorofila da confluência Brasil-Malvinas: Mecanismos inferidos por sensoriamento remoto. *Braz. J. Aquat. Sci. Technology.* 20, 10–20. doi: 10.14210/bjast.v20n1.4782

Arruda, R., Calil, P. H., Bianchi, A. A., Doney, S. C., Gruber, N., Lima, I., et al. (2015). Air-sea CO2 fluxes and the controls on ocean surface pCO2 seasonal variability in the coastal and openocean southwestern Atlantic Ocean: a modeling study. *Biogeosciences.* 12, 5793–5809. doi: 10.5194/bg-12-5793-2015

Azar, E., Piñango, A., Wallner-Kersanach, M., and Kerr, R. (2021). Source waters contribution to the tropical Atlantic central layer: New insights on the Indo-Atlantic exchanges. *Deep-Sea Res. Part II: Oceanographic Res. Papers* 168, 103450. doi: 10.1016/j.dsr.2020.103450

Azevedo, J. L. L., and Mata, M. M. (2010). O mecanismo de autopropulsão de vórtices oceânicos: uma revisão. *Rev. Bras. Geofísica.* 28, 331–347. doi: 10.1590/S0102-261X2010000300002

Bakker, D. C. E., Alin, S. R., Bates, N., Becker, M., Gkritzalis, T., Jones, S., et al. (2024). *Surface Ocean CO2 Atlas Database Version 2024 (SOCATv2024) (NCEI Accession 0293257)* (NOAA National Centers for Environmental Information). doi: 10.25921/9wpn-th28

Bakker, D. C. E., Pfeil, B., Landa, C. S., Metzl, N., O'Brien, K. N., Olsen, A., et al. (2016). A multi-decade record of high quality fCO2 data in version 3 of the Surface Ocean CO2 Atlas (SOCAT). *Earth System Sci. Data.* 8, 383–413. doi: 10.5194/essd-8-383-2016

Berghoff, C. F., Pierrot, D., Epherra, L., Silva, R. I., Segura, V., Negri, R. M., et al. (2023). Physical and biological effects on the carbonate system during summer in the Northern Argentine Continental Shelf (Southwestern Atlantic). *J. Mar. Syst.* 237, 103828. doi: 10.1016/j.jmarsys.2022.103828

Bianchi, A. A., Giulivi, C. F., and Piola, A. R. (1993). Mixing in the Brazil-Malvinas confluence. *Deep Sea Res. Part I: Oceanographic Res. Papers.* 40, 1345–1358. doi: 10.1016/0967-0637(93)90115-J

Bianchi, A. A., Ruiz-Pino, D., Perlender, H. G. I., Osiroff, A. P., Segura, V., Lutz, V., et al. (2009). Annual balance and seasonal variability of sea-air CO2 fluxes in the Patagonia Sea: their relationship with fronts and chlorophyll distribution. *J. Geophysical Res.* 114, 1345-1358. doi: 10.1029/2008JC004854

Boot, A., Heydt, A. S. V., and Dijkstra, H. A. (2022). Effect of the Atlantic Meridional Overturning Circulation on atmospheric pCO_2 variations. *Earth System Dynamics.* 13, 1041–1058. doi: 10.5194/esd-13-1041-2022

Bordin, L. H., MaChado, E. C., Carvalho, M., Freire, A. S., and Fonseca, A. L. D. O. (2019). Nutrient and carbon dynamics under the water mass seasonality on the continental shelf at the South Brazil Bight. *J. Mar. Systems.* 189, 22–35. doi: 10.1016/j.jmarsys.2018.09.006

Brandini, F. P., Tura, P. M., and Santos, P. P. G. M. (2018). Ecosystem response to biogeochemical fronts in the South Brazil Bight. *Progress in Oceanography* 164, 52-62. doi: 10.1016/j.pocean.2018.04.012

Campos, E. J. D., Gonçalves, J. E., and Ikeda, Y. (1995). Water mass characteristics and geostrophic circulation in the South Brazil Bight: Summer of 1991. *J. Geophysical Res.* 100, 18537. doi: 10.1029/95JC01724

Carvalho, A. C. O., Kerr, R., Mendes, C. R. B., Azevedo, J. L. L., and Tavano, V. M. (2021). Phytoplankton strengthen CO2 uptake in the South Atlantic Ocean. *Prog. Oceanography* 190, 102476. doi: 10.1016/j.pocean.2020.102476

Carvalho, A. C. O., Kerr, R., Tavano, V. M., and Mendes, C. R. B. (2022). The southwestern South Atlantic continental shelf biogeochemical divide. *Biogeochemistry.* 159, 139–158. doi: 10.1007/s10533-02200918-8

Carvalho, A. C. O., Mendes, C. R. B., Kerr, R., Azevedo, J. L. L., Galdino, F., and Tavano, V. M. (2019).) The impact of mesoscale eddies on the phytoplankton community in the South Atlantic Ocean: HPLC-CHEMTAX approach. *Mar. Environ. Res.* 144, 154-165. doi: 10.1016/j.marenvres.2018.12.003

Castro, B. M. d, and Miranda, L. B. d (1998). "Physical oceanography of the western Atlantic continental shelf located between 4 N and 34 S," in *The sea*, vol. 11. (John Wiley & Sons, New York), 209–251.

Chelton, D. B., Schlax, M. G., Witter, D. L., and Richmann, J. G. (1990). GEOSAT altimeter observations of the surface circulation of the Southern Ocean. *J. Geophysical Res.* 95, 877–903. doi: 10.1029/jc095ic10p17877

Chidichimo, M. P., Perez, R. C., Speich, S., Kersalé, M., Sprintall, J., Dong, S., et al. (2023). Energetic overtuning flows, dynamic interocean exchanges, and ocean warming observed in the South Atlantic. *Communication Earth Environ.* 4, 10. doi: 10.1038/s43247-022-00644-x

Chidichimo, M. P., Piola, A. R., Meinen, C. S., Perez, R. C., Campos, E. J. D., Dong, S., et al. (2021). Brazil current volume transport variability during 2009–2015 from a long-term moored array at 34.5 °S. *J. Geophysical Research: Oceans* 126, e2020JC017146. doi: 10.1029/2020JC017146

Combes, V., and Matano, R. P. (2014). Trends in the Brazil/Malvinas confluence region. *Geophysical Res. Letters.* 41, 8971–8977. doi: 10.1002/2014GL062523

D'Agostino, R. B., and Pearson, E. S. (1973). Tests for departure from normality. *Biometrika.* 60, 613–622. doi: 10.1093/biomet/60.3.613

De Souza, A. G. Q., Kerr, R., and Azevedo, J. L. L. (2018). On the influence of subtropical mode water on the south atlantic ocean. *J. Mar. System* 185, 13–24. doi: 10.1016/j.jmarsys.2018.04.006

FAPESP (Fundação de Amparo à Pesquisa do Estado de São Paulo) Grant 2018/09659-6; Cruise Report - Interannual Variability of the Meridional Transports across the SAMOC Basin-wide Array (SAMBAR). Available online at: https://inct.furg.br/images/Cruise_Report_SAM15_SAMBAR_A1_Low_Res.pdf (Accessed November 29, 2019).

FAPESP (Fundação de Amparo à Pesquisa do Estado de São Paulo) Grant 2019/09659-6; Cruise Report - Interannual Variability of the Meridional Transports across the SAMOC Basin-wide Array (SAMBAR). Available online at: https://www.bodc.ac.uk/resources/inventories/cruise_inventory/reports/alphacrucis_sambar_a2.pdf (Accessed November 29, 2019).

Fay, A. R., Munro, D. R., McKinley, G. A., Pierrot, D., Sutherland, S. C., Sweeney, C., et al. (2024). Updated climatological mean ΔfCO2 and net sea–air CO2 flux over the global open ocean regions. *Earth System Sci. Data.* 16, 2123–2139. doi: 10.5194/essd-16-2123-2024

Fernandes, T. F., Peixoto, R. B., Queiroz Pinho, L., da Cunha, L. C., Veloso Franklin, T., Pollery, R. C., et al. (2025). Eutrophication triggers diel and seasonal shifts of carbon dioxide and oxygen in tropical urban coastal waters. *Limnology Oceanography Letter.* 10, 329–339. doi: 10.1002/lol2.70006

Friedlingstein, P., O'Sullivan, M., Jones, M. W., Andrew, R. M., Hauck, J., Landschüter, P., et al. (2025). Global carbon budget 2024. *Earth System Sci. Data.* 17, 965–1039. doi: 10.5194/essd-2024-519

Gallego, M. A., Timmermann, A., Friedrich, T., and Zeebe, R. E. (2020). Anthropogenic intensification of surface ocean interannual pCO2 variability. *Geophysical Res. Lett.* 47. doi: 10.1029/2020GL087104

Ito, R. G., Garcia, C. A. E., and Tavano, V. M. (2016). Net sea-air CO2 fluxes and modelled pCO2 in the southwestern subtropical Atlantic continental shelf during spring 2010 and summer 2011. *Continental Shelf Res.* 119, 68–84. doi: 10.1016/j.csr.2016.03.013

Ito, R. G., Schneider, B., and Thomas, H. (2005). Distribution of surface fCO2 and air–sea fluxes in the Southwestern subtropical Atlantic and adjacent continental shelf. *J. Mar. Systems.* 56, 227–242. doi: 10.1016/j.jmarsys.2005.02.005

Kerr, R., Monteiro, T., Orselli, I. B. M., Tavano, V. M., and Mendes, C. R. B. (2024). Sea-air CO2 exchanges, pCO2 drivers and phytoplankton communities in the southwestern South Atlantic Ocean during spring. *Mar. Chem.* 267, 104472. doi: 10.1016/j.marchem.2024.104472

Kersalé, M., Meinen, C. S., Perez, R. C., Le Hénaff, M., Valla, D., Lamont, T., et al. (2020). Highly variable upper and abyssal overturning cells in the South Atlantic. *Sci. Adv.* 6, eaba7573. doi: 10.1126/sciadv.aba7573

Landschützer, P., Gruber, N., and Bakker, D. C. E. (2016). Decadal variationsand trends of the global ocean carbon sink. *Global Biogeochemical Cycles.* 0, 1396–1417. doi: 10.1002/2015GB005359

Lefèvre, N., Diverrès, D., and Gallois, F. (2010). Origin of CO2 undersaturation in the western tropical Atlantic. *Tellus B: Chem. Phys. Meteorology.* 62, 595–607. doi: 10.1111/j.1600-0889.2010.00475.x

Lefèvre, N., Veleda, D., and Hartman, S. E. (2023). Outgassing of dominates in the coastal upwelling off the northwest African coast. *Deep-Sea Res. Part I: Oceanographic Papers* 200, 104130. doi: 10.1016/j.dsr.2023.104130

Lencina-Avila, J. M., Ito, R. G., Garcia, C. A. E., and Tavano, V. M. (2016). Sea-air carbon dioxide fluxes along 35 S in the South Atlantic Ocean. *Deep Sea Res. Part I: Oceanographic Res. Papers.* 115, 175–187. doi: 10.1016/j.dsr.2016.06.004

Lima, C. R., Mendes, C. R. B., Tavano, V. M., Detoni, A. M. S., and Secchi, E. R. (2019). Chemotaxonomybased mapping of phytoplankton communities in the subtropical Southwestern Atlantic Ocean, with emphasis on the marine cyanobacterium *Trichodesmium*. *Prog. Oceanography*. 172, 77-88 doi: 10.1016/j.pocean.2019.01.008

Liu, M., and Tanhua, T. (2021). Water masses in the Atlantic Ocean: characteristics and distributions. *Ocean Science.* 17, 463–486. doi: 10.5194/os-17-463-2021

Liu, J., Wang, J., Wang, X., Zhou, Y., Hu, R., and Zhang, H. (2025). Research on Atlantic surface pCO2 reconstruction based on machine learning. *Ecol. Inf.* 87, 463–486. doi: 10.1016/j.ecoinf.2025.103094

Manta, G., Speich, S., Karstensen, J., Hummels, R., Kersalé, M., Laxenaire, R., et al. (2021). The South Atlantic meridional overturning circulation and mesoscale eddies in the first GO-SHIP section at 34.5°S. *J. Geophysical Research: Oceans* 126, e2020JC016962. doi: 10.1029/2020JC016962

Martínez-Moreno, J., Hogg, A.M., and England, M. H. (2022). Climatology, seasonality, and trends of spatially coherent ocean eddies. *J. Geophysical Research: Oceans* 127, e2021JC017453. doi: 10.1029/2021JC017453

Matthews, H. D., Tokarska, K. B., Nicholls, Z. R. J., Rogelj, J., Smith, C. J., and MacDougall, A. H. (2020). Opportunities and challenges in using remaining carbon budgets to guide climate policy. *Nat. Geoscience.* 13, 769–779. doi: 10.1038/s41561-020-00663-3

McGillicuddy, D. J. Jr., and Robinson, A. R. (1997). Eddy-induced nutrient supply and new production in the Sargasso Sea. *Deep Sea Res. Part I: Oceanographic Res. Papers* 44, 1427-1450. doi: 10.1016/S0967-0637(97)00024-1

Meinen, C. S., Garzoli, S. L., Perez, R. C., Campos, E., Piola, A. R., Chidichimo, M. P., et al. (2017). Characteristics and causes of Deep Western Boundary Current transport variability at 34.5° S during 2009–2014. *Ocean Sci.* 13, 175–194. doi: 10.5194/os-13-175-2017

Meinen, C. S., Speich, S., Perez, R. C., Dong, S., Piola, A. R., Garzoli, S. L., et al. (2013). Temporal variability of the Meridional Overturning Cir culation at 34.5° S: Results from two pilot boundary arrays in the South Atlantic. *J. Geophysical Research: Oceans* 118, 6461–6478. doi: 10.1002/2013JC009228

Meinen, C. S., Speich, S., Piola, A. R., Ansorge, I., Campos, E., Kersalé, M., et al. (2018). Meridional overturning circula tion transport variability at 34.5°S during 2009–2017: Baroclinic and barotropic f lows and the dueling influence of the boundaries. *Geophysical Res. Letters.* 45, 4180–4188. doi: 10.1029/2018GL077408

Möller, O. O. Jr, Piola, A. R., Freitas, A. C., and Campos, E. J. D. (2008). The effects of river discharge and seasonal winds on the shelf off Southeastern South America. *Continental Shelf Res.* 28, 1607–1624. doi: 10.1016/j.csr.2008.03.012

Moura-Falcão, R. H., Silva-Cunha, M. G. G., Borges, G. C. P., Ferreira, L. C., Farias, G. B., AlbergariaBarbosa, A. C. R., et al. (2024). Effects of environmental variability on phytoplankton structure, diversity and biomass at the Brazil-Malvinas Confluence (BMC). *Anais da Academia Bras. Ciências*. 96. doi: 10.1590/0001-3765202420230744

Nightingale, P. D., Liss, P. S., and Schlosser, P. (2000). Measurements of air-sea gas transfer during an open ocean algal bloom. *Geophysical Res. Letters.* 27, 2117–2120. doi: 10.1029/2000GL011541

Orselli, I. B. M., Goyet, C., Kerr, R., Azevedo, J. L. L., Araujo, M., Galdino, F., et al. (2019). The effect of Agulhas Eddies on absorption and transport of anthropogenic carbon in the South Atlantic Ocean. *Climate*. doi: 10.3390/cli7060084

Padin, X. A., Vázquez-Rodríguez, M., Castaño, M., Velo, A., Alonso-Pérez, F., Gago, J., et al. (2010). Air-Sea CO2 fluxes in the Atlantic as measured during boreal spring and autumn. *Biogeosciences.* 7, 1587–1606. doi: 10.5194/bg-7-1587-2010

Parc, L., Bellenger, H., Bopp, L., Perrot, X., and Ho, D. T. (2024). Global ocean carbon uptake enhanced by rainfall. *Nat. Geosci.* 17, 851–857. doi: 10.1038/s41561-024-01517-y

Pérez, F. F., Becker, M., Goris, N., Gehlen, M., López-Mozos, M., Tjiputra, J., et al. (2024). An assessment of CO_2 storage and sea-air fluxes for the Atlantic Ocean and Mediterranean Sea between 1985 and 2018. *Global Biogeochemical Cycles* 38, e2023GB007862. doi: 10.1029/2023GB007862

Pezzi, L. P., Souza, R. B., Acevedo, O., Wainer, I., Mata, M. M., Garcia, C. A., et al. (2009). Multiyear measurements of the oceanic and atmospheric boundary layers at the Brazil-Malvinas confluence region. *J. Geophysical Research: Atmospheres* 114, D19103. doi: 10.1029/2008JD011379

Pezzi, L. P., Souza, R. B. D., Dourado, M. S., Garcia, C. A. E., Mata, M. M., and Silva-Dias, M. A. F. (2005). Ocean-atmosphere in *situ* observations at the Brazil-Malvinas Confluence region. *Geophysical Res. Lett.* 32. doi: 10.1029/2005GL023866

Piola, A. R., Campos, E. J. D., Möller, O. O., Charo, M., and Martinez, C. M. (2000). Subtropical shelf front off eastern South America. *J. Geophysical Res.* 105, 6566–6578. doi: 10.1029/1999JC000300

Resplandy, L., Hogikyan, A., Müller, J. D., Najjar, R. G., Bange, H. W., Bianchi, D., et al. (2024). A synthesis of global coastal ocean greenhouse gas fluxes. *Global Biogeochemical Cycles* 38, e2023GB007803. doi: 10.1029/2023GB007803

Roobaert, A., Laruelle, G. G., Landschützer, P., Gruber, N., Chou, L., and Regnier, P. (2019). The spatiotemporal dynamics of the sources and sinks of CO2 in the global coastal ocean. *Global Biogeochemical Cycles*. 33, 1693–1714. doi: 10.1029/2019GB006239

Sabine, C. L., Feely, R. A., Gruber, N., Key, R. M., Lee, K., Bullister, J. L., et al. (2004). The oceanic sink for anthropogenic CO2. *Science*. 305, 367–371. doi: 10.1126/science.1097403

Sarmiento, J. L., and Gruber, N. (2006). *Ocean biogeochemical dynamics* (Princeton, NJ: Princeton University Press).

Schlitzer, R. (2021). Ocean Data View. Available online at: https://odv.awi.de (Accessed March 12, 2018).

Siddiqui, C., Rixen, T., Lahajnar, N., van der Plas, A. K., Louw, D. C., Lamont, T., et al. (2023). Regional and global impact of CO_2 uptake in the Benguela Upwelling System through preformed nutrients. *Nat. Commun.* 14, 2582. doi: 10.1038/s41467-023-38208-y

Silveira, I. C. A. d, Schmidt, A. C. K., Campos, E. J. D., Godoi, S. S. d, and Ikeda, Y. (2000). A corrente do Brasil ao largo da costa leste brasileira. *Rev. Bras. Oceanografia*. 48, 171–183. doi: 10.1590/S1413-77392000000200008

Smith, T. G., Nicholson, S.-A., Engelbrecht, F. A., Chang, N., Mongwe, N. P., and Monteiro, P. M. S. (2023). The heat and carbon characteristicsof modeled mesoscale eddies in the South–East Atlantic Ocean. *J. Geophysical Research: Oceans* 128, e2023JC020337. doi: 10.1029/2023JC020337

Souza, G. K., Von Ahn, C. M. E., Niencheski, L. F. H., and Andrade, C. F. F. (2021). Effects of coastal lagoon water level groundwater fluxes of nutrients to the coastal zone of southern Brazil. *J. Mar. Syst.* 213, 103459. doi: 10.1016/j.jmarsys.2020.103459

Takahashi, T., Olafsson, J., Goddard, J. G., Chipman, D. W., and Sutherland, S. C. (1993). Variação sazonal de CO2 e nutrientes nos oceanos superficiais de alta latitude: Um estudo comparativo. *Global Biogeochemical Cycles.* 7, 843–878. doi: 10.1029/93GB02263

Takahashi, T., Sutherland, S. C., Chipman, D. W., Goddard, J. G., Ho, C., Newberger, T., et al. (2014). Climatological distributions of pH, pCO2, total CO2, alkalinity, and CaCO3 saturation in the global surface ocean, and temporal changes at selected locations. *Mar. Chem.* 164, 95–125. doi: 10.1016/j.marchem.2014.06.004

Takahashi, T., Sutherland, S. C., Sweeney, C., Poisson, A., Metzl, N., Tilbrook, B., et al. (2002). Global sea–air CO2 flux based on climatological surface ocean pCO2, and seasonal biological and temperature effects. *Deep Sea Res. Part II: Topical Stud. Oceanography.* 49, 1601–1622. doi: 10.1016/S09670645(02)00003-6

Takahashi, T., Sutherland, S. C., Wanninkhof, R., Sweeney, C., Feely, R. A., Chipman, D. W., et al. (2009). Climatological mean and decadal change in surface ocean pCO2, and net sea–air CO2 flux over the global oceans. *Deep-Sea Res. Part II: Topical Stud. Oceanography.* 56, 554–577. doi: 10.1016/j.dsr2.2008.12.009

Talley, L., Pickard, G., Emery, W., and Swift, J. (2011). *Descriptive physical oceanography: an introduction* (Boston: Elselvier).

Villas Bôas, A. B., Sato, O. T., Chaigneau, A., and Castelão, G. P. (2015). The signature of mesoscale eddies on the air-sea turbulent heat fluxes in the South Atlantic Ocean. *Geophysical Res. Letters.* 42, 1856–1862. doi: 10.1002/2015GL063105

Wang, Z., Chen, G., Ma, C., and Liu, Y. (2023). Southwestern Atlantic oceans fronts detected from the fusion of the multi-source remote sensing data by a deep learning model. *Front. Mar. Sci.* 10. doi: 10.3389/fmars.2023.1140645

Wanninkhof, R. (1992). Relationship between wind speed and gas exchange over the ocean. *J. Geophysical Research: Oceans* 97, 7373–7382. doi: 10.1029/92JC00188

Wanninkhof, R. (2014). Relationship between wind speed and gas exchange over the ocean revisited. *Limnology Oceanography: Methods* 12, 351–362. doi: 10.4319/lom.2014.12.351

Weiss, R. F. (1974). Carbon dioxide in water and seawater: The solubility of a non-ideal gas. *Mar. Chem.* 2, 203–215. doi: 10.1016/0304-4203(74)90015-2

Weiss, R. F., and Price, B. A. (1980). Nitrous oxide solubility in water and seawater. *Mar. Chem.* 8, 347–359. doi: 10.1016/0304-4203(80)90024-9

frontiers | Frontiers in Marine Science

TYPE Original Research
PUBLISHED 06 October 2025
DOI 10.3389/fmars.2025.1606253

OPEN ACCESS

EDITED BY
Cecilia Chapa-Balcorta,
Universidad del Mar, Mexico

REVIEWED BY
Fiorella Prada,
Rutgers, The State University of New Jersey, United States
Francisco Medellín Maldonado,
National Autonomous University of Mexico, Mexico

*CORRESPONDENCE
Celeste Sánchez-Noguera
celeste.sancheznoguera@ucr.ac.cr

RECEIVED 04 April 2025
ACCEPTED 08 September 2025
PUBLISHED 06 October 2025

CITATION
Sánchez-Noguera C, Lange ID, Cortés J, Jiménez C, Wild C and Rixen T (2025) Environmental conditions and carbonate chemistry variability influencing coral reef composition along the Pacific coast of Costa Rica. *Front. Mar. Sci.* 12:1606253. doi: 10.3389/fmars.2025.1606253

Environmental conditions and carbonate chemistry variability influencing coral reef composition along the Pacific coast of Costa Rica

Celeste Sánchez-Noguera [1,2]*, Ines D. Lange [2,3], Jorge Cortés [1], Carlos Jiménez [4], Christian Wild [5] and Tim Rixen [2]

[1]Universidad de Costa Rica, Centro de Investigación en Ciencias del Mar y Limnología (CIMAR), San José, Costa Rica, [2]Leibniz Centre for Tropical Marine Research (ZMT), Bremen, Germany, [3]Faculty of Environment, Science and Economy, University of Exeter, Exeter, United Kingdom, [4]Enalia Physis Environmental Research Centre (ENALIA), Nicosia, Cyprus, [5]Marine Ecology Department, University of Bremen, Bremen, Germany

Coral reef development is influenced by a wide variety of factors, including temperature, salinity, nutrient concentrations, and carbonate chemistry. Studies focusing on physicochemical drivers of coral reef distribution and composition in the Eastern Tropical Pacific (ETP) are scarce, and carbonate chemistry and nutrient data for this region are limited. This study measured coral reef composition and physicochemical parameters along the Pacific coast of Costa Rica, over a one-year period at three locations: Santa Elena and Matapalo in the north, and Parque Nacional Marino Ballena in the south. Our results show high seasonal and spatial variability of physicochemical conditions with significant differences mainly explained by inorganic nutrient concentrations, with driving processes also having a strong influence on the variability of carbonate chemistry parameters. Coastal upwelling is the main driver of the seasonal variability in Santa Elena. Comparison of seasonal dissimilarity within locations confirms the presence of a geographical gradient, with stronger influence of the upwelling in Santa Elena relative to Matapalo, where several parameters displayed a lower seasonality and a carbonate system that supports reef development throughout the year. Conversely, in Marino Ballena the river discharges during rainy season exerted a strong control on the seasonal variability. The integrated analysis of coral reef composition and physicochemical parameters suggests that in addition to inorganic nutrients carbonate chemistry also plays a key role in coral distribution. Analyzing the spatial distribution of the main reef builders provides insights into the species-specific tolerance to varying conditions. *Pavona clavus* is widely distributed in both the northern and southern locations, suggesting that this massive coral is very tolerant to the high variability of physicochemical conditions. The dominant corals in the north (*Pavona gigantea* and *Pocillopora* spp.) are highly tolerant to nutrient-enriched cold waters with low aragonite saturation, while one of the main reef-builders in

southern locations (*Porites* cf. *lobata*) cope better with low salinity, low aragonite saturation and low light intensity caused by river discharges. Understanding the preferences of individual coral species at our study locations can shed light on the environmental factors driving coral reef distribution in other locations of the ETP.

KEYWORDS

coastal variability, coral reefs, drivers, Papagayo upwelling, Eastern Tropical Pacific

1 Introduction

Eastern Tropical Pacific (ETP) coral reefs extend from Mexico to northern Peru and are characterized by their small size and simple structure with discontinuous distribution. The relatively low diversity of corals in the ETP was increasingly attributed to the prevalence of extreme physical conditions along this coast (Dana, 1975; Cortés, 1997; Glynn et al., 2017a). Eastern boundary upwelling systems limit expansion of coral reefs in the north (California Upwelling system) and towards the south (Humboldt upwelling system). In between, major local wind-driven upwellings occur off Mexico in the Gulf of Tehuantepec, at the border between Nicaragua and Costa Rica in the Gulf of Papagayo (Papagayo upwelling) and in the Gulf of Panama (Panama upwelling). These wind-driven upwelling systems have a strong influence on the local physicochemical conditions in the ETP, particularly by lowering seawater temperature and increasing the availability of chlorophyll and inorganic nutrients (Fiedler and Talley, 2006; Lavín et al., 2006). Although less studied, it is also known that they drive changes in carbonate chemistry parameters. For example, during dry season the Panama upwelling produces a significant increase in total alkalinity (TA) and total dissolved inorganic carbon (DIC) of coastal waters in the Gulf of Panama, with the subsequent significant decrease in pH and aragonite saturation state (Ω_a) (Manzello et al., 2008; Manzello, 2010b). Only one study carried out over a 29-hour period in 2009 has measured carbonate chemistry parameters within the Gulf of Papagayo, reporting a sharp decrease in DIC, pH and Ω_a during the development of an upwelling event (Rixen et al., 2012). Additionally, the climate anomaly El Niño Southern-Oscillation (ENSO) strongly influences the upwelling conditions in the ETP (Fiedler and Lavín, 2017; Glynn et al., 2017b). During negative ENSO episodes known as El Niño, upwelling weakens, causing seawater temperatures to increase above the average. In the past, ENSO-induced warming events have caused bleaching and significant coral mortality in the Gulf of Papagayo (Jiménez et al., 2001). Conversely, positive ENSO episodes referred to as La Niña intensify local upwelling conditions.

Along the Pacific coast of Costa Rica, coral reef formations are restricted to northern and southern locations (Cortés and Jiménez, 2003; Cortés et al., 2010; Cortés, 2016), while in the middle sections of the littoral scleractinian corals appear as single colonies or in sparse coral communities. Near the coastline, branching corals of the genus *Pocillopora* built important reef structures in northern locations within the Gulf of Santa Elena and Gulf of Papagayo (Jiménez, 1997, 2001a; Jiménez et al., 2010; Méndez-Venegas et al., 2021), and smaller patch reefs in southern locations near Corcovado and Golfo Dulce (Guzmán and Cortés, 1989; Cortés, 1990; Cortés and Jiménez, 1996). The presence of massive species varies from north to south, with *Pavona gigantea*, *Pavona clavus* and *Gardineroseris planulata* as the main reef builders in the north, while *Porites* cf. *lobata* is the main reef-building coral in the south (Cortés, 1990; Jiménez, 2001a; Alvarado et al., 2005).

This observed longitudinal coral distribution (summarized by Cortés and Jiménez, 2003; Glynn et al., 2017a) raises the question of which environmental driver(s) regulate the reef development along this gradient. To address this question, we measured total alkalinity (TA), dissolved inorganic carbon (DIC), temperature, salinity and inorganic nutrient concentrations at three locations along the coast during the dry and rainy season. The selection of these physicochemical parameters responds to their natural variability along this coast due to different processes. For instance, seawater temperature, nutrients and carbonate chemistry are influenced by the Papagayo upwelling, which strongly affects northern locations (Alfaro et al., 2012; Fernández-García et al., 2012; Rixen et al., 2012). In contrast, seasonal changes in river runoff, which impact the southernmost locations, are likely to have a greater effect on nutrient concentrations and salinity (Alvarado and Aguilar, 2009; Alvarado et al., 2009), and likely in the carbonate chemistry during rainy season. In addition to the five physicochemical parameters measured during the study, percentages of benthic community composition were quantified in coral reefs at each location. The main goal of this study was to identify the key physicochemical factors controlling coral reef distribution and species composition at the local scale. Moreover, the specific objective of characterizing seawater carbonate chemistry will enhance baseline information within the ETP. The compiled data allowed the spatial and seasonal comparison of physicochemical conditions and coral reef status, to elucidate which factors can be controlling the differences of the benthic community structure along the Costa Rican Pacific coast.

2 Materials and methods

2.1 Study locations

To answer our research question about the environmental drivers controlling coral reef development and distribution along the Costa Rican Pacific coast, three study locations were chosen based on the presence of coral reefs, which are restricted to northern and southern locations (Cortés and Jiménez, 2003; Cortés et al., 2010; Cortés, 2016): Santa Elena and Matapalo in the north and Parque Nacional Marino Ballena in the south (also referred to as Marino Ballena in this paper) (Figure 1). The number of sampling sites in each location was determined by the presence of coral reef formations. A total of four reefs were selected in Santa Elena (Bajo Rojo: 10.95769, -85.73400; Matapalito: 10.93633, -85.79385; Pochote: 10.93151, -85.80002; Cabros: 10.942267, -85.81363), one in Matapalo (10.53922, -85.76553) and three in Marino Ballena (Tómbolo: 9.14481, -83.75819; Bajo Mauren: 9.11258, -83.74092; Tres Hermanas: 9.10408, -83.70686) (Table 1).

Most coral reefs in northern locations are directly exposed to the seasonal upwelling of Papagayo and are built by branching species (*Pocillopora* spp.), although there are also reefs that consist of massive corals (*Pavona* spp.) (Cortés, 1997; Jiménez, 1997, 2001a; Cortés et al., 2010). Two of the study locations selected for this project are located within the Gulf of Papagayo, as both display important reef formations built by different coral species. In southern locations, where the seasonal upwelling is absent, Marino Ballena features several coral communities and coral reefs built by *Porites* cf. *lobata* and *P. clavus* (Alvarado et al., 2005, 2006; Cortés et al., 2010). Golfo Dulce, which is also located in the south and has coral reefs primarily built by *Porites* cf. *lobata* (Cortés, 1990), was intentionally excluded from this study. The reason relies on the fact that Golfo Dulce is a tectonic basin with an anoxic layer (Vargas-Zamora et al., 2021), therefore this unique oceanographic

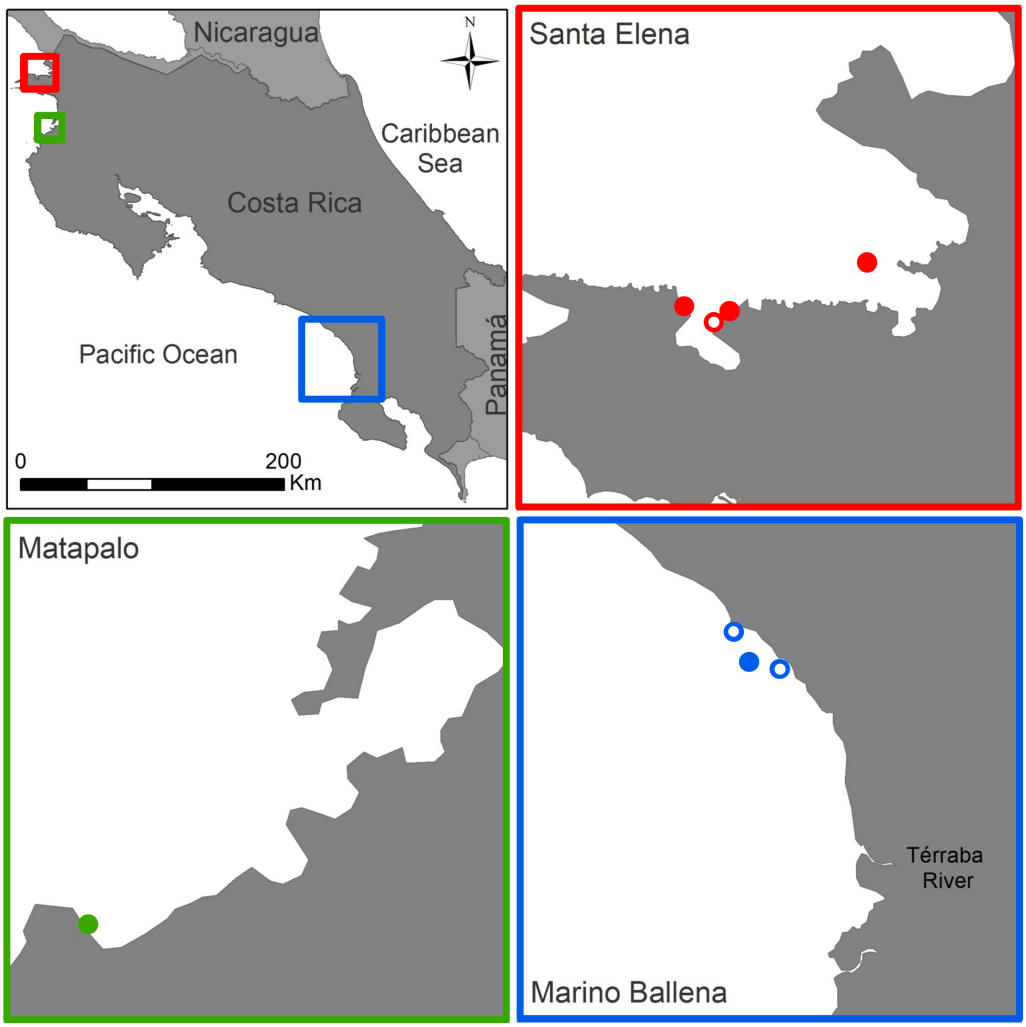

FIGURE 1
Study areas. Studied locations along the north (Santa Elena, Matapalo) and south (Marino Ballena) Pacific coast of Costa Rica. Circles indicate the sampling reefs in each location (close = water sampling + benthic survey, open = only water sampling).

10.3389/fmars.2025.1606253

TABLE 1 Samples were collected for eight consecutive days in each location over rainy (July-August 2013) and dry (January-February 2014) season. The reefs sampled are listed in each location and sampling dates are displayed in square brackets.

Location/ reefs	Non-upwelling [rainy season 2013]	Upwelling [dry season 2014]	Total
Santa Elena - Bajo Rojo - Matapalito - Pochote - Cabros	[7–14 August] 31 13 15 16	[5–13 February] 31 16 9 7	138
Matapalo	[29 July-5 August] 32	[20-21 & 23–28 January] 28	60
Marino Ballena (3) - Tombolo - Bajo Mauren - Tres Hermanas	[18–25 August] 18 30 28	[10–15 January] 9 9 9	103

Samples were collected for eight consecutive days in each location over rainy (July-August 2013) and dry (January-February 2014) season. The reefs sampled are listed in location and sampling dates are displayed in square brackets.

condition would have made challenging its comparison with the other locations.

The climate on the Pacific coast of Costa Rica features two well defined seasons, although their timing shows slight variations by location. In the north Pacific, the dry season runs from December to March while the rainy season occurs from May to November (Cambronero-Solano et al., 2021). In contrast, the dry season in the south Pacific is somewhat shorter, lasting from January to March, with the rainy season extending from May to December (Instituto Metereológico Nacional (IMN), 2008). In both regions April serves as a transition period between seasons. In the Gulf of Papagayo, major changes in seawater temperature, nutrient concentration and other physicochemical parameters occur mostly in pulses during the development of the upwelling events over the dry season (Alfaro et al., 2012; Fernández-García et al., 2012; Stuhldreier et al., 2015; Cambronero-Solano et al., 2021). Santa Elena is located in the northernmost section of this gulf and is thought to experience a strongest influence from the seasonal upwelling compared to Matapalo, which is located in the southernmost section of Papagayo. A previous study compared the seasonal changes of physicochemical parameters between these locations, reporting that the upwelling intensity is greater in Santa Elena than in Matapalo, characterized by a decrease in seawater temperature and increase in inorganic nutrient concentrations during the dry season (Stuhldreier et al., 2015). Conversely, during the dry season in Marino Ballena, seawater temperature and salinity increase, while the rainy season leads to higher sedimentation and nutrient levels, along with decreased seawater temperature and salinity (Alvarado and Aguilar, 2009; Alvarado et al., 2009).

Fieldwork for this research was conducted under the research permits No. 028-2013-SINAC and No. SINAC-SE-GASP-PI-R-096-2013, issued by the Sistema Nacional de Áreas de Conservación (SINAC), Ministry of the Environment, Costa Rica.

2.2 Water sampling

The seawater sampling was designed to capture the variability of physicochemical parameters in each location, not within reefs. At each location, water samples were collected during rainy (July-August 2013) and dry (January-February 2014) season (Table 1). Being aware that the Papagayo upwelling is wind-driven and can fluctuate significantly on weekly or daily timescales, the season sampling at each location was conducted during several days in a row. The sampling period per season ranged between 6–8 days in each location, depending on logistics, with the number of sampling days as replicates per season. When possible, samples in each reef were collected at two different tides and depths per day. Sampling depth ranged from 0.5 m below the surface to 11 m, based on the reef depth, tide and sea conditions. Sampling depth was not consistent across reefs, because water column depth varied with the tide range and the sampling hour. Samples were collected at different times of the day, from 05:30 to 16:30, depending on the tide cycles. The sampling was carried out as close as possible to the tide's peak, but there was a variability in the time of sampling due to the distance between reefs (time required to move from one reef to the next one) and other logistics. In some specific dates, not all reefs were sampled in Santa Elena or Marino Ballena, due to restrictive working conditions such as rough sea or fishing gear deployed near the reef. Additionally, in particular days, samples were collected only at one depth (near the surface or bottom indistinctly) or one tide (low or high indistinctly), due to limited amount of sampling bottles, the availability of boats for sampling (in Matapalo and Marino Ballena most sampling was done taking advantage of touristic trips), the navigation conditions or the distance between reefs.

Sampling was carried out with a 10 L volume Niskin bottle following best practices guidelines for ocean CO_2 measurements (Dickson et al., 2007). Discrete water samples for determination of carbonate chemistry parameters were collected in 250 mL air-tight borosilicate bottles, fixed immediately after collection with 200 µL of a 50% saturated $HgCl_2$ solution (35 g L^{-1} $HgCl_2$) and stored cold until analysis. Nutrient samples were filtered in the field through a 0.45 ?m pore size filter and frozen until analysis. Samples for salinity determination were collected in 50 mL plastic bottles and measured in the laboratory with a WTW probe (Cond3310). Seawater temperature (SWT) was measured *in situ* with HOBO®Pendant Temperature data loggers at Bajo Rojo and Matapalo (10–15 min intervals in dry season between December 2013 and January 2014 and every 30 min during rainy season). The SWT value used was the one recorded the closest to the seawater sampling time. In all the other reefs (Cabros, Matapalito, Pochote, Tómbolo, Tres Hermanas and Bajo Mauren) SWT was also measured *in situ*, with a WTW probe (Cond3310).

2.3 Reef surveys

To characterize the composition of the benthic community and the main coral reef builders at each location, percentages of benthic coverage were quantified across several reefs. Benthic surveys were carried out at three reefs in Santa Elena (Bajo Rojo, Matapalito, Cabros), one in Matapalo (Matapalo) and one in Marino Ballena (Bajo Mauren) (Figure 1). Due to fieldwork logistics and the fact that we did not intend to study the temporal changes in benthic community composition, reef surveys were conducted at one time point during dry season (Table 2). Data from different reefs were averaged by location. Benthic surveys were conducted following the chain method (Rogers et al., 1994) with five replicates per transect. A 10 m length chain with a known number of links (n = 532) was laid on top of the reef following its contours; nine categories (live coral at species level, dead coral, bleached coral, macroalgae, coralline algae, turf algae, substrate, cyanobacteria and others) were used to quantify the benthic composition under each link. Afterwards, the corresponding number of links for each category was converted to relative benthic cover.

2.4 Laboratory measurements

Total alkalinity (TA) and dissolved inorganic carbon (DIC) were measured with a VINDTA 3C system (Versatile instrument for the determination of total dissolved inorganic carbon and titration alkalinity), coupled with a UIC CO_2 coulometer (model CM5015) and a METROHM©Titrino (model 716 DMS). Instruments were calibrated with Dickson Certified Reference Material (Batch 127) (Dickson et al., 2003). The pH, aragonite saturation state (Ω_a) and fCO_2 were calculated with CO2SYS as a function of measured parameters (TA, DIC, salinity, nutrients and SWT), with dissociation constants of Mehrbach et al. (1973) for carbonic acid as refit by Dickson and Millero (1987), and Dickson (1990) for boric acid.

Five inorganic nutrients (phosphate, PO_4^{3-}; silicate, $SiO(OH)_3^-$; ammonium, NH_4^+; nitrite, NO_2^- and nitrate, NO_3^-) were measured through a reagent-based method with a Lachat'sQuikChem© 8500 Series 2 Flow Injection Analysis (FIA) System, following the Standard Operation Procedure from Centro de Investigación en Ciencias del Mar y Limnología (CIMAR) of the University of Costa Rica (PON Nut-08).

TABLE 2 Surveys were carried out in dry season between January and February 2014, with 10 m length chain transects and five replicates per site. The location of each reef is noted in squared brackets; SE = Santa Elena; MAT = Matapalo; MB = Marino Ballena. See Figure 1 for reference of study locations.

Reef	Sampling period	Transects (n)
Bajo Rojo [SE]	February 2014	5
Matapalito [SE]	February 2014	5
Cabros [SE]	February 2014	5
Matapalo [MAT]	February 2014	5
Bajo Mauren [MB]	January 2014	5

Surveys were carried out in dry season between January and February 2014, with 10 m length chain transects and five replicates per site. The location of each reef is noted in squared brackets; SE, Santa Elena; MAT, Matapalo; MB, Marino Ballena. See Figure 1 for reference of study locations.

2.5 Meteorological data

Meteorological data (rainfall and wind speed) were provided by the Instituto Meteorológico Nacional, from two stations located in the North Pacific (Santa Rosa and Liberia) and two in the South Pacific (Barú and Damas). Wind speed (m/s) and rainfall (mm) data used in this study corresponded to the same dates as the seawater sampling. Wind speed data corresponds to hourly averages and rainfall to daily values measured at each station. The values of wind speed used in this study corresponded to hourly averages closest to the seawater sampling time, and for rainfall values we used the daily value.

2.6 Data analysis

For a general comparison of the physicochemical and meteorological conditions during this study, all values were averaged by location and season (Supplementary Table S1). General statistical differences of physicochemical and meteorological parameters between locations (annual scale) and season were tested by Kruskal-Wallis. For statistical comparisons of carbonate chemistry, we used the salinity-normalized values (nTA, nDIC) (Equation 1):

$$nTA = TA \times \frac{35}{S} \qquad nDIC = DIC \times \frac{35}{S} \qquad (1)$$

where S is the measured salinity value of the sample.

Spatial and temporal variations in physicochemical parameters, as well as benthic community composition, were analyzed using the software programs PRIMER 7, R and PAST. The meteorological data was excluded from these statistical analyses and we expand on this at the end of this section. Moreover, to characterize the variability of the physicochemical conditions of the water column at each location, samples collected at different depths during the same tide were averaged together for each reef, as the sampling depth varied across the reefs. This averaging strategy avoid losing the seasonal replication of measured (SWT, salinity, phosphate, nitrate, nitrite, silicate, ammonium, TA, DIC) and calculated (pH, fCO_2, Ω_a) physicochemical parameters. Prior to analysis, the physicochemical parameters were log-transformed and standardized, and resemblance matrices were built using Euclidean distances. Differences in physicochemical parameters among locations and seasons were tested with a nested Permutational Multivariate Analysis of Variance (PERMANOVA), including season, location and tide as fixed factors, and reef as a random factor nested within location. Additionally, when the main test indicated significant differences,

PERMANOVA pairwise comparisons were conducted. A Similarity Percentage Analysis (SIMPER) was also performed to identify which parameters contributed the most to the observed differences between locations and seasons. To visualize patterns in physicochemical parameters, box-plots and Principal Component Analysis (PCA) were used.

To estimate the general contribution of the main processes driving the carbonate chemistry in our study locations on an annual basis, we did a simple linear regression analysis for each location and used an approach proposed by other authors (Albright et al., 2013); considering that net organic carbon production (photosynthesis-respiration) and net inorganic carbon production (calcification-dissolution) affect TA and DIC differently (Suzuki and Kawahata, 2004). According to the theoretical stoichiometric relationship between these processes and TA and DIC, for every mole of calcium carbonate ($CaCO_3$) produced, DIC decreases by two moles and TA decreases by one mole. In contrast, for every mole of organic carbon produced via photosynthesis, one mole of DIC is consumed while TA remains unchanged (Albright et al., 2013). Therefore, the slope of the simple linear regression (nDIC vs. nTA) indicates the general balance between the net inorganic and organic carbon production at each location. The ratio between these processes (inorganic carbon production:organic carbon production) is given by Equation 2, where m is the slope of the nDIC-nTA relationship (Albright et al., 2013):

$$Inorganic\ \ C\ \ production : Organic\ \ C\ \ production = \frac{1}{(2/m) - 1} \quad (2)$$

In Equation 2, a ratio < 1 points out to a system mainly controlled by organic processes. Conversely, a ratio > 1 indicates that inorganic processes are the main drivers of the system. Further data is needed to identify which specific processes (photosynthesis, respiration, calcification or dissolution) control the overall carbonate system, but this falls outside the objectives of this study.

For analysis of the benthic community composition, differences in percentages of benthic coverage between locations were tested with a nested PERMANOVA, including location as fixed factor and reef as a random factor nested within location. To reduce the influence of dominant taxa, benthic coverage data were fourth-root transformed prior to calculating a Bray-Curtis resemblance matrix. Average coverage values for each benthic category were calculated per location, followed by estimations of the Shannon-Wiener diversity index (H') and Pielou's evenness (J') to evaluate community diversity and distribution.

Finally, it is important to note that meteorological data were obtained from the nearest inland stations to our study areas, which do not measure the exact conditions at our sampling locations. Santa Rosa meteorological station (10.84111, -85.61944) for example, is about 20 km southeast from Santa Elena; Liberia station (10.83889, -85.55222) is about 25 km west from Matapalo; while Barú station (9.27139, -83.88139, rainfall) and Damas station (09.49528, -84.21472, wind speed) are located about 18 km and 70 km northwest from Marino Ballena, respectively. For this reason, we have used wind speed and rainfall data to explain general patterns and tendencies during sampling periods, but not for direct statistical correlations with the physicochemical parameters. Statistical differences of meteorological conditions between locations and season were tested by Kruskal-Wallis.

3 Results

3.1 Environmental parameters

Results of the nested PERMANOVA indicate that physicochemical conditions are significantly different between locations (Pseudo-F = 45.77, P(perm) = 0.003, perms = 8769) and between seasons (Pseudo-F = 38.63, P(perm) < 0.001, perms = 9941). Conversely, tide (Pseudo-F = 0.25, P(perm) = 0.779, perms = 9949) and reef (Pseudo-F = 1.28, P (perm) = 0.201, perms = 9899) did not have a significant effect in these parameters, suggesting that the tide cycle is not relevant for the changes in physicochemical conditions and that the variability within each location is not as important as the variability between locations and seasons. A comparison of the variability of physicochemical conditions on the annual scale indicates that within northern locations, Santa Elena reefs are exposed to a high variation with extreme values either end (Figure 2, Supplementary Table S1); while the variability in Matapalo is lower, particularly for salinity, temperature and carbonate chemistry parameters.

Pairwise tests suggest that the strongest differences in physicochemical conditions occur between the northernmost and the southernmost location (Pseudo-t = 9.53, P(perm) = 0.013, perms = 4322). Santa Elena displays the greatest internal variability, whereas Marino Ballena exhibits the most homogeneous conditions. Seasonal comparisons indicate significant differences between the rainy and the dry season (Pseudo-t = 6.22, p < 0.001, perms = 9940), with physicochemical parameters showing more heterogenous conditions during the dry season.

Average (± standard deviation) of measured parameters by location, independent of seasons, showed that in the northernmost location (Santa Elena) the coastal waters are cooler (25.3 ± 3.3 °C, H = 45.79, p < 0.001) and more saline (34.3 ± 0.8 psu, H = 131.03, p < 0.001), whilst at the southernmost location (Marino Ballena) coastal waters have a lower salinity (29.4 ± 1.7 psu, H = 131.03, p < 0.001) (Supplementary Tables S1, S2). Concentrations of PO_4^{3-} (H = 27.18, p < 0.001) and NO_3^- (H = 10.08, p = 0.006) were highest in Santa Elena, whereas Marino Ballena held the highest average concentrations of $SiO(OH)_3^-$ (H = 66.06, p < 0.001) and NO_2^- (H = 75.87, p < 0.001) (Supplementary Tables S1, S2). The average nTA values in Santa Elena and Matapalo (< 2300 µmol kg^{-1}) were lower than in Marino Ballena (> 2300 µmol kg^{-1}) (H = 109.31, p < 0.001). On the other hand, in Santa Elena and Marino Ballena annual average nDIC showed concentrations of > 2000 µmol kg^{-1} whereas nDIC concentrations were lower in Matapalo (< 2000 µmol kg^{-1}) (H = 57.95, p < 0.001) (Supplementary Tables S1, S2).

According to the PCA (Figure 3), five main water parameters explained 82.6% of the variance of the physicochemical conditions. Nitrate (0.663), phosphate (0.583) and ammonium (0.303)

10.3389/fmars.2025.1606253

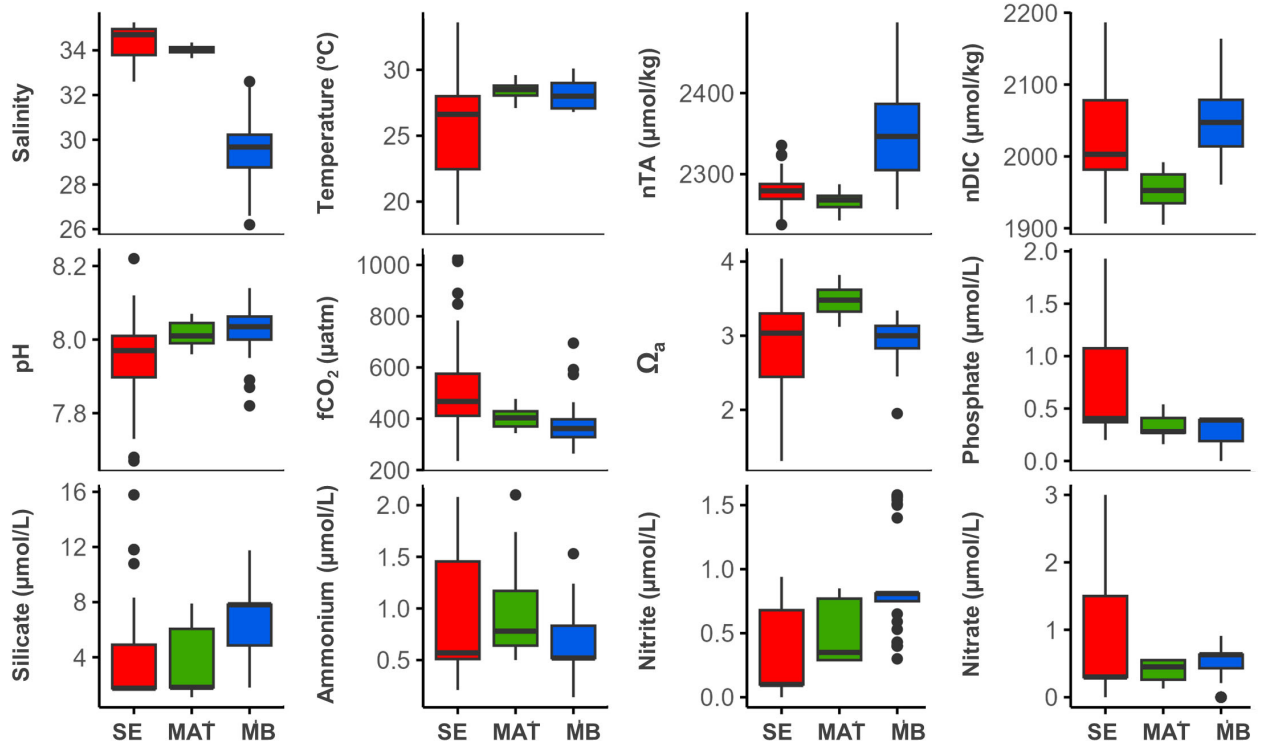

FIGURE 2
Variability of physicochemical conditions along the Pacific coast of Costa Rica. Annual mean values of physicochemical parameters from the study locations indicate a high spatial variability in seawater conditions, related to the distance from the upwelling of Papagayo. SE = Santa Elena; MAT = Matapalo; MB = Marino Ballena. See Figure 1 for the study locations.

contributed 57.2% to the variance (PC1); whilst nitrite (-0.829), phosphate (0.381) and silicate (-0.375) explained a further 25.4% (PC2). These findings were supported by SIMPER analysis, which identified the same five inorganic nutrients as the primary contributors to the observed differences between locations and seasons. According to the comparison between locations, the highest dissimilarity was found between the northernmost (Santa Elena) and the southernmost (Marino Ballena) location (average squared distance = 0.98), primarily driven by phosphate (28.23%), nitrite (27.94%) and nitrate (24.64%), with Santa Elena showing elevated phosphate and nitrate concentrations, whereas Marino Ballena exhibited higher nitrite levels. Meanwhile, there was a moderate dissimilarity (average squared distance = 0.83) between northern locations (Santa Elena and Matapalo), with nitrate (33.02%), phosphate (30.59%) and nitrite (16.17%) contributing nearly to 80% of the observed differences. Nutrient concentrations were generally higher at Santa Elena, except for nitrite, which was slightly greater at Matapalo. In contrast, Matapalo and Marino Ballena showed the lowest dissimilarity (average squared distance = 0.37), mainly due to differences in nitrite (38.32%), silicate (20.14) and ammonium (17.22%), all of which had higher concentrations at Marino Ballena. The SIMPER analysis between seasons indicated that three inorganic nutrients - nitrate (28.19%), phosphate (26.74%) and nitrite (21.56%) – are the primary contributors to the observed seasonal differences. Together, they accounted for over 76% of the dissimilarity between seasons, with notably higher concentrations during the dry season.

The PERMANOVA results also revealed a significant interaction between location and season (Pseudo-F = 54.86, P(perm) < 0.001, perms = 9960), indicating that the effect of the season on the physicochemical conditions is not equal in all locations. Pairwise test confirms this result, with the higher variability taking place during dry season in Santa Elena (Pseudo-t = 11.77, P(perm) = 0.026, perms = 7446) and Matapalo (Pseudo-t = 5.91, $p < 0.001$, perms = 9961). In Marino Ballena, the Pseudo-t value (8.95) also indicates a strong separation in physicochemical conditions between seasons. This difference is statistically significant based on the Monte Carlo p-value (P(MC) < 0.001, perms = 360), although permutation testing (P(perm) = 0.084, perms = 360) offers contradictory results, likely due to the limited permutation count which might affect robustness. SIMPER analysis revealed that seasonal dissimilarity within each location followed a decreasing gradient from north to south, with values of 1.69 for Santa Elena, 0.40 for Matapalo, and 0.31 for Marino Ballena.

During the dry season Santa Elena experienced an increase in salinity ($H = 44.38$, $p < 0.001$), nTA ($H = 17.83$, $p < 0.001$) and nDIC ($H = 48.21$, $p < 0.001$) as well as a sharp drop in SWT ($H = 65.34$, $p < 0.001$). At Marino Ballena the increase of nTA ($H = 35.781$, $p < 0.001$) and nDIC ($H = 33.12$, $p < 0.001$) during the rainy season was accompanied by a slight decrease of salinity ($H = 17.31$, $p < 0.001$) and SWT ($H = 48.26$, $p < 0.001$). Conversely, salinity ($H = 0.17$, p =

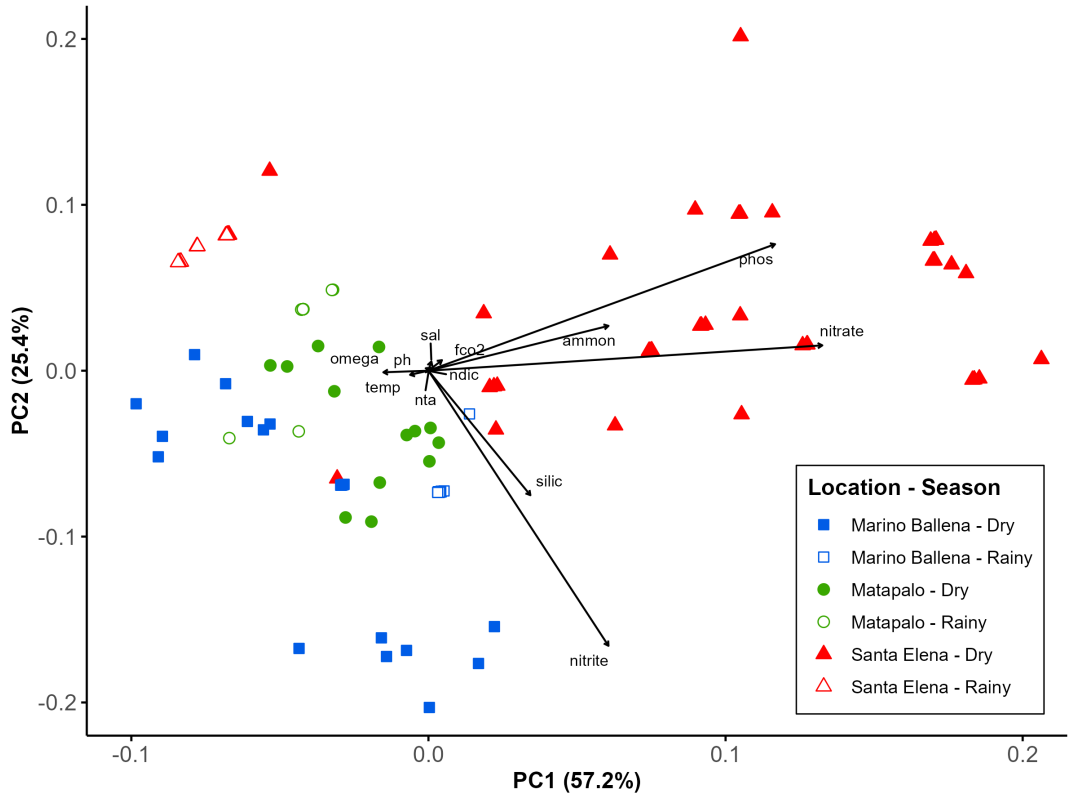

FIGURE 3
Spatial and temporal variation of physicochemical parameters. Seasonal sampling data from rainy season 2013 (July-August) and dry season 2014 (January-February) were analyzed by location and season based on Principal Component Analysis (PCA). The distance between data points indicates their similarity in seawater conditions. PC1 correlates positively to nitrate (0.663), phosphate (0.583) and ammonium (0.303). PC2 correlates positively to phosphate (0.381) and negatively nitrite (-0.829) and silicate (-0.375).

0.677), nTA (H = 0.76, p = 0.382) and nDIC (H = 0.68, p = 0.409) remained similar during both seasons in Matapalo (Supplementary Tables S1, S3).

The simple linear regression analysis of salinity-normalized values (nDIC vs. nTA) (Figure 4) indicates that Marino Ballena had higher nTA than the other locations, with a steep increase in nTA and nDIC during the rainy season. Santa Elena was the location with the highest nDIC values occurring specifically during the dry season. Measured parameters in Matapalo were the lowest and had similar values during both seasons, overlapping with values measured in Santa Elena during the rainy season. The estimated ratios between inorganic and organic carbon production (Equation 2) were lower in the northern locations, with values of 0.04 in Santa Elena and 0.18 in Matapalo. The estimated inorganic: organic production ratio in Marino Ballena was 0.88.

Meteorological parameters measured near Marino Ballena during the sampling period indicate that this was the location with the lowest wind speeds on the annual scale (1.3 ± 0.7 m s^{-1}, H = 56.33, p < 0.001) and highest rainfall during the rainy season (24.9 ± 12.9 mm day^{-1}, H = 49.28, p < 0.001) (Supplementary Tables S1-S3). The data obtained from the Liberia meteorological station show that Matapalo was the other extreme, with highest wind speeds during the dry season (7.1 ± 3.2 m s^{-1}, H = 6.74, p = 0.009) and lowest rainfall during the rainy season (1.1 ± 1.9 mm day^{-1}, H = 6.77, p = 0.009) (Supplementary Tables S1-S3). Near to Santa Elena, the annual average values of wind speeds and rain were 2.3 ± 1.3 m s^{-1} and 1.8 ± 3.6 mm day^{-1}, respectively (Supplementary Tables S1, S2).

3.2 Benthic community composition

In all locations, the category "Bleached" accounted for less than 0.2% of benthic coverage, and was excluded from the graphical representation of the percentages of benthic cover (Figure 5). Results from the nested PERMANOVA revealed no significant differences in benthic coverage between locations (Pseudo-F = 0.313, P(perm) = 1.000, perms = 10). In contrast, comparisons within each location indicated significant variation in benthic composition among reefs (Pseudo-F = 19.654, P(perm) = 0.000, perms = 9953). However, findings from within-location comparisons will not be discussed further, as Santa Elena was the only location where more than one reef was surveyed. Regarding benthic composition categories, richness (S) was consistent across all locations. Diversity (H') showed similar values in northern locations, with slightly higher levels in Marino Ballena. Evenness (J') was comparable between Matapalo and Marino Ballena, but somewhat lower in Santa Elena (Table 3). Reefs in Santa Elena were mainly composed of live coral (43.37 ± 38.11%), turf (27.67 ± 27.53%), coralline algae (17.24 ± 14.41%) and substrate (11.37 ±

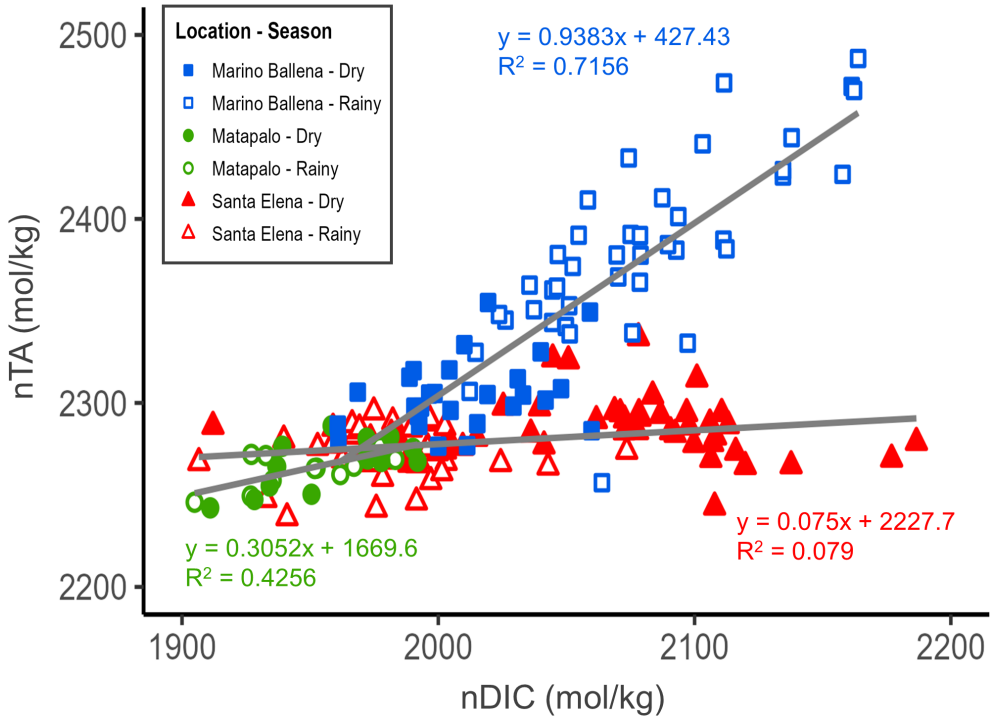

FIGURE 4
Seasonal variation of carbonate chemistry in three locations at the Pacific coast of Costa Rica. Total alkalinity (TA) and dissolved inorganic carbon (DIC) were normalized to a salinity of 35 (Equation 1). The slope of the nDIC-nTA relationship indicates the balance between the inorganic (calcification-dissolution) and organic processes (photosynthesis-respiration). The ratio between inorganic carbon production:organic carbon production is given by Equation 2.

14.96%). Matapalo reef had three dominant categories, live coral (41.39 ± 15.67%), coralline algae (31.50 ± 5.43%) and turf (20.94 ± 6.10%). In the reef evaluated in Marino Ballena the three dominant categories of the benthic composition were coralline algae (44.02 ± 20.19%), live coral (25.71 ± 10.44%) and substrate (13.80 ± 29.29%). Macroalgae were only observed in Santa Elena (0.08 ± 0.21%) and Matapalo (4.92 ± 9.99%). Cyanobacteria were present in all locations but had a very low coverage; with the highest quantified value in Marino Ballena (3.20 ± 2.08%) (Figure 5A). Regarding scleractinian corals, all locations showed low diversity indexes (H') with values < 1.0, suggesting that these coral reefs are built by few species (Table 3). The reefs in the north were mainly built by *P. gigantea* and *Pocillopora* spp., whereas southern reefs are built by *P. clavus* and *P.* cf. *lobata* with minor contribution of *Porites panamensis* and *Psammocora stellata* (Figure 5B). Matapalo was the location with lower coral diversity (Table 3), with *Pocillopora* sp. as the dominant reef builder (Figure 5B).

4 Discussion

4.1 Evidence of geographical and seasonal variability in the physicochemical conditions along the Pacific coast of Costa Rica

This study shows high spatial variability in the physicochemical parameters on coral reefs along the Costa Rican Pacific coast (Figure 2), and their seasonality seems to be controlled by different processes in each location. The Papagayo upwelling is the main driver of seasonal variability in water parameters in the north, while the rainfall during rainy season controls the variability in the south (Figure 3). Complementing previous studies that described the physical conditions caused by this coastal upwelling (Jiménez, 2001b; Fernández-García et al., 2012), our results show that the changes extend beyond a decrease in SWT and an increase in nutrient concentrations. The Papagayo coastal upwelling is also marked by an increase in nDIC, with the corresponding decline in pH and aragonite saturation state (Ω_a) (Figure 4, Supplementary Table S1). Data from this study furthermore confirms the findings of a parallel survey conducted within the same research project which found a geographical gradient in the upwelling intensity between Santa Elena and Matapalo (Stuhldreier et al., 2015), with a greater range in the variability of physicochemical parameters in Santa Elena and a relatively low seasonality in Matapalo (Figures 2, 3, Supplementary Table S1). Therefore, we can affirm that in northern locations the variability in physicochemical parameters depends on the distance from the coastal upwelling. Our results allow comparisons not only within northern locations but also with southern reefs. In the following sections we will discuss the individual environmental parameters and their spatial and seasonal variability in more detail.

4.1.1 Seawater temperature and salinity

The SWT exhibits a reverse seasonality between northern (Santa Elena and Matapalo) and southern (Marino Ballena) locations. Coastal waters in the north are colder from December

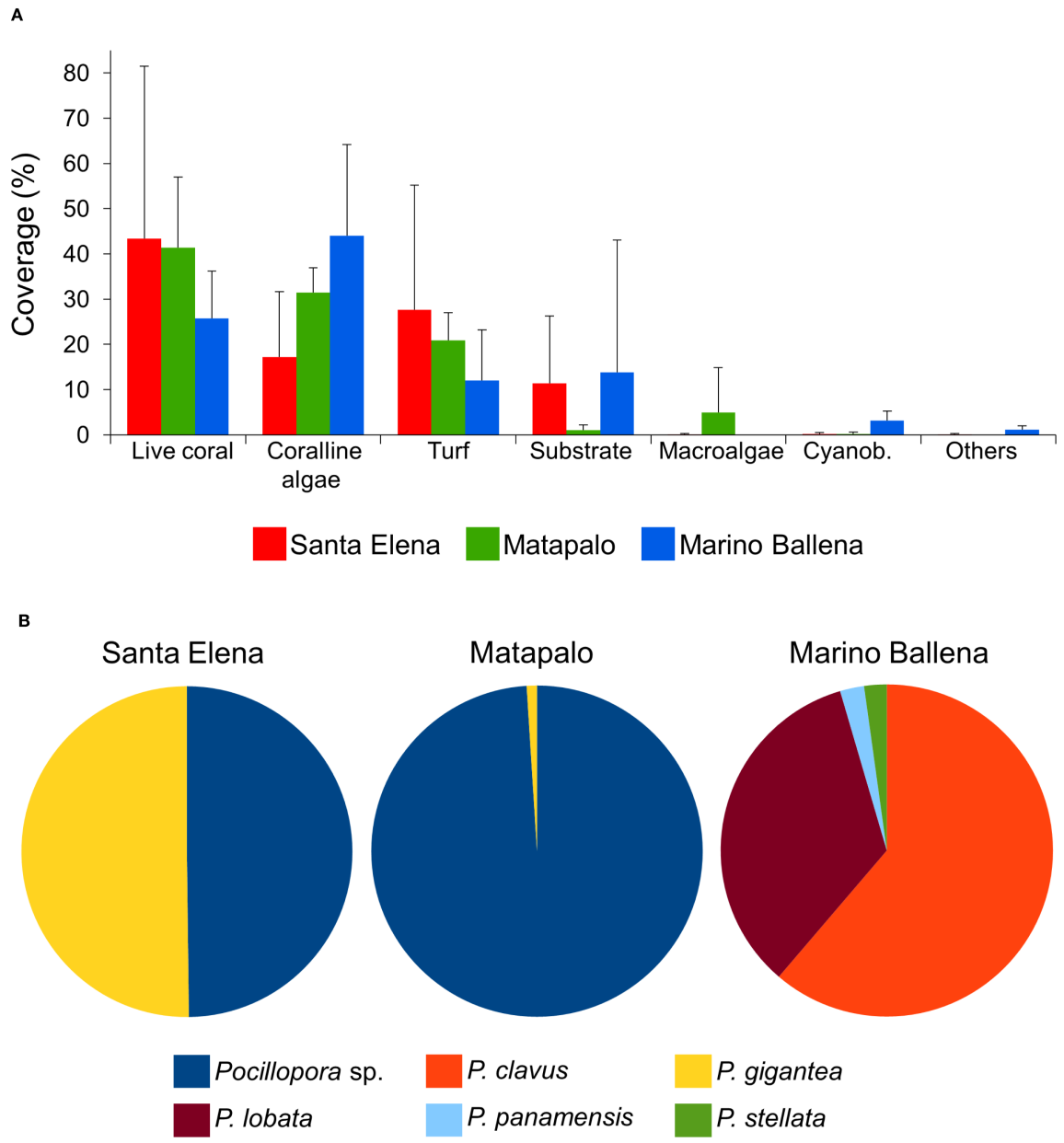

FIGURE 5
Benthic cover along the Pacific coast of Costa Rica. **(A)** Percentages of benthic cover reveal the dominant organisms in coral reefs from three locations, Cyanob. = cyanobacteria. **(B)** Contribution (%) of scleractinian coral species to coral coverage in the study locations.

to April due to the occurrence of the Papagayo upwelling and start to get warmer around May (Alfaro and Cortés, 2012; Alfaro et al., 2012) during the transition to the rainy season. The range of SWT fluctuations in Santa Elena is very high during upwelling season (Cortés et al., 2014; Stuhldreier et al., 2015) and although the lowest value measured during our study was 18 °C, previous studies indicated that SWT in this area can drop to values below 14.0 °C for a few hours during strong upwelling events (Jiménez, 2001b). Conversely, in southern reefs the coastal waters experience a slight cooling during the second half of the year, as the rainy season develops.

This cooling in the south during the rainy season is related to greater freshwater input from numerous rivers near Marino Ballena. The Grande de Térraba River, for example, is located about 10 km southwest of Marino Ballena and drains one of the largest basins in the country (Krishnaswamy et al., 2001). Mean annual precipitation and flow discharge are significantly higher than in any other basin in the north (Waylen and Laporte, 1999). The average water temperature of this river is 25 °C (Umaña-Villalobos and Springer, 2006) and the river discharge is enhanced between the months of May and November (Rojas and Rodríguez, 2008), producing the cooling of the surface waters and a decrease in

TABLE 3 Richness (S), diversity (H′) and evenness (J′) of benthic categories and scleractinian coral species in coral reefs at three locations in the Pacific coast of Costa Rica.

Location	Categories			Coral species		
	S	H′	J′	S	H′	J′
Santa Elena	7	1.29	0.52	2	0.69	1.00
Matapalo	6	1.26	0.59	2	0.05	0.53
Marino Ballena	7	1.41	0.58	4	0.84	0.58

salinity to values of 26.0 psu (this study and Alvarado and Aguilar, 2009).

4.1.2 Nutrients

This study revealed that inorganic nutrients are the main contributors to the observed differences between locations and seasons in coastal waters along the Costa Rican Pacific. Our results confirm that the high variability of nutrient concentrations in Santa Elena during the dry season is driven by the Papagayo upwelling, with a significant increase of the mean values by 69% in phosphate, 80% in nitrate and 65% in ammonium, as compared to the non-upwelling rainy season. In contrast, most of the inorganic nutrient concentrations in Marino Ballena increased during the rainy season. In these southern reefs, agricultures, land erosion and runoff strongly contribute to the nutrient input carried by the Grande de Térraba River discharge (Alvarado et al., 2009) and other rivers in the area. Consequently, the average concentration of silicate in Marino Ballena during the rainy season was 48% higher as compared to the dry season (Figure 3), and phosphate and nitrate also had a significant increase in their concentrations during the rainy season of up to 125% and 74%, respectively.

4.1.3 Carbonate chemistry parameters

The spatial and temporal analysis of our data supports two major assumptions: 1) the northern Pacific coast of Costa Rica experiences an upwelling-driven geographic gradient in alkalinity, dissolved inorganic carbon and pH, and 2) seasonal variability in seawater carbonate chemistry is mainly driven by the Papagayo upwelling during the dry season in northern locations and by river discharges during the rainy season in the south. Dynamics of Ω_a and pH in coastal areas are driven by several processes: i) upwelling of high-CO_2 waters (Feely et al., 2008; Rixen et al., 2012; Harris et al., 2013; Sánchez-Noguera et al., 2018b), ii) metabolic processes controlled by planktonic communities and coral reefs (inorganic: organic carbon production ratios) (Gray et al., 2012; Albright et al., 2013, 2015) and iii) inputs from land (Vargas et al., 2016; Dong et al., 2017; Carstensen and Duarte, 2019). In this study, the northernmost location (Santa Elena) and southern location (Marino Ballena) experienced low Ω_a values; however, the source of these reduced values and their variability differed between the two locations. In Santa Elena, the lower pH and Ω_a was linked to the upwelling of waters with high-CO_2 concentrations (Rixen et al., 2012). In contrast, in Marino Ballena the dilution effect by freshwater input was likely responsible for the observed decrease in Ω_a values, due to river discharges and increased runoff during the rainy season (Chierici and Fransson, 2009; Harris et al., 2013).

By analyzing the coupled changes of salinity-normalized alkalinity and dissolved inorganic carbon (Figure 4) in combination with the estimated inorganic:organic carbon production ratios, we can shed light on which processes are exerting a major control over the carbonate system in our study locations. In Santa Elena, the observed high variability of nDIC between seasons confirms that the upwelling of CO_2-enriched waters is partially responsible for the seasonal fluctuation in seawater carbonate chemistry. This result agrees with other studies (Rixen et al., 2012; Sánchez-Noguera et al., 2018b), showing that in the Papagayo upwelling system deep waters hauled to the surface are enriched in CO_2. Additionally, the estimated inorganic:organic carbon production ratio in Santa Elena (< 1) suggests that organic carbon production and respiration also play a role in the seasonal variability of carbonate chemistry. The linear regression analysis of nDIC vs. nTA (Figure 4) suggests that organic carbon production via photosynthesis was enhanced during the rainy season and respiration during the dry season. In line with our findings, other authors have indicated that enhanced primary production can be responsible for decreasing the concentrations of dissolved inorganic carbon, nitrite and nitrate (He et al., 2025), as occurred in Santa Elena during the rainy season. In terms of the enhanced respiration during the dry season, previous studies reported that the abundance of zooplankton in the Gulf of Papagayo is higher during the dry season (Bednarski and Morales-Ramírez, 2004; Rodríguez-Sáenz and Morales-Ramírez, 2012). Therefore, upwelled nutrient-enriched waters can boost the respiration of zooplankton communities, partially contributing to the observed increase in dissolved inorganic carbon during the upwelling season. Similarly, in the California Current System the high concentration of dissolved inorganic carbon is mostly attributed to respiration-derived CO_2 (Hauri et al., 2009). On the other hand, the slight enrichment of alkalinity measured in Santa Elena during the dry season could be attributed to the dissolution of $CaCO_3$ in deep waters. Similar to Santa Elena, the estimated inorganic:organic carbon production ratio in Matapalo was also < 1, highlighting the importance of organic production and respiration processes in the carbonate system of northern locations. Moreover, the small seasonal variability in alkalinity and dissolved inorganic carbon measured in Matapalo, in combination with higher pH (> 8.0) and Ω_a (> 3.4) values, suggests that $CaCO_3$ is precipitated all year round in this location.

Moving southward to Marino Ballena, the coupled increase of nDIC and nTA (Figure 4) suggest that inorganic processes (i.e. carbonate production or dissolution) could play a key role in the seawater chemistry of this location. However, the estimated inorganic:organic carbon production ratio (0.88) challenges this assumption, indicating that organic processes also play a dominant role in driving the seasonal variability of the carbonate system in this location. Nevertheless, the carbon production ratio in Marino Ballena is considerably higher than in northern locations (Santa

TABLE 4 Comparison of local conditions in reefs from the Pacific coast of Costa Rica using as reference values the global suitable environmental ranges for potential coral reef habitats, as previously defined by other authors (Guan et al., 2015). The data shown for this study correspond to the extreme average values measured in different seasons (d = dry season, r = rainy season).

Parameter	Global (Guan et al., 2015)	Santa elena	Matapalo	Marino ballena
		[Extreme mean seasonal values; this study]		
Temperature (°C) (range)	21.7-29.6	22.0-28.1	28.0-28.8	27.5-29.0
Salinity (range)	28.7-40.4	33.9-34.9	34.0-34.0	29.1-34.0
NO_3^- (µmol l^{-1}) (maximum)	4.51	1.47	0.52	0.64
PO_4^{3-} (µmol l^{-1}) (maximum)	0.63	1.14 ^{d}	0.40^{d}	0.39^{r}
Omega - Ω_a (minimun)	2.82	2.38 ^{d}	3.44^{d}	2.93^{r}

Comparison of local conditions in reefs from the Pacific coast of Costa Rica using as reference values the global suitable environmental ranges for potential coral reef habitats, as previously defined by other authors (Guan et al., 2015). The data shown for this study correspond to the extreme average values measured in different seasons (d, dry season; r,= rainy season).

Elena = 0.04, Matapalo = 0.18) and closer to a value of 1, implying that the inorganic processes may have a relatively stronger influence on the dynamics of the carbonate system, potentially linked to $CaCO_3$ formation, which is somehow promoted during the dry season. Considering that the Grande de Térraba River drains the largest karstic region in Costa Rica (about 185 km^2 of extension) (Ulloa et al., 2011, 2024; Bolz and Calvo, 2018), is very likely that surface and groundwater discharges supply dissolved carbonates to the reefs in this area (Krishnaswamy et al., 2001; Tamše et al., 2014; Kapsenberg et al., 2017; He et al., 2025). This could help explain the slightly elevated nTA observed in Marino Ballena during the dry season, in comparison to Matapalo, a northern location where seasonal upwelling exerts a less pronounced influence on the variability of the carbonate system parameters. A thorough analysis of other carbonate system parameters showed that the fluctuations of nDIC and nTA in Marino Ballena did not correspond with seasonal variations in pH values. The pH levels in Marino Ballena remained consistent across both seasons, with values of about 8.0, which might be caused by the enhanced outwelling of carbonates from nearby mangroves (i.e. Térraba-Sierpe National Wetland) during the rainy season. This is consistent with conclusions from another study, suggesting that mangroves can contribute to buffer coastal acidification (Sippo et al., 2016).

4.2 Environmental conditions shape coral reef composition in the Costa Rican Pacific coast

Even though all study locations displayed a similar benthic richness and diversity; the main reef-building corals are different along the Costa Rican Pacific coast (Figure 5B). Reefs from northern locations are dominated by massive and branching species, whereas reefs from the southern part of this coast are mostly dominated by massive species (this study and Glynn et al., 2017a). A few and small patch reefs of branching-corals have been reported in southern locations (Guzmán and Cortés, 1989; Cortés and Jiménez, 1996), but they are surpassed in number by massive-coral reefs and mostly found in Caño Island, 16 km northwest from the coast. The coral distribution patterns described above (Figure 5B) raise two key questions: 1) Why are the massive reef-building species in the north different from the massive reef-building species in the south? 2) Why are branching corals not among the main reef-builders in the south?

The measured physicochemical parameters revealed spatial and seasonal differences in the conditions along the Costa Rican Pacific coast (Figures 2, 3). However, changes of physicochemical parameters seem to be insufficient to explain why the main reef-building species differ between locations (Figure 5). To find a possible explanation for the observed coral distribution patterns, we also compared our local values with the established global environmental ranges suitable for potential coral reef habitats (Table 4) (Guan et al., 2015). These global values were used to update the ReefHab model (Kleypas, 1995, 1997), originally developed to predict the potential distribution of coral reefs according to the available environmental data. Kleypas' work was a milestone that stated for the first time the environmental tolerance limits for coral reefs, contributing to understanding and predicting their global distribution. Comparing the physicochemical conditions on the Pacific coast of Costa Rica (this study) with the global thresholds established by the updated ReefHab model (Guan et al., 2015) helps to explain the presence of coral reefs in our study locations, but does not necessarily capture the variability in species composition. Nevertheless, given the limited information available on the environmental tolerance ranges for individual coral genera, we also used these global thresholds as a proxy to understand the differences in the dominant coral species observed at our three study locations. This combined analysis suggests that the composition of the dominant coral species in this study can be mainly explained by phosphate and Ω_a, as these parameters divert from the global tolerance thresholds in different ways (Table 4).

In the following paragraphs, we will use the presence of coral reefs as an indicator of the success of those coral species to cope with the combination of the measured physicochemical parameters, therefore a proxy of the suitability of local conditions for the reef development along this coast. To address the first question regarding the observed differences in massive coral species building reefs along this coast (Figure 5B), it is important to mention that even though *P. clavus* was not present in the reefs surveyed in Santa Elena and Matapalo, this massive coral was reported in the past as the main reef-builder (Jiménez, 1997) or among the most ubiquitous massive species (Palmer et al., 2022) in other northern location. We excluded that *P. clavus* reef from this study because it experienced a mass mortality several years before, thus the benthic coverage at the time of our study was mainly dominated by turf algae (Sánchez-Noguera et al., 2018a). By considering the historical record of coral reefs in the north Pacific of Costa Rica in addition to our data, we can say that *P. clavus* succeeds to build reefs in both northern and southern locations. This indicates that this massive coral is highly tolerant to the wide range of physicochemical conditions measured along this coast. Nevertheless, it is likely that they were already living near their physiological tolerance limits in northern locations, which might explain their historical mortality in those areas (Mena et al., 2025). Now we will focus our attention on the massive coral species that are building reefs exclusively in northern or southern locations and are not widely distributed as *P. clavus*. Our data suggests that *P. gigantea*, one of the main massive reef-builders in the north Pacific coast of Costa Rica, is highly tolerant to the episodic exposition to low- Ω_a cool waters and eutrophic conditions occurring in pulses during upwelling season. This agrees with results from the Pacific coast of Panama, where corals from the genus *Pavona* exhibited a high tolerance to the combination of thermal stress (lower SWT) and acidification in the coastal upwelling impacted Gulf of Panama (Manzello, 2010a). In contrast, *P.* cf. *lobata* building reefs in Marino Ballena indicates that this massive coral thrives in constant conditions of lower Ω_a (< 3.0) and lower salinity, and copes very well with low light intensity due to the influx of terrigenous materials occurring predominantly during the rainy season (Alvarado et al., 2009). Despite the mechanisms by which inorganic nutrients affect coral reefs are subject to debate, there is a consensus that unbalanced nutrient enrichment from anthropogenic sources poses negative effects for coral reef functioning (D'Angelo and Wiedenmann, 2014). For example, high nutrient loads have the potential to affect corals indirectly by favoring primary producers, which can outcompete stony corals (Fernández-García et al., 2012), and increasing bioerosion by facilitating shifts to larger and more effective bioeroders (Wizemann et al., 2018). Furthermore, a study from Galapagos concerning reefs affected by different upwelling levels suggested that the skeletal density of *P. lobata* was diminished due to exposure to elevated phosphate conditions (Manzello et al., 2014). This can contribute to explaining why *P.* cf. *lobata* was one of the main reef builders in Marino Ballena. The average seasonal phosphate levels in Marino Ballena were lower than those in Santa Elena, which likely promotes stronger skeletons in Marino Ballena and allows their persistence over time. This suggests that the lower phosphate levels enable *P.* cf. *lobata* to build reefs in Marino Ballena, despite the steady Ω_a values < 3.0 measured in southern locations. Moreover, other studies involving corals from the genus *Porites* support our assumption that changes driven by river discharges significantly shape the structure of local coral reefs. For instance, *Porites* corals in Biscayne Bay, Florida show a high tolerance to changes in salinity (Manzello and Lirman, 2003), while those in Golfo Dulce, Costa Rica, are particularly resilient to high sedimentation (Cortés, 1990). In consequence, this species contributes the most to the reef building under riverine impacted locations.

Now we will move forward to our second question, regarding the minor contribution of branching corals in southern locations. In Costa Rica, most reefs built by *Pocillopora* spp. have experienced severe mortalities, frequently attributed to warming during ENSO events and to recurrent occurrence of harmful algal blooms (Guzmán et al., 1987, 1990; Glynn et al., 2017a; Sánchez-Noguera et al., 2018a; Palmer et al., 2022). Nevertheless, the current distribution of branching corals and the remaining structures of former reefs can be used as a proxy to identify the most favorable conditions for the success of this genus along the Costa Rican coast. For example, the precipitation of $CaCO_3$ over the whole year at Matapalo, along with its sheltered location, helps explain the presence of a reef built by branching species. This combination of factors contributes to the branching species' prevalence and relatively high contribution to coral coverage compared to other coral reefs in the same area, which have experienced significant degradation over the last decade (Mena et al., 2025). While branching corals are not entirely absent from southern locations (Guzmán and Cortés, 1989; Cortés and Jiménez, 1996), they contribute much less to the benthic coverage than massive corals in Marino Ballena. This is likely due to the reduced light availability caused by river discharge. Grande de Térraba River, located near Marino Ballena, is the second largest catchment of the country (Granados-Bolaños et al., 2024). Other authors (Alvarado et al., 2005) have previously discussed that the limited presence of *Pocillopora* spp. in Marino Ballena may be linked to low light penetration in the water column, due to high concentrations of suspended matter derived from river discharge (Alvarado et al., 2009). This hypothesis is confirmed by another study from the Great Barrier Reefs, which showed that the genus *Pocillopora* is very sensitive to reduced light resulting from high turbidity (Jones et al., 2020). Therefore, we can infer that reduced light availability is one of the main factors limiting reef development by branching corals in southern locations, while high tolerance to salinity fluctuations promotes the prevalence of reefs built by massive corals such as *Porites* sp.

The results presented in this study provide insights into adaptation limits of individual coral species to local physicochemical conditions. For example, *Pavona* spp. and *Pocillopora* spp. reefs from Santa Elena indicate that these species have adapted to the episodic exposition to low- Ω_a conditions occurring during upwelling season (2.38, Table 4), when Ω_a values are lower than the proposed local (Sánchez-Noguera et al., 2018b)

and global thresholds (2.82, Table 4) (Guan et al., 2015) for reef development. Even though the success of the massive and branching species to build coral reefs along the Pacific coast is a good example of adaptation to high local variability, it does not guarantee their survival under climate change scenarios, when the rate of changes will be enhanced (Howes et al., 2015). Costa Rican coral reefs have suffered several ENSO-induced bleaching events over the last decades (Guzmán et al., 1987; Guzmán and Cortés, 1992, 2001; Jiménez and Cortés, 2001, 2003; Jiménez et al., 2001; Cortés et al., 2010; Alvarado et al., 2018), while the current lapse between global bleaching events is shortening the temporal window for reef recovery after associated mass mortality (Hughes et al., 2018). This implies that physicochemical conditions in the ETP are close to the limits that warm water reef ecosystems can tolerate.

4.3 Outlook

The results from our study demonstrate that seawater chemistry properties of coastal waters along the Costa Rican Pacific coast display a high spatial and temporal variability, which is driven by the Papagayo upwelling system during the dry season in the north and river discharge during the rainy season in the south. Matapalo reef, located between the northernmost (Santa Elena) and the southernmost location (Marino Ballena), reveals a relatively low seasonality of physicochemical conditions. This confirms that the seasonal upwelling has a stronger influence further north, in Santa Elena relative to Matapalo. Although carbonate chemistry plays a significant role in determining the composition of coral reefs along the Pacific coast of Costa Rica, it is not the only controlling factor, as inorganic nutrients explain a higher percentage of the observed variability. Our findings indicate that carbonate chemistry is key for promoting favorable physicochemical conditions for reef development in northern locations like Matapalo. However, the sensitivity of coral species to other physicochemical conditions, such as lower salinity and lower light intensity, are responsible for shaping the reef composition in Marino Ballena (Figure 6).

Corals from the Pacific coast of Costa Rica have adapted to the local variability in physicochemical parameters. Nevertheless, their tolerance to this variability appears to be species-specific, and does not imply that they can withstand external disturbances that push physicochemical conditions beyond the limits for reef development. Regarding future conservation efforts and reef protection, Matapalo and Marino Ballena seem to be very promising locations. This is mainly to the relatively stable carbonate chemistry conditions in Matapalo and the buffering effect against ocean acidification in Marino Ballena, which is most probably caused by the dissolved carbonates entering from land. However, this calls for integrated

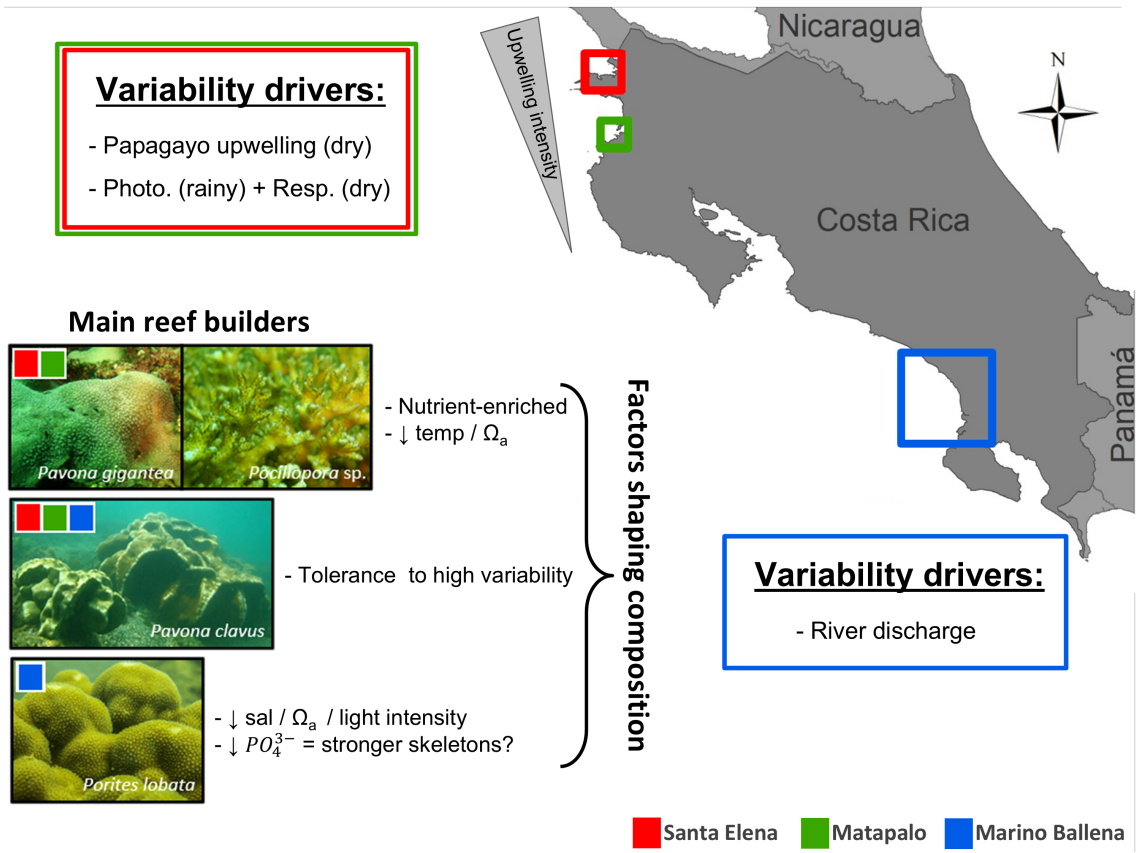

FIGURE 6
Graphic summary of main findings. Drivers of spatial and seasonal variability in nutrient concentrations and carbonate chemistry, and main factors controlling coral reef composition along the Pacific coast of Costa Rica.

coastal management actions to reduce the pressures of local stressors such as siltation, pollution, fishing and tourism.

Data availability statement

The datasets generated and analyzed for this study are publicly available and can be found in PANGAEA (https://www.pangaea.de/), under the following DOI: https://doi.pangaea.de/10.1594/PANGAEA.920884, https://doi.pangaea.de/10.1594/PANGAEA.920876, https://doi.pangaea.de/10.1594/PANGAEA.920881, https://doi.pangaea.de/10.1594/PANGAEA.920883, https://doi.pangaea.de/10.1594/PANGAEA.920882.

Ethics statement

The manuscript presents research on animals that do not require ethical approval for their study.

Author contributions

CS-N: Conceptualization, Formal analysis, Methodology, Writing – original draft, Investigation, Data curation. IL: Methodology, Writing – review & editing. JC: Writing – review & editing. CJ: Writing – review & editing. CW: Writing – review & editing, Funding acquisition. TR: Supervision, Writing – review & editing, Funding acquisition, Project administration.

Funding

The author(s) declare financial support was received for the research and/or publication of this article. This study was funded by the Leibniz Association as part of COSTACID project from the Leibniz Centre for Tropical Marine Research (ZMT). The publication (APC) of this article was funded by Universidad de Costa Rica through Vicerrectoría de Investgación and Red de Mujeres en Ciencias, Ingenierías y Humanidades (CIHRED-UCR).

Acknowledgments

Special thanks to Minor Lara and family, Fernando Monge and the staff from Scuba Caribe Diving Center for their support in the field. We also thank Centro de Investigación en Ciencias del Mar y Limnología (CIMAR), Hotel RIU Guanacaste (Alberto Leónard) and Scuba Caribe for logistic support. Juan José Alvarado, Gustavo Arias and Jeffrey Sibaja-Cordero provided valuable advice in statistical analysis. The constructive comments of two reviewers improved the manuscript.

Conflict of interest

The authors declare that the research was conducted in the absence of any commercial or financial relationships that could be construed as a potential conflict of interest.

Generative AI statement

The author(s) declare that no Generative AI was used in the creation of this manuscript.

Any alternative text (alt text) provided alongside figures in this article has been generated by Frontiers with the support of artificial intelligence and reasonable efforts have been made to ensure accuracy, including review by the authors wherever possible. If you identify any issues, please contact us.

Publisher's note

Supplementary material

The Supplementary Material for this article can be found online at: https://www.frontiersin.org/articles/10.3389/fmars.2025.1606253/full#supplementary-material

SUPPLEMENTARY TABLE 1
Overall average values (95% confidence intervals) by location and season of measured and calculated (*) physicochemical and meteorological parameters at three locations in the Pacific coast of Costa Rica. Seawater temperature (SWT) was measured *in situ* and the values for the other parameters were obtained from discrete water samples. For abbreviations of listed parameters please referred to the manuscript. Meteorological data collected at meteorological stations located near the study locations was provided by the Instituto Meteorológico Nacional.

SUPPLEMENTARY TABLE 2
Statistical differences of physicochemical and meteorological parameters between locations. Asterisks indicate significant differences ($p < 0.05$).

SUPPLEMENTARY TABLE 3
Statistical differences of physicochemical and meteorological parameters between seasons. Asterisks indicate significant differences ($p < 0.05$).

References

Albright, R., Benthuysen, J., Cantin, N., Caldeira, K., and Anthony, K. (2015). Coral reef metabolism and carbon chemistry dynamics of a coral reef flat. *Geophys Res. Lett.* 42, 3980–3988. doi: 10.1002/2015gl063488

Albright, R., Langdon, C., and Anthony, K. (2013). Dynamics of seawater carbonate chemistry, production, and calcification of a coral reef flat, central Great Barrier Reef. *Biogeosciences* 10, 6747–6758. doi: 10.5194/bg-10-6747-2013

Alfaro, E. J., and Cortés, J. (2012). Atmospheric forcing of cool subsurface water events in Bahía Culebra, Gulf of Papagayo, Costa Rica. *Rev. Biol. Trop.* 60, 173–186. doi: 10.15517/rbt.v60i2.20001

Alfaro, E. J., Cortés, J., Alvarado, J. J., Jiménez, C., León, A., Sánchez-Noguera, C., et al. (2012). Clima y temperatura sub-superficial del mar en Bahía Culebra, Golfo de Papagayo, Costa Rica. *Rev. Biol. Trop.* 60, 159–171. doi: 10.15517/rbt.v60i2.20000

Alvarado, J. J., and Aguilar, J. F. (2009). Batimetría, salinidad, temperatura y oxígeno disuelto en aguas del Parque Nacional Marino Ballena, Pacífico, Costa Rica. *Rev. Biol. Trop.* 57, 19–29. doi: 10.15517/rbt.v57i0.21273

Alvarado, J., Beita-Jiménez, A., Mena, S., Fernández-García, C., Cortés, J., Sánchez-Noguera, C., et al. (2018). Cuando la conservación no puede seguir el ritmo del desarrollo: Estado de salud de los ecosistemas coralinos del Pacífico Norte de Costa Rica. *Rev. Biol. Trop.* 66, S280–S308. doi: 10.15517/rbt.v66i1.33300

Alvarado, J. J., Cortés, J., Fernández, C., and Nivia-Ruiz, J. (2005). Coral communities and coral reefs of Ballena Marine National Park, Pacific coast of Costa Rica. *Cienc Mar.* 31, 641–651. doi: 10.7773/cm.v31i4.1140

Alvarado, J. J., Fernández, C., and Cortés, J. (2009). Water quality conditions on coral reefs at the Marino Ballena National Park, Pacific Costa Rica. *Bull. Mar. Sci.* 84, 137–152.

Alvarado, J. J., Fernández, C., and Nielsen, V. (2006). "Arrecifes y Comunidades Coralinas," in *Informe técnico: Ambientes Marino Costeros de Costa Rica*. Eds. V. Nielsen-Muñoz and M. Quesada-Alpízar (San José, Costa Rica: The Nature Conservancy), 51–68.

Bednarski, M., and Morales-Ramírez, A. (2004). Composition, abundance and distribution of macrozooplankton in Culebra Bay, Gulf of Papagayo, Pacific coast of Costa Rica and its value as bioindicators of pollution. *Rev. Biol. Trop.* 53, 105–118.

Bolz, A., and Calvo, C. (2018). Carbonate platform development in an intraoceanic arc setting: Costa Rica's largest limestone sequence - the fila de cal formation (Middle eocene to lower oligocene). *Rev. Geológica América Cent.* 58, 85–114. doi: 10.15517/rgac.v58i0.32845

Cambronero-Solano, S., Tisseaux-Navarro, A., Vargas-Hernández, J. M., Salazar-Ceciliano, J. P., Benavides-Morera, R., Quesada-ávila, I., et al. (2021). Hydrographic variability in the Gulf of Papagayo, Costa Rica during 2017-2019. *Rev. Biol. Trop.* 69, S74–S93. doi: 10.15517/rbt.v69is2.48308

Carstensen, J., and Duarte, C. (2019). Drivers of pH variability in coastal ecosystems. *Environ. Sci. Technol.* 53, 4020–4029. doi: 10.1021/acs.est.8b03655

Chierici, M., and Fransson, A. (2009). Calcium carbonate saturation in the surface water of the Arctic Ocean: undersaturation in freshwater influenced shelves. *Biogeosciences* 6, 2421–2431. doi: 10.5194/bg-6-2421-2009

Cortés, J. (1990). The coral reefs of Golfo Dulce, Costa Rica: distribution and community structure. *Atoll Res. Bull.* 339–346, 1–37. doi: 10.5479/si.00775630.344.1

Cortés, J. (1997). Biology and geology of eastern Pacific coral reefs. *Coral Reefs* 16, S39–S46. doi: 10.1007/s003380050240

Cortés, J. (2016). "The Pacific Coastal and Marine Ecosystems," in *Costa Rican Ecosystems*. Ed. M. Kappelle (The University of Chicago Press, Chicago), 97–138.

Cortés, J., and Jiménez, C. (1996). Coastal-marine environments of Parque Nacional Corcovado, Puntarenas, Costa Rica. *Rev. Biol. Trop.* 44, 35–40.

Cortés, J., and Jiménez, C. (2003). "Corals and Coral Reefs of the Pacific of Costa Rica: History, Research and Status," in *Latin American Coral Reefs*. Ed. J. Cortés (Elsevier Science B.V, Amsterdan, The Netherlands), 361–385.

Cortés, J., Jiménez, C., Fonseca, A., and Alvarado, J. (2010). Status and conservation of coral reefs in Costa Rica. *Rev. Biol. Trop.* 58, 33–50. doi: 10.15517/rbt.v58i1.20022

Cortés, J., Samper-Villarreal, J., and Bernecker, A. (2014). Seasonal phenology of Sargassum liebmannii J. Agardh (Fucales, Heterokontophyta) in an upwelling area of the Eastern Tropical Pacific. *Aquat Bot.* 119, 105–110. doi: 10.1016/j.aquabot.2014.08.009

D'Angelo, C., and Wiedenmann, J. (2014). Impacts of nutrient enrichment on coral reefs: new perspectives and implications for coastal management and reef survival. *Curr. Opin. Environ. Sustain* 7, 82–93. doi: 10.1016/j.cosust.2013.11.029

Dana, T. (1975). Development of contemporary Eastern Pacific coral reefs. *Mar. Biol.* 33, 355–374. doi: 10.1007/bf00390574

Dickson, A. (1990). Thermodynamics of the dissociation of boric acid in synthetic seawater from 273.15 to 318.15 K. *Deep Sea Res. Part A. Oceanographic Res. Papers* 37, 755–766. doi: 10.1016/0198-0149(90)90004-F

Dickson, A., Afghan, J., and Anderson, G. (2003). Reference materials for oceanic CO2 analysis: a method for the certification of total alkalinity. *Mar. Chem.* 80, 185–197. doi: 10.1016/S0304-4203(02)00133-0

Dickson, A., and Millero, F. (1987). A comparison of the equilibrium constants for the dissociation of carbonic acid in seawater media. *Deep Sea Res. Part A. Oceanographic Res. Papers* 34, 1733–1743. doi: 10.1016/0198-0149(87)90021-5

Dickson, A., Sabine, C., and Christian, J. (2007). *Guide to best practices for ocean CO2 measurements* PICES Special Publication 3. Sidney, BC, Canada: North Pacific Marine Science Organization (PICES).

Dong, X., Huang, H., Zheng, N., Pan, A., Wang, S., Huo, C., et al. (2017). Acidification mediated by a river plume and coastal upwelling on a fringing reef at the east coast of Hainan Island, Northern South China Sea. *J. Geophysical Resarch Oceans* 122, 7521–7536. doi: 10.1002/2017JC013228

Feely, R., Sabine, C., Hernández-Ayón, J., Ianson, D., and Hales, B. (2008). Evidence for upwelling of corrosive "Acidified" Water onto the continental shelf. *Sci. (1979)* 320, 1490–1492. doi: 10.1126/science.1155676

Fernández-García, C., Cortés, J., Alvarado, J., and Nivia-Ruiz, J. (2012). Physical factors contributing to the benthic dominance of the alga Caulerpa sertularioides (Caulerpaceae, Chlorophyta) in the upwelling Bahía Culebra, north Pacific of Costa Rica. *Rev. Biol. Trop.* 60, 93–107. doi: 10.1007/s003380050240

Fiedler, P., and Lavín, M. (2017). "Oceanographic Conditions of the Eastern Tropical Pacific," in *Coral Reefs of the Eastern Tropical Pacific: Persistence and Loss in a Dynamic Environment*. Eds. P. Glynn, D. Manzello and I. Enochs (Springer Netherlands, Dordrecht), 59–83.

Fiedler, P., and Talley, L. (2006). Hydrography of the eastern tropical Pacific: A review. *Prog. Oceanogr* 69, 143–180. doi: 10.1016/j.pocean.2006.03.008

Glynn, P., Alvarado, J., Banks, S., Cortés, J., Feingold, J., Jiménez, C., et al. (2017a). "Eastern Pacific Coral Reef Provinces, Coral Community Structure and Composition: an Overview," in *Coral Reefs of the Eastern Tropical Pacific: persistence and loss in a dynamic environment*. Eds. P. Glynn, D. Manzello and I. Enochs (Springer Science +Business Media B.V. Dordrecht, Dordrecht), 107–176. doi: 10.1007/978-94-017-7499-4_5

Glynn, P., Mones, A., Podestá, G., Colbert, A., and Colgan, M. (2017b). "El Niño-Southern Oscillation: Effects on Eastern Pacific Coral Reefs and Associated Biota," in *Coral reefs of the Eastern tropical Pacific: Persistence and loss in a dynamic environment*. Eds. P. Glynn, D. Manzello and I. Enochs (Springer Science+Business Media B.V. Dordrecht, Dordrecht), 251–290.

Granados-Bolaños, S., Surian, N., Birkel, C., Alvarado, G. E., Quesada-Román, A., Galve, J. P., et al. (2024). "Fluvial Landscapes of Costa Rica: An Overview of Dynamic Rivers," in *Landscapes and Landforms of Costa Rica*. Ed. A. Quesada-Román (Springer International Publishing, Cham), 91–111. doi: 10.1007/978-3-031-64940-0_5

Gray, S., DeGrandpre, M., Langdon, C., and Corredor, J. (2012). Short-term and seasonal pH, pCO2 and saturation state variability in a coral-reef ecosystem. *Global Biogeochem Cycles* 26, 1–13. doi: 10.1029/2011GB004114

Guan, Y., Hohn, S., and Merico, A. (2015). Suitable environmental ranges for potential coral reef habitats in the tropical ocean. *PloS One* 10, e0128831. doi: 10.1371/journal.pone.0128831

Guzmán, H., and Cortés, J. (1989). Coral reef community structure at Caño Island, Pacific Costa Rica. *Mar. Ecol.* 10, 23–41. doi: 10.1111/j.1439-0485.1989.tb00064.x

Guzmán, H., and Cortés, J. (1992). Cocos Island (Pacific of Costa Rica) coral reefs after the 1982–83 El Niño disturbance. *Rev. Biol. Trop.* 40, 309–324.

Guzmán, H., and Cortés, J. (2001). Changes in reef community structure after fifteen years of natural disturbances in the Eastern Pacific (Costa Rica). *Bull. Mar. Sci.* 69, 133–149.

Guzmán, H., Cortés, J., Glynn, P., and Richmond, R. (1990). Coral mortality associated with dino-flagellate blooms in the eastern Pacific (Costa Rica and Panama). *Mar. Ecol. Prog. Ser.* 60, 299–303. doi: 10.3354/meps060299

Guzmán, H., Cortés, J., Richmond, R., and Glynn, P. (1987). Efectos del fenómeno de "El Niño Oscilacion Sureña" 1982/83 en los arrecifes coralinos de la Isla del Caño, Costa Rica. *Rev. Biol. Trop.* 35, 325–332.

Harris, K., DeGrandpre, M., and Hales, B. (2013). Aragonite saturation state dynamics in a coastal upwelling zone. *Geophys Res. Lett.* 40, 2720–2725. doi: 10.1002/grl.50460

Hauri, C., Gruber, N., Plattner, G., Alin, S., Feely, R., Hales, B., et al. (2009). Ocean acidification in the california current system. *Oceanography* 22, 60–71. doi: 10.5670/oceanog.2009.97

He, S., Gordon, S., and Maiti, K. (2025). Carbonate and nutrient dynamics in a mississippi river influenced eutrophic estuary. *Estuaries Coasts* 48, 63. doi: 10.1007/s12237-025-01494-4

Howes, E., Joos, F., Eakin, M., and Gattuso, J. (2015). An updated synthesis of the observed and projected impacts of climate change on the chemical, physical and biological processes in the oceans. *Front. Mar. Sci.* 2. doi: 10.3389/fmars.2015.00036

Hughes, T., Anderson, K., Connolly, S., Heron, S., Kerry, J., Lough, J., et al. (2018). Spatial and temporal patterns of mass bleaching of corals in the Anthropocene. *Sci. (1979)* 359, 80–83. doi: 10.1126/science.aan8048

Instituto Metereológico Nacional (IMN) (2008). *El clima, su variabilidad y cambio climático en Costa Rica* (San José: Comité Regional de Recursos Hidráulicos (CRRH)).

Jiménez, C. (1997). Corals and coral reefs of Culebra Bay, Pacific coast of Costa Rica: Anarchy in the reef. *Proc. 8th Int. Coral Reef Symposium* 1, 329–334.

Jiménez, C. (2001a). Arrecifes y ambientes coralinos de Bahía Culebra, Pacífico de Costa Rica: Aspectos biológicos, económico-recreativos y de manejo. *Rev. Biol. Trop.* 49, 215–231.

Jiménez, C. (2001b). Seawater temperature measured at the surface and at two depths (7 and 12 m) in one coral reef at Culebra Bay, Gulf of Papagayo, Costa Rica. *Rev. Biol. Trop.* 49, 153–161.

Jiménez, C., Bassey, G., Segura, A., and Cortés, J. (2010). Characterization of the coral communities and reefs of two previously undescribed locations in the upwelling region of Gulf of Papagayo (Costa Rica). *Rev. Mar. Cost.* 2, 95–108. doi: 10.15359/revmar.2.8

Jiménez, C., and Cortés, J. (2001). Effects of the 1991–92 El Niño on scleractinian corals of the Costa Rican central Pacific coast. *Rev. Biol. Trop.* 49, 239–250.

Jiménez, C., and Cortés, J. (2003). Coral cover change associated to El Niño, Eastern Pacific, Costa Rica 1992-2001. *Mar. Ecol.* 24, 179–192. doi: 10.1046/j.1439-0485.2003.03814.x

Jiménez, C., Cortés, J., León, A., and Ruíz, E. (2001). Coral bleaching and mortality associated with the 1997–98 El Niño in an upwelling environment in the Eastern Pacific (Gulf of Papagayo, Costa Rica). *Bull. Mar. Sci.* 69, 151–169.

Jones, R., Giofre, N., Luter, H. M., Neoh, T. L., Fisher, R., and Duckworth, A. (2020). Responses of corals to chronic turbidity. *Sci. Rep.* 10, 4762. doi: 10.1038/s41598-020-61712-w

Kapsenberg, L., Alliouane, S., Gazeau, F., Mousseau, L., and Gattuso, J.-P. (2017). Coastal ocean acidification and increasing total alkalinity in the northwestern Mediterranean Sea. *Ocean Sci.* 13, 411–426. doi: 10.5194/os-13-411-2017

Kleypas, J. (1995). "A Diagnostic Model for Predicting Global Coral Reef Distribution," in *Recent Advances in Marine Science and Technology*. Eds. O. Bellwood, H. Choat and N. Saxena (Honolulu, HI, USA: PACON International and James Cook University), 211–220.

Kleypas, J. (1997). Modeled estimates of global reef habitat and carbonate production since the last glacial maximum. *Paleoceanography* 12, 533–545. doi: 10.1029/97PA01134

Krishnaswamy, J., Halpin, P., and Richter, D. (2001). Dynamics of sediment discharge in relation to land-use and hydro-climatology in a humid tropical watershed in Costa Rica. *J. Hydrol (Amst)* 253, 91–109. doi: 10.1016/S0022-1694(01)00474-7

Lavín, M., Fiedler, P., Amador, J., Ballance, L., Färber-Lorda, J., and Mestas-Nuñez, A. (2006). A review of eastern tropical Pacific oceanography: Summary. *Prog. Oceanogr* 69, 391–398. doi: 10.1016/j.pocean.2006.03.005

Manzello, D. (2010a). Coral growth with thermal stress and ocean acidification: lessons from the eastern tropical Pacific. *Coral Reefs* 29, 749–758. doi: 10.1007/s00338-010-0623-4

Manzello, D. (2010b). Ocean acidification hotspots: Spatiotemporal dynamics of the seawater CO2 system of eastern Pacific coral reefs. *Limnol Oceanogr.* 55, 239–248. doi: 10.4319/lo.2010.55.1.0239

Manzello, D., Enochs, I., Bruckner, A., Renaud, P., Kolodziej, G., Budd, D., et al. (2014). Galaípagos coral reef persistence after ENSO warming across an acidification gradient. *Geophys Res. Lett.* 41, 9001–9008. doi: 10.1002/2014GL062501

Manzello, D., Kleypas, J., Budd, D., Eakin, C., Glynn, P., and Langdon, C. (2008). Poorly cemented coral reefs of the eastern tropical Pacific: possible insights into reef development in a high-CO2 world. *Proc. Natl. Acad. Sci. U.S.A.* 105, 10450–10455. doi: 10.1073/pnas.0712167105

Manzello, D., and Lirman, D. (2003). The photosynthetic resilience of Porites furcata to salinity disturbance. *Coral Reefs* 22, 537–540. doi: 10.1007/s00338-003-0327-0

Mehrbach, C., Culberson, C., Hawley, J., and Pytkowicz, R. (1973). Measurement of the apparent dissociation constants of carbonic acid in seawater at atmospheric pressure. *Limnol Oceanogr* 18, 897–907. doi: 10.4319/lo.1973.18.6.0897

Mena, S., Quesada-Perez, F., Sánchez-Noguera, C., Salas-Moya, C., Alvarado, J. J., López-Garro, A., et al. (2025). Estructura comunitaria de ecosistemas coralinos en sitos de importancia para la conservación de la biodiversidad marina del Pacífico Norte de Costa Rica. *Rev. Biol. Trop.* 73, e63715. doi: 10.15517/rev.biol.trop.v73iS1.63715

Méndez-Venegas, M., Jiménez, C., Bassey-Fallas, G., and Cortés, J. (2021). Condición del arrecife coralino de Playa Blanca, Punta Gorda, uno de los arrecifes más extensos de la costa Pacífica de Costa Rica. *Rev. Biol. Trop.* 69, 194–207. doi: 10.15517/rbt

Palmer, C., Jimenez, C., Bassey, G., Ruiz, E., Cubero, T. V., Diaz, M. M. C., et al. (2022). Cold water and harmful algal blooms linked to coral reef collapse in the Eastern Tropical Pacific. *PeerJ* 10, e14081. doi: 10.7717/peerj.14081

Rixen, T., Jiménez, C., and Cortés, J. (2012). Impact of upwelling events on the sea water carbonate chemistry and dissolved oxygen concentration in the Gulf of Papagayo (Culebra Bay), Costa Rica: Implications for coral reefs. *Rev. Biol. Trop.* 60, 187–195. doi: 10.15517/rbt.v60i2.20004

Rodríguez-Sáenz, K., and Morales-Ramírez, A. (2012). Composición y distribución del mesozooplanDICon en una zona de afloramiento costero (Bahía Culebra, Costa Rica) durante La Niña 1999 y el 2000. *Rev. Biol. Trop.* 60, 143–157. doi: 10.15517/rbt.v60i2.19998

Rogers, C., Garrison, G., Grober, R., Hillis, Z.-M., and Franke, M. (1994). *Coral Reef Monitoring Manual for the Caribbean and Western Atlantic*. St. John, U.S. Virgin Islands: National Park Service, Virgin Islands National Park. p. 114.

Rojas, J., and Rodríguez, O. (2008). Diversidad y abundancia ictiofaunística del río Grande de Térraba, sur de Costa Rica. *Rev. Biol. Trop.* 56, 1429–1447. doi: 10.15517/rbt.v56i3.5720

Sánchez-Noguera, C., Jiménez, C., and Cortés, J. (2018a). Desarrollo costero y ambientes marino-costeros en Bahía Culebra, Guanacaste, Costa Rica. *Rev. Biol. Trop.* 66, S309–S327. doi: 10.15517/rbt.v66i1.33301

Sánchez-Noguera, C., Stuhldreier, I., Cortés, J., Jiménez, C., Morales, A., Wild, C., et al. (2018b). Natural ocean acidification at Papagayo upwelling system (north Pacific Costa Rica): Implications for reef development. *Biogeosciences* 15, 2349–2360. doi: 10.5194/bg-15-2349-2018

Sippo, J. Z., Maher, D. T., Tait, D. R., Holloway, C., and Santos, I. R. (2016). Are mangroves drivers or buffers of coastal acidification? Insights from alkalinity and dissolved inorganic carbon export estimates across a latitudinal transect. *Global Biogeochem Cycles* 30, 753–766. doi: 10.1002/2015GB005324

Stuhldreier, I., Sánchez-Noguera, C., Rixen, T., Cortés, J., Morales, A., and Wild, C. (2015). Effects of seasonal upwelling on inorganic and organic matter dynamics in the water column of eastern Pacific coral reefs. *PloS One* 10, e0142681. doi: 10.1371/journal.pone.0142681

Suzuki, A., and Kawahata, H. (2004). "Reef water CO2 system and carbon production of coral reefs: Topographic control of system-level performance," in *Global Environmental Change in the Ocean and on Land*. Eds. M. Shiyomi, H. Kawahata, H. Koizumi, A. Tsuda and Y. Awaya (TERRAPUB, Tokyo), 229–248. Available online at: http://faculty.petra.ac.id/dwikris/docs/cvitae/docroot/html/www.terrapub.co.jp/e-library/kawahata/pdf/229.pdf (Accessed March 7, 2017).

Tamše, S., Ogrinc, N., Walter, L., Turk, D., and Faganeli, J. (2014). River Sources of dissolved inorganic carbon in the gulf of trieste (N adriatic): stable carbon isotope evidence. *Estuaries Coasts* 38, 151–164. doi: 10.1007/s12237-014-9812-7

Ulloa, A., Aguilar, T., Goicoechea, C., and Ramirez, R. (2011). Descripción, clasificación y aspectos geológicos de las zonas kársticas de Costa Rica. *Rev. Geológica America Cent.* 45, 53–74. doi: 10.15517/rgac.v0i45.1910

Ulloa, A., Vargas, M., Argüello, A., Álvarez, Y., Hidalgo, A., and Deleva, S. (2024). "Main karstic Landscapes and Caves of COSTA RICA," in *Landscapes and Landforms of Costa Rica*. Ed. A. Quesada-Román (Springer International Publishing, Cham), 133–149. doi: 10.1007/978-3-031-64940-0_7

Umaña-Villalobos, G., and Springer, M. (2006). Variación ambiental en el río Grande de Térraba y algunos de sus afluentes, Pacífico sur de Costa Rica. *Rev. Biol. Trop.* 54, 265–272. doi: 10.15517/rbt.v54i1.26850

Vargas, C., Contreras, P., Pérez, C., Sobarzo, M., Saldías, G., and Salisbury, J. (2016). Influences of riverine and upwelling waters on the coastal carbonate system off Central Chile and their ocean acidification implications. *J. Geophys Res. Biogeosci* 121, 1468–1483. doi: 10.1002/2015JG003213

Vargas-Zamora, J. A., Gómez-Ramírez, E., and Morales-Ramírez, Á. (2021). A fjord-like tropical ecosystem, Pacific coast of Costa Rica : overview of research in Golfo Dulce. *Rev. Biol. Trop.* 69, 773–796. doi: 10.15517/rbt.v69i3.46406

Waylen, P., and Laporte, M. (1999). Flooding and the El Niño-Southern Oscillation phenomenon along the Pacific coast of Costa Rica. *Hydrol Process* 13, 2623–2638. doi: 10.1002/(SICI)1099-1085(199911)13:16<2623::AID-HYP941>3.0.CO;2-H

Wizemann, A., Nandini, S., Stuhldreier, I., Sánchez-Noguera, C., Wisshak, M., Westphal, H., et al. (2018). Rapid bioerosion in a tropical upwelling coral reef. *PloS One* 13, e0202887. doi: 10.1371/journal.pone.0202887

frontiers | Frontiers in Marine Science

TYPE Original Research
PUBLISHED 22 October 2025
DOI 10.3389/fmars.2025.1676610

OPEN ACCESS

EDITED BY
Jun Sun,
Tianjin University of Science and Technology, China

REVIEWED BY
Zong-Pei Jiang,
Zhejiang University, China
Luis Amado Ayala-Pérez,
Universidad Autónoma Metropolitana, Mexico

*CORRESPONDENCE
Emily R. Hall
emily8@mote.org

RECEIVED 30 July 2025
ACCEPTED 06 October 2025
PUBLISHED 22 October 2025

CITATION
Hall ER, Hu X, Vreeland-Dawson J, Yates KK, Besonen M, Brenner J, Barbero L, Herzka SZ, Hernández-Ayon JM, Simoes N and González-Díaz P (2025) A tri-national initiative to advance understanding of coastal and ocean acidification in the Gulf of Mexico/Gulf of America. *Front. Mar. Sci.* 12:1676610. doi: 10.3389/fmars.2025.1676610

A tri-national initiative to advance understanding of coastal and ocean acidification in the Gulf of Mexico/Gulf of America

Emily R. Hall[1*], Xinping Hu[2], Jennifer Vreeland-Dawson[3], Kimberly K. Yates[4], Mark Besonen[5], Jorge Brenner[4], Leticia Barbero[6], Sharon Z. Herzka[2], Jose Martín Hernández-Ayon[7], Nuno Simoes[5,8,9] and Patricia González-Díaz[5,10]

[1]Mote Marine Laboratory, Ocean Acidification Program, Sarasota, FL, United States, [2]Marine Science Institute, University of Texas at Austin, Austin, TX, United States, [3]Ocean Associates, Inc., Arlington, VA, United States, [4]Gulf of America Coastal Ocean Observing System, College Station, TX, United States, [5]Harte Research Institute, Texas A&M University-Corpus Christi, Corpus Christi, TX, United States, [6]Cooperative Institute for Marine and Atmospheric Sciences, University of Miami, Miami, FL, United States, [7]Instituto de Investigaciones Oceanológicas, Universidad Autónoma de Baja California, Ensenada, Mexico, [8]Unidad Multidisciplinaria de Docencia e Investigación Sisal, Universidad Nacional Autónoma de México, Sisal, Mexico, [9]Laboratorio Nacional de Resiliencia Costera, Laboratorios Nacionales, Sisal, Mexico, [10]Centro de Investigaciones Marinas, Universidad de La Habana, La Habana, Cuba

The Gulf of Mexico's (also recognized by the United States government as the Gulf of America; herein referred to as "the Gulf") valuable and diverse marine, coastal, and estuarine environments sustain many habitats, species, and economically important fisheries that are vulnerable to open ocean and coastal acidification (OOCA), including shellfish, coral reefs, and other carbonate reefs and seafloor. OOCA poses an economic threat to the Gulf's economy, which is estimated to have a combined value of $2.04 trillion (US) per year across Cuba, Mexico and the United States (U.S.). Scientists from Cuba, Mexico, and the U.S. co-organized and co-hosted the first Gulf International Ocean Acidification Summit on Oct. 18-19, 2022 in Mérida, Yucatan, Mexico to exchange information and begin development of a new tri-national network to address the socioeconomic and ecological impacts of OOCA in the Gulf based on common needs. The meeting included representatives from government agencies, universities, research institutes, non-governmental organizations, and was sponsored by the Furgason Fellowship of the Harte Research Institute at Texas A&M University-Corpus Christi. Discussions focused on each country's challenges, including known and potential socioeconomic vulnerabilities and biological and ecosystem responses to OOCA. Shared priorities were identified for observational, biological, environmental needs, socioeconomic research, outreach, and communications. Priority geographic locations for the study and short and long-term monitoring of OOCA were identified based on the group's knowledge of oceanographic conditions and vulnerable regions. Longer-term actions that will help support multinational collaborations include: identifying shared data and information platforms; standardizing chemical and biological

sampling methodologies; coordinating communications with regulatory agencies and resource managers; and coordinating monitoring activities, collaborative research projects, and tri-national comparisons and synthesis of findings. We present guidance from this effort for an integrated, multinational approach to understanding the causes and consequences of OOCA in the Gulf.

KEYWORDS

coastal acidification, ocean acidification, tri-national, Gulf of America, Gulf of Mexico

1 Introduction

The Gulf, the ninth largest ocean basin in the world, is home to highly diverse marine, coastal, and estuarine environments, including ecosystems that contribute significantly to the economy of the three nations surrounding the Gulf (the U.S., Mexico, and Cuba; Figure 1). The Gulf is home to multiple species potentially susceptible to OOCA impacts such as shellfish, coral reefs, mesophotic corals, phytoplankton and other economically important fisheries. These organisms occupy a variety of habitats in the Gulf, including carbonate reefs and seafloor environments that can change as a result of acidification. The Gulf is highly biodiverse, with over 15,000 described species (Felder and Camp, 2009). This number is likely underestimated due to limited surveys on the slope and in deepwater regions.

Understanding, predicting, and responding to local and global stressors and responsive changes within the Gulf requires an integrated geographical approach due the interconnectedness of its waters through the current systems of the central, deep Gulf, estuaries, the shelves, and inshore/offshore flows (Morey et al., 2003; Oey et al., 2005; Martínez-López and Zavala-Hidalgo, 2009). Therefore, developing a tri-national network to exchange information and address the socioeconomic and ecological impacts of ocean and coastal acidification in the Gulf, based on mutually understood needs or shared needs, is of utmost importance.

Open ocean and coastal acidification (OOCA) throughout the Gulf is due to elevated atmospheric carbon dioxide (CO_2) as well as other chemical, biological, and physical processes (Osborne et al., 2022). Approximately one quarter to one third of annual CO_2 emissions are absorbed by the ocean, which lowers seawater pH (an indicator of ocean acidification). Coastal acidification is caused by a combination of ocean acidification and land-based pollution sources (for example, regional excess nutrient inputs to estuaries or coastal waters that can lead to eutrophication, hypoxia, and remineralization) that can contribute to localized acidification. Harmful algal blooms, freshwater inflows, biological production and respiration, anaerobic respiration, calcium carbonate ($CaCO_3$) dissolution, other benthic inputs, and episodic storm events have all been shown to contribute to or are affected by coastal acidification (Cai et al., 2021; Hicks et al., 2022; Hall et al., 2024; Zhang and Xue, 2022). Riverine systems are poorly buffered, have variable total alkalinity, and are often high in pCO_2 (Cai et al., 2011; 2021). A long-term time-series of OOCA does not currently exist in the Gulf (Hu, 2019); however, several studies have documented that OOCA is occurring in both the open Gulf and within estuarine environments (Hu et al., 2015; Robbins and Lisle, 2017; Kealoha et al., 2020; Osborne et al., 2022).

Much of the research on OOCA in the Gulf has primarily focused on US waters (Hu, 2019). The shelves of the northern Gulf (a tropical-subtropical region) are dominated by rivers and eutrophication (Laurent et al., 2017), with localized coral reefs in the Florida Keys and Flower Garden Banks in Texas (Gil-Agudelo et al., 2020), mesophotic reefs (30–150 m; Turner et al., 2017) and karst geology in the southern FL peninsula. Historically, the National Oceanic and Atmospheric Administration (NOAA) leads the effort to monitor OOCA across the Gulf through the Gulf Ecosystems and Carbon Cruises (GOMECC) and Ship of Opportunity-OA (SOOP-OA) programs. The data obtained demonstrate the importance of ocean circulation, temperature seasonality, and the influence of rivers on carbon chemistry dynamics in the Gulf (Wang et al., 2013; Wanninkhof et al., 2015; Kealoha et al., 2020). In Mexican waters, the XIXIMI program has conducted total alkalinity (TA) and dissolved inorganic carbon (DIC) measurements in the southern Gulf offshore waters since 2010. Data from the XIXIMI expeditions show similar vertical structures in the DIC and TA profiles over time in the central and southern Gulf, comparable to the Caribbean profiles generated during the World Ocean Circulation Experiment (WOCE) in 1994. Like the northern Gulf, these regions exhibit high TA/DIC ratios, indicating a strong buffering capacity against acidification (https://www.ncei.noaa.gov/products/world-ocean-circulation-experiment Gledhill et al., 2008). The Research Network of Marine-Coastal Stressors in Latin America and the Caribbean (Red de Investigació n Marino-Costera; REMARCO) has established a network across the Caribbean and Latin America to increase measurements of OA (Espinosa, 2023). Despite these efforts, existing programs do not provide robust temporal coverage at subannual or subseasonal water column carbon chemistry scales, especially in the central Gulf region.

Cuba, while bordering the Gulf, is the largest island in the Caribbean. Its surrounding waters are generally oligotrophic, coral

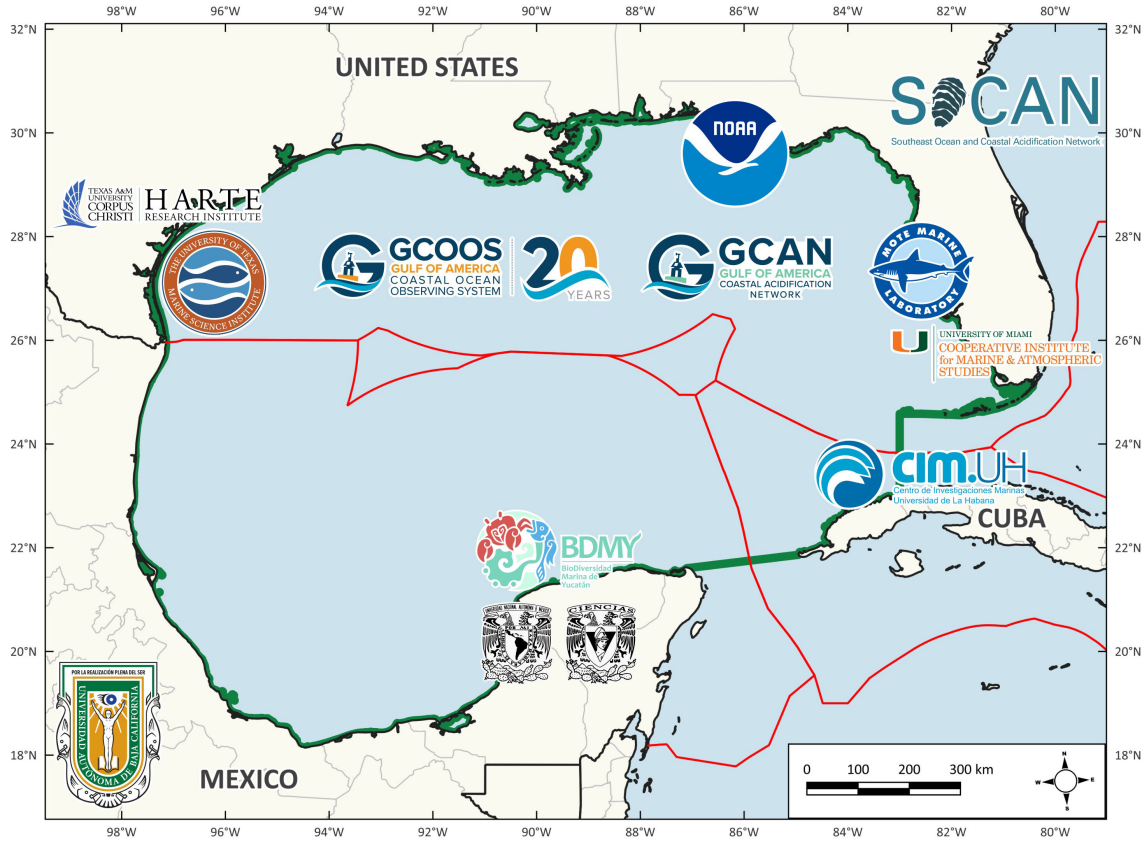

FIGURE 1
Map of the Gulf and surrounding nations. Red lines indicate exclusive economic zones of each nation. Green boundary line indicates official Gulf boundary. Representative logos from participating institutions are included.

reef ecosystems dominate its nearshore habitats, and studies indicate an increase in OOCA (Gledhill et al., 2008). The productive Yucatan Peninsula coast is characterized by karstic geology and submarine groundwater discharges (SGDs), deep water upwellings in the northeast, and seasonal wind-driven upwelling along the coast. Different seasonal conditions affect OOCA. Cold fronts typically approach from the north in the fall and winter and are accompanied by elevated values of dissolved inorganic carbon and total alkalinity near the coast. OOCA is also affected by geophysical characteristics, including the influence of SGD, oxidation of organic matter, and dissolution of carbonate minerals (Barranco et al., 2022). Monitoring efforts that encompass seasonal variability would help broaden understanding of the carbonate system dynamics in these regions.

The Loop Current, which enters through the Yucatan Channel and exits through the Straits of Florida, dominates the mesoscale circulation of the central Gulf in the top ca. 1000 m (Oey et al., 2005; Candela et al., 2019). All nations bordering the Gulf are influenced by the Loop Current and the anticyclonic eddies that detach from it periodically. They are transported west and southwest, demonstrating the region's oceanographic interconnectedness (Hamilton et al., 1999). The upper layer is also influenced by near-surface freshwater discharge from rivers; water mass hydrographic and biogeochemical properties are altered through water density differences, mixing, and bathymetry, and are spatially variable and dynamic (Portela et al., 2018; McKinney et al., 2021; Cervantes-Díaz et al., 2022). Over the past several decades, human interactions have led to changes and impacts on natural resources throughout the Gulf, including fisheries resources, recreational facilities, offshore oil drilling, land use changes, and changes in organism and ecosystem diversity.

OOCA poses an economic threat to the Gulf's economy, which is estimated to be worth $2.04 trillion per year across Cuba, Mexico, and the US (Shepard et al., 2013). According to National Marine Fisheries (2024), the Gulf's commercial seafood landings for revenue in 2022 in the US was $921 million, accounting for 17.4% of national landings and 15.6% of the total revenue. Of the total Gulf commercial landings in 2021-22, shellfish contributed $66 million and almost 7% of the revenue. Recreational finfish fisheries accounted for catches of 580,375 individuals, which corresponds to 52% of the US total (National Marine Fisheries Service, 2024). Oyster fisheries alone brought in an estimated revenue of $76.9 and 93.4 million in 2023 and 2022, respectively (https://www.fisheries.noaa.gov/foss/f?p=215:200:3384444710405). Mexico's 2023 Statistical Yearbook of Aquaculture, published by the Fisheries National Commission of Aquaculture and Fisheries (CONAPESCA), indicates that the value of the Gulf's fisheries was approximately $440 million, with oyster production

contributing $3.4 million (Comisión Nacional de Acuacultura y Pesca, 2023). Major fisheries for Cuba include export of spiny lobster, penaid shrimp, and tuna. Since 1992, average annual value of fishery export in Cuba is ~$107 million annually (Adams et al., 2000).

The Gulf ecosystems are subject to multiple local (e.g., overfishing, eutrophication, hypoxia, and oil spills) and global (e.g., ocean warming and acidification) anthropogenic stressors. The Gulf U.S. shell fisheries are particularly vulnerable to ocean and coastal impacts because of a combination of environmental (e.g., eutrophication and high river input), biological (e.g., low diversity of shellfish fishery harvest), and social factors (e.g., low political engagement in OOCA, ocean warming, and relatively low science accessibility; Ekstrom et al., 2015). In Mexico, the lack of long-term surveys of environmental conditions and biological communities, limited enforcement of fishery regulations, overexploitation, and coastal eutrophication and pollution threaten ecosystem health (Caso et al., 2014). Socioeconomic risks from ocean and coastal acidification impacts to fisheries' species are largely unknown. In addition to elevated carbon dioxide (CO_2) in the atmosphere, acidification in the region is influenced by a complex interplay of processes and multiple stressors such as increasing water temperature, changing ocean circulation, runoff of both river water and excess nutrients, as well as regionally low oxygen over the shelf, harmful algal blooms (HABs), storms, and oil spills. For example, blooms of *Sargassum* spp. have been problematic throughout the Caribbean. However, more recent studies show blooms persisting throughout the Gulf as well (Zhang et al., 2024). Decaying *Sargassum* spp. blooms could contribute to localized OOCA events (Liu et al., 2024) but may also have positive effects under OOCA on coral physiology (Lankes et al., 2025).

The Gulf seawater chemistry is highly complex but remains relatively under-studied concerning acidification (Osborne et al., 2022). Critical knowledge, research, and monitoring gaps limit our current understanding of environmental, ecological, and socioeconomic impacts needed to improve models for predicting acidification and its consequences. The diversity of habitats found in the Gulf spanning multiple climatic zones and the connection between bordering nations' ocean and coastal resources through ocean circulation and migration makes international collaboration critical to understanding the influence of acidification, its causes, and impacts in the Gulf. A shared, multi-national vision of a Gulf that is prepared to respond and adapt to ocean acidification united an international team of scientists from the US, Cuba, and Mexico to organize and conduct the Gulf's first International Ocean Acidification Summit.

2 Materials and methods

2.1 Meeting purpose and scope

Thirty-one participants from the US, Cuba, and Mexico met in Mérida, Yucatán, Mexico, from October 18-19, 2022, for the first "Gulf International Ocean Acidification Summit". Organizing institutions included: Harte Research Institute (HRI), Texas A&M University-Corpus Christi; the Gulf of America Coastal Ocean Observing System (GCOOS, a Regional Association of the U.S. Integrated Ocean Observing System); Gulf of America Coastal Acidification Network (GCAN); Centro de Investigaciones Marinas, Universidad de La Habana (CIM-UH); Centro de Estudios Ambientales de Cienfuegos (CEAC); UMDI-Sisal, Facultad de Ciencias, Universidad Nacional Autónoma de México (UNAM); Instituto de Investigaciones Oceanológicas, Universidad Autonoma de Baja California (IIO-UABC); and Kalanbio A.C. – Mexico. Meeting participants included representatives from government agencies, universities, research institutes, non-governmental organizations, and graduate students. The primary meeting objectives included: fostering communication among international colleagues; sharing information on OOCA science, identifying gaps, research, and monitoring needs; and exploring approaches and opportunities for collaboration.

Prior to the in-person meeting, GCAN hosted a virtual coordination meeting that included activities to prioritize topics for discussion at the in-person meeting based on common needs across the nations. The results of the discussion were used to develop the summit's agenda. Participants were also asked to join a virtual meeting to introduce each other as a group, identify other stakeholders who may wish to participate, provide summaries of each participant's information needs related to OOCA for the organizing committee, and to allow participants to assist with determining what was required to ensure a productive meeting that met the overall objectives.

The meeting in Mérida, Mexico, began with a social activity and introductory presentations from the sponsors and representatives of each of the three countries, covering meeting goals, potential outcomes, and brief overviews of the state of the science, gaps, and challenges from each country. These presentations were followed by topic-specific breakout sessions and group discussions on gaps, challenges, common regional issues, and scientific and geographic priorities related to: exposure to OOCA and region-specific special considerations affecting exposure; biological response to OOCA, including species, habitats, and ecosystem-level responses; and known and potential socioeconomic vulnerabilities. Due to the varying levels of expertise among the participants, protocols for sample collection, analysis, and QA/QC were discussed, as were the challenges of using optical sensors for continuous monitoring (sensor availability, cost, and deployment locations). The final group discussion focused on approaches for developing a tri-national network for ocean acidification and acknowledging the shared commitment to working toward this goal. The group agreed upon short-term actions to begin facilitating the development of this network, including establishing pathways and platforms to facilitate group communication, increasing awareness of the tri-national effort to stakeholders, policy-makers, and managers, and building on existing collaborative efforts and networks such as GCAN. Additionally, the group identified shared priorities for observational, biological, and socioeconomic research; outreach and communications; priority geographic locations for study; and

longer-term actions needed to facilitate multi-national collaboration such as: identification or development of shared data and information platforms; standardization of chemical and biological methods; joint training activities for research and monitoring practices and procedures; coordinated interaction and communication with regulatory agencies and resource managers for guidance to science; and coordination of monitoring activities, collaborative research experiments, and tri-national comparison of results.

2.2 Anticipated outcomes

In addition to working toward development of a tri-national network to foster collaboration among the three nations on ocean acidification research and monitoring, other anticipated outcomes from this meeting included: co-development of a report by the participant group describing meeting topics and discussions in detail; development of a tri-national Gulf regional gap analysis to assist with identifying nation-specific as well as shared research and monitoring gaps; development of a multi-national Gulf socioeconomic risk and vulnerability assessment/report; and development of special topical work groups to facilitate international collaborative research activities, training opportunities, and funding needs.

3 Results

3.1 Preliminary meeting

During the virtual meeting with participants, the highest priority communication needs were identified as exchanging experiences with colleagues related to science and working with stakeholders, learning different perspectives across regions and sectors on OOCA's impacts, and developing a tri-national network to facilitate multi-national collaboration on OOCA research and monitoring.

3.2 Meeting introductions

Social activities were conducted at the beginning of each day of the summit to provide an opportunity for participants to meet, engage in informal conversation, and to begin working together as a team. For example, one group activity included all participants working together to map the Gulf on the floor with a rope. Participants were grouped by region (U.S., Cuba, or Mexico) and the rope was placed in the shape of the coastline adjacent to their county (Figure 2). Then participants were asked to work together across regions to evaluate and improve the map as a way to facilitate interaction and conversation. Introductions were provided on the meeting agenda, the summit organizing institutions (GCOOS and HRI), GCAN, state of the science on ocean and coastal acidification, and summaries of recent or ongoing research cruises that encompass most of the Gulf. After introductions, participants were asked to participate in topic-specific group discussions on gaps, challenges, common regional issues, scientific and geographic priorities related to three different themes including: 1. exposure to ocean acidification and region-specific special considerations influencing their vulnerability; 2. potential biological responses to ocean acidification including specific species, habitats, and ecosystem responses; and 3. known and potential socioeconomic vulnerabilities. A final group discussion focused on approaches for developing a tri-national network for OOCA and acknowledging the shared commitment to working toward this goal.

3.3 Breakout session 1: exposure

The exposure breakout session consisted of four subgroups focusing on identification of knowledge gaps, measurement protocols, communications, and solutions. Geographic gaps for OOCA research and monitoring were identified as:

- nearshore and estuarine measurements (<10 m depth),
- the deep-water region of the Gulf,
- Usumacinta River outflow and impacts,

FIGURE 2
The social activity involved participants being asked to form the shape of the Gulf.

- Veracruz Region and National Park, and
- ocean and coastal impacts to the karst environments of Florida and the Yucatan Peninsula.

OOCA measurement priorities were identified as:

- all countries needing higher temporal and spatial resolution measurements to pair with biological studies and address resource management issues,
- establishing laboratories with the capacity to integrate chemical and biological studies,
- need for identifying OOCA indicator species that are charismatic and relatable to the public,
- ensuring the availability of reference samples, especially in Mexico and Cuba, and
- making sure the sampling and analytical methodology is standardized (by establishing best practices) for chemistry and biology measurements.

Communications priorities were identified as:

- conveying OOCA information to non-experts in understandable terms,
- emphasizing that although OOCA is underemphasized as a problem in the Gulf, the system has been shown to have some of the fastest acidification rates measured as declining carbonate saturation states,
- a need for a transdisciplinary approach to communicating OOCA issues,
- improving efforts oriented toward stakeholder outreach through interaction with local and regional groups, and
- expanding awareness through student education programs.

Potential solutions identified included:

- collaboration and development of common communication strategies and practices,
- using the expertise within the summit's participants to share best practices for OOCA studies,
- implementing training activities to promote professional development in the field of OOCA that are oriented toward early career researchers,
- initiate laboratory inter-comparisons across nations, and develop sampling kits to train people for sample collection and expanding monitoring through citizen science,
- identify common (Gulf-wide) indicator species and establish baselines of biological responses to OOCA,
- developing an approach for elevating perception of impact such as designing a multi-national sampling effort and strategy for the most impacted areas and events,
- exploring collaboration with the National Association of Marine Labs (NAML) for help with obtaining and distributing certified reference materials, and
- identifying or developing cost-effective alternatives for pH measurements.

3.4 Breakout session 2: biological response

The biological response breakout session was broken out into three subgroups covering gaps, challenges, and solutions. Knowledge gaps were identified as

- OOCA impacts on marine fish and shellfish,
- studies on other Gulf marine organisms (e.g. megafauna), and
- research on food web implications from plankton to higher species.

Challenges were identified as:

- no standardized methods across regions and
- difficulty of studying physiological effects on larger coastal and marine organisms.

Solutions were identified as:

- the need to identify common species of interest across nations and involve fisheries regulatory agencies in the process to provide guidance for biological research focus and
- the need for vulnerability models for species groups.

3.5 Breakout session 3: socioeconomic considerations

The socioeconomic session was divided into two subgroups, centered on knowledge gaps and potential activities. The socioeconomic impacts of OOCA throughout the Gulf can be linked to recreational tourism (diving, hotel occupancy along the coast, etc.), ecotourism, shellfish farming, and commercial, recreational, and subsistence fishing. The total economic value of fisheries is well-studied by each country surrounding the Gulf, but the current or future estimates if impacted by OOCA have not been assessed. Additionally, socioeconomic impacts are likely to differ among nations and regions (such as states in the U.S. and Mexico and provinces in Cuba), and specific evaluation and assessment are required. The gaps the workshop participants identified include:

- need for assessing potential socioeconomic impacts and potential values within each region,
- a pressing need for public, community leader, managers, and policy maker education about OOCA, particularly in Mexico and Cuba, and
- development of educational content in English and Spanish to promote public and stakeholder education.

Potential activities include:

- mining socioeconomic data from each country to evaluate the realized or potential effect of OOCA and updating as a tri-national effort,

- identifying socio-economists who understand the effects of OOCA on economic value,
- implementing community listening sessions,
- increasing partnership development (e.g., working with organizations that function as liaisons),
- targeted public engagement, and
- creative communication.

3.6 Development of a tri-national network

The final group discussion focused on approaches for developing a "Tri-National Network for OOCA" and acknowledging their shared commitment toward this goal. The group agreed upon short- and long-term actions to begin facilitating the development of the network, including establishing pathways and platforms to facilitate group communication, increasing awareness of this tri-national effort, and building on existing collaborative efforts (Table 1). Additionally, the group identified shared priorities for observational, biological, and socioeconomic research, including environmental justice needs; outreach and communication; and pursuing funding and longer-term actions needed to facilitate multinational collaboration. Priority locations within each region for monitoring and research were also identified (Table 2).

TABLE 1 Short- and long-term action items for a tri-national OA network.

Short-term action items
Continuation of tri-national network communications
Follow-up meetings
Search for funding for international collaborations
Long-term action items:
Identification or development of shared data and information platforms
Standardization of analytical methods
Joint training activities for research, monitoring practices, and protocols
Coordinated interaction and communication with regulatory agencies and resource managers to identify and guide scientific needs
Coordination of monitoring activities, collaborative research experiments, and tri-national comparison of results

TABLE 2 Priority locations for pilot studies within each region.

U.S.	Cuba	Mexico
Florida Keys	Guanahacabibes MPA	Veracruz MPA
Northwest Gulf	La Habana	Laguna de Términos MPA
Florida Shelf	Cayo Santa María MPA	Celestún MPA
		Alacranes MPA

MPA, Marine Protected Areas.

4 Discussion

The Gulf is a semi-enclosed oceanic basin of approximately 1.6 million km^2 that connects Mexico, the US, and Cuba (Turner and Rabalais, 2019). These nations are aware of risks to the Gulf, including the degradation of coastal areas that support local communities, loss of habitat and marine and coastal natural resources; overfishing; increasing harmful algal blooms; hypoxia; vessel groundings on coral reefs; coastal subsidence; energy exploration (including oil spills); increased production in coastal areas; increases in the frequency of environmental changes in the ecosystem (such as fluctuations in abundance and distribution of fish, birds and mammals due to anthropogenic stressors linked to climate change); and the need for climate change monitoring (UNIDO, 2014). OOCA, currently understood as both a water quality and a climate change issue (Doney et al., 2009; Wallace et al., 2014), is increasing throughout the Gulf estuaries, coasts, and open ocean (Wanninkhof et al., 2015; Robbins and Lisle, 2017; Osborne et al., 2022; Jiang et al., 2024), yet the connectivity of populations and communities throughout the Gulf has not been fully evaluated. Developing a tri-national network to foster collaboration among the three nations on OOCA research and monitoring is imperative to understand the Gulf's oceanographic and biological interconnectedness.

During this first International OA Meeting, participants concluded that exposure to OOCA is poorly understood, particularly in shared waters and adjacent national coastlines. Several research and monitoring gaps were identified; although some previous studies within each region have been conducted and published, they were either short-term or lacked a broader context. For example, only a handful of studies on nearshore and estuarine measurements throughout the Gulf have been published, and these are predominantly in the U.S. (e.g., Cai et al., 2011; Hu et al., 2015; Robbins and Lisle, 2017; McCutcheon and Hu, 2022; Hall et al., 2024; Martínez-Trejo et al., 2024). Some coral reefs, like the Flower Garden Banks, and the northern Gulf (e.g., Mississippi River outflow), have been relatively well-studied (e.g. see Hall et al., 2020; Osborne et al., 2022; and references therein). However, studies in deep Gulf waters (>300 m depths) are generally limited because of difficult access and high costs. In addition, benthic landers are promising for deep water acidification studies at the sediment-water interface (Berelson et al., 2019). The Grijalva-Usumacinta River System provides the highest freshwater inflow into the southern Gulf, yet the impact on OOCA is poorly understood. Studies in that system are only beginning to evaluate changes in carbon cycles (Soria-Reinoso et al., 2022). The coast and shelf of the state of Veracruz in the southwestern Gulf has the main commercial port in Mexican waters, an extensive network of coral reef systems that includes endemic species of fishes and is one of the largest marine protected areas in Mexico. Studies on high population centers that are popular fishing and recreational areas, like the Grijalva-Usumacinta River System and the state of Veracruz, can serve as models to promote and enhance public awareness, motivate effective management for current or projected OOCA impacts, with the ultimate goal of protecting or restoring ecosystems (Duarte et al., 2008). Other poorly understood systems

include karst environments. Much of the geology in the Gulf (east of Louisiana in the U.S., Cuba, and Mexico) is karst. These systems are unique in that the dissolution of carbonate rocks can increase TA and DIC, yet how these systems influence OOCA is uncertain (Patin et al., 2021; Barranco et al., 2022; Martínez-Trejo et al., 2024). Limited *in-situ* studies have been conducted in coral reef ecosystems in the Gulf (e.g. Crook et al., 2012; Dee et al., 2019; Guan et al., 2020; Lawman et al., 2022).

To tackle these gaps, participants determined that all three nations need higher temporal and spatial resolution measurements. Short term or temporally infrequent data collections can provide some information (e.g. Hall et al., 2024), however frequent and sustained data collection (e.g. from *in situ* sensors) can more effectively capture key parameter measurements under variable environmental conditions, allowing for a better characterization of daily to seasonal trends in carbonate chemistry across a range of estuarine, coastal and marine settings (Rosenau et al., 2021). The group also recognized that higher temporal and spatial resolution measurements should be paired with biological studies. A unified set of indicator species that are charismatic and relatable to the public would contribute to developing management responses to OOCA (Ducarme et al., 2013). Many species of coral have been well studied for the effects of OOCA (e.g. Lunden et al., 2014; Kurman et al., 2017; Muller et al., 2021; Bove et al., 2022), yet corals are distributed in isolated locations throughout the Gulf and OOCA exposure and impacts do not exist entirely throughout the Gulf. Other, less-studied, yet ecologically and economically relevant organism studies are needed. Impacts of OOCA on marine fish species and food web interactions throughout the Gulf are limited (Osborne et al., 2022). A challenge is that there are currently no standardized methods to assess the effects of OOCA on marine organisms across the Gulf regions. Common species of interest that are found across the Gulf should be identified, and fisheries regulatory agencies should be involved to guide biological research focus (e.g. Galindo-Cortes et al., 2019). Lastly, OOCA vulnerability models are needed for species groups to support ecosystem-based management decisions across nations (Ekstrom et al., 2015; Ocaña et al., 2019).

Addressing these gaps requires increased funding. Funding for marine research in Mexico, Cuba, and the U.S. could come from various sources, including government agencies, private foundations, and international organizations. Participants agree that shared strategies and best practices can be established effectively despite funding limitations. Collaboration on best practices for methods of OOCA sampling and analyses, including standard protocols for biological sampling, is imperative for cross-nation studies. There are currently several best practices manuals for studies on OOCA (e.g. Dickson et al., 2007; Riebessel et al., 2011; Boyd et al., 2019; Sutton et al., 2022); however, some institutions do not have access to the materials, instruments, and methods described in these manuals. To define these best practices throughout the Gulf, joint training activities and shared students can be utilized to grow human capacity. Programs like international internships and fellowships offered by universities or non-government organizations can increase participation (Torres et al., 2017; Sharma, 2024).

Another potential action to overcome these gaps is to begin collaborative interlaboratory comparisons on sampling and carbonate chemistry analyses across nations. Shared data and the usefulness of these measurements will depend on data quality and consistency. Historically, interlaboratory comparisons for OOCA analyses have been conducted throughout the U.S. using certified reference materials provided by the Dickson Lab; however, these comparisons have not occurred since 2017 (Bockmon and Dickson, 2015). Likewise, laboratories across the U.S., Mexico, and Cuba have not performed interlaboratory comparisons. As previously stated, many institutions lack the proper equipment and materials to perform interlaboratory comparisons. Organizations like the Global Ocean Acidification Observing Network (GOA-ON) have created low-cost kits for collecting ocean acidification measurements. The GOA-ON in a Box kits have been distributed to scientists in sixteen countries in Africa, Pacific Small Island Developing States, and Latin America, and can be used to train people in the measurement, collection of OOCA indicators and expanding monitoring through citizen science (Valauri-Orton et al., 2025).

There will be socioeconomic impacts from OOCA throughout the Gulf, including tourism and commercial, recreational, and subsistence fishing sectors. Understanding socioeconomic impacts due to OOCA in the Gulf can be improved by better defining the economic values of impacted sectors within each region. The total value of fisheries is well-studied by each country surrounding the Gulf (e.g. Sánchez-Gil et al., 2004; Valle et al., 2011; Ekstrom et al., 2015; Anuario Estadístico de Acuacultura y Pesca 2023), but not the species-specific potential losses if impacted by OOCA. Additionally, valuation of resources may differ depending on the country leading the study and available data (Adams et al., 2004). Understanding the impacts of OOCA on tourism remains a challenge to define.

Another challenge is public education and awareness about OOCA as it relates to the potential impacts on socioeconomic activities. Evaluating and identifying regions or environmental conditions that are conducive to OOCA is critical to mitigating its impacts, yet is hindered by a lack of a sense of urgency in the general public and a lack of media coverage (Tiller et al., 2019). Multiple efforts throughout the US are working toward better public awareness (which are also directed and coordinated with managers and policy-makers), such as the Coastal Acidification Networks, the Ocean Acidification Alliance, NOAA Ocean Acidification Program, the National SeaGrant Programs, and others (Cook and Kim, 2019; Cross et al., 2019; Hall et al., 2020; Osborne et al., 2022). While these efforts are starting to extend across nations, they remain insufficient in certain regions. For example, the Global Ocean Acidification Network (GOA-ON) is an international collaborative network that monitors ocean acidification in marine environments to understand its causes and impacts. It supports the development of mitigation and adaptation strategies. The network encourages the formation of regional centers, such as the North American and Caribbean Hubs, where EUA, Mexico, and Cuba are all included, to collect comparable data and support predictive models. In addition, in Mexico, the Mexican carbon Program (PMC) also seeks to coordinate scientific activities related to carbon cycle studies carried out, act as

Mexico's scientific counterpart to similar programs in other countries, develop and promote scientific research related to the carbon cycle in the country, and systematize scientific information on carbon.

Results from this meeting indicated a strong need for a tri-national network on OOCA. Since the summit, some progress has occurred, laying a foundation toward achieving some of the identified priorities. Short-term and long-term communication needs were determined. In the short term, a web page was developed by HRI (https://www.harteresearch.org/collaboration/trinational-initiative-mexico-and-cuba-0, accessed 03/29/25) including a linked page to the tri-national network on OOCA (https://gcoos.org/oa-trinational/, accessed 03/29/25) and multiple press releases were developed. In the long-term, priority international OOCA projects were agreed upon (Table 2). A more comprehensive Gulf of Mexico Ecosystems and Carbon Cycle (GOMECC) cruise began in 2017. It continued with the 2021 cruise, sampling international waters of Mexico and Cuba for the first time to establish an OOCA monitoring network to quantify the increase in near-surface water carbon dioxide and associated changes in inorganic carbon speciation (Barbero et al., 2019). Supported by NOAA OAP, GOMECC-5 is scheduled for the fall of 2025. A series of webinars were presented virtually and focused on establishing collaborative opportunities among the US Marine Biodiversity Observation Network (MBON), GCAN and the Southeast Ocean and Coastal Acidification Network (SOCAN) (https://gcoos.org/webinars2024/; accessed 3/25/25). The goal of building synergy across networks to advance science in support of resource management and the Blue Economy aligns with the goals of the tri-national OOCA network. Topics of discussion included advancing the state of MBON and OOCA science, identifying opportunities to bridge MBON and OOCA science, synthesizing lessons learned, and developing new partnerships. GCOOS has since opened membership to international collaborators. These initiatives are also synergistic with ongoing efforts to facilitate cross-national collaboration (Machlis et al., 2012; Ayala-Castañares and Knox, 2000; UNIDO, 2014; Zaldívar-Jiménez et al., 2017).

There has also been progress from each represented nation's policies on OOCA throughout the Gulf since this initiative occurred. In 2023, the US Ocean Acidification Action Plan was established, which outlines strategies for mitigation, adaptation, and resilience to OOCA (Interagency Working Group on Ocean Acidification, 2023). This plan also aligns with the International Alliance to Combat Ocean Acidification (OA Alliance), which the US joined in 2022. In this plan, the US commits to working with communities worldwide to share knowledge and build capacity to address the shared challenges of OOCA. The US has also added a new Coastal Acidification Network (The Caribbean CAN [Cari-CAN]) to its network within NOAA. Cari-CAN engages with international bodies like the UNESCO Intergovernmental Oceanographic Committee and other research networks to address OOCA. Cuba continues to be a part of the Research Network of Marine-Coastal Stressors in Latin America and the Caribbean (REMACO) project (www.remarco.org/en/cuba/, accessed 9/22/2025). This network aims to establish current levels of OOCA and promote policies aimed at reducing CO_2 emissions. Most recently, Cuba is participating in the project *Strengthening Regional Capabilities on the Application of Nuclear and Isotopic Techniques to Increase Knowledge about Stressors that Affect Marine and Coastal Sustainable Management* (ARCAL CLXXXIX; https://remarco.org/en/cuba/) as part of their participation in the Research Network of Marine-Coastal Stressors in Latin America and the Caribbean (REMARCO; https://remarco.org/en/). (Nuclear techniques refer to contaminant detection.) Data from Cuba is currently being uploaded to the United Nations SDG 14.3.1 Monitoring Portal and a monitoring tool developed by UNESCO's Intergovernmental Oceanographic Commission to share ocean acidification data (Grabb et al., 2025). Mexico is expected to publish an updated national policy for the sustainable management of Mexico's seas and coasts during the latter half of 2025: *Política Nacional para el Manejo Sustentable de Mares y Costas 2025* (https://sdgs.un.org/partnerships/publication-updated-national-policy-sustainable-management-mexicos-seas-and-coasts). This policy will serve as Mexico's Sustainable Ocean Plan, is part of the country's commitments to the High-Level Panel for a Sustainable Ocean Economy and preliminarily includes a focus on OOCA. Some initiatives will likely overlap between the three nations. Future efforts should support collaborative efforts that complement existing monitoring efforts and the understanding of the drivers of OOCA in the Gulf.

A trinational initiative involving the US, Mexico, and Cuba is crucial for understanding OOCA in the Gulf due to the shared nature of marine ecosystems and the transboundary challenges they face. The Gulf's diverse habitats and species, including shellfish and coral reefs, are vulnerable to OOCA, which poses significant ecological and economic threats. Collaborative efforts enable the pooling of resources, expertise, and data, leading to a more comprehensive understanding of acidification patterns and impacts across the entire Gulf region. Such cooperation fosters the development of unified strategies and policies to mitigate adverse effects, benefiting all nations involved.

Data availability statement

The original contributions presented in the study are included in the article/supplementary material. Further inquiries can be directed to the corresponding author.

Ethics statement

Written informed consent was obtained from the individual(s) for the publication of any potentially identifiable images or data included in this article.

Author contributions

EH: Investigation, Writing – review & editing, Methodology, Funding acquisition, Conceptualization, Writing – original draft.

XH: Writing – review & editing, Investigation, Conceptualization, Funding acquisition, Methodology, Project administration. JV: Writing – review & editing, Investigation, Methodology, Conceptualization, Project administration. KY: Methodology, Conceptualization, Project administration, Investigation, Funding acquisition, Writing – review & editing. MB: Methodology, Project administration, Conceptualization, Investigation, Funding acquisition, Writing – review & editing. JB: Funding acquisition, Conceptualization, Writing – review & editing, Project administration, Methodology, Investigation. LB: Conceptualization, Writing – review & editing, Methodology, Investigation. SH: Funding acquisition, Methodology, Project administration, Conceptualization, Investigation, Writing – review & editing. JH: Methodology, Writing – review & editing, Investigation, Conceptualization. NS: Conceptualization, Methodology, Investigation, Writing – review & editing. PG: Conceptualization, Methodology, Writing – review & editing, Project administration, Investigation.

Funding

The author(s) declare financial support was received for the research and/or publication of this article. This effort was supported by the Furgason Fellowship of the Harte Research Institute (HRI) at Texas A&M University-Corpus Christi. Funding was also provided to EH by NOAA OAP (NA21NOS0120097).

Acknowledgments

The authors would like to acknowledge all participants of the workshop including Gabriela Aquilera Pérez, Christian Appendini, Miguel Batista, Matt Bethel, José Cardoso Mohedano, Cecilia Chapa Balcorta, Dorka Cobián Rojas, Adolfo Gracia, Yusmila Helguera Pedraza, Aracely Hernández, Jorge Herrera-Silveira, Claire McGuire, Alain Muñoz Caravaca, Alejandra Navarrete, Daniel Pech, and Armando Toyokazu Wakida Kusunoki.

Conflict of interest

Author JV-D was employed by Ocean Associates, Inc.

The remaining authors declare that the research was conducted in the absence of any commercial or financial relationships that could be construed as a potential conflict of interest.

Generative AI statement

The author(s) declare that no Generative AI was used in the creation of this manuscript.

Any alternative text (alt text) provided alongside figures in this article has been generated by Frontiers with the support of artificial intelligence and reasonable efforts have been made to ensure accuracy, including review by the authors wherever possible. If you identify any issues, please contact us.

Publisher's note

References

Adams, C. M., Hernandez, E., and Cato, J. C. (2004). The economic significance of the Gulf of Mexico related to population, income, employment, minerals, fisheries and shipping. *Ocean Coast. Manage.* 47, 565–580. doi: 10.1016/j.ocecoaman.2004.12.002

Adams, C., Vega, P. S., and Alvarez, A. G. (2000). *An overview of the Cuban commercial fishing industry and recent changes in management structure and objectives* (Gainesville, FL: EDIS document FE 218, Department of Food and Resource Economics, Florida Cooperative Extension Service, Institute of Food and Agricultural Science, University of Florida).

Ayala-Castañares, A., and Knox, R. A. (2000). Opportunities and challenges for Mexico-US cooperation in ocean sciences. *Oceanography* 13, 79–82. Available online at: http://www.jstor.org/stable/43924372 (Accessed February 21, 2025).

Barbero, L., Pierrot, D., Wanninkhof, R., Baringer, M., Hooper, J., Zhang, J. Z., et al. (2019). *Third Gulf of Mexico Ecosystems and Carbon Cycle (GOMECC-3) Cruise* (Atlantic Oceanographic and Meteorological Laboratory). doi: 10.25923/y6m9-fy08

Barranco, L. M., Martín Hernández Ayón, J., Pech, D., Enriquez, C., Herrera, J., Mariño, I., et al. (2022). Physical and biogeochemical controls of the carbonate system of the Yucatan Shelf. *Continent. Shelf Res.* 244, 104807. doi: 10.1016/j.csr.2022.104807

Berelson, W. M., McManus, J., Severmann, S., and Rollins, N. (2019). Benthic fluxes from hypoxia-influenced Gulf of Mexico sediments: Impact on bottom water acidification. *Mar. Chem.* 209, 94–106. doi: 10.1016/j.marchem.2019.01.004

Bockmon, E. E., and Dickson, A. G. (2015). An inter-laboratory comparison assessing the quality of seawater carbon dioxide measurements. *Mar. Chem.* 171, 36–43. doi: 10.1016/j.marchem.2015.02.002

Bove, C. B., Davies, S. W., Ries, J. B., Umbanhowar, J., Thomasson, B. C., Farquhar, E. B., et al. (2022). Global change differentially modulates Caribbean coral physiology. *PLoS One.* 17 (9), e0273897. doi: 10.1371/journal.pone.0273897

Boyd, P. W., Collins, S., Dupont, S., Fabricius, K., Gattuso, J.-P., Havenhand, J., et al. (2019). SCOR WG149 Handbook to support the SCOR Best Practice Guide for Multiple Drivers Marine Research. (Hobart, Tasmania: University of Tasmania for Scientific Committee on Oceanic Research (SCOR)), 42pp. doi: 10.25959/5c92fdf0d3c7a

Cai, W. J., Feely, R. A., Testa, J. M., Li, M., Evans, W., Alin, S. R., et al. (2021). Natural and anthropogenic drivers of acidification in large estuaries. *Annu. Rev. Mar. Sci.* 13, 23–55. doi: 10.1146/annurev-marine-010419-011004

Cai, W. J., Hu, X., Huan, W. J., Murrell, M. C., Lehrter, J. C., Lohrenz, S. E., et al. (2011). Acidification of subsurface coastal waters enhanced by eutrophication. *Nat. Geosci.* 4, 766–770. doi: 10.1038/ngeo1297

Candela, J., Ochoa, J., Sheinbaum, J., López, M., Pérez-Brunius, P., Tenreiro, M., et al. (2019). The flow through the Gulf of Mexico. *J. Phys. Oceanogr.* 49, 1381–1401. doi: 10.1175/JPO-D-18-0189.s1

Caso, M., Pisanty, I., and Ezcurra, E. (2004). *Diagnóstico ambiental del Golfo de México. Volumen II.* Secretaría de Medio Ambiente y Recursos Naturales : Instituto Nacional de Ecología : Instituto de Ecología, A.C. : Harte Research Institute for Gulf of Mexico Studies.

Cervantes-Díaz, G. Y., Hernández-Ayón, J. M., Zirino, A., Herzka, S. Z., Camacho-Ibar, V., Norzagaray, O., et al. (2022). Understanding upper water mass dynamics in the Gulf of Mexico by linking physical and biogeochemical features. *J. Mar. Syst.* 225, 103647. doi: 10.1016/j.jmarsys.2021.103647

Cooke, S. L., and Kim, S. C. (2019). Exploring the "evil twin of global warming": public understanding of ocean acidification in the United States. *Sci. Commun.* 41 (1), 66–89.

Comisión Nacional de Acuacultura y Pesca (2023). *Anuario Estadístico de Acuacultura y Pesca*. Available online at: https://nube.conapesca.gob.mx/sites/cona/dgppe/2023/ANUARIO_ESTADISTICO_DE_ACUACULTURA_Y_PESCA_2023.pdf (Accessed February 21, 2025).

Crook, E. D., Potts, D., Rebolledo-Vieyra, M., Hernandez, L., and Paytan, A. (2012). Calcifying coral abundance near low-pH springs: implications for future ocean acidification. *Coral Reefs* 31, 239–245. doi: 10.1007/s00338-011-0839-y

Cross, J. N., Turner, J. A., Cooley, S. R., Newton, J. A., Azetsu-Scott, K., Chambers, R. C., et al. (2019). Building the knowledge-to-action pipeline in North America: Connecting ocean acidification research and actionable decision support. *Front. Mar. Sci.* 6. doi: 10.3389/fmars.2019.00356

Dee, S. G., Torres, M. A., Martindale, R. C., Weiss, A., and DeLong, K. L. (2019). The future of reef ecosystems in the Gulf of Mexico: insights from coupled climate model simulations and ancient hot-house reefs. *Front. Mar. Sci.* 6. doi: 10.3389/fmars.2019.00691

Dickson, A. G., Sabine, C. L., and Christian, J. R. (Eds.) (2007). *Guide to Best Practices for Ocean CO2 Measurements* (Sidney, BC, Canada: PICES Special Publication 3), 191 pp.

Doney, S. C., Fabry, V. J., Feely, R. A., and Kleypas, J. A. (2009). Ocean acidification: the other CO2 problem. *Annu. Rev. Mar. Sci.* 1, 169–192. Available online at: https://digitalcommons.law.uw.edu/wjelp/vol6/iss2/3.

Duarte, C. M., Dennison, W. C., Orth, R. J., and Carruthers, T. J. (2008). The charisma of coastal ecosystems: addressing the imbalance. *Estuar. Coasts* 31, 233–238. doi: 10.1007/s12237-008-9038-7

Ducarme, F., Luque, G. M., and Courchamp, F. (2013). What are "charismatic species" for conservation biologists. *Biosci. Master. Rev.* 10, 1–8.

Ekstrom, J. A., Suatoni, L., Cooley, S. R., Pendleton, L. H., Waldbusser, G. G., Cinner, J. E., et al. (2015). Vulnerability and adaptation of US shellfisheries to ocean acidification. *Nat. Climate Change* 5, 207–214. doi: 10.1038/nclimate2508

Espinosa, L. F. (2023). *REMARCO – Network for Research on Marine–Coastal Stressors in Latin America and the Caribbean (UNEP(DEPI)/CAR)*.

D. L. Felder and D. K. Camp (Eds.) (2009). *Gulf of Mexico origin, waters, and biota: Biodiversity* (Texas A&M University Press).

Galindo-Cortes, G., Jiménez-Badillo, L., and Meiners, C. (2019). "Moving from stock assessment to fisheries management in Mexico: the finfish fisheries from the southern Gulf of Mexico and Caribbean Sea," in Viability and Sustainability of Small-Scale Fisheries in Latin America and the Caribbean, *MARE Publication Series*, vol. 19 . Eds. S. Salas, M. Barragán-Paladines and R. Chuenpagdee (Springer), 243–263. doi: 10.1007/978-3-319-76078-0_11

Gil-Agudelo, D. L., Cintra-Buenrostro, C. E., Brenner, J., González-Díaz, P., Kiene, W., Lustic, C., et al. (2020). Coral reefs in the Gulf of Mexico large marine ecosystem: conservation status, challenges, and opportunities. *Front. Mar. Sci.* 6, 807. doi: 10.3389/fmars.2020.00807

Gledhill, D. K., Wanninkhof, R., Millero, F. J., and Eakin, M. (2008). Ocean acidification of the greater Caribbean region 1996–2006. *J. Geophys. Res.: Oceans* 113, C10031. doi: 10.1029/2007JC004629

Grabb, K. C., Lord, N., Dobson, K. L., Gordon-Smith, D.-A.D.S., Escobar-Briones, E., Ford, M. C., et al. (2025). Building ocean acidification research and policy capacity in the wider Caribbean region: a case study for advancing regional resilience. *Front. Mar. Sci.* 12. doi: 10.3389/fmars.2025.159591

Guan, Y., Hohn, S., Wild, C., and Merico, A. (2020). Vulnerability of global coral reef habitat suitability to ocean warming, acidification and eutrophication. *Global Change Biol.* 26, 5646–5660. doi: 10.1111/gcb.15293

Hall, E. R., Wickes, L., Burnett, L. E., Scott, G. I., Hernandez, D., Yates, K. K., et al. (2020). Acidification in the U.S. Southeast: causes, potential consequences and the role of the Southeast Ocean and Coastal Acidification Network. *Front. Mar. Sci.* 7, 548. doi: 10.3389/fmars.2020.00548

Hall, E. R., Yates, K. K., Hubbard, K. A., Garrett, M. J., and Frankle, J. D. (2024). Nutrient and carbonate chemistry patterns associated with *Karenia brevis* blooms in three West Florida Shelf estuaries 2020-2023. *Front. Mar. Sci.* 11. doi: 10.3389/fmars.2024.1331285

Hamilton, P., Fargion, G. S., and Biggs, D. C. (1999). Loop Current eddy paths in the western Gulf of Mexico. *J. Phys. Oceanogr.* 29, 1180–1207. doi: 10.1175/1520-0485(1999)029<1180:LCEPIT>2.0.CO;2

Hicks, T. L., Shamberger, K. E., Fitzsimmons, J. N., Jensen, C. C., and DiMarco, S. F. (2022). Tropical cyclone-induced coastal acidification in Galveston Bay, Texas. *Commun. Earth Environ.* 3, 297. doi: 10.1038/s43247-022-00608-1

Hu, X., Pollack, J. B., McCutcheon, M. R., Montagna, P. A., and Ouyang, Z. (2015). Long-term alkalinity decrease and acidification of estuaries in northwestern Gulf of Mexico. *Environ. Sci. Technol.* 49, 3401–3409. doi: 10.1021/es505945p

Hu, X. (2019). 1.3.3 Ocean Acidification Studies in the Gulf of Mexico—Current Status and Future Research Needs. *Proc. Gulf Mexico Workshop International Res.*, (Houston, TX).

Interagency Working Group on Ocean Acidification (IWG-OA) (2023). *United States Ocean Acidificaiton Action Plan* (US Department of State. 88 FR 31578).

Jiang, Z. P., Qin, C., Pan, Y., Le, C., Rabalais, N., Turner, R. E., et al. (2024). Multi-decadal coastal acidification in the northern Gulf of Mexico driven by climate change and eutrophication. *Geophys. Res. Lett.* 51, p.e2023GL106300. doi: 10.1029/2023GL106300

Kealoha, A. K., Shamberger, K. E. F., DiMarco, S. F., Thyng, K. M., Hetland, R. D., Manzello, D. P., et al. (2020). Surface water CO2 variability in the Gulf of Mexico, (1996-2017). *Sci. Rep.* 10, 12279. doi: 10.1038/s41598-020-68924-0

Kurman, M. D., Gómez, C. E., Georgian, S. E., Lunden, J. J., and Cordes, E. E. (2017). Intra-specific variation reveals potential for adaptation to ocean acidification in a cold-water coral from the Gulf of Mexico. *Front. Mar. Sci.* 4. doi: 10.3389/fmars.2017.00111

Lankes, J. D., Page, H. N., Quasunella, A., Torkelson, J. F., Lemaire, C., Nowicki, R. J., et al. (2025). Quantifying coral-algal interactions in an acidified ocean: Sargassum spp. exposure mitigates low pH effects on *Acropora cervicornis* health. *Front. Mar. Sci.* 12. doi: 10.3389/fmars.2025.1487102

Laurent, A., Fennel, K., Cai, W. J., Huang, W. J., Barbero, L., and Wanninkhof, R. (2017). Eutrophication-induced acidification of coastal waters in the northern Gulf of Mexico: Insights into origin and processes from a coupled physical-biogeochemical model. *Geophys. Res. Lett.* 44, 946–956. doi: 10.1002/2016GL071881

Lawman, A. E., Dee, S. G., DeLong, K. L., and Correa, A. M. S. (2022). Rates of future climate change in the Gulf of Mexico and the Caribbean Sea: Implications for Coral Reef Ecosystems. *J. Geophys. Res.: Biogeosci.* 127, p.e2022JG006999. doi: 10.1002/2016GL071881

Liu, Z., Chen, J., Zhang, J., Wang, K., and Zhang, S. (2024). The evaluation of C, N, P release and contribution to the aquatic environment during Sargassum litters biomass decay. *Regional Stud. Mar. Sci.* 80, 3892. doi: 10.1016/j.rsma.2024.103892

Lunden, J. J., McNicholl, C. G., Sears, C. R., Morrison, C. L., and Cordes, E. E. (2014). Acute survivorship of the deep-sea coral Lophelia pertusa from the Gulf of Mexico under acidification, warming, and deoxygenation. *Front. Mar. Sci.* 1. doi: 10.3389/fmars.2014.00078

Machlis, G., Frankovich, T. A., Alcolado, P. M., García-MaChado, E., Caridad Hernández-Zanuy, A., Hueter, R. E., et al. (2012). Ocean policy—US-Cuba scientific collaboration: Emerging issues and opportunities in marine and related environmental sciences. *Oceanography* 25, 227–231. doi: 10.5670/oceanog.2012.63

Martínez-López, B., and Zavala-Hidalgo, J. (2009). Seasonal and interannual variability of cross-shelf transports of chlorophyll in the Gulf of Mexico. *J. Mar. Syst.* 77, 1–20. doi: 10.1016/j.jmarsys.2008.10.002

Martínez-Trejo, J. A., Cardoso-Mohedano, J. G., Sanchez-Cabeza, J. A., Ayón, J. M. H., Ruiz-Fernández, A. C., Gómez-Ponce, M. A., et al. (2024). Variability of dissolved inorganic carbon in the most extensive Karst Estuarine-Lagoon System of the southern Gulf of Mexico. *Estuar. Coasts* 47, pp.2573–2588. doi: 10.1016/j.jmarsys.2008.10.002

McCutcheon, M. R., and Hu, X. (2022). Long-term trends in estuarine carbonate chemistry in the northwestern Gulf of Mexico. *Front. Mar. Sci.* 9. doi: 10.3389/fmars.2022.793065

McKinney, L. D., Shepherd, J. G., Wilson, C. A., Hogarth, W. T., Chanton, J., Murawski, S. A., et al. (2021). The gulf of Mexico. *Oceanography* 34, 30–43. doi: 10.5670/oceanog.2021.115

Morey, S. L., Martin, P. J., O'Brien, J. J., Wallcraft, A. A., and Zavala-Hidalgo, J. (2003). Export pathways for river discharged fresh water in the northern Gulf of Mexico. *J. Geophys. Res.: Oceans* 108, 3303. doi: 10.1029/2002JC001674

Muller, E. M., Dungan, A. M., Million, W. C., Eaton, K. R., Petrik, C., Bartels, E., et al. (2021). Heritable variation and lack of tradeoffs suggest adaptive capacity in *Acropora cervicornis* despite negative synergism under climate change scenarios. *Proc. R. Soc. B* 288, 20210923. doi: 10.1098/rspb.2021.0923

National Marine Fisheries Service (2024). *Fisheries of the United State* (U.S. Department of Commerce, NOAA Current Fishery Statistics No. 2022). Available online at: https://www.fisheries.noaa.gov/national/sustainable-fisheries/fisheries-united-states (Accessed February 21, 2025).

Ocaña, F. A., Pech, D., Simões, N., and Hernández-Ávila, I. (2019). Spatial assessment of the vulnerability of benthic communities to multiple stressors in the Yucatan Continental Shelf, Gulf of Mexico. *Ocean Coast. Manage.* 181, 104900. doi: 10.1016/j.ocecoaman.2019.104900

Oey, L., Ezer, T., and Lee, H. (2005). Loop Current, rings and related circulation in the Gulf of Mexico: A review of numerical models and future challenges. *Geophys. Monograph American Geophys. Union* 161, 31.

Osborne, E., Hu, X., Hall, E. R., Yates, K., Vreeland-Dawson, J., Shamberger, K., et al. (2022). Ocean acidification in the Gulf of Mexico: Drivers, impacts, and unknowns. *Prog. Oceanogr.* 209, 102882. doi: 10.1016/j.pocean.2022.102882

Patin, N. V., Dietrich, Z. A., Stancil, A., Quinan, M., Beckler, J. S., Hall, E. R., et al. (2021). Gulf of Mexico blue hole harbors high levels of novel microbial lineages. *ISME J.* 15, 2206–2232. doi: 10.1038/s41396-021-00917-x

Portela, E., Tenreiro, M., Pallàs-Sanz, E., Meunier, T., Ruiz-Angulo, A., Sosa-Gutiérrez, R., et al. (2018). Hydrography of the central and western Gulf of Mexico. *J. Geophys. Res.: Oceans* 123, 5134–5149. doi: 10.1029/2018JC013813

Riebesell, U., Fabry, V. J., Hansson, L., and Gattuso, J. P. (2011). *Guide to best practices for ocean acidification research and data reporting*. Office for Official Publications of the European Communities.

Robbins, L. L., and Lisle, J. T. (2017). Regional acidification trends in Florida shellfish estuaries: a 20+ year look at pH, oxygen, temperature, and salinity. *Estuar. Coasts* 41, 1268–1281. doi: 10.1007/s12237-017-0353-8

Rosenau, N. A., Galavotti, H., Yates, K. K., Bohlen, C. C., Hunt, C. W., Liebman, M., et al. (2021). Integrating high-resolution coastal acidification monitoring data across seven United States estuaries. *Front. Mar. Sci.* 8. doi: 10.3389/fmars.2021.679913

Sánchez-Gil, P., Yáñez-Arancibia, A., Ramírez-Gordillo, J., Day, J. W., and Templet, P. H. (2004). Some socio-economic indicators in the Mexican states of the Gulf of Mexico. *Ocean Coast. Manage.* 47, 581–596. doi: 10.1016/j.ocecoaman.2004.12.003

Sharma, D. R. (2024). IMO internship programme-opportunity and challenges for novice maritime researchers. *J. Maritime Res.* 21, 1–5.

Shepard, A. N., Valentine, J. F., D'Elia, C. F., Yoskowitz, D., and Dismukes, D. E. (2013). Economic impact of Gulf of Mexico ecosystem goods and services and integration into restoration decision-making. *Gulf Mexico Sci.* 31. doi: 10.18785/goms.3101.02

Soria-Reinoso, I., Alcocer, J., Sánchez-Carrillo, S., García-Oliva, F., Cuevas-Lara, D., Cortés-Guzmán, D., et al. (2022). The seasonal dynamics of organic and inorganic carbon along the tropical Usumacinta River Basin (Mexico). *Water* 14, 2703. doi: 10.3390/w14172703

Sutton, A. J., Battisti, R., Carter, B., Evans, W., Newton, J., Alin, S., et al. (2022). Advancing best practices for assessing trends of ocean acidification time series. *Front. Mar. Sci.* 9, 1045667. doi: 10.3389/fmars.2022.1045667

Sutton, A. J., Battisti, R., Carter, B., Evans, W., Newton, J., Alin, S., et al. (2022). Advancing best practices for assessing trends of ocean acidification time series. *Front. Mar. Sci.* 9. doi: 10.3389/fmars.2022.1045667

Tiller, R., Arenas, F., Galdies, C., Leitão, F., Malej, A., Romera, B. M., et al. (2019). Who cares about ocean acidification in the Plasticine? *Ocean Coast. Manage.* 174, 170–180. doi: 10.1016/j.ocecoaman.2019.03.020

Torres, P. Á., Rabalais, N. N., Gutiérrez, J. M. P., and López, R. M. P. (2017). Research and community of practice of the Gulf of Mexico large marine ecosystem. *Environ. Dev.* 22, 166–174. doi: 10.1016/j.envdev.2017.04.004

Turner, J. A., Babcock, R. C., Hovey, R., Kendrick, G. A., and Degraer, S. (2017). Deep thinking: a systematic review of mesophotic coral ecosystems. *ICES J. Mar. Sci.* 74, 2309–2320. doi: 10.1093/icesjms/fsx085

Turner, R. E., and Rabalais, N. N. (2019). "The Gulf of Mexico," in *World seas: An environmental evaluation* (Academic Press), 445–464.

UNIDO (2014). *Strategic action programme. Integrated Assessment and Management of the Gulf of Mexico Large Marine Ecosystem* (Vienna, Austria: United Nations Industrial Development Organization).

Valauri-Orton, A., Lowder, K., Currie, K., Sabine, C., Dickson, A., Chu, S., et al. (2025). Perspectives from developers and users of the GOA-ON in a box kit: A model for capacity sharing in ocean sciences. *Oceanography* 38. doi: 10.5670/oceanog.2025.135

Valle, S. V., Sosa, M., Puga, R., Font, L., and Duthit, R. (2011). "Coastal fisheries of Cuba," in *Coastal Fisheries of Latin America and the Caribbean. FAO Fisheries and Aquaculture Technical Paper. No. 544*. Eds. S. Salas, R. Chuenpagdee, A. Charles and J. C. Seijo (FAO, Rome), 155–174.

Wallace, R. B., Baumann, H., Grear, J. S., Aller, R. C., and Gobler, C. J. (2014). Coastal ocean acidification: The other eutrophication problem. *Estuar. Coast. Shelf Sci.* 148, 1–13. doi: 10.1016/j.ecss.2014.05.027

Wang, Z. A., Wanninkhof, R., Cai, W.-J., Byrne, R. H., Hu, X., Peng, T.-H., et al. (2013). The marine inorganic carbon system along the Gulf of Mexico and Atlantic coasts of the United States: Insights from a transregional coastal carbon study. *Limnol. Oceanogr.* 58, 325–342. doi: 10.1073/pnas.1203849109

Wanninkhof, R., Barbero, L., Byrne, R., Cai, W. J., Huang, W. J., Zhang, J. Z., et al. (2015). Ocean acidification along the Gulf Coast and East Coast of the USA. *Continent. Shelf Res.* 98, 54–71. doi: 10.1016/j.csr.2015.02.008

Zaldívar-Jiménez, A., Ladrón-de-Guevara-Porras, P., Pérez-Ceballos, R., Díaz-Mondragón, S., and Rosado-Solórzano, R. (2017). US-Mexico joint Gulf of Mexico large marine ecosystem based assessment and management: Experience in community involvement and mangrove wetland restoration in Términos lagoon, Mexico. *Environ. Dev.* 22, 206–213. doi: 10.1016/j.envdev.2017.02.007

Zhang, Y., Hu, C., McGillicuddy, D. J. Jr., Barnes, B. B., Liu, Y., Kourafalou, V. H., et al. (2024). Pelagic Sargassum in the Gulf of Mexico driven by ocean currents and eddies. *Harmful Algae* 132, 102566. doi: 10.1016/j.hal.2023.102566

Zhang, L., and Xue, Z. G. (2022). A Numerical reassessment of the Gulf of Mexico carbon system in connection with the Mississippi River and global ocean. *Biogeosciences* 19, 4589–4618. doi: 10.5194/bg-19-4589-2022

frontiers | Frontiers in Marine Science

TYPE Original Research
PUBLISHED 29 October 2025
DOI 10.3389/fmars.2025.1645755

OPEN ACCESS

EDITED BY
Eva Chatzinikolaou,
Hellenic Centre for Marine Research (HCMR), Greece

REVIEWED BY
M. Roberto García-Huidobro,
Universidad Santo Tomás, Chile
Gurucharan Sudarshan,
Ben-Gurion University of the Negev, Israel

*CORRESPONDENCE
Ricardo Sahade
rsahade@unc.edu.ar
Natalia Servetto
nservetto@mi.unc.edu.ar

RECEIVED 12 June 2025
ACCEPTED 13 October 2025
PUBLISHED 29 October 2025

CITATION
Servetto N, De Troch M, Alurralde G, Ferrero L, de Aranzamendi MC and Sahade R (2025) Effects of ocean acidification on fatty acid composition in the Antarctic snail *Neobuccinum eatoni*. *Front. Mar. Sci.* 12:1645755. doi: 10.3389/fmars.2025.1645755

Effects of ocean acidification on fatty acid composition in the Antarctic snail *Neobuccinum eatoni*

Natalia Servetto[1,2]*, Marleen De Troch[3], Gastón Alurralde[4,5], Luciana Ferrero[1,2], M. Carla de Aranzamendi[1,2] and Ricardo Sahade[1,2]*

[1]Facultad de Ciencias Exactas Físicas y Naturales, Universidad Nacional de Córdoba, Córdoba, Argentina, [2]Consejo Nacional de Investigaciones Científicas y Técnicas (CONICET), Instituto de Diversidad y Ecología Animal (IDEA), Ecosistemas Marinos Polares, Córdoba, Argentina, [3]Marine Biology, Ghent University, Gent, Belgium, [4]Department of Environmental Science, Stockholm University, Stockholm, Sweden, [5]Baltic Marine Environment Protection Commission Helsinki Commission (HELCOM) Secretariat, Helsinki, Finland

Introduction: Ocean acidification (OA), resulting from the absorption of increasing atmospheric CO_2 by the oceans, represents a major threat to marine organisms. Despite growing concern, the biochemical responses of Antarctic species to OA remain poorly understood.

Methods: This study investigated the impact of OA (pH 7.70 ± 0.09) on the fatty acid (FA) composition of the Antarctic snail *Neobuccinum eatoni* over a two-month experimental period (December 2015–March 2016). Fatty acid profiles were analyzed in multiple tissues to assess potential alterations induced by low-pH (LpH) conditions.

Results: Significant tissue-specific changes in FA composition were detected, particularly in the mantle and gill. Under LpH exposure, notable modifications occurred in long-chain polyunsaturated fatty acids (LC-PUFAs) such as 22:5n-3, 22:6n-3, and 24:5n-6. Elevated LC-PUFA levels in the mantle suggested a compensatory response to oxidative stress, while shifts in the n-3/n-6 ratios in the gill pointed to potential alterations in immune and anti-inflammatory functions.

Discussion: Indicators of homeoviscous adaptation (HVA), including PUFA/SFA ratios and mean chain length (MCL), revealed biochemical strategies used by N. eatoni to maintain membrane fluidity under acidified conditions. This study provides the first evidence of FA-based responses to elevated pCO_2 in an Antarctic gastropod, highlighting the potential of fatty acids as sensitive biomarkers of physiological adaptation to environmental stressors.

KEYWORDS

Southern Ocean, gastropod, CO_2 anthropogenic emissions, lipid biochemistry, benthos

1 Introduction

The Anthropocene, which began with the Industrial Revolution in the 18th century, is characterized by significant human impact on a global scale, marked by an unprecedented and rapid increase in atmospheric CO_2 levels (Gingerich, 2019). Oceanic uptake of excess CO_2 helps mitigate anthropogenic emissions at the expense of inducing ocean acidification (OA). This process alters the physicochemical properties of seawater, profoundly affecting marine organisms and ecosystem functions (Findlay and Turley, 2021). Key marine species are already experiencing significant impacts, threatening biodiversity and essential ecosystem services (Gattuso et al., 2015; Shi and Li, 2024; Teixidó et al., 2024).

The severity of OA impacts is expected to vary across regions, with high-latitude areas experiencing more intense effects at finer spatial scales. The Southern Ocean (SO) plays a disproportionately large role in global carbon uptake, accounting for 30–40% of anthropogenic CO_2 absorption (Fisher et al., 2025). This, combined with naturally low calcium carbonate ($CaCO_3$) levels and the increased solubility of CO_2 in cold waters (Hancock et al., 2020), contributes to its already low buffering capacity, making the SO ecosystem particularly vulnerable to OA. Aragonite saturation is biologically important because it determines the availability of carbonate ions necessary for calcifying organisms to form and maintain their shells and skeletons. For example, pteropods and corals rely on supersaturated aragonite conditions to precipitate calcium carbonate structures, and declines in aragonite saturation due to ocean acidification can lead to shell dissolution and impaired growth (Fabry et al., 2008; Orr et al., 2005). These physiological effects on key species can cascade through the web, ultimately impacting ecosystem structure and function. For instance, projections based on an ensemble of ten Earth system models indicate that aragonite undersaturation events will begin to spread rapidly around 2030, affecting approximately 30% of the SO surface waters by 2060, and more than 70% by 2100 (Hauri et al., 2015). Moreover, from 2003 to 2022, CO_2 absorption increased by 0.076 gC m^{-2} per month in the Atlantic region of the SO, largely due to enhanced westerly winds linked to the Antarctic Oscillation (AO) and events related to the El Niño Southern Oscillation (ENSO) (de Carvalho et al., 2025). This means that Antarctic biota are exposed to potentially accelerated and more severe OA conditions than elsewhere.

OA not only impedes biomineralization and leads to shell dissolution in calcifiers, but it also exerts broader impacts on marine biota through cascades of physiological and biochemical mechanisms, often involving energetic trade-offs and complex cellular adjustments (Johnson and Hofmann, 2017; Servetto et al., 2023, 2025). Under elevated partial pressure of carbon dioxide (pCO_2), meeting these physiological and metabolic demands requires significant energy, which forces a reallocation of limited energy budgets away from other vital functions. Thus, beyond direct physiological impacts, reproduction, growth, and development can also be adversely affected (Kroeker et al., 2013; Turner et al., 2016). To meet this energetic demand, organisms generally rely on lipid reserves and adjust fatty acid (FA) composition (Gibbs et al., 2021), diverting resources toward processes such as enhanced glycolipid metabolism as observed in *Crassostrea gigas* under acid stress (Wang et al., 2025). These energetic trade-offs generally manifest as reductions in total lipid content and a shift in key fatty acid ratios (e.g., decreased polyunsaturated fatty acids (PUFAs)/saturated fatty acids (SFA)), providing a sensitive proxy for potential hidden costs of OA (Valles-Regino et al., 2015). The close link between FAs and fundamental physiological processes makes them powerful biomarkers for assessing health and stress responses in marine organisms (Capitão et al., 2017; Ericson et al., 2019). FAs are essential components of cellular membranes and key energy sources for metabolism (Arts and Kohler, 2009; Hedberg et al., 2023). Within immune and physiological functions, polyunsaturated fatty acids (PUFAs) such as docosahexaenoic acid (DHA, 22:6n-3) and eicosapentaenoic acid (EPA, 20:5n-3) play critical roles in lipid metabolism, reproduction, and anti-inflammatory processes (Corsolini and Borghesi, 2017; Schmitz and Ecker, 2008). Although less abundant, arachidonic acid (ARA, 20:4n-6) acts as a precursor of eicosanoids that regulate immune responses and other physiological pathways (Stanley-Samuelson et al., 1988). Ratios such as n-6/n-3 PUFAs provide further insight into stress and inflammation (Ericson et al., 2019; Van Anholt et al., 2004).

In addition, homeoviscous adaptation—where organisms adjust membrane fluidity in response to environmental change—is commonly evaluated through PUFA/SFA ratios and mean carbon chain length (MCL) (Bennett et al., 2018; Ericson et al., 2019). For instance, temperature-driven shifts in MCL have been documented in the sponge *Rhopaloeides odorabile* (Bennett et al., 2018), while reductions in saturated and monounsaturated fatty acids were observed in *Artemia sinica* and the gastropod *Dicathais orbita* under short-term acidifying CO_2 conditions (Valles-Regino et al., 2015; Gao et al., 2018). These findings underscore the sensitivity of FA composition to environmental stress in aquatic organisms and ecosystems (Fadhlaoui and Lavoie, 2021). Gastropods are key components of benthic ecosystems, driving nutrient cycling, grazing, and serving as prey for higher trophic levels (Dennis et al., 2021). Their heavily calcified shells make them especially vulnerable to OA, which not only impairs calcification but also inhibits growth and development (Kroeker et al., 2013). Additionally, if the cost of coping with acidic conditions compromises lipid reserves (particularly essential FAs like EPA and DHA), it may reduce their nutritional value and jeopardize predator health and survival throughout the food web (Gladyshev et al., 2013; Zhukova, 2019). While research on Antarctic gastropods is still limited, studies on other Antarctic mollusks have shown that elevated CO_2 levels can impair physiological performance (Cummings et al., 2011; Johnson and Hofmann, 2017; de Aranzamendi et al., 2021). For example, de Aranzamendi et al. (2021) examined the impact of OA on the Antarctic limpet *Nacella concinna*. During a 15-day controlled laboratory exposure to low pH, sublittoral individuals displayed downregulation of heat-shock protein genes (HSP70A and HSP70B), indicating a stress response to acidified conditions. These results suggest that OA alone can substantially disrupt the

physiological functioning of *N. concinna*, potentially reducing their resilience under future OA scenarios.

This study focuses on *Neobuccinum eatoni*, an Antarctic gastropod found in shallow coastal areas to over 2000 meters deep. As an endemic species dominating Antarctic benthic ecosystems (Schiaparelli et al., 2006; Norkko et al., 2007), *N. eatoni* represents a relevant model species to assess the impacts of OA. Model projections under elevated CO_2 emissions suggest a substantial decline in suitable habitat for *N. eatoni*, underscoring both its susceptibility to ocean acidification and the need to prioritize research on this species (González et al., 2024). This study examines the specific effects of OA on the FA composition of *N. eatoni*, aiming to determine the effect of OA on the FA composition of the Antarctic snail *N. eatoni*, by comparing individuals exposed to acidified conditions with those maintained under control conditions. Recognizing the established link between FA profiles and environmental stressors (including temperature, pH, and nutrient availability), the research focuses on key FA indicators associated with immune functions (such as the 22:6n-3/20:4n-6 and n-3/n-6 ratios), and HVA (including MCL and PUFA/SFA ratios). These metrics were analyzed across tissues (mantle, gill, gonads, and foot) with distinct metabolic roles and lipid requirements. Experimental exposures were conducted under current ambient CO_2 levels and elevated concentrations projected for 2100 under the high-emission RCP8.5 scenarios (IPCC, 2019), simulating future ocean conditions.

The central hypothesis posits that *N. eatoni* exposed to elevated CO_2 levels will exhibit significant alterations in FA composition, reflecting changes in immune function and membrane fluidity compared to controls (individuals under current ambient conditions). Using FA profiles, the study addresses this question: could FA composition serve as a potential biomarker of stress in snails exposed to OA? By exploring these questions, the research aims to elucidate the mechanisms by which OA affects marine organisms at the biochemical level, enhancing our understanding of the potential impacts on Antarctic marine life.

2 Materials and methods

2.1 Study area

The experiment was carried out for 66 days in Potter Cove (PC) (62°14′S., 58°40′W; King George/25 de Mayo Island - South Shetlands - Antarctica) during the summer campaign of 2015-2016 (from December to March) (Figure 1). *N. eatoni* was collected by scuba diving at approximately 15 m depth, and they were immediately placed in seawater containers and transported to the experimental aquarium at the Argentinian research station Carlini. Prior to altering the pCO_2, the snails were placed for seven days in an individual acclimation tank [with a continuous flow of seawater, maintained at *in situ* natural conditions (approximately 8.03)].

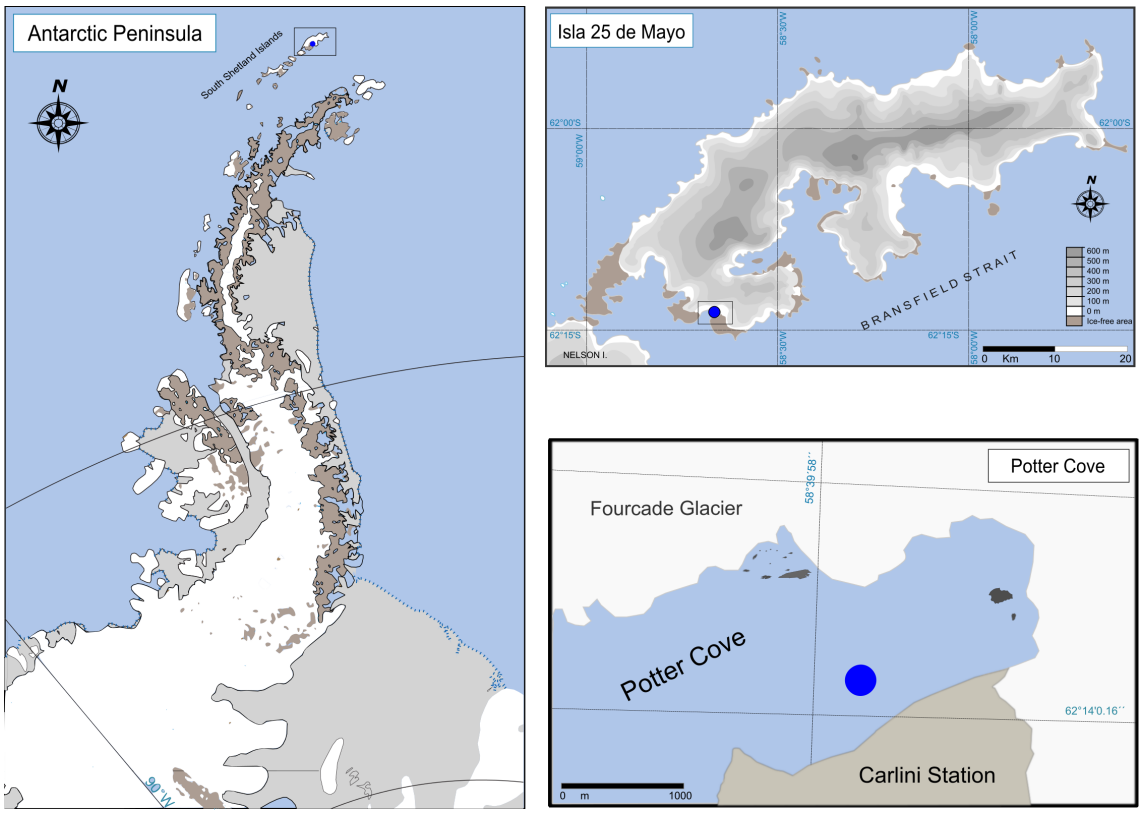

FIGURE 1
Study area. Antarctic Peninsula showing the location of 25 de Mayo Island. 25 de Mayo Island, with the location of Potter Cove indicated, and Potter Cove detailing the sampling area.

2.2 Experimental design

We implemented an experimental CO_2-manipulation system following the same experimental design utilized in previous studies on zoo-benthic Antarctic species exposed to OA (de Aranzamendi et al., 2021; Servetto et al., 2021, 2023, 2025) (Figure 2). Seawater was continuously supplied from the field to two main header tanks (150 L each), designated as the acidified treatment (hereafter referred to as low pH, LpH) and the control. pH levels were continuously monitored using glass electrodes (LL Ecotrodeplus, Metrohm) connected to a pH controller (Consort R3610, Turnhout, Belgium). The LpH tank was gradually acidified by bubbling CO_2 gas (99.9% purity) until reaching a target pH of 7.68 ± 0.17, representing ~1000 µatm pCO_2, a reduction of approximately 0.3–0.4 pH units relative to the control. The control tank was maintained to reflect the natural pH variability recorded at the snails' collection depth (15 m). It continuously received unaltered seawater directly supplied from the PC. Individual snails (N = 6; two individuals per tank) were placed in separate subsidiary smaller aquaria (~6 L), each connected to a continuous flow of seawater supplied from either the LpH or control head tank (Figure 2). The experimental sample size (5–6 cm) was carefully selected to minimize potential impacts on the individuals. As these snails are Antarctic organisms and little is known about their population in PC (Sahade et al., 2015; personal observation), a precautionary approach was taken by limiting the number of specimens collected. To minimize evaporation and reduce gas exchange with the air, each tank was covered with a methacrylate lid. Electrodes were calibrated daily using Tris buffers of known pH values, following standard procedures (SOP6a of Dickson et al., 2007). Weekly, 50 mL water samples were collected from the head tanks and fixed with $HgCl_2$ for subsequent total alkalinity (TA) analysis. TA was quantified via Gran titration (Smith and Kinsey, 1978) employing a sample exchanger coupled to a TitroLine alpha plus titration system (SI Analytics, Mainz, Germany) equipped with an A157–1 M-DIN-ID pH electrode, and conducted in accordance with standard operating procedure SOP 3a (Dickson et al., 2007). Carbonate chemistry parameters were calculated with the CO2SYS spreadsheet (Pierrot et al., 2006), using dissociation constants for carbonate determined by Mehrbach et al. (1973) and refitted by Dickson and Millero (1987). A summary of the physicochemical parameters of seawater is provided in Table 1. Temperature and salinity were not experimentally manipulated; instead, natural conditions from the cove were maintained throughout the study. Nevertheless, both parameters were continuously monitored during the experimental period to account for natural oscillation and support data interpretation (Table 1).

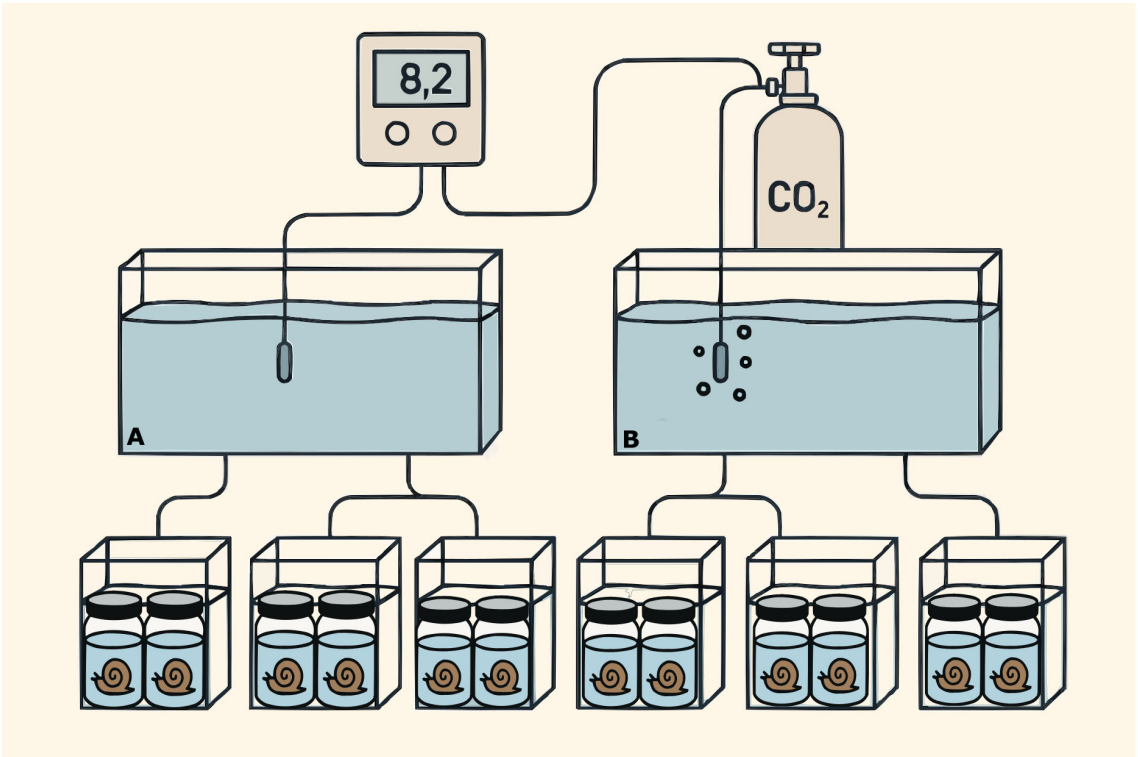

FIGURE 2
Experimental setup (following Servetto et al., 2021). *Neobuccinum eatoni* were collected by scuba divers in the Antarctic summer campaign 2015–2016 and acclimated until the start of experimentation. Seawater was continuously supplied to two head tanks: **(A)** control and **(B)** low pH head tank (7.70 ± 0.09). From each head tank, seawater was delivered to three smaller aquaria where the animals were placed separately. After exposure, tissue samples from the snail (mantle, gill, gonads, and foot) were taken for fatty acid analyses.

TABLE 1 Summary of seawater physicochemical conditions during the experiment with the Antarctic snail *Neobuccinum eatoni* (Servetto et al., 2023).

Treatment	Measured parameters		Calculated parameters				
	TA	pH_T	HCO_3	pCO_2	$[CO_2]_{aq}$	Ω_{Ca}	Ω_{Ar}
Low pH	2747 ± 669	7.70 ± 0.09	3065.5 ± 975.9	975.74 ± 130	62.26 ± 8.15	1.37 ± 0.59	0.85 ± 0.37
Ambient pCO_2	2849 ± 640	8.00 ± 0.16	2442.8 ± 484.74	473.4 ± 129.36	30.06 ± 8.20	2.73 ± 1.43	1.71 ± 0.89

Temperature (1.04 ± 0.26°C), Salinity (32.51 ± 0.67), TA total alkalinity (µmol/kg SW), and pH in total scale [pH_T] were measured. The partial pressure of CO_2 [pCO_2] (µatm), bicarbonate ion concentration [HCO_3^-] (µmol/kg SW), CO_2 concentration in seawater [CO_2]aq (µmol/kg SW), Ω_{Ca} saturation state of seawater to calcite and Ω_{Ar} saturation state of seawater to aragonite were calculated using CO_2SYS (Lewis et al., 1998). Data are expressed as mean ± SD. N = 643 for pH and N = 9 for the rest of the variables.

After two months of incubation under experimental conditions, the animals were dissected. Different tissues were selected for the FA analysis based on their functional and metabolic roles. Samples of mantle, gill, gonads, and foot were separated, stored at −80°C, and subsequently transported to Ghent University (Ghent, Belgium) for FA analysis. Results are expressed as both percentages and in $\mu g \cdot mg^{-1}$ dry weight (DW).

2.3 Fatty acid profiling

FA methyl esters (FAME) were prepared via a direct transesterification procedure with 2.5% (v:v) sulfuric acid in methanol as described by De Troch et al. (2012) to achieve total FA analysis. An internal standard (FA 19:0 5 µg) was added to the freeze-dried tissue samples (~ 10 mg). FAME was extracted twice with hexane. FA composition was carried out using a gas chromatograph (GC) (HP 7890B. Agilent Technologies, Diegem. Belgium) equipped with a flame ionization detector (FID) and connected to an Agilent 5977A Mass Selective (MS) Detector (Agilent Technologies). The GC was equipped with a PTV injector (CIS-4. Gerstel. Mülheim an der Ruhr. Germany). A 60 m×0.25 mm×0.20 µm film thickness HP88 fused silica capillary column (Agilent Technologies) was used for the GC analysis at a constant Helium flow rate (2 mL min^{-1}). The injection sample volume was 2 µL, and the oven temperature program was set as Boyen et al. (2020) described. The signal obtained with the FID detector was used to generate quantitative data on all compounds (MassHunter Quantitative Analysis Software, Agilent Technologies). Chromatogram peaks were identified based on their retention times. Quantification was done through the external standards (Supelco 37 Component FAME Mix, Sigma-Aldrich). Mean FA chain length (MCL) was calculated using the equation from Guerzoni et al. (2001):

$$MCL = \sum(FAP \times C)/100$$

where FAP is the percentage of fatty acid; C number of carbon atoms.

QC/QA procedures included repeated measurements of water chemistry parameters using calibrated instruments, verification of FA identification against reference standards, and cross-validation of statistical outputs. Residuals and diagnostic plots were systematically examined to ensure model assumptions were met, and all analyses were independently reproduced to confirm consistency.

2.4 Data analysis

To verify the consistency of experimental conditions, a *t*-test was performed on the measured water parameters (pH, $CaCO_3$, total alkalinity (TA), and temperature) to detect any significant differences between control and LpH treatments. FA profiles of different tissues were analyzed using Principal Component Analysis (PCA), while Non-Metric Multidimensional Scaling (nMDS) was conducted separately for each tissue type. The homogeneity of variances was assessed using Bartlett's test, and homoscedasticity and normality were further evaluated through residual analysis. Differences in FA composition among treatments were tested using an ANOVA (with tanks nested within treatments to account for potential tank effects). Additionally, a *t*-test was performed to compare the LpH treatment and control groups within each tissue after 66 days of the experimental condition. All statistical analyses were conducted using R version 3.6 for Microsoft Windows (R Core Team, 2020), with significance set at $p < 0.05$.

3 Results

3.1 Experimental conditions

The experimental setup successfully verified the targeted pH conditions (7.70 ± 0.09) despite variability in the incoming natural seawater throughout the experiment. The treatment was consistently maintained at a lower pH (7.70) compared to the control (8.00) (*t*-test, T = 4.94, p < 0.01) (Table 1). Additionally, the average bicarbonate ion concentration (HCO_3^-) and aragonite saturation state (Ω_{Ar}) differed significantly between the two conditions over the 66-day exposure period (T = -7.95, $p < 0.01$ and T = 2.60, $p = 0.0266$, respectively). In contrast (Table 1). Similarly, pCO_2 (µatm) was significantly higher in the LpH treatment compared to ambient conditions (mean ± SD: 975.74 ± 61.25 *vs.* 473.43 ± 40.24; T = -9.45, $p < 0.0001$), and aqueous CO_2 concentration ([CO_2]aq, µmol kg^{-1}) also increased significantly under elevated pCO_2 (62.26 ± 7.49 *vs.* 30.06 ± 3.99; T = -9.65, $p < 0.0001$). TA did not vary significantly between treatments for either variable (T = -1.53, $p > 0.1407$).

10.3389/fmars.2025.1645755

3.2 Fatty acid composition

A total of 20 FAs were identified in *N. eatoni*, grouped as saturated (SFA), monounsaturated (MUFA), and polyunsaturated (PUFA) fatty acids (Table 2). PUFA was the predominant group across all tissues (Supplementary Figure S1). FA composition varied among tissues and treatments, with the foot and mantle showing similar ranges, while the gonads exhibited the highest MUFA content (19.43–40.40%).

Multivariate analyses supported these tissue-specific patterns. Principal Component Analysis (PCA) revealed a clear separation along PC1, differentiating the gonad's FA composition from that of gill, foot, and mantle tissues (Figure 3). Within this framework, differences between control and LpH conditions were most evident in the gills. Similarly, non-metric Multidimensional Scaling (nMDS) indicated a marked distinction between control and LpH treatments in gill and mantle tissues, while this separation was less pronounced in the other tissues (Figure 4).

Under LpH conditions, opposite patterns were observed in gill and mantle tissues. In the gills, total SFA, MUFA, PUFA, and LC-PUFA contents were significantly higher in the control group than in LpH-exposed snails (Figure 5; Supplementary Table S1). The PUFA/SFA and MCL ratios followed the same trend, whereas the 20:5n-3/20:4n-6 and n-3/n-6 ratios were elevated under LpH. EPA was the most abundant FA in the gills, although no significant difference was detected between treatments. Several other FAs, including 20:2n-6, ARA, DHA, 22:5n-3, and MUFAs such as 18:1n-7, 20:1n-11, and 20:1n-9, were significantly higher in control samples (Table 2).

Conversely, in the mantle, SFA, MUFA, PUFA, and LC-PUFA levels were significantly higher under LpH exposure. The PUFA/SFA ratio and MCL indicator also increased in LpH samples compared to controls (Figure 5; Supplementary Table S1). Most mantle FAs were significantly altered by acidification, with EPA, DHA, 22:5n-3, 22:6n-3, and 24:5n-6 showing particularly elevated levels under LpH conditions (Table 2; Supplementary Table S2).

4 Discussion

This study represents the first investigation into the response of *N. eatoni* to projected OA scenarios, providing novel evidence of tissue-specific sensitivity through FA composition analyses. Our findings demonstrate that exposure to LpH conditions induces significant alterations in FA profiles, with distinct patterns observed between gill and mantle tissues.

4.1 Tissue-specific fatty acid profiles

FA composition varied considerably among tissues, with PUFAs predominating across all samples. The gonads displayed the highest MUFA content, likely reflecting their reproductive function and energy storage role. In contrast, the gills and mantle were more responsive to OA exposure. In gills, total SFA, MUFA,

TABLE 2 Total concentrations (mg/µg DW) in various tissues of the Antarctic snail *Neobuccinum eatoni* under control conditions and low pH exposure (LpH).

Tissue	FA	Media (LpH)	Media (C)	T	*p*-valor
Foot	14:0	0.11	0.10	1.09	0.3019
Foot	15:0	0.11	0.11	0.32	0.7590
Foot	16:0	2.09	1.97	0.63	0.5460
Foot	17:0	0.28	0.24	1.46	0.1953
Foot	18:0	1.42	1.30	1.14	0.2819
Foot	16:1 n-7	0.08	0.06	0.98	0.3497
Foot	18:1 n-9	0.44	0.41	0.52	0.6119
Foot	18:1 n-7	0.28	0.27	0.33	0.7493
Foot	20:1 n-11	0.77	0.75	0.15	0.8853
Foot	20:1 n-9	0.27	0.31	-1.03	0.3276
Foot	20:1 n-7	0.43	0.33	2.27	0.0634
Foot	18:2 n-6	0.15	0.13	0.59	0.5704
Foot	18: 2	0.09	0.08	1.37	0.1996
Foot	20:2 n-6	0.35	0.33	0.29	0.7747
Foot	20:4n-6 (ARA)	1.18	1.19	-0.07	0.9462
Foot	20:5n-3 (EPA)	2.96	2.68	1.35	0.2056
Foot	22:4n-6 (DHA)	0.18	0.15	1.24	0.2442
Foot	22:5 n-3 (DPA)	0.93	0.83	1.38	0.1981
Foot	22:6 n-3	0.47	0.42	0.78	0.4546
Foot	24:5 n-6	0.12	0.11	0.51	0.6218
Gill	14:00	0.08	0.09	-0.74	0.4741
Gill	15:00	0.12	0.2	-2.26	0.0474
Gill	16:00	1.53	2.71	-2.68	0.0232*
Gill	17:00	0.19	0.33	-3.64	0.0045*
Gill	18:00	0.87	1.35	-2.23	0.0496
Gill	16:1 n-7	0.06	0.11	-1.85	0.0942
Gill	18:1 n-9	0.28	0.33	-0.68	0.5142
Gill	18:1 n-7	0.25	0.54	-2.59	0.0268*
Gill	20:1 n-11	0.62	1.45	-3.03	0.0126*
Gill	20:1 n-9	0.18	0.43	-3.21	0.0093*
Gill	20:1 n-7	0.3	0.48	-2.03	0.0694
Gill	18:2 n-6	0.12	0.54	-3.29	0.0081*
Gill	18:02	0.08	0.12	-1.86	0.0923
Gill	20:2 n-6	0.3	0.87	-3.39	0.0069*
Gill	20:4n-6 (ARA)	0.86	2	-2.93	0.0151*
Gill	20:5n-3 (EPA)	2.37	3.51	-1.99	0.0744
Gill	22:4n-6 (DHA)	0.12	0.24	-2.3	0.0446*

(Continued)

TABLE 2 Continued

Tissue	FA	Media (LpH)	Media (C)	T	*p*-valor
Gill	22:5 n-3 (DPA)	0.58	1.04	-2.51	0.0309*
Gill	22:6 n-3	0.2	0.53	-3.07	0.0118*
Gill	24:5 n-6	0.09	0.12	-1.45	0.197
Gonad	14:00	0.37	0.63	-1.17	0.2705
Gonad	15:00	0.2	0.24	-0.56	0.5896
Gonad	16:00	4.91	5.25	-0.26	0.8019
Gonad	17:00	0.6	0.56	0.3	0.7714
Gonad	18:00	2.29	2.3	-0.02	0.9867
Gonad	16:1 n-7	0.5	0.65	-0.61	0.5577
Gonad	18:1 n-9	0.73	1.33	-1.12	0.2889
Gonad	18:1 n-7	1.64	1.95	-0.38	0.7154
Gonad	20:1 n-11	3.21	3.7	-0.53	0.6106
Gonad	20:1 n-9	0.76	1.77	-1.54	0.1557
Gonad	20:1 n-7	3.18	3.96	-0.61	0.5527
Gonad	18:2 n-6	1.39	0.7	1.57	0.1485
Gonad	18:02	0.42	0.51	-0.39	0.7022
Gonad	20:2 n-6	1.96	1.04	1.62	0.1359
Gonad	20:4n-6 (ARA)	0.98	1.15	-0.54	0.6015
Gonad	20:5n-3 (EPA)	7.36	7.28	0.04	0.9703
Gonad	22:4n-6 (DHA)	0.46	0.45	0.04	0.9663
Gonad	22:5 n-3 (DPA)	1.89	1.77	0.12	0.906
Gonad	22:6 n-3	2.7	2.59	0.18	0.8593
Gonad	24:5 n-6	0.11	0.13	-0.57	0.5928
Mantle	14:00	0.11	0.09	1.8	0.131
Mantle	15:00	0.11	0.07	4.03	0.003*
Mantle	16:00	1.74	1.32	3.58	0.0059*
Mantle	17:00	0.2	0.14	4.14	0.0025
Mantle	18:00	1.16	0.92	3.16	0.0116*
Mantle	16:1 n-7	0.08	0.05	2.48	0.0353*
Mantle	18:1 n-9	0.29	0.24	1.36	0.2079
Mantle	18:1 n-7	0.22	0.15	2.3	0.0615
Mantle	20:1 n-11	0.84	0.62	2.97	0.0158*
Mantle	20:1 n-9	0.21	0.19	0.35	0.7308
Mantle	20:1 n-7	0.4	0.28	3.98	0.0032*
Mantle	18:2 n-6	0.13	0.09	2.38	0.0412
Mantle	18:02	0.07	0.04	4.05	0.0067*
Mantle	20:2 n-6	0.33	0.24	2.74	0.0228*
Mantle	20:4n-6 (ARA)	1.22	0.98	1.42	0.1893

(Continued)

TABLE 2 Continued

Tissue	FA	Media (LpH)	Media (C)	T	*p*-valor
Mantle	20:5n-3 (EPA)	2.42	1.76	3.85	0.0039*
Mantle	22:4n-6 (DHA)	0.17	0.1	2.73	0.0342*
Mantle	22:5 n-3 (DPA)	0.77	0.5	3.12	0.0124*
Mantle	22:6 n-3	0.4	0.29	2.73	0.0232*
Mantle	24:5 n-6	0.12	0.09	3.62	0.0056*

Statistical analyses were performed using a *t*-test, with asterisks denoting significant differences ($p < 0.05$).

PUFA, and LC-PUFA levels were significantly reduced under LpH conditions, indicating a reorganization of FA composition in response to environmental stress. Notably, ARA (20:4 n-6) levels also decreased, which could reduce the production of eicosanoids, potentially compromising inflammatory signaling and immune plasticity (Supplementary Table S3). Conversely, in the mantle, these same FA classes were elevated under LpH. The increased LC-PUFA content in the mantles may represent an adaptive response to mitigate oxidative damage and maintain membrane integrity under environmental stress. LC-PUFAs, particularly DHA and EPA, play a crucial role in modulating oxidative stress, as they are involved in the regulation of antioxidant defense mechanisms and inflammatory responses (Monroig et al., 2013). While this mechanism has been previously documented in marine microorganisms (Okuyama et al., 2008), studies have also shown the involvement of LC-PUFAs in oxidative stress responses in marine invertebrates, such as mollusks and crustaceans (Monroig et al., 2013; Lv et al., 2021).

The observed tissue-specific variations in DHA levels between the mantle and gill tissues of *N. eatoni* under LpH conditions may be attributed to the distinct physiological roles and environmental exposures of these tissues. The mantle, primarily responsible for shell formation and protection, exhibited elevated DHA levels under LpH conditions, suggesting an adaptive mechanism to maintain membrane fluidity and integrity in response to environmental stressors. This lipid remodeling could enhance the mantle's resilience to oxidative stress induced by ocean acidification. However, this strategy may involve a metabolic cost, diverting resources from other physiological processes such as growth or reproduction.

In contrast, the gills, which are directly exposed to the external environment and are the main site for respiration and ion regulation, contained higher DHA concentrations in the control samples. Under LpH conditions, the reduced DHA levels in the gills likely reflect increased lipid peroxidation caused by elevated reactive oxygen species (ROS) (Fadhlaoui and Lavoie, 2021; Lushchak, 2021). Gills are known to be particularly susceptible to environmental stressors, including changes in pH, which can lead to oxidative damage and lipid degradation (Harms et al., 2014; Zutshi et al., 2019). This susceptibility necessitates efficient antioxidant defenses to mitigate oxidative damage and maintain cellular function (Mathieu-Resuge et al., 2020). Moreover, the loss

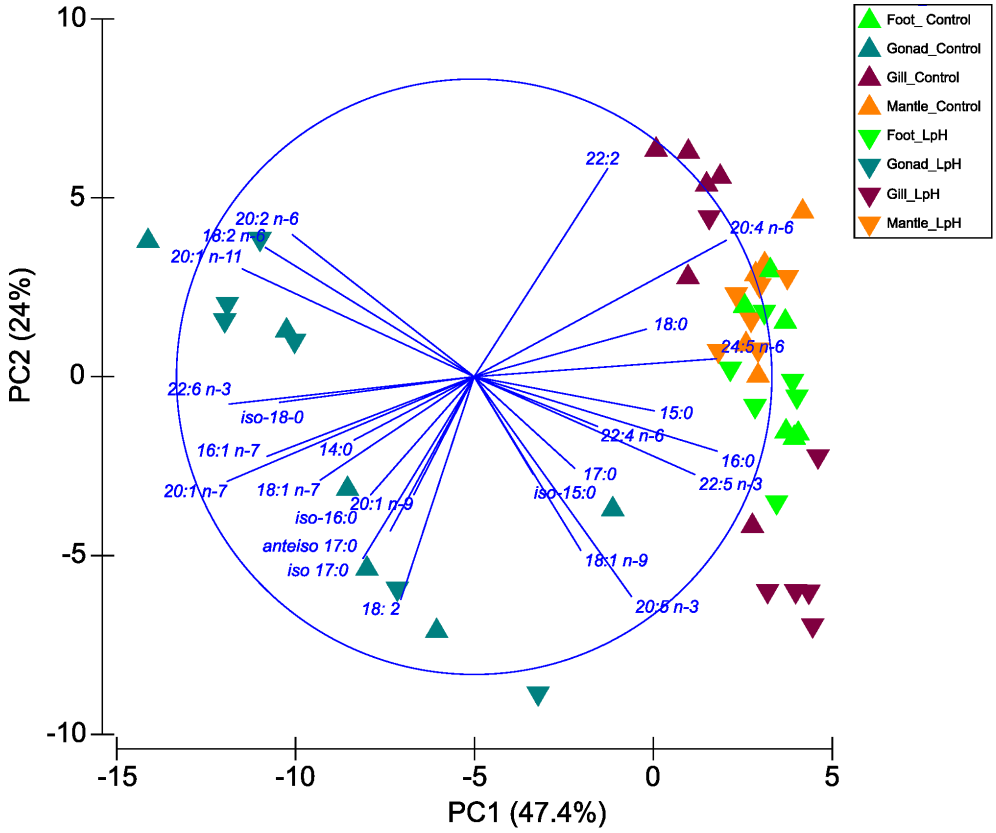

FIGURE 3
Principal Component Analysis (PCA) illustrating the relative (%) composition of fatty acids in different tissues (gonad, gill, mantle, and foot) of the Antarctic snail *Neobuccinum eatoni* under acidified conditions (LpH = low pH; (7.70 ± 0.09)) compared to control conditions.

of PUFA and increased SFA content in gills could reduce membrane fluidity, potentially impairing critical physiological functions such as ion transport, respiration efficiency, and filtration. These findings underscore the importance of DHA in modulating tissue-specific responses to environmental stress, reflecting the organism's strategic allocation of lipid resources to maintain functionality under varying conditions.

In mantle tissue, EPA levels were elevated in individuals exposed to LpH conditions. These FAs are well known for their anti-inflammatory properties and their ability to modulate membrane-associated proteins, such as ion channels and transporters (Banaszak et al., 2024). Additionally, they play a crucial role in defining key biophysical properties of biological membranes, including organization, ion permeability, elasticity, and the formation of microdomains (Bruno et al., 2007). A similar pattern was observed by Silva et al. (2017) in *Gibbula umbilicalis* exposed to metal contamination, further supporting the idea that DHA and EPA serve as reliable biomarkers of environmental stressors, in that particular case, metal pollutants.

Additionally, independent of the OA experiment, we observed differences in FA concentrations between the gonads and the other three analyzed tissues. These differences are primarily driven by the higher abundance of MUFAs in the gonads, where MUFAs represent the predominant FA class. The elevated MUFA suggests a critical role in reproductive processes, likely associated with energy storage and the maintenance of membrane fluidity during gametogenesis. In *N. eatoni*, this pattern may indicate a physiological adaptation to meet the energetic and structural requirements of gamete development. For example, Kapranova et al. (2019) reported that in the mussel *Mytilus galloprovincialis*, MUFA concentrations peak in male gonads at the onset of stage 2, whereas SFAs predominate in female gonads throughout stages 1 to 4. This pattern is consistent with our findings in *N. eatoni*, where the predominance of MUFAs in gonads suggests a comparable role of these fatty acids in supporting reproductive processes. These findings highlight the necessity for further research to elucidate the specific FA composition patterns associated with the reproductive cycle of *N. eatoni* and their potential ecological implications. Overall, the comparison underscores that differences in gonadal FA profiles across species can inform interpretations of reproductive status and resilience in *N. eatoni* under changing environmental conditions.

4.2 Immune modulation and n-3/n-6 balance

In addition to their structural and energetic roles, fatty acids contribute to immune regulation. In particular, the balance between n-3 and n-6 PUFAs influences the production of pro- and anti-

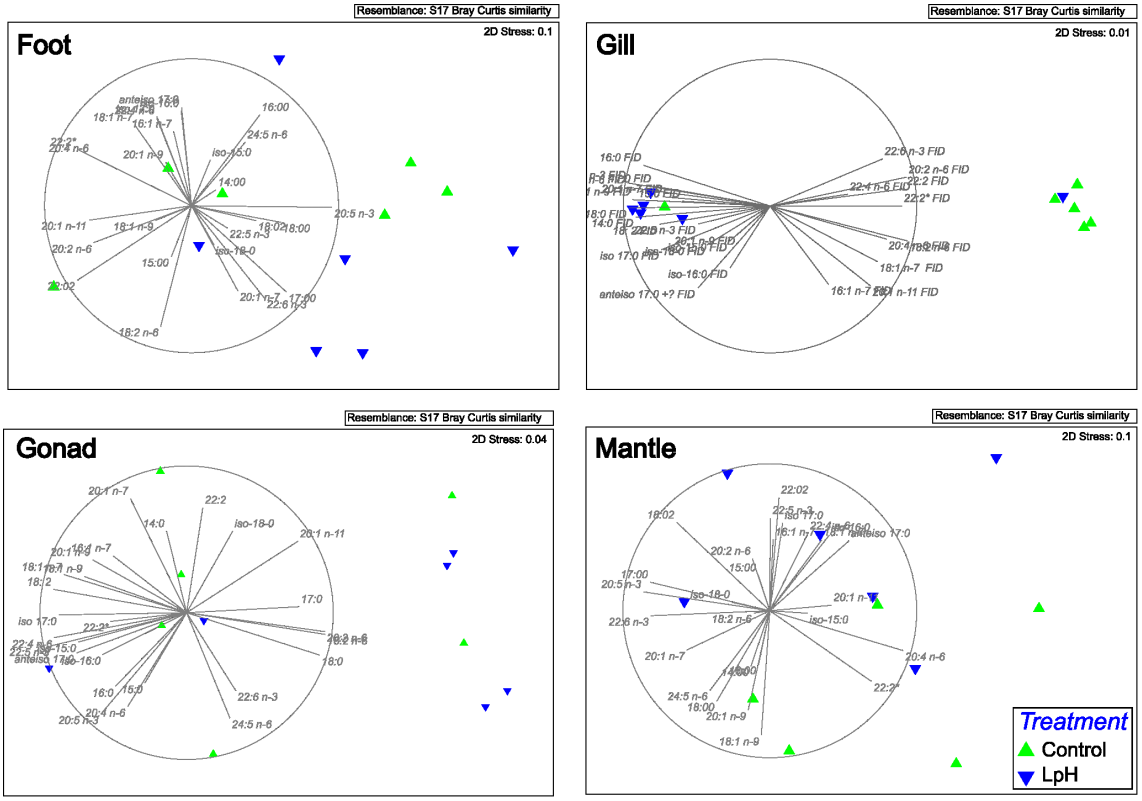

FIGURE 4
Non-metric Multidimensional Scaling (MDS) analysis depicting tissue fatty acid composition variability. LpH = low pH (7.70 ± 0.09).

inflammatory eicosanoids, as both groups compete for the same desaturation and elongation pathways (Monroig and Kabeya, 2018). In our study, the n-3/n-6 ratio remained largely unchanged in mantle, foot, and gonadal tissues, suggesting a stable immune–lipid balance under OA conditions. However, in gill tissues, this ratio was significantly elevated in the LpH group, indicative of a potential shift toward an anti-inflammatory lipid profile under acidified conditions.

Similar findings have been reported in *Crassostrea gigas*, where OA exposure increased n-3 PUFA content in gills, influencing immune performance and disease susceptibility (Wang et al., 2016). In *N. eatoni*, this tissue-specific shift may serve as a compensatory immune response to the heightened oxidative and ionic challenges posed by OA. However, whether this adjustment enhances or compromises immune competency remains to be further investigated.

4.3 Homeoviscous adaptation

Homeoviscous adaptation (HVA) refers to modifications in the chemical and mechanical properties of the lipid bilayer that help preserve membrane fluidity under changing stress conditions (Parrish, 2013). In this study, HVA biomarkers—specifically PUFA/SFA ratios and mean chain length (MCL)—revealed effects of elevated CO_2 exposure in both mantle and gill tissues. In the gills, a higher PUFA/SFA index under control conditions suggests a decrease in membrane fluidity in response to acidification, potentially indicating an adaptive mechanism for maintaining membrane function. This aligns with known functions of PUFAs enhancing membrane fluidity, and SFAs contributing to membrane stability (Hąc-Wydro and Wydro, 2007). Elevated seawater pCO_2 in treatment also influenced MCL in both tissues. The mantle exhibited higher MCL under LpH conditions, suggesting a reduced membrane fluidity as a compensatory response to acidification (Guerzoni et al., 2001). These findings are evidence that OA can modulate HVA pathways in polar invertebrates. In addition, under stress, HVA, through the regulation of lipid class ratios (e.g., ST/PL ratio), may be more energy-efficient than modifications in PUFA/SFA ratios and MCL. HVA pathways have been previously reported as adaptive responses to abiotic stressors in other marine organisms (Somero, 2022). For example, the impact of increasing seawater CO_2 and temperature on HVA has been studied in marine sponges (Bennett et al., 2018). They found that certain species used the additional carbon to enhance sterol biosynthesis, which likely reflects an HVA mechanism, providing a potential pathway where elevated CO_2 helps to mitigate thermal stress (Bennett et al., 2018).

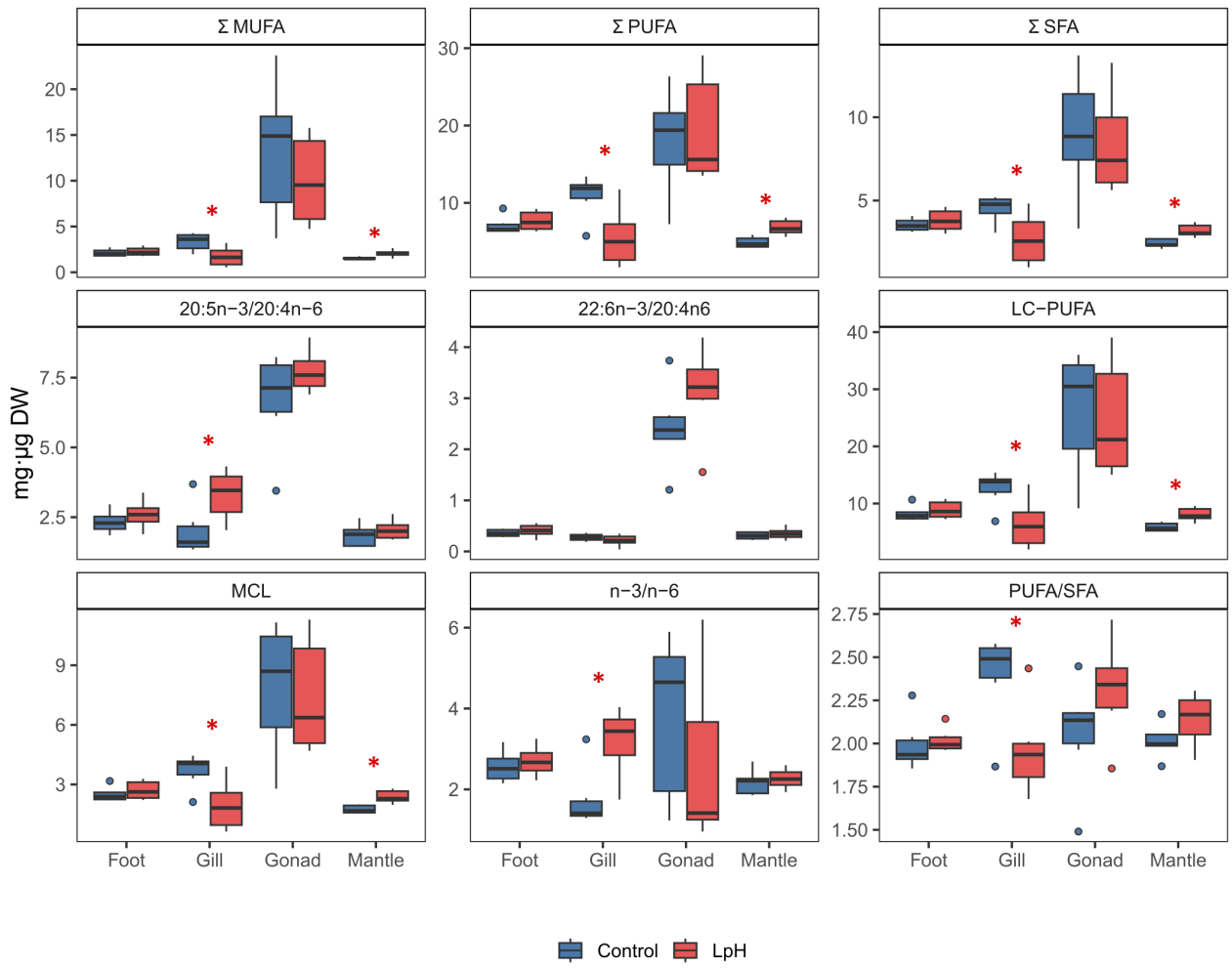

FIGURE 5
Fatty acid composition (mg/µg DW) across various Antarctic snail *Neobuccinum eatoni* tissues under low pH (LpH) (7.70 ± 0.09) and control conditions, with asterisks denoting significant differences ($p < 0.05$).

4.4 Biochemical drivers of FA shifts

While our results support the use of FA profiles as tissue-specific biomarkers of physiological stress in *N. eatoni*, a more mechanistic understanding of the biochemical underpinnings driving these shifts under pCO_2/pH variability is essential. FA composition in marine invertebrates is not static, but rather dynamically regulated through enzymatic pathways such as desaturation and elongation, mediated by desaturases and elongases whose activities are often sensitive to environmental stressors (Monroig et al., 2013; Bell et al., 2016). Changes in pH and CO_2 availability can alter cellular acid-base balance, indirectly affecting enzymatic efficiency and gene expression linked to lipid metabolism (Tocher, 2010). Moreover, the remodeling of membrane lipid composition, particularly increases in LC-PUFAs like EPA and DHA, may reflect adaptive strategies to maintain membrane fluidity and functionality under acidified conditions, as observed in both invertebrate and vertebrate systems (Mourente et al., 2022). In gill tissues, reductions in PUFAs under LpH (7.70 ± 0.09) may be associated with impaired membrane-bound processes such as ion transport or respiration, whereas the mantle's elevated LC-PUFA content could suggest compensatory regulation aimed at preserving cellular performance. Collectively, these tissue-specific FA shifts likely represent a balance between maintaining membrane integrity, oxidative defense, and energetic allocation, highlighting the complex trade-offs faced by *N. eatoni* under OA stress. Such tissue-specific responses align with broader findings across phyla, including mollusks and crustaceans, where FA remodeling serves as a plastic response to environmental change (Arts and Kohler, 2009; Soudant et al., 2020). Thus, interpreting FA shifts not solely as stress indicators, but as reflections of underlying biochemical and physiological strategies, provides a richer framework for understanding organismal resilience to ocean acidification.

5 Conclusion

This study provides new evidence of tissue-specific alterations in the FA composition of *N. eatoni* under LpH exposure. Significant changes were observed, particularly in mantle and gill tissues, with

shifts in n-3/n-6 ratios and lipid-related indicators (e.g., PUFA/SFA ratio, MCL), suggesting possible effects on membrane properties and immune-related pathways. The depletion of ARA in gills and elevation of LC-PUFAs in the mantle highlight tissue-specific trade-offs between immune regulation and membrane resilience. While our study did not directly measure physiological processes, these FA patterns may serve as biochemical signals of tissue remodeling under OA conditions. Overall, these findings highlight that different tissues of *N. eatoni* respond distinctly to acidified seawater, offering valuable baseline information on potential sensitivity to OA. Given the scarcity of data on Antarctic gastropods, this work represents a step toward understanding their responses, but longer-term and integrative studies are needed to clarify the physiological and ecological implications, particularly regarding organismal performance and population resilience in polar environments. Considering the ecological and reproductive implications, longer-term and integrative studies are needed to clarify the consequences for organismal performance, survival, and population resilience in polar environments.

Data availability statement

The raw data supporting the conclusions of this article will be made available by the authors, without undue reservation.

Ethics statement

The study was conducted in accordance with the local legislation and institutional requirements.

Author contributions

NS: Formal analysis, Investigation, Methodology, Writing – original draft, Writing – review & editing, Funding acquisition, Project administration. MD: Conceptualization, Supervision, Writing – review & editing, Methodology. GA: Formal analysis, Methodology, Writing – review & editing, Conceptualization, Investigation. LF: Formal analysis, Methodology, Writing – review & editing. MD: Methodology, Writing – review & editing. RS: Conceptualization, Formal analysis, Funding acquisition, Investigation, Supervision, Writing – review & editing, Project administration.

Funding

The author(s) declare financial support was received for the research and/or publication of this article. This study was supported by PADI Foundation (#81356), Dirección Nacional del Antártico (DNA)/Instituto Antártico Argentino (IAA), Consejo Nacional de Investigaciones Científicas y Técnicas (CONICET), Alfred Wegener Institute (AWI, Germany), and Universidad Nacional de Córdoba. Partial funding was provided by PICT-2018-02125, PICT-2021-I-GRF1, PICT-2020-SERIEA-02956, and the EU project CoastCarb, Marie Curie Action RISE (H2020-MCSA-RISE 872690). The research presented here was conducted with infrastructure funded by EMBRC Belgium-FWO International Research Infrastructure I001621N.

Acknowledgments

The authors extend their sincere thanks to the staff of the Carlini Station. Special thanks to Dr. Bruno Vlaeminck (UGent, Marine Biology) for his assistance with lab work.

Conflict of interest

The authors declare that no commercial or financial relationships were present that could be perceived as a potential conflict of interest in the conduct of this research.

Generative AI statement

The author(s) declare that no Generative AI was used in the creation of this manuscript.

Any alternative text (alt text) provided alongside figures in this article has been generated by Frontiers with the support of artificial intelligence and reasonable efforts have been made to ensure accuracy, including review by the authors wherever possible. If you identify any issues, please contact us.

Publisher's note

Supplementary material

The Supplementary Material for this article can be found online at: https://www.frontiersin.org/articles/10.3389/fmars.2025.1645755/full#supplementary-material

References

Banaszak, M., Dobrzyńska, M., Kawka, A., Górna, I., Woźniak, D., Przysławski, J., et al. (2024). Implementation of and systems-level barriers to cancer clinical trials: a qualitative study. *JCO Precis Oncol.* (2024) 8:1-8. doi: 10.1200/PO.23.00518

Bell, M. V., Tocher, D. R., and Sargent, J. R. (2016). Biosynthesis of polyunsaturated fatty acids in aquatic ecosystems: general pathways and species differences. *Prog. Lipid Res.* 62, 1–17. doi: 10.1016/j.plipres.2016.01.001

Bennett, H., Bell, J. J., Davy, S. K., Webster, N. S., and Francis, D. S. (2018). Elucidating the sponge stress response; lipids and fatty acids can facilitate survival under future climate scenarios. *Glob. Chang. Biol.* 24, 3130–3144. doi: 10.1111/gcb.14116

Boyen, J., Fink, P., Mensens, C., Hablützel, P. I., and De Troch, M. (2020). Fatty acid bioconversion in harpacticoid copepods in a changing environment: a transcriptomic approach. *Philos. Trans. R. Soc Lond. B Biol. Sci.* 375, 20190645. doi: 10.1098/rstb.2019.0645

Bruno, M. J., Koeppe, R. E., and Andersen, O. S. (2007). Docosahexaenoic acid alters bilayer elastic properties. *PNAS* 104, 9638–9643. doi: 10.1073/pnas.0701015104

Capitão, A., Lyssimachou, A., Castro, L. F. C., and Santos, M. M. (2017). Obesogens in the aquatic environment: an evolutionary and toxicological perspective. *Environ. Int.* 106, 153–169. doi: 10.1016/j.envint.2017.06.003

Corsolini, S., and Borghesi, N. (2017). A comparative assessment of fatty acids in Antarctic organisms from the Ross Sea: Occurrence and distribution. *Chemosphere* 174, 747–753. doi: 10.1016/j.chemosphere.2017.02.031

Cummings, V., Hewitt, J., Van Rooyen, A., Currie, K., Beard, S., Thrush, S., et al. (2011). Ocean acidification at high latitudes: potential effects on functioning of the Antarctic bivalve Laternula elliptica. *PloS One* 6, e16069. doi: 10.1371/journal.pone.0016069

de Aranzamendi, M. C., Servetto, N., Movilla, J., Bettencourt, R., and Sahade, R. (2021). Ocean acidification effects on the stress response in a calcifying Antarctic coastal organism: The case of *Nacella concinna* ecotypes. *Mar. pollut. Bull.* 166, 112218. doi: 10.1016/j.marpolbul.2021.112218

de Carvalho, G. T., Pezzi, L. P., Lefèvre, N., Rodrigues, C. C. F., Santini, M. F., and Mejia, C. (2025). Spatio-temporal variability in CO_2 fluxes in the Atlantic sector of the southern ocean. *Atmosphere* 16, 319. doi: 10.3390/atmos16030319

Dennis, M. M., Molnár, K., Kriska, G., and Lőw, P. (2021). Mollusca: gastropoda. *Histol. Invertebr.*, 87–132. doi: 10.1002/9781119507697.ch4

De Troch, M., Boeckx, P., Cnudde, C., Van Gansbeke, D., Vanreusel, A., Vincx, M., et al. (2012). Bioconversion of fatty acids at the basis of marine food webs: insights from a compound-specific stable isotope analysis. *Mar. Ecol. Prog. Ser.* 465, 53–67. doi: 10.3354/meps09920

Dickson, A. G., Sabine, C. L., and Christian, J. R. (2007). *Guide to best practices for ocean CO_2 measurements* (North Pacific Marine Science Organization, Canada: PICES Special Publication), 191.

Dickson, A. G., and Millero, F. J. (1987). A comparison of the equilibrium constants for the dissociation of carbonic acid in seawater media. *Deep-Sea Res. I: Oceanogr. Res. Pap.* 34, 1733–1743. doi: 10.1016/0198-0149(87)90021-5

Ericson, J. A., Hellessey, N., Kawaguchi, S., Nichols, P. D., Nicol, S., Hoem, N., et al. (2019). Near-future ocean acidification does not alter the lipid content and fatty acid composition of adult Antarctic krill. *Sci. Rep.* 9 (1), 12375. doi: 10.1038/s41598-019-48665-5

Fabry,V. J., Seibel,B. A., Feely,R. A., and Orr,J. C. (2008). Impacts of ocean acidification on marine fauna and ecosystem processes. *ICES J. Mar. Sci.* 65, 414–432. doi: 10.1093/icesjms/fsn048

Fadhlaoui, M., and Lavoie, I. (2021). Effects of temperature and glyphosate on fatty acid composition, antioxidant capacity, and lipid peroxidation in the gastropod lymneae sp. *Water* 13 (8), 1039. doi: 10.3390/w13081039

Findlay, H. S., and Turley, C. (2021). *Ocean acidification and climate change, in: Climate Change: Observed Impacts on Planet Earth. 3rd ed.* (Elsevier), 251–279. doi: 10.1016/B978-0-12-821575-3.00013-X

Fisher, B. J., Poulton, A. J., Meredith, M. P., Baldry, K., Schofield, O., and Henley, S. F. (2025). Climate-driven shifts in Southern Ocean primary producers and biogeochemistry in CMIP6 models. *Biogeosciences* 22, 975–994. doi: 10.5194/bg-22-975-2025

Gao, Y., Zheng, S. C., Zheng, C. Q., Shi, Y. C., Xie, X. L., Wang, K. J., et al. (2018). The immune-related fatty acids are responsive to CO_2-driven seawater acidification in a crustacean brine shrimp *Artemia sinica*. *Dev. Comp. Immunol.* 81, 342–347. doi: 10.1016/j.dci.2017.12.022

Gattuso, J. P., Magnan, A., Billé, R., Cheung, W. W., Howes, E. L., Joos, F., et al. (2015). Contrasting futures for ocean and society from different anthropogenic CO_2 emissions scenarios. *Science* 349, aac4722. doi: 10.1126/science.aac4722

Gibbs, M. C., Parker, L. M., Scanes, E., Byrne, M., O'Connor, W. A., and Ross, P. M. (2021). Energetic lipid responses of larval oysters to ocean acidification. *Mar. pollut. Bull.* 168, 112441. doi: 10.1016/j.marpolbul.2021.112441

Gingerich, P. D. (2019). Temporal scaling of carbon emission and accumulation rates: modern anthropogenic emissions compared to estimates of PETM onset accumulation. *Paleoceanogr. Paleoclimatol.* 34, 329–335. doi: 10.1029/2018PA003379

Gladyshev, M. I., Sushchik, N. N., and Makhutova, O. N. (2013). Production of EPA and DHA in aquatic ecosystems and their transfer to the land. *PGs* 107, 117–126. doi: 10.1016/j.prostaglandins.2013.03.002

González, R., Pertierra, L. R., Guerrero, P. C., and Díaz, A. (2024). High vulnerability of the endemic Southern Ocean snail *Neobuccinum eatoni* (Buccinidae) to critical projected oceanographic changes. *Sci. Rep.* 15, 3799. doi: 10.1038/s41598-024-80353-x

Guerzoni, M. E., Lanciotti, R. , and Cocconcelli, P. S. (2001). Alteration in cellular fatty acid composition as a response to salt, acid, oxidative and thermal stresses in *Lactobacillus helveticus*. *Microbiology* 147, 2255–2264. doi: 10.1099/00221287-147-8-2255

Hąc-Wydro, K., and Wydro, P. (2007). The influence of fatty acids on model cholesterol/phospholipid membranes. *Chem. Phys. Lipids.* 150, 66–81. doi: 10.1016/j.chemphyslip.2007.06.213

Hancock, A. M., King, C. K., Stark, J. S., McMinn, A., and Davidson, A. T. (2020). Effects of ocean acidification on Antarctic marine organisms: A meta-analysis. *Ecol. Evol.* 10, 4495–4514. doi: 10.1002/ece3.6205

Harms, L., Frickenhaus, S., Schiffer, M., Mark, F. C., Storch, D., Held, C., et al. (2014). Gene expression profiling in gills of the great spider crab *Hyas araneus in* response to ocean acidification and warming. *BMC Genomics* 15, 1–17. doi: 10.1186/1471-2164-15-789

Hauri, C., Doney, S. C., Takahashi, T., Erickson, M., Jiang, G., and Ducklow, H. W. (2015). Two decades of inorganic carbon dynamics along the West Antarctic Peninsula. *BG* 12, 6761–6779. doi: 10.5194/bg-12-6761-2015

Hedberg, P., Lau, D. C. P., Albert, S., and Winder, M. (2023). Variation in fatty acid content among benthic invertebrates in a seasonally driven system. *Limnol. Oceanogr. Lett.* 8, 751–759. doi: 10.1002/lol2.10333

IPCC (2019). *IPCC Special Report on the Ocean and Cryosphere in a Changing Climate* H.-O. Pörtner, D.C. Roberts, V. Masson-Delmotte, P. Zhai, M. Tignor, E. Poloczanska, K. Mintenbeck, A. Alegría, M. Nicolai, et al (eds.) Cambridge University Press, Cambridge, UK and New York, NY, USA, 755 pp. doi: 10.1017/9781009157964

Johnson, K. M., and Hofmann, G. E. (2017). Transcriptomic response of the Antarctic pteropod *Limacina helicina Antarctica* to ocean acidification. *BMC Genomics* 18, 1–16. doi: 10.1186/s12864-017-4161-0

Kapranova, L. L., Nekhoroshev, M. V., Malakhova, L. V., Ryabushko, V. I., Kapranov, S. V., and Kuznetsova, T. V. (2019). Fatty acid composition of gonads and gametes in the Black Sea bivalve mollusk *Mytilus galloprovincialis* Lam. at different stages of sexual maturation. *J. Evol. Biochem. Phys.* 55, 448–455. doi: 10.1134/S0022093019060024

Kroeker, K. J., Kordas, R. L., Crim, R., Hendriks, I. E., Ramajo, L., Singh, G. S., et al. (2013). Impacts of ocean acidification on marine organisms: quantifying sensitivities and interaction with warming. *Glob. Change Biol.* 19, 1884–1896. doi: 10.1111/gcb.12179

Lushchak, V. I. (2021). Interplay between bioenergetics and oxidative stress at normal brain aging. Aging as a result of increasing disbalance in the system oxidative stress–energy provision. *Pflugers Arch.* 473, 713–722. doi: 10.1007/s00424-021-02531-4

Lv, D., Zhang, F., Ding, J., Chang, Y., and Zuo, R. (2021). Effects of dietary n-3 LC-PUFA on the growth performance, gonad development, fatty acid profile, transcription of related genes and intestinal microflora in adult sea urchin (*Strongylocentrotus intermedius*). *Aquac. Res.* 52, 1431–1441. doi: 10.1111/are.14997

Mathieu-Resuge, M., Le Grand, F., Schaal, G., Lluch-Cota, S. E., Racotta, I. S., and Kraffe, E. (2020). Specific regulations of gill membrane fatty acids in response to environmental variability reveal fitness differences between two suspension-feeding bivalves (*Nodipecten subnodosus* and *Spondylus crassisquama*). *Conserv. Physiol.* 8. doi: 10.1093/conphys/coaa079

Mehrbach, C., Culberson, C. H., Hawley, J. E., and Pytkowicx, R. M. (1973). Measurement of the apparent dissociation constants of carbonic acid in seawater at atmospheric pressure. *Limnol. Oceanogr.* 18, 897–907. doi: 10.4319/lo.1973.18.6.0897

Monroig, Ó., and Kabeya, N. (2018). Desaturases and elongases involved in polyunsaturated fatty acid biosynthesis in aquatic invertebrates: a comprehensive review. *Fish. Sci.* 84, 911–928. doi: 10.1007/s12562-018-1254-x

Monroig, Ó., Tocher, D. R., and Navarro, J. C. (2013). Biosynthesis of polyunsaturated fatty acids in marine invertebrates: recent advances in molecular mechanisms. *Mar. Drugs* 11, 3998–4018. doi: 10.3390/md11103998

Mourente, G., Bell, J. G., and Tocher, D. R. (2022). Polyunsaturated fatty acids and eicosanoids in marine invertebrates: recent advances and perspectives. *Prog. Lipid Res.* 86, 101166. doi: 10.1016/j.plipres.2022.101166

Norkko, A., Thrush, S. F., Cummings, V. J., Gibbs, M. M., Andrew, N. L., Norkko, J., et al. (2007). Trophic structure of coastal Antarctic food webs associated with changes in sea ice and food supply. *Ecology* 88, 2810–2820. doi: 10.1890/06-1396.1

Okuyama, H., Orikasa, Y., and Nishida, T. (2008). Significance of antioxidative functions of eicosapentaenoic and docosahexaenoic acids in marine microorganisms. *Appl. Environ. Microbiol.* 74, 570–574. doi: 10.1128/AEM.02256-07

Orr, J. C., Fabry, V. J., Aumont, O., Bopp, L., Doney, S. C., Feely, R. A., et al. (2005). Anthropogenic ocean acidification over the twenty-first century and its impact on calcifying organisms. *Nature* 437, 681–686. doi: 10.1038/nature04095

Parrish, C. C. (2013). Lipids in marine ecosystems. *Int. Sch. Res. Notices.*, 2356–7872. doi: 10.5402/2013/604045

Pierrot, D., Lewis, E., and Wallace, D. W. R. (2006). *CO2SYS DOS Program Developed for CO_2 System Calculations* (Oak Ridge, TN: ORNL/CDIAC-105. Carbon Dioxide Information Analysis Center, Oak Ridge National Laboratory, US Department of Energy).

R Core Team. (2020). R: A language and environment for statistical computing. R Foundation for Statistical Computing, Vienna, Austria. Available at: https://www.R-project.org.

Schiaparelli, S., Lörz, A. N., and Cattaneo-Vietti, R. (2006). Diversity and distribution of mollusc assemblages on the Victoria Land coast and the Balleny Islands, Ross Sea, Antarctica. *Antarct. Sci.* 18, 615–631. doi: 10.1017/S0954102006000654

Schmitz, G., and Ecker, J. (2008). The opposing effects of n-3 and n-6 fatty acids. Prog. *Lipid Res.* 47, 147–155. doi: 10.1016/j.plipres.2007.12.004

Sahade, R., Lagger, C., Torre, L., Momo, F., Monien, P., Schloss, I., et al. (2015). Climate change and glacier retreat drive shifts in an Antarctic benthic ecosystem. *Sci. Adv.* 1, e1500050. doi: 10.1126/sciadv.1500050

Servetto, N., de Aranzamendi, M. C., Bettencourt, R., Held, C., Abele, D., Movilla, J., et al. (2021). Molecular mechanisms underlying responses of the Antarctic coral *Malacobelemnon daytoni* to ocean acidification. *Mar. Environ. Res.* 170, 105430. doi: 10.1016/j.marenvres.2021.105430

Servetto, N., De Troch, M., Gazeau, F., de Aranzamendi, C., Alurralde, G., González, G., et al. (2025). Fatty acid response of calcifying benthic Antarctic species to ocean acidification and warming. *Mar. pollut. Bull.* 217, 118111. doi: 10.1016/j.marpolbul.2025.118111

Servetto, N., Ruiz, M. B., Martínez, M., Harms, L., de Aranzamendi, M. C., Alurralde, G., et al. (2023). Molecular responses to ocean acidification in an Antarctic bivalve and an ascidian. *Sci. Total Environ.* 903, 166577. doi: 10.1016/j.scitotenv.2023.166577

Shi, Y., and Li, Y. (2024). Impacts of ocean acidification on physiology and ecology of marine invertebrates: a comprehensive review. *Aquat. Ecol.* 58, 207–226. doi: 10.1007/s10452-023-10058-2

Silva, C. O., Simões, T., Novais, S. C., Pimparel, I., Granada, L., Soares, A. M., et al. (2017). Fatty acid profile of the sea snail *Gibbula umbilicalis* as a biomarker for coastal metal pollution. *Sci. Total Environ.* 586, 542–550. doi: 10.1016/j.scitotenv.2017.02.015

Smith, S. V., and Kinsey, D. (1978). "Calcification and organic carbon metabolism as indicated by carbon dioxide," in *Coral Reef: Research Methods, UNESCO Monographs on Oceanographic Methology*, vol. 5 . Eds. D.-R. Stoddart and R. E. Johannes, 462–484.

Somero, G. N. (2022). Solutions: how adaptive changes in cellular fluids enable marine life to cope with abiotic stressors. *Mar. Life Sci. Technol.* 4, 389–413. 3. doi: 10.1007/s42995-022-00140-3

Soudant, P., Gonçalves, J. G., Quere, C., and Rittschof, D. (2020). Environmental effects on fatty acid composition and functional implications in marine bivalves. *Front. Physiol.* 11. doi: 10.3389/fphys.2020.576237

Stanley-Samuelson, D. W., Jurenka, R. A., Cripps, C., Blomquist, G. J., and de Renobales, M. (1988). Fatty acids in insects: composition, metabolism, and biological significance. *Arch. Insect Biochem. Physiol.* 9, 1–33. doi: 10.1002/arch.940090102

Teixidó, N., Carlot, J., Alliouane, S., Ballesteros, E., De Vittor, C., Gambi, M. C., et al. (2024). Functional changes across marine habitats due to ocean acidification. *Glob. Change Biol.* 30, e17105. doi: 10.1111/gcb.17105

Tocher, D. R. (2010). Fatty acid requirements in ontogeny of marine and freshwater fish. *Aquac. Res.* 41, 717–732. doi: 10.1111/j.1365-2109.2008.02150.x

Turner, L. M., Ricevuto, E., Massa Gallucci, A., Lorenti, M., Gambi, M. C., and Calosi, P. (2016). Metabolic responses to high pCO_2 conditions at a CO_2 vent site in juveniles of a marine isopod species assemblage. *Mar. Biol.* 163, 1–11. doi: 10.1007/s00227-016-2984-x

Valles-Regino, R., Tate, R., Kelaher, B., Savins, D., Dowell, A., and Benkendorff, K. (2015). Ocean warming and CO_2-induced acidification impact the lipid content of a marine predatory gastropod. *Mar. Drugs* 13, 6019–6037. doi: 10.3390/md13106019

Van Anholt, R. D., Spanings, F. A. T., Koven, W. M., Nixon, O., and Wendelaar Bonga, S. E. (2004). Arachidonic acid reduces the stress response of gilthead seabream *Sparus aurata* L. *J. Exp. Biol.* 207, 3419–3430. doi: 10.1242/jeb.01166

Wang, Q., Cao, R., Ning, X., You, L., Mu, C., Wang, C., et al. (2016). Effects of ocean acidification on immune responses of the Pacific oyster *Crassostrea gigas*. *Fish Shellfish Immunol.* 49, 24–33. doi: 10.1016/j.fsi.2015.12.025

Wang, S. T., Yang, Q., Liu, M. K., Li, L., Wang, W., Zhang, S. D., et al. (2025). Comparative transcriptomic analysis reveals a differential acid response mechanism between estuarine oyster (*Crassostrea ariakensis*) and Pacific oyster (*Crassostrea gigas*). *Ecotoxicol. Environ. Saf.* 297, 118210. doi: 10.1016/j.ecoenv.2025.118210

Zhukova, N. V. (2019). Fatty acids of marine mollusks: Impact of diet, bacterial symbiosis and biosynthetic potential. *Biomolecules* 9, 857. doi: 10.3390/biom9120857

Zutshi, B., Singh, A., and Dasgupta, P. (2019). Outcome of prolonged pH exposure on oxidative stress indices and glucose levels in gills and muscles of juvenile koi (*Cyprinus carpio*). *Fish. Aquat. Life.* 27 (4). doi: 10.2478/aopf-2019-0023

frontiers | Frontiers in Marine Science

TYPE Original Research
PUBLISHED 30 October 2025
DOI 10.3389/fmars.2025.1633653

OPEN ACCESS

EDITED BY
Jun Sun,
Tianjin University of Science and Technology, China

REVIEWED BY
Peisong Yu,
Ministry of Natural Resources, China
Vincenzo Alessandro Laudicella,
National Institute of Oceanography and Applied Geophysics, Italy

*CORRESPONDENCE
Simón Gutiérrez Duque
gutierrezds@javeriana.edu.co

RECEIVED 23 May 2025
ACCEPTED 25 September 2025
PUBLISHED 30 October 2025

CITATION
Gutiérrez Duque S, Acosta A, Murcia A, Garcia AP, Corredor-Acosta A, Hernandez-Ayon JM, Coronado Álvarez LdLA, Kahl LC and Ruiz-Pino D (2025) Seasonal air-sea CO_2 flux dynamics in Colombia's Gorgona Marine Area during La Niña 2021–2022. *Front. Mar. Sci.* 12:1633653. doi: 10.3389/fmars.2025.1633653

Seasonal air-sea CO_2 flux dynamics in Colombia's Gorgona Marine Area during La Niña 2021–2022

Simón Gutiérrez Duque[1]*, Alberto Acosta[1], Andrea Murcia[1], Alejandro P. Garcia[1], Andrea Corredor-Acosta[2,3], José Martin Hernandez-Ayon[4], Luz de Lourdes Aurora Coronado Álvarez[4], Lucía Carolina Kahl[5] and Diana Ruiz-Pino[6]

[1]UNESIS (Unidad de Ecología y Sistemática), Departamento de Biología, Facultad de Ciencias, Pontificia Universidad Javeriana, Bogotá, Colombia, [2]División de Investigación en Acuicultura, Instituto de Fomento Pesquero (IFOP), Putemún, Chile, [3]Centro FONDAP de Investigación en Dinámica de Ecosistemas Marinos de Altas Latitudes (IDEAL), Instituto de Acuicultura y Ciencias Ambientales, Universidad Austral de Chile, Puerto Montt, Chile, [4]Instituto de Investigaciones Oceanológicas, Universidad Autónoma de Baja California, Ensenada, Baja California, Mexico, [5]Departamento Oceanografía, Servicio de Hidrografía Naval, Buenos Aires, Argentina, [6]Sorbonne Universités (IPSL-CNRS-IRD-MNHN), LOCEAN Laboratory, Paris, France

Air–sea CO_2 fluxes in tropical coastal zones are strongly influenced by ENSO variability, but in situ measurements in the Eastern Tropical Pacific remain scarce. We assessed seasonal CO_2 dynamics around Gorgona Island (Panama Bight, Colombian Pacific) under La Niña 2021–2022. From November 2021 to July 2022, we conducted monthly sampling at seven stations spanning the Guapi River plume to the open ocean, measuring physical (SST, SSS, thermocline depth), chemical (TA, DIC, pH, carbonate system parameters), and biological (chlorophyll-a) variables, and estimating net CO_2 fluxes (FCO_2) with the Liss and Merlivat (1986) parameterization and atmospheric CO_2 from NOAA. La Niña featured a cool-water anomaly (–0.78 °C), enhanced precipitation (+59%) and river discharge (+44%) relative to multi-year means. The nine-month mean CO_2 flux was near neutral (–0.01049 ± 0.00014 mol C m^{-2}) but strongly seasonal: six post-upwelling months showed slightly positive fluxes (0.00929 ± 0.000147 mol C m^{-2}) associated with high precipitation (746.4 ± 214.7 mm), warmer SST (27.5 ± 0.4 °C), elevated pCO_2w (567 ± 97.5 µatm) and lower pH (7.869 ± 0.040), whereas three upwelling months showed slightly negative fluxes (–0.00119 ± 0.00010 mol C m^{-2}) with reduced precipitation (165.8 ± 82.4 mm), cooler SST (26.5 ± 0.2 °C), lower pCO_2w (461 ± 92.8 µatm) and higher pH (7.968 ± 0.048). La Niña amplified pCO_2w variability (316–839 µatm) via vertical Ekman pumping, horizontal transport (Zonal Ekman Transport, tides), and freshwater inputs, while a persistent thermocline (10–40.1 m) restricted deep CO_2-rich waters from

10.3389/fmars.2025.1633653

reaching the surface. Biological uptake further modulated outgassing, as evidenced by chlorophyll-a and ΔDIC dynamics. Overall, CO_2 fluxes were relatively low compared with other tropical estuarine and oceanic sources. These results underscore the need for sustained in situ observations in estuarine–ocean systems to refine predictive models of CO_2 fluxes under ENSO conditions.

KEYWORDS

ENSO, CO_2 Flux, Gorgona, Panama Bight, Eastern Tropical Pacific, estuarine systems, seasonal variability

1 Introduction

Oceanic carbon fluxes have become a central focus in marine biogeochemistry and are increasingly studied for their potential in carbon sequestration (Lal, 2024; Gerrard, 2023; Santos et al., 2022). The oceans absorb around 31% of CO_2 emissions from fossil fuels (Friedlingstein et al., 2023; Parv et al., 2023). However, not all parts of the ocean have the same absorption capacity, with the poles acting as sinks and tropical areas considered sources of CO_2 to the atmosphere (Legge et al., 2015; Yilmaz et al., 2022; Swesi et al., 2023). The largest carbon sinks are found in the Arctic and polar waters, with fluxes between -3.8 mol C m^{-2} yr^{-1} and -4.4 mol C m^{-2} yr^{-1-1} (Olafsson et al., 2021), due to carbon "drawdown" from high primary productivity, deep convective mixing, water heat loss and strong seasonal winds (Olafsson et al., 2021). On the other hand, coastal zones, which only contain 7-8% of the ocean's surface area, are nutrient-rich and account for 25% of global primary production (Smith and Hollibaugh, 1993), which allows them to be more effective than the open ocean in retaining the atmospheric CO_2 (Andersson, 2005). However, some coastal tropical areas are sources (Kryzhova and Semkin, 2023) and others are sinks (Roobaert et al., 2021; Watanabe et al., 2024), depending on many factors, which are seldom explored (Chen and Borges, 2009; Borges and Abril, 2011; Cai et al., 2011; Kahl, 2018; Rosentreter et al., 2023; Roobaert et al., 2025). Similarly, in tropical areas, CO_2 flux can vary between source or sink depending on atmospheric and oceanographic conditions in space, which also change during different seasons of the year, with the net flux further influenced by complex biogeochemical processes (Monteiro et al., 2022; Swesi et al., 2023).

Among the global drivers of carbon flux, biological processes predominantly influence equatorial and subpolar zones, while sea surface temperature (SST) and salinity (SSS) play a fundamental role in subtropical areas (Roobaert et al., 2021). Additionally, the direction and magnitude of flux in each location depend on atmospheric processes such as wind stress and ENSO events (Ford et al., 2022). La Niña event in particular has a significant effect on the direction and magnitude of CO_2 flux, as it increases coastal upwelling and Ekman pumping (Amos and Castelao, 2022), enabling outgassing events (facilitating carbon flux to the atmosphere) of around 1 billion tons of carbon (CO_2) per year, where deep waters rich in dissolved inorganic carbon (DIC) rise to the surface. This contrasts with the inherent capacity of coastal upwelling regions to act as significant carbon sinks through the biological pump they promote (Lanson et al., 2009). Moreover, rainfall during La Niña events tends to be more intense (Chung and Power, 2014), shifting coastal systems from upwelling to post-upwelling (river-dominated ocean margin; Dai et al., 2022).

Thus, the ENSO-driven oscillations between cold (La Niña) and warm periods (El Niño) in the Tropical Pacific involve massive redistributions of heat content in the surface ocean (Amos and Castelao, 2022), thereby altering the net carbon flux. Despite this, few studies focus on what happens in the Eastern Tropical Pacific and specifically in the Panama Bight (*e.g.*, Kao and Yu, 2009; Corredor-Acosta et al., 2020; Torres et al., 2023). Recent findings in the Colombian Caribbean indicated that ENSO events are the most important influence over marine biogeochemistry as increased upwelling anomalies bring up water's rich in DIC (Ricaurte-Villota et al., 2025). Therefore, the question arises as to whether the same patterns and drivers apply in the Colombian Pacific as those observed for the Caribbean area.

Latitudinal trends reveal distinct patterns in whether coastal zones act as sources or sink of CO_2. In low latitudes, coastal zones are expected to release CO_2 due to physical processes such as high sea temperature (average SST above 26 °C) and relatively low salinity (25.7–32 units), which cause higher partial pressures of CO_2 in water (pCO_{2w}) compared to the atmosphere (Borges et al., 2005; Cai, 2011). However, whether low latitudes emit CO_2 depends on the drivers in each coastal zone (Dai et al., 2013), and this is why the fine balance between the promoters of pCO_{2w} and those that help to reduce it must be studied locally. For example, in upwelling zones (high DIC and pCO_{2w}), phytoplankton blooms can capture large amounts of CO_2, reducing DIC excesses and resulting in exceptionally low pCO_{2w} values, thereby altering the direction of net carbon flux to negative values (Li et al., 2022). According to Strutton et al. (2008), the equatorial Pacific would be a much larger carbon emitter if not for photosynthetic processes, which convert a billion tons of DIC/CO_2 into living organisms.

One of the main issues in the Pacific Ocean regarding the net CO_2 flux is the discrepancy between models and *in situ* air-sea CO_2 observations (Polavarapu et al., 2018; Rastogi et al., 2021). This is due to the limited amount of data, particularly in the coastal zones of the Pacific, and specifically in the Panama Bight, which includes the Pacific coast of Colombia and Panama (Herrera Carmona et al., 2022). The uncertainty in predictions stems from the fact that there are many complex atmospheric and oceanographic variables—physical (*e.g.*, wind; Takahashi et al., 2002; Kim et al., 2019), chemical (*i.e.*, Total Alkalinity-TA and Dissolved Inorganic Carbon- DIC), and biological (biological uptake, remineralization; Takahashi et al., 1997) that cause significant spatial and temporal variations in pCO_{2w} at different scales (DeGrandpre et al., 1998), and consequently, in the magnitude and direction of the net flux. Moreover, the lack of technical, technological, infrastructural, and financial resources in Latin American countries makes it challenging to quantify pCO_{2w} values and the magnitude of the flux, particularly in the coastal zone, where multiple drivers converge in time and space (Roobaert et al., 2024).

According to Dai et al. (2022), calculating pCO_{2w} and CO_2 flux in tropical coastal margins dominated by rivers and deltas is particularly complex. The dissolved inorganic carbon (DIC), dissolved organic carbon (DOC; 49.5% of DOC export is by rivers concentrated in the tropics, 23.5°S to 23.5°N; Fabre et al., 2020), particulate organic matter (POM), dissolve organic matter (DOM), and nutrients (NO_3 and PO_4; Li et al., 2020) are mainly contributed by rivers. These contributions promote phytoplankton growth (a CO_2 sink) and the consequent remineralization of dead particulate organic matter (a CO_2 source), where the resultant flux is the product of all these interactions. In a system with predominant river inputs, the fresher waters of the river plume gradually mix with oceanic waters both horizontally and vertically (Gan et al., 2009), creating an estuarine ecosystem, like the one found in the Colombian Pacific around Gorgona Island. In consequence, Dai et al. (2022) suggest that the air-sea CO_2 flux is determined by the sum of DIC inputs and outputs at the coast-ocean boundary over time, net ecological productivity (gross primary production – ecosystem respiration), and net ecological calcification (Andersson and Gledhill, 2013; Courtney and Andersson, 2019). However, systems dominated by river inputs can transition to predominantly oceanic inputs depending on the water volume it receives from the open sea, for example, during coastal upwelling events (Ekman Pumping - WEK) and horizontal transport (Zonal Ekman Transport – ZET) when cold, CO_2- and DIC-rich subsurface ocean water emerges (Hu et al., 2015; Weber et al., 2021), or through surface water movement by ocean currents toward the coast and tides. Changes from a river to oceanic coastal regimes and vice versa alter the direction and intensity of the CO_2 flux and should be explored further according to Dai et al. (2022). This is the reason why this study focuses on the Gorgona's continental island, located 55 km from the continent but strongly influenced by many rivers, upwelling events and sustained primary productivity (Corredor-Acosta et al., 2020).

The Gorgona Island (2° 55' 45" – 3° 00' 55" N; 78° 09' – 78° 14' 30" W; Figure 1) is located on the continental margin of the Colombian Pacific Basin (CPB) in the Panama Bight region, and is part of the largest Marine Natural National Park in the Colombian Pacific (Guzmán et al., 2023; UAESPNN, 2005). The island is characterized by a wide and shallow continental shelf to the east (less than 100 m deep; Figure 1) and a deep slope a few kilometers to the west, with canyons and submarine mountains according to Murcia and Giraldo (2007; Figure 1B).

Precipitation on Gorgona Island follows a bi-seasonal pattern (periods of less and more rain), with an annual total rainfall up to ~6000 mm (Blanco, 2012). At seasonal scale, we performed a multi-year analysis of precipitation on the Gorgona Island (2006-2021, data source IDEAM) which indicated low relative rainfall from January to April (Figure 2), when the northern trade winds dominate and the wind field of the Chocó Jet is weak. In contrast,

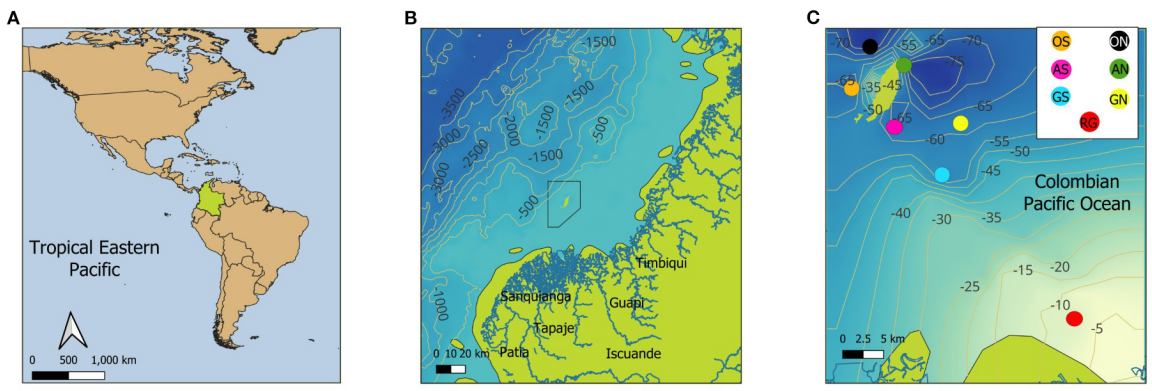

FIGURE 1
The study area is the Colombian Pacific Ocean (Tropical Eastern Pacific). **(A)** Location of the Colombian Pacific, as part of the Panama Bight. **(B)** The polygon representing the protected area of the Gorgona National Natural Park is shown, along with its proximity to the coastline and the main continental watersheds that discharge their waters into the area (marked in blue): Patía River, Sanquianga River, Tapaje River, Iscuandé River, Guapi River, and Timbiquí River. **(C)** The colored points show the seven stations where discrete water samples were collected from November 2021 to July 2022 along the coast-ocean gradient; Guapi River in red (RG), South Guapi in blue (GS), North Guapi in yellow (GN), South Reef in pink (AS), North Reef in green (AN), South Ocean in orange (OS), and North Ocean in black (ON). The underwater topography lines are represented in meters.

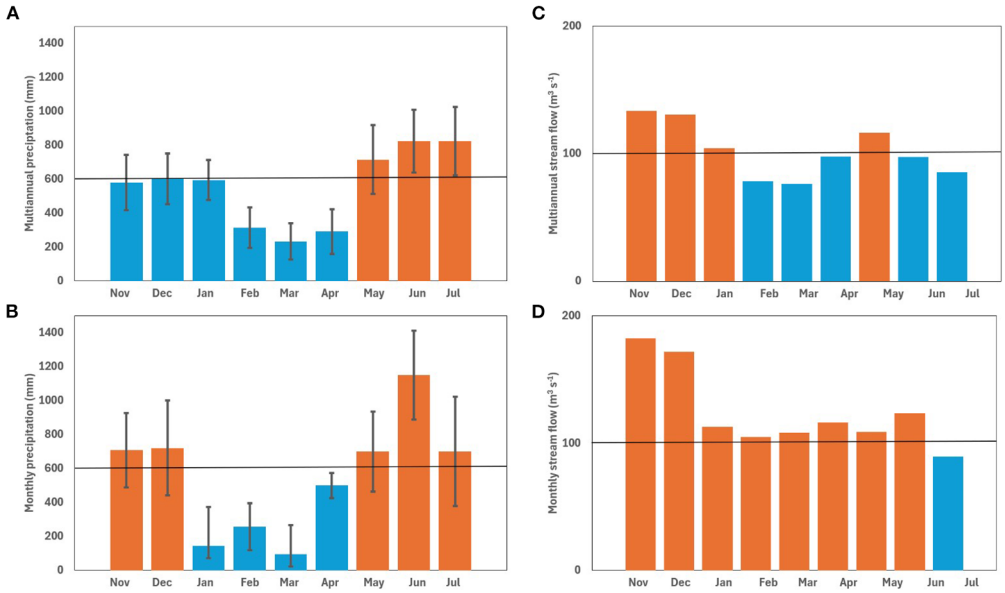

FIGURE 2
Time scale comparison of precipitation and streamflow (Río Guapi) in the study area. **(A)** Multiannual total precipitation as monthly averages (2006-2021). The black horizontal line marks the historic (2006-2021) annual mean total precipitation (605 mm) for the "Isla Gorgona station". Standard deviation is illustrated on each month's data. **(B)** Average monthly total precipitation for the sampled year (November 2021 to July 2022). Black horizontal line marks the historic annual mean (2006-2021). Standard deviation is illustrated on each month's data. **(C)** Multiannual total streamflow as monthly averages (2006-2021) from the "57025020 Isla Gorgona" IDEAM station. Black horizontal line marks the historic (2006-2021) annual mean discharge (103 m^{-3} s^{-1}). **(D)** Average total monthly streamflow for the sampling year (November 2021 to July 2022) at the "53047010 Río Guapi" station of IDEAM. Black horizontal line marks the historic (2006-2021) annual mean discharge (103 m^{-3} s^{-1}). Months below the multiannual records are shown in blue, and above in orange.

the period with higher precipitation conditions were found from May to December (not shown), when the southern trade winds dominate and the Chocó Jet winds are stronger (September to October). Figure 2 shows extreme precipitation during the 2021–2022 sampling year, with monthly rainfall exceeding 700 mm for several months. Only four months recorded precipitation below the multiannual average (Figure 2B). The precipitation regime on Gorgona Island is primarily governed by the latitudinal migration of the Intertropical Convergence Zone (ITCZ), which provides the context for understanding the atypical precipitation observed. According to Schneider et al. (2014), this pattern dictates that the relative driest period occurs in January and February, when the ITCZ is at its southernmost position (2°N) near the study area (2° 55' – 3° 00'). Then, from March to May, it moves to the north, occupying a latitudinal range between 2 and 7°N. Conversely, the wettest period is expected between June and July as the ITCZ moves north (reaching 8 to 10°N). Finally, between September and December, the ITCZ returns to its southernmost position.

In the study area, the northeastern trade winds dominate between December and March, generating the Panama Jet, which causes a strong upwelling extending from north to south in the Panama Bight (Rodríguez-Rubio et al., 2003; Corredor-Acosta et al., 2020; Crawford et al., 2023). Similarly, in the second half of the year, the Chocó Jet occurs (Rodríguez-Rubio et al., 2003; Crawford et al., 2023), which travels from west to east until it collides with the continent. The Chocó Jet is strongest in November and weakest between February and March, so the heavy rainfall from November to December on Gorgona Island is attributed to this climatic phenomenon (Crawford et al., 2023). The intense rain creates a layer of brackish water on the surface, up to 2 meters thick (Gassen et al., 2024), which reduces salinity on the Colombian Pacific coast, and river runoff from the Guapi river and deltaic complex into the sea increases. The Guapi River characterized by a sea water temperature of 26.34 °C at 10 meters (Palacios Moreno and Pinto Tovar, 1992), had an average NBS pH of 7.3 between 2018 and 2021, and salinity (PSU) between 0 and 0.25 at 1-meter depth (INVEMAR, 2019, 2020, 2022).

The island is influenced to the east by several rivers and deltas from the mainland, and on the oceanic side (west) by oceanic currents from the Northern Hemisphere, such as the California and Northern Equatorial currents, and from the Southern Hemisphere, by the Peru and Humboldt currents (Diaz, 2001; Willett et al., 2006; Fiedler and Lavín, 2017). The hydrodynamic pattern around the island is dominated by ocean currents and numerous mesoscale eddies, both cyclonic and anticyclonic occurring throughout the year. The direction and intensity of those geostrophic field and mesoscale eddies around Gorgona are determined by wind stress, the Panama Jet, the Chocó Jet, and the position of the Intertropical Convergence Zone (Rodríguez-Rubio et al., 2003; Díaz Guevara et al., 2008; Corredor-Acosta et al., 2011; Lorenzoni et al., 2011). Specifically, the Panama cyclonic current (Amaya, 2024) is fed from the south by a branch of the Peru current, forming the so-called Colombia current (Stevenson, 1970; Corredor-Acosta et al., 2011), which flows from south to north along the Colombian coast. The

surface water masses flows through the area of Gorgona National Natural Park in a northeastward direction, with a velocity ranging between 0.2 and 0.9 m s^{-1} (Diaz, 2001). During La Niña, the North Equatorial Countercurrent (warm water with high salinity) flowing from west to east (Torres et al., 2023) loses it prevalence around 3° N, while the Peru Current, flowing in a northeastward direction, brings cold water from the South Pacific to the Colombian coast. Therefore, the sampling carried out in this present study (2021-2022) corresponds to a period of relatively cold water (La Niña; ONI -1.0; McLean et al., 2024) contrasting with what happens during El Niño events. Also, at more local scale, the oceanographic circulation is affected by semidiurnal tides (two highs and two lows) oscillating between -40 cm and 5 m per day (Tide-Forecast.com, map of tide stations in Colombia 2021-2022).

According to Restrepo and Kjerfve (2004) and Blanco (2012), La Niña events significantly influences river discharge in the Colombian Pacific due to increased precipitation and, consequently, water flow especially during the sampled year (Figure 2). The Colombian Pacific watershed covers an area of 76,852 km^2 and consists of more than 200 rivers, which a total discharge of ~9,000 m^3 s^{-1} and 96 million tons of sediment per year (Díaz, 2008). The Gorgona National Natural Park is in front of the Patía-Sanquianga delta complex, the largest in the country, which contributes approximately 23% of the total freshwater discharged into the Colombian Pacific (2,045 m^3 s^{-1}; Díaz, 2008). The delta complex is made up of the Patía-Sanquianga rivers, which discharge 1,300 m^3 s^{-1}, the Guapi River at 357 m^3 s^{-1}, the Iscuandé River at 213 m^3 s^{-1}, and the Tapaje River at 175 m^3 s^{-1} (Restrepo and Kjerfvel, 2004; Díaz, 2008; Figure 1). The Patía-Sanquianga delta, covering an area of 23,000 km^2, contributes freshwater, nutrients, and organic and inorganic material (both particulate and dissolved) from the western Andes mountains to the Pacific Ocean (Restrepo and Kjerfve, 2004; Giraldo et al., 2011). The Guapi River multi-year average monthly flow (station "53047010 IDEAM") was 103 m^3 s^{-1} from 2000 to 2021. However, during La Niña event (2021-2022), the stream flow exceeded the multi-year monthly average, with a maximum value in November 2021, exceeding the average by over 77% (182 m^3 s^{-1}), with a minimum in February 2022 being also 2% above the multi-year monthly mean (105 m^3 s^{-1}; Figure 2). On average, the flow exceeded expectations, except for July 2022 when it was 14% below the multi-year average (89 m^3 s^{-1}).

In this context, this study aims to: (1) evaluate the net CO_2 flux in the Panama Bight to address a gap in the current knowledge of the region, as no similar studies have been addressed it in the coastal zone of the Colombian Pacific; and (2) review the predictions made by the models proposed by Wong et al. (2022) and Dai et al. (2022), assessing their accuracy and applicability in the context of this study. To do so, we estimate the seasonal direction and intensity of the CO_2 flux under the effects of La Niña conditions (2021-2022), characterized by intense precipitation and river discharge promoting an estuarine system. Lastly, we discuss the potential drivers explaining the dynamics of the pCO_{2w} and CO_2 flux variability.

2 Methods

2.1 Sampling design

Seven stations were sampled and used to estimate CO_2 fluxes and carbonate system chemistry in Gorgona National Natural Park from the coast to the open ocean. The closest station to the coast was "Río Guapi - RG", located approximately 25 km from Guapi-Nariño, Colombia, and the furthest was "North Ocean - ON", approximately 60 km from the coastline. The stations were distributed along two parallel transects separated by five kilometers, with GPS-WGS84 coordinates. The southern transect was formed by "South Guapi - GS", "South Reef - AS", and "South Ocean - OS", while the northern transect was formed by "North Guapi - GN", "North Reef - AN", and "North Ocean - ON" (Figure 1). Monitoring began in November 2021 and extended until July 2022 (nine months), with monthly sampling during the first week of each month. In addition, the "Río Guapi" station was added in January 2022 to characterize its influence.

2.2 Measurements

On site, salinity, temperature, pH millivolts (total protons), percent oxygen, and depth were measured using a Hanna multiparameter sounder (previously calibrated), a CTD-Castaway, and a YSI equipment (accurate to ±2% of reading or ±0.01 PSU, whichever is greater; ± 0.15 °C; ± 0.02 pH/± 0.5 mV; and ranging from 0.00 to 30.00 ppm (mg/L) with an accuracy of ±0.25% of full range.

Discrete water samples were collected at seven stations (GS, GN, AS, AN, OS, ON, and RG; Figure 1) using a 5 L Niskin bottle at depths between 1.8 and 3 meters. The water collected on site was not murky, sampling sites were right after the river plume limit (35 km away from the continent). Seawater samples were stored in 250 mL borosilicate bottles and preserved with 50 µL of a saturated mercuric chloride ($HgCl_2$) solution for later TA analysis in the laboratory, following recommended best practices (Best Practice Guide for Ocean CO_2 Measurements, SOP 2, SOP-specified concentration range of 0.02-0.05%). Additionally, DIC samples were taken in 50 mL dark bottles (silicone seal), leaving no headspace; and wrapping the cap in parafilm paper. All samples were packed in a Styrofoam refrigerator and sent by plane to our new lab in Bogotá (Javeriana University) in less than four hours from the Pacific region. Then, the samples were kept without exposing them to light and maintaining temperature conditions below 15 °C in the laboratory. TA was measured within two weeks, as well as other parameters such as pH. Regarding DIC samples, those were kept in our lab for two months after the sampling was finished and then sent to the Autonomous University of Baja California in Mexico. They were processed in a maximum of one week after arrival in the UABC.

In the laboratory, total alkalinity (TA) measurements were performed on seawater samples following a standardized protocol (SOP 3b of the open-cell titration method; Dickson et al., 2007) using the GOA-ON titration kit. For titrant, Dickson Lab reference HCl solutions were used (Batch A17: 0.100362 ± 0.000009 mol kg^{-1}; Batch A24: 0.099922 ± 0.000005 mol kg^{-1}), buffered with 0.6 M NaCl to match seawater ionic strength. A 50 g sample (~50 g or mL, ± 0.0001 mL) was weighed into a jacketed titration cell (maintained at ~25 °C via a circulating water bath) and titrated. The analytical balance used (Ohaus Pioneer AX225D, ± 0.0001 g) yielded a reproducibility of ±0.001 g for 50 g samples, corresponding to a coefficient of variation<0.003%, well within the precision requirements for TA analysis (0.01 g). The titration involved two stages: first, the addition of a small amount of acid (0.2 mL) with a HandyStep® Touch S, first by adding to drop the pH to ~3.5 (~0.2100 mV) and waiting 5 minutes to allow for degassing, and second, titration resumed in 0.05 mL steps until a pH close to 3.0 was reached (~0.2300 mV), with pH and temperature measurements taken at each step. Data, including sample volume, titrant volumes (to pH 3.5 and 3.0), salinity, final temperature, and voltage per addition was compiled in an Excel spreadsheet program, which employed a non-linear least squares regression to calculate total alkalinity (Dickson et al., 2007). Approximately 50% of surface samples (n = 31) were analyzed in triplicate. Only triplicate sets with a maximal variation of ±5 µmol kg^{-1} TA were retained (± 9 µmol kg^{-1}, Batch #182: 2230.91 ± 0.71 µmol kg^{-1}; Batch # 202: 2215.13 ± 0.57 µmol kg^{-1}; all data set available at NOAA; https://doi.org/10.25921/gfan-3e30).

Dissolved Inorganic Carbon (DIC) was measured at UABC (Mexico) using the UIC C-CM5014 instrument, following the coulometric methodology described by Johnson et al. (1987) and Dickson et al. (2007). Measurements were performed with high precision and accuracy, ensuring that the difference in DIC from the reference values of the standards did not exceed 3 µmol kg^{-1} (error of 0.1%). The Dickson Certified Reference Material (CRM) was prepared at the Institute of Oceanography, University of California, San Diego (USA). The substandards and analyzed samples were carried out in parallel at the Oceanographic Research Institute of the Autonomous University of Baja California (Mexico). For a more comprehensive DIC measurement methodology, see Supplementary Table 1.

Similarly, quality "flags" (scale 1 to 5) were reviewed and assigned to the TA and DIC data (equipment accuracy and potential errors in the field or laboratory). Outliers (n=6) were removed from the matrix; this was done by reviewing multiple graphical relationships between temperature, salinity, TA, and DIC.

The Liss and Merlivat (1986) equation allowed for the calculation of the flux magnitude for each of the nine months and seasons in Gorgona. The estimated CO_2 flux in Gorgona was compared with the IPACOA, OOI, NOAA, and SOCAT databases.

The CO_2 fluxes (FCO_2 direction, magnitude, and variability) were calculated following the equation proposed by Liss and Merlivat (1986):

$$FCO_2 = k \times K' \times (\Delta pCO_2)(mmol \cdot m^2 \cdot year^{-1})$$

Where, the constant k is the gas transfer coefficient of CO_2 as a function of wind (U_{10}) at 10 meters above sea level (Wanninkhof, 2014), expressed as:

$$k = 0.251(\frac{Sc}{660})0.5(U_{10})^2$$

K′ is the solubility of CO_2 and is a function of temperature and salinity (Weiss, 1974); Sc is the Schmidt number and depends on temperature; ΔpCO_2 is the difference between the partial pressure of carbon dioxide (pCO_2) in the surface seawater (pCO_{2w}) and the pCO_2 of the atmosphere (pCO_{2A}). ΔpCO_2 determines the direction of the flux, with positive FCO_2 indicating CO_2 moving from the sea to the atmosphere, and negative indicating movement from the atmosphere to the sea. The magnitude of the gas exchange is controlled not only by ΔpCO_2 but also by the gas transfer rate between the two media, which in turn varies with wind speed.

The hourly wind speed from the seven sampling sites - U_{10} (m s^{-1}) was extracted from: https://earth.nullschool.net/, taking the 24-hour wind average of the sampling day. For months with sampling of all stations on two consecutive days (adverse weather conditions in two months), 48-hour wind values were averaged. The wind average was also calculated and compared using only the exact sampling hours at each station and by averaging the wind over a month, finding no significant changes in the flow results compared to the daily/monthly wind average (which was finally used).

Since the atmosphere is a well-mixed fluid, the pCO_{2A} values for the flow calculation were extracted from NOAA/GML https://gml.noaa.gov/ccgg/trends/data.html (NOAA 2021, 2022), which come from the Mauna Loa climate station, Hawaii, file "Mauna Loa CO_2 monthly mean data." The pCO_{2A} data for the sampling months (Nov 2021 to Jul 2022) were extracted.

The pCO_{2w} was calculated from TA, DIC, salinity, and temperature data resolving the carbonate system equation in seawater using the CO2SYS v3.0 software (Pierrot et al., 2021). In the carbonate system equation solution, the following constants were used: (i) Dissociation constants for K1 and K2 from Millero (2010) for waters ranging from 0 to 40, given that the study area the salinities variation are between 27.03 to 31.29, (ii) KHSO4 dissociation constant from Dickson (1990), (iii) KHF from Perez and Fraga (2003), (iv) Total pH scale (mol-kg SW), (v) [B]T value from Lee et al. (2010), and (vi) EOS-80 standard. The pCO_{2w} was estimated with an error of ±1.79 concerning the determined fluxes (mmol C m^2 day^{-1}). Out of 66 flux data points, six were flagged as possible outliers (flags three onward). The CO2SYS was also used with DIC and TA pairs to estimate the Revelle factor, omega aragonite (Ω_{AR}), HCO_3, and CO_3. Lastly, the pH in total scale was derived through the CO2SYS using the same specific settings and found to be less variable than *in situ* measurements, displaying a smaller error. We performed a full uncertainty propagation analysis, which yielded the following average errors: pH_T (± 0.022), pCO_{2W} (± 30.17 µatm), total alkalinity (TA: ± 9 µmol kg^{-1}), dissolved inorganic carbon (DIC: ± 3 µmol kg^{-1}), salinity (± 0.20 PSU), and temperature (± 0.08 °C). These values fall within acceptable ranges for carbonate system studies and support the reliability of our calculated FCO_2 values at Gorgona.

Daily images of Chl-a were downloaded from the Ocean Colour Climate Change Initiative (OC-CCI; version 3.1) for the studied period. The OC–CCI is a merged Level 3 product with a spatial resolution of 4 km, available at http://www.oceancolour.org/. The OC-CCI Chl-a dataset is retrieved by combining the observational data from the MERIS (MEdium spectral Resolution Imaging Spectrometer) sensor of the European Space Agency, the SeaWiFS (Sea-viewing Wide-Field-of-view Sensor) and MODIS-Aqua (Moderate-resolution Imaging Spectroradiometer-Aqua) sensors from the National Aeronautics and Space Administration (NASA-USA), and the VIIRS (Visible and Infrared Imaging Radiometer Suite) from the National Oceanic and Atmospheric Administration (NOAA-USA). The remote sensing reflectance data derived from the sensors were merged by band-shifting and bias-correcting the MERIS, MODIS, and VIIRS data to match the SeaWiFS data. Due to the complexity of the study region, version 3.1 of the OC-CCI product was selected as it improves the performance of the ocean color data in coastal Case-2 waters compared to earlier versions that primarily focus on open ocean waters. Finally, total monthly Chl-a values were obtaining by averaging the Chl-a of the seven sampling stations, resulting in a relative total Chl-a concentration for the entire sampling region.

2.3 Statistical analyses

The analysis began with a Shapiro-Wilk test, which indicated that the flux magnitude data does not follow a normal distribution (S-W, P = 0.01877, W = 0.95, n = 60), repeating this for pCO_{2w} and ΔpCO_2 components, respectively (S-W, p = 0.147 and 0.134, W = 0.97 and 0.96, n = 60 and 60), indicating that the variables associated with flux do not follow a normal distribution either. Hence, the Box-Cox methodology was applied to transform FCO_2 data into a normal distribution. Furthermore, a Welch *F* test in the case of unequal variances was applied to all the variables of interest (FCO_2, pCO_{2w}, ΔpCO_2, SST, SSS, TA, DIC, and Chl-a) which showed that these different data groups have equal variance (W-F, F = $2.512E^{-4}$, df = 200.3, p = $1.855E^{-304}$). Moreover, a t-test (parametric) was used to analyze differences between the two flux periods: Upwelling (January to March of 2022) and Post-upwelling (November to December of 2021 and April to July of 2022). We used a One-way ANOVA to compare different flux magnitudes across the nine months, and then an a posteriori t-test. Additionally, a Spearman linear correlation was run to explore relationships between pCO_{2w} and SST, SSS, TA, DIC, and Chl-a.

Normalizations to observe the pCO_{2w} sensitivity were conducted as follows: we used the maximum values for salinity and temperature (32.06 units and 28.1 °C, respectively) setting the maximum value for salinity first, as a constant, while leaving the TA, DIC, and temperature values corresponding to each data point to evaluate the effect of salinity over the pCO_{2w}, repeating the same process but substituting the temperature for the recorded maximum, and leaving salinity as measured (CO2SYS). Then, we recalculated the pCO_{2w} and plot the difference between the pCO_{2w} with *in situ* salinity against the recalculated pCO_{2w} that uses the maximum recorded salinity. 49 µatm higher, in average, was the pCO_{2w} difference by using max salinity effect. Regarding a normalization with maximum temperature, the same procedure was followed where the maximum recorded temperature was constant, and the remaining variables used the corresponding values, revealing an average pCO_{2w} difference of 31 µatm higher than with the observed temperatures (Supplementary Figure 1) in the CO2SYS (Lewis and Wallace, 1998). Thus, it is clear that salinity has a larger influence (relative percentage) than temperature regarding the pCO_{2w} variability observed throughout the year. To complement these normalizations, we assessed the uncertainty associated with pCO_{2w} by incorporating the potential error of ±30.17 µatm into our flux calculations, recalculating them and comparing them to the original estimates.

In addition, to define climatic-oceanographic periods, a Principal Component Analysis (PCA) was performed using the latest version of R Studio software. The PCA used the following variables: month, season, SST, SSS, pCO_2w, pH_T, DIC, Chl-a, to review if there are spatio-temporal FCO_2 groups. Furthermore, to clearly separate both seasons we used several atmospheric/climatic variables, such as total monthly precipitation (mm), average sea surface temperature (SST), average pH (total), average surface water partial CO_2 pressure (pCO_{2w}), and average CO_2 fluxes (mmol m^{-2} d^{-1}).

2.4 Zonal Ekman Transport and Ekman pumping

The Zonal Ekman Transport (ZET) was obtained following the methodology of Bakun and Nelson (1991) by using weekly wind data obtained from the CCMP product (https://www.remss.com/measurements/ccmp/). For the calculation, we follow the equation:

$$ZET = \frac{1}{\rho_w f}\tau$$

where ρ_ω is the density of seawater, which is assumed constant at 1025 kg m^{-3}; f is the Coriolis parameter and τ is the wind stress for the studied area.

The wind stress (τ) was computed from the weekly wind fields as follows:

$$\tau = \rho_a C_d |V_{10}| V_{10}$$

where C_d = 0.0015 is the drag coefficient, ρ_a = 1.2 kg m^{-3} is the mean air density, and V_{10} is the wind speed at 10 m above the sea surface. The wind stress curl was estimated using the zonal and meridional components of the weekly wind stress:

$$(\nabla \times \tau)_z = \frac{\partial \tau_y}{\partial x} - \frac{\partial \tau_x}{\partial y}$$

This procedure was performed for each grid point of the wind field by applying the centered finite difference algorithm, and the Ekman pumping velocity was estimated as follows:

$$WEK = \frac{(\nabla \times \tau)_z}{f\rho_w} + \frac{\beta\tau_x}{f^2\rho_w}$$

where τ_x is the zonal wind stress component, $\beta = (2\Omega cos\varphi/R)$ is the latitudinal variability of the Coriolis parameter ($f = 2\Omega sen\varphi$), R = 6,371,000 m is the radius of the earth and ρ_w = 1025 kg m^{-3} is the mean water density. This methodology has been previously used on the Northeast Tropical Pacific (Kessler, 2006) and Panama Bight region (Devis-Morales et al., 2008; Corredor-Acosta et al., 2020).

Previous studies have indicated an interplay between the Ekman transport due to alongshore winds and Ekman pumping due to offshore wind stress curl playing an important role due to their relative contributions for upwelling/downwelling dynamics. For instance, in the northern Chilean upwelling system, the vertical transport induced by coastal divergence (ZET) represented the 60% of the annual total upwelling, however, the Ekman pumping also displayed an important contribution of 40%, indicating that the largest differences between these mechanisms occur at spatial scale. That is, coastal ZET predominated in areas with low orography and headlands, whereas WEK was higher in regions with high orography and the presence of embayments (Bravo et al., 2016). Similar findings were observed in three typical upwelling systems of the South China Sea, showing temporal and spatial differences, highlighting regions where WEK had the same intensity as ZET, even doubling the amount of upwelling predicted solely considering the coastal divergence (Wang et al., 2013). Those physical mechanisms and their coupling are important to be explored because the physical transfer of water properties and nutrients from the deep to the surface ocean is strongly related to the vertical supply, which also involves important effects on primary productivity, changes in the water column mixing/stratification and associated water masses, as well as, in the local chemical processes (e.g., Williams and Follows, 2003; Pasquero et al., 2005). According to this, we assess both mechanisms (ZET and WEK) in this study, in order to relate its contributions to the maintenance of biological production (in terms of Chl-a) and key changes of the carbonate system.

2.5 Mix model

To identify potential processes (physical mixing and biological) and explain the variability observed in carbonate system parameters (*e.g.*, $pCO_{2w,}$ DIC, TA, and O_2), we employed a three-endmember mixing model following established methodologies in oceanographic studies that developed the analysis of sea water from mixing triangles without assumption of isopycnic mixing (Tomczak, 1981; Paulmier et al., 2011; Kahl et al., 2018). This approach identifies water endmembers, in order to describe the thermohaline variability due to mixing, using conservative tracers (salinity and potential temperature) to construct a mixing triangle. The contribution of the water masses considered ($M_{k,i}$) to a given sample 'i' can be calculated by solving the followings determined system of three linear equations:

$$1 = \Sigma\ M_{K,i}$$

$$S_i = \Sigma\ M_{K,i} \cdot\ S_k$$

$$\theta_i = \Sigma\ M_{K,i} \cdot\ \theta_k$$

Where k is the water mass endmembers (1,2 and 3) and 'i' is the sample number (from 1 to 60). S_k and θ_k are the thermohaline characteristics of the k-water mass endmember (Tomczak, 1981). Finally, it computes expected conservative values due to physical mixing processes (DIC_{mix}, TA_{mix}, and O_{2mix}) for the non-conservative variables measured *in situ* (DIC, TA, and O_2). DIC_{mix} is defined as the fraction of dissolved inorganic carbon whose variability (R^2 from the regression DIC_{mix} vs. DIC) can predominantly be attributed to physical mixing. The complementary variability (1 – R^2) is then attributed to biogeochemical processes, isolated through residual analysis (*e.g.*, ΔDIC = observed DIC – DIC by mixing) and quadrant plots of ΔDIC vs. ΔO_2, where quadrants indicate net production (positive ΔDIC, positive ΔO_2), photosynthesis (negative ΔDIC, positive ΔO_2) ammonification (negative ΔDIC, negative ΔO_2) or respiration/remineralization (positive ΔDIC, negative ΔO_2) (Paulmier et al., 2011; Kahl et al., 2018).

Initially, we constructed T-S diagrams from the full spatiotemporal dataset (13 months, 7 stations, 0–80 m depth) to define three endmembers representing distinct sources of variability and mixing in the area. The river endmember (1; river-influenced) exhibited low salinity (26.81), TA (1750 µmol kg^{-1}), and DIC (1763 µmol kg^{-1}), with high temperature (27.94 °C) and O_2 (174 µmol kg^{-1}). The transitional endmember (2) showed intermediate values: salinity (33.06), TA (2138 µmol kg^{-1}), DIC (1867 µmol kg^{-1}), temperature (27.28 °C), and O_2 (123 µmol kg^{-1}). Finally, the oceanic endmember (3; oceanic influenced) featured high salinity (35.38), TA (1999 µmol kg^{-1}), and DIC (1989 µmol kg^{-1}), with low temperature (14.26 °C) and O_2 (40 µmol kg^{-1}; Preciado et al., in Progress). All three water endmembers incorporate signals from multiple upstream sources, reflecting the complex dynamics of this estuarine system. For instance, the oceanic (3) endmember exhibited influence from at least four diverse origins, including Antarctic Intermediate Water signals (Kawabe and Fujio, 2010); the intermediate endmember (2) blends subsurface and riverine inputs; and the river endmember (1) primarily mixes freshwater with marine waters, potentially including remote eddy-transported surface waters and local coastal currents. We could not directly measure riverine carbonate parameters due to differences in instrumentation and chemistry, river itself even showed tidal intrusion of seawater from below during high tides, further complicating pure freshwater end-member isolation. Instead, riverine influence is inferred through its dilution effects on salinity and biogeochemistry, following a similar approach to Huang et al. (2022) and Sun et al. (2023).

Once the mixing fractions are applied to compute expected DIC_{mix} values under conservative mixing assumptions. Deviations from these expected values then highlighted non-conservative processes affecting DIC, which is a key objective of our biogeochemical analysis. DIC, TA, and O_2 are used as complementary information for the characterization of the

endmembers, enabling us to perform the mixing model analysis and determine the sources of variability (physical-mixing or biogeochemical processes) for the non-conservative variables DIC, TA, and O_2. This approach aligns with standard practices in estuarine and oceanic studies, where salinity and TA are often normalized or used to account for dilution and mixing effects before assessing non-conservative variables like DIC (Cai & Wang, 1998; Oliveira et al., 2017; Courtney et al., 2021). For instance, while TA behaves conservatively in many open-ocean settings and correlates linearly with salinity (Millero et al., 1998; Jiang et al., 2014), the T-S framework was chosen due to its effectiveness in capturing thermohaline distinctions in Pacific Colombian dynamic estuarine system, influenced by high rainfall and runoff. In addition, to validate the implication of the biological removal in pCO_2w concentration, we used a complementary approach, such as ΔDIC together with cumulative monthly *in situ* Chl-a data to explain CO_2 consumption. These results (biological/temperature implications) were also validated by an analysis to calculate if physical or biological factors are implicated in the pCO_{2w} concentrations found around Gorgona island, following the methodology described by Takahashi et al. (2002), for more detail on the equations used see Supplementary Table 2.

3 Results

The PCA (Figure 3) revealed two distinct seasonal clusters: an upwelling period (January–March) and a post-upwelling period (May–July, November–December) distributed across the space. Together, PC1 (45.5%) and PC2 (28.2%) explained 73.7% of the total variability. The biplane shows that post-upwelling months were characterized by warmer, CO_2-enriched surface waters, whereas upwelling months reflected cooler, saltier, DIC-rich conditions and elevated pH_T. Chlorophyll-a displayed an intermediate position, reflecting its role across both seasons. No spatial separation among sampling sites was detected, implying that despite local variability, temporal changes through upwelling and post-upwelling dynamics (e.g. rainfall and stratification) were the main driver of environmental variability around Gorgona Island.

The two seasonal periods were verified through the atmospheric/climatic variables showing significant differences between upwelling and post-upwelling. That is, total monthly precipitation (M-W, Z = 2.203, p = 0.027, n Post-upwelling = 6 months, n Upwelling = 3), average sea surface temperature (SST; M-W, Z = 2.2132, p = 0.0268, n Post-upwelling = 6, n Upwelling = 3), average pH (total; M-W, Z = 2.2039, p = 0.027532, n Post-upwelling = 6, n Upwelling = 3), average surface water partial CO_2 pressure (pCO_{2w}; M-W, Z = 2.1947, p = 0.028186, n Post-upwelling = 6, n Upwelling = 3) and average CO_2 fluxes (mmol m^{-2} d^{-1}; M-W, Z = 2.0045, p = 0.071429, n Post-upwelling = 6, n Upwelling = 3). Specifically, during post-upwelling we found significantly higher: (I) Monthly average precipitation (746 ± 214 vs 165 ± 82 mm) due to the increased influence of the ITCZ and a moderate La Niña year; (II) Average sea surface temperature (27.5 ± 0.4 °C vs. 26.5 ± 0.2 °C); and (III) Average pCO_{2w} and CO_2 Fluxes (567 ± 64 µatm vs. 450 ± 55 µatm, and 0.2 ± 0.09 mmol CO_2 m^{-2} d^{-1} vs. 0.1 ± 0.06 mmol CO_2 m^{-2} d^{-1}, respectively). Contrasting, in upwelling, we found a higher significant total pH mean (7.8697 vs 7.9686, respectively).

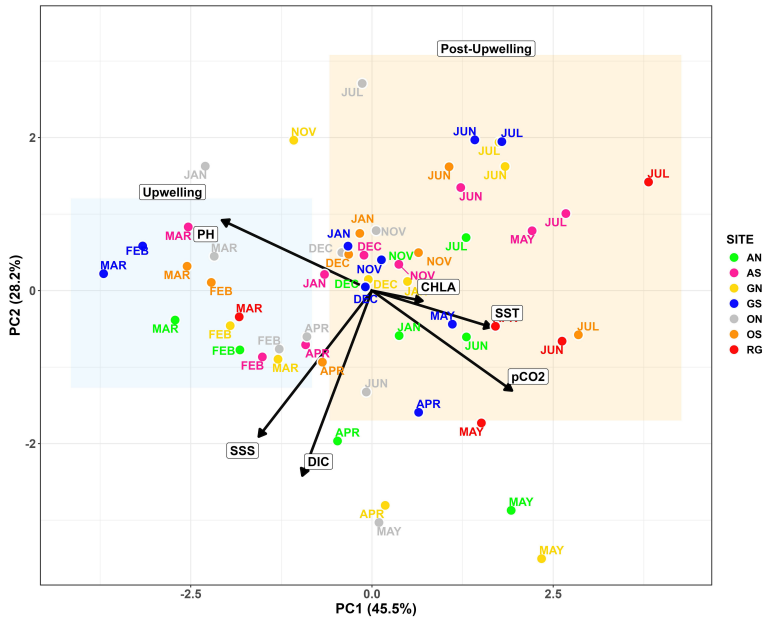

FIGURE 3
PCA test for stations and months considering the physicochemical variables SST, SSS, pCO_2, pH, DIC, and Chl-a. Note the grouping in the left quadrants for the months of February and March (upwelling, blue rectangle), from the upper right quadrant, May, June, and July (rainier season; post-upwelling, orange rectangle), highlighting the two contrasting seasons. The x axes explain the main variability 45.5% and the second axis y 28.1%. The colors represent the different sites and their corresponding sampling months.

10.3389/fmars.2025.1633653

3.1 Air–sea CO_2 exchange

During the moderate 2021–2022 La Niña event, surface waters around Gorgona displayed a near-neutral net CO_2 flux (0.0105 ± 0.0001 mol C m^{-2}) over the nine sampled months, with a bimodal pattern driven by upwelling and post-upwelling wet season (Figure 4). Throughout the upwelling season, cooler, saltier waters reached the surface (shallow thermocline), coinciding with the observed low pCO_{2w} values (below atmospheric levels, mean pCO_{2A} = 461 ± 92.8 µatm and negative ΔpCO_2, see Figures 4A–E), resulting in near-zero to weakly negative FCO_2 (February–March, Figure 4F). This is additionally in line with elevated DIC and TA (Figures 4G, H). In contrast, during the post-upwelling period, the fluxes were slightly positive (0.0093 ± 0.0001 mol C m^{-2}) with an average pCO_{2w} of 567 ± 97.5 µatm (Figure 4D). Similarly, monthly fluxes also differed significantly between periods (Welch test, $F = 2.5 \times 10^{-4}$, $p < 1 \times 10^{-300}$; n = 9), peaking in June (2.5 mmol C m^{-2} $month^{-1}$) and reaching a minimum in March (–0.1 mmol C m^{-2} $month^{-1}$). Therefore, markedly higher fluxes were observed during the post-upwelling compared to the upwelling season when including the seven stations sampled per month (t = 4.91, critical t = 2.00, $p = 7.8 \times 10^{-6}$; n = 21 vs. 39; Figure 4F).

Comparably, the average pCO_{2w} trend (Figure 4D) during the upwelling season evidences surface pCO_{2w} hovering moderately above atmospheric values in January (near 513 µatm Figure 4D; atmospheric reference value ~418 µatm, horizontal black line), but dips towards/just below atmospheric level by March (minimum average 397 µatm). Correspondingly, a post-upwelling spike in pCO_{2w} increases values up to ~700 µatm in May, around 1.7 times higher than atmospheric values, which drives a large positive ΔpCO_2 and outgassing (Figure 4E). Thereafter, pCO_{2w} slightly decreases until July, but remains well above atmospheric values (~580 – 590 µatm).

The ΔpCO_2 values in eight of the nine months were above the atmospheric pCO_{2A} - (between 50 and 260 micro atmospheres). However, during the upwelling season, there is a reduction in pCO_{2w}, causing it to be less saturated than the pCO_2 of the surrounding atmosphere. Thus, March evidenced less pCO_2 in the water than in the air (negative ΔpCO_2, Figure 4E) which is reflected with near-zero/negative FCO_2 (Figure 4F). Transition to the post-upwelling (higher rain and streamflow season; April-July) was also evident through the progressive increment in CO_2 peaking during May ($\Delta pCO_2 \gtrsim +250$ µatm; more pCO_2 in the ocean than in the surrounding air) and then stabilizing, as reflected in the average CO_2 flux (Figure 4F).

3.2 Physical oceanographic conditions of sea surface temperature and salinity

The coolest temperatures were recorded during upwelling (~26–26.5 °C). Rapid warming of the surface water was observed in April (~28 °C) lasting until July (>27 °C). The shown warming is concurrent with the sharp rise in pCO_{2w} (Figures 4A, D). Average salinity was< 31 during the nine months, meanwhile, the highest salinity was recorded during upwelling (31.2 in March). From April to July (post-upwelling months) a steady drop in salinity was measured, coinciding with the peak of precipitation/river discharge (Figure 2). Hence, markedly brackish water was observed (low-alkalinity via dilution), related to pCO_{2w} increase (Figures 4B, D, H).

3.3 Key parameters of the carbonate system: total alkalinity, pH_T, and dissolved inorganic carbon

The highest pH_T was measured in March (8.01), chemically consistent with reduced pCO_{2w} values and less riverine/precipitation influence (Figure 4I). Then, pH_T began to decline during April and May (recorded a minimum of 7.81 in May) and stabilized after during June and July. Meanwhile, DIC start increasing between November and January (~1,700–1750 µmol kg^{-1}) reaching its highest values in April (1,815 µmol kg^{-1}) and May (~1800 µmol kg^{-1}). After, there was a general decrease from May onward (~1,790–1,650 µmol kg^{-1} by July; Figure 4G).

The dominant DIC species, bicarbonate (HCO_3^-), remained relatively stable from November to February (~1,550–1,600 µmol/kg, Figure 4J) then increased sharply from March–April (~1,720 µmol/kg) in line with the highest DIC/TA values. Thereafter, HCO_3^- decreased gradually during the post-upwelling season (May–July) mirroring the reduction in DIC/TA.

Carbonate ion (CO_3^{2-}) values showed a clearer seasonal signal. They peaked during the upwelling months (January–March: ~170 and 180 µmol/kg, Figure 4K) in agreement with higher pH_T and Ω_{AR} (Figures 4I, L). Afterwards, CO_3^{2-} concentrations decreased during the post-upwelling period, sharply decreasing in April to ~150 µmol/kg, then rebounding slightly during May to ~170 µmol/kg, and finally steadily decreasing to its minimum values from June to July (114–118 µmol/kg) coinciding with lower pH_T, elevated Revelle Factor, and reduced Ω_{AR}.

3.4 Biological proxy signals

Monthly accumulated Chl-a (sum of seven stations) was relatively high during the sampling period (~16–19 mg m^{-3}, Figure 4M), with average Chl-a of 1.09 – 2.77 mg m^{-3} per sampled site (see Supplementary Figure 2). A marked increase from February to March was observed (16 – 19.4 mg m^{-3}). Afterwards, Chl-a values remain high during May (17.2 mg m^{-3}) until July with ~18 mg m^{-3} (Figure 4).

3.5 Key chemistry parameters of oceanic chemistry: Revelle Factor and omega aragonite

The Revelle Factor (RF, Figure 4N) and Ω-aragonite (Ω_{AR}) displayed an inverse relationship. The lowest RF values (9.9)

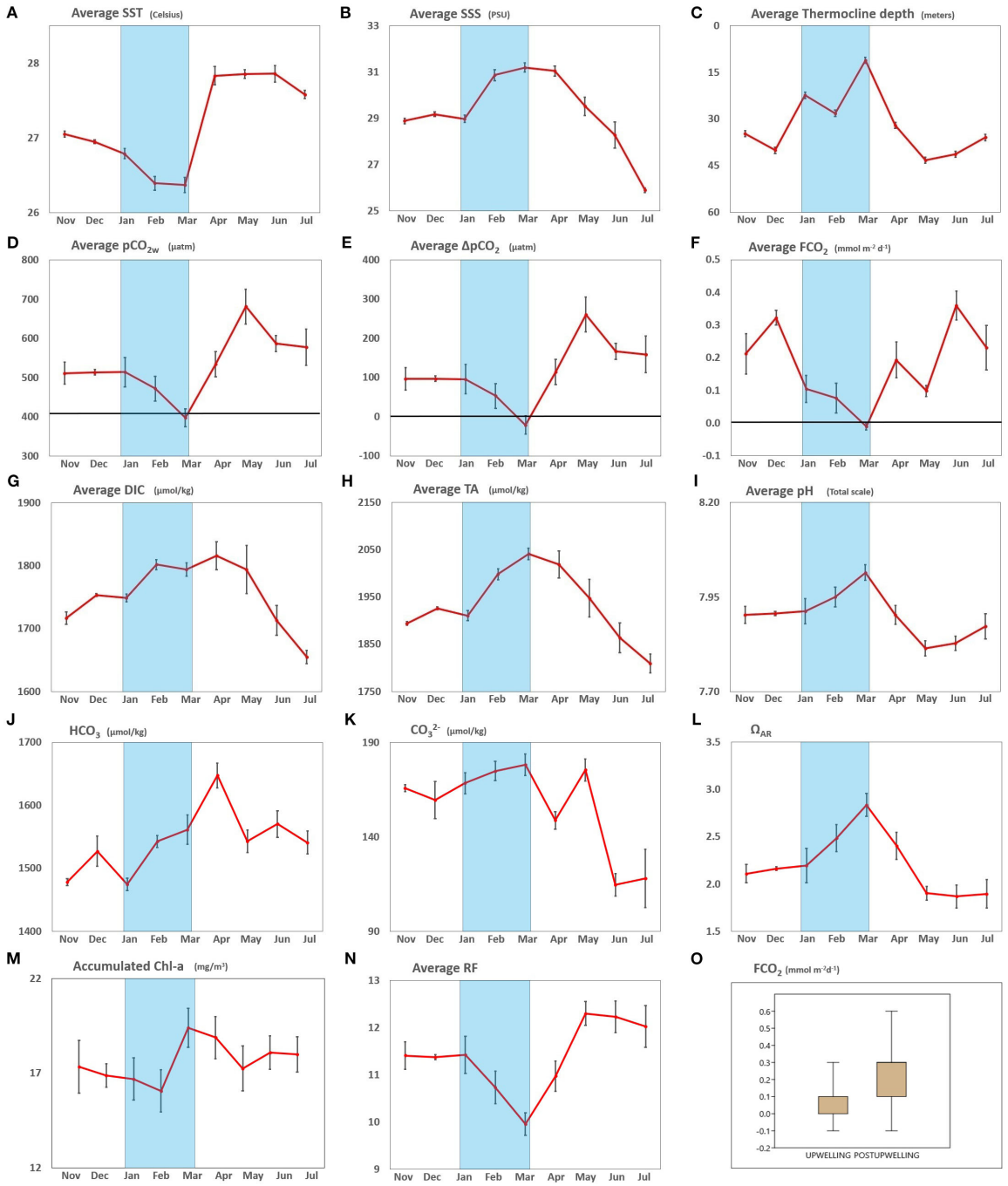

FIGURE 4
Monthly cycle of: **(A)** Average sea surface temperature (SST). **(B)** Average sea surface salinity (SSS). **(C)** Average thermocline depth (meters). **(D)** Average pCO_{2W} with average pCO_{2A} mark (418 µatm) indicated with a black horizontal line. **(E)** Average ΔpCO_2 with zero delta mark indicated with a black horizontal line. **(F)** Average FCO_2 with zero magnitude mark indicated with a black horizontal line. **(G)** Average Dissolved Inorganic Carbon (DIC). **(H)** Average Total Alkalinity (TA). **(I)** Average pH in total scale. **(J)** Average bicarbonate (HCO3). **(K)** Average carbonate (CO32-). **(L)** Average Saturation state of aragonite (ΩAR). **(M)** Accumulated Chlorophyll concentration (Chl-a). **(N)** Average Revelle Factor. **(O)** Boxplot comparing FCO2 values between upwelling (January, February, March) and post-upwelling (November, December, April, May, June, July) evidencing statistical differences (T test, T = 4,908, Tc = 2.001, p = 7.80E-6, N = 21 vs 39, respectively). Monthly measurements around Gorgona near the surface (≤ 3 m), standard error is illustrated as a black vertical line on each data point. Note that Ω AR data starts above 1.2, indicating possible but suboptimal calcification throughout the sampled period.

occurred in March, coinciding with weakened or even collapsed stratification (Figure 4C), when Ω_{AR} reached its peak (2.8). In contrast, RF increased during the post-upwelling season, rising from April and reaching ≥12 by July, concurrent with the lowest Ω_{AR} values (1.9), indicating suboptimal conditions for calcification. As expected, Ω_{AR} was inversely proportional to pH_T (Figures 4I, L), while RF varied inversely with SST.

3.6 Seasonal drivers of the carbonate system variability

Seasonal variability in dissolved inorganic carbon (DIC), its mixing component (DIC_{mix}), and related drivers highlighted the coupled influence of physical circulation and biological activity (Figure 5). During the upwelling season, lower ΔDIC values coincided with reduced pCO_{2w} and CO_2 fluxes, whereas in the post-upwelling season both DIC and pCO_{2w} increased together with intensified Ekman transport and pumping (Figures 5B–D). Regional chlorophyll-a distributions also followed these seasonal shifts, with peaks during February–March and again in May–July (Figure 5C).

Complementary evidence from a temperature–salinity (T–S) diagram (Figure 6A) underscored the role of mixing in shaping carbonate chemistry. Mixing calculations indicated that up to ~79% of the observed DIC could be explained by conservative mixing of three endmembers, while the residual ~19% reflected non-conservative processes (Figure 6B). The correlation between ΔDIC and ΔO_2 (Figure 6C) suggested that aerobic remineralization and nitrification were the dominant biological drivers of this residual variability. Physical processes dominated DIC variability, as indicated by the strong correlation between DICmix and DIC (R^2 = 0.79, Figure 6B). In contrast, respiration explained a smaller but measurable fraction of the variance (ΔDIC–ΔO_2, R^2 = 0.19; Figure 6C). Together, these results highlight that both physical and biological controls on DIC ultimately influenced its relationship with pCO_{2w}, consistent with the significant negative correlation observed between the two variables (Q = −0.71, p< 0.001, n = 60; Figures 4D, G).

4 Discussion

4.1 DIC dynamics

The physical mixing of the water mass contributes significantly to explaining the DIC values in the system (Figure 6A) as validated by the relationship between DIC_{mix} and DIC (Figure 6B; ~78% of variability) and the seasonal variability of WEK and ZET (Figures 5C, D). Therefore, DIC increased from November to May (Figure 5A) and then decreased from June to July. During La Niña 2021-2022, estuarine dynamics were strongly modulated by horizontal and vertical exchanges between marine and freshwater sources. High-frequency tides (up to 4 per day, with amplitudes of 5 m; Cauca tide table 2021–2022) mixed riverine and oceanic waters, while mesoscale eddies and Ekman-Zonal transport introduced deep offshore waters into the system (Corredor-Acosta et al., 2020; Figures 5C, D). Wind speed and direction generate local

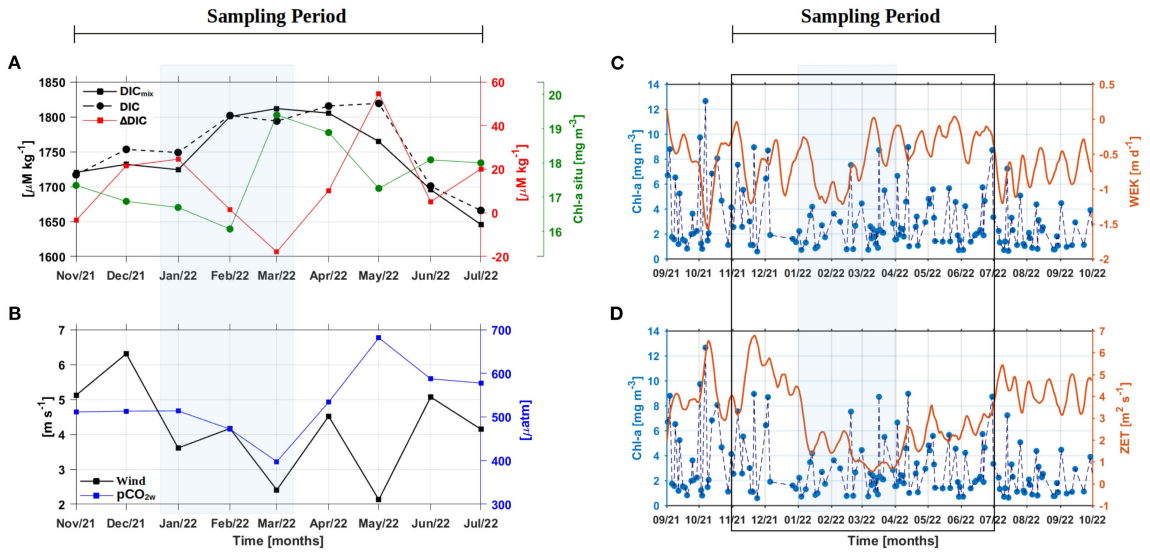

FIGURE 5
Temporal variability of DIC, DIC_{mix}, DeltaDIC and accumulated *in situ* Chl-a values in **(A)**. Monthly average values of wind and pCO_{2w} of the *in situ* sampling stations in **(B)**. For comparison and higher resolution analysis, weekly data of regional satellite Chl-a data from the OC-CCI product (https://www.oceancolour.org/) was coupled with weekly Ekman pumping (WEK in **C**) and Zonal Ekman Transport values (ZET in **D**). Weekly wind fields for the above calculations were obtained from the CCMP Wind Vector Analysis Product (https://www.remss.com/measurements/ccmp/). Note that the left-panels consider the *in situ* sampling period between Nov/2021 to Jul/2022, while the right-panels consider a full year of variability including months before, during (black rectangular box), and after the sampling period (Sept/2021 to Sept/2022). Transparent blue rectangle indicates the upwelling period from January to March 2022.

10.3389/fmars.2025.1633653

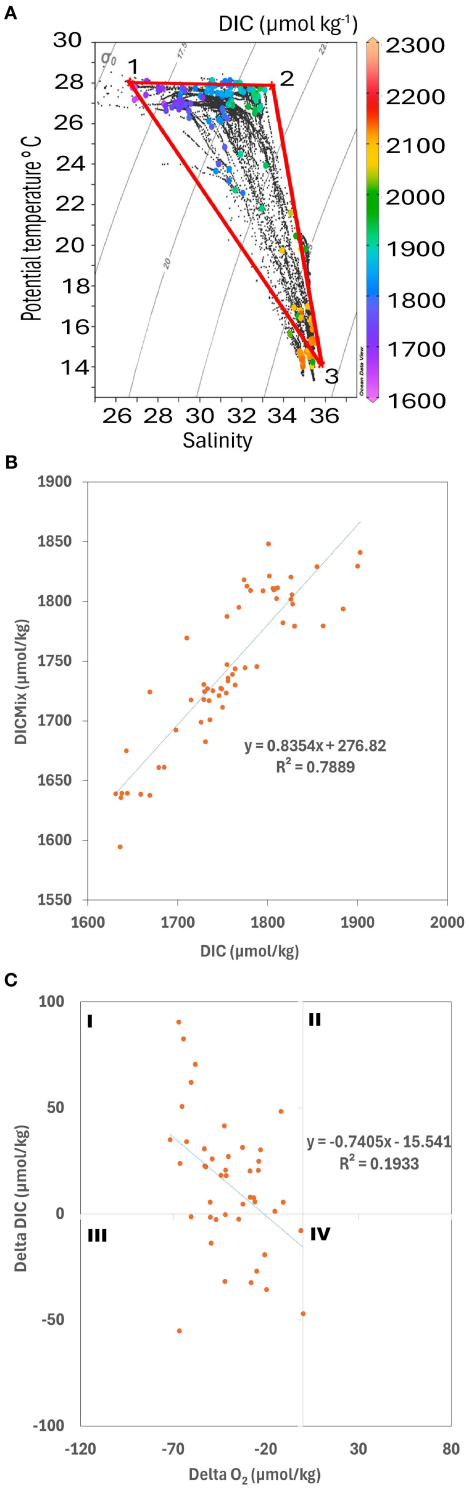

FIGURE 6
Temperature-salinity (T-S) diagram **(A)**. Data points color-coded by dissolved inorganic carbon (DIC) concentration (µmol kg^{-1}). The points represent observed oceanographic sampled depths throughout the year. The numbered labels (1-3) denote the end members of distinct water masses, with their respective salinity (S), potential temperature (T), and DIC values. The solid red lines connecting these end members outline the considered mixing triangles. Positive regression between DIC_{mix} and DIC **(B)**. Physical process explains 78.8% of the DIC measured (DIC_{mix}). The remaining percentage is explained by biogeochemical processes (19%). ΔDIC (biological processes) and ΔO_2 (µmol/kg) relationship (**C**; explaining 19%), where sampling points were mainly distributed within quadrants I and III (as shown in Kahl, 2018), suggesting aerobic remineralization and nitrification, respectively.

coastal currents, with north-south surface flow above the thermocline and south-north flow in subsurface waters (*in situ* observations); and upwelling and subsidence cycles (downwelling; Figures 5C, D) producing three water masses with different densities along the vertical profile (up to 80 m; see Figure 6A). Peaks in DIC between January and March coincided with intensified WEK and ZET which enhanced vertical injection of CO_2 and TA rich subsurface waters, when freshwater dilution and stratification was weaker (lower relative rain and precipitation; Figures 2B, D). Even so, elevation of DIC values could also be due to a gradual increase of bicarbonate and carbonate in the system (Figures 4J, K), when acidic sub-superficial waters (Ω_{AR} values sometimes below 1.5, Preciado A., unpublished data) could dissolve the reef structure, bringing the increased DIC signal to the surface. From April to July, the relative decrease in DIC reflected dilution by enhanced river discharge and weaker zonal inputs. The residual variability (~19%) was linked to respiration and remineralization, as evidenced by the correlation between ΔDIC and ΔO_2 where DIC increased but O_2 decreased (Figure 6C; O_2 levels reached 60 µmol/kg) and pCO_{2w} values were elevated. However, this respiration hypothesis requires further studies in the study site, to understand its contribution in DIC variability.

4.2 Seasonal FCO_2 variability

The seasonal variability of FCO_2 in Gorgona during the study period resulted from the system shifting from post-upwelling, dominated by southerly trade winds, higher precipitation and river dominated system to upwelling, dominated by northern winds, less precipitation, and lower river discharge, and then back to post-upwelling season. During post-upwelling, a slight positive increase in FCO_2 is related to the extensive plume of water from coastal rivers (Figure 2) originating from a 44% increase in river flow during the study period (*e.g.*, the Guapi River with 103 m^3 s^{-1}; Figure 2D), this plume extended for more than 60 km from the coast (as observed by floating logs on the field), forming a large estuary with an average salinity of 29.51 units (SD ± 1.56). Thus, following the definitions of Dai et al. (2013) and McKee et al. (2004), our study area can be classified as a system dominated by riverine inputs. During the post-upwelling season, pCO_{2W} values were relatively high (Figure 4D), ranging from 378 to 839 µatm (average 567 µatm), peaking in May, in line with high SST (Figure 4A), and ΔpCO_2 ranging from 47 µatm to 418 µatm. Our results agree with Ricaurte-Villota et al. (2025), where rivers via remineralization could explain the high pCO_{2w} values during moderate La Niña years (see Figure 6C). But also, the increased freshwater discharge could also diminish CO_2 fluxes, simultaneously, under La Niña (Reimer et al., 2013; Ricaurte-Villota et al., 2025), via nutrient excess and phytoplankton bloom. During upwelling season, the average water temperature decreased to 26.53 °C, but the average salinity remained below 30, confirming the rivers influence on surface waters. Likewise, the pCO_{2W} was relatively lower, ranging from 316 to 626 µatm (average 461 ± 92 µatm), with minimum values in March, coinciding with the lowest surface temperature (26.11 °C) and highest salinity (28.39). During this period, FCO_2 reached negative or near neutral values (between 0.3 and -0.1 mmol m^{-2} d^{-1}), with similarly low ΔpCO_2 values, ranging from –101 µatm to 93 µatm. Despite theory indicating that upwelling during a moderate La Niña should increase the CO_2 flux to the atmosphere (Kim et al., 2017), this was not observed in our study site. Similar dynamics *i.e.*, low or negative net fluxes despite upwelling have been reported in tropical estuarine systems where upwelled DIC is rapidly consumed by phytoplankton blooms which counterbalance the physical delivery of dissolved carbon (*e.g.*, Vargas et al., 2007; Bouillon, 2011; Giraldo et al., 2011). Monthly patterns and flux directions were preserved when calculated using the propagated pCO_{2w} error, including the neutral/slight sink observed in March, with only December and June showing greater variability. Net flux differences over the nine-month period remained negligible (original net flux = 0.0105 mol C m^{-2}, positive error net flux = 0.0133 mol C m^{-2}, negative error net flux = 0.0077 mol C m^{-2}) indicating a net total difference of ±0.0028 mol C m^{-2}, confirming the robustness of our results.

4.3 Temporal pCO_{2W} variability and key associated variables: salinity, temperature, dissolved inorganic carbon and ΔO_2

The temporal variability of pCO_{2W} was shaped by the combined effects of salinity, temperature, DIC, and ΔO_2 variables were correlated with pCO_{2W} values. Salinity showed the strongest and most significant correlation with pCO_{2w} (Q = –0.96; p = $1.77E^{-36}$, n = 60) reflecting the strong influence of river discharge and freshwater dilution, particularly during post-upwelling months, which differs from many oceanic regions where temperature is typically the main driver of FCO_2 variability (Séférian et al., 2013). Ekman-driven processes contributed to FCO_2 variability by vertical mixing processes (upwelling, downwelling; Figure 5C) that reduce salinity up to 40-60m, modifying the depth of the mixed layer over time. Sea surface temperatures recorded at the study site were relatively high (26.1–28.1 °C), as foreseen at equatorial latitudes, due to maximum solar insolation (Saraswat, 2011). On the other hand, sea surface temperature also correlated positively with pCO_{2w} (Spearman Q = 0.42313, p = 0.0007, n = 61; Figure 4A), in line with previous findings by Zhai et al. (2005), who reported higher pCO_{2w} values during warmer seasons. During the post-upwelling, the increase in SST from April to June aligned with increases in pCO_{2W}, ΔpCO_2, and FCO_2. As a result, the observed trend is consistent with the thermodynamic relationships between temperature and CO_2 solubility (Johnson et al., 2010), even though sea surface temperature alone did not fully explain the FCO_2 variability. Furthermore, we assessed the relative influence of salinity and temperature to pCO_{2W} by performing a sensitivity test which fixed one of the variables (salinity or temperature) while allowing the other to vary in the CO2SYS, recalculating pCO_{2w}. This approach allowed us to isolate the individual effect of each parameter (see Supplementary Figure 1). Results showed that salinity explained a larger proportion of the variance –

particularly in June and July when riverine CO_2 inputs were strongest, supporting the findings of Ricaurte-Villota et al. (2025) who also observed that river influence on salinity in the Colombian Caribbean exerts a greater control on pCO_{2w} than temperature. The lower salinity observed in June (post-upwelling) was associated with higher pCO_{2w} values, consistent with dilution by freshwater input and potential organic and inorganic matter increase from riverine mangrove sources (Palacios Peñaranda et al., 2019). The observed negative relationship between DIC and pCO_{2W} reflects the seasonal interplay of physical and biological processes at Gorgona. During upwelling, physical mixing and water mass advection introduced CO_2-rich subsurface waters, but biological drawdown suppressed pCO_{2w} provided by the sea and rivers. On the contrary, during the post-upwelling phase, the DIC increases and then decreases, due to the antagonistic relationship between the mixture (ZET, WEK; Figure 5) that, like respiration processes (oxygen reduction; Figure 6), provide pCO_{2w} (and DIC), and the photosynthetic activity, which consumes it or the excess of fresh water that dilutes the DIC (Figure 4).

Overall, the patterns in Figure 6 suggest that physical mixing and dilution were the primary controls of DIC variability, consistent with estuarine systems where hydrodynamic forcing often dominates carbon system fluctuations (Clark et al., 2022). Nevertheless, biological processes such as respiration and photosynthesis clearly modulated the signal, producing seasonal configurations of DIC–pCO_{2W} values that reflect the co-occurrence of both physical and biogeochemical drivers. Similar interactions have been reported in estuarine environments by Ahad et al. (2008) and Quiñones-Rivera et al. (2022), where strong physical control is complemented by meaningful, localized biological contributions. As anticipated, pH's relationship to pCO_{2w} was inverse (Peng et al., 2013; Hans-Rolf and Fritz, 2023; Ramaekers et al., 2023), and direct with Ω_{AR} (See Figure 4I), which is similar to the relationship described by Feely et al. (2009), in our case also in agreement with the highest salinity values. In addition, high pH_T values during March were coupled with consumption of CO_2 by phytoplankton (lowered pCO_{2w}), and higher buffer capacity in the system (high TA; Figure 4), which is similar to cases reported by Cai et al. (2011) and Macdonald et al. (2009) in coastal and estuarine systems (low SSS), despite relatively high DIC values. This condition favors coral reef or marine organisms' calcification, although the Ω_{AR} remained below 3, suggesting thermodynamically possible, yet suboptimal conditions (Ries et al., 2009). On the other hand, pH_T decreased during post-upwelling, to its minimum values (May; 7.81), as did TA (~1800 μmol kg^{-1}, Refer to Figure 4H), when the pCO_{2w} was at its maximum, thereby lowering the Ω_{AR} below 2.

4.4 Biological processes

The apparent suppression of CO_2 fluxes under upwelling conditions contradicted expectations from classical upwelling theory (*e.g.*, Kim et al., 2017), which generally predicts enhanced CO_2 outgassing as deeper, carbon-rich waters reach the surface. Instead, rapid phytoplankton uptake offset the physical inputs (rivers, subsurface water, advection, atmosphere, and other sources). Evidence for this mechanism comes from strongly negative ΔDIC values in February and March (Figure 6D), indicating intense CO_2 consumption, and from the inverse relationship between surface pCO_{2w} and cumulative Chl-a concentrations (Figures 4D, M; Figure 5A). This agrees with the findings of Corredor-Acosta et al. (2020) who reported peak productivity around Gorgona during March, based on multi-annual satellite observations. Both their long-term satellite information and our average and accumulated Chl-a data (Figure 4M) confirm that the coastal waters near Gorgona sustain relatively high phytoplankton biomass throughout the year, with average concentrations exceeding 2.45 mg m^{-3} in both seasons, and accumulated values surpassing 16 mg m^{-3} (Figure 4M; Supplementary Figure 2).

According to Corredor-Acosta et al. (2020) the sustained Chl-a signal on the Colombian Pacific coast is modulated by rising waters along the Panama Bight during the upwelling season and river discharges (see also Rodríguez-Rubio et al., 2003; Devis-Morales et al., 2008; Giraldo et al., 2008; 2008; 2011). Therefore, the productivity observed in Gorgona is attributed to the constant input of nutrients (Giraldo et al., 2011), coming from both, subsurface waters and the nearby Patía–Sanquianga deltaic complex (~50 km), which contributes total suspended solids (23.2 mg L^{-1}), nitrates (33.55 μg L^{-1}), and phosphates (<2 μg L^{-1}; Giraldo et al., 2011). These inputs, according to INVEMAR (2019–2022) result in high Chl-a concentrations near the coast (~0.9 mg m^{-3}) compared to areas farther from the island (~0.3 mg m^{-3}). Additionally, the coastal phytoplankton around Gorgona is dominated by large diatoms and dinoflagellates which support a zooplankton biomass up to seven times greater (89 g/100 m^3) than the regional average for the Colombian Pacific (12 g/100 m^3; Murcia Riaño and Giraldo López, 2007; Giraldo et al., 2011). Therefore, zooplankton also facilitates carbon export through marine snow, contributing to remineralization in the water column and up approximately 90–100 m depth (Alldredge, 1984; Vargas et al., 2007) which further aids in pCO_{2w} modulation at the surface (WEK, Figure 5C). The persistence of such high productivity effectively modulates surface pCO_{2w} by enhancing phytoplanktonic CO_2 uptake, thereby reducing the magnitude of air-sea fluxes. Without this sustained biological activity, surface waters around Gorgona would likely accumulate greater CO_2 excesses and display substantially higher efflux to the atmosphere during La Niña years.

4.5 Potential drivers for low CO_2 flux

The near-neutral to slightly positive CO_2 fluxes observed around Gorgona can be understood as the outcome of several interacting climatic–oceanographic processes. As shown, the system displays marked seasonal variability, yet overall fluxes remained low to neutral compared with other tropical Pacific or estuarine sites. Three main drivers appear to regulate this behavior: wind-driven exchange, vertical stratification, and the buffering capacity of surface waters.

Wind speeds during the study period were consistently low (mean<5 m s^{-1}; range: 2.1–6.4 m s^{-1}; Figure 5), which limited the efficiency of gas transfer. Since air–sea CO_2 fluxes are jointly governed by wind speed and the air–sea CO_2 partial pressure gradient (ΔpCO_2), the absence of high-wind events (>10 m s^{-1}; Prytherch et al., 2010) meant that surface–atmosphere exchange remained weak throughout most of the year. Even when ΔpCO_2 values were favorable for outgassing, limited wind-driven turbulence constrained fluxes to the atmosphere.

Vertical stratification further reinforced this suppression. The water column at Gorgona remained strongly stratified for most of the year, with the thermocline–halocline–pycnocline complex typically lying between 11 and 40 m depth (Figure 4C). This effectively isolated subsurface CO_2-enriched waters from the surface, preventing their sustained transfer into the mixed layer. Only in March, during the shoaling of the thermocline (to ~11 m), did subsurface waters briefly reach the surface, temporarily breaking stratification. Yet even under these conditions, fluxes remained near-neutral rather than shifting strongly positive.

This apparent contradiction can be explained by the buffering capacity of surface waters. Revelle Factor (RF) values were lowest during upwelling (January–March; Figure 4N), indicating a high resistance of surface waters to changes in pCO_{2W} despite inputs of dissolved inorganic carbon (DIC) from below. As a result, increases in subsurface DIC did not translate into proportional rises in surface pCO_{2W}, thus preventing strong efflux. By contrast, RF increased during the post-upwelling period (May–July; Figure 4N), when surface waters became more sensitive to DIC changes. Nevertheless, stratification was then strongest, reducing the vertical supply of CO_2-rich subsurface waters and limiting fluxes.

Taken together, these mechanisms explain why Gorgona exhibited suppressed CO_2 efflux during both upwelling and post-upwelling conditions. Wind limitation constrained the physical transfer of CO_2, stratification acted as a barrier separating sources from the surface, and buffering capacity modulated the extent to which subsurface DIC inputs could alter surface pCO_{2W}. This combination is consistent with earlier findings in the Colombian Caribbean (Reimer et al., 2013; Ricaurte-Villota et al., 2025), where La Niña–driven stratification similarly reduced CO_2 outgassing. At Gorgona, therefore, the interplay of seasonal stratification and surface carbonate chemistry set the stage for fluxes that remained near-neutral, even under physical conditions that would normally favor enhanced CO_2 release.

4.6 Gorgona's CO_2 fluxes in the context of global and regional estimates

To enable comparison of our nine-month flux record with annual estimates reported in literature, we estimated the three missing post-upwelling months (August to October 2020) in order to derive a potential annual flux. This approximation was based on our *in situ* measurements from six post-upwelling months that correspond to the rainy (wetter) season, a period which also encompasses the missing months. From these six months, we calculated a mean monthly flux of 0.00024 ± 0.0001 mol C m^2. Using this value, we estimated the flux for the three missing months (0.0007 mol C m^2; net positive flux) and added it to the nine-month total (0.01049 ± 0.000148 mol C m^2) yielding a potential annual flux of 0.0112 ± 0.00015 mol C m^2 yr^{-1}. Interpolation of missing FCO_2 data has been applied previously (e.g., Kahl, 2018). Nevertheless, we emphasize that the estimated three-month flux is a hypothetical approximation intended only for comparison purposes, and should be validated with additional *in situ* measurements.

This approach revealed a neutral to weakly positive net air-sea CO_2 flux at Gorgona Island (FCO_2 = 0.0112 ± 0.00015 mol C m^{-2} yr^{-1}; ~0.031 mmol C m^{-2} d^{-1}) being an order of magnitude lower than those reported by Dai et al. (2022) for non-ENSO years (0.8–1.0 mol C m^{-2} yr^{-1}), and close to the lower limit of the global range reported by Wong et al. (2022) for surface ocean carbon fluxes (0–1.5 mol C m^{-2} yr^{-1}); highlighting potential regional divergence from global modeling outputs (Table 1).

The Gorgona fluxes were also markedly lower than those observed in other tropical and coastal systems. For instance, at similar equatorial latitudes (~3°N), Jersild et al. (2017) and Landschützer et al. (2022) reported fluxes exceeding 0.3 ± 0.1 mol C m^{-2} yr^{-1} during moderate La Niña conditions. Pacific Ocean continental shelves exhibit values between 0.2 and 0.35 mol C m^{-2} yr^{-1} (Jersild et al., 2017; Vaittinada Ayar et al., 2022), while the North Pacific shelf, even under non-ENSO conditions, registers around 0.043 mol C m^{-2} yr^{-1} (Reimer et al., 2013). These regional differences suggest that local environmental controls strongly limit the air-sea CO_2 exchange in the Eastern Tropical Pacific, particularly near Gorgona. Consistent with this interpretation, Ricaurte-Villota et al. (2025) documented similarly low to near-neutral fluxes in the Colombian Caribbean under La Niña conditions, attributing them to high rainfall, enhanced stratification, and strong biological uptake. These drivers mirror those identified in our study, reinforcing the idea that La Niña exerts a suppressive effect on CO_2 release in this region. Comparable mechanisms have also been described in Arctic continental shelves, where freshwater inputs from rivers and ice melts (together with seasonal ice coverage) enhanced stratification, restricting gas exchange and contributing to low or near-neutral fluxes (Else et al., 2013; Miller et al., 2019; Mu et al., 2020).

Furthermore, comparison with other tropical systems reinforces our findings. Similar low or near-neutral fluxes have been reported in Costa Rica's Gulf of Nicoya (Pfeil et al., 2013) and other areas of the Eastern Tropical Pacific (Laurelle et al., 2013).

Estuarine systems by contrast, tend to show higher fluxes and yearly variability (Chen et al., 2013). For example, the Matla estuary in India exhibits high annual fluxes of 2.3 mol C m^{-2} yr^{-1} (Akhand et al., 2016) over 10 times greater than the estimated CO_2 flux around Gorgona, and the Patos Lagoon in Brazil ranges from -13.9 to 19.7 mol C m^{-2} yr^{-1} attributed to changes in freshwater input and phytoplankton activity (Albuquerque et al., 2022). Meanwhile Asian tropical estuaries average around 8.1 mol C m^{-2} yr^{-1} (Chen et al., 2013) which are also substantially higher than our estimated yearly fluxes. However, comparable near-neutral fluxes were reported in the Arafura and Red Seas under similar La Niña conditions (Hydes et al., 2012).

TABLE 1 CO_2 fluxes between air and sea in different geographic areas.

Location	Long.	Lat.	Continent	CO_2 Flux (mol C m^{-2} yr^{-1})	ENSO state	Reference
Southeast Asia	115°E	2.2°S	AS	0.86 ± 17	Moderate Niño	Laurelle et al. (2013)
Northern Australia	125°E	8.9°S	OC	0.11 ± 15.7	Moderate Niño	Laurelle et al. (2013)
Caribbean Sea	75°W	14.5°N	SA	0.66 ± 4.5	Moderate Niño	Laurelle et al. (2013)
Tropical Ocean	90°E – 90°W	20°S – 20°N	NA/SA	2.4 ± 0.05	Moderate Niño	Laurelle et al. (2013)
Matla Estuary	88°E	20°N	AS	2.3 + 0.5	Strong Niño	Akhand et al. (2016)
Patos Lagoon	52.5°W	6°N	SA	-13.9 – 19.7	Moderate Niña	Albuquerque et al. (2022)
Omani coast	59°E	20°N	AS	-0.9 ± 0.03	Strong Niña	Millero et al. (1998)
South China Sea (North)	116°E	22°N	AS	0.86 ± 0.04	Weak Niño	Zhai et al. (2005)
South China Sea (North)	116°E	22°N	AS	0.4 ± 0.2	Weak Niña	Li et al. (2022b)
Eastern Equatorial Pacific Ocean	90°W - 165°E	5°N - 10°S	NA/SA - OC	2 ± 1	Weak Niña	Cosca et al. (2003)
Equatorial Pacific Ocean	270°E	3°N	SA	0.20 ± 0.02	Moderate Niña	Vaittinada Ayar et al. (2022)
Red Sea	42.8°E	13.4°N	AS/AF	0.01 ± 0.001	Moderate Niña	Hydes et al. (2012)
Gulf of Nicoya	-84.9°W	9.6°N	CA	-0.02 ± 0.001	NA	Palacios Moreno and Pinto Tovar (1992) (SOCAT)
Arafura Sea	136.3°E	-9.9°S	OC	-0.01 ± 0.001	Moderate Niña	Hydes et al. (2012)
Amazon River plume	-52.5°W	6°N	SA	-12.78 ± 0.02	Weak Niña	Kortzinger (2003)
Equatorial Pacific	125°W	3°N	SA	0.3 ± 0.1	Moderate Niña	Landschützer et al. (2022)
Equatorial Pacific	125°W	3°N	SA	1.5 ± 0.03	Strong Niño	Cosca et al. (2003)
Tropical Eastern Pacific	-81°W	4.7°N	SA	-0.05 ± 0.01	NA	Laurelle et al. (2013)
Subarctic Pacific	145°E	50°N	AN	0.7 ± 0.5	Moderate Niño	Wang et al. (2018)
North Pacific Shelf	118°W	28°N	NA	0.35 ± 0.07	Weak Niña	Jersild et al. (2017)
North Pacific Shelf	117°W	31°N	NA	0.043 ± 0.01	NA	Reimer et al. (2013)
Colombian Atlantic	77°W	10°N	SA	0.25 ± 0.05	Weak Niña	Vaittinada Ayar et al. (2022)
Caribbean Coast	74°W	11°N	SA	0.02 ± 0.01	Moderate Niña	Ricaurte-Villota et al. (2025)
Equatorial Pacific Coast	78°W	3°N	SA	0.0112 ± 0.0001	Moderate Niña	This study (2021-2022)

It is important to note the flux difference when comparing systems at low latitudes, even during ENSO years. The similarity of the flux in the Colombian Pacific with tropical systems in the western Pacific Ocean is observed, even if they are located in Asia or Oceania. The abbreviations for continents are: AS, Asia; OC, Oceania; SA, South America; NA, North America; AF, Africa; CA, Central America; AN, Antarctica; EN, El Niño and LN, La Niña. The ENSO state is based on the ONI index from NOAA. Note that the value for this study is the predicted yearly flux for easier literature comparison.

Although global models (*e.g.*, Dai et al., 2022) and some regional studies do not explicitly separate ENSO phases, this distinction is essential for accurately characterizing flux dynamics in equatorial regions such as Gorgona. Prior literature indicates that La Niña conditions can reduce FCO_2 by 0.2–0.4 mol C m^{-2} yr^{-1} in the Pacific region, compared to El Niño or neutral years, aligning with the low values observed in this study (Chavez et al., 1999; Landschützer et al., 2016; McKinley et al., 2020; Park et al., 2010).

Our findings challenge the assumption that upwelling-dominated systems and estuarine environment are high CO_2 emitters, especially under La Niña conditions. Since in our tropical coastal area FCO_2 is sensitive to atmospheric conditions (wind velocity, precipitation, solar radiation), freshwater discharge, physical dynamic (vertical-horizontal water movement), vertical stratification, upwelling events, carbonate chemistry and biological uptake. Future research should incorporate higher-resolution temporal data, uncertainty analyses in ΔpCO_2, and ENSO-phase-specific studies (and neutral/non-ENSO years) to improve carbon flux estimates in this and similar tropical estuarine systems.

4.7 Methodological considerations and recommendations

Our study did not include measurements of δ^{13}C-DIC, which limits our ability to trace the biogeochemical sources and transformations of dissolved inorganic carbon. This isotopic parameter is a powerful tool for distinguishing between marine, terrestrial, and anthropogenic carbon inputs, and for assessing the extent of biological activity and remineralization. Its absence constrains our interpretation of carbon cycling dynamics, particularly under varying ENSO conditions. We suggest that future sampling campaigns incorporate δ^{13}C-DIC analysis to enhance source attribution and improve the mechanistic understanding of CO_2 flux variability in coastal upwelling systems. Additionally, we did not directly measure nutrients, which limits our ability to consider them in the CO2SYS calculations, specifically those which are proton acceptors (e.g. phosphates, silicates, ammonia), which can have effects on the computation of certain carbonate system parameters under high nutrient loads. We recommend that future sampling efforts incorporate nutrient measurements for improved flux and carbonate system calculations.

It is important to consider methodological differences when comparing with other studies. Although references such as Feely et al. (2004, 2006) and Hydes et al. (2012) offer context, disparities in sampling protocols, spatial resolution, and ecosystem type limit the scope of direct comparison. Finally, we recommend a long-term monitoring program taking water samples to estimate in the lab the couple DIC/TA, this will allow to compare the CO_2 flux variability between ENSO events and neutral conditions. An inexpensive discrete sampling based on our experience for Gorgona National Park could be to take water samples for 2–4 contrasting months.

5 Conclusions

The estimated air-sea CO_2 flux at Gorgona Island (near 3°N in the Eastern Equatorial Pacific) was close to neutral (0.0104 mol C m^{-2}) during the nine sampled months under La Niña conditions. Gorgona displayed a bimodal regime: (I) a predominantly post-upwelling system for six months, characterized by slightly positive to near-neutral fluxes, augmented river discharge and rainfall, elevated sea surface temperatures (>27.4 °C), and high pCO_{2W} (567 µatm in average); and (II) three months of upwelling, with neutral or weakly negative fluxes (–0.1 ± 0.07 g C m^{-2} day^{-1}), associated with CO_2 rich subsurface waters (nutrient rich) and phytoplankton uptake (minimum values of DeltaDIC aligned with the Chl-a maximum).

Although subsurface waters and coastal rivers deliver CO_2 to the surface, the intense and persistent stratification from low TA/DIC freshwater (high Revelle factor values; stratification starting at 10 to 45 m), reinforced by warmer surface waters, and freshwater downwelling, effectively limits CO_2 venting to the atmosphere. The estimated air-sea CO_2 flux at Gorgona Island aligns with global estimates proposed by Wong et al. (2022). Still is lower than those predicted by the model of Dai et al. (2022), suggesting the influence of local biogeochemical processes. In summary, under La Niña conditions, characterized by rainfall and river runoff (mean SSS = 29.5 ± 1.5) the combined effects of low wind speeds (<5 m s^{-1}), vertical stratification, and the biological activity appear to explain the net neutral balance in the air-sea CO_2 flux in this region. This study highlights the importance of integrating local physical and biological coastal processes (hydrography) when estimating region-specific CO_2 fluxes (in both magnitude and direction); additionally, long temporal *in situ* measurements under ENSO events such as El Niño and Neutral conditions are needed to compare with La Niña FCO_2 findings.

Nevertheless, the overall trend of low fluxes during La Niña, as shown across tropical estuaries and coastal systems, supports the hypothesis that this event suppresses CO_2 efflux through enhanced freshwater delivery and weakened ocean-atmosphere coupling. However, the hypothesis of high positive fluxes during El Niño or neutral years, when rainfall and upwelling are reduced at Gorgona, needs further investigation through seasonal and interannual monitoring campaigns including physical and biogeochemical variables.

Data availability statement

The datasets generated for this study can be found in the NOAA - National Centers for Environmental Information (NCEI; Accession Number 0300558). (NCEI; URL, https://www.ncei.noaa.gov/data/oceans/ncei/ocads/metadata/0300558.html).

Author contributions

SG: Writing – original draft, Formal analysis, Data curation, Writing – review & editing, Visualization, Software, Investigation, Validation, Methodology. AA: Conceptualization, Validation, Data curation, Supervision, Methodology, Project administration, Investigation, Resources, Writing – review & editing, Funding acquisition, Visualization, Formal analysis. AM: Methodology, Investigation, Visualization, Writing – review & editing. AG: Investigation, Data curation, Methodology, Writing – review & editing. AC-A: Conceptualization, Visualization, Writing – review & editing, Formal analysis. JH-A: Conceptualization, Writing – review & editing, Visualization. LC: Writing – review & editing, Validation, Methodology, Formal analysis, Visualization. LK: Visualization, Methodology, Formal analysis, Writing – review & editing. DR-P: Writing – review & editing, Supervision, Validation, Methodology.

Funding

The author(s) declare financial support was received for the research and/or publication of this article. The Principal Investigator (PI), AA, acknowledges receiving financial support for various research activities, including the purchase of

equipment, acquisition of laboratory and field materials, and funding for field trips. Additionally, these funds were used to establish and equip a laboratory at the Pontificia Universidad Javeriana. Partial resources from the same fund were also allocated to cover the publication costs of this article (ID 21346). This research was funded by the National Geographic Explorer program through the project titled *"Ocean Acidification Vulnerability in Colombia: First Monitoring Program in the Tropical Pacific"* (Grant No. NGS-64756R-19), with additional COVID-19 grant support (Grant No. NGS-81727R-20). Further funding was provided by the Pontificia Universidad Javeriana under the project *"Monitoreo de acidificación marina en el Pacífico colombiano"* (Project ID: 120132C0401200, No. 20019; Grant ID 21347).

Acknowledgments

The Ocean Foundation donated the GOA-ON in a Box kit, OA training, and grant support for equipment maintenance under the Memorandum of Understanding between Pontificia Universidad Javeriana and The Ocean Foundation ("TOF"). This research is part of the collaboration with the International COCAS project (2021-2030), Ocean Decade-United Nations (Leader Diana Ruiz Pino and Alban Lazar) https://oceandecade.org/fr/actions/coastal-observatory-for-climate-co2-and-acidification-for-the global-south-society-cocas/. Dra. Andrea Corredor-Acosta thanks FONDECYT Postdoctoral Project No. 3230740 granted by the Chilean Agency for Research and Development (ANID). We also thank Parques Nacionales Naturales de Colombia - Gorgona for their logistical support at Gorgona (Christian Díaz – research head & Monitoring of the Gorgona park), accommodation and boat, and the research permit No. 004 de 2020 - file number: OTRP 004-2020. To Camilo, Freddy, and Jaime for their help in the Ocean Acidification laboratory. To Juan Felipe Cifuentes for his field assistance (monitoring) and also to Gabriela Cervantes Diaz for her help in the laboratory analysis at the UABC. Thanks to Dr. Alan Giraldo of Universidad del Valle for funding research interns Cristian Claros, Sebastián Ortiz, and Natalia Londoño, who collaborated with us in the field sampling. We thank Camilo Rodríguez and Enrique Herman for their help during the long days of boat sampling and for hosting us in their home during our stay at Guapi. Finally, a huge thanks to my friends, Hugo Barata, Catalina Infante, Iván Gonzales, Vinny Preiss, and my family, Mónica Duque, Juan Pablo Gutiérrez, and Emma Gutiérrez for their never-ending support, without which this research would not have been possible.

Conflict of interest

The authors declare that the research was conducted in the absence of any commercial or financial relationships that could be construed as a potential conflict of interest.

Generative AI statement

The author(s) declare that no Generative AI was used in the creation of this manuscript.

Any alternative text (alt text) provided alongside figures in this article has been generated by Frontiers with the support of artificial intelligence and reasonable efforts have been made to ensure accuracy, including review by the authors wherever possible. If you identify any issues, please contact us.

Publisher's note

Supplementary material

The Supplementary Material for this article can be found online at: https://www.frontiersin.org/articles/10.3389/fmars.2025.1633653/full#supplementary-material

References

Ahad, J. M. E., Barth, J. A. C., Ganeshram, R. S., Spencer, R. G. M., and Uher, G. (2008). Controls on carbon cycling in two contrasting temperate zone estuaries: The Tyne and Tweed, UK. *Estuarine. Coast. Shelf. Sci* 78, 685–693. doi: 10.1016/j.ecss.2008.02.006

Akhand, A., Chanda, A., Manna, S., Das, S., Hazra, S., Roy, R., et al. (2016). A comparison of CO_2 dynamics and air-water fluxes in a river-dominated estuary and a mangrove-dominated marine estuary. *Geophys. Res. Lett.* 43. doi: 10.1002/2016gl070716

Albuquerque, C., Kerr, R., Monteiro, T., MaChado, E.da C., Carvalho, A. da C.d., and Mendes, C. R. B. (2022). Water-air exchanges in the lower estuary of the patos lagoon: seasonal variability, drivers, and sources of CO_2. doi: 10.21203/rs.3.rs-1336400/v1

Alldredge, A. L. (1984). "The quantitative significance of gelatinous zooplankton as pelagic consumers," In: M. J. R. Fasham (eds) *Flows of Energy and Materials in Marine Ecosystems* (Boston, MA: Springer US), 407–433. doi: 10.1007/978-1-4757-0387-0_16

Amaya, C. A. A. (2024). "Las corrientes superficiales en la cuenca de Colombia observadas con boyas de deriva," in *Revisa de la Academia Colombiana de Ciencias Exactas, Físicas y Naturales*, vol. 25. Bogotá, Colombia: Academia Colombiana de Ciencias Exactas, Físicas y Naturales (ACCEFYN), 321–336. doi: 10.18257/raccefyn.25(96).2001.2796

Amos, C. M., and Castelao, R. M. (2022). Influence of the El Niño-Southern oscillation on SST fronts along the west coasts of north and South America. *J. Geophys. Res.: Oceans.* 127. doi: 10.1029/2022JC018479

Andersson, A. J. (2005). Coastal ocean and carbonate systems in the high CO2 world of the Anthropocene. *Am. J. Sci* 305, 875–918. doi: 10.2475/ajs.305.9.875

Andersson, A. J., and Gledhill, D. (2013). Ocean acidification and coral reefs: effects on breakdown, dissolution, and net ecosystem calcification. *Annu. Rev. Mar. Sci* 5, 321–348. doi: 10.1146/annurev-marine-121211-172241

Bakun, A., and Nelson, C. (1991). The seasonal cycle of wind-stress curl in subtropical eastern boundary current regions. *J. Physical Oceanography* 21 (12), 1815–1834. Available online at: https://journals.ametsoc.org/view/journals/phoc/21/12/1520-0485_1991_021_1815_tscows_2_0_co_2.xml

Bouillon, S. (2011). Storage beneath mangroves. *Nature Geoscience* 4 (5), 282–283. doi: 10.1038/ngeo1130

Blanco, J. F. (2012). The hydroclimatology of Gorgona Island: seasonal and ENSO-related Patternsa. *Actualidades. Biológicas.* 31, 111–121. doi: 10.17533/udea.acbi.331494

Borges, A. V., and Abril, G. (2011). "Carbon dioxide and methane dynamics in estuaries," in *Treatise on Estuarine and Coastal Science* (Elsevier), 119–161. doi: 10.1016/B978-0-12-374711-2.00504-0

Borges, A. V., Delille, B., and Frankignoulle, M. (2005). Budgeting sinks and sources of CO_2 in the coastal ocean: Diversity of ecosystems counts. *Geophys. Res. Lett.* 32. doi: 10.1029/2005GL023053

Bravo, L., Ramos, M., Astudillo, O., Dewitte, B., and Goubanova, K. (2016). Seasonal variability of the Ekman transport and pumping in the upwelling system off central-northern Chile (∼ 30° S) based on a high-resolution atmospheric regional model (WRF). *Ocean. Sci* 12, 1049–1065. doi: 10.5194/os-12-1049-2016

Cai, W.-J. (2011). Estuarine and coastal ocean carbon paradox: CO 2 sinks or sites of terrestrial carbon incineration? *Annu. Rev. Mar. Sci* 3, 123–145. doi: 10.1146/annurev-marine-120709-142723

Cai, W.-J., Hu, X., Huang, W.-J., Murrell, M. C., Lehrter, J. C., Lohrenz, S. E., et al. (2011). Acidification of subsurface coastal waters enhanced by eutrophication. *Nat. Geosci.* 4, 766–770. doi: 10.1038/ngeo1297

Cai, W.-J., and Wang, Y. (1998). The chemistry, fluxes, and sources of carbon dioxide in the estuarine waters of the Satilla and Altamaha Rivers, Georgia. *Limnology and Oceanography* 43 (4), 657–668. doi: 10.4319/lo.1998.43.4.0657

Chavez, F. P., Service, S. K., and Buttrey, S. E. (1996). Temperature-nitrate relationships in the central and eastern tropical Pacific. *J. Geophys. Res.: Oceans.* 101, 20553–20563. doi: 10.1029/96JC01943

Chavez, F. P., Strutton, P. G., Friederich, G. E., Feely, R. A., Feldman, G. C., Foley, D. G., et al. (1999). Biological and chemical response of the equatorial pacific ocean to the 1997–98 El Niño. *Science* 286, 2126–2131. doi: 10.1126/science.286.5447.2126

Chen, C.-T. A., and Borges, A. V. (2009). Reconciling opposing views on carbon cycling in the coastal ocean: Continental shelves as sinks and near-shore ecosystems as sources of atmospheric CO_2. *Deep. Sea. Res. Part II.: Topical. Stud. Oceanogr.* 56, 578–590. doi: 10.1016/j.dsr2.2009.01.001

Chen, C., Huang, T. S., Chen, Y., Bai, Y., He, X.-T., and Kang, Y.J. (2013). Air–sea exchanges of CO_2 in the world's coastal seas. *Biogeosciences* 10, 6509–6544. doi: 10.5194/bg-10-6509-2013

Chung, C. T. Y., and Power, S. B. (2014). Precipitation response to La Niña and global warming in the Indo-Pacific. *Climate Dynamics.* 43, 3293–3307. doi: 10.1007/s00382-014-2105-9

Clark, J. B., Uz, S. S., Tsontos, V., Huang, T., Scott, J., and Rogers, L. (2022). Assessing carbon properties in coastal waters with a new observing system testbed. *Oceans*, 1–6. doi: 10.1109/OCEANS47191.2022.9977358

Corredor-Acosta, A., Acosta, A., Gaspar, P., and Calmettes, B. (2011). Variation in the surface currents in the Panama Bight during El Nino and LA Nina events from 1993 to 2007. *Bull. Mar. Coast. Res.* 40. doi: 10.25268/bimc.invemar.2011.40.0.127

Corredor-Acosta, A., Cortés-Chong, N., Acosta, A., Pizarro-Koch, M., Vargas, A., Medellín-Mora, J., et al. (2020). Spatio-temporal variability of chlorophyll-A and environmental variables in the Panama bight. *Remote Sens.* 12, 2150. doi: 10.3390/rs12132150

Cosca, C. E., Feely, R. A., Boutin, J., Etcheto, J., McPhaden, M. J., Chavez, F. P., et al. (2003). Seasonal and interannual CO_2 fluxes for the central and eastern equatorial Pacific Ocean as determined from fCO_2 -SST relationships. *J. Geophys. Res.: Oceans.* 108. doi: 10.1029/2000JC000677

Courtney, T. A., and Andersson, A. J. (2019). Evaluating measurements of coral reef net ecosystem calcification rates. *Coral. Reefs.* 38, 997–1006. doi: 10.1007/s00338-019-01828-2

Courtney, T. A., Cyronak, T., Griffin, A. J., and Andersson, A. J. (2021). Implications of salinity normalization of seawater total alkalinity in coral reef metabolism studies. *PloS One* 16, e0261210. doi: 10.1371/journal.pone.0261210

Crawford, G., Mepstead, M., and Díaz-Ferguson, E. (2023). Characterizing oceanographic conditions near Coiba Island and Pacific Panama using 20 years of satellite-based wind stress, SST and chlorophyll-a measurements. *Mar. Fish. Sci. (MAFIS)* 37, 391–411. doi: 10.47193/mafis.37X2024010112

Dai, X., Ma, J., Zhang, H., and Xu, W. (2013). Evaluation of ecosystem health for the coastal wetlands at the Yangtze Estuary, Shanghai. *Wetlands. Ecol. Manage.* 21, 433–445. doi: 10.1007/s11273-013-9316-4

Dai, M., Su, J., Zhao, Y., Hofmann, E. E., Cao, Z., Cai, W.-J., et al. (2022). Carbon fluxes in the coastal ocean: synthesis, boundary processes, and future trends. *Annu. Rev. Earth Planet. Sci.* 50, 593–626. doi: 10.1146/annurev-earth-032320-090746

DeGrandpre, M. D., Hammar, T. R., and Wirick, C. D. (1998). Short-term pCO_2 and O_2 dynamics in California coastal waters. *Deep. Sea. Res. Part II.: Topical. Stud. Oceanogr.* 45, 1557–1575. doi: 10.1016/S0967-0645(98)80006-4

Devis-Morales, A., Schneider, W., Montoya-Sánchez, R. A., and Rodríguez Rubio, E. (2008). Monsoon-like winds reverse oceanic circulation in the Panama Bight. *Geophys. Res. Lett.* 35, L20607. doi: 10.1029/2008GL035172

Diaz, R. J. (2001). Overview of hypoxia around the world. *J. Environ. Qual.* 30, 275–281. doi: 10.2134/jeq2001.302275x

Díaz Guevara, D. C., Málikov, I., and Villegas Bolaños, N. L. (2008). Características de las zonas de surgencia de la cuenca del Pacífico Colombiano y su relación con la zona de convergencia intertropical. *Boletín. Científico. CIOH.* 26, 59–71. doi: 10.26640/01200542.26.59_71

Dickson, A. G. (1990). Standard potential of the reaction: AgCl (s)+ 12H2 (g)= Ag (s) + HCl (aq), and the standard acidity constant of the ion HSO_4^- in synthetic sea water from 273.15 to 318.15 K. *J. Chem. Thermodynamics.* 22, 113–127. doi: 10.1016/0021-9614(90)90074-z

Dickson, A. G., Sabine, C. L., and Christian, J. R. (Eds.) (2007). Guide to best practices for ocean CO_2 measurements (PICES Special Publication 3), 191. ("Guide" in one PDF file). Available online at: https://www.ncei.noaa.gov/access/ocean-carbon-acidification-data-system/oceans/Handbook_2007/Guide_all_in_one.pdf

Doney, S. C., Lima, I., Feely, R. A., Glover, D. M., Lindsay, K., Mahowald, N., et al. (2009b). Mechanisms governing interannual variability in upper-ocean inorganic carbon system and air–sea CO_2 fluxes: Physical climate and atmospheric dust. *Deep. Sea. Res. Part II.: Topical. Stud. Oceanogr.* 56, 640–655. doi: 10.1016/j.dsr2.2008.12.006

Else, B. G. T., Papakyriakou, T. N., Galley, R. J., Mucci, A., Gosselin, M., Miller, L. A., et al. (2013). Annual cycle of air–sea CO_2 exchange in an Arctic Polynya region. *J. Geophys. Res.: Biogeosci.* 118, 681–703. doi: 10.1002/jgrg.20023

Engel, A., Kiko, R., and Dengler, M. (2022). Organic matter supply and utilization in oxygen minimum zones. *Annu. Rev. Mar. Sci* 14, 355–378. doi: 10.1146/annurev-marine-041921-090849

Fabre, C., Sauvage, S., Probst, J.-L., and Sánchez-Pérez, J. M. (2020). Global-scale daily riverine DOC fluxes from lands to the oceans with a generic model. *Global and Planetary Change* 194, 103294. doi: 10.1016/j.gloplacha.2020.103294

Feely, R., Doney, S., and Cooley, S. (2009). Ocean acidification: present conditions and future changes in a high-CO_2 world. *Oceanography* 22, 36–47. doi: 10.5670/oceanog.2009.95

Feely, R. A., Takahashi, T., Wanninkhof, R., McPhaden, M. J., Cosca, C. E., Sutherland, S. C., et al. (2006). Decadal variability of the air-sea CO_2 fluxes in the equatorial Pacific Ocean. *J. Geophys. Res.: Oceans.* 111. doi: 10.1029/2005JC003129

Feely, R. A., Wanninkhof, R., McGillis, W., Carr, M.-E., and Cosca, C. E. (2004). Effects of wind speed and gas exchange parameterizations on the air-sea CO_2 fluxes in the equatorial Pacific Ocean. *J. Geophys. Res.: Oceans.* 109. doi: 10.1029/2003JC001896

Fiedler, P. C., and Lavín, M. F. (2017). *Oceanographic Conditions of the Eastern Tropical Pacific*. Berlin: Springer Nature Link 59–83. doi: 10.1007/978-94-017-7499-4_3

Ford, D. J., Tilstone, G. H., Shutler, J. D., and Kitidis, V. (2022). Identifying the biological control of the annual and multi-year variations in South Atlantic air–sea CO_2 flux. *Biogeosciences* 19, 4287–4304. doi: 10.5194/bg-19-4287-2022

Friedlingstein, P., O'Sullivan, M., Jones, M. W., Andrew, R. M., Bakker, D. C. E., Hauck, J., et al. (2023). Global carbon budget 2023. *Earth Syst. Sci Data* 15, 5301–5369. doi: 10.5194/essd-15-5301-2023

Gan, J., Li, L., Wang, D., and Guo, X. (2009). Interaction of a river plume with coastal upwelling in the northeastern South China Sea. *Continent. Shelf. Res.* 29, 728–740. doi: 10.1016/j.csr.2008.12.002

Gassen, L., Esters, L., Ribas-Ribas, M., and Wurl, O. (2024). The impact of rainfall on the sea surface salinity: a mesocosm study. *Sci. Rep.* 14, 6353. doi: 10.1038/s41598-024-56915-4

Gerrard, M. B. (2023). "The role of ocean CDR in mitigating climate change," in *Ocean Carbon Dioxide Removal for Climate Mitigation* (Edward Elgar Publishing), 12–19. doi: 10.4337/9781802208856.00009

Giraldo, A., Rodríguez-Rubio, E., and Zapata, F. (2008). Condiciones oceanográficas en isla Gorgona, Pacífico oriental tropical de Colombia. *Latin. Am. J. Aquat. Res.* 36, 121–128. doi: 10.3856/vol36-issue1-fulltext-12

Giraldo, A., Valencia, B., and Ramírez, D. G. (2011). Productividad planctónica y condiciones oceanográficas locales en Isla Gorgona durante julio 2006. *Bol. Invest. Mar. Cost.* 40, 185–201. doi: 10.25268/bimc.invemar.2011.40.1.108

Giraldo López, A. (2008). Variabilidad espacial de temperatura, salinidad y transparencia en el ambiente pelágico del PNN Gorgona durante septiembre 2007 y marzo 2008. *Boletín. Científico. CIOH.* 26, 157–163. doi: 10.26640/22159045.192

Guzmán, D. H., Mier, R. L., Vergara, A., and Milanes, C. B. (2023). Marine protected areas in Colombia: A historical review of legal marine protection since the late 1960s to 2023. *Marine Policy*, 155, 105726. doi: 10.1016/j.marpol.2023.105726

Hans-Rolf, D., and Fritz, V. (2023). Oceans' surface pH-value as an example of a reversible natural response to an anthropogenic perturbation. *Ann. Mar. Sci* 7, 034–039. doi: 10.17352/ams.000036

Herrera Carmona, J. C., Selvaraj, J. J., and Giraldo, A. (2022). Dynamic regionalization of the Panama Bight, Eastern Tropical Pacific, using remote sensing data. *Int. J. Remote Sens.* 43, 3131–3151. doi: 10.1080/01431161.2022.2063040

Hu, J., Lan, W., Huang, B., Chiang, K.-P., and Hong, H. (2015). Low nutrient and high chlorophyll a coastal upwelling system – A case study in the southern Taiwan Strait. *Estuarine. Coast. Shelf. Sci* 166, 170–177. doi: 10.1016/j.ecss.2015.05.020

Huang, J., Li, Q., Wu, P., Wang, S., Gu, S., Guo, M., et al. (2022). The buffering of a riverine carbonate system under the input of acid mine drainage: Example from a small karst watershed, southwest China. *Front. Environ. Sci.* 10 doi: 10.3389/fenvs.2022.1020452

Hydes, D., Jiang, Z.-P., Hartman, M. C., Campbell, J. M., Hartman, S. E., Pagnani, M. R., et al. (2012). *Surface DIC and TALK measurements along the M/V Pacific Celebes VOS Line during the 2007–2012 cruises*. Carbon Dioxide Information Analysis Center, Oak Ridge National Laboratory, US Department of Energy, Oak Ridge, TN. doi: 10.3334/CDIAC/OTG.VOS_PC_2007-2012

Ianson, D., Feely, R. A., Sabine, C. L., and Juranek, L. W. (2009). Features of coastal upwelling regions that determine net air-sea CO_2 flux. *J. Oceanogr.* 65, 677–687. doi: 10.1007/s10872-009-0059-z

INVEMAR. (2019). Informe del Estado de los Ambientes Marinos y Costeros en Colombia 2019 (Santa Marta: Instituto de Investigaciones Marinas y Costeras INVEMAR). Available online at: https://portal.invemar.org.co/inf-ier (Accessed July 28, 2023).

INVEMAR. (2020). Informe del Estado de los Ambientes Marinos y Costeros en Colombia 2020 (Santa Marta: Instituto de Investigaciones Marinas y Costeras INVEMAR). Available online at: https://portal.invemar.org.co/inf-ier (Accessed July 28, 2023).

INVEMAR. (2022). Informe del Estado de los Ambientes Marinos y Costeros en Colombia 2022 (Santa Marta: Instituto de Investigaciones Marinas y Costeras INVEMAR). Available online at: https://portal.invemar.org.co/inf-ier (Accessed July 28, 2023).

Jersild, A., Landschützer, P., Gruber, N., and Bakker, D. C. E. (2017). *An observation-based global monthly gridded sea surface pCO_2 and air–sea CO_2 flux product from 1982 onward (NCEI Accession 0160558)*. NOAA National Centers for Environmental Information. doi: 10.7289/V5Z899N6

Jiang, Z.-P., Tyrrell, T., Hydes, D. J., Dai, M., and Hartman, S. E. (2014). Variability of alkalinity and the alkalinity-salinity relationship in the tropical and subtropical surface ocean, Global Biogeochem. *Cycles* 28, 729–742. doi: 10.1002/2013GB004678

Johnson, M. S., Billett, M. F., Dinsmore, K. J., Wallin, M., Dyson, K. E., and Jassal, R. S. (2010). Direct and continuous measurement of dissolved carbon dioxide in freshwater aquatic systems—method and applications. *Ecohydrology* 3, 68–78. doi: 10.1002/eco.95

Johnson, K., Sieburth, J. M., Williams, P.J. le., and Brändström, L. (1987). Coulometric total carbon dioxide analysis for marine studies: Automation and calibration. *Mar. Chem.* 21, 117–133. doi: 10.1016/0304-4203(87)90033-8

Kahl, L. C. (2018). Dinámica del CO_2 en el Océano Atlántico Sudoccidental (Buenos Aires, Argentina: Universidad de Buenos Aires, Facultad de Ciencias Exactas y Naturales). Available online at: https://hdl.handle.net/20.500.12110/tesis_n6525_Kahl (Accessed May 17, 2025).

Kao, H.-Y., and Yu, J.-Y. (2009). Contrasting eastern-pacific and central-pacific types of ENSO. *J. Climate* 22, 615–632. doi: 10.1175/2008jcli2309.1

Kawabe, M., and Fujio, S. (2010). Pacific Ocean circulation based on observation. *J. Oceanogr.* 66, 389–403. doi: 10.1007/s10872-010-0034-8

Kessler, W. S. (2006). The circulation of the eastern tropical Pacific: A review. *Prog. Oceanogr.* 69, 181–217. doi: 10.1016/j.pocean.2006.03.009

Kim, D., Choi, Y., Kim, T.-W., and Park, G.-H. (2017). Recent increase in surface fCO_2 in the western subtropical North Pacific. *Ocean. Sci J.* 52, 329–335. doi: 10.1007/s12601-017-0030-7

Kim, H. J., Kim, T., Hyeong, K., Yeh, S., Park, J., Yoo, C. M., et al. (2019). Suppressed CO_2 outgassing by an enhanced biological pump in the eastern tropical pacific. *J. Geophys. Res.: Oceans.* 124, 7962–7973. doi: 10.1029/2019JC015287

Körtzinger, A. (2003). A significant CO2 sink in the tropical Atlantic Ocean associated with the Amazon River plume. *Geophysical Research Letters* 30 (24), 2287. doi: 10.1029/2003GL018841

Kryzhova, K. A., and Semkin, P. Y. (2023). *Carbonate System and CO_2 Fluxes in the Partizanskaya River Estuary*. Berlin: Springer Nature Link 268–279. doi: 10.1007/978-3-031-47851-2_32

Lal, R. B. (2024). Recent trends in carbon sequestration technique. *J. Biochemical Sciences*. doi: 10.61577/jbs.2024.100003

Landschützer, P., Gruber, N., and Bakker, D. C. E. (2016). Decadal variations and trends of the global ocean carbon sink. *Global Biogeochem. Cycles.* 30, 1396–1417. doi: 10.1002/2015GB005359

Landschützer, P., Keppler, L., and Ilyina, T. (2022). *Ocean systems* (Elsevier eBooks), 427–452. doi: 10.1016/b978-0-12-814952-2.00004-6

Lanson, D., Feely, R. A., Sabine, C. L., and Juranek, L. W. (2009). Features of coastal upwelling regions that determine net air–sea CO2 flux. *J. Oceanography* 65 (5), 677–687. doi: 10.1007/s10872-009-0059-z

Laruelle, G. G., Dürr, H. H., Slomp, C. P., Borges, A. V., Gypens, N., Lauerwald, R., et al. (2013). Air–sea CO2 exchanges in the world's coastal seas. *Biogeosciences* 10, 6509–6544. doi: 10.5194/bg-10-6509-2013

Lee, K., Kim, T. W., Byrne, R. H., Millero, F. J., Feely, R. A., and Liu, Y. M. (2010). The universal ratio of boron to chlorinity for the North Pacific and North Atlantic oceans. *Geochim. Cosmochim. Acta* 74, 1801–1811. doi: 10.1016/j.gca.2009.12.027

Legge, O. J., Bakker, D. C. E., Johnson, M. T., Meredith, M. P., Venables, H. J., Brown, P. J., et al. (2015). The seasonal cycle of ocean-atmosphere CO_2 flux in Ryder Bay, west Antarctic Peninsula. *Geophys. Res. Lett.* 42, 2934–2942. doi: 10.1002/2015GL063796

Lewis, E., and Wallace, (1998). *Program Developed for CO_2 System Calculations* OSTI OAI (U.S. Department of Energy Office of Scientific and Technical Information). doi: 10.15485/1464255

Li, J., Cao, R., Lao, Q., Chen, F., Chen, C., Zhou, X., et al. (2020). Assessing seasonal nitrate contamination by nitrate dual isotopes in a monsoon-controlled bay with intensive human activities in South China. *Int. J. Environ. Res. Public Health* 17, 1921. doi: 10.3390/ijerph17061921

Li, H., Zhang, J., Xuan, J., Wu, Z., Ran, L., Wiesner, M. G., et al. (2022). Asymmetric response of the biological carbon pump to the ENSO in the south China sea. *Geophys. Res. Lett.* 49. doi: 10.1029/2021gl095254

Liss, P. S., and Merlivat, L. (1986). Air–sea gas exchange rates: Introduction and synthesis, in P. Buat-Ménard (ed.), *The Role of Air–Sea Exchange in Geochemical Cycling*, NATO ASI Series (Series C: Mathematical and Physical Sciences), vol. 185, Springer, Dordrecht, 113–127. doi: 10.1007/978-94-009-4738-2_5

Lorenzoni, L., Hu, C., Varela, R., Arias, G., Guzmán, L., and Muller-Karger, F. (2011). Bio-optical characteristics of Cariaco Basin (Caribbean Sea) waters. *Continent. Shelf. Res.* 31, 582–593. doi: 10.1016/j.csr.2010.12.013

Macdonald, H. S., Baird, M. E., and Middleton, J. H. (2009). Effect of wind on continental shelf carbon fluxes off southeast Australia: A numerical model. *J. Geophys. Res.: Oceans.* 114. doi: 10.1029/2008JC004946

McKee, B. A., Aller, R. C., Allison, M. A., Bianchi, T. S., and Kineke, G. C. (2004). Transport and transformation of dissolved and particulate materials on continental margins influenced by major rivers: benthic boundary layer and seabed processes. *Continent. Shelf. Res.* 24, 899–926. doi: 10.1016/j.csr.2004.02.009

McKinley, G. A., Fay, A. R., Eddebbar, Y. A., Gloege, L., and Lovenduski, N. S. (2020). External forcing explains recent decadal variability of the ocean carbon sink. *AGU. Adv.* 1. doi: 10.1029/2019AV000149

McLean, P., Bulmer, C., Davies, P., Dunstone, N., Gordon, M., Ineson, S., et al. (2024). Predictability of European winter 2021/2022: Influence of La Niña and stratospheric polar vortex. *Atmospher. Sci Lett.* 25. doi: 10.1002/asl.1255

Miller, L. A., Shadwick, E. H., and Thomas, H. (2019). Air–sea CO_2 fluxes in the Hudson Bay system: The role of stratification. *Geophys. Res. Lett.* 46, 541–549. doi: 10.1029/2018GL080099

Millero, F. J. (2010). Carbonate constants for estuarine waters. *Mar. Freshw. Res.* 61, 139–142. doi: 10.1071/mf09254

Millero, F. J., Degler, E. A., O'Sullivan, D. W., Goyet, C., and Eischeid, G. (1998). The carbon dioxide system in the Arabian Sea. *Deep Sea Research Part II* 45, 2225–2252.

Millero, F. J., Lee, K., and Roche, M. P. (1998). Distribution of alkalinity in the surface waters of the major oceans. *Marine Chemistry* 60 (1–2), 111–130. doi: 10.1016/S0304-4203(97)00084-4

Monteiro, T., Batista, M., Henley, S., MaChado, E., da, C., Araujo, M., et al. (2022). Contrasting sea-air CO_2 exchanges in the western tropical atlantic ocean. *Global Biogeochem. Cycles.* 36. doi: 10.1029/2022GB007385

Mu, L., Gruber, N., and Doney, S. C. (2020). Seasonality of air–sea CO_2 fluxes in the Arctic Ocean: The role of sea ice, freshwater input, and biological uptake. *Global Biogeochem. Cycles.* 34, e2020GB006574. doi: 10.1029/2020GB006574

Murcia Riaño, M., and Giraldo López, A. (2007). Condiciones oceanográficas y composición del Mesozooplancton en la zona oceánica del Pacífico Colombiano, durante septiembre-octubre 2004. *Boletín. Científico. CCCP.* 14, 83–94. doi: 10.26640/01213423.14.83_94

NOAA. (2021). *Mauna Loa CO_2 monthly mean data*. NOAA Global Monitoring Laboratory. Available online at: https://gml.noaa.gov/ccgg/trends/data.html (Accessed September 2022)

NOAA. (2022). *Mauna Loa CO_2 monthly mean data*. NOAA Global Monitoring Laboratory. Available online at: https://gml.noaa.gov/ccgg/trends/data.html (Accessed September 2022)

Olafsson, J., Olafsdottir, S. R., Takahashi, T., Danielsen, M., and Arnarson, T. S. (2021). Enhancement of the north atlantic CO_2 sink by arctic waters. *Biogeosciences* 18, 1689–1701. doi: 10.5194/bg-18-1689-2021

Oliveira, A. P., Fernandes, A. M., Fonseca, V. F., Vale, C., and Mendonça, A. M. M. (2017). Inorganic carbon distribution and CO_2 fluxes in a large tropical estuary (Tagus, Portugal). *Scientific Reports*. doi: 10.1038/s41598-017-06758-z

Palacios Moreno, M. A., and Pinto Tovar, C. A. (1992). Estudio de la influencia de la marea en el río Guapi. *Boletín. Científico. CCCP.* 3, 3–13. doi: 10.26640/01213423.3.3_13

Palacios Peñaranda, M. L., Cantera Kintz, J. R., and Peña Salamanca, E. J. (2019). Carbon stocks in mangrove forests of the Colombian Pacific. *Estuarine. Coast. Shelf. Sci* 227, 106299. doi: 10.1016/j.ecss.2019.106299

Park, G.-H., Wanninkhof, R., Doney, S. C., Takahashi, T., Lee, K., Feely, R. A., et al. (2010). Variability of global net sea air CO_2; fluxes over the last three decades using empirical relationships. *Tellus. B.: Chem. Phys. Meteorol.* 62, 352. doi: 10.1111/j.1600-0889.2010.00498.x

Parv, S., Chen, Z., Shutler, J., and Watson, A.. (2023). Assessing Air–sea CO2 flux products with constraints from atmospheric inverse analyses. *EGU General Assembly 2023*. doi: 10.5194/egusphere-egu23-10224

Pasquero, C., Bracco, A., and Provenzale, A. (2005). Impact of the spatiotemporal variability of the nutrient flux on primary productivity in the ocean. *J. Geophys. Res.: Oceans.* 110. doi: 10.1029/2004JC002738

Paulmier, A., Ruiz-Pino, D., and Garçon, V. (2011). CO_2 maximum in the oxygen minimum zone (OMZ). *Biogeosciences* 8, pp.239–pp.252. doi: 10.5194/bg-8-239-2011

Peng, C., Crawshaw, J. P., Maitland, G. C., Martin Trusler, J. P., and Vega-Maza, D. (2013). The pH of CO_2-saturated water at temperatures between 308K and 423K at pressures up to 15MPa. *J. Supercrit. Fluids.* 82, 129–137. doi: 10.1016/j.supflu.2013.07.001

Perez, F. F., and Fraga, F. (2003). Association constant of fluoride and hydrogen ions in seawater. *Mar. Chem.* 21, 161–168. doi: 10.1016/0304-4203(87)90036-3

Pierrot, D., Epitalon, J.-M., Orr, J. C., and Lewis, E. R. (2021). and Wallace, D.: MS Excel program developed for CO_2 system calculations – version 3.0. Available online at: https://github.com/dpierrot/co2sys_xl (Accessed May 17, 2025).

Polavarapu, S. M., Deng, F., Byrne, B., Jones, D. B. A., and Neish, M. (2018). A comparison of atmospheric CO2 flux signals obtained from GEOS-Chem flux inversions constrained by in situ or GOSAT observations. doi: 10.5194/acp-2017-1235

Prytherch, J., Yelland, M. J., Pascal, R. W., Moat, B. I., Skjelvan, I., and Srokosz, M. A. (2010). Open ocean gas transfer velocity derived from long-term direct measurements of the CO_2 flux. *Geophys. Res. Lett.* 37. doi: 10.1029/2010GL045597

Quiñones-Rivera, Z. J., Wissel, B., Turner, R. E., Rabalais, N. N., Justić, D., Finlay, K. P., et al. (2022). Divergent effects of biological and physical processes on dissolved oxygen and dissolved inorganic carbon dynamics on a eutrophied and hypoxic continental shelf. *Limnol. Oceanogr.* 67, 2603–2616. doi: 10.1002/lno.12225

Ramaekers, L., Vanschoenwinkel, B., Brendonck, L., and Pinceel, T. (2023). Elevated dissolved carbon dioxide and associated acidification delays maturation and decreases calcification and survival in the freshwater crustacean Daphnia magna. *Limnol. Oceanogr.* 68, 1624–1635. doi: 10.1002/lno.12372

Rastogi, B., Miller, J. B., Trudeau, M., Andrews, A. E., Hu, L., Mountain, M., et al. (2021). Evaluating consistency between total column CO2 retrievals from OCO-2 and the in situ network over North America: implications for carbon flux estimation. *Atmospheric Chemistry and Physics* 21 (18), 14385–14401. doi: 10.5194/acp-21-14385-2021

Reimer, J. J., Vargas, R., Smith, S. V., Lara-Lara, R., Gaxiola-Castro, G., Martín Hernández-Ayón, J., et al. (2013). Air-sea CO_2 fluxes in the near-shore and intertidal zones influenced by the California Current. *J. Geophys. Res.: Oceans.* 118, 4795–4810. doi: 10.1002/jgrc.20319

Restrepo, J. D., and Kjerfve, B. (2004). "The pacific and caribbean rivers of Colombia: water discharge, sediment transport and dissolved loads," in *Environmental Geochemistry in Tropical and Subtropical Environments* (Springer Berlin Heidelberg), 169–187. doi: 10.1007/978-3-662-07060-4_14

Ricaurte-Villota, C., Murcia-Riaño, M., and Hernádez-Ayón, J. M. (2025). Dynamics and drivers of the carbonate system: response to terrestrial runoff and upwelling along the Northeastern Colombian Caribbean coast. *Front. Mar. Sci* 11. doi: 10.3389/fmars.2024.1305542

Ries, J. B., Cohen, A. L., and McCorkle, D. C. (2009). Marine calcifiers exhibit mixed responses to CO_2-induced Ocean acidification. *Geology* 37, 1131–1134. doi: 10.1130/G30210A.1

Rodríguez-Rubio, E., Schneider, W., and Abarca del Río, R. (2003). On the seasonal circulation within the Panama Bight derived from satellite observations of wind, altimetry and sea surface temperature. *Geophys. Res. Lett.* 30. doi: 10.1029/2002GL016794

Roobaert, A., Goulven, L., Resplandy, L., Landschützer, P., Gruber, N., Liao, E., et al. (2021). The spatiotemporal dynamics of the sources and sinks of CO2 in the global coastal ocean. *MPG.PuRe (Max Planck Society).* doi: 10.5194/egusphere-egu21-10048

Roobaert, A., Regnier, P., Landschützer, P., and Laruelle, G. G. (2024). A novel sea surface pCO_2-product for the global coastal ocean resolving trends over 1982–2020. *Earth Syst. Sci Data* 16, 421–441. doi: 10.5194/essd-16-421-2024

Roobaert, A., Regnier, P., Landschützer, P., and Laruelle, G. G. (2025). Global coastal ocean CO_2 trends over the 1982–2020 period. doi: 10.5194/egusphere-egu24-14775

Rosentreter, J. A., Laruelle, G. G., Bange, H. W., Bianchi, T. S., Busecke, J. J. M., Cai, W.-J., et al. (2023). Coastal vegetation and estuaries are collectively a greenhouse gas sink. *Nat. Climate Change* 13, 579–587. doi: 10.1038/s41558-023-01682-9

Santos, I. R., Hatje, V., Serrano, O., Bastviken, D., and Krause-Jensen, D. (2022). Carbon sequestration in aquatic ecosystems: Recent advances and challenges. *Limnol. Oceanogr.* 67. doi: 10.1002/lno.12268

Saraswat, R. (2011). "Global equatorial sea-surface temperatures over the last 150,000 years: an update from foraminiferal elemental analysis," in *current science*, vol. 100. Bangalore, India: Current Science, 1201–1206.

Schneider, T., Bischoff, T., and Haug, G. H. (2014). Migrations and dynamics of the intertropical convergence zone. *Nature* 513, 45–53. doi: 10.1038/nature13636

Séférian, R., Bopp, L., Swingedouw, D., and Servonnat, J. (2013). Dynamical and biogeochemical control on the decadal variability of ocean carbon fluxes. *Earth Syst. Dynamics.* 4, 109–127. doi: 10.5194/esd-4-109-2013

Smith, S. V., and Hollibaugh, J. T. (1993). Coastal metabolism and the oceanic organic carbon balance. *Rev. Geophys.* 31, 75–89. doi: 10.1029/92RG02584

Stevenson, M. (1970). Circulation in the Panama bight. *J. Geophys. Res.* 75, 659–672. doi: 10.1029/JC075i003p00659

Strutton, P. G., Evans, W., and Chavez, F. P. (2008). Equatorial Pacific chemical and biological variability 1997–2003. *Global Biogeochem. Cycles*. 22. doi: 10.1029/2007GB003045

Sun, Q., Li, D., Wang, B., Xu, Z., Miao, Y., Lin, H., et al. (2023). Massive nutrients offshore transport off the Changjiang Estuary in flooding summer of 2020. *Front. Mar. Sci* 10. doi: 10.3389/fmars.2023.1076336

Swesi, A., Yusup, Y., Ahmad, M. I., Almdhun, H. M., Jamshidi, E. J., Sigid, M. F., et al. (2023). Seasonal and yearly controls of CO_2 fluxes in a tropical coastal ocean. *Earth Interact.* 27. doi: 10.1175/EI-D-22-0023.1

Takahashi, T., Feely, R. A., Weiss, R. F., Wanninkhof, R. H., Chipman, D. W., Sutherland, S. C., et al. (1997). Global air-sea flux of CO_2: An estimate based on measurements of sea–air pCO_2 difference. *Proc. Natl. Acad. Sci.* 94, 8292–8299. doi: 10.1073/pnas.94.16.8292

Takahashi, T., Sutherland, S. C., Sweeney, C., Poisson, A., Metzl, N., Tilbrook, B., et al. (2002). Global sea–air CO_2 flux based on climatological surface ocean pCO_2, and seasonal biological and temperature effects. *Deep. Sea. Res. Part II.: Topical. Stud. Oceanogr.* 49, 1601–1622. doi: 10.1016/S0967-0645(02)00003-6

Tide-Forecast.com (2022). Map of tide Stations in Colombia. Available online at: https://www.tide-forecast.com/weather_maps/Colombia (Accessed May 17, 2025).

Tomczak, M. (1981). A multi-parameter extension of temperature/salinity diagram techniques for the analysis of non-isopycnal mixing. *Prog. Oceanogr.* 10, 147–171. doi: 10.1016/0079-6611(81)90010-0

Torres, R. R., Giraldo, E., Muñoz, C., Caicedo, A., Hernández-Carrasco, I., and Orfila, A. (2023). Seasonal and El Niño–Southern oscillation-related ocean variability in the Panama bight. *Ocean. Sci* 19, 685–701. doi: 10.5194/os-19-685-2023

UAESPNN (2005). Parque Nacional Natural Gorgona: Plan de Manejo 2005–2009 (Cali: Unidad Administrativa Especial del Sistema de Parques Nacionales Naturales de Colombia). Available online at: https://koha.parquesnacionales.gov.co/cgi-bin/koha/opac-detail.pl?biblionumber=3899 (Accessed May 17, 2025).

Vaittinada Ayar, P., Bopp, L., Christian, J. R., Ilyina, T., Krasting, J. P., Séférian, R., et al. (2022). Contrasting projections of the ENSO-driven CO_2 flux variability in the equatorial Pacific under high-warming scenario. *Earth Syst. Dynamics.* 13, 1097–1118. doi: 10.5194/esd-13-1097-2022

Vargas, C. A., Martínez, R. A., Cuevas, L. A., Pavez, M. A., Cartes, C., GonzÁlez, H. E., et al. (2007). The relative importance of microbial and classical food webs in a highly productive coastal upwelling area. *Limnol. Oceanogr.* 52, 1495–1510. doi: 10.4319/lo.2007.52.4.1495

Wang, D., Wang, H., Li, M., Liu, G., and Wu, X. (2013). Role of Ekman transport versus Ekman pumping in driving summer upwelling in the South China Sea. . *J. Ocean. Univ. China* 12, 355–365. doi: 10.1007/s11802-013-1904-7

Wang, J., Zeng, N., Wang, M., Jiang, F., Wang, H., and Jiang, Z. (2018). Contrasting terrestrial carbon cycle responses to the 1997/98 and 2015/16 extreme El Niño events. *Earth Syst. Dynamics.* 9, 1–14. doi: 10.5194/esd-9-1-2018

Wanninkhof, R. (2014). Relationship between wind speed and gas exchange over the ocean revisited. *Limnology and Oceanography: Methods* 12, 351–362. doi: 10.4319/lom.2014.12.351

Watanabe, K., Tokoro, T., Moki, H., and Kuwae, T. (2024). Contribution of marine macrophytes to pCO_2 and DOC variations in human-impacted coastal waters. *Biogeochemistry* 167, 831–848. doi: 10.1007/s10533-024-01140-4

Weber, E. D., Auth, T. D., Baumann-Pickering, S., Baumgartner, T. R., Bjorkstedt, E. P., Bograd, S. J., et al. (2021). State of the California current 2019–2020: back to the future with marine heatwaves? *Front. Mar. Sci* 8. doi: 10.3389/fmars.2021.709454

Weiss, R. F. (1974). Carbon dioxide in water and seawater: the solubility of a non-ideal gas. *Mar. Chem.* 2, 203–215. doi: 10.1016/0304-4203(74)90015-2

Willett, C. S., Leben, R. R., and Lavín, M. F. (2006). Eddies and Tropical Instability Waves in the eastern tropical Pacific: A review. *Prog. Oceanogr.* 69, 218–238. doi: 10.1016/j.pocean.2006.03.010

Williams, R. G., and Follows, M. J. (2003). "Physical transport of nutrients and the maintenance of biological production," in *Ocean biogeochemistry: The role of the ocean carbon cycle in global change* (Springer Berlin Heidelberg, Berlin, Heidelberg), 19–51.

Wong, S. C. K., McKinley, G. A., and Seager, R. (2022). Equatorial pacific pCO_2 interannual variability in CMIP6 models. *J. Geophys. Res.: Biogeosci.* 127. doi: 10.1029/2022JG007243

Yilmaz, E., Bernardello, R., and Martin, A. P. (2022). *Natural processes behind the CO_2 sink variability in the Southern Ocean during the last three decades*. Göttingen, Germany: Copernicus GmbH doi: 10.5194/egusphere-egu22-7827

Zhai, W., Dai, M., Cai, W.-J., Wang, Y., and Hong, H. (2005). The partial pressure of carbon dioxide and air–sea fluxes in the northern South China Sea in spring, summer and autumn. *Mar. Chem.* 96, 87–97. doi: 10.1016/j.marchem.2004.12.002

Frontiers in Marine Science

Explores ocean-based solutions for emerging global challenges

The third most-cited marine and freshwater biology journal, advancing our understanding of marine systems and addressing global challenges including overfishing, pollution, and climate change.

Discover the latest Research Topics

See more →

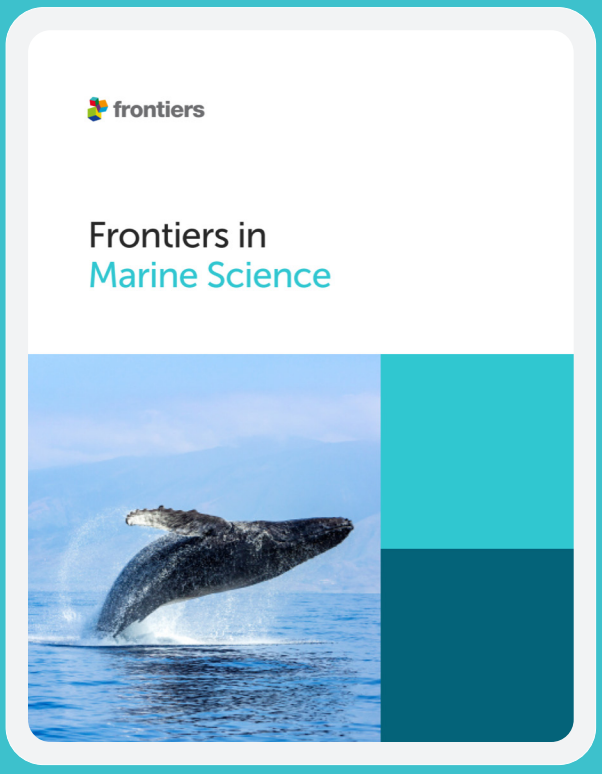

Frontiers

Avenue du Tribunal-Fédéral 34
1005 Lausanne, Switzerland
frontiersin.org

Contact us

+41 (0)21 510 17 00
frontiersin.org/about/contact